Verification
of Crystal Growth
Models by Detailed
Surface Microtopography
and X-Ray Diffraction Topography

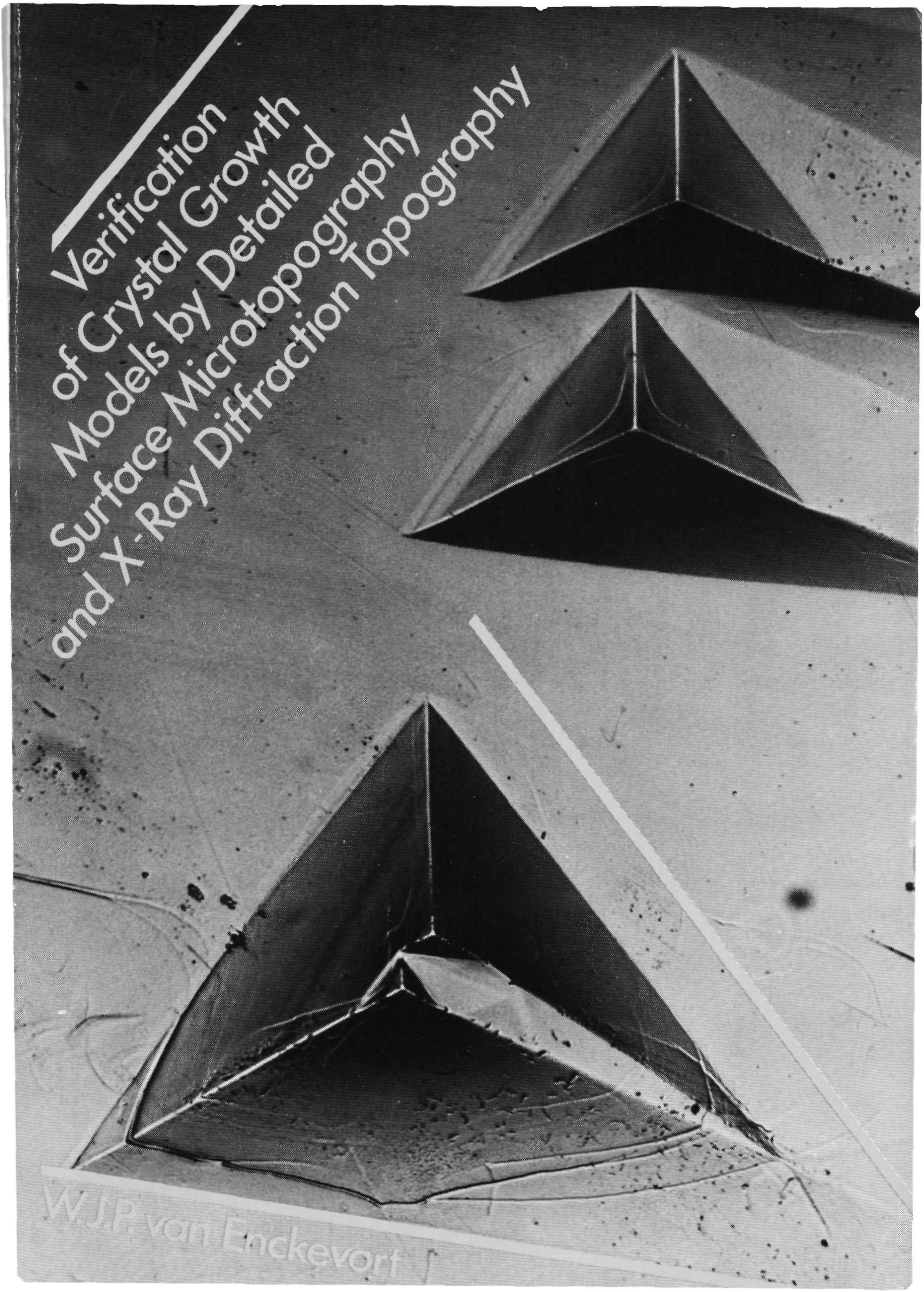

W.J.P. van Enckevort

Front cover:
Trigonal dislocation etch pits formed after slight disolution of an [1 1 1] face of a potash alum single crystal in water.

VERIFICATION OF CRYSTAL GROWTH MODELS BY DETAILED SURFACE MICROTOPOGRAPHY AND X-RAY DIFFRACTION TOPOGRAPHY

Promotoren: Prof. Dr. P. Bennema
Prof. Dr. J. Bloem

VERIFICATION OF CRYSTAL GROWTH MODELS BY DETAILED SURFACE MICROTOPOGRAPHY AND X-RAY DIFFRACTION TOPOGRAPHY

PROEFSCHRIFT
TER VERKRIJGING VAN DE GRAAD VAN DOCTOR
IN DE WISKUNDE EN NATUURWETENSCHAPPEN
AAN DE KATHOLIEKE UNIVERSITEIT TE NIJMEGEN,
OP GEZAG VAN DE RECTOR MAGNIFICUS
PROF. DR. P.G.A.B. WIJDEVELD
VOLGENS BESLUIT VAN HET COLLEGE VAN DEKANEN
IN HET OPENBAAR TE VERDEDIGEN
OP VRIJDAG 26 FEBRUARI 1982
DES NAMIDDAGS OM 4 UUR

DOOR

WILHELMUS JOHANNUS PETRUS VAN ENCKEVORT

GEBOREN TE BLERICK

1982
DRUK · STICHTING STUDENTENPERS NIJMEGEN

This thesis contains the results of a number of characterization studies of several crystal types in relation to their growth properties.

I am greatly indepted to the co-authors of the papers presented in this thesis as well as to all the members of the department(s) of solid state chemistry, for supplying all kinds of crystals and theories, for their invaluable help in characterizing the specimens and, most importantly, for their pleasant companionship.
I am especially grateful to Katsuo Tsukamoto, who introduced me into the highest level of the art of characterizing crystals, during his stay of two years at our laboratory.

Further I want to thank the two departments of electron microscopy (especially Ing. A.W. Dicke), the department of photography and the other technical departments at the University of Nijmegen for their assistance in the investigations.

These investigations were supported by the Netherlands Foundation for Chemical Research (SON), with financial aid from the Netherlands Organisation for Pure Scientific Research (ZWO).

Aan mijn moeder

CONTENTS

INTRODUCTION

IONIC CRYSTALS GROWN FROM AQUEOUS SOLUTIONS

Potash alum

Potassium hydrogen phthalate

Potassium dihydrogen phosphate

CRYSTALS WITH A DIAMOND-LIKE STRUCTURE

Silicon

$CuInS_2$ and $CuGaS_2$

Synthetic diamond

INTRODUCTION

In the present-day technological society, growth of crystals is of essential importance, especially in the fields of high quality single crystal growth for products like electronic devices (e.g. Si, Ge and GaAs), oscillators (quartz) and optical components (e.g. garnet, calcite, and KH_2PO_4) and, on a larger scale, of industrial crystallization of bulk materials, like sugar, fertilizers and NaCl.

However, despite that in industry crystallization is employed extensively, the understanding of the fundamental aspects of the crystal growth process is limited. This is still due to "a lack of really powerful experimental tools for studying the critical steps of the growth process" as Gilman (1) already stated about twenty years ago. The fact that the relevance of the theoretical models is hardly determined, implies that it is often very difficult to apply them to real crystal growth systems, so that growth of good crystals, both on laboratory and on industrial scale, necessarely remains an art, and often can only be achieved by trial and error.

On the other hand also the development of relevant theoretical models is hindered by the limited number of sufficiently precise experimental methods to study crystal growth processes from a fundamental point of view, because almost no "feed-back" from "real" crystal growth systems is possible.

The fact that crystal growth and dissolution are surface processes, implies that detailed examination of the crystal surfaces in relation to growth conditions is the obvious means for testing the possibilities and limitations of crystal growth models. To achieve this, surface examination by modern optical microscopy plays a main role. However, the surface morphology is to a large extent determined by the internal defect structure of the crystals, so that it is essential to complement surface microtopography with X-ray diffraction topography. Finally it is to be mentioned that, in general, the theoretical models have to be adjusted to specific non-idealized cases, to allow for a proper -in the present thesis mostly qualitative- correlation between theory and experiment.

The three tools to study the crystal growth process from a more fundamental point of view, will be treated in some detail below.

I. OPTICAL METHODS FOR CRYSTAL SURFACE EXAMINATION

The main object in the application of optical reflection microscopy for investigating crystal surfaces is to

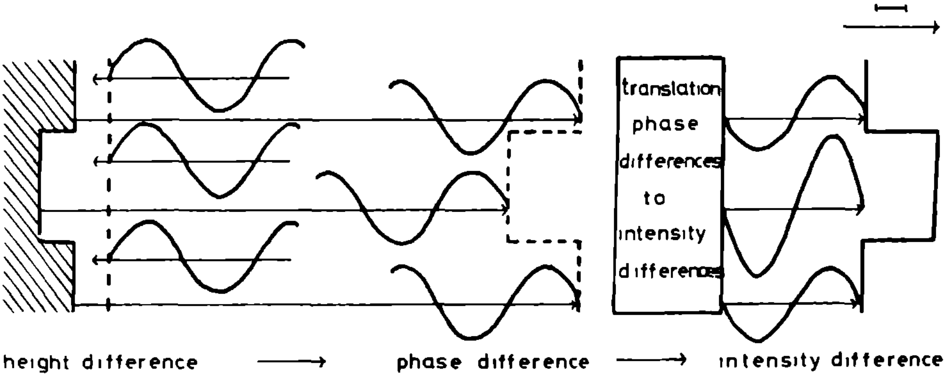

Fig.1. Fundamental principle of the detection of height differences on -crystal- surfaces by optical microscopy.

reveal growth steps and all kinds of undulations on the crystal surfaces. This implies that the optical microscope must be capable to detect both extremely low height differences, as low as one atomic layer, and very low inclinations, down to about 0.05 degrees. The only way to achieve this is to convert height differences into phase differences, which finally are transformed into intensity differences as illustrated schematically in figure 1. The conversion of phase differences into intensity differences has to be done for the simple reason, that only intensity but no phase differences can be detected by eye, photographic emulsion or video system. This transformation can be carried out in two fundamentally different ways:

(A) By manipulation of the fourier transform of the wave front reflected from the crystal surface;
(B) By interferometric techniques.

(A) "Fourier methods"

In figure 2a a simple schematic representation of an ordinary microscope is presented. Here an image of the object, located in the object plane ,OP, is created in the image plane ,IP, by the objective lens according to

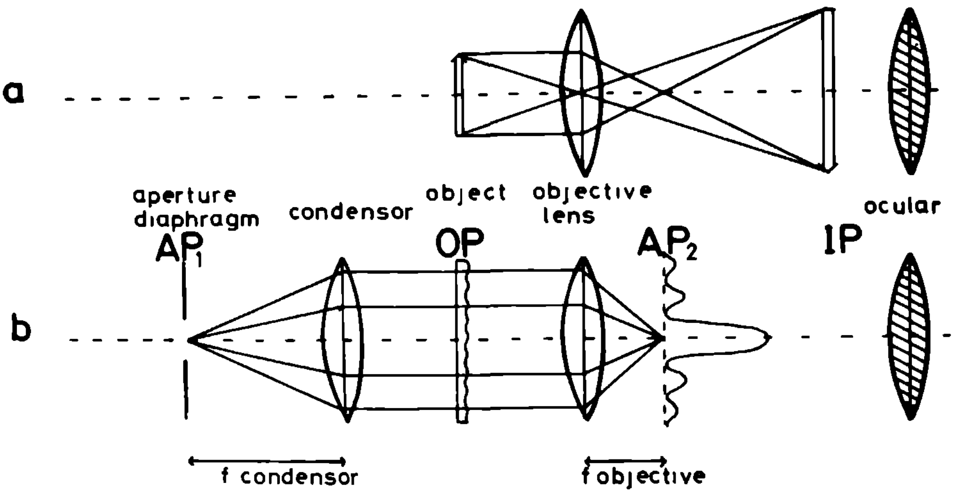

Fig.2. Kohler illumination in modern microscopy:
(a) Simple microscope consisting of an objective lens and an ocular. The objective lens creates an image in the image plane IP of the object in the object plane OP.
(b) The same microscope as (a) but now fitted with a condensor lens and an aperture diaphragm AP_1 in its front focus. The system condensor - objective lens creates an image of AP_1 at AP_2, being the fourier tranform of the object "smeared out" with the image of AP_1.

the principles of conventional geometrical optics. Nowadays, nearly all better quality microscopes are fitted with an illumination system according to th principle of Kohler (2) as shown in figure 2b. In this case, among others, a condensor lens and an aperture diaphragm AP_1, located at the front focus of this condensor is added to the system in order to obtain an homogeneous illumination of the object OP. It is to be noted, that for simplification in figure 2 the case of transmission instead of reflection microscopy has been presented, but no essential differences exist between both systems. In the case of reflection microscopy, which is commonly used for crystal surface examination the object located at OP corresponds to the crystal surface.

From figure 2b it can be seen that the optical system condensor-objective lens creates an image of the aperture diaphragm AP_1 at AP_2, located at the focus of the objective lens. However, the image in AP_2 is deformed by the presence of the object OP in the path of rays. Formulated in terms of modern fourier optics this means, that the image created in AP_2 is the fourier transform (i.e. the diffraction pattern) of the object located at OP, "smeared out" with the image of the aperture diaphragm (3). A typical fourier transform of an arbitrary phase object (2), for instance a crystal surface, using a relatively closed aperture diaphragm AP_1 is given in figure 3 by the solid line. Clearly a large zero order peak, containing no information on phase details and some smaller peaks having the information on phase details, such as steps and hillocks for the case of crystal surfaces can be seen.

It is easily to be understood that by recombining the components of this "smeared" fourier transform to an image of the object in the image plane ,IP, the central peak overradiates the weaker components, so that phase information gets lost, which occurs in the case of ordinary bright field microscopy.

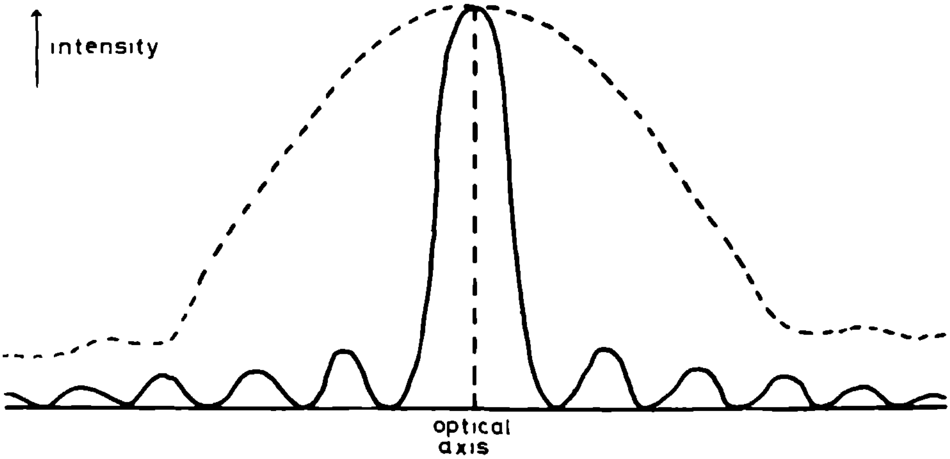

Fig.3. Diffraction patterns ("fourier transforms") of an arbitrary phase object: Solid line, case of nearly closed aperture diaphragm; dashed line case of open aperture diaphragm AP_1.

Several methods exist to "manipulate" the fourier transform of the phase object, such as:

(i) Removal of the central peak, so that the reconstructed image is only formed by first and higher order peaks, containing the phase information. This method is known as "dark field illumination". The elimination of the zero order peak is achieved by a wide variety of methods, for instance by placing a small opaque beam stop at the centre of the diffracted image at AP_2.

(ii) Closure of the aperture diaphragm AP_1 to a large extent, resulting in a lower "smearing out" of the zero order peak in the diffracted image in AP_2. In figure 3 the fourier transform for the case of a completely opened aperture diaphragm AP_2 is given by the dashed line, whereas for a nearly closed aperture diaphragm the diffracted image of OP is presented by the solid line. It can clearly be seen that in contrast to an open aperture AP_2, in the case of a nearly closed aperture (also called pencil illumination) the central peak does not overwhelm the smaller peaks containing the phase information.

(iii) Exclusion of the fourier components at one side of the central peak, by placing a "knife-edge" in AP_2 (Schlieren method (3)) or by oblique illumination in such a way that the, now eccentrically positioned, central peak is just half obscured by the edge of a diaphragm placed in AP_2. The latter method combined with a closure of the incident beam aperture diaphragm as described in (ii) has been applied for the in situ crystal surface examinations described in Chapter VII.

(iv) Strong reduction in intensity, combined with a phase shift of a quarter of a wavelength of the light used, of the central peak gives the best manner to translate phase differences into intensity differences. This technique, in 1935 proposed by Zernike (4) is now well known as phase contrast microscopy and has been used as the most important surface microtopographic technique throughout this thesis.

(B) Interference methods

Interference microscopy covers two fields:
(i) Interferometry, by which quantitative information on the phase object (i.e. the crystal surface) can be obtained.
(ii) Interference contrast, by which phase differences are translated into intensity or colour differences.

(i) Interferometry

The most simple and most commonly used interferometric technique is the two beam method, based on the

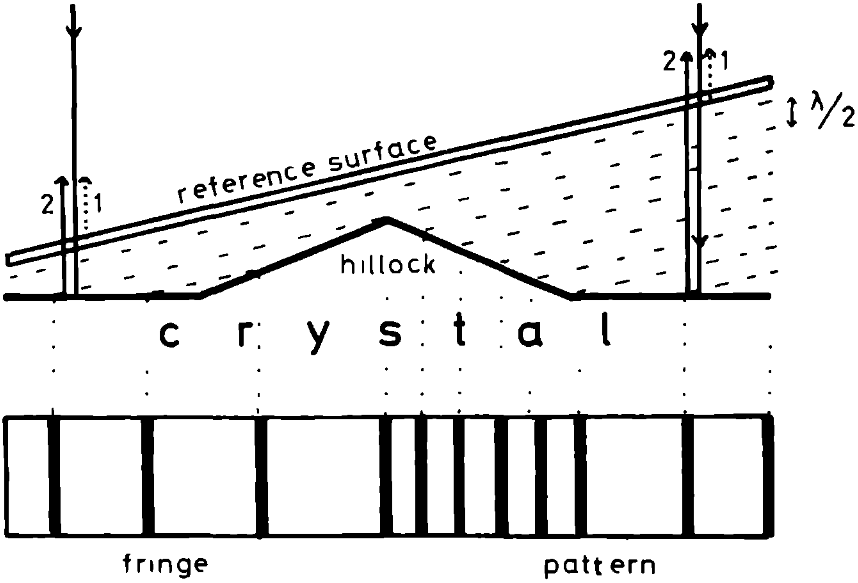

Fig.4. Principle of two-beam interferometry, demonstrated for the case of a two-dimensional growth hillock on a crystal surface.

principle of the formation of Newton rings, produced by the interference of two reflected beams of monochromatic light (2,5): one from the specimen surface (the solid lines 2 in figure 4) and another from a reference surface (the dotted lines in figure 4), being a very flat glas plate. To obtain clear interference fringes the separation between the specimen and the reference surface has to be less than a few microns. From the fringe pattern created by this method (in figure 4 presented for the case of a growth hillock) inclinations or step heights can be determined.

By coating the specimen and the reference surfaces with a thin layer of silver, so that the reflectivity of both surfaces become higher than 80%, the fringes in the interference pattern become much sharper, due to multiple reflection between both surfaces (5). As a result of this increased sharpness of the fringes the accuracy of the height or inclination measurements is increased strongly. This method, which has extensively been used by Tolansky (6) is known as multiple beam interferometry.

(ii) Interference contrast

Of the numerous interference contrast techniques described in literature (2), in this thesis only differential interference contrast methods have been used to examine the crystal surfaces. Therefore only this method to translate height (i.e. phase) differences to intensity differences will be treated here.

The fundamental principle of all types of differential interference contrast microscopes is shown in figure 5: Firstly a plane wave (the incident beam), which is indicated by the dotted line is reflected at a surface with one step of height h. Then the reflected beam, the wave front of which is drawn by the dashed line, passes an optical device, that splits the original wave into two coherent waves of varying or equal intensity, which are laterally shifted over a small distance Δ. Interference of the two coherent waves, finally results in an intensity distribution, which is constant over the whole surface, except for the region Δ, where a phase difference exists between both waves, being equal to 4π h/λ. In this way the step on the -crystal- surface becomes visible as a line of different intensity in the microscopic image.

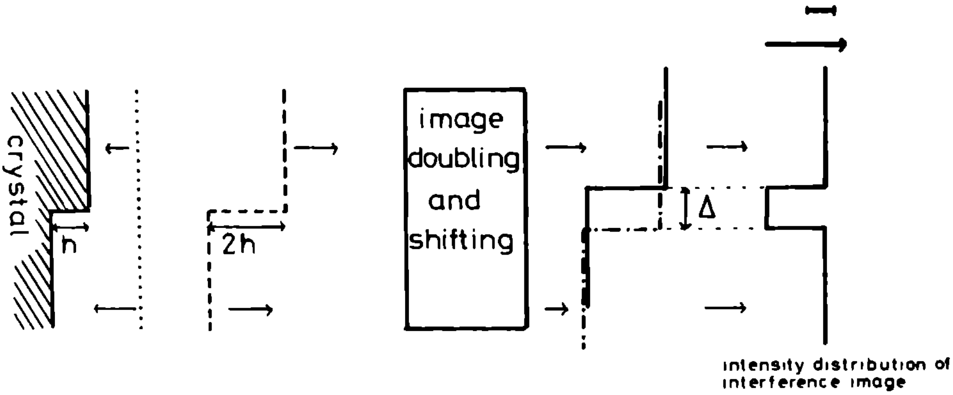

Fig.5. Fundamental principle of differential interference contrast microscopy, demonstrated for the case of a step on a -crystal- surface.

To achieve this image doubling, many systems have been designed (2), among which the method of Nomarski (7,8) has mostly been employed for the surface micro-topographic investigations presented in this thesis.

II. X-RAY DIFFRACTION TOPOGRAPHY

Among the numerous experimental techniques developed during the last thirty years, the Lang method (9) is the most popular and widely used technique of X-ray diffraction topography. In this thesis this method has been used to study the defect structure of crystals in relation to their growth properties.

The principle of Lang's transmission tecnique is illustrated in figure 6: A "point focus" X-ray source emits a beam of monochromatic X-rays, which passes through a collimator, being a slit of varying width. This collimated beam enters the crystal, which is very accurately adjusted in such a manner that diffraction from a particular set of lattice planes is obtained. The diffracted beam is recorded on a fine grain photographic emulsion, whereas the direct beam is stopped by a slit. Two methods for obtaining an image exist, namely (i) Section topography (10), in which case the crystal and the film are not translated and a collimating slit of ∿10μ in width is used and (ii) Projection topography (11) by scanning the crystal and the film across the beam, using a collimating slit of 0.5 mm in width. In this thesis only the projection technique, by which complete images of the crystals can be obtained has been employed.

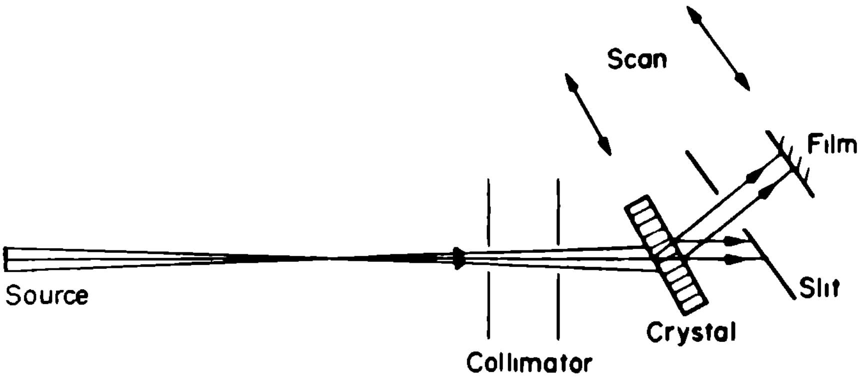

Fig.6. Schematic representation of Lang's transmission X-ray diffraction topographic technique.

Using Lang's topographic technique it is possible to detect lattice bendings as low as about 5.10^{-4} rad (9), which can be recognized as local differences in diffracted intensity on the topographs. This means that defects inducing such or larger lattice deformations over an area larger than the spatial resolution of this method (1-3μ) can directly be observed on the topographic images of the crystals. To this group of defects belong, among others, dislocations, stacking faults, growth bands, growth sector boudaries and larger point defects.

The difference in contrast of the -slightly- distorted regions with respect to the unperturbated background regions of the crystal images on the Lang topographs can manifest in three different ways, depending on the linear absorption coefficient (μ) and the thickness of the crystal ($\sim$t) (9,12):

(i) For thin crystals with low absorption ($\mu t < 1$) the direct image is the most dominant one. In this case the deformed crystal regions exhibit an increased intensity, visible as dark areas on the topographs.

(ii) For thick, highly absorbing crystals ($\mu t < 10$) the dynamical image is most predominant. In this case the deformed crystal regions appear as white -i.e. less intense with respect to the background region- images on the topographs.

(iii) On the topographs of crystals with intermediate thickness and absorption coefficient ($1 < \mu t < 10$) the images of defects can show an oscillatory contrast. This is known as the intermediary image.

The majority of the dislocations on the Lang topographs presented in this thesis have a direct image contrast.

III SURVEY OF CRYSTAL GROWTH THEORIES

The phenomenon of crystal growth can be described theoretically at five different scales:

1) Molecular or atomistic level, at which individual growth or dissolution units, interacting with each other are considered (fig. 7-1).

The foundation of this approach was laid by Kossel and Stranski (13), who formulated the molecular-kinetic theory of crystal growth, by following the successive stages of each crystal growth process (viz. attachment at the surface → surface diffusion → step integration) at molecular scale. Later on this molecular description has been extended by theoretical physicists, using highly sophisticated statistical mechanics, both in an ana-

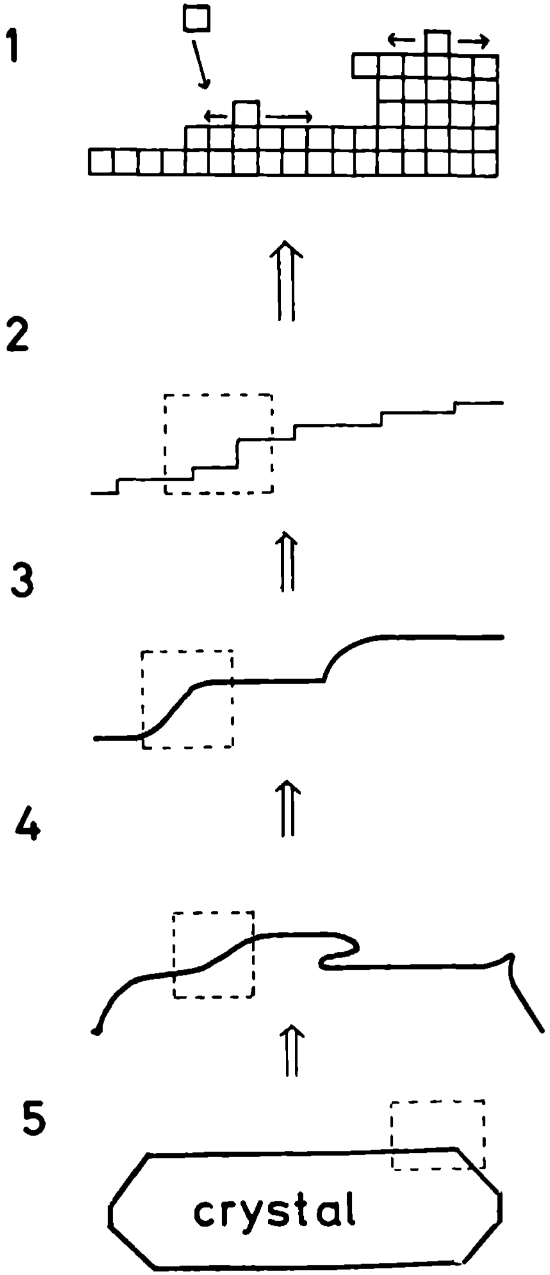

Fig.7. Schematic illustration of the five successive levels of describing crystal growth processes.

lytical way (14) and with the aid of Monte Čarlo computer simulations (15). The most important conclusion drawn from this work is that, very probably for each F-face (16) a critical temperature exists above which the crystal surface is rough and growth proceeds according to a modified Wilson-Frenkel law (15). Below this critical temperature, the value of which depends on the crystal type and the growth system (17), the surface is flat at a molecular level and growth proceeds via a step flow mechanism, which can better be described at the subsequent scale 2.

2) Step flow models, in which no individual growth units are considered, but steps on a crystal surface are described as "advancing lines", functioning as sinks (or in the case of dissolution as sources) of fluxes of molecules on or above the crystal surface (fig.7-2).

At this level the spiral growth theory of Burton, Cabrera and Frank (18), as well as the Birth and Spread model for two-dimensional nucleation growth (19) have been formulated. The appropriate method to study crystal growth processes at this scale is application of phase contrast microscopy in combination with theoretical interpretation based on recently developed step flow models (20).

3) Kinematic wave models for step flow, in which individual steps are no longer considered, but growth of a crystal face is described in terms of step densities and step fluxes (fig. 7-3).

The kinematic wave theory describes the advancement of extended step trains on crystal surfaces in a similar way as traffic flows on roads. When somewhere a perturbation in a equidistant train of steps occurs (a "street accident"), it may develop into a macroscopic compilation of steps (a "traffic jam"), called a bunch (21,22). To study these phenomena, differential interference contrast and two- or multiple beam interferometry are the most suitable characterization methods.

4) Models describing morphological instabilities of crystal faces in transport limited growth systems (fig. 7-4).

If the mass or heat transport processes are slow compared with the interface processes, the surface morphology is to a large extent determined by the gradients in supersaturation in the liquid or gas phase, as was described by Sekerka (23) for smooth and by Chernov (24) for facetted interfaces. At this level the formation of "hoppers", dendrites and inclusions, phenomena which can most appropriately be studied by means of scanning electron microscopy, are formulated.

5) Macroscopic morphology, i.e. the external crystal shape, in relation to the crystallographic structure (fig.7-5).

The most sophisticated way to obtain a relationship between the crystallographic structure (at molecular scale) and the crystal shape (at macroscopic scale) is application of the Periodic Bond Chain (PBC) method developed by Hartman and Perdok (16). The morphology of single crystals can most easily and accurately be characterized by means of an optical goniometer.

Recently it was shown that the PBC method is also a very important tool to allow application of the various crystal growth theories at molecular level, mostly only developed for the ideal Kossel crystal, to "real" crystals having a more or less complicated crystallographic structure (25). By this connection between the largest, macroscopic, scale and the molecular scale the cycle of the successive levels of describing crystal growth theories is closed.

SCOPE AND SUMMARY OF THIS THESIS

Up to now the three methods described above to study crystal growth processes, viz. surface microtopography, X-ray diffraction topography and theoretical interpretation have mostly been used separately to tackle the problems in crystal growth. In the present work it is attempted to combine these three "voices" to one complicated "fugue" in order to get a deeper understanding of the relation between theory and experiment for several kinds of crystals, which can be distinguished in two main categories:

(i) Ionic crystals grown from aqueous solutions (Chapters I-XI)

For three typical representatives of this group of crystals, namely potash alum, potassium hydrogen phthalate and potassium dihydrogen phosphate, it is shown by ex situ and in situ surface microtopography that growth proceeds via a spiral growth or two-dimensional nucleation mechanism, involving higher and lower steps. These observations put an end to earlier speculations on the growth mechanism of this class of compounds, deduced from growth kinetics. During the microtopographic studies, for the first time unit lattice height and lower steps were revealed and measured on aqueous solution grown crystals (Chapters II and VI). However, a new and quite unexpected problem did arise, namely the occurrence of an as yet unexplained complete standstill in growth or step advancement (not related to changes in dislocation structure or the supersaturation), for {100} and {110} potash alum (Chapters III and IV), {100} and {101} KH_2PO_4 (Chapter XI) and for {010} potassium hydrogen phthalate (Chapter VII). This phenomenon, noted earlier by Chernov et al. for $(NH_4)H_2PO_4$ (26), probably will be one of the main topics for studies on crystal growth from solution in the near future.

A final point to be mentioned is that the very first results of the in situ observations of the growth behaviour of {010} potassium hydrogen phthalate (Chapter VII) are thus promising, that it can safely be concluded that such direct observations will lead to an -up till now never realized- unambiguous quantitative comparison of crystal growth theories to solution growth experiments in the coming decade.

(ii) Crystals with a diamond-like structure (Chapters XII-XX)

In the second part of the thesis attention is focussed to four different compounds having a diamond or a related structure, i.e. silicon, $CuInS_2$, $CuGaS_2$ and synthetic diamond, which all are of major importance in the field of materials science.

For this category of crystals, in addition to spiral growth and two-dimensional nucleation, also found for the aqueous solution grown ionic crystals, three other specific growth phenomena were studied in detail:

(a) Bunch formation on gas phase etched {111} silicon, which was interpreted by an extended version of the kinematic wave theory, developed by Frank (21) and by Cabrera and Vermilya (22) (Chapter XV).

(b) Generation of growth steps at the outcrops of twin planes at the crystal surface, resulting in fast growth according to a Twin Plane Reentrant Edge (TPRE) growth mechanism, for the case of growth of poly-crystalline silicon on -or better "in"- a molten metal layer, on top of a graphite substrate (Chapter XIV).

(c) Vapour-Liquid-Solid (VLS) growth of $CuInS_2$ and $CuGaS_2$ crystals, grown by the chemical vapour transport method, using iodine as a transporting agent. In this case growth from the gas phase proceeds via a liquid layer of CuI, covering the crystal surface, which enhances two-dimensional nucleation due to a lowering of the edge free energy at the liquid-solid interface with respect to the gas-solid interface (Chapters XVI and XVII).

The thesis is closed with a characterization study on both the surface morphology and the inner structure of synthetic diamond, by employing a wide variety of complementary topographic techniques, in order to unravel the growth mechanism of the man-made diamonds. This integral approach leads to the important conclusion that synthetic diamond is a typical case of a solution grown crystal (Chapter XIX and XX).

(1) J.J. Gilman, in: The Art and Science of Growing Crystals, Ed. J.J. Gilman (J. Wiley and Sons, New York, 1963) p. vii.

(2) H. Beyer, Theorie und Praxis der Interfenzmikroskopie (Akad. Verlaggeselschaft Geest & Portig K.-G, Leipzig, 1974).

(3) J.W. Goodman, Introduction to Fourier Optics (Mc Graw - Hill Book Company, San Francisco).

(4) F. Zernike, Z. Tech. Phys. 16 (1935) 454.

(5) H. Komatsu, in: Crystal Growth and Characterization, Proc. ISSCG2 Springschool, Japan, 1974, Eds. R.Ueda and J.B. Mullin (North Holland, Amsterdam, 1975) p. 333.

(6) S. Tolansky, Surface Microtopography (Longmans, London, 1960).

(7) G. Nomarski and A.R. Weill, Bull. Soc. Franc. Mineral. Crist. 77 (1954) 840.

(8) G. Nomarski and A.R. Weill, Rev. Met. 52 (1955) 121.

(9) B.K. Tanner, X-Ray Diffraction Topography, I.S. Science of the Solid State, Vol. 10 (pergamon, 1976).

(10) A.R. Lang, J. Appl. Phys. 29 (1958) 597.

(11) A.R. Lang, Acta Cryst. 12 (1959) 249.

(12) A. Authier, in: Modern Diffraction and Imaging Techniques, Eds. Amelinckx et al. (North Holland, Amsterdam, 1970) p.481.

(13) R. Kaischew, J. Crystal Growth 51 (1981) 643.

(14) D.E. Temkin in, Crystallization processes, Eds. N.N. Sirota et al. (Plenum, New York, 1966) p.15.

(15) J.P. van der Eerden, P. Bennema and T.A. Cherepanova, Progr. Crystal Growth Charact. Vol. 1 pp 219-254.

(16) P. Hartman in: Crystal growth: An Introduction, Ed. P. Hartman (North Holland, Amsterdam, 1973) p. 367.

(17) P. Bennema and J.P. van der Eerden, J. Crystal Growth 42 (1977) 201.

(18) W.K. Burton, N. Cabrera and F.C. Frank, Phil. Trans. Roy. Soc. London A243 (1951) 299.

(19) W.B. Hillig, Acta Met. 14 (1966) 1968.

(20) J.P. van der Eerden, J. Crystal Growth 52 (1981) 14; 53 (1981) 305,315.

(21) F.C. Frank, in: Growth and Perfection of Crystals (J. Wiley and Sons, New York, 1958) p.411.

(22) N. Cabrera and D.A. Vermilya, in: Growth and Perfection of Crystals (J. Wiley and Sons, New York, 1958) p.393.

(23) R.F. Sekerka, in: Crystal growth: An introduction, Ed. P. Hartman (North Holland, Amsterdam, 1973) p. 403.

(24) A.A. Chernov, Sov. Phys. Cryst. 8 (1963) 63 and 16 (1971) 734 and J. Crystal Growth 24/25 (1974) 11.

(25) T.A. Cherepanova, G.T. Didrichons, P. Bennema and K. Tsukamoto, work in progrees.

(26) A.A. Chernov, I.L. Smolski, V.F. Parvov, Yu. G. Kuznetsov and V.N. Rozhanskii, Sov. Phys. Dokl. 24 (1979) 760.

IONIC CRYSTALS GROWN FROM AQUEOUS SOLUTIONS

POTASSIUM ALUMINIUM ALUM

Journal of Crystal Growth 47 (1979) 196–202

ON THE RELATION BETWEEN ETCH PITS OR GROWTH HILLOCKS AND DISLOCATIONS ON THE (111) FACES OF POTASSIUM ALUMINIUM ALUM

W.J.P. VAN ENCKEVORT and W.H. VAN DER LINDEN
R.I.M. Laboratory of Solid State Chemistry, Faculty of Science, Catholic University, Toernooiveld, Nijmegen, The Netherlands

Received 3 January 1979; manuscript received in final form 18 March 1979

A correlation has been made between etch pits formed on the (111) faces of potassium aluminium alum after etching in water and dislocations in the crystal by application of a simple etch polish and reetch technique and by relating the observed optical stress birefringence images of edge dislocations with higher Burgers vectors in the crystal to etch pits at the surface. Growth hillocks observed on solution grown potash alum (111) could be related to dislocation outcrops at the crystal surface, giving a direct evidence for a spiral growth mechanism.

1. Introduction

It is known for a considerable time that after etching in water the octrahedral faces of potash alum show well developed trigonal etch pits [1,2]. A more detailed phenomenological study on this subject has been given recently by Omar and Youssef [3]. Growth hillocks on the other hand have been observed on the (111) faces of solution grown potash alum crystals as long as three decennia ago [4]. Recent work on potash alum has for example been carried out by Emara et al. [5] who studied the dislocation structure in these crystals by means of X-ray topography and by Bennema [6] and Garside et al. [7], who both concluded after a detailed investigation of the dependence of the crystal growth rate versus supersaturation that growth must take place according to a spiral growth mechanism. However, a direct proof for this statement could not be given.

The purpose of this study is to correlate the above mentioned phenomena to each other and to get direct evidence for the spiral growth mechanism on potash alum. For this purpose we applied reflection interference contrast microscopy to observe the surfaces and transmission polarization microscopy to detect the birefringence images of dislocations in the crystals.

2. Experimental procedure

The potash alum crystals have been grown in the following way [8]. A well developed seed crystal of about 0.25 cm^3 is mounted on a plastic rod and is placed in a thermostated (±0.01 deg) saturated aqueous solution, which is allowed to cool down at a rate of 0.2°C per 24 h. After a period of a few weeks a clear and well formed octahedral crystal of about 2.5 cm^3 can be obtained in this way.

Before the observation of growth phenomena the crystal is picked up quickly from the supersaturated solution and is dipped for a moment in n-hexane (kept at the same temperature as the solution) in order to remove the adsorbed water layer from the crystal. After this the adhering n-hexane is soaked up with a piece of blotting paper. This procedure has to be done to minimize secundary effects as, e.g., local growth or etching of the crystal.

For obtaining an etch pattern for observation, the crystal is dipped for a few seconds in deionized water at room temperature, after this the same procedure to eliminate secundary effects as described above is carried out.

In order to polish the (111) faces of the crystals a soft felty cloth pasted on a metal disc and wetted with a saturated aqueous potash alum solution has been used.

3. Observations and discussion

3.1. Etch pits formed after dissolution in water

Fig. 1 shows a typical pattern of etch pits on potash alum (111) after a slight etch in water. Many triangular pits, sometimes ordered in rows, can be seen [3,9], showing their side faces parallel to the $\langle\bar{1}10\rangle$ directions. These trigons are oriented in such a way that their angular points point to the $\langle 11\bar{2}\rangle$ directions.

For a better understanding of the origin of the etch pits a repeated alternating etching and polishing technique has been applied. The result is demonstrated in fig. 2: Fig. 2b shows the etch pit pattern after polishing (during which so much material was removed that the original pattern could no longer be observed) and reetching of the same area as in fig. 2a. It can clearly be seen that there is no change in the pattern; this indicates strongly that these pits are related to line-defects (in other words these trigons are *dislocation etch pits*).

Keeping this in mind the observed rows of etch pits (fig. 1) can be interpreted as low angle grain boundaries. It also can be understood that during continuous etching the etch pits rarely disappear, because a dislocation line cannot end within a crystal. However, in the few cases when a dislocation line ends on an inclusion, this can be identified by the appearance of flat-bottomed etch pits, which disappear soon after continued etching. The conclusion drawn by Gülzow et al. [9] from their growth experiments, that during growth of potash alum crystals defects of the nucleus propagate as so called "primary distortions" in the growing crystal, can now easily be understood by identifying these "primary distortions" as dislocations.

The distribution of the etch pits on the {111} faces of very carefully grown crystals is not homogeneous: At the center of the {111} surfaces the pit density is about 10^4–10^5 cm^{-2}, near the edges about 10^2–10^3 cm^{-2} or sometimes even less. A similar etch pit distribution on potash alum (111) has also been reported by Gülzow et al. [9].

This is in complete agreement with the examina-

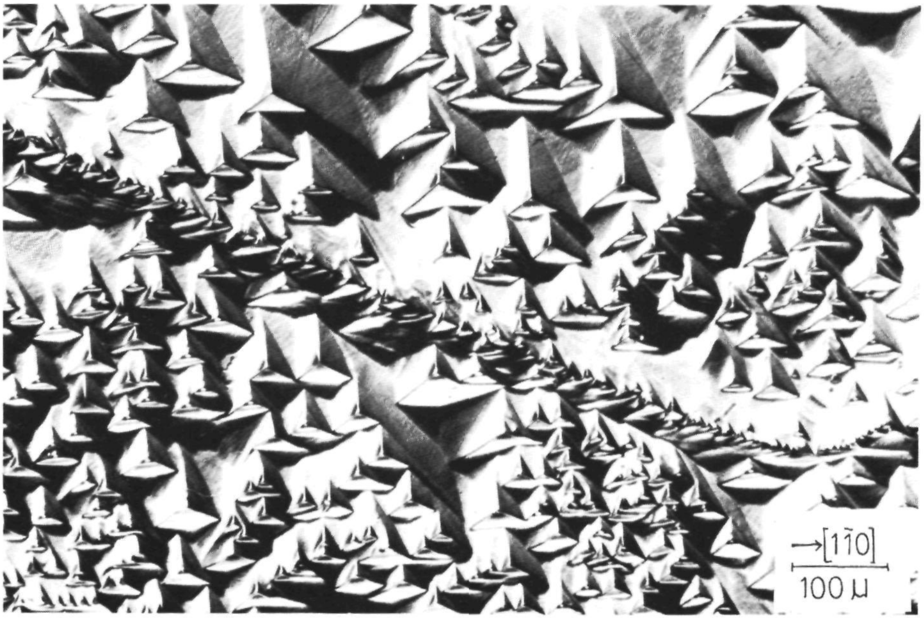

Fig. 1. Typical etch pit pattern, including a small angle grainboundary, on potash alum (111) after slight dissolution in water.

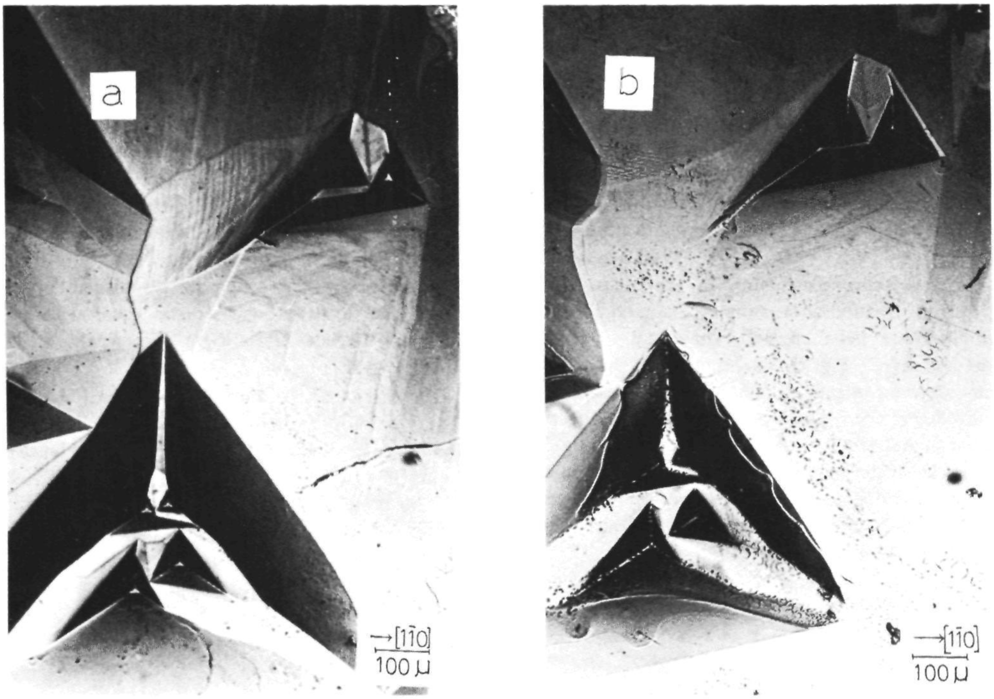

Fig. 2. Relation between etch pits and dislocations: (a) etch pit pattern on the (111) face of potash alum after slight etching in water; (b) etch pit pattern after polishing and reetching of the same area as (a).

tion of the dislocation structure in potash alum by means of X-ray topography done by Emara et al. [5] and by Gits-Leon et al. [14], who observed that the dislocations radiate from a central nucleus (in this case the seed crystal) and grow nearly perpendicularly to the $\{111\}$ surfaces of the crystal (this phenomenon has not only been observed for potash alum, but for a long range of solution grown crystals [10]). This implies that the density of dislocation outcrops at the central area of the $\{111\}$ faces will be higher than near the edges.

Interesting points for future investigation are to check by means of X-ray topography whether every dislocation outcrop at the surface results in an etch pit after etching and to study the properties of these pits in dependence of the undersaturation of the etching solution.

3.2. Optical birefringence images of edge dislocations

Fig. 3 is a photograph of an alum crystal placed between the crossed polarizing plates of a polarization microscope. The alum crystal was sliced parallel to the (111) face and had a thickness of about 6 mm. The patterns labelled A are all images of edge dislocations having their dislocation lines more or less perpendicular to the (111) surface and their Burgers vectors parallel to the $[\bar{1}10]$ vector [11,12]. The same Burgers vector orientation has been observed by Gits-Leon et al. by means of X-ray topography [14]. The feature labelled B is an image of a dislocation similar to the patterns denoted as A, with the difference that in this case the edge component of the Burgers vector is parallel to $[\bar{1}\bar{1}2]$. This is consistent with the observation done by Gits-Leon et al. [14], that for a num-

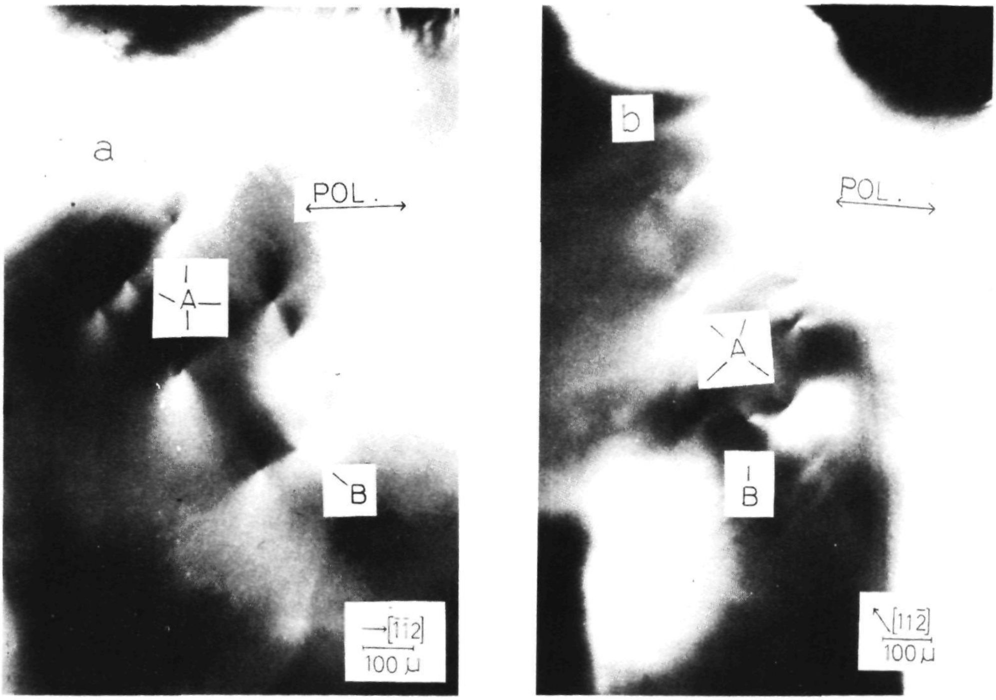

Fig. 3. Stress birefringence images of edge dislocations with higher Burgers vectors having their dislocation lines nearly perpendicular to the (111) face. (a) Polarizer orientated parallel to the [$\bar{1}\bar{1}2$] direction; dislocations denoted as A have Burgers vectors parallel to [$\bar{1}10$], the dislocation called B has a Burgers vector with an edge component parallel to [$\bar{1}\bar{1}2$]. (b) The same situation as in fig. 3a except that the crystal has been rotated over about 45° with respect to the polarizer and analyser.

ber of dislocations having their dislocation lines nearly normal to the octahedral faces the Burgers vectors are parallel to the ⟨100⟩ directions, because for a mixed [001] dislocation of this kind the Burgers vector has an edge component parallel to [$\bar{1}\bar{1}2$].

The intensity distributions of the dislocation images is in complete qualitative agreement with the calculated intensity contours of edge dislocations in a homogeneous strained isotropic (the point group of alum is cubic, so we can consider it as isotropic) medium as done by Tanner and Fathers [12].

By changing the height of the plane imaged in sharp focus by raising or lowering the specimen with regard to the front lens of the microscope, it is possible to trace the dislocation line through the crystal. Nearly all dislocation lines emerge in the case of slightly etched crystals at the bottom of an etch pit at the surface; sometimes they end in an inclusion. The ratio between the number of etch pits at the surface and the number of observed dislocation images in the crystal is in our case about (10^2–10^3) : 1, which means that the observed optical dislocation images belong to dislocations with a higher Burgers vector. The strain field around the numerous single dislocations most probably is too low to allow for detection by optical polarization microscopy.

3.3. Correlation between growth hillocks and etch pits

Typical growth phenomena on the (111) faces of potash alum can be seen in fig. 4, showing numerous trigonal growth hillocks [4], having an inclination of

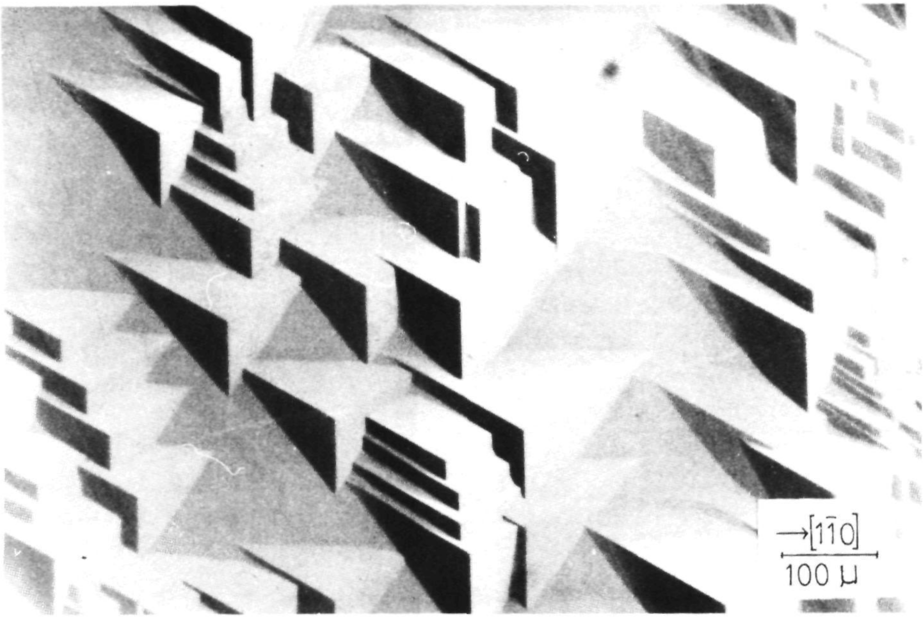

Fig. 4. Typical hillock pattern on potash alum (111) after growth from the solution.

a few tenths of a degree (depending on the supersaturation). The trigonal hillocks have an orientation of 180° rotated with respect to the etch pits formed after dissolution, so the angular points of the "growth trigons" point to the ⟨$\bar{1}\bar{1}$2⟩ directions.

To get more insight in the origin of these growth hillocks the following simple experiment has been carried out: First a suitable area with some growth hillocks is selected and photographed (fig. 5a), then the same area is slightly etched and rephotographed (fig. 5b). It can be seen clearly that without any exception every growth hillock is converted to an etch pit after slight dissolution. This experiment has been repeated several times, but always exactly the same result could be obtained and also numerous additional etch pits have been observed. From this result the conclusion can be drawn that the center of each growth hillock coincides with a dislocation outcrop at the surface, i.e. these elevations are spiral hillocks. So the growth of potash alum crystals indeed takes place according to a spiral growth mechanism, confirming the conclusions of Bennema [6,8] and Garside [7]. The etch pits not related to growth hillocks very probably originate from edge dislocations and perhaps some of them from screw dislocations with high Burgers vectors [13], so the prefered dissolution at dislocation outcrops is due to the elastic energy stored in the lattice around the dislocation or to the energy of the dislocation core, but not due to a spiral mechanism.

Theoretically it has been deduced by Bennema et al. [13] that during growth, spirals originating from screw dislocations with smaller Burgers vectors (in fact unit dislocations) will dominate the growth spirals related to dislocations having larger Burgers vectors. This means that probably most of the observed growth hillocks originate from dislocations whose part of the screw component of the Burgers vector normal to the octahedral surface is equal to the minimum growth slice thickness on the (111) face.

Mixed unit dislocations with ⟨100⟩ and especially with ⟨110⟩ Burgers vectors as observed by Gits-Leon

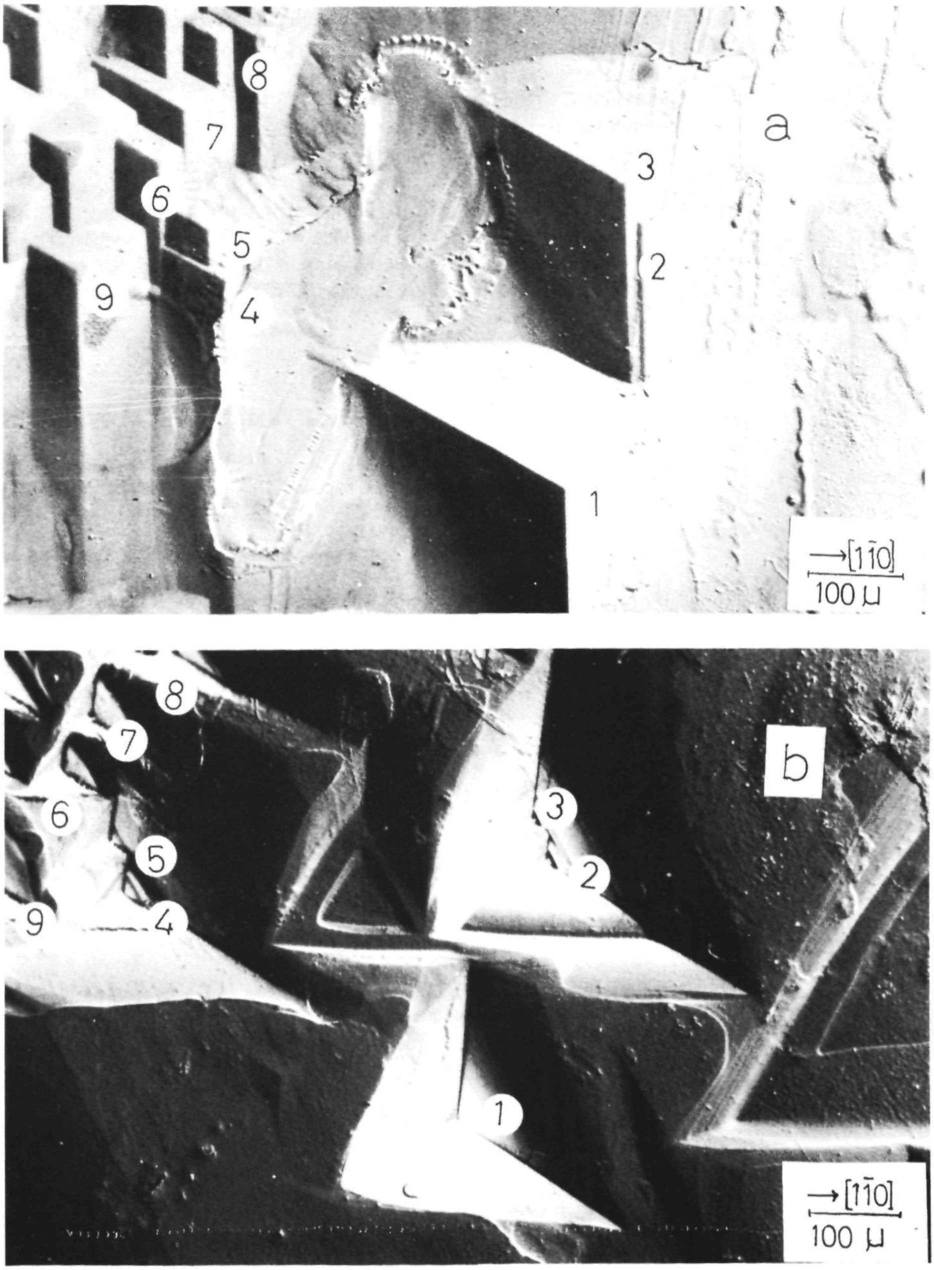

Fig. 5. Relation between growth hillocks and etch pits on potash alum (111). (a) Hillock pattern on the (111) face after growth from aqueous solution. (b) Etch pit pattern on the same area as a. after slight dissolution in water; the numbers indicate the corresponding pairs of hillocks and pits.

et al [14] fulfil this requirement for growth of spirals with unit step height, so the observation that after etching every growth hillock, without exception, becomes a pit suggests that even unit ⟨110⟩ and unit ⟨100⟩ dislocations result in an etch pit after dissolution in water, In a few cases steeper growth hillocks originating from dislocations whose part of the screw component of the Burgers vector perpendicular to the growth face is higher than the unit step height or from dislocation bundles have been observed

An interesting point for more detailed examination in future is to determine the inclination of the growth hillocks versus the supersaturation in order to check the reability of the BCF theory in the case of solution growth of potash alum crystals

4 Conclusions

From the foregoing investigation it can be concluded

(1) The etch pits formed on the (111) faces of potash alum crystals after dissolution in water are almost without exception correlated with dislocation outcrops at the surface Some indication exists that every dislocation outcrop at the surface results in an etch pit, but a direct proof has not yet been given

(2) Edge and mixed dislocations with higher Burgers vectors, having their dislocation lines nearly perpendicular to the {111} faces can be observed by means of the optical birefringence method These dislocation lines almost always end at the bottom of an etch pit at the crystal surface or end at an inclusion inside the crystal

(3) The correspondence between growth hillocks and dislocation etch pits gives a very strong evidence for the spiral growth mechanism on potash alum (111)

Acknowledgements

The authors wish to thank Dr K Tsukamoto and Dr P Bennema for their stimulating and helpful discussions One of us (W J P van Enckevort) acknowledges the support of the Netherlands Foundation for Pure Research, ZWO/SON

References

[1] H Bauhans, Verhandl Naturh Med Ver Heidelberg 12 (1913) 319
[2] Friedel Compt Rend (Paris) 179 (1924) 796
[3] M Omar and T H Youssef, Phil Mag 6 (1961) 791
[4] H E Buckley, in Crystal Growth (Wiley, New York 1951) p 325
[5] S H Emara, B R Lawn and A R Lang, Phil Mag 19 (1969) 7
[6] P Bennema, J Crystal Growth 1 (1967) 278, 287
[7] J Garside, R Janssen van Rosmalen and P Bennema, J Crystal Growth 29 (1975) 353 366
[8] P Bennema, Thesis Tech Univ Delft (1965) p 41
[9] G Gulzow, Hj Gulzow and W Ludke, Phys Status Solidi 11 (1965) 205
[10] A R Lang, in Crystal Growth, An Introduction, Ed P Hartman (North-Holland, Amsterdam, 1973) pp 503-507
[11] R Bullough, Phys Rev 110 (1958) 620
[12] B K Tanner and D J Fathers, Phil Mag 29 (1974) 1081
[13] P Bennema B van der Hoek, J P van der Eerden and I Sunagawa, J Crystal Growth, to be published
[14] S Gits Leon, F Lefaucheux and M C Robert, J Crystal Growth 44 (1978) 345

Zeitschrift für Physikalische Chemie Neue Folge Bd 124 S 171–191 (1981)
© by Akademische Verlagsgesellschaft, Wiesbaden 1981

CHAPTER II:

On the Observation of Growth Spirals with very Low Step Heights on Potash Alum Single Crystals

By

W J P. van Enckevort, P Bennema and W H van der Linden

R I M Laboratory of Solid State Chemistry, Faculty of Science Catholic University
Toernooiveld, Nijmegen, The Netherlands

(Received July 4 1980 revised October 8, 1980)

In memory of Ivan N Stranski

Potash alum / Growth spirals Dislocations Mono-molecular growth steps Interlacing

Surface microtopographic observations by application of highly sensitive phase contrast microscopy revealed numerous growth spirals with very low step heights on both the {111} and the {100} faces of potash alum single crystals grown from aqueous solutions The observed and by means of two-beam interferometry measured step heights of the spirals equaled about 14 and 12 Å for the {111} and the {100} faces respectively In interlaced regions of spirals on the {100} surfaces even lower step heights of 6 Å which is equivalent to half a unit lattice height were observed The observation of steps of one unit lattice height and lower gives direct evidence that the atomistic layer model developed among others by Stranski is also applicable to potash alum crystals and therefore probably also for other aqueous solution grown crystals Several kinds of growth spirals such as single, double and multiple spirals (and in some cases no spirals) were observed on the {001} faces which gives an explanation for the extremely high dispersion in growth rate of these faces reported in literature Also some other typical phenomena of these spirals, such as step accelerations in reentrant corners and interlacing are observed and discussed

Bei mikrotopographischen Beobachtungen der Oberflächen mit Hilfe sehr empfindlicher Phasenkontrast-Mikroskopie wurden viele Wachstumsspiralen mit sehr niedrigen Stufenhöhen auf {111}- und {100}-Flächen von Kaliumaluminiumalaun gefunden Die beobachtete und durch Zweistrahl-Interferometrie ermittelte Stufenhöhe der Spiralen betrug etwa 12–14 Å für die {100}- und {111} Flächen Im Gebiet verschränkter Spiralen auf den {100}-Flächen wurden Stufen mit einer Höhe von nur 6 Å beobachtet die mit dem halben Gitterabstand übereinstimmen Die Beobachtung von Stufen mit einer Höhe von einem Gitterabstand und niedriger gibt den direkten Beweis für die Anwendbarkeit des u a von Stranski entwickelten atomistischen Schichtenmodelles auf Kaliumaluminiumalaun-Kristalle und somit wahrscheinlich auch auf viele andere aus wäßriger Lösung gewachsene Kristalle

Viele verschiedene Arten von Wachstumsspiralen, solche mit ein, zwei oder mehreren kooperierenden Spiralen (und in einigen Fällen gar keine), wurden auf {100}-Flächen beobachtet. Damit würde die in der Literatur angegebene große Streuung in der Wachstumsgeschwindigkeit dieser Fläche zu erklären sein. Auch einige typische Phänomene dieser Spiralen, wie Stufenbeschleunigungen in einspringenden Ecken und Verschränkung wurden beobachtet und diskutiert.

1. Introduction

Since the postulation by Frank [1] that a screw dislocation emerging from a crystal face provides a continuous step source on the surface leading to the formation of a growth spiral, numerous successful attempts were made to observe these spirals. The first observation of a growth feature, which was recognized as a growth spiral, was made by Griffin [2]. Verma was the first who succeeded to observe a – decorated – growth step of unit lattice height using a highly sensitive optical phase contrast microscope [3]. Soon numerous surface microtopographic studies of growth spirals, performed by several investigaters, followed [4–6]. The earliest observations and measurements of step heights less than one unit lattice height were carried out by Sunagawa and Tolanski on hematite crystals [7]. The step heights were measured by application of the multiple beam interferometric technique, developed by Tolansky [8].

Until now these very low steps of one unit lattice height or less were only observed and measured on natural minerals (e.g. [9]), crystals grown from the vapour phase (e.g. [4–6, 9, 10]) and from the flux (e.g. [9, 11, 12]), but hardly on crystals grown from aqueous solutions. As far as known to us until very recently the observation and measurement of the lowest step height on an aqueous solution crystal was carried out by Trigunayat and Verma, who reported a step height of 83 Å on a CdI_2 crystal [13]. Lower steps were observed by Sunagawa and Tsukamoto on KCl, but no step heights were measured [14]. However, very recently van Enckevort and Klapper succeeded to observe and to measure steps of one unit lattice height (18 Å) and of half an unit lattice height (9 Å) on the {001} faces of $NiSO_4 \cdot 6H_2O$ crystals grown from aqueous solutions [15, 16].

In contrast to surface microtopography, a considerable amount of work was done on growth kinetics of crystals grown from aqueous solutions (e.g. [17–19]). A very extensively investigated crystal is potash alum: both for the {111} faces [20–22] and for the {100} faces [22] the dependence of the growth rate on the supersaturation was measured.

For the {111} faces of potash alum the growth rate versus supersaturation curve for higher supersaturations could be interpreted in terms of the spiral growth model of Burton Cabrera and Frank [17, 23] adapted to growth from solutions [24, 25]. For lower supersaturations this curve was interpreted in terms of cooperating spirals giving rise to a second linear law [26, 27]. That spiral growth on {111} potash alum indeed occurs was strongly confirmed by a surface microtopographic investigation carried out by van Enckevort and van der Linden [28], who were able to show that the growth hillocks on these faces are growth spirals.

On the other hand the {100} faces of potash alum crystals show a high dispersion in growth rate [22, 29], which could be explained by an occurrence or a non-occurrence of screw dislocation outcrops at these faces leading to spiral growth or nucleation growth respectively. Strong evidence for this interpretation of the growth rate dispersion was given by Gits-Leon *et al.* [30] on basis of X-ray diffraction topographic studies.

At this moment very detailed growth kinetics measurements of both the {111} and the {100} faces are performed by Human *et al.* [29, 31].

The aims of this paper are: (i) To investigate the possibilities of the optical phase contrast method on the very difficult class of aqueous solution grown crystals. (ii) To obtain direct evidence that spirals indeed occur on {111} and {100} potash alum. (iii) To prove that growth of crystals in aqueous solutions proceeds via steps with unit lattice height or lower, in order to show that the atomistic layer model for crystal growth, among others developed by Stranski [32], also holds for this catogory of crystals. Until now this was assumed by many authors (e.g. [17, 33]), but was never proved.

2. Experimental

2.1. Specimen preparation

The potash alum crystals were grown as follows [28, 34]: A high quality seed crystal of about 0.25 cm^3, mounted on a plastic rod, was placed in a thermostated (± 0.01 °C) saturated aqueous potash alum solution, which was cooled down at a rate of about 0.1 °C per 24 h. After a period of a few weeks a clear and well formed octahedral crystal of about 4 cm^3 could be obtained in this way.

In order to allow observation of a {001} face one of the tops of the octahedral crystals was cut off by means of a metal-wire saw in such a way that a large {001} surface area was produced.

After this the crystal was allowed to grow for a few days in a vessel, specially constructed for easy removal of the crystal prior to surface observation in such a way that no secondary effects as local growth or etching of the surfaces arise. The construction of this vessel is shown in Fig. 1. The supersaturated solution (S) is kept in a double-jacket well thermostated (± 0.01 °C) stirred vessel. The crystal (C) is mounted on the stirrer: This increases the quality of stirring and in addition the removal of the crystal out of the solution becomes more convenient. The supersaturated solution is covered by a layer of n-hexane of about 5 cm in thickness (H), which prevents

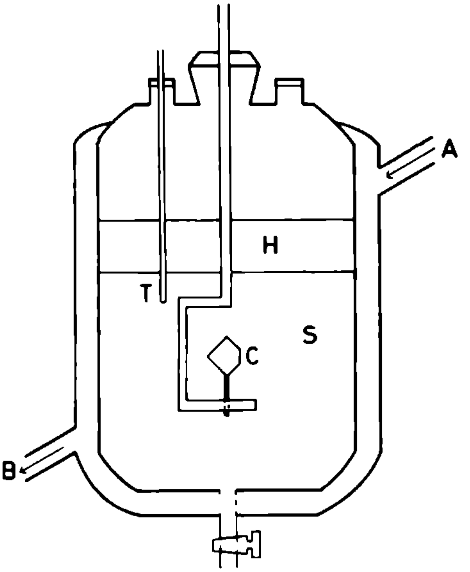

Fig 1 Schematic diagram of the growth vessel especially constructed for removal of the crystal out of the solution in such a way that very clean surface areas, suitable for surface microtopography, can be obtained *S* Supersaturated solution *H* n hexane layer covering the solution, *C* crystal, *T* thermocouple, *A* thermostated water inlet, *B* thermostated water outlet

evaporation of water, leading to undesired changes in supersaturation. A well defined supersaturation of the potash alum solution was obtained by careful saturation at a well known temperature, followed by a temperature decrease until the desired experimental temperature (here 25°C) was reached. The differences between both temperatures is a measure for the supersaturation of the solution [27].

After surface defects and the misorientation of the cut face with respect to the exact crystallographic {100} plane, due to a non-exact cutting, were well overgrown, so that the crystal was bounded by perfect {111} and {100} faces, the crystal was carefully separated from the solution. This separation from the solution, a process which is extremely critical for observation of unit lattice height steps, was carried out as follows: First the crystal was removed out of the solution in the vessel, during which procedure the crystal was passed through the n-hexane layer covering the solution. This n-hexane, which is not miscible with water, replaces the adhering aqueous solution film on the crystal faces to a great extent. Then the crystal was dipped for a few seconds into n-hexane having the same temperature as the solution and finally the adhering n-hexane was soaked up with a piece of blotting paper or a paper tissue. By this separation procedure it was prevented that evaporation or cooling down of the adhering solution on the crystal faces would lead to artifacts caused by a sudden increase in growth rate, so that very clean surface areas suitable for microtopography could be obtained [15, 28, 35]

Observation of the crystal faces had to be carried out within a few hours after separation of the crystal from the solution, since the surfaces were easily corroded by too dry or too moisty air Because of the fact that the alum faces were heavely attacked in vacuum – probably due to evaporation of some water of crystallization – it was not possible to silver or to gild the crystal surfaces, which would enhance the weak contrasts of the growth features in the application of phase contrast microscopy [35, 36]. Despite that silvering was not carried out it was still feasible to observe very low step heights, but now the efforts were somewhat higher

2.2 Observation techniques

Most observations were carried out by means of a highly sensitive optical phase contrast microscope, provided with a high absorption phase plate [36] (95 % instead of the commonly used 60 % absorption) In order to reveal extremely low contrasts, a high contrast photographic emulsion was used Since observations of unit lattice step heights at lower and high magnifications, which had to be used in the case of potash alum, makes great demands on the instrument, only high quality microscopes can be used For this study a Reichert Me F II was used.

General views of growth features were obtained by means of a reflection Nomarsky differential interference contrast microscope

For measurements of height differences and inclinations two beam interferometry [36], using a mercury light source combined with a monochromator filter ($\lambda = 5460$ Å) was applied.

Excellent reviews on the characterization of crystal surfaces by optical microscopy were given by Komatsu [36] and Sunagawa [37]

3. Observations and interpretation

3 1. {111} faces

Fig. 2 presents an interference contrast micrograph of a typical growth hillock pattern on a {111} face of a potash alum crystal grown from a slightly supersaturated aqueous solution The trigonal growth hillocks, which can be seen, were extensively described in a previous paper [28] In this work it was shown that these hillocks were related to dislocation outcrops at the crystal surface, so that these elevations must be spiral hillocks.

A more elegant proof for spiral growth on the {111} faces would be a direct observation of growth helixes. To allow for this the distance between

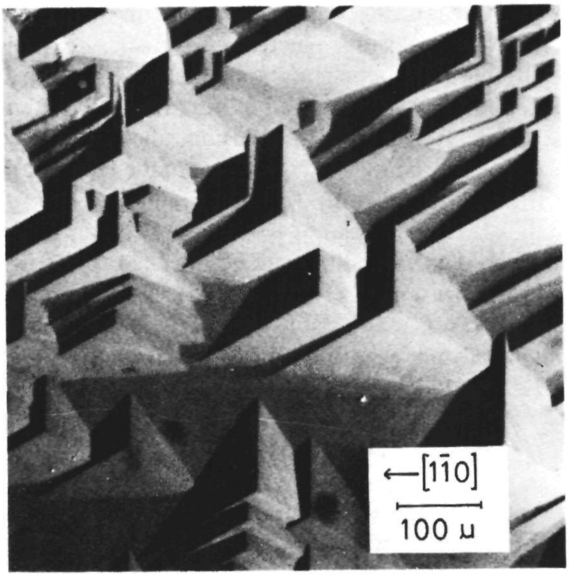

Fig. 2. Characteristic trigonal growth hillock pattern on the {111} faces of potash alum after growth from a slightly supersaturated aqueous solution (Interference contrast micrograph)

successive spiral arms has to be more than the resolution of the optical microscope used (about 5000 Å). This can be acheaved by growing the crystals at the lowest supersaturations possible (less than 0.2%), since for a given spiral the separation between its arms is roughly inversely proportional to the supersaturation [23]. One of the results is shown in Fig. 3: Photograph 3a is an interference contrast micrograph giving a general view of some shallow growth hillocks, whereas 3b presents a phase contrast micrograph at a higher magnification, clearly showing that these hillocks are growth spirals. From the contrasts the step height is estimated to be 10–30 Å.

For a more exact measurement of the step height, a well formed growth hillock with a clear step pattern was selected. This hillock is presented in Fig. 4: Interference contrast micrograph 4a gives a general survey, where the hillock in question is denoted by an arrow. Phase contrast micrograph 4b gives a detailed view of the step pattern on the growth hillock. A two-beam interferogram of the same surface area as 4a is shown in Fig. 4c. On this micrograph the location of the hillock is indicated by an arrow. Clearly a slight perturbation in the interference fringe pattern due to the height difference of the growth hillock with respect to the "background" can be seen. From the ratio of the magnitude of this perturbation, which was carefully measured, to the distance between two successive fringes it can be

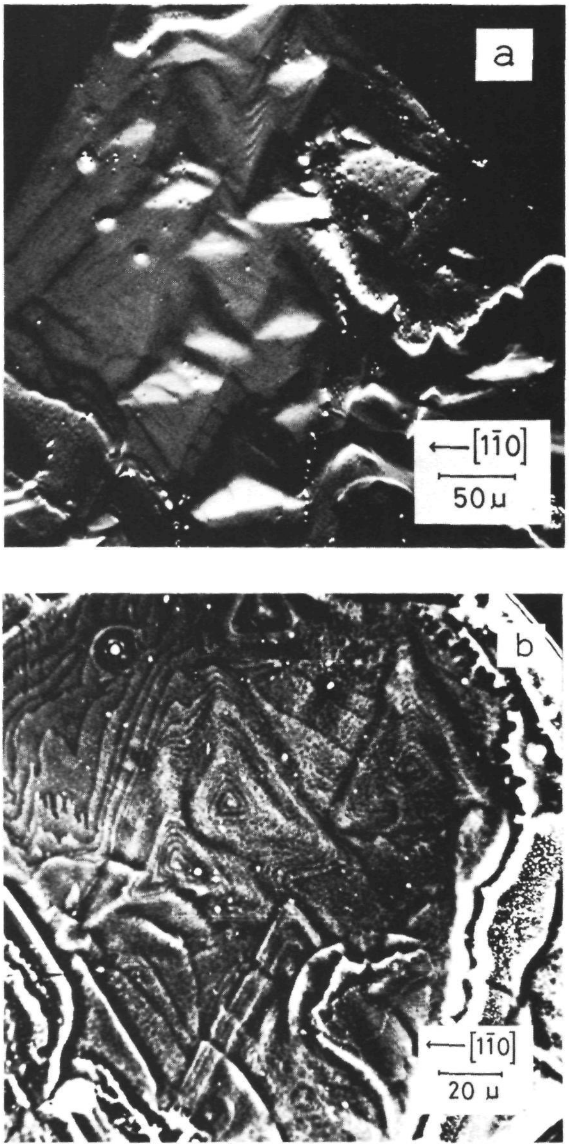

Fig. 3. Growth spirals on {111} alum: (*a*) General view showing some shallow trigonal growth hillocks (Interference contrast photograph). (*b*) Detailed view revealing the spiral patterns

deduced that the height of the growth hillock equals 310 ± 30 Å. Counting of steps, visible on photograph 4b, gives after a correction for the "background" (region B), which is crowded with steps, that this height cor-

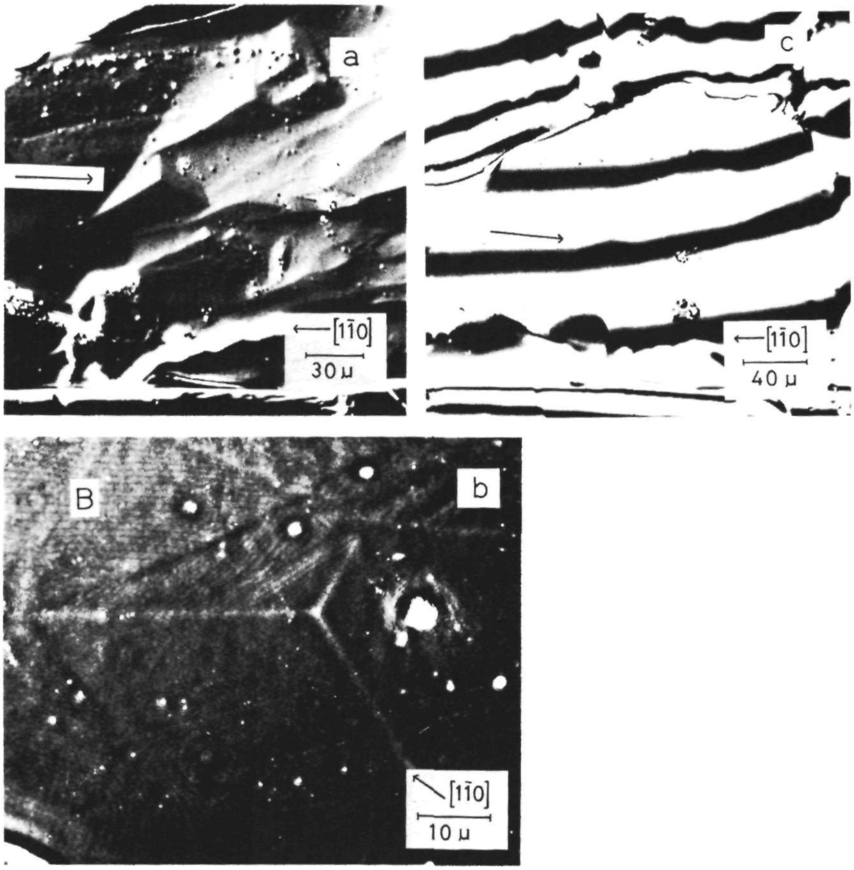

Fig. 4. Step height measurement of a given growth hillock: (*a*) General view (Interference contrast micrograph). (*b*) High magnification phase contrast micrograph showing the step pattern on the growth hillock in question. (*c*) Two beam interferogram of the surface area of Fig. 4a

responds to 23 ± 2 steps. From these data it can now be concluded that the step height of the spiral arms of this growth hillock equals 13.5 ± 2 Å.

Since the step height of the spiral arms is equal to the magnitude of that part of the screw component of the Burgers vector of the dislocation in the center of the spiral, which is perpendicular to the $\{111\}$ growth face, it is clear that this normal component must be equivalent to the vector $\frac{2}{3}$ [111]. A dislocation type which fulfils this requirement and so can account for this growth hillock is the pure screw dislocation with Burgers vector [110] and line direction [110], observed by means of X-ray diffraction topography [38].

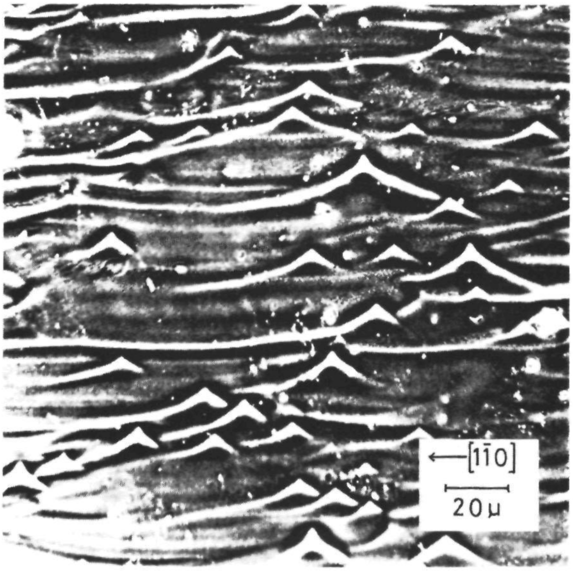

Fig. 5. Growth hillocks emerging from a step train pattern, as a result from a short-time increase in supersaturation during removal of the crystal out of the solution (Phase contrast micrograph)

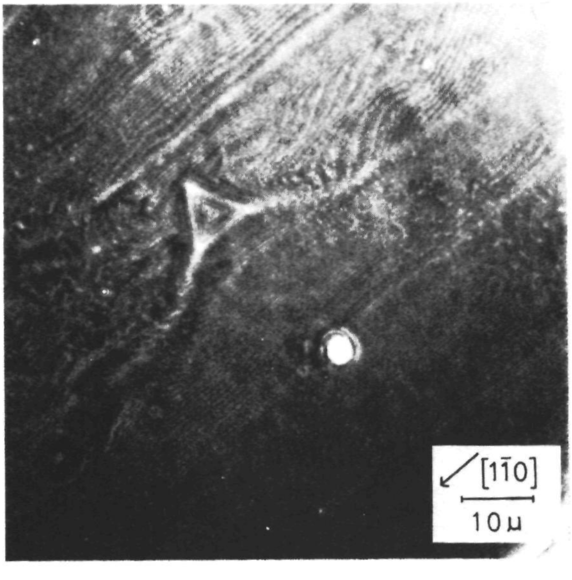

Fig. 6. High magnification phase contrast photograph of a growth spiral rising from a step train

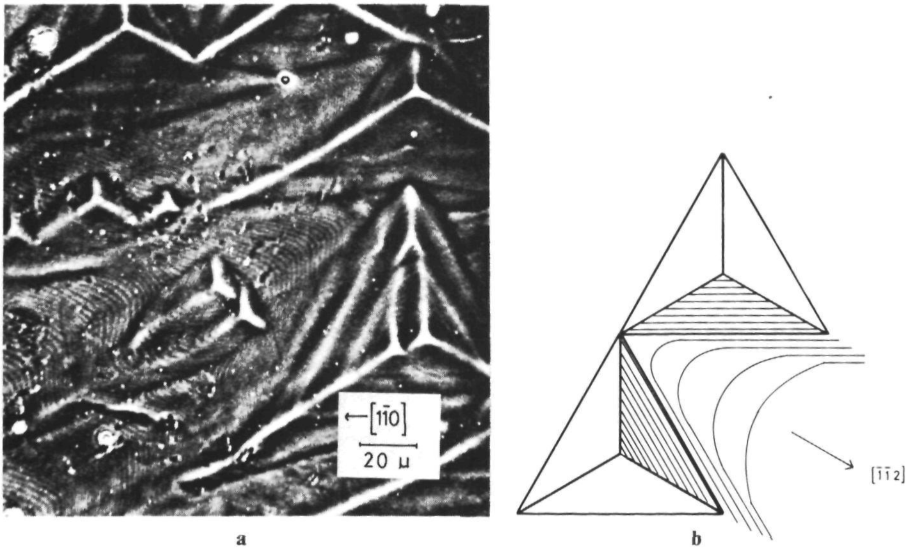

Fig. 7. Increase of the step advancement rate on {111} alum as a result of lateral anisotropy and of the occurrence of a reentrant corner in the step pattern: (*a*) Phase contrast micrograph, (*b*) Schematic representation

Very often growth of the {111} faces is governed by one single or a few dominating growth centers, for instance macroscopic spirals [35] or groups of spirals in surface regions with higher supersaturations in consequence of hydrodynamical reasons. These centers lead to the formation of extended step trains running over a large surface area, by which they overwhelm numerous screw dislocation outcrops, which are potential spiral sources. However, despite the precautions taken, still a very short time increase in supersaturation at the surfaces does occur during separation of the crystal from the solution. During this increase in supersaturation the step distance of the step train does not change, but the spiral arm separation of the overflown screw dislocation outcrops – which is more or less inversely proportional to the supersaturation [23] – becomes less than the step distance of the step train. This results in the formation of numerous growth hillocks rising from the step train pattern (Figs. 5 and 6). The size of these hillocks gives a rough estimate of the influence of this short time increase in supersaturation during separation of the crystals from the solution on the surface pattern.

Fig. 6, which clearly shows a spiral rising from a step train, also gives a better view on the bunching phenomena of the step train. This bunching consists of a fluctuation in step separation, which is related to the emerging growth spirals. In all cases the effects arising from the separation of the

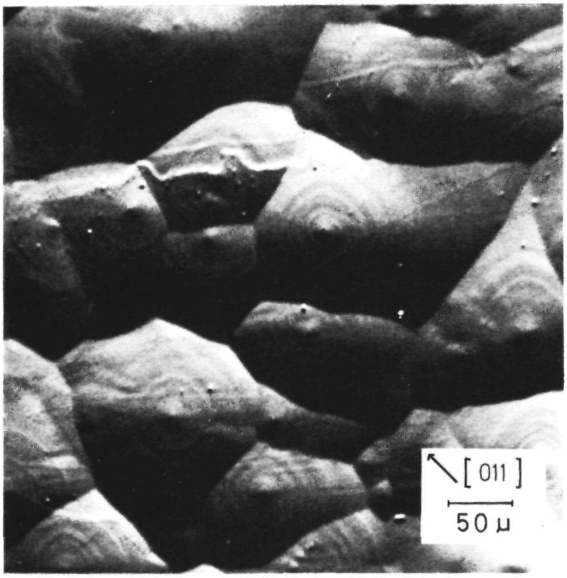

Fig. 8. Representative growth hillock pattern on $\{100\}$ potash alum (Interference contrast micrograph)

crystal from the solution were so large, that it was impossible to estimate the supersaturation of the solution quantitatively.

Fig. 7a and b give a clear indication that steps having a reentrant corner and advancing roughly towards the $\langle\bar{1}\bar{1}2\rangle$ directions move much faster – as can be seen from the larger step separation – than steps running towards the $\langle 11\bar{2}\rangle$ directions. That the advancement rate of steps varies for the different directions on the $\{111\}$ faces probably can be explained in terms of anisotropy in surface diffusion or in step integration of the ad-atoms. Step acceleration due to a reentrant corner in the step pattern is also a well known effect, which can easily be understood from the dependence of the step advancement rate on the step curvature derived by Burton, Cabrera and Frank [23].

The faster running steps amidst the growth hillocks lead to the formation of relatively flatter surface area in these regions. Similar flat regions were also observed between etch pits on potash alum crystals [28, 39] and on diamond [39].

3.2. $\{100\}$ faces

Typical growth phenomena on the $\{100\}$ faces of potash alum can be seen in Fig. 8, an interference contrast micrograph showing numerous tetragonal growth hillocks with low (less than about 0.1 degree) inclinations. The side

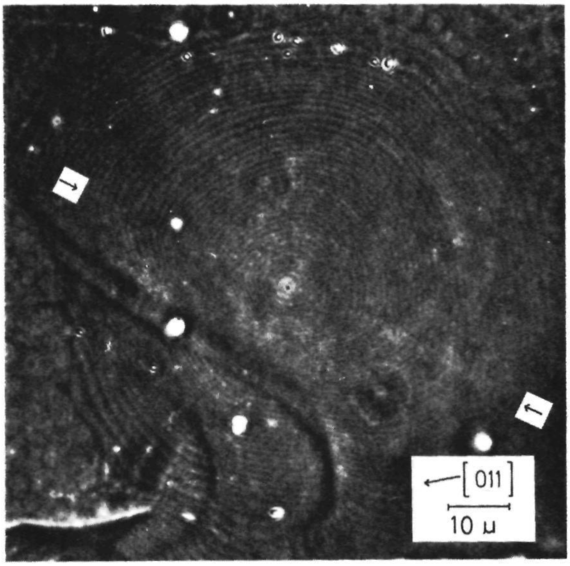

Fig. 9. Detailed view of one single growth hillock, revealing its step pattern. The black dot at the centre indicates the occurrence of a hole, caused by a slight dissolution around the strained dislocation outcrop area, during separation of the crystal from the solution (Phase contrast micrograph)

faces of these slightly polygonized growth hillocks are parallel to the two ⟨011⟩ vectors laying in the {100} plane. A closer look to the hillocks, given in Fig. 9, shows that in the center a small hole, visible as a black dot – on all the phase contrast micrographs presented here dark areas have a lower level than adjacent bright areas – can be revealed. This hole, which is observed on the summit of several growth hillocks, probably is formed due to an extreme slight dissolution around the – strained – dislocation outcrop during removal of the crystal out of the solution. It is not likely that these holes are endings of hollow tubes around dislocations as described by Cabrera and Levine [40, 41], since the observed width of such a hole (about 0.5 µ) is an order of magnitude too high and many hillocks with the same step heights do not reveal such a hole. The observation of these holes at the centres of numerous growth hillocks gives strong evidence that these hillocks are related to dislocations, i.e. these hillocks are growth spirals.

In order to measure the step height of the growth spirals a particularly beautiful and isolated growth hillock was selected. This spiral is shown in Fig. 10: Interference micrograph 10a gives a general view of the elevation, Fig. 10b is a two-beam interferogram of the same region as 10a and Fig. 10c is a high magnification phase contrast micrograph of the growth spiral, revealing numerous steps. With the help of the interferogram it can be

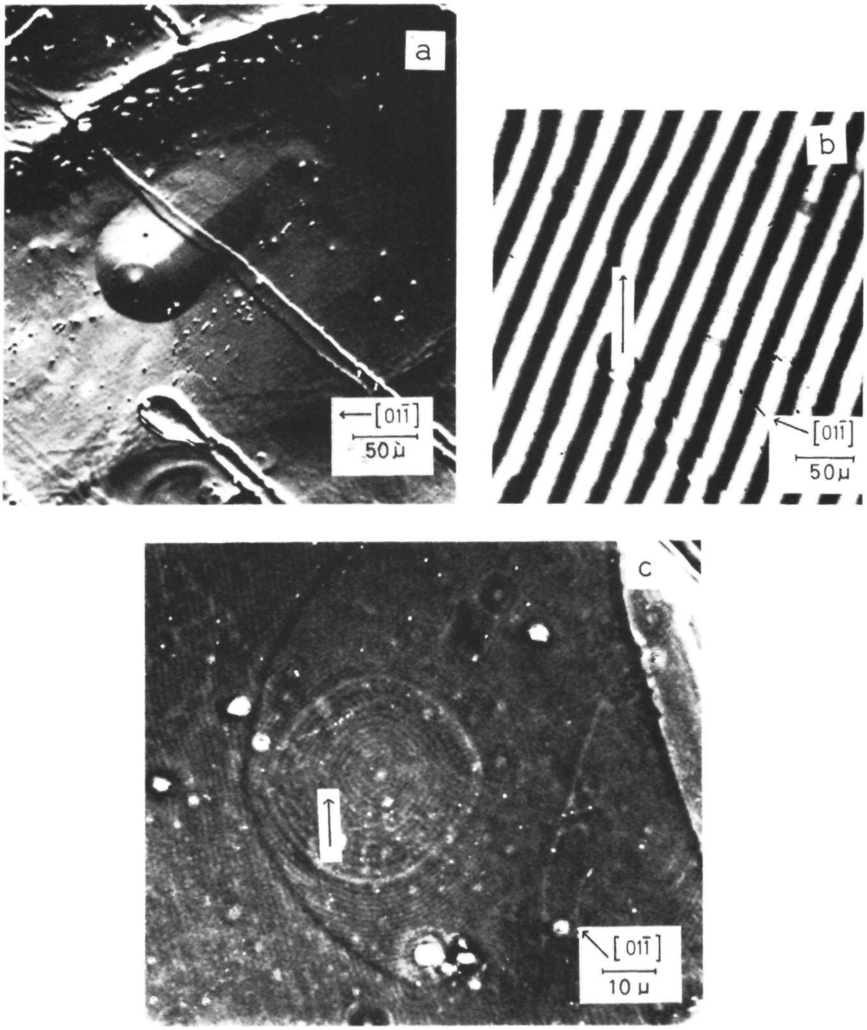

Fig. 10. Step height measurement of a growth hillock on {100} potash alum: (*a*) General view of the hillock (Interference contrast micrograph). (*b*) Two beam interferogram of the same-surface area as *a*. (*c*) High magnification phase contrast micrograph of the growth spiral showing numerous steps

deduced from the ratio of the amount of bending outwards of the interference fringes near the center of the spiral – this region is denoted by an arrow in Fig. 10b – to the fringe separation that the height of the hillock equals 450 ± 50 Å. This height corresponds to 39 ± 2 steps, which can be infered from counting of steps in photograph 10c, as well as on the spiral as in the

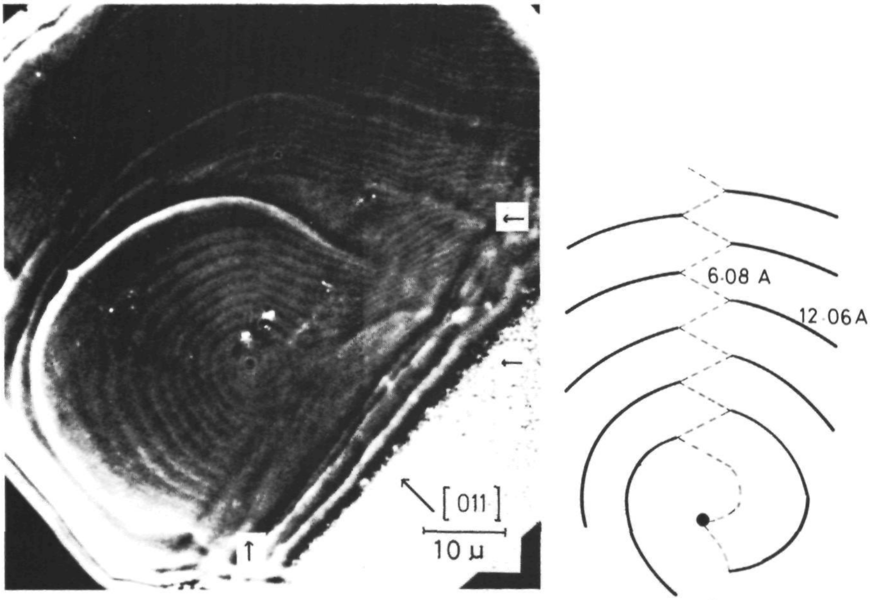

a b

Fig. 11. Interlacing of 12.16 Å and 6.08 A steps on the {100} faces: (*a*) Phase contrast micrograph, (*b*) Schematic illustration

background region. From the foregoing it can now be concluded that the step height of the arms of this spiral equals 11.5 ± 1.4 Å.

From this step height it can be concluded that the height of that part of the screw component of the Burgers vector of the dislocation at the center of the spiral, which is perpendicular to the {100} growth face, must be equal to the vector ⟨100⟩, which has a length of 12.16 Å [42]. From X-ray diffraction topographic studies of potash alum [30, 38] it can be concluded that dislocations with Burgers vectors ⟨100⟩, ⟨110⟩ and ⟨111⟩ fulfil this condition, since all types of dislocations end perpendicularly to the {100} growth faces.

All the observed growth hillocks, with a step height of 12 Å – this step height was estimated by comparison of the contrasts of the steps to the step contrasts of the measured spiral – revealed a rectilinear surface area where the step pattern could not be resolved and where opposite steps do not fit together. These areas which appear as a single diagonal on the growth hillocks are indicated by arrows on Figs. 9 and 10c. A well developed spiral with an extraordinary wide step separation is shown in Fig. 11a, in which the rectilinear area where the steps don't fit together are denoted by arrows. It can clearly be recognized that here each higher (12.16 Å) layer splits up into two lower layers of the same height. The height of such a lower step is equal to

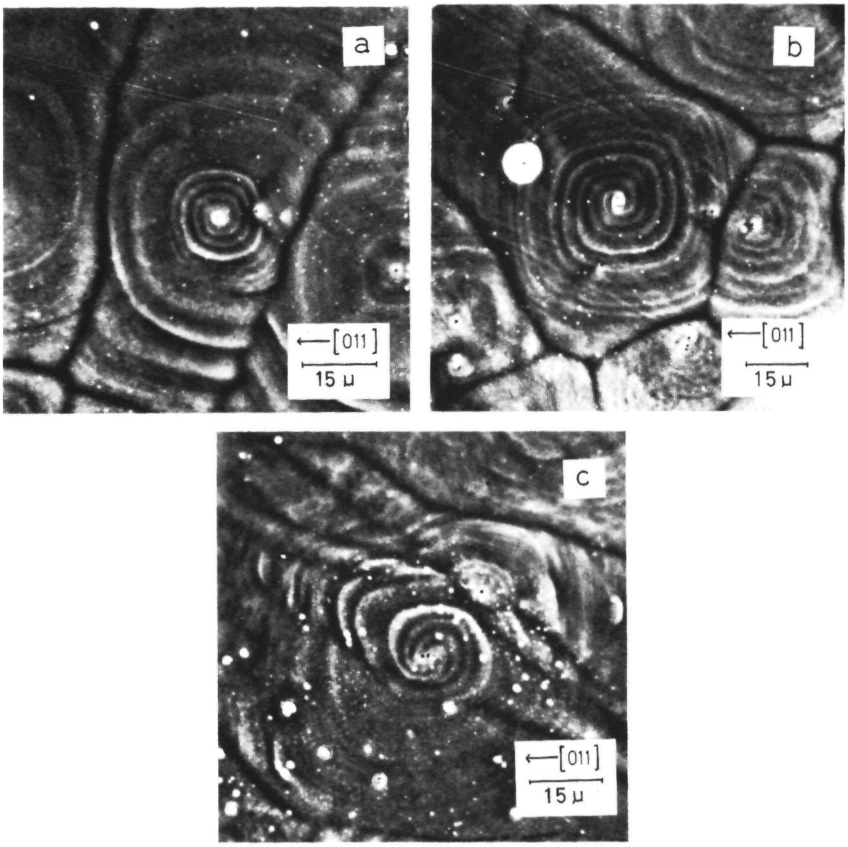

Fig. 12. Several different types of growth spirals observed on {100} alum: (*a*) single spiral, (*b*) double spiral, (*c*) multiple spiral

6.08 Å (Fig. 11b). Such a decomposition of a spiral layer into two thinner layers, leading to the formation of an interlaced step pattern has been observed on numerous crystals, such as Si *C* [6, 43], hematite [43], garnet [11] and $NiSO_4 \cdot 6\,H_2O$ [16].

The lower steps are not bended outwards, which means that these 6 Å steps have no higher advancement rate than the double 12 Å steps. From this it can be concluded that surface diffusion can not be the rate determining step in the crystal growth process, since in that case a lower step should move faster than a higher one [43–45]. So it can be concluded that integration of growth units in the step must be the rate determining step in the growth of {100} alum. Since similar conclusions were drawn from other surface topographic studies [16, 35], it is suggested that it may be quite common for crystals grown from aqueous solutions that step integration of the growth units is the rate determining step in the crystal growth process

Several kinds of growth spirals, such as single (Fig 12a), double (Fig 12b) and multiple (Fig 12c) ones were observed on {100} potash alum On some cubic faces no growth hillocks could be observed, which means that in these cases no screw dislocation outcrops were present so that growth was governed by nucleation This variation in surface morphology of {100} potash alum gives a direct insight into the extremely high dispersion in growth rate of these faces observed by Botsaris and Denk [22], Human *et al* [31] and Gits-Leon *et al* [30] This can be explained as follows When no spiral occurs growth must be governed by a nucleation mechanism, which means that the growth rate will be lower This is in agreement with the X-ray topographic work carried out by Gits-Leon *et al* [30], who showed that the presence of one or more screw dislocation outcrops on {100} alum gave a much higher growth rate of these faces than when no screw dislocation outcrop was present

Further it is a well established fact that double and multiple spirals give higher growth rates than single spirals [23,46] The "strength" of such a group of cooperating spirals depends on the number of dislocations belonging to this group and their separation with respect to each other From the observation of different types of growth spirals it is suggested that for cubic faces with many dislocation outcrops the growth rate dispersion can be interpreted in terms of a domination of the growth process by different kinds of groups of cooperating spirals, each having its own growth rate

4. Discussion

4.1 Relation between step height and growth unit size

From the crystallographic structure and from the slice thickness of the *F*-faces {111} and {100} as was evaluated from a Periodic Bond Chain analysis [47], for alums carried out by Hartman [48], it can be concluded that the observed step height of 14 Å on {111} alum corresponds to two slices d_{111} The step height of 12 Å on the {100} faces is equivalent to two slices d_{200}, whereas the interlaced steps of 6 Å have a thickness of one slice d_{200}

Seen in the [111] direction the alum structure consists of successive layers of Al^{3+} and K^+ ions One slice d_{111} corresponds to one layer Al^{3+} plus one layer K^+ This means that the observed step height on {111} must be equivalent to two $Al^{3+} - K^+$ layers Thus here the maximal size of the growth units is equivalent to a few molecules $KAl(SO_4)_2 \cdot 12H_2O$, but probably they are smaller

For the {100} faces the observed step height of one slice thickness corresponds to the height of one single potash alum molecule This means that for growth of alum the dimensions of one growth unit must be in the order of one molecule or less

From the foregoing it can be concluded that the growth units have such small dimensions that the atomistic layer models for crystal growth — in which growth is assumed to take place by a horizontal advancement of more or less monomolecular growth layers caused by an addition of roughly monomolecular growth units — as developed by among others Stranski [32], Kossel [49] and Burton, Cabrera and Frank [23] can be applied in the case of potash alum This is of importance, since numerous growth rate versus supersaturation curves of crystals grown from aqueous solutions were interpreted on basis of this presupposition (see for instance [17]) for which up to now only indirect evidence was available.

4.2 Interpretation of interlaced spirals on the {100} faces

From X-ray structure analyses, carried out by several authors [42, 50] it was concluded that potash alum crystallizes in space group $P\frac{2_1}{a}\bar{3}$. This means that in the analysis of the interlaced step pattern on the {100} faces both the occurrence of a two-fold screw axis and of a glide plane perpendicular to the growth face has to be taken into account. In what follows, firstly only the influence of the two-fold screw axis on the step pattern will be considered, whereas in a later stage also the effects of the glide plane will be elucidated

From the X-ray diffraction topographic observation that all dislocations in the {100} growth sectors end perpendicularly to the {100} faces [30], it can be concluded that when a dislocation has a part of its screw component normal to the growth face, this normal component of the Burgers vector must have a minimum length of one unit lattice height d_{100}, which is equivalent to 12.16 Å The thickness of a slice parallel to {100}, defined in the Hartman-Perdok theory [47], is given by $d_{200} = 6.08$ Å In this slice, it is for example possible to construct two *PBC*'s $[011]$ and $[0\bar{1}1]$, which are connected to each other by strong bonds [48]

The stacking of two (200) layers is demonstrated in Fig. 13. A straight step seen in the $[0\bar{1}1]$ direction will have a certain configuration, which is symbolically indicated by a hatched area. This will be defined as configuration *A*. Half d_{100} $(= d_{200})$ higher another step type occurs, called configuration *B*, which is not equivalent to *A* after operation of the two-fold screw axis. Due to the 2_1, axis step configuration *A* is repeated seen in the $[01\bar{1}]$ direction, but now $\frac{1}{2}$ d_{100} lower (and higher). This also holds for step configuration *B*, which is repeated in the same way as *A*, giving seen in the $[0\bar{1}1]$ direction an equivalent configuration *B*, which is also d_{200} higher (and lower) than the original one. Thus due to the 2_1 axis perpendicular to the

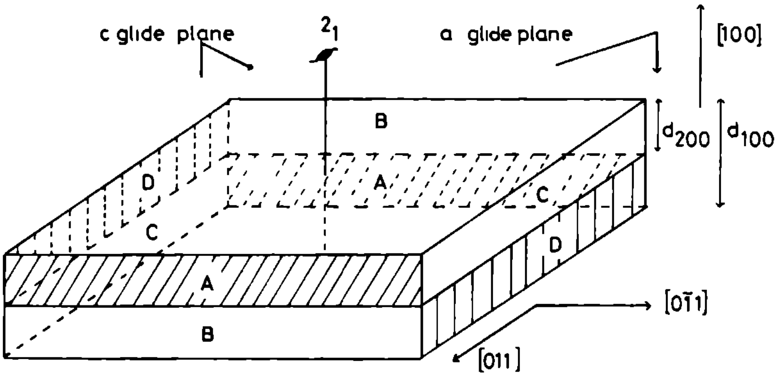

Fig 13 Stacking sequence of d_{200} layers perpendicular to a two-fold screw axis In contrast to space group $P2, 3$ for $Pa3$, the advancement rate of layer A equals that of B

growth face (100) one gets seen in the $[0\bar{1}\bar{1}]$ direction an AB stacking and seen in the [011] direction a BA stacking

The same holds for the $[0\bar{1}1]$ direction. If a DC stacking occurs for the $[0\bar{1}1]$ direction, then for the [011] direction a CD stacking must occur due to the two-fold screw axis.

Using the stacking model as given in Fig. 13, the observed interlacing can now easily be interpreted. This will be demonstrated with the help of Fig. 14.

Firstly it is assumed that polygonization occurs, i.e. spirals are limited by the $[0\bar{1}1]$ and [011] PBC directions. In a previous section it was pointed out that the observed heights of steps along these $[0\bar{1}1]$ and [011] directions are about 12 Å, which corresponds to d_{100} Obviously most spirals are generated by dislocations, whose part of the screw component normal to the growth face of the Burgers vector have the lowest possible non-zero height of d_{100}.

Now the hypothesis is introduced that along both the directions $[0\bar{1}1]$ and [011] one of the two possible double step configurations, say AB and CD, is stable, but that the other step configuration, say BA and DC, is unstable and decomposes soon after leaving the spiral centre in a faster advancing B and D step and a slower moving A and C step. Then the B (D) step runs away quickly and overtakes the adjacent A (C) step. It can now be seen from Fig. 14 that this leads to interlacing in one diagonal only. Interlacing means that, say in the [010] direction, double steps decompose into two single steps and vice versa A similar interpretation of interlaced step patterns was given by Frank for the case of Si C [51].

Upon introducing perpendicularly to the growth face an a-glide plane, transforming (x, y, z) to $(x + \frac{1}{2}, y, \frac{1}{2} - z)$ and a c-glide plane transforming (x, y, z) to $(x, \frac{1}{2} - y, z + \frac{1}{2})$ (both are also symmetry elements in space group $Pa3$) the situation does not change essentially In this case, due to both the glide planes, step configurations A and C as well as B and D become

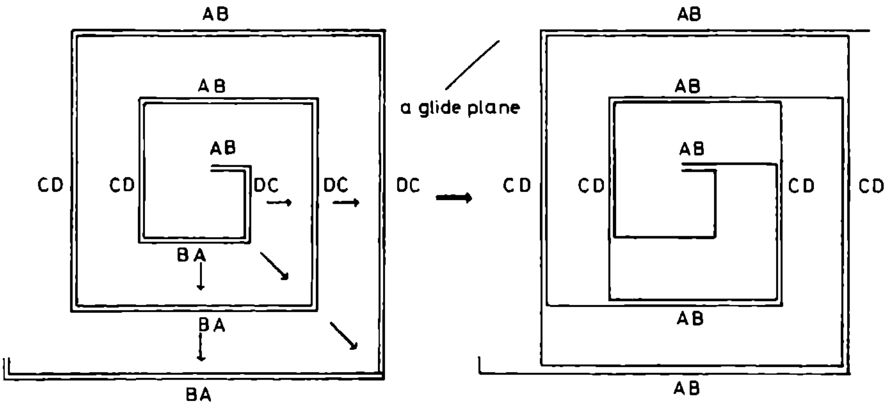

Fig. 14. The formation of a spiral with an interlaced step pattern along its diagonal as a result of the occurrence of a two-fold screw axis perpendicular to the growth face

equivalent to each other. Therefore the advancement rates of the slower moving steps *A* and *C* and also of the faster moving steps *B* and *D* equal each other, so that configurations *AB* and *CD* remain stable, whereas *BA* and *DC* remain unstable and decompose into two lower steps as mentioned before.

This means that the interlacing pattern along one diagonal direction remains unaffected by the glide planes. The rectilinear interlaced diagonal corresponds to the direction of the intersection line of the *a*-glide plane with the {100} growth face as shown in Fig. 14. The only difference compared to the situation without glide planes is that now the advancement rates of the stable double step configurations *AB* and *CD* equal each other, leading to, aside from the interlacing pattern, the two dimensional *mm* (*m* parallel to [010] and [001]) symmetry of the growth hillocks.

It is to be noticed that in reality spirals are not completely polygonized, but rounded off, but this does not change the preceding interpretation essentially.

In the foregoing it is shown that the interlacing of unit lattice height spiral arms on {100} alum can be interpreted on basis of a "crystallographic" consideration in which the screw axis plays an essential role. Similar interlaced spirals on garnet and nickel sulphate, which were interpreted in an analogous way will be published elsewhere [11, 16].

It is interesting to note that interlaced spirals were never observed on the {111} faces of potash alum. This is due to the fact that here the thickness of an *F*-slice is d_{111}. This means that a given configuration located in a certain slice (111) can also be found at a translated position in all the other higher and lower slices (111). Thus every possible step configuration on the (111) face has an identical configuration for all the other slices (111), which means that every multiple step configuration becomes stable and so no interlacing can occur, because now there is no difference in advancement rate of adjacent steps.

5. Conclusions

From the present surface microtopographic study of the {111} and {100} faces of potash alum the following conclusions can be formulated:

(a) Unit lattice height and even lower steps can be observed on crystals grown from aqueous solutions by means of optical reflection phase contrast microscopy.

(b) Growth of potash alum proceeds via a layer (step flow) mechanism involving unit lattice height and lower steps. This gives direct evidence that the atomistic layer model for crystal growth also holds for potash alum crystals grown from aqueous solutions.

(c) Both for the {111} and for the {100} faces of potash alum crystal growth proceeds according to a spiral growth mechanism. In a few cases when no screw dislocation outcrop is present, growth of the {100} faces is governed by nucleation.

(d) The occurrence of interlaced steps on {100} alum can be interpreted in terms of the morphological Periodic Bond Chain method and of crystallographic symmetry.

Acknowledgements

The authors wish to thank Drs. S. Gits-Leon, F. Lefaucheux and M. C. Robert for their hint to observe the particularly interesting {100} potash alum faces.

One of us (W. J. P. van Enckevort) acknowledges the support of the Netherlands Foundation for Pure Research, ZWO/SON.

References

1. F. C. Frank, Disc. Faraday Soc. **5** (1949) 48.
2. L. J. Griffin, Phil. Mag. **41** (1950) 196, **42** (1951) 775, 1337, **43** (1952) 651
3. Ajit Ram Verma, Phil. Mag. **42** (1951) 1005
4. Ajit Ram Verma, Nature **167** (1951) 939
5. S. Amelinckx, Nature **167** (1951) 939, **168** (1951) 431.
6. S. Amelinckx and G. Strumane, in. *Silicon Carbide: A high Temperature Semidonductor*, Proc. Conf. of Silicon Carbide, Boston, 1959, Eds. J. R. O'Connor and J. Smiltens Pergamon, New York 1960, pp. 162–201
7. I. Sunagawa, Am. Mineral **46** (1961) 1216
8. S. Tolansky, *Surface Microtopography* Longmans, London 1960
9. I. Sunagawa, J. Cryst. Growth **45** (1978) 3.

10 M Shimbo I Nishizawa and T Terasaki J Cryst Growth **23** (1974) 267

11 P Bennema K Tsukamoto and W Tolksdorf, J Cryst Growth, to be published

12 K Watanabe Y Sumiyoshi and I Sunagawa J Cryst Growth **42** (1977) 293

13 Ajit Ram Verma and P Krishna, *Polymorphism and Polytypism in Crystals* J Wiley and Sons New York 1966 p 297

14 I Sunagawa and K Tsukamoto, J Cryst Growth **15** (1972) 73

15 P Bennema J P van der Eerden W J P van Enckevort, B van der Hoek and K Tsukamoto, Phys Status Solidi (a) **55** (1979) 403

16 W J P van Enckevort and H Klapper, J Cryst Growth, to be published

17 P Bennema, J Boon, C van Leeuwen and G H Gilmer, Krist Tech **8** (1973) 659

18 J W Mullin and A Amatavivadhana J Appl Chem **17** (1967) 151

19 A V Valcic J Cryst Growth **30** (1975) 129

20 P Bennema Phys Status Solidi **17** (1966) 555 563

21 J W Mullin and J Garside, Trans Inst Chem Eng **45** (1967) T 285, T 291, **46** (1968) T 11

22 G D Botsaris and E G Denk, Ind Eng Chem Fundam **9** (1970) 277

23 W K Burton, N Cabrera and F C Frank, Philos Trans R Soc London **243** (1951) 299

24 P Bennema, J Cryst Growth **1** (1967) 287

25 P Bennema, J Cryst Growth **5** (1969) 29

26 P Bennema and G H Gilmer in *Crystal Growth An introduction* Ed P Hartman, North-Holland, Amsterdam 1973, ch 10

27 P Bennema, Thesis, Tech Univ Delft (1965)

28 W J P van Enckevort and W H van der Linden, J Cryst Growth **47** (1979) 196

29 H Human, W J P van Enckevort and J Odekerken, work in progress

30 S Gits-Leon, F Lefaucheux and M C Robert, J Cryst Growth **44** (1978) 345

31 H Human, work in progress

32 I N Stranski, Z Phys Chem **136** (1928) 259

33 O Sohnel, J Garside and S J Jancic J Cryst Growth **39** (1977) 307

34 P Bennema, Thesis, Tech Univ Delft (1965), p 41

35 W J P van Enckevort, R Janssen- van Rosmalen and W H van der Linden, J Cryst Growth **49** (1980) 502

36 H Komatsu, in *Crystal Growth and Characterization* Eds R Ueda and J B Mullin North Holland, Amsterdam 1975, p 333

37 I Sunagawa in *Crystal Growth and Characterization*, Eds R Ueda and J B Mullin North Holland, Amsterdam 1975, p 347

38 W J P van Enckevort and J Odekerken, Philos Mag , to be published

39 M Omar and I H Youssef, Philos Mag **6** (1961) 791

40 N Cabrera and M M Levine, Philos Mag **1** (1956) 450

41 N Cabrera, M M Levine and J S Plaskett Phys Rev **96** (1954) 1153

42 R W G Wykoff, *Crystal Structures*, vol 3 John Wiley and Sons, New York 1965, p 872

43 I Sunagawa and P Bennema, J Cryst Growth **46** (1979) 451

44 C van Leeuwen, R van Rosmalen and P Bennema, Surf Sci **44** (1974) 213

45 B A Mason in *The Art and Science of Growing Crystals*, Ed J J Gilman John Wiley and Sons, New York 1963, p 139

46 J P van der Eerden, J Cryst Growth, to be published

47 P Hartman, in *Crystal Growth an introduction*, Ed P Hartman North Holland, Amsterdam 1973, pp 358- 402

48 P Hartman, in *Growth of Crystals*, vol 7, Ed N N Sheftal Cons Bureau, New York 1969, p 53

49 W Kossel, Nachr Ges Wiss Goettingen, Math Physik Kl IIa (1927) 135- 143

50 A C Larson and D T Cromer, Acta Crystallogr **22** (1967) 793

51 F C Frank, Philos Mag **42** (1951) 1014

CHAPTER III:

ON DISPERSION IN THE GROWTH RATES OF THE DIFFERENT FACES OF POTASH ALUM CRYSTALS

Part II: Surface topography as a tool for interpretation of the growth mechanism of the {110} faces

W.J.P. van Enckevort and H.J. Human and W.H. van der Linden

RIM Laboratory of Solid State Chemistry,
Faculty of Science, Catholic University,
Toernooiveld, Nijmegen, The Netherlands

ABSTRACT

In situ measurements of the growth rates of the {110} faces of potash alum crystals, as well as inspection of the course of the sector boundary between the growth sector of a {110} face and its two adjacent {111} faces by means of stress birefringence microscopy, revealed the existence of a considerable dispersion in the growth rate of these faces. A posteriori surface topography with the aid of optical differential interference contrast and phase contrast microscopy showed that crystal growth of these faces proceeds via very low (∿ 10 - 20Å) steps, which can bunch to higher ones. As step sources may function: (i) Elliptical growth hillocks related to dislocation outcrops (i.e. growth spirals) and (ii) The edges of the {110} faces acting as active places for two-dimensional nucleation. Application of Lang-topography demonstrated, that growth sectors related to fast growing {110} faces show a much higher dislocation density, than those corresponding to slower growing {110} faces. From these characterization studies of the dodecahedral faces some of the observed growth phenomena could be interpreted in terms of an appearance and disappearance of dislocation outcrops at the {110} faces leading to spirals or two-dimensional nucleation growth respectively. Also a not yet understood mechanism, not related to dislocations, which can completely inhibit crystal growth for some time, plays an essential role in the growth dispersion of these faces.

1. INTRODUCTION

In a previous paper [1] a flowsystem is described in which the growth rates of crystal faces, growing under very well defined and constant conditions, can be measured with high accuracy. One of the intriguing results obtained from the measurements of the growth rates of the {111} faces of potash alum in this system is the occurrence of a considerable variation in growth rate of these faces, both in time for one single face throughout a run and for one crystal from one face to another. Despite this variation it was still possible to measure growth rate, R, versus supersaturation, σ, curves, although these differed for each individual octahedral face. Attempts to measure R-σ curves for the {110} faces occurring between two {111} faces of the octahedron-like shaped crystals (see figure 1), in the same manner as described in ref. [1], completely failed because of an extremely large dispersion in the growth rate of these dodecahedral faces. Since it was impossible to obtain interpretable information from - in situ - growth rates measurements of

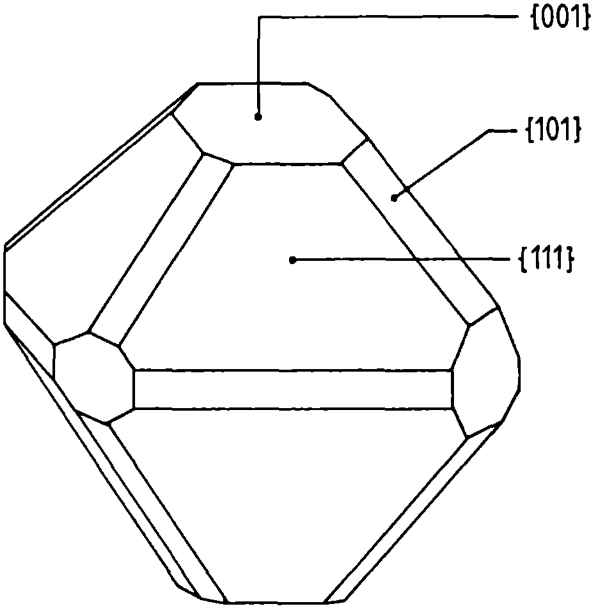

Fig. 1. Morphology of aqueous solution grown potash alum crystals, bounded by {111}, {101} and {001} faces.

these faces it is useful to apply - a posteriory - characterization methods, such as surface microtopography and X-ray diffraction topography to get more information about the growth characteristics of the {110} faces.

Surface microtopography with the aid of optical reflection differential interference or phase contrast microscopy is a powerful tool to get a better understanding of the growth behaviour of gas phase [2,3] and liquid phase [3,4] grown crystals. Recently it has been shown that this observation method, which is capable to reveal growth steps as low as 2.3Å [5,6], is also suited to observe very low steps on crystals such as KCl [7], potash alum [8,9], $NiSO_4.6H_2O$ [9,10] and potassium hydrogen phthalate [11] grown from the aqueous solutions. For these crystals it was demonstrated that crystal growth generally proceeds via a spiral growth mechanism involving very low (generally unit lattice height) steps. In these works it was directly prooved for the first time, that the atomistic layer models for crystal growth, developed by Stranski and Kossel [12] are probably also applicable to aqueous solution grown crystals. In addition several properties of the step patterns, such as interlacing, asymmetry, step acceleration in reentrant corners and bunching were described.

In contrast to surface microtopography, X-ray diffraction topography is a well known and frequently used method for characterizing aqueous solution grown crystals [13,14,15]. Especially the relation between dislocation structure and growth rate of the crystal faces has been studied by several investigators in order to get evidence for the occurrence of spiral growth for this catagory of crystals. For instance Mussard and Goldstaub [16] observed that for $NaClO_3$ crystals, faces to which screw dislocations end perpendicularly grow faster, than those without screw dislocation outcrops. Further work on $NaClO_3$ by Matsunaka et al. [17] however, pointed out that for higher supersaturations the screw dislocation outcrops at the {100} surfaces are not necessarely the growth centres. Other work in this field was carried out by Gits-Leon et al. [18] for potash alum and by van Enckevort et al. [19] for the {101} faces of KDP. Both were able to establish a correlation between the dislocation structure and the growth rates of the crystal faces.

The aim of the present paper is to get a deeper insight in the causes of the observed dispersion in the growth rate of the dodecahedral faces of potash alum. The main tool to tackle this problem is surface microtopography by means of optical differential interference or phase contrast microscopy. These observations are completed by X-ray diffraction topography (Lang method [20]) in order to relate the internal dislocation structure to the growth rates of the {110} crystal faces.

2. EXPERIMENTAL

2.1. *In situ observations*

The growth of the dodecahedral alum faces was studied in situ by means of a microscope placed over a flowsystem, in which crystal growth takes place under extremely well defined and constant conditions. Throughout one single growth run the temperature of the supersaturated solution was kept constant within 0.03°C. The displacement of a {110} face with time was observed by an optical microscope, applying transmission bright field illumination, using time lapse photography. The crystal was oriented in such a way that the normals of the {110} face and of the two adjacent {111} faces in question are oriented perpendicularly to the optical axis of the microscope. A detailed description of recording the growth process of crystals growing in a flowsystem has been given before [1].

2.2. *Stress birefringence microscopy*

In order to study within a certain crystal the sector boundaries between adjacent {110} and {111} growth sectors - which give the positions of the edges between the dodecahedral and octahedral faces during the growth process of the crystal [18,19,21] - the stress birefringence method was used [22,23,24]. The specimen plates for this polarization microscopic method were cut parallel to (110) as shown in fig. 2a. Then these plates were carefully polished and placed in immersion oil between a thoroughly cleaned microscope slide and a cover glas. After this preparation the specimens were photographed via a high quality polarization microscope at low magnifications, using high contrast photographic emulsions. A detailed description of the application of the stress birefringence method to potash alum crystals is given in an other paper [24].

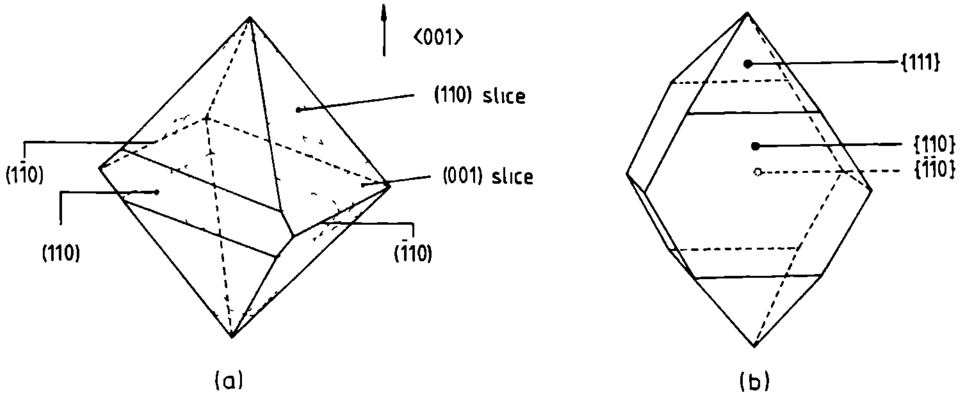

Fig. 2. (a) Cutting plan of alum crystals for characterization of the internal structure. The (110) slices are used for stress birefringence microscopy; the (001) slices, containing one large and one adjacent non-developed {110} face for Lang topography. (b) Cutting plan of an alum crystal to be used for surface microtopography: Two dodecahedral edges are cut off in order to obtain large {110} surface areas.

2.3. *Surface microtopography*

2.3.1. Specimen preparation

The main problem for the application of - a posteriori - highly sensitive surface microtopographic observation techniques to aqueous solution grown crystals is, that the surface patterns may be ruined during the separation of the crystal from the supersaturated solution at the end of the growth experiment (the so-called shut off effect) [8,9,25]. To overcome this difficulty a crystal growth vessel especially constructed to minimize this shut off effect was used to grow the specimen crystals for surface microtopography. The essential point of this vessel, which has been described extensively in previous work [8], is, that the supersaturated solution in which the crystal grows is covered by a layer of n-hexane of a few centimeters in thickness. During separation of the crystal from the solution at the end of the growth experiment, the crystal was passed through the n-hexane layer, which replaces the adhering aqueous solution film on its surface to a great extent. Then the crystal was dipped for a few seconds into n-hexane having the same temperature as the solution and after this the adhering hexane was finally soaked up with a paper tissue. By this separation procedure it was prevented, that due to evaporation or cooling down of the adhering solution artifacts were created on the crystal surfaces by a sudden final increase in growth rate. In this way very clean areas on the crystal surface, suitable for detailed observation of very low steps or inclinations, can be obtained.

In the present case, specimen preparation was carried out as follows: In order to obtain a large {110} surface area, from a good quality octahedral potash alum crystal (about 4 cm^3 in size; grown by standard methods [26,27]) one or two of the dodecahedral edges were cut off by means of a metal wire saw as shown in fig. 2b. After this the crystal, mounted on a plastic rod, was placed in the earlier mentioned vessel, where it was allowed to grow for a time sufficient long to overgrow both surface defects and the misorientation of the surface with respect to the exact {110} plane due to non-exact cutting. The temperature of the solution was kept constant within a range of 0.1°C at about 24°C, the supersaturation being 1% or less. Then the crystal, now bounded by a perfect {110} plane, was carefully separated from the supersaturated solution, according to the previously given procedure to minimize the shut off effect.

Observation of the dodecahedral faces was carried out within a few hours after separation of the crystal from the solution, since the surfaces are easily affected by too dry or too moisty air [8].

2.3.2. Observation methods

To observe the crystal surfaces, use was made of optical reflection differential interference contrast (after Nomarski [28]) and phase contrast microscopy, combined with high contrast photographic emulsion (orthochromatic documentary film).

Differential interference contrast microscopy was mainly applied to obtain general views of surface features and to reveal very low inclinations.

On the other hand for observation of extremely low step heights, use was made of the phase contrast microscope, fitted with a high absorption phase plate (95% instead of the commonly used 60% absorption). Using such a high absorption phase plate and high contrast film phase contrast is capable to reveal step heights as low as 2Å.

Detailed treatises on the characterization of crystal surfaces by optical microscopy are given by Komatsu [28] and Sunagawa [6].

2.4. *X-ray diffraction topography*

In order to study the correlation between the growth rate of a {110} face and the dislocation structure in the corresponding {110} growth sector, good quality octahedral crystals, with one large, well developed thus slowly growing (110) face and one non-developed (thus fast growing) adjacent ($\bar{1}10$) or ($1\bar{1}0$) face were selected. From each crystal a plate (about 1.5 mm in thickness) parallel to (001), containing both in size differing dodecahedral faces, was cut according to the cutting plan given in fig. 2a. In order to prevent interference of surface defects with the X-ray topographic image, these plates were slightlu polished using a wetted cloth and subsequently etched in deionized water.

All topographs of the specimen plates were taken by the Lang method [20], using AgKα_1 (λ = 0.5594Å) radiation and X-ray film Structurix D7 and D4 (Agfa gevaert). For all the (001) plates the strong reflections (220) and ($2\bar{2}0$) were used.

3. OBSERVATIONS AND DISCUSSIONS

3.1. *In situ observations*

As was pointed out in the introductory part, a quantitative measurement of the growth rate of {110} potash alum in dependence on the supersaturation is impossible, because of a large dispersion in the growth rate. This variation in the growth rate throughout a growth run is convincingly demonstrated by - in situ - time lapse photography of a growing dodecahedral face as shown in fig. 3. In figure 3a no {110} face can be observed between the two adjacent {111} faces. This means that the growth rate of the dodecahedral face, $R_{\{110\}}$, equals or exceeds 1/2 $\sqrt{6}$ times the growth rates of the two neighbouring octahedral faces, $R_{\{111\}}$. Then often suddenly a {110} face becomes visible (fig. 3b) indicating that $R_{\{110\}} < 1/2 \sqrt{6}.\ R_{\{111\}}$, which again vanishes after a

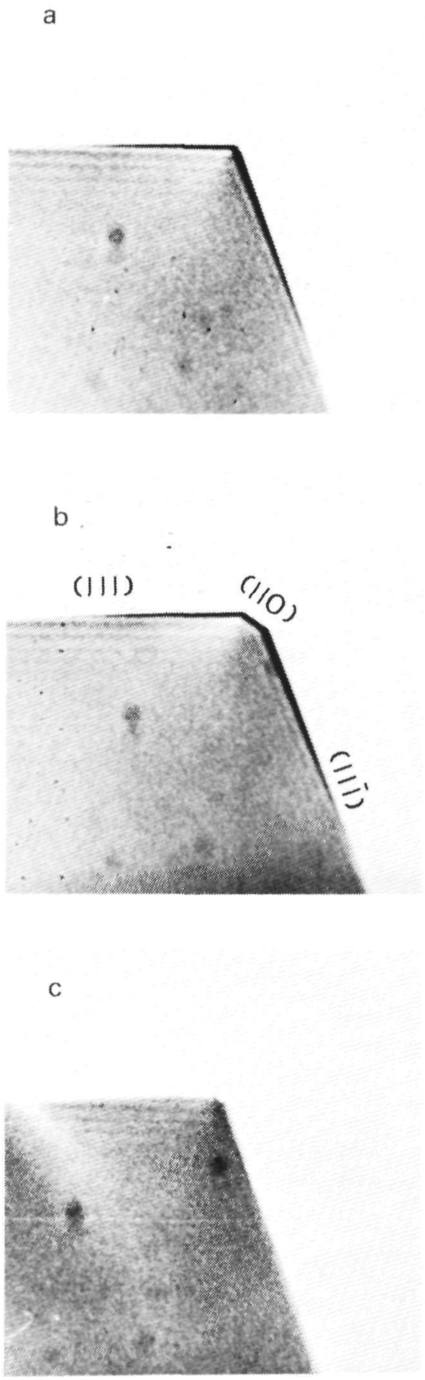

Fig. 3. In situ observation of the dispersion in growth rate of a {110} face . (a) t = 0.0 min., (b) t = 180.0 min., (c) t = 420.0 min.

while (fig. 3c) showing that $R_{\{110\}} > 1/2 \;\; 6 . R_{\{111\}}$. This appearance and disappearance of {110} faces is a quite commonly occurring phenomenon. On some high quality (without inclusions, veils or cracks and with a low dislocation density) crystals some of the {110} faces were persistent and could grow to considerable dimensions.

The variation in size of the {110} faces during crystal growth is practically completely due to variations in growth rate of these {110} faces and not of the {111} faces. This will be demonstrated with the aid of the stress birefringence method in the next section.

3.2. *Stress birefringence microscopy*

Fig. 4 presents a polarization micrograph of a {110} slice photographed between crossed polarizers. Clearly three growth sectors can be recognized: Two {111} growth sectors and between them a $\{1\bar{1}0\}$ sector. The difference in intensity for each sector on the stress birefringence micrographs is caused by a difference in deviation from the ideal cubic symmetry, leading to differing amounts of birefringence for the three growth sector areas. The sawtooth-like patterns of the boundaries between the {110} and the {111} sectors point to an extremely large variation in growth rate of the {110} faces as was discussed in detail in previous work [24]. In this paper it was shown that the ratio of the growth rates of the {110} and {111} faces could vary from 0 to 4.2. at several "pseudo-discrete" levels. The sawtooth-like structure of the growth sectors of the $(1\bar{1}0)$ face given in figure 4 is symmetrical with respect to the $[1\bar{1}0]$ direction (or better: to the (001) plane). Since the growth rates of the two adjacent $(1\bar{1}1)$ and $(1\bar{1}\bar{1})$ faces are not related to each other, it can be concluded from this symmetry, that the observed variation in $R_{(1\bar{1}0)}/R_{(111)}$, mentioned in section 3.1. is almost completely due to changes in growth rate of the $(1\bar{1}0)$ faces. Moreover, in ref. [1] it has been shown by in situ observations in a flowsystem, that during an experiment the growth rate of the {111} faces is almost constant. Hence, the growth dispersion of the dodecahedral faces, deduced from in situ observations, is confirmed by the analysis of growth sector boundaries, observed by stress birefringence microscopy. A similar use of sector boundaries to unravel the history of the relative growth rates of adjacent faces was made by Gits-Leon et al. for potash alum [18], by

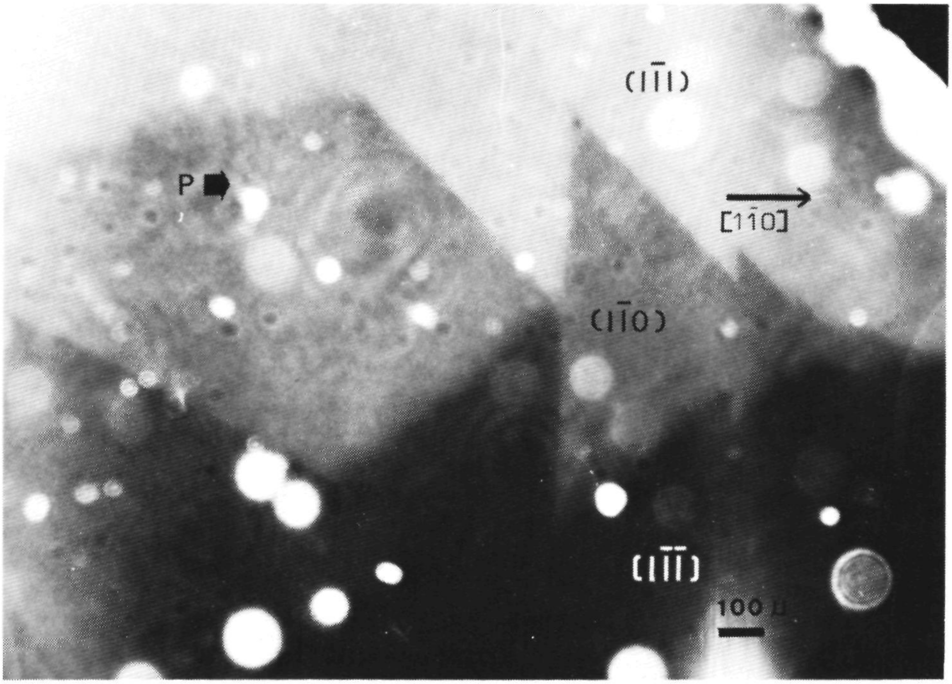

Fig. 4. Stress birefringence micrograph showing irregularly shaped sector boundaries between the $(1\bar{1}0)$ and the $(1\bar{1}1)$ and $(1\bar{1}\bar{1})$ growth sectors. P denotes the orientation of the polarizer; the analyser is oriented perpendicular to this direction.

van Enckevort et al. [19] and B. Dam et al. [21] for KDP and most beautifully by Lang for natural diamond [29].

3.3. *Surface microtopography*

3.3.1. General features

Figure 5a is a differential interference contrast micrograph, giving a general view of a typical growth hillock pattern on the {110} faces of potash alum. From this photograph, as well as from the high magnification interference contrast micrograph presented in figure 5b it is clear, that the hillocks, which have an inclination of the order of one or a few tenths of a degree, are highly asymmetric in shape. Without exception these elevations show an elliptical growth form, for

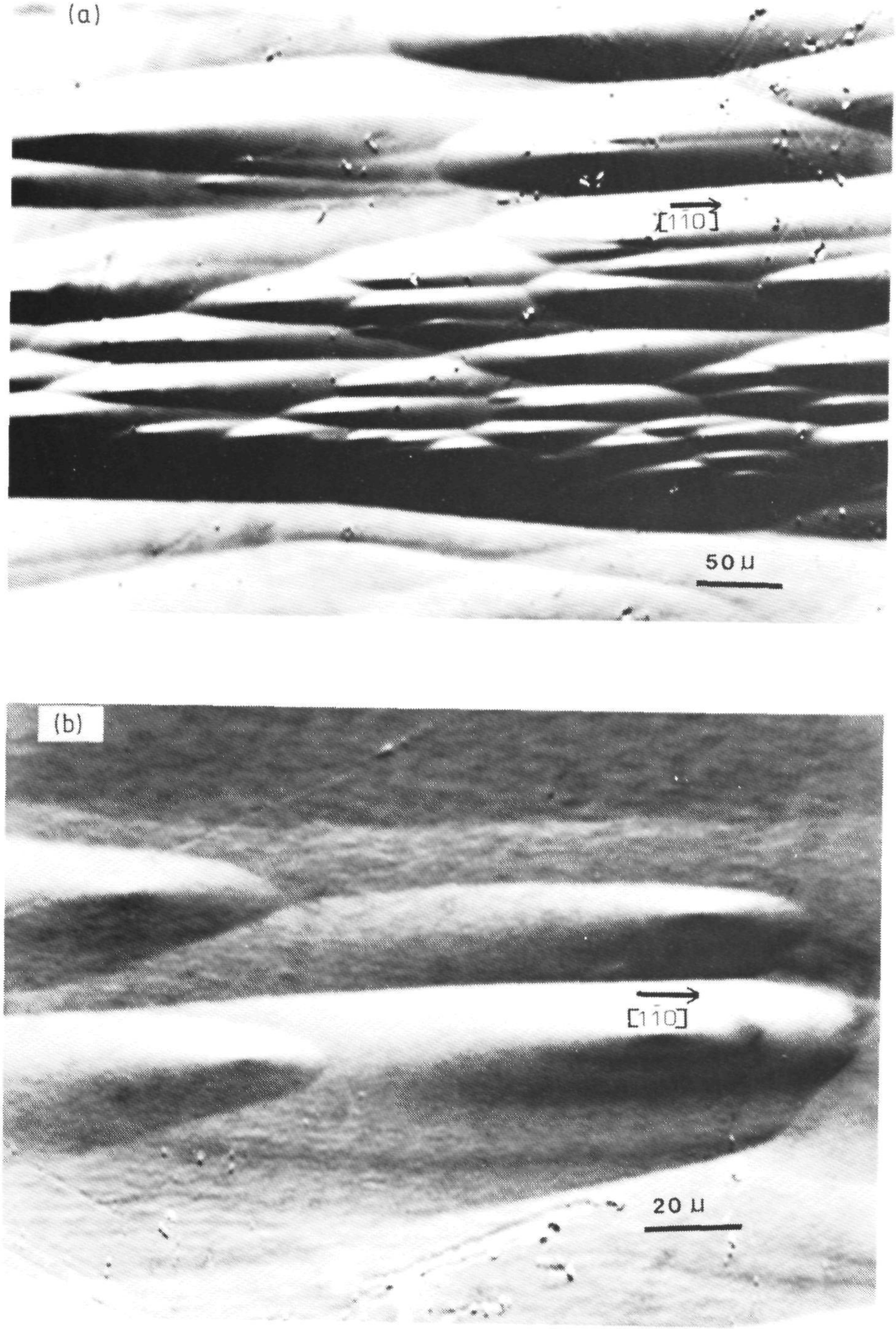

Fig. 5. Differential interference contrast micrographs of growth hillocks on {110} potash alum: (a) General view. (b) Detailed view.

which the ratio between length and width amounts to about 5.5. With respect to the external crystal morphology, the elongated hillocks are oriented in such a way, that their longitudinal directions are parallel to the direction <$\bar{1}10$> as presented schematically in figure 6. In the following section it will be shown, that these hillocks consist of concentric elliptical step trains originating from their centres. So it can now be concluded, that the advancement rate of steps parallel to <$\bar{1}10$> is about 5.5 times lower than for steps parallel to the perpendicular direction <001>.

From a periodic bond chain (PBC) [30] analysis of several alums, carried out by Hartman [31], it was found, that {110} potash alum is an

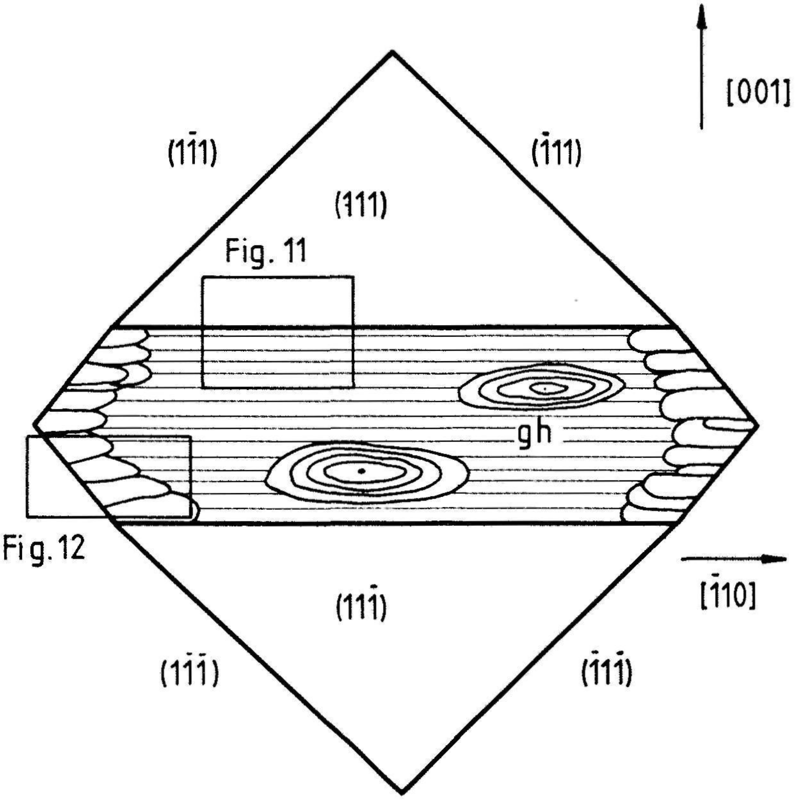

Fig. 6. Schematic representation of all the growth phenomena occurring on {110} potash alum, viz. spiral growth, manifesting as growth hillocks (gh) and two-dimensional nucleation starting from the edges of the face, in relation to the external morphology of the crystal.

F-face since its growth layer contains the two interconnected PBC s <$\bar{1}$10> and <001>. Because according to the morphological PBC theory on an F-face steps always run parallel to periodic bond chains [30], it is to be expected, that the step orientations on {110} alum are parallel to the two direction <$\bar{1}$10> and <001>. As the core of the PBC <1$\bar{1}$0> contains only the strong Al^{3+}-SO_4^2-bonds and the core of the PBC <001> also the weaker K^+-SO_4^{2-} interactions, it can be concluded, that the PBC <$\bar{1}$10> is stronger than the PBC <001>. Now assuming, that steps parallel to the PBC with the strongest bonds have the lowest advancement rate (because of a lower kink density), it can be concluded, that the hillocks should have a rectangular shape with the longitudinal direction parallel to <$\bar{1}$10>.

The observed shape of the elliptical growth hillocks is in agreement with the theoretically deduced rectangular form to such an extent, that the advancement velocity of the <$\bar{1}$10> steps is much lower, than of the <001> steps. However, "polygonized" steps parallel to <001> have never been observed; probably the PBC <001> is too weak to form more or less straight steps, as a result of an extreme amount of step roughening. Another phenomena, which may explain the rounding off of the growth hillocks is the possibility, that the anisotropy of the surface diffusion may be different from the anisotropy of the step edge free energy or step integration kinetics of ad-atoms.

3.3.2. Detailed observations with the aid of highly sensitive phase contrast microscopy

Application of phase contrast microscopy, which is more sensitive than differential interference contrast microscopy, reveals numerous steps on the {110} faces, as can be seen in figure 7. The height of the steps (estimated from the contrast: 50 - 500Å) is not extremely low, so probably these steps are formed due to a bunching of lower steps. The formation of such macrosteps, which are oriented parallel to the strongest PBC direction <$\bar{1}$10>, can only be understood, if growth of {110} potash alum proceeds via a step flow mechanism. Also non-bunched steps with very low step heights, as shown in figure 8 were commonly observed. The height of these steps equals about 10 - 20Å as was estimated

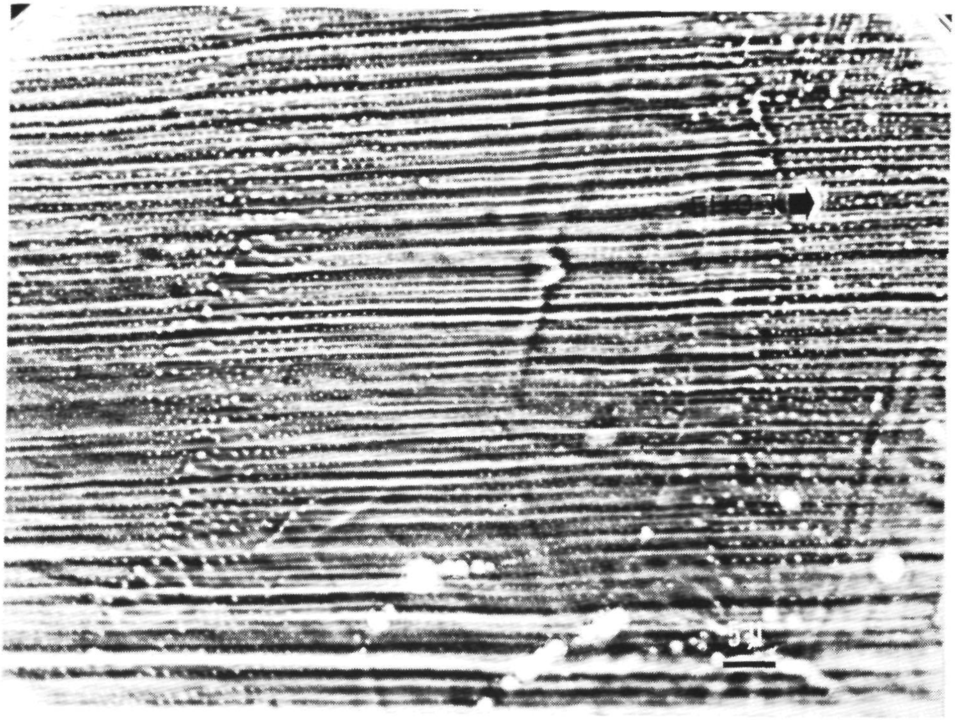

Fig. 7. Step train on {110} potash alum consisting of somewhat higher steps parallel to [$1\bar{1}0$] *(phase contrast micrograph).*

by comparison of their contrasts on the phase contrast micrographs with the contrast of steps of well known heights on {111} and {100} potash alum [8].

Observation of very low steps on {110} alum is extremely difficult, even more than on the {100} and {111} faces, because of the high anisotropy of the bonds within a growth layer of {110}. The {110} faces do not only contain the strong PBC <$\bar{1}$10>, but also the weaker PBC <001>. Such anisotropy, due to the occurrence of some weak lateral bonds in the growth layer of the {110} face leads to a lowering of the edge free energy of a two-dimensional nucleus, this promoting two-dimensional nucleation as was shown by Monte Carlo simulations [33]. So, due to an enhanced probability of nucleation growth at somewhat higher supersa-

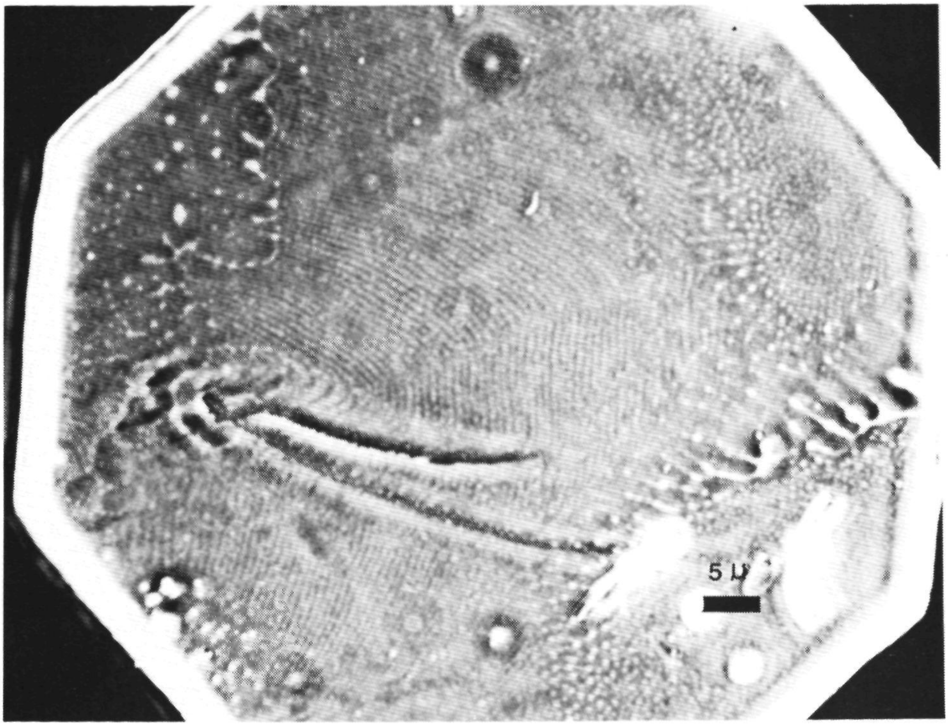

Fig. 8. Very low steps (step height ∿ 10 - 20A) on {110} potash alum (phase contrast micrograph).

turations, which may occur for a short time during the removal of the crystal from the solution, the original step pattern may be not longer visible by optical microscopy because of interference of this step pattern by two-dimensional nucleii.

Careful examination of growth hillocks by phase contrast microscopy revealed "concentric" elliptical step patterns (at least when the surface is not contaminated by nucleation during removal of the crystal out of the solution), as can be seen in figures 9 and 10. The step heights of these hillocks are about 10 - 20Å. A typical feature of many hillocks is the occurrence of a small hole at the centre, visible as a black dot - on all the phase contrast micrographs presented in this paper, dark areas have a lower level, than adjacent bright areas - in the figures 9 and 10. Probably these holes are formed due to an extremely slight dissolution resulting from the stress fields of the dislo-

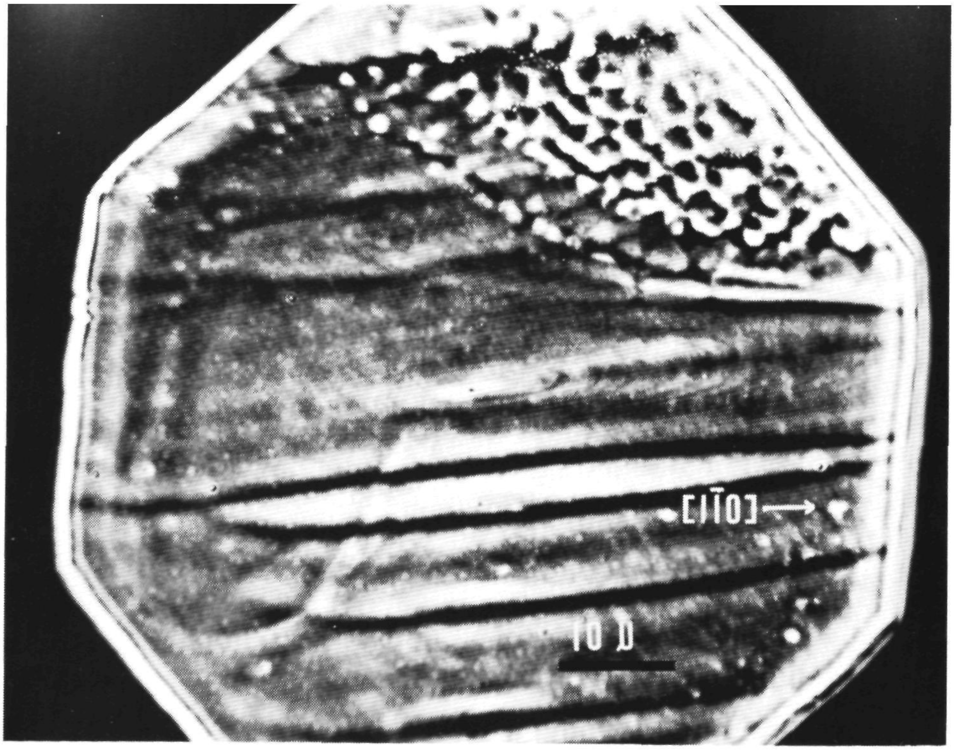

Fig. 9. High magnification phase contrast micrograph of an elliptical growth hillock revealing its step pattern.

cation outcrops at the centres of the hillocks during removal of the crystals from the solution as was pointed out for {100} alum in previous work [8]. From the presence of hollows at the centres of numerous growth hillocks (which turn into elongated etchpits upon etching in water), it can be concluded, that these elevations are related to dislocation outcrops. The mutual relation between growth hillocks and dislocation outcrops is confirmed by the observation, that the hillocks often occur in extended rows, which can be interpreted by the occurrence of low angle grain boundary outcrops at the crystal surface. From the correspondence between growth hillocks and dislocation outcrops, it can be concluded, that very probably these elevations are growth spirals.

During the present investigation spiral hillocks with different step height have been observed on {110} alum, which may be understood

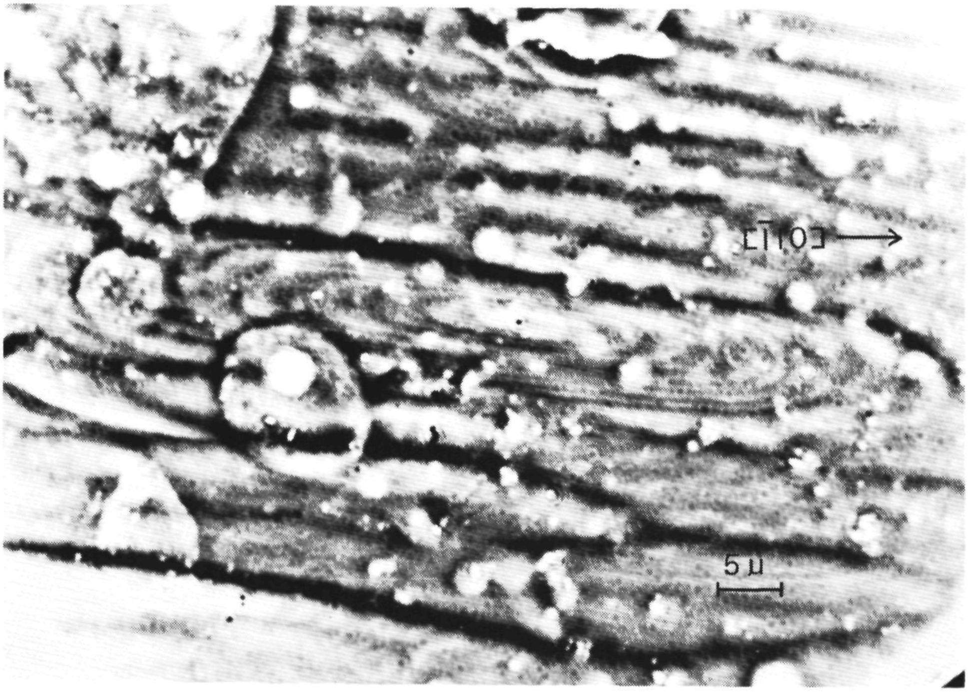

Fig. 10. Detailed view of an elliptical growth hillock, revealing its step pattern. The black dot at the centre indicates the occurrence of a hole, probably caused by a slight dissolution around the strained dislocation outcrop area during separation of the crystal from the solution (phase contrast micrograph).

in terms of the occurrence of different types of dislocations ending on the {110} faces, having different screw components normal to the growth face.

3.3.3. Nucleation growth

In cases, when no or a few growth hillocks were present at the dodecahedral faces, nearly always extended step trains originating from the edges of the {110} faces could be seen. Figure 11 shows such a parallel step train generated at the edge of the {110} face formed by the intersection line of the {110} and {111} faces (see also figure 6). It can clearly be seen, that at further distances from the edge, the height as well as the separation of the steps increases. This can be explained in terms of bunching of the very low steps formed at the <$\bar{1}$10> edges of

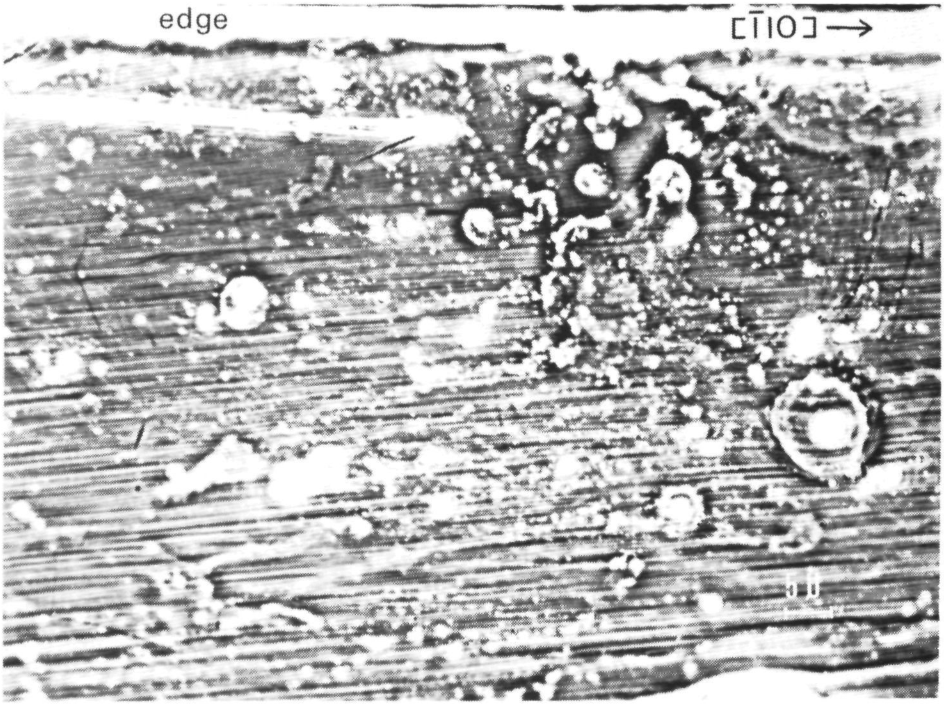

Fig. 11. Step train generated by two-dimensional nucleation starting from the $\langle\bar{1}10\rangle$ edge of the dodecahedral face (phase contrast micrograph).

the dodecahedral $\{110\}$ face.
Also the $\langle 1\bar{1}2\rangle$ intersection line of the $\{110\}$ and $\{1\bar{1}\bar{1}\}$ faces (see figure 6) quite commonly acts as a step source as shown in figure 12. In this case the step configuration is, due to the large anisotropy in step advancement rate on the dodecahedral faces, completely different from the step pattern generated at the $\langle\bar{1}10\rangle$ edges of the same face.

The formation of steps at the edges of the $\{110\}$ faces can be interpreted in terms of two-dimensional nucleation at the perifery of these crystal faces. Two possible explanations can be given for the - compared to the central region - enhanced formation of 2D nuclei at the edges of the $\{110\}$ faces:

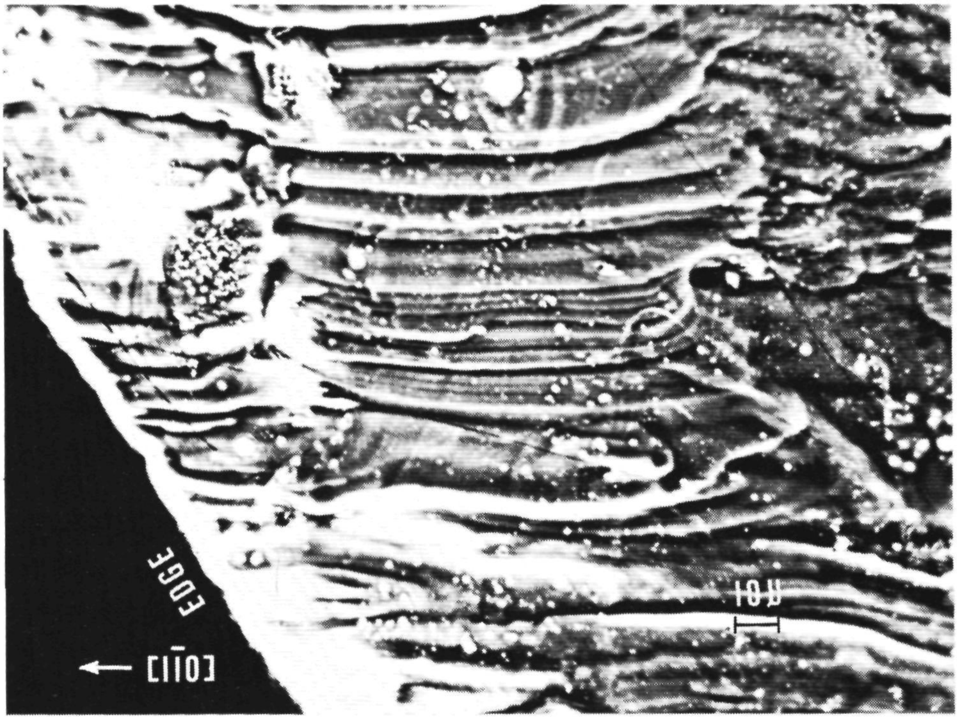

Fig. 12. Step train generated by two-dimensional nucleation starting from the <1$\bar{1}$2> edge of the {110} face (phase contrast micrograph).

(i) The supersaturation of the solution is higher near the edges and corners of the crystal, when crystal growth is - at least to some extent - mass or heat transport limited [34]. A similar step generation at edges and corners of a crystal face was observed by, among others: Bunn and Emmet [35] and by van Enckevort et al. on {101} KDP [25].

(ii) For a given interface supersaturation the size of a critical 2D nucleus and so also the energy barrier for the formation of such a nucleus, may be smaller near the edge of the dodecahedral faces, than at the central region. Such a difference in energy of surface atoms, which may constitute a 2D nucleus, in dependence on the location (edge, corner or central region) on the crystal face, has been calculated for the {100} faces of the ionic NaCl lattice by Stransky [12] and by Piela and Andzelm [36]. In order to verify this possibility for {110} alum a detailed Madelung energy calculation has to be carried out.

When it is assumed, that in periods of low growth rates, growth is determined by 2D nucleation, the observed high step density on the {110} face is in contradiction with the arrest of growth, which can be deduced from the stress birefringence microtopograph in figure 4. This contradiction in the relation between the growth rate and the observed surface morphology will be discussed later on, at the end of section 3.4.

Finally it is to be mentioned, that the steps starting from the edges of the {110} faces are not steps coming from adjacent {111} faces, which after arrival at the <$\bar{1}$10> and <1$\bar{1}$2> edges continue on the {110} faces. If this indeed would be the case, it is to be expected, that the growth rate of the {110} faces, $R_{\{110\}}$, is completely determined by the growth rate of the adjacent {111} faces, $R_{(111)}$. This is apparently not the case, because from the course of the sector boundaries between the {111} and the {110} sector, as given in the stress birefringence microtopograph in figure 4, it can be deduced, that the ratio of $R_{\{110\}}$ and $R_{\{111\}}$ can vary considerable and sometimes approaches zero. Moreover, the step patterns on adjacent {111} and {110} faces are not correlated to each other.

3.4. *X-ray diffraction topography*

In order to verify the correlation between growth rate and dislocation outcrop density on the {110} faces, use was made of Lang topography. Figures 13a and b present Lang topographs of the same {001} plate, with different diffraction vectors. This slice, which was cut according to the plan given in figure 2a, contains one well developed (thus slow growing) dodecahedral face, a, and one non-developed (thus fast growing) {110} face, b, as represented schematically in figure 13c. It can clearly be seen that the number of dislocations in the sector, belonging to face a is small, approaching zero. This in contrast to the sector belonging to the non-developed faster growing {110} face b, where the dislocation density is high. From this observation, it can now be concluded, that a high dislocation outcrop density on a {110} face leads to an increased growth rate of such a face.

Combining the surface topographic observations and the results obtained by Lang topography the following explanation for the growth rate dispersion of the dodecahedral faces of potash alum can be given: When

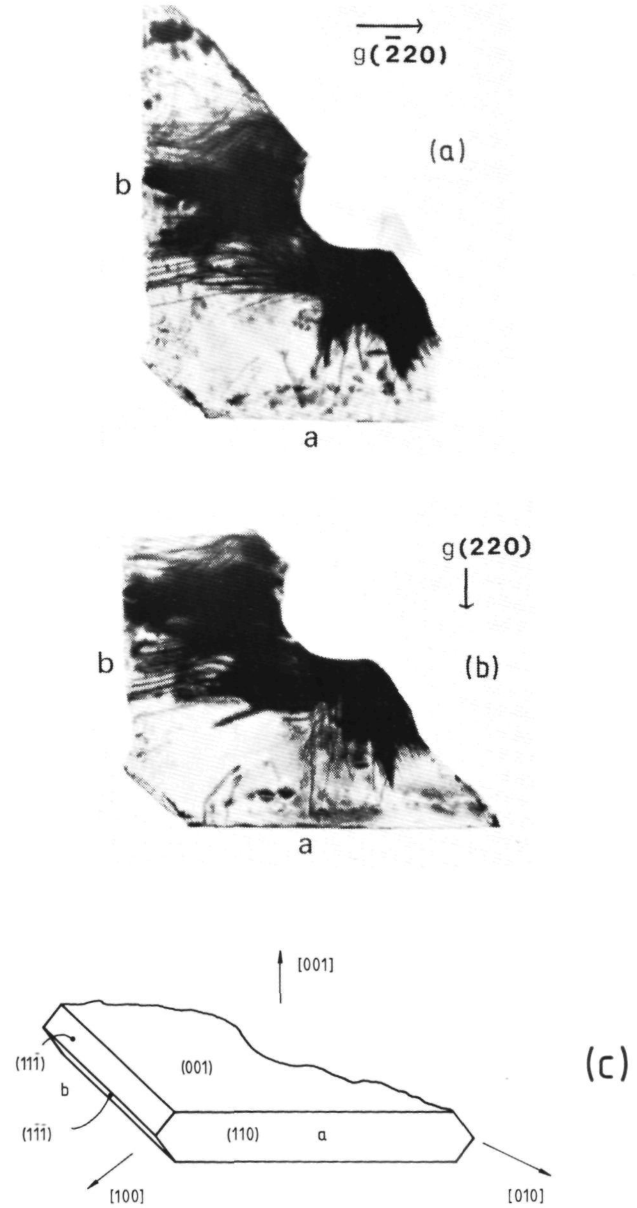

Fig. 13. Relation between the growth rate of {110} potash alum and the dislocation density:

(a) Lang topograph of an (001) slice, with one large {110} face, a, and one non-visible {110} face, b. $\vec{g} = (\bar{2}20)$.

(b) Lang topograph of the same slice as in (a) but now with $\vec{g} = (220)$.

(c) Schematic illustration of the (001) slice presented in (a) and (b).

outcrops of dislocations, having a screw component perpendicular to the growth face, equivalent to one growth slice thickness or more, are present on these faces, then the growth rate is high due to a spiral growth mechanism. The growth spirals manifest as elliptical growth hillocks. The fast growth of a {110} face with active dislocation outcrops, leads to a decrease in size of this face, since its growth rate is higher than $1/2\ \sqrt{6}.\ R_{\{111\}}$. At a given moment, all the endpoints of dislocations, which may function as active centres of growth spirals, are "refracted" from the in size decreasing dodecahedral face to the adjacent octahedral faces, so that growth proceeds via two-dimensional nucleation starting from the edges. This nucleation growth leads to an enormous decrease in growth rate and thus to an increase in size of the {110} face, which again may lead to a "capture" of screw dislocation endpoints from adjacent {111} faces, resulting in renewed fast spiral growth. Also a "spontaneous" formation of dislocations, in a {110} sector corresponding to a slowly growing face, may result in a sudden increase in growth rate of this face.

So the dispersion in growth rate can be understood in terms of an appearance and disappearance of - screw - dislocation outcrops at the {110} faces, leading to respectively spiral or two-dimensional nucleation growth. A similar explanation for the growth rate dispersion of crystal faces was given earlier by Gits-Leon et al. for {001} potash alum [18] and by Chernov et al. for {101} ADP [37].

It is to be noted, however, that the sudden arrest of growth of a {110} face after a period of fast growth, which can be deduced from the stress birefringence micrographs, can not be attributed to a "refraction" of an active dislocation outcrop from the {110} face to an adjacent {111} or {100} face. If this was the case, after refraction in the adjacent {111} or {100} growth sector, the dislocation line should run parallel to the {110} face otherwise renewed growth of the {110} face should occur immediately. Such dislocation line orientations have never been observed, neither during the present investigation, nor in literature [18,24]. From this it can be concluded that aside from the above mentioned dislocation mechanism, also another mechanism, which can give at "unpredictable" moments a more or less complete arrest of growth plays an essential role in the growth dispersion of {110} alum. A similar sudden arrest in crystal growth, not related to the dislocation structure was also observed for {001} faces of potash alum, which properties will be described extensively in a subsequent paper [38] and for {101} ADP [37].

Finally it is to be mentioned, that in addition to the long time variations in growth rate, often also short time fluctuations in the relative growth rate of the {110} faces could be observed with the aid of polarization microscopy. A similar fine structure in the growth rate dispersion was deduced from sector boundary profiles for {101} KDP [21], however in the present case no conclusive explanation can be given for this phenomenon.

4. CONCLUSIONS

From in situ observations and detailed a posteriori characterization by means of transmission polarization, reflection differential interference and phase contrast microscopy and Lang topography of the growth characteristics of the dodecahedral faces of potash alum the following can be concluded:

(i) The growth rate of the {110} potash alum faces shows a high dispersion. This variation in growth rate even occurs throughout one growth experiment - during which the supersaturation was kept constant - for one single face!

(ii) Growth of the {110} faces proceeds via a step flow model, involving low steps with a height of roughly 10 - 20Å. These low steps can "bunch" to macrosteps, having a height of a few hundred Angströms. The growth steps generally run parallel to the PBC-directions $<\bar{1}10>$.

(iii) As step sources may function:

(a) Dislocation outcrops, resulting in spiral growth, which leads to the formation of elliptical spiral hillocks with very low inclinations. In several cases an asymmetric step pattern (step height ∿ 10 - 20Å) was observed in relation to these hillocks.

(b) When no or a few growth hillocks are present: the edges of the {110} faces. In this case growth is governed by 2D nucleation, starting from the edges.

(iv) Dislocations can be the immediate cause for the variations in the growth rate of the {110} faces of potash alum. This can be concluded from the observed higher growth rates of dodecahedral faces with high dislocation outcrop densities than faces with very low (approaching zero) dislocation densities.

(v) The observed variations in the growth rate of the dodecahedral faces and the occurrence of a sudden arrest in growth at "unpredictable" moments can not be attributed to an appearance and disappearance of dislocation outcrops on the {110} faces alone. To account for this phenomenon an additional unknown mechanism by which steps are retarded or even become immobile must be postulated.

ACKNOWLEDGEMENTS

The authors wish to thank Ing. H.J. Böshaar for his assistence in making the Lang topographs and Prof. P. Bennema for stimulating discussions and critical reading of the manuscript.

One of us (W.J.P. van Enckevort) acknowledges the support of the Netherlands Foundation for Pure Research, ZWO/SON.

REFERENCES

[1] H.J. Human, J. Crystal Growth to be published.
See also: H.J. Human, Ph. D. Thesis, Catholic University of Nijmegen, The Netherlands (1981) Chapter IV).

[2] S. Amelinckx and G. Strumane in: Silicon Carbide: A High Temperature Semiconductor, Proc. Conf. of Silicon Carbide, Boston, 1959, Eds. J.R. O'Connor and J. Smiltens (Pergamon, 1960) pp. 162-201.

[3] I. Sunagawa, J. Cryst. Growth 45 (1978) 3.

[4] E. Bauser and K.S. Löchner, to be published.

[5] I. Sunagawa, Am. Mineral. 46 (1961) 1216.

[6] I. Sunagawa, in: Crystal Growth and Characterization, Proc. ISSCG-2 Spring School, Japan, 1974. Eds. R. Ueda and J.B. Mullin (North-Holland, Amsterdam, 1975) p. 347.

[7] I. Sunagawa and K. Tsukamoto, J. Crystal Growth 15 (1972) 73.

[8] W.J.P. van Enckevort, P. Bennema and W.H. van der Linden, Z. Phys. Chemie 124 (1981) 171.

[9] P. Bennema, J.P. van der Eerden, W.J.P. van Enckevort, B. van der Hoek and K. Tsukamoto, Phys. Status Solidi (a) 55 (1979) 403.

[10] W.J.P. van Enckevort and H. Klapper, J. Crystal Growth, to be published.

[11] W.J.P. van Enckevort and L. Jetten, J. Crystal Growth, to be published.

[12] See for instance: B. Honigmann, Gleichgewichts- und Wachstumformen von Kristallen, in: Fortschritte der physikalischen Chemie, Band 4, Ed. W. Jost (Dr. Dietrich Steinkopf Verlag, Darmstadt, 1958).

[13] V.G. Lutsau, Ju.M. Fishman and I.S. Res, Kristall Tech. 5 (1970) 445.

[14] N. Kato, J. Crystal Growth 3/4 (1968) 683.

[15] H. Klapper, Z. Naturforsch. 28a (1973) 614.

[16] F. Mussard and S. Goldstraub, J. Crystal Growth 13/14 (1972) 445.

[17] M. Matsunaka, M. Kitamura and I. Sunagawa, J. Crystal Growth 48 (1980) 425.

[18] S. Gits-Leon, F. Lefaucheux and M.C. Robert, J. Crystal Growth 44 (1978) 659.

[19] W.J.P. van Enckevort, R. Janssen- van Rosmalen, H. Klapper and W.H. van der Linden, J. Crystal Growth to be published.

[20] A.R. Lang, Acta Cryst. 12 (1959) 249.

[21] B. Dam and W.J.P. van Enckevort, J. Crystal Growth 51 (1981) 607.

[22] A.R. Lang, Nature 213 (1967) 248.

[23] B.K. Tanner, Phys. Stat. Sol. (a) 14 (1972) k9.

[24] W.J.P. van Enckevort and J.G.M. Odekerken, Phyl. Mag. to be published.

[25] W.J.P. van Enckevort, R. Janssen- van Rosmalen and W.H. van der Linden, J. Crystal Growth 49 (1980) 502.

[26] W.J.P. van Enckevort and W.H. van der Linden, J. Crystal Growth 47 (1979) 196.

[27] P. Bennema, Thesis, Tech. Univ. Delft (1965).

[28] See for instance: H. Komatsu in: Crystal Growth and Characterization, Proc. ISSCG-2 Spring School, Japan, 1974, Eds. R. Ueda and J.B. Mullin (North-Holland, Amsterdam, 1975) p. 347.

[29] A.R. Lang in: Properties of Diamond, Ed. J. Field (Academic press, 1979) p. 425.

[30] P. Hartman in: Crystal Growth: An introduction, Ed. P. Hartman (North-Holland, Amsterdam, 1973) p.p. 358-402.

[31] P. Hartman in: Growth of Crystals, vol. 7, Ed. N.N. Sheftal (Cons. Bureau, New York, 1969) p. 53.

[32] H. Müller-Krumbhaar, T.W. Burkhardt and D.M. Kroll, J. Crystal Growth 38 (1977) 13.

[33] J.P. van der Eerden, C. van Leeuwen, P. Bennema, W.L. van der Kruk and B.P.Th. Veltman, J. Appl. Phys. 48 (1977) 2124.

[34] A. Seeger, Phil. Mag. ser. 7, vol. 44 (1953) 1.

[35] C.W. Bunn and H. Emmet, Discuss. Faraday Soc. 5 (1949) 144.

[36] L. Piela and J. Andzelm, Surface Science 84 (1979) 179.

[37] A.A. Chernov, I.L. Smolski, V.F. Parvov, Yu.G. Kuznetsov and V.N. Rozhanskii, Sov. Phys. Dokl. 24 (1979) 760.

[38] H.J. Human and W.J.P. van Enckevort, J. Crystal Growth, to be published.

CHAPTER IV:

ON DISPERSION IN THE GROWTH RATES OF THE DIFFERENT FACES OF POTASH ALUM CRYSTALS

Part III: Relation between the growth rates of the {100} faces and the dislocation structure

H.J. Human and W.J.P. van Enckevort

RIM Laboratory of Solid State Chemistry,
Faculty of Science, Catholic University,
Toernooiveld, Nijmegen, The Netherlands

ABSTRACT

Highly accurate in situ growth rate measurements of the {100} faces of potash alum revealed an extremely large variation in growth rate inherent to the growth process itself. Three more or less discrete levels could be distinguished for the growth rate: 1) Complete arrest in growth, 2) Fast growth, 3) Growth at moderate speeds. Lang topography applied to crystals from which the growth rates had been measured, showed no positive correlation between the changes in growth rate and the dislocation structure. It was found, that complete standstill in growth of a {100} face might occur despite the presence of at least one screw dislocation outcrop at this face, which is capable to provide for spiral growth. Subsequent detailed investigation of the relation between surface morphology and internal defect structure of crystals grown in another system, using advanced optical techniques, Lang topography and stress birefringence microscopy resulted in the following conclusions:

(i) Sometimes the variations in the growth rates of the {100} faces can can be related to changes in the dislocation structure. Fast growth occurs, when screw dislocations are terminating on the {100} faces and growth proceeds via a spiral growth mechanism. On the other hand moderate growth rates were found, when growth is determined by either spiral growth from a dislocation outcropping near one of the edges of the {100} faces or by two dimensional nucleation growth.

(ii) Complete arrest of growth for longer periods - not related to changes in the dislocation structure - may occur at unpredictable moments. To

clarify this phenomenon an as yet unknown mechanism, by which steps are retarded or even become immobile, has to be postulated.

1. INTRODUCTION

The main interest of investigations concerning crystal growth from solution is the relation between the growth rate of a crystal face and the driving force, for which normally the relative supersaturation is used. In general it is assumed, that there exists an unambiguous relation between growth rate and relative supersaturation, i.e. it is supposed, that under identical experimental conditions (relative velocity between crystal and solution, actual working temperature etc.), the relative supersaturation is the only parameter determining the growth rate of a crystal face. However, in the past quite a lot of experimental evidence has been found, that this is not always the case and that at a fixed relative supersaturation the value of the growth rate can vary considerably. This phenomenon has been called elsewhere [1] dispersion in the growth rate.

From investigations of the concentration profiles around growing crystals in stagnant solutions [2-5] it has been shown, that the concentration distribution around a crystal is not uniform. Moreover, it has been observed, that the crystal face in contact with the solution with the highest concentration, was not necessarily the one with the highest growth rate. These observations indicate, that there exists no unambiguous relation between the growth rate and the relative supersaturation.

Measurements of the linear growth rate as a function of the relative supersaturation by various techniques [6-14] quite often result in a considerable scatter in the positions of the experimental points in the plots of linear growth rate versus relative supersaturation. Although, it is not always clear, whether this scatter in growth rate should be completely attributed to "real variations" in the growth rate, this scatter in the positions of the experimental points again indicates, that no unambiguous relation exists between growth rate and relative supersaturation.

Another experimental method, which is frequently applied in the world of industrial crystallization, to obtain the relation between the growth rate of a crystal and the relative supersaturation is the determination of the crystal size distributions (CSD) of crystals, growing in an agitated vessel or a mixed suspension mixed product removal (MSMPR) crystallizer, as a function of time. From this type of experiments, the growth rates of the crystals can be obtained by using McCabes ΔL law [15]. This law, which states, that growth of geometrically similar crystals of the same material, suspended in the same solution proceeds with the same linear growth rate, is frequently violated [16-21]. This indicates, that either there exists no unambiguous relation between the linear growth rate and the relative supersaturation, or that the solubility of the crystals is size dependent. Much more direct evidence, from this type of experiments, for the non-existence of an one to one relation between the growth rate and the relative supersaturation was obtained by White et al. [22] and Wright et al. [23], who observed a considerable broadening of the crystal size distribution during growth of a batch of seed crystals of a very narrow sieve fraction.

Finally from the large variation in the directions of the boundaries between the growth sectors belonging to two different faces - which can sometimes be observed in slices cut from crystals, grown under almost constant experimental conditions, by means of Lang topography, stress birefringence microscopy or etching methods [24-31] - it can be deduced, that the growth rate of one crystal face may vary considerably in comparison to the growth rate of the adjacent crystal faces. However, by means of these techniques it is in principle not possible to give absolute values of the magnitude of the variations in the growth rate, because the direction of a sector boundary is determined by the ratio of the growth rates of the two relevant faces. Nevertheless it is quite safe to conclude from these observations, that there exists no unambiguous relation between the linear growth rate and the relative supersaturation.

The aim of the present investigation is to get a better understanding of the origins of the observed dispersion in the growth rates of the {100} faces of potash alum ($KAL(SO_4)_2.12H_2O$) crystals. Up to now only in a restricted number of cases, the dispersion in the growth rates of crystal faces, growing under fixed experimental conditions have been investigated systematically [32,33]. Despite the negative results of the attempts in these investigations to correlate the dispersion in the growth rates with the presence or absence of active growth centres on a crystal face, it was decided to try to correlate the variations in growth rate of the {100} faces of potash alum to changes in the dislocation structure in the growth sectors belonging to these faces. Reasons, why it was decided to investigate the {100} faces are the following: In general the most obvious origin for changes in the growth rate under fixed experimental conditions are changes in the dislocation structure in the growth sector of the crystal face under consideration. Whenever, there exists a correlation between the changes in the dislocation structure and the changes in the growth rate, it is obvious, that this can be observed most easily in the growth sector of the {100} alum faces, because in this sector the dislocation structure is rather simple [24,29].

2. EXPERIMENTAL

2.1. Measurements of the linear growth rate

To study the growth rate of {100} potash alum ($KAL(SO_4)_2.12H_2O$) in dependence on time and relative supersaturation, simultaneously the growth rates of at least one and sometimes two {111} faces and one {100} face were measured for five crystals. As it is assumed to be essential for this part of the investigation to measure the growth rates under constant and reproducible experimental conditions for sufficient long times, use was made of the flowsystem, which was also used for the measurements of the linear growth rates of the {111} faces of potash alum. This flowsystem, its advantages and imperfections, the possible experimental errors, the accuracy of the measurements, the preparation of the solution and the experimental procedure has been described elsewhere [1]. The growth rates used in the present paper are equivalent to the differential linear growth rate as defined in ref. [1], which can be calculated from the displacement of a face in the time between successive measurements (exposures) and the magnitude of the time interval. Slices parallel to {100} cut by means of a wetted metal wire saw from almost perfect large single crystals - grown by a slow temperature decrease technique on a rotating crystal tree in a two litre vessel - were used as seed crystals. These seeds were mounted onto the crystal holder by means of a contact cement on cyanoacrylate base (Permacol, Industrial

Contact Cement, type 301) in the way as shown in fig. 2c of reference [1].

2.2. Determination of the dislocation structure

In order to investigate the dislocation structure in the growth sectors related to those {100} faces, of which the linear growth rates had been measured, slices parallel to {110} were cut from the crystals in question, by means of a wetted metal wire saw. As shown in figure 1, this can be done in two ways. From this illustration it is clear, that it is not possible to trace the course of the dislocations over all the four sector boundaries between the {100} and {111} faces. When the slice is cut from the crystal as indicated by the dashed lines, it is not possible to follow completely the course of the dislocations crossing the sector boundaries AA'D'D and BB'C'C. When the slice is cut from the crystal according to the dotted lines, the trajectory of the dislocations crossing the sector boundaries AA'B'B and DD'C'C cannot be followed completely.

To prevent interference of surface defects with the X-ray topographic image, the slices were slightly etched with deionized water. All topographs were made by the Lang technique [41], using $CuK\alpha_1$ ($\lambda = 1.5406Å$) or $AgK\alpha_1$ ($\lambda = 0.5594Å$) radiation. Several reflections such as {220} and {004} were used.

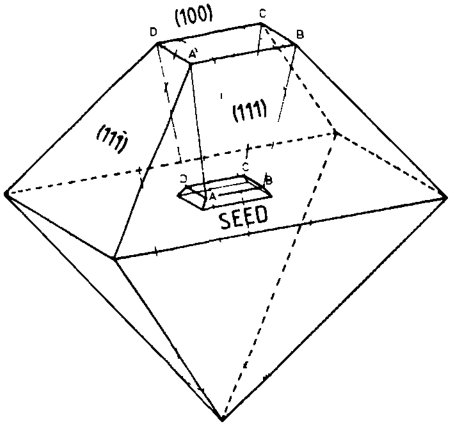

Fig. 1. The two possibilities to cut a slice parallel to {110} out of a crystal.

2.3. Observations of the surface morphology

To carry out a posteriory surface observation of aqueous solution grown crystals by means of highly sensitive phase contrast and differential interference contrast microscopy, special attention must be paid to the separation of the crystals from the supersaturated solution. Therefore the specimen crystals were grown in a vessel, especially designed to facilitate the removal of the crystal from its mother liquor, under experimental conditions comparable to the conditions in the flowsystem. In this way clean surface areas, suitable for surface microtopography can be obtained. This vessel, as well as the separation procedure have been described in detail elsewhere [34]. It is to be noted, however, that in contrast to this earlier work, now not one of the tops or edges of the octahedral crystals were cut off, but that "complete" as-grown crystals were placed in the vessel, where they were allowed to grow for a few days.

The observations of the as-grown {100} faces, were carried out by making use of a highly sensitive optical phase contrast microscope, fitted with a 95% absorption phase plate. By using this microscope, combined with high contrast photographic emulsion, it is possible to reveal extremely low step heights (as low as 2.3Å [35,36]. The application of optical microscopy to study surfaces of aqueous solution grown crystals has been treated in several papers [34,37-40].

2.4. Observations of the growth sectors

In order to investigate the relative positions of the growth sectors, belonging to different faces and the course of the boundaries between them, stress birefringence microscopy was applied to the same {110} slices, which were cut from the crystals to inspect the dislocation structure within these growth sectors, by means of Lang topography. For further details on the application of stress birefringence microscopy to potash alum, the reader is referred to [30].

3. RESULTS AND OBSERVATIONS

3.1. The linear growth rate and the dislocation structure

3.1.1. *The differential linear growth in dependence on relative supersaturation and time*

In the figures 2a and 2b the growth rates - measured at a restricted number of relative supersaturations for a {100} and a {111} face simultaneously - are given as a function of time for the crystals 25, 26, 27 and 28. On top of the relevant parts of these figures, the average values of the relative supersaturations, σ, during an experiment and the registration numbers of the experiments are given for each crystal. For most of the experiments, the absolute error in the growth rate is equal to 0.7 nm/s and sometimes even smaller. Only for a small number of experiments, the absolute error in the differential linear growth rate is higher, being 1.4 nm/s. A detailed description of the way in which the value of the absolute error in the differentail linear growth rate can be obtained is given elsewhere [1].

From the figures 2a and b it can be seen, that at the beginning of the experiments with the crystals 25, 26, 27 and 28, the growth rates of the {100} faces show a sharp decline. After this period, which varies from 8 hours for crystal 26 to 30 hours for crystal 25, the growth rate reaches a minimum value - equal to 0.0 nm/s - and starts fluctuating very irregularly with very large variations. As can be seen from the figures 2a and b, the growth rates of the {100} faces of all crystals vary from complete arrest of growth up to values, which can be about 10 times larger than the values of the more or less constant growth rate of the {111} faces. The variations in the growth rate of the {100} faces are twenty to fifty times larger, than the absolute error of this quantity and about 10 times larger, than the variations in the growth rate of the {111} faces. From a comparison of the magnitudes of the variations in the simultaneously measured growth rates of the {100} and {111} faces, it can be inferred, that the variations in the growth rates of the {100} faces are due to unnoticed changes in the experimental conditions only to a very small extent. Moreover in previous work [1] it has been shown, that the variations in the growth rates of the {111} faces cannot be

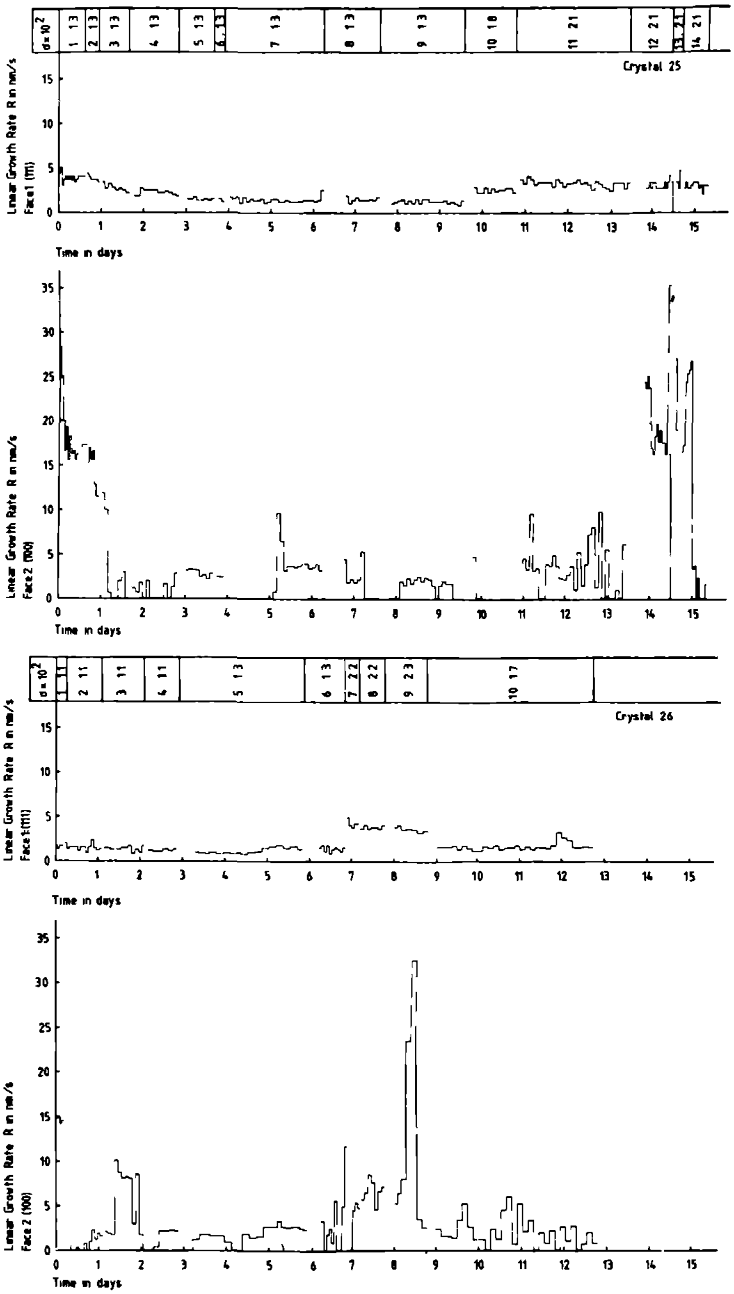

Fig. 2a. The differential linear growth rate in nm/s of the crystals 25 and 26 in days. On top the registration number of the experiments and the average relative supersaturations are given.

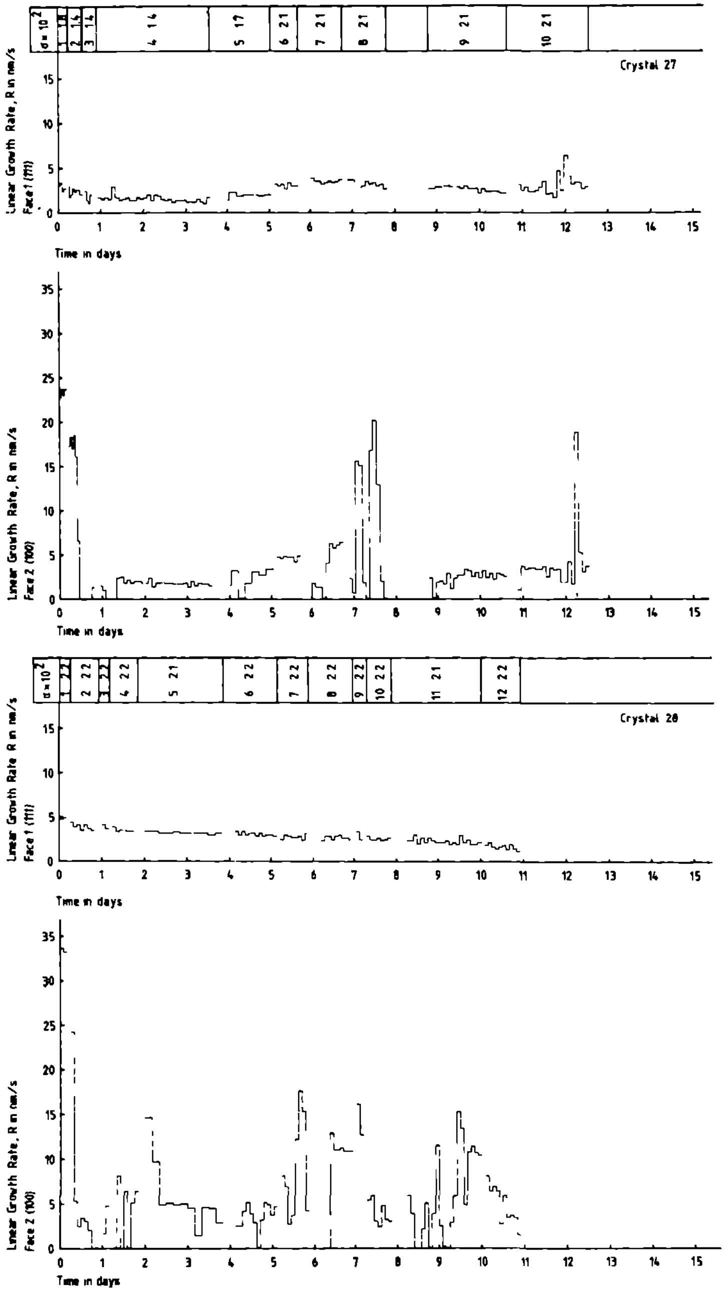

Fig. 2b. The differential linear growth rate in nm/s of the crystals 27 and 28 in days. On top the registration number of the experiments and the average relative supersaturations are given.

attributed completely to experimental errors, but must be - at least partly - inherent to the growth process itself. So, the conclusion can be drawn, that the much larger variations in the growth rates of the {100} faces are caused by "real" changes in the growth process. Now, it is clear, that also for the {100} faces of potash alum there exists no unambiguous relation between growth rate and relative supersaturation and that it is not possible to construct a sensible curve through the experimental points for the growth rate versus the relative supersaturation.

Even the construction of a "maximum" growth rate versus relative supersaturation curve, from the values for the "maximum" growth rates of the {100} faces given in table 1, seems not to be very useful, because it should be realized, that the values given in this table are average values of the growth rate between two exposures. As can be seen from the figures 2a and b, it is neither possible to distinguish any regular periodicity in the fluctuations of the growth rate, nor to obtain an idea about the length of the periods of the fluctuations. The abrupt way, in which the changes in the growth rate take place suggests, that growth occurs according to an "ON/OFF" mechanism. When this is indeed the case, it should be kept in mind, that the average values of the growth rates of the {100} faces given in the figures 2a and b and table 1 may differ considerably from the real momentary growth rates, because in the period between two exposures the momentary growth rate might have been much larger and smaller for a couple of minutes than the average value of the growth rate. So, it can be concluded, that even the in table 1 given "maximum" values for the growth rate are not very reliable.

3.1.2. *The relation between changes in the growth rates of the {100} faces and changes in the dislocation structure in the growth sectors of the {100} faces*

From simple goniometry the following relation for the angle, β, between the sector boundary, located between the {100} and 111 sectors and the {100} face can be derived:

$$\mathrm{cotg}\beta = \frac{R_{\{111\}}}{R_{\{100\}}} \cdot \frac{1}{\cos\alpha} - \mathrm{tg}\alpha \qquad (3.1)$$

where $R_{\{100\}}$ and $R_{\{111\}}$ are the growth rates of respectively the {100}

TABLE 1

Maximum and minimum linear growth rate at 3 different intervals for the relative supersaturation

Crystal	Rel. Supersat.: $1.1-1.3.10^{-2}$		Rel. Supersat.: $1.7-1.8.10^{-2}$		Rel. Supersat.: $2.1-2.3.10^{-2}$	
	Max. Lin. Gr. Rate (nm/s)	Min. Lin. Gr. Rate (nm/s)	Max. Lin. Gr. Rate (nm/s)	Min. Lin. Gr. Rate (nm/s)	Max. Lin. Gr. Rate (nm/s)	Min. Lin. Gr. Rate (nm/s)
25	9.7	0.0	4.8	0.0	35.3	0.0
26	10.2	0.0	6.0	0.0	30.5	0.0
27	2.5	0.0	3.2	0.0	20.2	0.0
28	-	-	-	-	17.6	0.0
31	5.8	0.0	7.8	3.0	10.2	0.0

face and the adjacent {111} face and α is the angle between these faces. As can be seen from the figures 2a and b the growth rate of the {111} face - except for a slow decrease - is more or less constant. So, from equation 3.1 it follows, that abrupt changes in the growth rate of the {100} faces will show up as a sudden change in the direction of the sector boundary. From this argument it is clear, that a convenient way to look for dispersion in the growth rate of the {100} faces, is to investigate the course of the sector boundary between the growth sectors of the {100} and {111} faces in the crystal. In order to correlate sudden changes in the growth rate of {100} faces to changes in the dislocation structure in the growth sector of the {100} faces, it is necessary to know the course of the sector boundary within the Lang topographs of the {110} slices, cut from the investigated crystals.

Since in contrast to the work by Gits-Leon et al. [24] in the present investigation no sector boundaries could be observed on the Lang topographs, it was decided to reconstruct the sector boundary from the data obtained by in situ measurements of the growth rates of the {100} and {111} faces. In the figures 3c and 4c, in which also the positions of the {100} and {111} faces at the beginning and the end of an experiment are given, the paths of the sector boundaries between the {100} and {111} growth sectors are reconstructed in this way, using the dimensions of the crystal in the end situation, i.e. after the removal of the crystal out of the flowsystem, as a reference. Upon comparison of the figures 3c and 4c with the Lang topographs given in the figures 3a, b and 4a, b respectively a discrepancy with respect to the size of the seed may be observed. This is due to the fact, that the slice from which the Lang topographs have been taken, is cutted from the crystal according to the dotted lines in figure 1, while the growth rates of the {100} and {111} faces have been measured instead of the {100} and $\{11\bar{1}\}$ faces. Also with regard to the ultimate size of the crystal a deviation may be observed upon comparing the figures 3c and 4c with respectively the figures 3a, b and 4a, b. It is clear, that due to these discrepancies the course of the sector boundary in the crystal can not be determined very accurately by the above described method. Another factor hindering the investigation of the correlation between dispersion in the growth

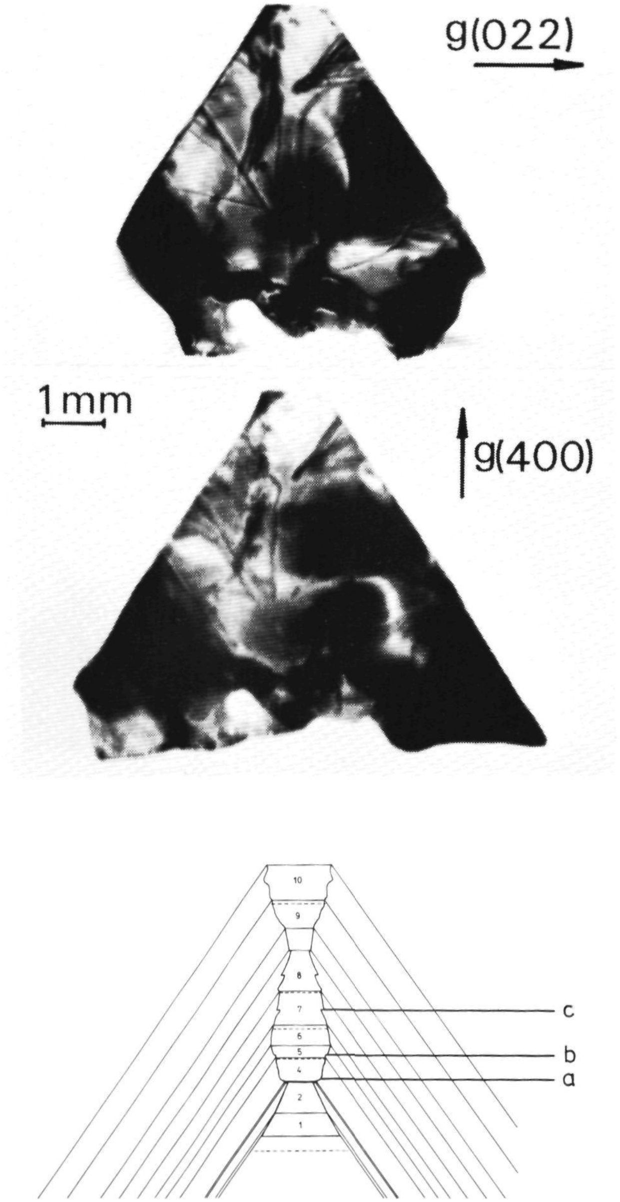

Fig. 3. Relation between the growth rate of {100} potash alum and the dislocation structure of crystal 27.

(a) Lang topograph of a $(01\bar{1})$ *slice.* $\vec{g} = (022)$.

(b) Lang topograph of the same $(01\bar{1})$ *slice as in (a), but now with* $\vec{g} = (400)$.

(c) Schematic illustration of the growth history and the trajectory of the sector boundary.

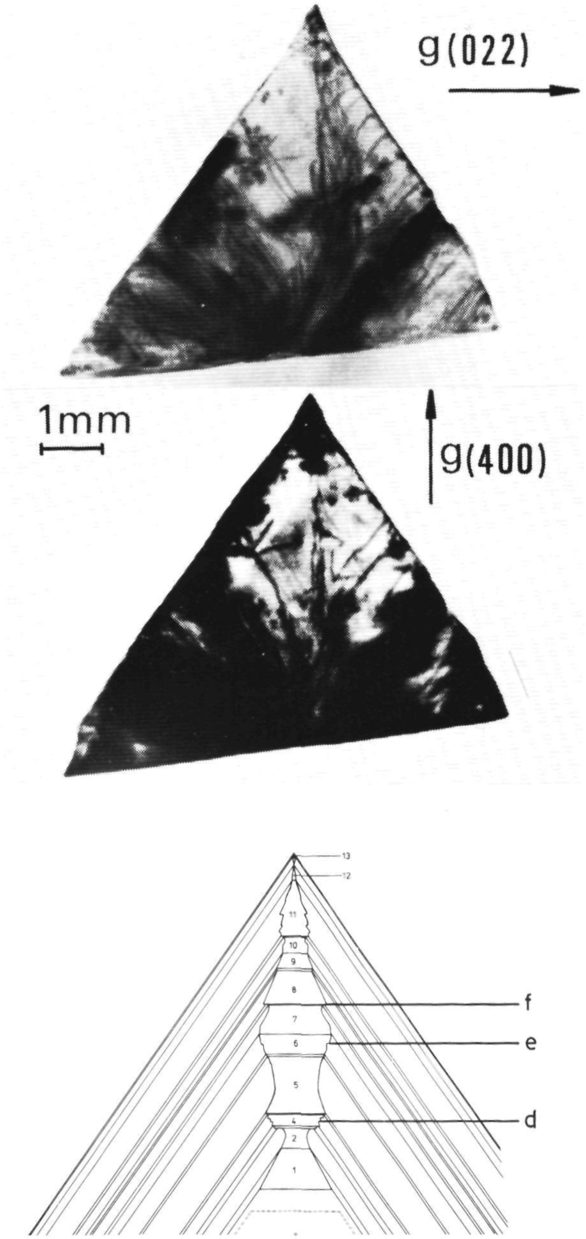

Fig. 4. Relation between the growth rate of {100} potash alum and the dislocation structure of crystal 28.

(a) Lang topograph of a $(01\bar{1})$ slice. $\vec{g} = (022)$.

(b) Lang topograph of the same $(01\bar{1})$ slice as in (a), but now with $\vec{g} = (400)$.

(c) Schematic illustration of the growth history and the trajectory of the sector boundary.

rate of the {100} face and the dislocation structure in its growth sector is the limited resolution of the Lang technique. However, despite the above mentioned problems, from the specific course of the dislocation lines on the Lang topographs, it can unambiguously be deduced in which growth sector the dislocations were included during growth.

In the figures 3a, b respectively 4a, b Lang topographs made of the {110} slices cut from the crystals 27 and 28, using the (022) and (400) reflections are given. In the figures 3c and 4c the positions of a {100} face and two adjacent {111} faces and the boundaries between the growth sectors of these faces are constructed for the crystals 27 and 28 respectively. From these figures it is clear, that only at the very first beginning of the experiments there exists a positive correlation between the growth rate and the dislocation structure. High growth rates as a result of a large number of outcrops of screw dislocations, which probably are formed at liquid inclusions, resulting from a "healing" process of the seed crystal after it has been mounted into the cell of the flow-system and the experiment has been started. However, after the first arrest of growth of the {100} face of the crystal, no clear positive correlation between changes in the growth rate and changes in the dislocation structure - i.e. a sudden increase or decrease in growth rate of the {100} face after respectively appearance or disappearance of a screw dislocation within the growth sector of this face - is found. This observation does not necessarily imply that such a correlation does not exist, because it must be kept in mind, that the course of a dislocation can be traced over only two of the four sector boundaries.

One of the interesting aspects, which can be observed from the figures 4a and b is the asymmetry in growth rate of the left {111} face with respect to the right {111} face. Probably due to a much higher number of screw dislocation outcrops on the left {111} face than on the right {111} face, the growth rate of the left {111} face is much higher than of the right {111} face. This observation is in agreement with the conclusion, that growth of the {111} faces proceeds via a cooperating spiral mechanism; a preliminary explanation given elsewhere [1] in order to understand the slow decrease of the growth rates of the {111} faces with time at constant relative supersaturations.

One of the most intriguing and unexpected features, which can be deduced from the figures 3 and 4 is, that growth of the {100} faces may be arrested even when outcrops of dislocations with a screw component are present on these faces. For crystal 27 this situation can be observed during the experiments 4, 5 and 7, indicated in figure 3c by respectively a, b and c. For crystal 28 this situation can be observed during the experiments 4, 6 and 8, indicated in figure 4c by respectively d, e and f. This negative correlation between changes in growth rate and changes in dislocation structure suggests, that outcrops of screw dislocations do not always function as active step sources or, that steps on a crystal face can be retarded or even become immobile. In order to investigate this phenomenon more precisely, it was decided to investigate the surface morphology of crystals grown under almost identical experimental conditions. The result of this part of the investigation will be presented and discussed in the following section.

3.2. The surface morphology and the dislocation structure

In this part of the paper the results will be described of an investigation of the surface morphology of the well developed {100} faces of three crystals, grown in a vessel especially designed to facilitate the removal of the crystal from its mother liquor in such a way, that "ruination" of the surface patterns is prevented as much as possible [34]. The experimental conditions in this vessel are not significantly different from the experimental conditions in the flowsystem. This means, that the information of the surface morphology obtained by way of a posteriori observation by advanced optical techniques on crystals grown in this vessel, is also relevant for the crystals grown in the flowsystem. In the subsequent part some features of each of these three crystals will be discussed.

Crystal 1: In figure 5 two phase contrast micrographs of a well developed {100} face of this crystal are given. In Figure 5a a growth hillock can be seen near the edge parallel to the direction $[0\bar{1}1]$, being the intersection line between this {100} face and an adjacent {111} face. Figure 5b shows a nearly equidistant step train with very low step height (12.2Å being one unit lattice height, as can be estimated from the contrast [34]), parallel to [011] and located somewhat more near to the centre of this {100} face. A more elaborate inspection of this {100} face by means of phase contrast microscopy showed, that the whole step pattern

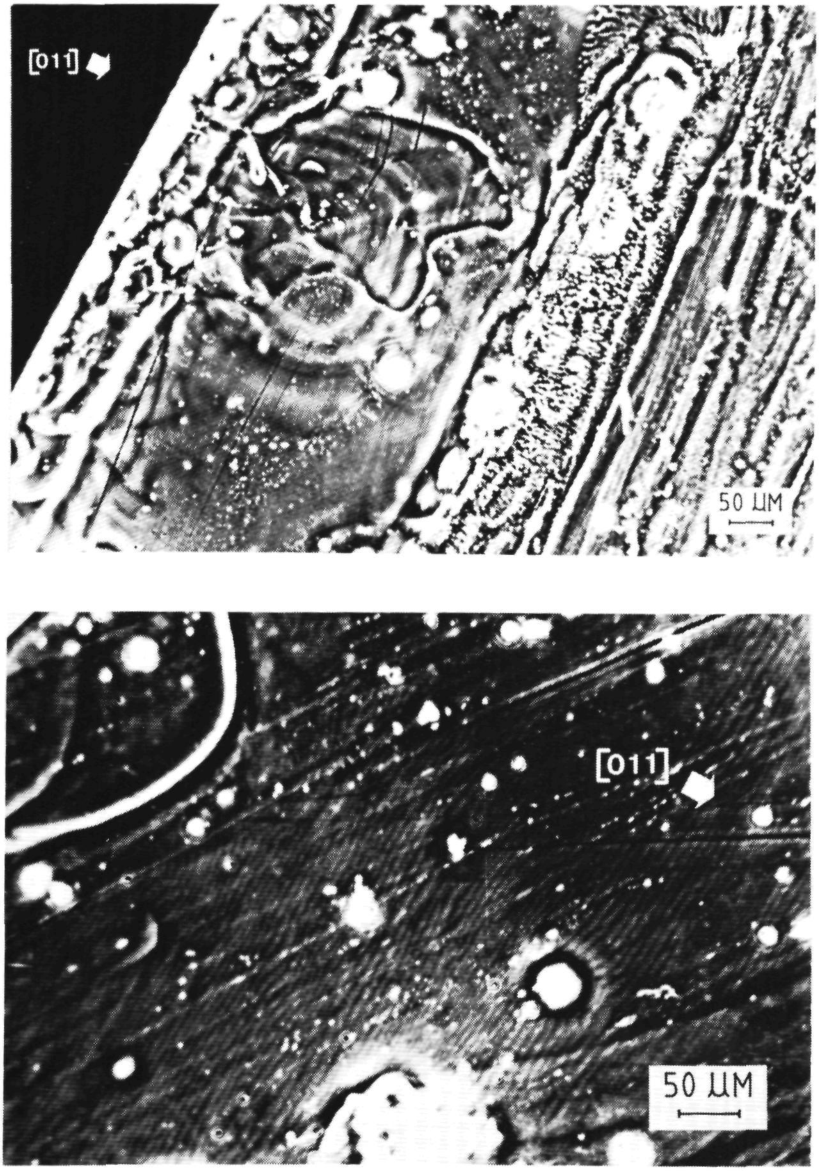

Fig. 5. Phase contrast microphotographs of the surface of the (100) face of crystal 1 showing:

(a) Growth hillock near the edge of the crystal, resulting from the outcrop of the "refracted" dislocation, shown in the Lang topograph of Fig. 6.

(b) Train of very low steps (step height: 12.2Å) at the centre of the (100) face, originating from the growth hillock of (a).

on this face originates from the growth hillock presented in figure 5a. In order to examine, whether this growth hillock is related to the outcrop of a screw dislocation, a {110} slice cut from this crystal was investigated by means of X-ray diffraction topography. From the Lang topograph - which was made of this slice using the (400) reflection - presented in figure 6, it can be seen that in the main part of the growth sector of this {100} face no dislocations with a screw component perpendicular to this face are present. Only just before the removal of the crystal from the vessel, a dislocation with a screw component perpendicular to the {100} face (indicated by the arrow in figure 6) is refracted from the growth sector of a {111} face into the growth sector of this {100} face. The Burgers vector ($\vec{b} = [100]$) was deduced from the orientation of the dislocation line and its extinction in another Lang topograph using the

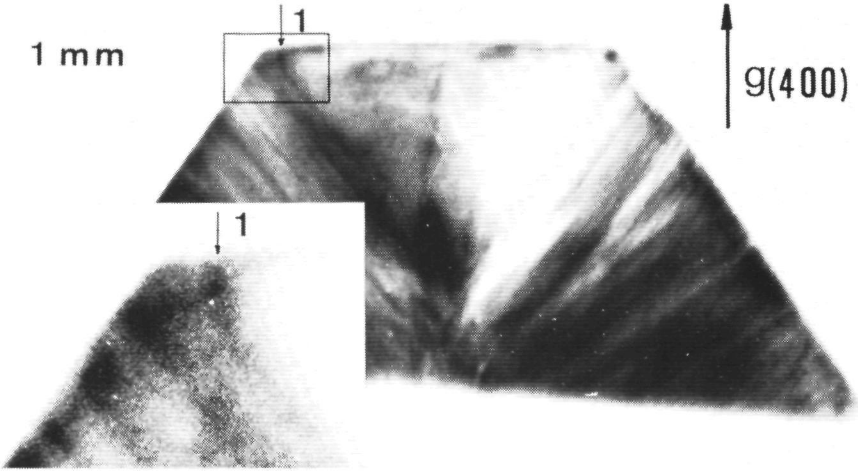

Fig. 6. Lang topograph showing the "refraction" of a dislocation from a {111} face to the adjacent (100) face of crystal 1.

reflection (022) (not shown in this paper) [30]. Careful measurements of the distance between the outcrop of the screw dislocation and the edge of this {100} face with an adjacent {111} face on the Lang topograph given in figure 6 (150 ± 20 μm) and on the phase contrast micrograph shown in figure 5a (140 μm) indicates, that most probably the growth hillock presented in figure 5 is related to the refracted dislocation indicated by the arrow in figure 6.

Crystal 2: In figure 7a a drawing is presented in which some characteristics of crystal 2 are given. In this illustration the step pattern observed on one of the {100} faces of this crystal is given in a schematic way. The location of the more or less equidistant step train with unit lattice height presented in the phase contrast micrograph of figure 7b, is indicated by the rectangle in figure 7a. The step train shown on the surface micrograph of figure 7b originates from a growth centre, A, near an edge of the {100} face. In order to verify, whether this growth centre, A, is related to an outcrop of a dislocation with a screw component perpendicular to this {100} face, a {110} slice cut from this crystal in the way as indicated by the dashed lines in figure 7a, was investigated by means of X-ray diffraction topography. From the Lang topograph of this {110} slice in figure 7c (diffraction vector $\vec{g} = (400)$) it can be seen, that this growth centre is related to a screw dislocation, entraped in the boundary between the {100} growth sector and one of its adjacent {111}growth sectors. The direction of the Burgers vector ($\vec{b} = [100]$) of this dislocation line, indicated by an arrow in figure 7c was again deduced from its orientation and its extinction in the Lang topograph using the reflection (022) (not shown in this paper) [30].

Crystal 3: In the schematic illustration of crystal 3 given in figure 8a, the creation of bundles of dislocations originating from a row of liquid inclusions (resulting from a small accident during the growth process) is sketched. As can be seen from this drawing these bundles of dislocations run into the growth sector of a {100} face, as well as into the growth sector of a {111} face and result in the formation of low angle grain boundaries ending on both faces. In figure 8b a phase contrast micrograph is presented, showing a group of growth hillocks, probably located at the outcrops of the dislocations in the low angle grain boundary ending on the {100} face. Etching of the same surface area as shown in figure 8b, using deionized water, revealed the etch pit pattern given in the differential interference contrast micrograph presented in figure 8c. From the resemblance of the pattern of growth hillocks given in figure 8b to the pattern of etch pits in figure 8c, it can be concluded, that each growth hillock turns into an etch pit after etching. This prooves, that the growth hillocks of figure 8b are related to the outcrops of the dislocations in the low angle grain boundary ending on the {100} face. A similar correspondence between growth hillocks or spirals

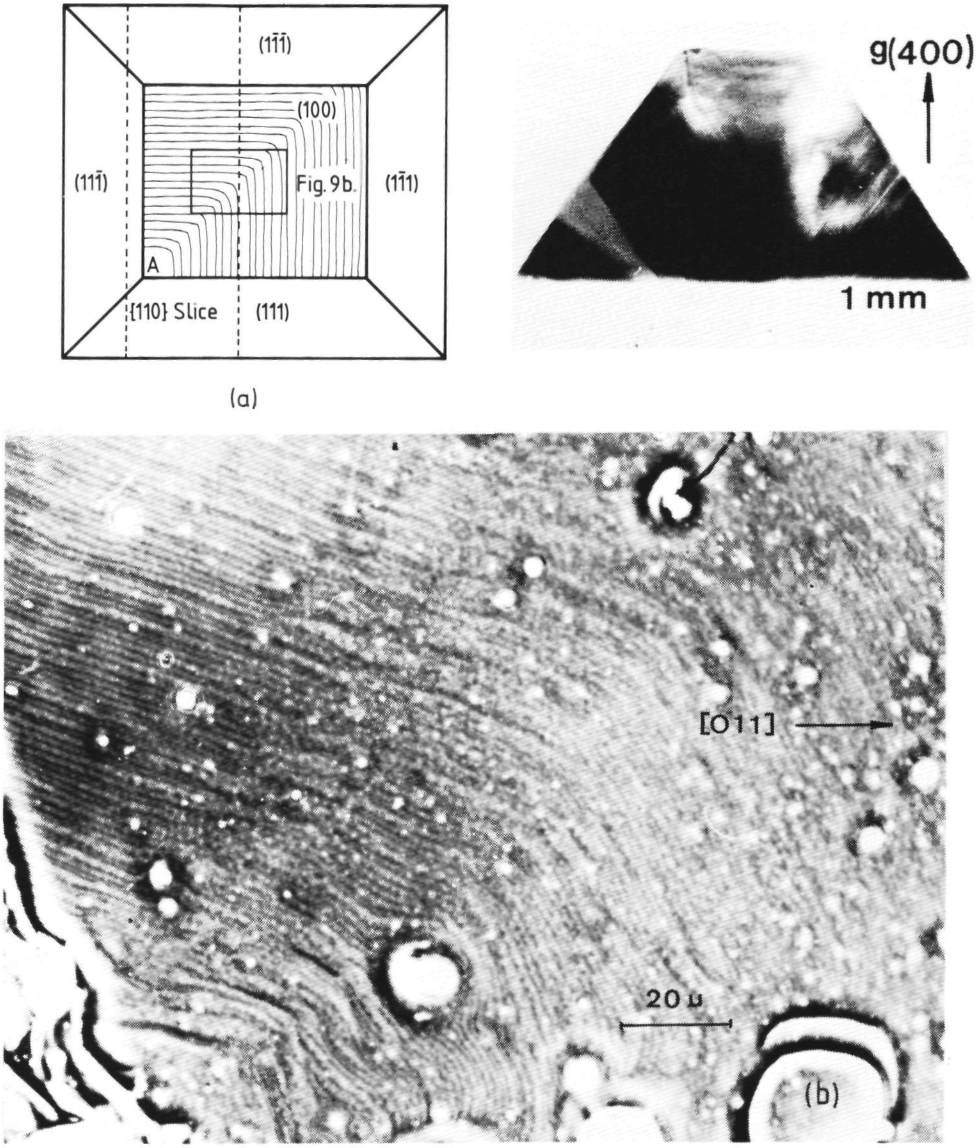

Fig. 7. Some growth characteristics of crystal 2:
(a) Schematic illustration of the growth phenomena on its (100) face and the way, in which the slice parallel to {110} is cut out of crystal 2, for the Lang topograph presented in (b).
(b) Phase contrast microphotograph of its (100) face, showing a step train with very low step height: 12.2Å.
(c) Lang topograph showing the dislocation structure in the growth sector of its (100) face.

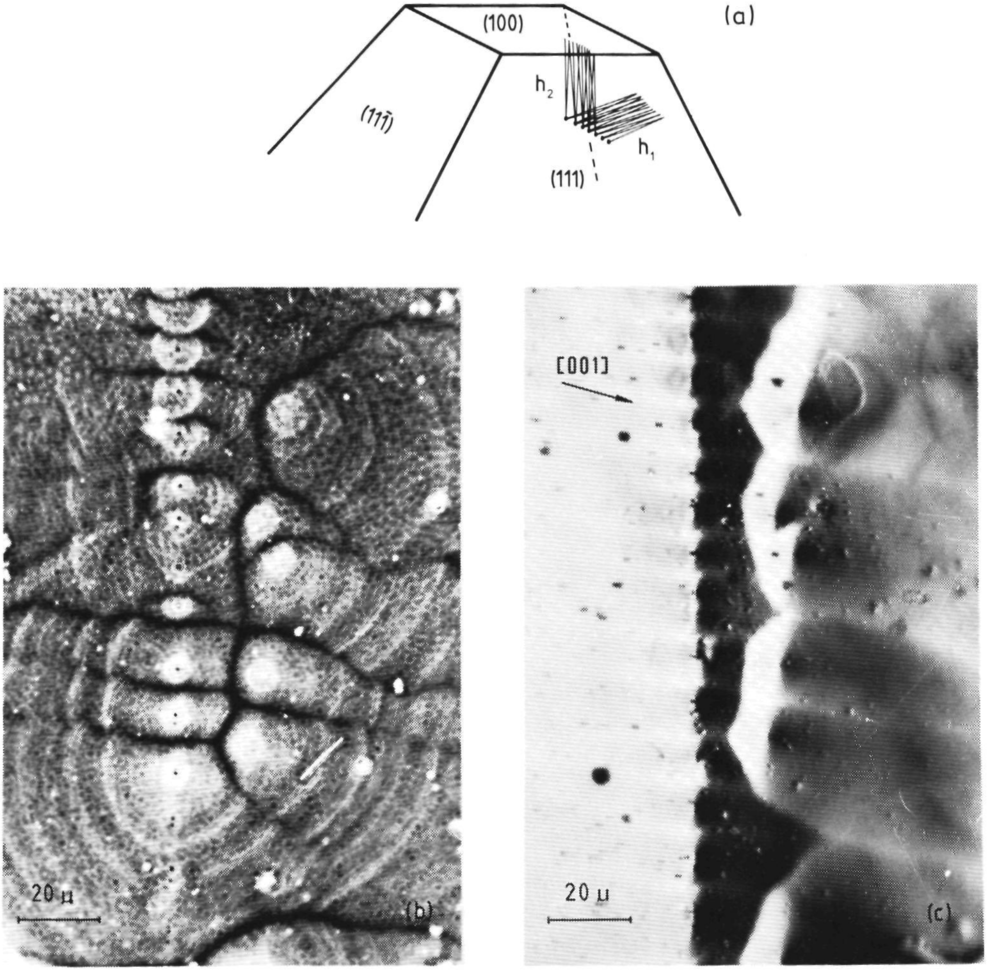

Fig. 8. Some growth characteristics of crystal 3:

(a) Schematic illustration of the crystal, showing a row of liquid inclusions, formed simultaneously as a result from a small accident during growth. From the liquid inclusions originate bundles of dislosections, leading to low angle grain boundaries on its (100) face and an adjacent {111} face.

(b) Phase contrast microphotograph, showing the growth hillocks of the low angle grain boundary.

(c) Differential interference microphotograph, showing the etchpit pattern, which was obtained after the etching of the same area as in (b), indicating, that the growth hillocks of (b) are related to screw dislocations.

and outcrops of dislocations on as-grown crystal surface has been shown earlier for, among others, SiC by Amelinckx et al. [42], stearic acid by Sato et al. [43], {111} potash alum by one of us [44] and on {101} KDP [45].

As extensive step trains have been observed on all the {100} faces (also on the {100} faces not described in this paper), it can be concluded, that most probably growth of the {100} faces proceeds via a step flow mechanism. Normally, these steps on the {100} faces originate from growth hillocks, which are related to outcrops of dislocations with a screw component perpendicular to the {100} faces.

3.3. The growth sectors and their dislocation structure

In figure 9 a polarization micrograph of the same crystal slice as used for the Lang topograph of figure 6, photographed between crossed polarizers, is presented. Clearly three growth sectors can be recognized: Two {111} growth sectors and between the two a {100} sector. The difference in intensity for each sector on this picture is caused by a different amount of birefringence, resulting from differences in deviation from the ideal cubic structure, for each of these sectors. For further details on the application of stress birefringence microscopy to potash alum, one is referred to ref. [30]. From the saw-tooth like pattern of the boundaries between the {100} and {111} sectors, it can be deduced, that the growth rate of the {100} face varies considerably with respect to the growth rates of the adjacent {111} faces. A similar saw-tooth like pattern has been observed earlier for the boundaries between the growth sectors of the {101} and {111} faces of potash alum [30,31].

A saw-tooth like pattern for the boundaries between the growth sectors of the {100} and {111} faces can also be observed in the figures 3c and 4c, in which the course of these sector boundaries and the positions of the {100} and {111} faces at the beginning and end of an experiment has been reconstructed from the growth rate data, obtained by in situ measurements of the crystal 27 and 28 respectively. So, the result of this a posteriori investigation by means of stress birefringence microscopy is in good agreement with the results from the in situ measurements of the growth rates given in the figures 3c and 4c and it can be concluded, that the observed variations in the growth rates of the {100} face are no artefacts, but are inherent to the crystal growth process itself.

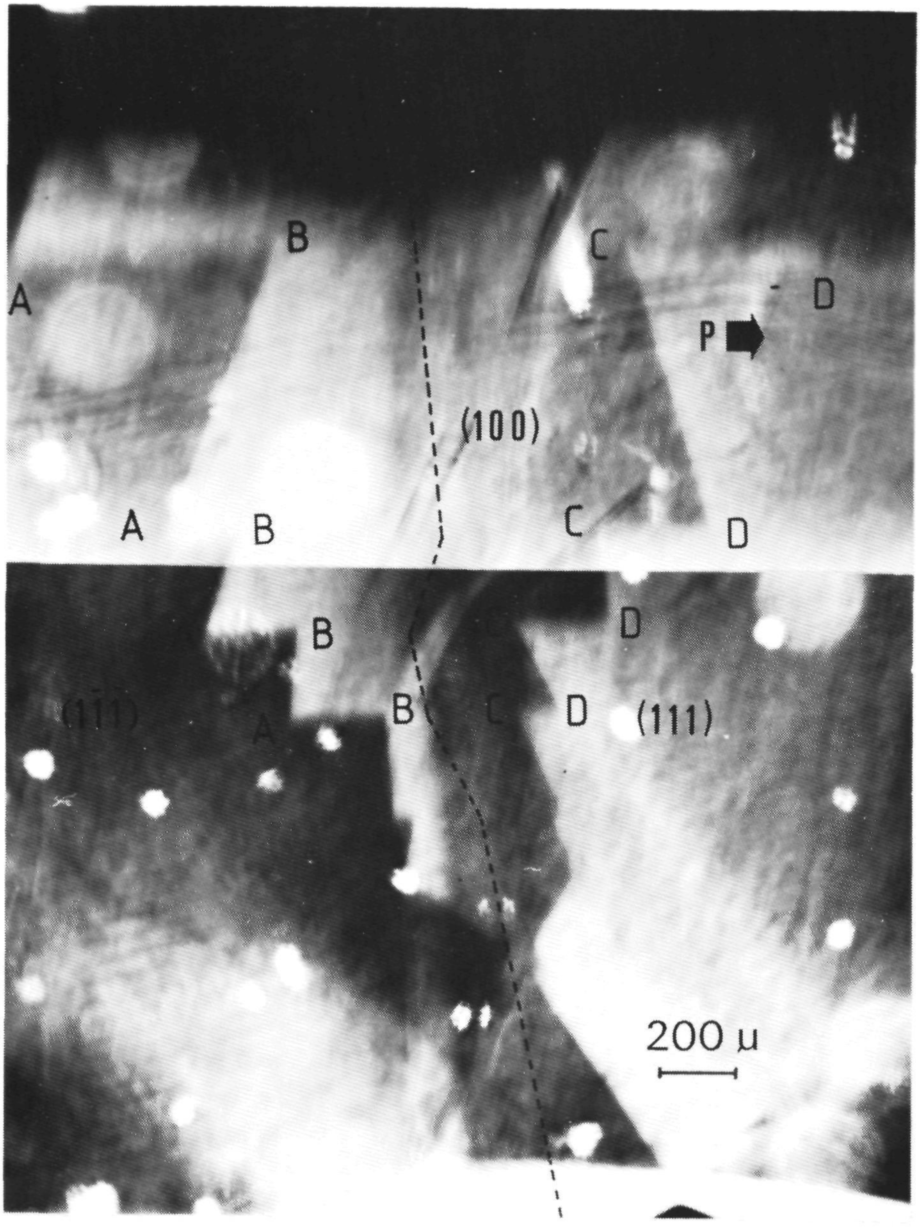

Fig. 9. Stress birefringence micrograph showing irregularly shaped sector boundaries between the (100), the $(1\bar{1}1)$ and the $(\bar{1}11)$ growth sectors of crystal 1. P denotes the orientation of the polariser; the analyzer is oriented perpendicular to this direction.

Another interesting aspect, which can be deduced from the variations in the position of the centre of the (100) face - indicated in figure 9 by the dashed line - is, that also the {111} faces of potash alum exhibit a considerable variation in their growth rates. In figure 9 it can easily be seen, that at first the growth rate of the left {111} face, $R^1_{\{111\}}$, is much larger than the growth rate of the right {111} face, $R^2_{\{111\}}$, then they become equal, next $R^2_{\{111\}}$ is somewhat larger than $R^1_{\{111\}}$ and finally $R^1_{\{111\}}$ is again larger than $R^2_{\{111\}}$. By means of simple goniometry it can be deduced from the ratios AB/CD in figure 8, that the ratio $R^1_{\{111\}}/R^2_{\{111\}}$ varies from 0.6 to 3.3. Other indications about considerable dispersion in the growth rates of the {111} faces of potash alum have been found by one of us [1].

4. DISCUSSION

One of the most remarkable aspects, which can be observed from the figures 3c, 4c and 9 is, that roughly three more or less discrete directions for the boundaries between the growth sectors of the {100} and {111} face can be distinguished. These three directions are presented schematically in figure 10. When a {100} face does not grow at all, or when its growth rate is very low as compared to the growth rate of a {111} face, the boundary between the growth sectors of these faces will "grow" into direction 1. However, when the growth rate of a {100} face is large with respect to the growth rate of a {111} face, the sector boundary will "grow"

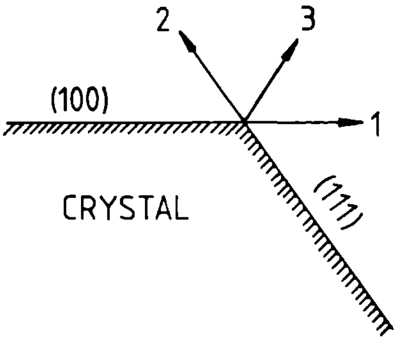

Fig. 10. The three possibilities for the direction of the sector boundary between the growth sectors of a {100} and a {111} face.

into direction 2. Finally, at growth rates of the {100} faces, which are moderate as compared to the growth rates of the {111} faces, the boundaries between the growth sectors of these faces will "grow" into direction 3. In the following, the possibilities and limitations of two explanations for changes in the course of sector boundaries, given in literature, will be discussed. Moreover an additional possible explanation for changes in the direction of the sector boundaries, which can cover all the observed phenomena, will be presented.

According to Gits-Leon et al. [24], the changes in the growth rates of the cubic faces of potash alum are directly related to the elimination of screw dislocations out of the growth sectors of these faces, as was deduced from the changes in the direction of the boundaries between the growth sector of cubic and octahedral faces and by assuming, that the growth rate of octahedral faces is constant. In periods of fast growth, when the boundary between the growth sector of the cubic and of the octahedral face "grows" into direction 2, it is assumed, that dislocations with a screw component perpendicular to the cubic faces, end on these faces and growth occurs according to a spiral growth mechanism. In periods of slow growth, when the sector boundary between the cubic faces and the octahedral faces "grows" into direction 3, it is assumed, that no dislocation with a screw component perpendicular to the cubic faces is terminating on these faces, but no opinion is given upon the growth mechanism. Complete arrest of growth of the cubic faces has never been observed by Gits-Leon et al. and for the time being it is not possible to give a reasonable explanation for the discrepancy between the results of their investigation and the present investigation.

The main result of the investigation of the growth kinetics of ADP crystals by in situ X-ray topography by Chernov et al. [46] is, that also the changes in the growth rates of the {011} faces of ADP are directly related to changes in the dislocation structure in the growth sectors of these faces. In periods, when two or more dislocations with a screw component perpendicular to this bipyramidal face are terminating on this face, or when the outcrop of the last screw dislocation is not situated near the edge with one of its adjacent faces, the growth rate of the {011} face is not related to the growth rate of an adjacent face. However, as soon as the outcrop on the {011} face of the last screw dislocation is situated near the edge with an adjacent face, the growth rates of these faces are related to each other.

When it is assumed, that the changes in the growth rates of the {100} faces of potash alum take place in a similar way as described by Chernov et al., by simple goniometry it can be shown that, when the outcrop of the last screw dislocation on the {100} face has approached the edge with an adjacent {111} face, the following relation between the growth rates of the {100} faces, $R_{\{100\}}$, and the growth rates of the {111} faces, $R_{\{111\}}$, is valid

$$R_{\{100\}} = \frac{\sin\delta}{\sin(\alpha + \delta)} R_{\{111\}} \quad , \qquad (4.1)$$

where δ is the angle between the dislocation line and the {100} face and α is the angle between the {111} and {100} faces. When it is assumed - as suggested by Chernov et al. [46] - that growth is completely arrested, when no screw dislocation outcrops are present on a {100} face, it can easily be demonstrated, that it is impossible for the last screw dislocation within the growth sector of this {100} face to "grow" out of this growth sector. As can be seen from formula (4.1) according to this mechanism complete arrest of growth of the {100} face can only occur, when the direction of the dislocation line is changed into a direction parallel to the {100} face: $\delta = 0$ (arrest of growth of the {111} face ($R_{\{111\}} = 0$) has never been observed). Dislocations with this direction have only been observed in the growth sectors of the {111} and {110} faces and have a Burgers vector $\vec{b} = <011>$, which would be of pure edge type in the {100} growth sector [30]. Therefore a dislocation of this type can not attribute to growth of the {100} face by means of spiral growth and it can be concluded, that complete arrest of growth of the {100} face can not be explained by this type of mechanism.

According to the experiences of Gits-Leon et al. [24] the {100} faces of potash alum are always growing. Sometimes fast, due to spiral growth, when at least one screw dislocation is terminating at these faces. In other occasions slowly due to a nucleation mechanism, when no outcrops of screw dislocations are present on the {100} face. For this reason it is obvious, that the mechanism as proposed by Gits-Leon et al. is also not capable to explain the observed arrest of growth of the {100} faces of potash alum.

In order to explain all the phenomena observed during the present investigation, it is suggested that parallel to spiral growth or nucleation growth another "ON/OFF" mechanism is active. A similar mechanism was found by Chernov et al. [46], who observed complete arrest of growth of the {011} faces of ADP, even when outcrops of screw dislocations are present on these faces. More evidence for the existence of such a mechanism is given in part 3.1.2, where it was pointed out for the crystal 27 and 28, that complete arrest of growth of the {100} face can occur, even in the presence of a screw dislocation outcrop on this face. In table 2 a survey is presented, in which the relation between the growth mechanism and the direction of the boundary between the growth sectors of the {100} face and the {111} face is given. The sector boundary will "grow" into direction 2, when growth proceeds via a step flow mechanism, resulting from spiral growth, when two or more dislocations with a screw component perpendicular to the {100} face are terminating on this face, or when the outcrop of the last screw dislocation on the {100} face is not situated near the edge with an adjacent {111} face. The sector boundary will "grow" into direction 3, when growth occurs according to step flow mechanism, resulting from either spiral growth, when the outcrop of the last screw dislocation is situated on the {100} face near the edge with an adjacent {111} face - an example of this possibility can be seen in figure 7c for crystal 2 - or nucleation growth. The sector boundary will "grow" into direction 1, when the {100} face does not grow at all.

Table 2

The direction of the sector boundary between the {111} and {100} faces in relation to the growth mechanism

Mechanism Growth	Spiral Growth dislocation: outcrop not near edge	Spiral Growth dislocation: outcrop near edge	Nucleation dislocation: Growth
ON	2	3	3
OFF	1	1	1

From the extensive step patterns observed on the {100} faces of all the investigated crystals it can be concluded, that the above mentioned "ON/OFF" switching of growth originates from a mechanism, which starts and stops the step movement. Although no detailed model for this mechanism can be presented, some preliminary ideas, which may serve as a starting point for further theoretical and experimental investigation, will be given. First of all, it is to be remarked, that this mechanism can not be a local one, but must be able to govern the growth process over the whole crystal face, since it has been observed, that the whole {100} face stopped growing, even when one or more screw dislocation outcrops were present on these faces. The first idea, which comes into mind to explain the observed blocking in growth rate of the {100} faces, is to relate this phenomenon to absorption of impurities on the crystal surface. Growth may be arrested, when the whole {100} surface or only the steps on the surface are covered by the impurity. A possibility to explain the irregular way in which this "ON/OFF" switching of growth of the {100} faces takes place, is to assume that the formation of such an impurity layer proceeds via a nucleation mechanism. In this case growth of the {100} face can be stopped abruptly, when a critical nucleus of impurity has been formed and the whole surface becomes covered by impurity as a result of layer growth. In a similar way growth of the {100} face may suddenly start again as a result of the formation of a critical two-dimensional nucleus of the original substance on top or on the same level of the impurity layer, followed by layer growth of potash alum. With regard to the nature of this impurity nothing is known, but since no growth bands were observed in the investigated crystals, it must be realized, that this impurity may be one of the growth units from the solution. Other possibilities to explain dispersion in the growth rates may be offered by surface reconstruction or surface strain relaxation and by changes in the absorption layer, which as was pointed out in ref. [1], may exist around a growing crystal.

Recently the starting and stopping of step trains at considerable supersaturations have been observed in situ on the {010} faces of potassium hydrogen phthalate [47].

5. CONCLUSIONS

From the combined measurements of the growth rates of the {100} and {111} faces of potash alum, Lang topographic studies of the dislocation structure of the same crystals and seperate studies of the surface morphology of crystals grown under almost identical conditions the following conclusions can be formulated:

1. The observed variations in the growth rate of the {100} faces of potash alum are inherent to the crystal growth process itself, i.e. the {100} faces of potash alum exhibit a considerable dispersion in their growth rates.
2. Due to dispersion in growth rate, no unambiguous relation exists between growth rate and relative supersaturation. As a consequence it is not possible to determine whether growth of the {100} faces proceeds via spiral growth or two-dimensional nucleation from the information obtained from the theoretical spiral growth and two-dimensional nucleation growth curves, which by means of a least square method, fit the best to the experimental points.
3. Growth of the {100} faces proceeds via a step flow mechanism, involving steps with a height of roughly 10 - 20Å. Sometime these steps "bunch" into macrosteps, with heights up to 100Å. Dislocation outcrops, resulting in spiral growth hillocks, normally function as step sources.
4. Changes in the growth rate of the {100} faces can not always be attributed to changes in the dislocation structure in the growth sectors of the {100} faces.
5. Complete arrest of growth of a {100} face can occur even when a dislocation with a screw component perpendicular to this face is terminating on this face. As extensive step patterns were always observed on the {100} faces of all crystals, this implies, that due to an as yet unknown mechanism steps can be retarded or even become immobile.

REFERENCES

[1] H.J. Human, J. Crystal Growth to be published
See also: H.J. Human, Ph. D. Thesis, Catholic University of Nijmegen, The Netherland (1981) Ch. IV

[2] W.F. Berg, Proc. Roy. Soc. A, 164 (1938) 79

[3] S.P.F. Humphreys-Owen, Proc. Roy. Soc. A., 197 (1949) 218

[4] S.P.F. Humphreys-Owen, Discuss. Faraday Soc., 5 (1949) 144-149

[5] C.W. Bunn, Discuss. Faraday Soc., 5 (1949) 132-144

[6] P. Bennema, Ph. D. Thesis, Technical University of Delft, The Netherlands, (1965)

[7] P. Bennema, Phys. Stat. Sol., 17 (1966) 563

[8] J.W. Mullin and J. Garside, Trans. Inst. Chem. Eng. London, 45 (1967) T285

[9] J.W. Mullin and J. Garside, Trans. Inst. Chem. Eng. London, 46 (1968) T11

[10] G.D. Botsaris and E.G. Denk Jr., Ind. Eng. Chem. Fundam., 9 [2] (1970) 276

[11] E.G. Denk and G.D. Botsaris, J. Crystal Growth, 6 (1970) 241-244

[12] P. Bennema and H.B. Klein Haneveld, J. Crystal Growth, 1 (1970) 232-237

[13] R.W. Rousseau, C.Y. Tai and W.L. McCabe, J. Crystal Growth, 32 (1976) 73-76

[14] C.Y. Tai, W.L. McCabe and R.W. Rousseau, A.I.Ch.E.J., 21 (1975) 351

[15] W.L. McCabe, Ind. Eng. Chem., 21 (1929) 30-33

[16] J. Garside and S.J. Jancic, Chem. Eng. Sci., 33 (1978) 1623-1630

[17] J. Garside and S.J. Jancic, A.I.Ch.E.J., 22 (1976) 887

[18] H.N. Rosen and H.M. Hulburt, Chem. Eng. Progr. Symp. Ser. No 110, 67 (1971) 27

[19] J. Garside, J.W. Mullin and S.N. Das, Ind. Eng. Chem. Fundam., 13 (1971) 299

[20] E.T. White, L.L. Bending and M.A. Larson, Chem. Eng. Progr. Symp. Ser. No 153, 72 (1976) 41

[21] W.L. McCabe and R.P. Stevens, Chem. Eng. Progr., 47 [4] (1951) 168

[22] E.T. White and P.G. Wright, Chem. Eng. Progr. Symp. Ser., 67 [10] (1971) 81

[23] P.G. Wright and E.T. White, Thirty Sixth Conference (1969) 299

[24] S. Gits-Leon, F. Lefaucheux and M.C. Robert, J. Crystal Growth, 44 (1978) 659

[25] W.J.P. van Enckevort, R. Janssen- van Rosmalen, H. Klapper and W.H. van der Linden, J. Crystal Growth, to be published

[26] B. Dam and W.J.P. van Enckevort, J. Crystal Growth, 51 (1981) 607

[27] A.R. Lang in: Properties of Diamond, Ed. J. Field (Academic press, 1979) p. 425

[28] Sayeda H. Emara, B.R. Lawn and A.R. Lang, Phil. Mag., 19 [157] (1969) 7

[29] S. Gits-Leon, M.C. Robert et Albert Zarka, Bull. Minéral, 101 (1978) 399

[30] W.J.P. van Enckevort and J.G.M. Odekerken, Phyl. Mag. to be published

[31] W.J.P. van Enckevort and H.J. Human to be published

[32] L.N. Natalina and E.B. Treivus, Sov. Phys. Crystallogr., 19 [3] (1974) 389

[33] A.P. Kasatkin, Sov. Phys. Crystallogr., 10 [4] (1966) 459

[34] W.J.P. van Enckevort, P. Bennema and W.H. van der Linden, Z. Phys. Chem. Wiesbaden, 124 (1981) 171-191

[35] I. Sunagawa, Am. Mineral, 46 (1961) 1216

[36] I. Sunagawa in: Crystal Growth and Characterization, Proc. ISSCG-2 Spring School, Japan, 1974, Eds. R. Ueda and J.B. Mullin (North-Holland, Amsterdam, 1975) p. 347

[37] I. Sunagawa and K. Tsukamoto, J. Crystal Growth, 15 (1972) 73

[38] P. Bennema, J.P. van der Eerden, W.J.P. van Enckevort, B. van der Hoek and K. Tsukamoto, Phys. Status Solidi (a) 55 (1979) 403

[39] W.J.P. van Enckevort and L.A.M.J. Jetten, J. Crystal Growth, to be published

[40] W.J.P. van Enckevort and H. Klapper, J. Crystal Growth to be published

[41] A.R. Lang, Acta Cryst., 12 (1959) 249

[42] S. Amelinckx in: Solid State Physics, Suppl. 6, The direct observation of dislocations , ed. F. Seitz and D. Turnbull (Academic Press, New York, 1964) p. 16

[43] K. Sato, K. Yokoyama, H. Kouchi and M. Okada, Jap. J. Appl. Phys., 17 [9] (1968) 1483

[44] W.J.P. van Enckevort and W.H. van der Linden, J. Crystal Growth, 47 (1979) 196

[45] W.J.P. van Enckevort, R. Janssen- van Rosmalen and W.H. van der Linden, J. Crystal Growth, 49 (1980) 502

[46] A.A. Chernov, I.L. Smolski, V.F. Parvov, Yu.G. Kuznetzov and V.N. Rozhanskii, Sov. Phys. Dokl., 24 (1979) 760

[47] W.J.P. van Enckevort, B. van der Hoek and L.A.M.J. Jetten, J. Crystal Growth, to be published

CHAPTER V:
ON THE COMPARISON BETWEEN THE X-RAY DIFFRACTION TOPOGRAPHIC AND THE STRESS BIREFRINGENCE IMAGE OF POTASH ALUM SINGLE CRYSTALS

W.J.P. van Enckevort and J.G.M. Odekerken

RIM Laboratory of Solid State Chemistry, Faculty of Science,
Catholic University, Toernooiveld, Nijmegen, The Netherlands

ABSTRACT

It has been shown that dislocations -viewed from side- in the optically isotropic potash alum crystals can be observed by the stress birefringence method. Comparison with Lang topography demonstrated that all dislocations could be revealed by polarization microscopy, except the ones with the lowest possible Burgers vector <001>. The extinction orientations of the dislocations were not in agreement with theoretical predictions; the reason for this anomalous behaviour is not understood. The birefringence method appeared to be an extremely powerful tool for relating the dislocation structure to -liquid- inclusions in the crystals. This showed that often inclusions can act as a source as well as an ending point of dislocations and dislocation bundles. In many cases inclusions not related to line defects were found, whereas in other cases inclusions and hollow tubes lying on or near continuous dislocation lines were discernable. In contradistinction to Lang topography, application of the stress birefringence method also clearly revealed the {111} and {110} -but never the {100}- growth sectors as well as growth bands in the {111} sectors. From the stepped patterns of the boundaries between the {111} and {110} sectors it was shown that during crystal growth the {110} facets suffered a high dispersion in growth rate.

1. INTRODUCTION

Since the discovery by Bond and Andrus (1956), about 25 years ago, that stress fields of dislocations can be imaged by means of stress birefringence microscopy, the optical birefringence method was extensively used for studying crystal perfection. This method was especially employed for semiconductor crystals, which have large elasto-optical coefficients and large refractive indices. In the late 1950's and in the 1960's especially the for visible light opaque, but for infrared light transparant semiconductor crystals such as Si and Ge were studied extensively (Bond and Andrus, 1956, Indenbom and Tomilovskii, 1957, Bullough, 1958, Indenbom, 1961, Indenbom, Nikitenko and Milevskii, 1962, Nikitenko and Dedukh, 1970).

Recently a number of electronic materials that are more or less transparant for the visible region of light became more important (for instance GaP (Matthews, Plaskett and Blum, 1977) and garnet (Matthews, Plaskett and Ahn, 1976)). Since the stress birefringence method is non-destructive, quick and simple to be carried out, it can be quite important for characterization of these for visible light non-opaque materials on industrial scale. This is the main reason for the recently strongly increased interest for this method, both experimentally (Fathers and Tanner, 1973 a and b, Matthews, Klokholm, Plaskett and Sadogopan, 1973, Löschke, Gottschalch, Jacobs and Tempel, 1979) and theoretically (Tanner and Fathers, 1973, Fathers and Tanner, 1973 a, Jenkins and Hren, 1976). In general, the birefringence method for observation of dislocations was only applied to cubic -optically isotropic- crystals however, it can also be applied to non-cubic -optically anisotropic- materials as was shown by Fathers and Tanner (1973 b).

In contrast to semiconductor crystals, for ionic crystals the birefringence method is far less simply to be carried out, because of their lower elasto-optical coefficients and refractive indices. Nevertheless, still some stress birefringence studies of this catagory of crystals were made. For example Kear and Pratt (1958) applied the birefringence method to LiF, Tanner (1972) to fluorite and van Enckevort and van der Linden (1979) (who were able to relate the birefringence images of the dislocations to etch pits) to potash alum, however, individual dislocations of unit length could not be resolved.

Another -aside from slice cutting- nondestructive method, for direct observation of dislocations is X-ray diffraction topography, especially Lang-topography (Lang, 1959). At the moment the Lang method, which is capable to resolve single dislocations of unit height in all kinds of materials, can be considered as one of the standard techniques for characterization of single crystals. Excellent reviews on this method are given by Lang (1970) and Tanner (1976).

Despite the fact that it would be highly interesting, only a few authors made a direct comparison of the stress birefringence method with Lang topography. Examples of comparisons of dislocation images observed by both techniques are given by Lang (1967) for diamond, Tanner (1972) for fluorite and Fathers and Tanner (1973 b) for barium titanate. However, a systematic on this topic has not yet been carried out.

The aim of the present paper is to present a more detailed study of the relation between the Lang topographic and the stress birefringence image for the case of potash alum crystals. From this comparison the limits as well as the advantages and diadvantages of both methods can be verified. Potash alum was selected as a model compound for the following reasons: (i) It is a well known, easily obtainable crystal, whose dislocation structure has been studied extensively (Emara, Lawn and Lang, 1969, Gits-Leon, Lefaucheux and Robert, 1978). (ii) The crystals are -because of their cubic symmetry- optically isotropic. (iii) The cell dimensions of the primitive lattice are quite large (unit lattice length = 12.16 A (Wykoff, 1965)), therefore the length of the Burgers vectors must be rather high. This strongly enhances the contrasts of their stress birefringence images, compensating more or less the low refractive index and the lower elasto-optical constants, both being typical for ionic crystals.

A second aim of this work is to study the correlation between liquid inclusions and the dislocation structure in potash alum, especially by means of the birefringence method. When dislocations can be made visible by means of a transmission optical polarization microscope, the birefringence method appears to be extremely powerful for relating them to -liquid- inclusions, since the latter can be seen directly by means of the same microscope, now using bright field illumination or phase contrast.

2. EXPERIMENTAL

2.1. Crystal Growth

The potash alum crystals were grown in the following way (Bennema, 1965, van Enckevort and van der Linden, 1979, van Enckevort, Bennema and van der Linden, 1980) : A well developed seed crystal of about 0.25 cm^3, mounted on a plastic rod was placed in a thermostated (± 0.01 °C) saturated aqueous potash alum solution, of which the temperature was lowered at rates between 0.05 °C, or less, and 0.3 °C per 24 h. After a period varying from a few days to a few weeks a clear and well formed octahedral crystal of about 4 cm^3 could be obtained in this way. In general, crystals grown at high rates contained more liquid inclusions than slowly grown crystals, which is in conformity with the observations made by Gülzow, Gülzow and Lüdke (1965).

2.2. X-ray diffraction topographic procedure

Specimen plates (about 1 mm in thickness) were cut parallel to (110) in the same way as by Gits-Leon et al. (1978). Then the plates were slightly etched in deionized water in order to remove surface defects due to cutting, which can interfere the X-ray topographic image.

All topographs of these plates were taken by the Lang method (Lang, 1959), using Cu $K\alpha_1$ ($\lambda = 1.5406$ A) or Ag $K\alpha_1$ ($\lambda = 0.5594$ A) radiation and X-ray film Structurix D7 and D4 (agfa Gevaert). Several reflections, such as {220} and {004} were used.

2.3. Polarization microscopy

In order to carry out the stress birefringence studies of the dislocation structure of the alum crystals use was made of a high quality polarization microscope. In the present case an Olympus Vanox microscope was used, because of its highly contrasted image at lower magnifications. Since the image contrast of the dislocations was still very low, a high contrast photographic film (agfaortho 25, developed during 5 minutes in G117 C (Agfa-Gevaert)) was used. This emulsion is capable to reveal extremely low contrasts, so that details, which could not be observed visually, could be photographed. In general, the intensity of the image in the polarization microscope was very low, which means that exposure times varying from a few minutes to one hour were needed.

The specimens, being the same (110) slices as used for the Lang topographs, had to be prepared very carefully in order to obtain a clear stress birefringence pattern. This was carried out by whiping the crystal gently with a slightly wetted cotton tissue in order to remove dust particles. After this the "cleaned" crystal plate was placed in immersion oil (with roughly the same refractive index as the crystal) between a slide and a cover-glass (both being thoroughly cleaned!), so that the surface pattern of the crystal plate can not interfere the image (Ehringhaus and Trapp). Good care should be taken that the number of dust particles between the glass plates and the crystal is as low as possible, because they give a large amount of stray radiation, which can obscure the image completely

3. OBSERVATIONS AND DISCUSSION

3.1. Dislocations

3.1.1. General features

Fig. 1a presents a Lang topograph of a {110} slice of a good quality alum crystal. Several dislocations radiating outwards from a central region (the seed crystal) can be discerned, which is in similarity to the observations by Emara, Lawn and Lang (1968) and by Gits-Leon et al. (1978). Figs 1b to e are stress birefringence micrographs of the same areas as marked on fig. 1a. Nearly all single dislocations and dislocation bundles visible on the X-ray topograph can clearly be recognized on the polarization micrographs. The white dots, blots or stripes are images of miniscule dust particles, mostly out of focus, giving a large amount of stray radiation. This clearly demonstrates that thoroughly cleaning of the specimens is of extreme importance for the birefringence method

Fig. 1b shows two parallel dislocations, of more or less the same sign, whereas 1c gives two dislocations of opposite sign starting from one common point (P). A difference in contrast -especially in the region intermediate the two dislocation lines- can clearly be recognized.The contrast between two dislocations with the same, but opposite, Burgers vectors will be discussed in the following section.

Fig. 1d gives a detailed birefringence micrograph of a dislocation bundle: the occurrence of numerous parallel

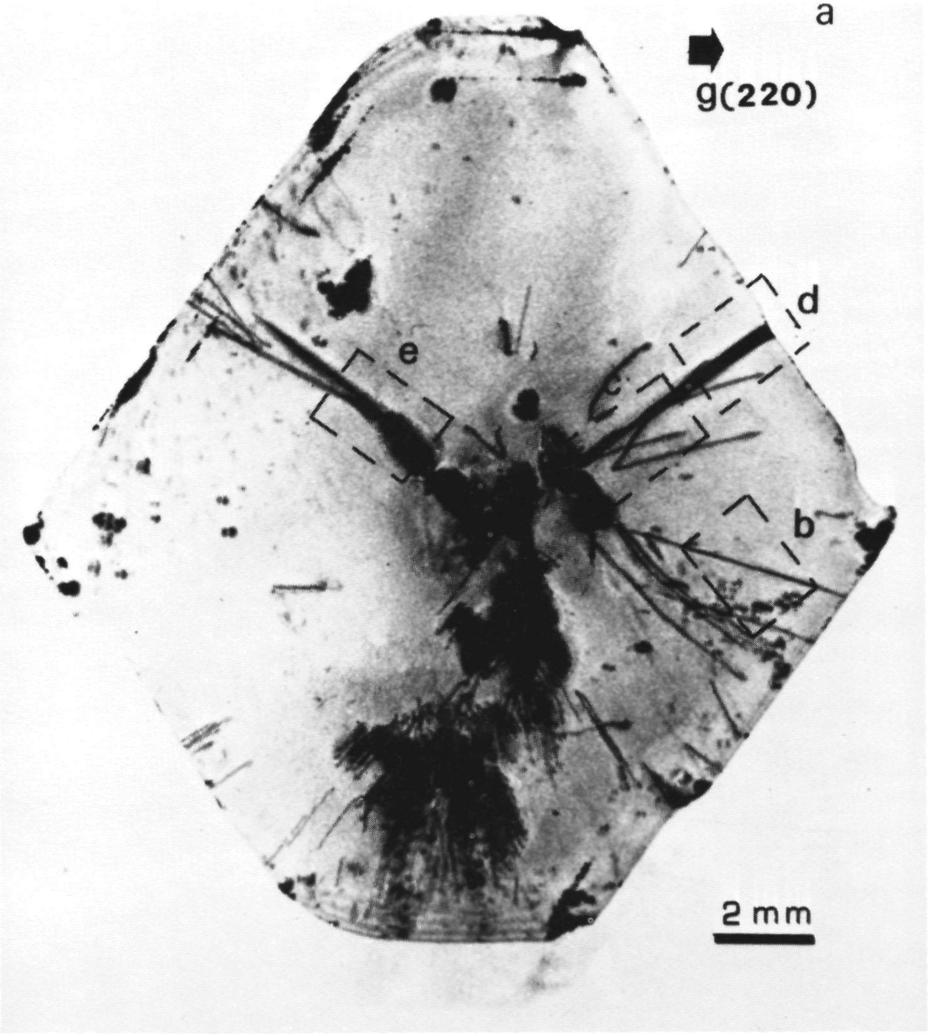

Fig. 1. Correspondence between Lang topographs and stress birefringence micrographs:
(a) Lang topograph of an (110) potash alum plate.

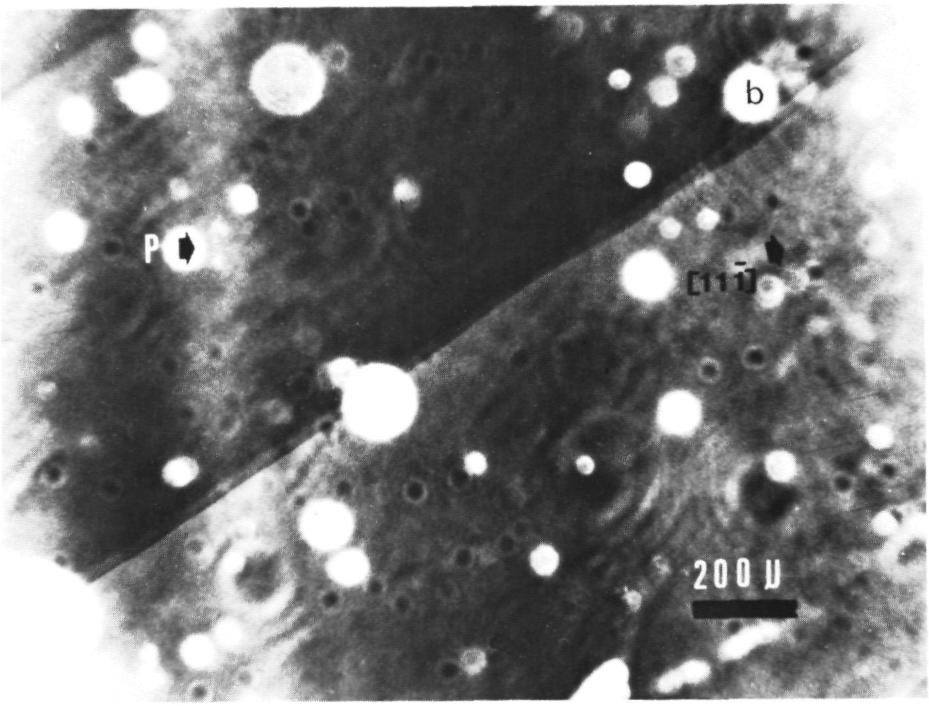

Fig. 1. (continued) (b) and (c) Stress birefringence micrographs of the boxed areas in (a).

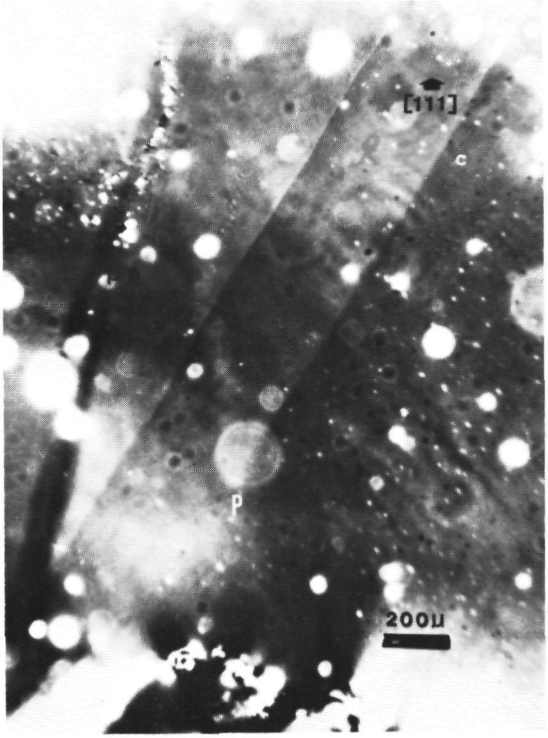

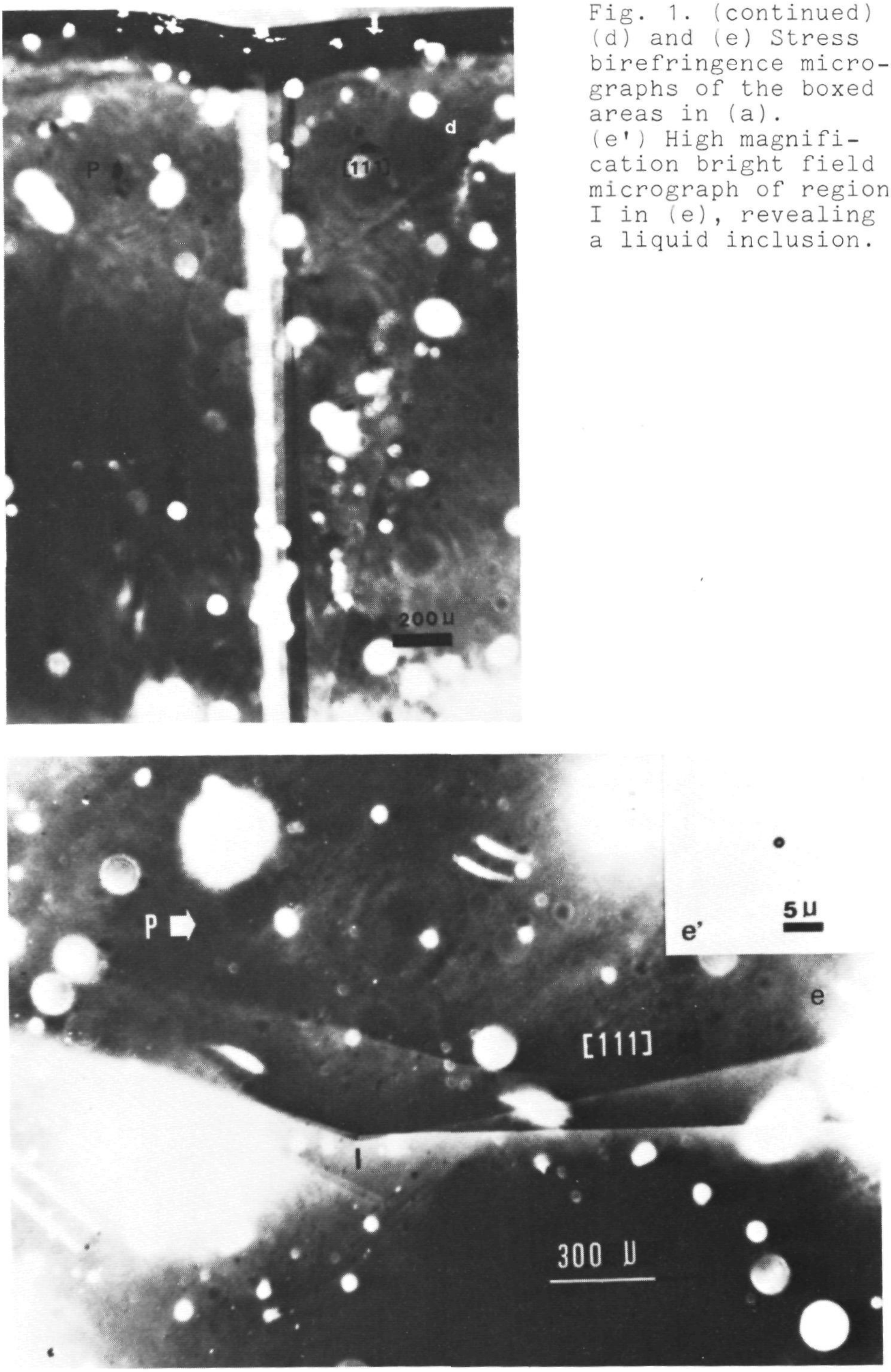

Fig. 1. (continued)
(d) and (e) Stress birefringence micrographs of the boxed areas in (a).
(e') High magnification bright field micrograph of region I in (e), revealing a liquid inclusion.

dislocations with various Burgers vector directions and signs leads to the formation of various rectilinear -compared to the background- contrasted regions. Fig. le shows two well developed dislocations (no single dislocations of unit height, as can be deduced from the large image width on the X-ray topograph) which are refracted at a certain point (I). Application of bright field transmission microscopy shows that for one of the dislocation lines this refraction is accompanied by the occurrence of a liquid inclusion as can be seen in fig. le'.

3.1.2. A more quantitative comparison of the dislocation images

From the dependece of the contrasts and the occurrence of extinctions of the X-ray topographic dislocation images on the diffraction vector it was possible to classify the dislocations occurring in the {111} growth sectors into three main categories. Fig. 2a gives a schematic representation of

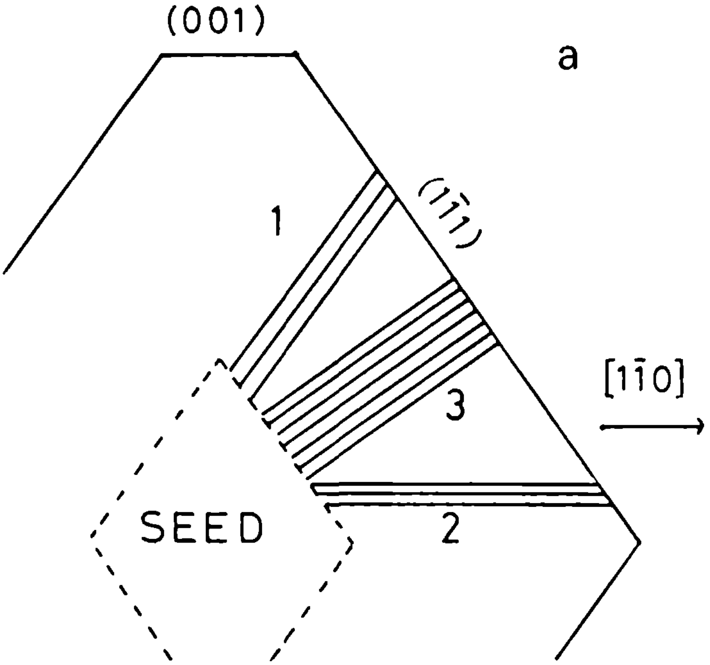

Fig.2. Three categories of dislocations occurring in the {111} growth sectors of potash alum:
(a) Schematic representation of the line directions of the different dislocation types.

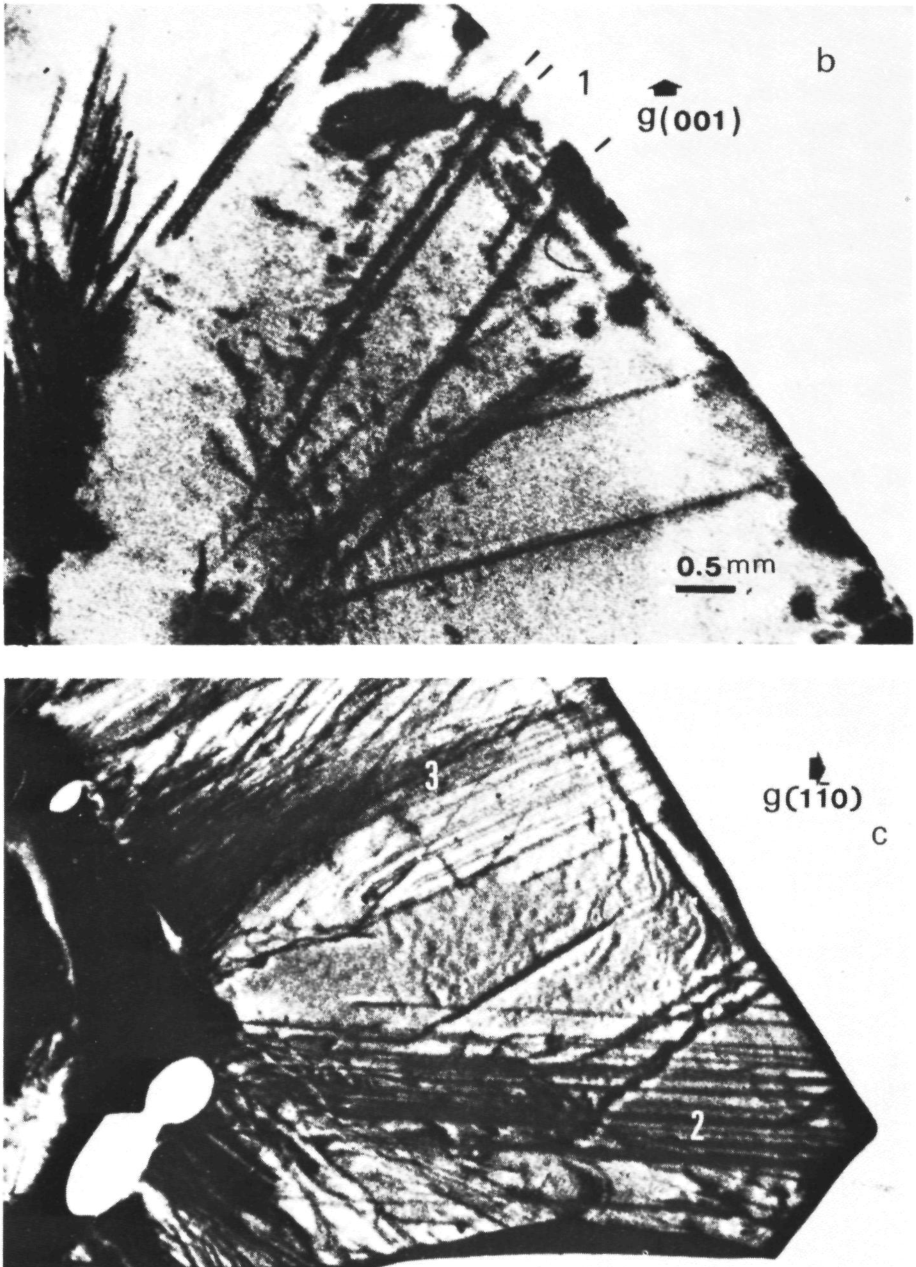

Fig.2. (continued) (b) Lang topograph showing a few type 1 dislocations (g = (004)).
(c) Lang topograph showing type 2 and type 3 dislocations (g = (2$\bar{2}$0)).

a {110} slice indicating the line directions of the three types of dislocations. Type 1 (See also fig. 2b) runs parallel to the (110) plane at an angle of about 54° with respect to the $<1\bar{1}0>$ direction. Its Burgers vector was determined to be <001> . Type 2 (See also fig. 2c) runs parallel to $<1\bar{1}0>$, so it always lies in the {110} plane. The Burgers vector was determined to be $<1\bar{1}0>$; hence type 2 dislocations are pure screw ones. To the dislocations of type 3, the most abounding ones, no Burgers vector could be assigned by means of the Lang method: Nor extinction, nor a strong variation in contrast of the dislocation images in dependence of the diffraction vector, necessary for Burgers vector determination, was found. Probably here the second order term in the expression for the atomic displacement around dislocations (Tanner, 1976) plays an essential role, so that no extinction can occur, or the dislocations are decorated by impurities or -liquid- inclusions. In general, type 3 dislocations lie more or less in the (110) plane and end roughly perpendicularly to the $\{1\bar{1}1\}$ growth faces (See fig. 2). However, many exceptions, such as dislocation lines not lying in the (110) plane or lines parallel to (110) but not ending perpendicularly to $\{1\bar{1}1\}$were found, which suggests that type 3 dislocations do not all have the same Burgers vector.

By application of the stress birefringence method dislocations of type 3 could nearly always be discerned clearly. Examples of such dislocations are given in figs. 1b to e. Type 2, whose contrast is much lower, could just be revealed. Fig. 3 shows both a Lang topograph and a stress birefringence micrograph of such a dislocation. Since type 2 dislocations are pure screw in character, it is possible to estimate the absolute magnitude of the Burgers vector, $|\vec{b}|$, from their image widths on Lang topographs, of which the diffraction vector, $\vec{g}$, is parallel to the line direction $|1\bar{1}0|$ of the screw dislocations (Authier, 1967, Klapper, 1970). This is done by making use of the relation $|\vec{b}| = \pi W C \Delta O_{\frac{1}{2}}$ where W refers to the width of the dislocation image, C is the polarization factor, in the present case being roughly equal to 1 and $\Delta\Theta_{\frac{1}{2}}$ is the width of the half maximum hight of the rocking curve of the perfect crystal. Using among others the structure factor 220 calculated by Lipson and Bragg (1935) this half width can be derived theoretically, which leads to a value of $1.14.10^{-5}$ rad for $\vec{g} = (2\bar{2}0)$ and Cu-$K\alpha_1$ radiation. Taking the measured width of the $|1\bar{1}0|$ dislocation in fig. 3a, W = 50 + 5 μ , it can now be deduced that $|\vec{b}|$ equals about 18 A. This means that the dislocation shown in fig. 3 must be of unit length, since the unit translation parallel to <110> equals 17.20 A. So it can be concluded that by means of the stress birefringence method single $|1\bar{1}0|$ dislocations with unit Burgers vectors can be observed in potash alum. In contradistinction to dislocations of type 2 and 3, type 1 dislocations, with the lowest possible Burgers vector ($\vec{b} = |001|$) of 12.16 A, were never observed by the stress birefringence method. Probably the stress field of these dislocations is too low to allow for detection by polarization microscopy.

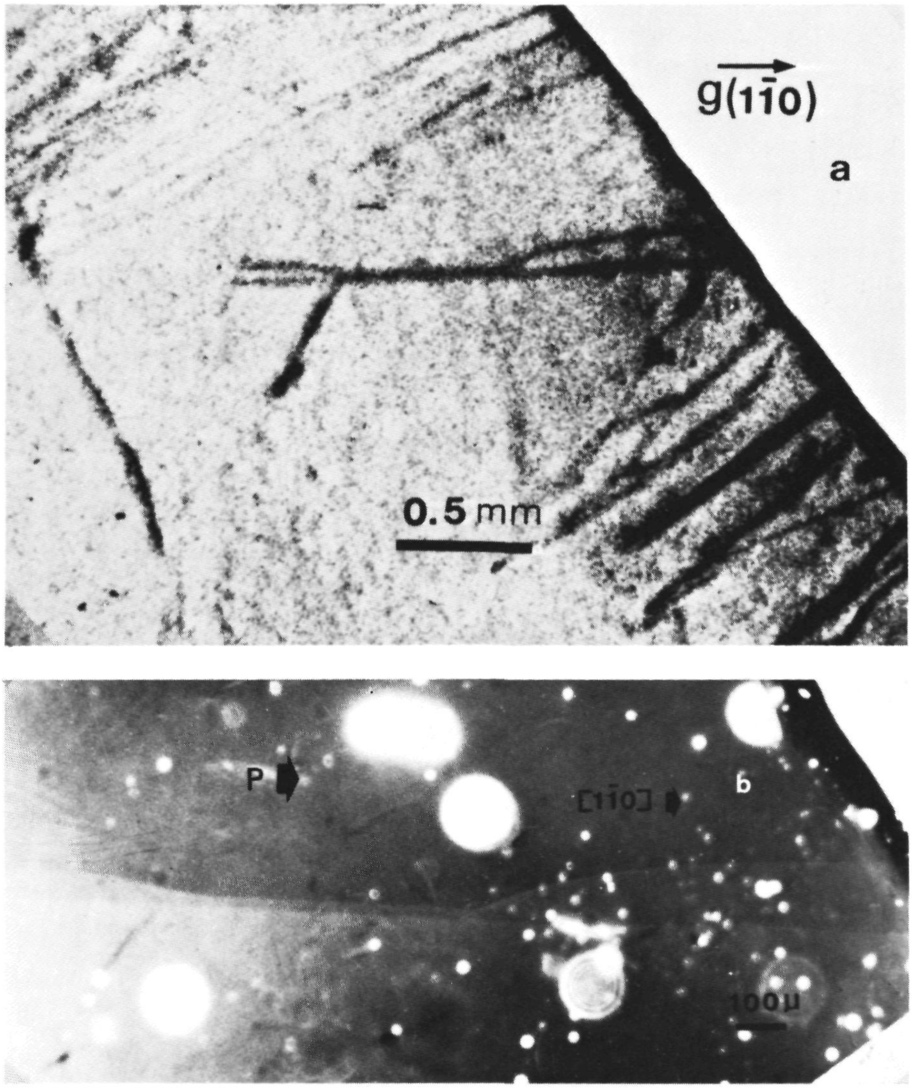

Fig.3. Observation of a single, unit height type 2 ($\vec{b} = |1\bar{1}0|$) dislocation:
(a) Lang topograph ($\vec{g} = (2\bar{2}0)$)
(b) Stress birefringence micrograph of the same area as (a). Polarizer and analyser are oriented in such a way that maximum contrast is obtained.

By rotating the crystal slice with respect to the crossed polarizers, it was shown that the contrasts of all visible dislocations (both type 2 and type 3) decreased to minimal or mostly to zero when the polarizer and analyser were orientated parallel or perpendicular to the $|1\bar{1}0|$ direction. Maximum contrast was obtained when the polarizer and analyser were rotated about 45 degrees. Now using the visibility criteria for dislocations with lines perpendicular to the optical axis of the microscope, derived by Fathers and Tanner (1973 b) and Tanner and Fathers (1974), the dislocations of type 2 should be more or less edge type, since these are invisible, when their lines are parallel to the polarizer and analyser. On the other hand dislocations of type 3, at least those that end perpendicularly to the $\{1\bar{1}1\}$ growth face, should be screw type, because these vanish when their lines are orientated at about 45 degrees with respect to the polarizer and analyser. The conclusion, drawn from the extinctions of the birefringence images, that type 2 dislocations are edge type is in complete contradiction to the observation by the Lang method that these are pure screw dislocations. The fact that practically all dislocation images, regardless of orientation or type, vanish when the polarizer or analyzer is parallel to $|1\bar{1}0|$ makes the situation concerning the stress birefringence images even more "suspected". So at this moment no conclusions can be drawn from the extinction orientations of the stress birefringence images, which means that type 2 dislocations are pure screw type conform the X-ray topographic observations and the Burgers vector of type 3 dislocations, that should mostly be $|1\bar{1}1|$ after the polarization microscopic observations, still remain uncertain. The reason for this anomalous behaviour of the stress birefringence images of dislocations in potash alum is not clear. Possibilities are anisotropy of the elastic medium, decoration of thedislocations (however, both should also affect the X-ray topographic images) or some other effect which leads to birefringence.

A very interesting phenomenon, already adumbrated in section 3.1.1. is the occurrence of domain-like birefringence patterns, consisting of areas, which are -more or less uniformly- brighter or darker than the background region. Fig. 4a gives an example of such an area; comparison with the inserted Lang topograph unambiguously shows that the boundaries of these "domains" are formed by dislocations, as represented schematically in fig. 4b. In fig. 4 it can clearly be seen that both dislocations originate from one single point, where no other dislocations end, so that the Burgers vectors of both dislocations must be equal but of opposite sign (Kovacs and Zsoldos, 1973). From this and other observations it can be concluded that the domain-like patterns are a result of overlapping birefringence images of roughly parallel dislocations with the same Burgers vectors but of opposite sign. Whether the central area between both dislocations is brighter or darker than elswhere depends on the relative positions of the parallel dislocation lines and on the orientation of the uniform background strain tensor. In fig. 4 both a bright and a dark area can be recognized.

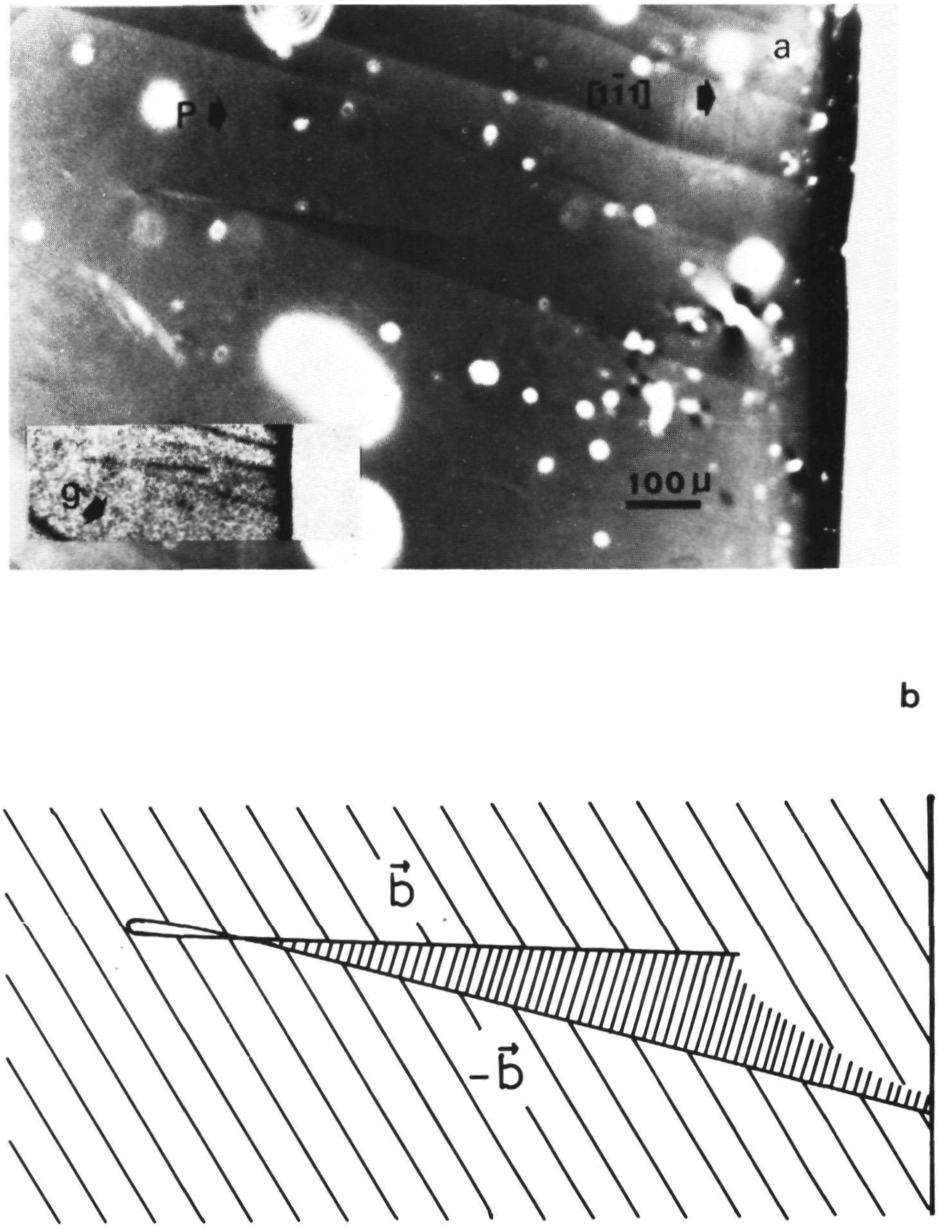

Fig.4. Domain-like pattern as a result of the occurrence of two more or less paralleling dislocations with the same, but opposite, Burgersvectors:
(a) Stress birefringence micrograph.
(b) Schematic representation of the same area as (a).

3.2. Relation between the occurrence of -liquid- inclusions and dislocations

The birefringence method is extremely powerful for investigation of the correlation between inclusions and dislocations, since both can directly be observed by means of the same -polarization- microscope. Application of the stress birefringence method and bright field microscopy, combined with Lang topography to potash alum crystals showed that for the interaction between liquid inclusions and dislocations four different cases can be distinguished:

3.2.1. Inclusions as a source of dislocations

Due to some disturbances during the growth process often

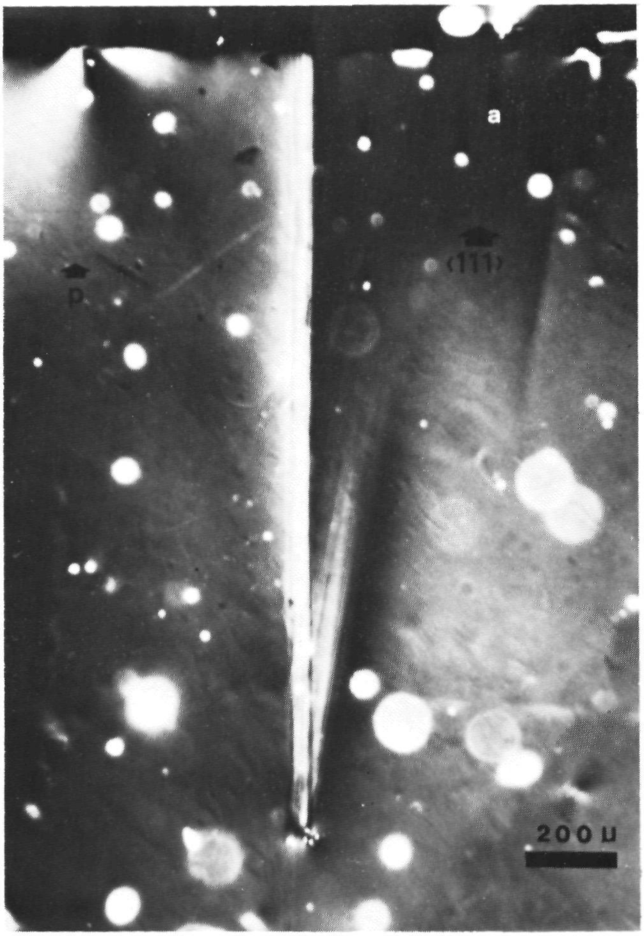

Fig.5. Liquid inclusions as a source of dislocations:
(a) Stress birefringence micrograph of a well developed dislocation bundle originating from a few liquid inclusions.

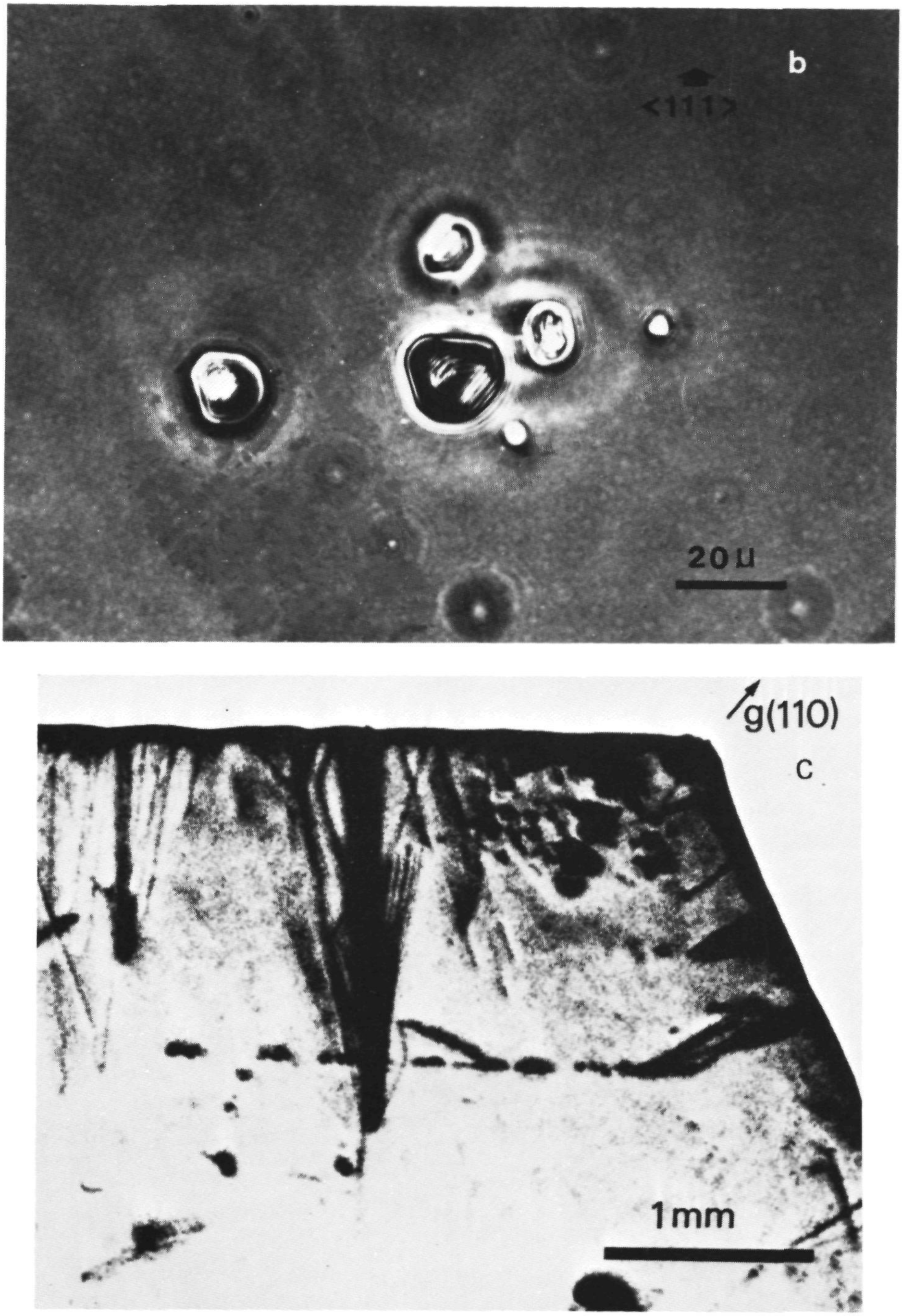

Fig.5. (continued) (b) High magnification transmission phase-contrast micrograph of the incclusions in (a).
(c) Lang topograph of the same area as (a).

liquid inclusions are formed in the crystals. After formation of these inclusions a few dislocations (Sato 1980 a, b) or a dislocation bundle (van Enckevort, Janssen- van Rosmalen and van der Linden 1980, van Enckevort, Janssen- van Rosmalen, Klapper and van der Linden 1982) may be generated due to the occurrence of a lattice enclosure error, as was shown by etching techniques and Lang topography. Stress birefringence micrographs of potash alum crystal slices demonstrate this generation of dislocations from liquid inclusions with a dramatic clearness, as can be seen in fig. 5. Fig. 5a is a polarization micrograph of a well developed dislocation bundle originating from a few liquid inclusions, which are represented in detail by fig. 5b. Fig. 5c is a Lang topograph of the same area, clearly showing the dislocation bundle. From this and other observations it can now be concluded that lattice enclosure errors after the formation of liquid inclusions may be a source of dislocations or dislocation bundles in potash alum crystals.

3.2.2. Inclusions as ending points of dislocations

In contrast to the foregoing, inclusions can also act as termination points of dislocations. This phenomenon has been observed by Emara et al. (1969) and studied extensively by Gits-Leon et al. (1978), who were able to obtain rather perfect crystals by making use of this effect. A similar termination of dislocations at liquid inclusions has also been observed during the present study, both by X-ray diffraction and by the stress birefringence method.

3.2.3. No correlation between inclusions and dislocations

Quite often layers of liquid inclusions (veils) parallel

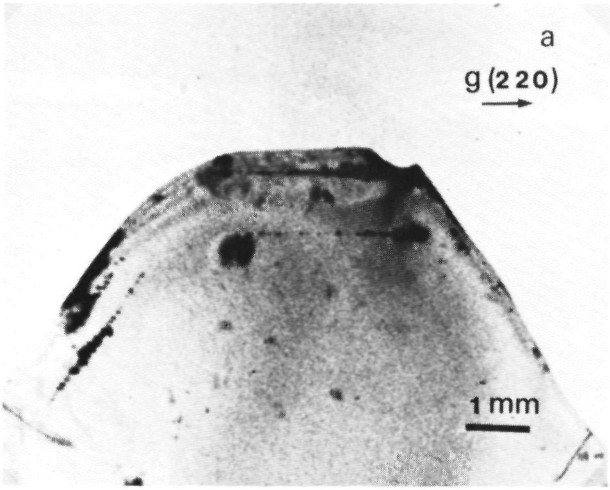

Fig.6. Liquid inclusions not related to dislocations:
(a) Lang topograph of inclusion row parallel to the growth faces. Note that no dislocations end or start from the bubbles.

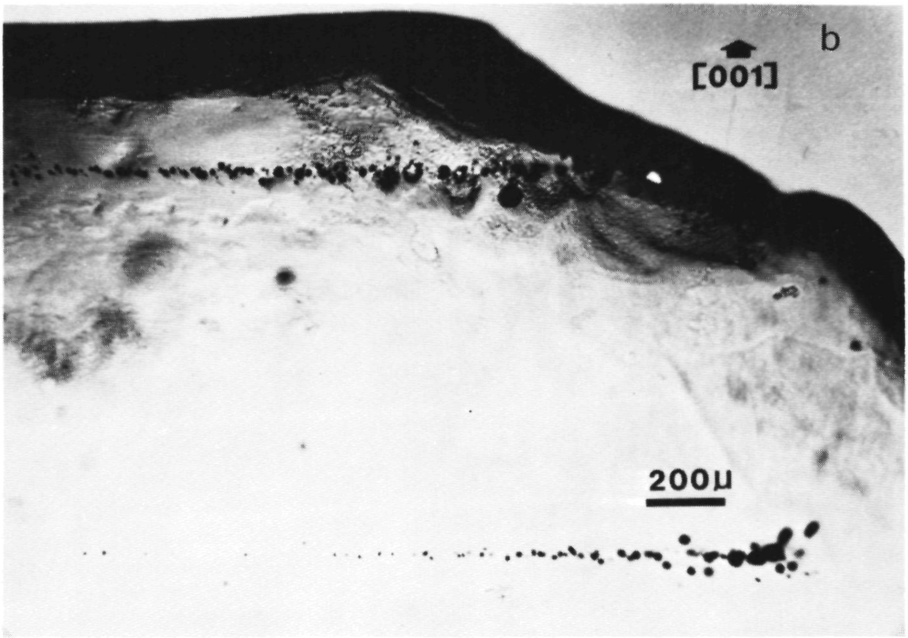

Fig.6. (continued) (b) Bright field micrograph showing two of the inclusion arrays given in (a).

to the {111} or {100} growth faces were observed. X-ray diffraction topography as well as birefringence microscopy showed that often neither dislocations terminate, nor start from these bubbles. An example is given in fig. 6a showing a detail of the Lang topograph presented in fig. 1a. Fig. 6b gives a bright field micrograph, showing two rows of liquid inclusions. From both photographs it can clearly be deduced that no dislocations are related to the inclusions. Earlier observations of this kind of liquid inclusions in potash alum were made by Gülzow, Gülzow and Lüdke (1965) and by Hähnert (1972), who showed by etching that the bubbles occurring in veils and rows parallel to the growth faces are not laterally connected with each other by dislocation lines. The present study as well as the work by Gots-Leon et al. (1978) show that this kind of inclusions are also not related to dislocations normal to the veil planes.

3.2.4. Formation of liquid inclusions due to the stress fields of dislocations

All the liquid inclusions, which are formed near or on a dislocation line as a result of its stress field belong to

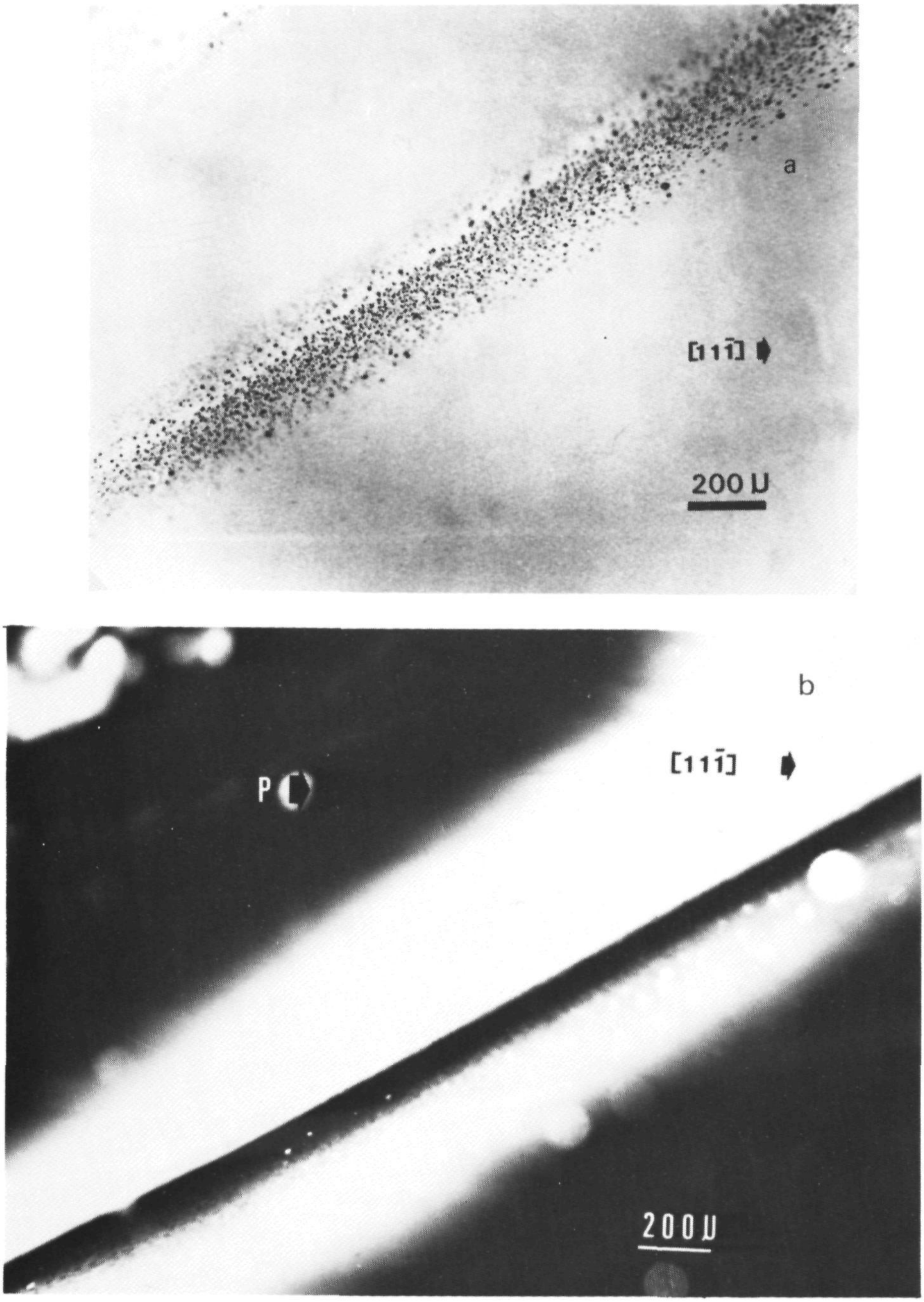

Fig.7. Inclusion strings related to large dislocation bundles:
(a) Bright field transmission micrograph of an inclusion string showing numerous small -liquid- inclusions
(b) Birefringence micrograph of the same region as (a): a well developed strain field due to a dislocation bundle can be seen.

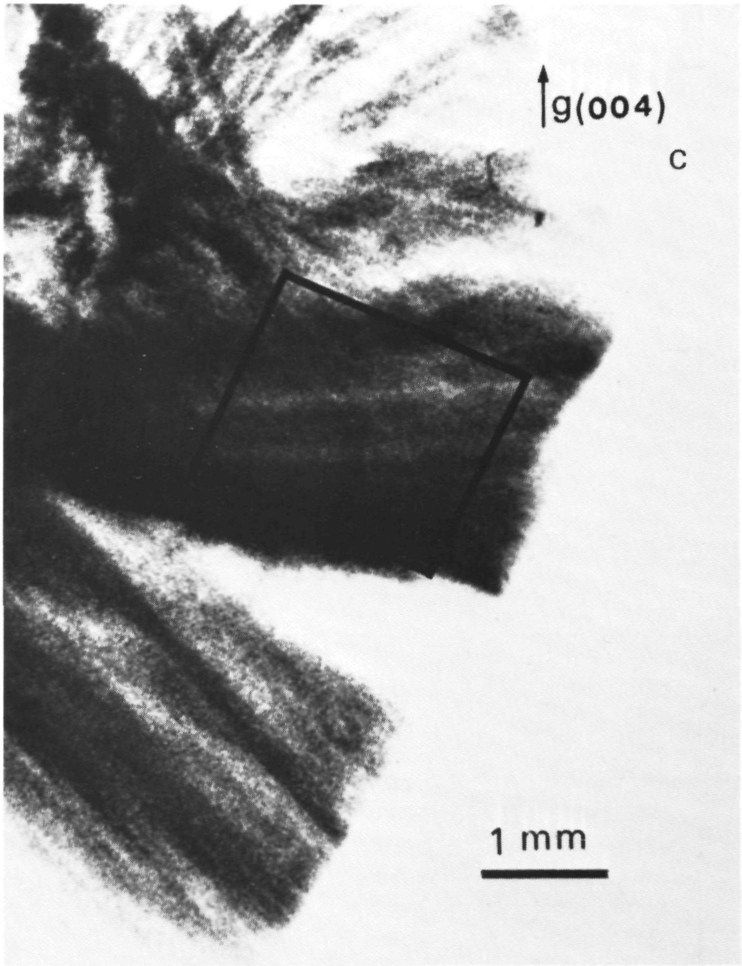

Fig.7. (continued) (c) Lang topograph of the dislocation bundle corresponding to the inclusion string. The boxed area corresponds to (a) and (b).

this class. Two catagories can be distinguished:
(i) Inclusion strings

Often in quickly grown lower quality alum crystals numerous liquid inclusions, distributed as strings radiating (mostly parallel to the $<1\bar{1}0>$ and $<1\bar{1}1>$ directions) from the seed to the $\{1\bar{1}1\}$ growth faces were found. A typical example of such a rectilinear group of inclusions is given in fig. 7a, which is a bright field micrograph showing multitudinous small (∿5μ in diameter) inclusions. Application of stress birefringence microscopy shows that this region is heavely strained as can be seen in fig. 7b. Lang topography (fig. 7c) shows that this row of inclusions coincides with a strongly developed dislocation bundle. Recently a similar inclusion string related to a dislocation bundle was also found for potassium hydrogen phtalate, where below the centre of a macroscopic growth spiral an extended row of inclusions, which was inclined to the growth face, could be identified (van Enckevort and Jetten, 1981).

Concerning the formation history of the inclusion strings, this is very similar as for the development of isolated or hollow tube inclusions near or on dislocation lines, which will be pointed out elswere.

(ii) Isolated inclusions and hollow tubes

Quite commonly isolated liquid inclusions lying near or on dislocation lines were revealed by comparison of stress birefringence and bright field micrographs. On the polarization micrographs often near dislocation lines four lobe rosette images, typical for spherical stress fields around inclusions or precipitates in an uniform background stress field, were recognized (figs. 1e and 8a). Detailed observation

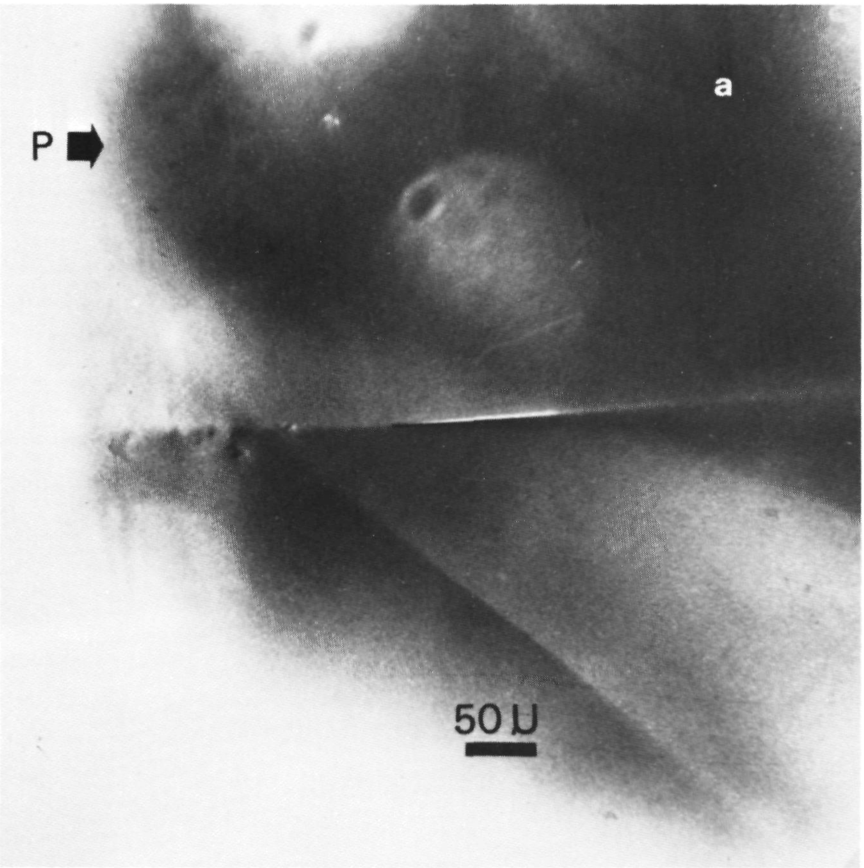

Fig.8. Correlations between hollow -liquid- tubes and dislocations: (a) and (b) Stress birefringence micrographs of both the extreme points of a hollow tube, where it changes into a dislocation line.

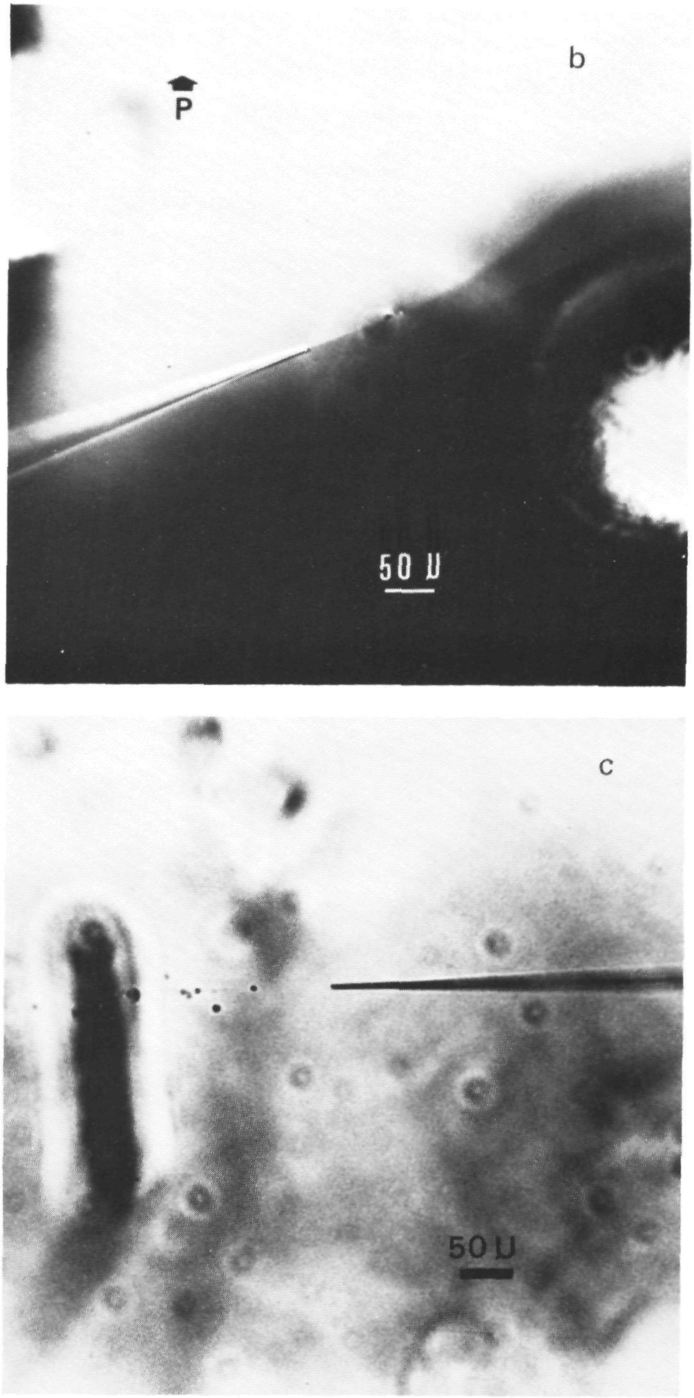

Fig. 8. (continued) (b); (c) Bright field micrograph of the same region as (a), showing the tube and some liquid inclusions.

of these strained area with the aid of a bright field microscope often revealed small liquid inclusions as for example can be seen in figs. le' and 8c. However, in many other cases neither inclusions, nor precipitates could be seen; probably their sizes are too small to be detected by optical bright field microscopy.

In a few cases, especially for lower quality, quickly grown crystals,"hollow" tubes related to dislocation lines were identified. A beautiful example of such a tube is given in fig. 8: Figs. 8a and 8b are stress birefringence micrographs of both extreme points of the tube, where it changes into a dislocation line. Fig. 8c presents a bright field micrograph of the same region as given in fig. 8a, showing the tube-like and some spherical inclusions. From the observation that at both extremities the hollow tube passes into a dislocation of roughly the same strength -as can be estimated from the contrasts on the birefringence photographs- it can be concluded that the dislocation leaving the tube is not formed via a lattice enclosure error, but that the tube itself has the same Burgers vector as the dislocation. This is confirmed by the fact that the birefringence image remains unaffected when the dislocation changes into a tube as can be seen in fig. 8a.

In spite of the similarity of the present situation to the hollow cores around dislocation lines at equilibrium and non-equilibrium conditions as described by Frank (1951), Cabrera, Levine and Plaskett (1954) and van der Hoek, van der Eerden and Bennema (1981 a) the origin of the tubes in potash alum must be rather different. This can be understood from the following arguments: (a) The observed widths of the tubes (a few microns) are one order of magnitude higher than to be expected after a rough estimation on basis of the relation derived by Cabrera et al. (1954), using some standard values of this class of compounds for the shear modulus and surface free energy. (b) Dislocation lines in the same crystal, having the same or higher birefringence contrasts and so with similar or larger Burgers vectors than the few dislocations corresponding to tubes, mostly do not reveal hollow pipes. (c) Since during crystal growth the supersaturation was kept more or less constant, the abrupt beginning and ending of the tubes along the dislocation lines, without any evidence for a dislocation splitting, can not be interpreted in terms of the hollow core model of Cabrera et al. (1954).

It is suggested that the inclusion strings, isolated inclusions and tubes are formed via the following -dynamic- mechanism (see also fig. 9): Firstly a step train generated by a dominant growth spiral, is passing a dislocation outcrop at the crystal surface (fig.9a). Due to its stress field a step retardation takes place in the same way as described in the work by van der Hoek, van der Eerden and Bennema (1981 b), which leads to bunch formation (fig. 9b). This bunch hampers mass transport to the region near the dislocation outcrop, which can result in the formation of a cavity (fig. 9c). After lattice enclosure the inclusion is formed. A similar mechanism

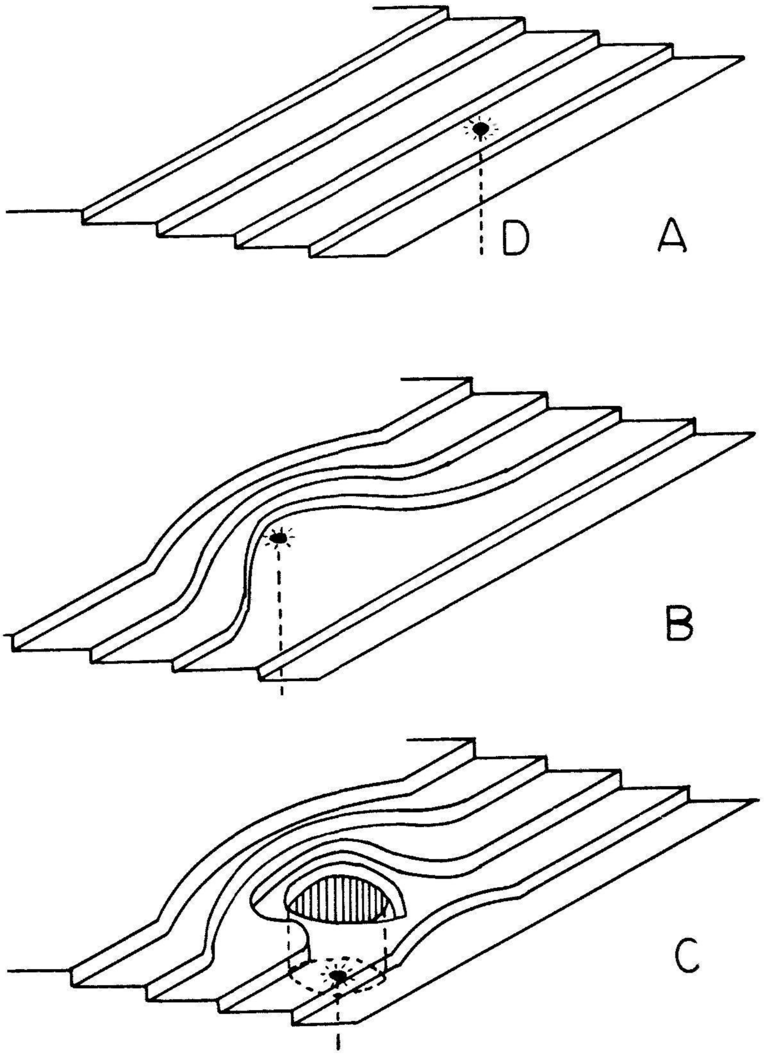

Fig.9. Successive stages of the development of a liquid inclusion -or tube- around a dislocation outcrop at the crystal surface

based on the interplay of stress fields and mass transport, can also occur when the dislocation acts as a growth -spiral-centre.

The inclusions near the dislocation line are not formed via a movement towards these line defects, giving a release in elastic strain, because no moving inclusions were observed, neither during growth (Hähnert,1972 and Akizuki, 1965) nor after growth.

3.3. Growth sector boundaries and growth bands

In contradistinction to the observations made by Gits-Leon et al. (1978) and Klapper (1980) in the present case no, or in some cases very weakly, sector boundaries and growth bands could be identified on the X-ray topographs. Probably this is due to the use of a more pure starting material for crystallization, leading to a lower variation in impurity content between adjacent regions, which is the origin of both defect types (Dam and van Enckevort,1981). On the other hand, on the birefringence micrographs the {1$\bar{1}$1} and {1$\bar{1}$0} growth sectors and so also their boundaries were clearly identified as shown in fig. 10. Theoretically the -cubic- alum should be optically isotropic, but due to impurity contents a slight amount of birefringence is introduced, which differs for each growth sector as a result of a difference in impurity absorption or growth mechanism. This leads to the ob-

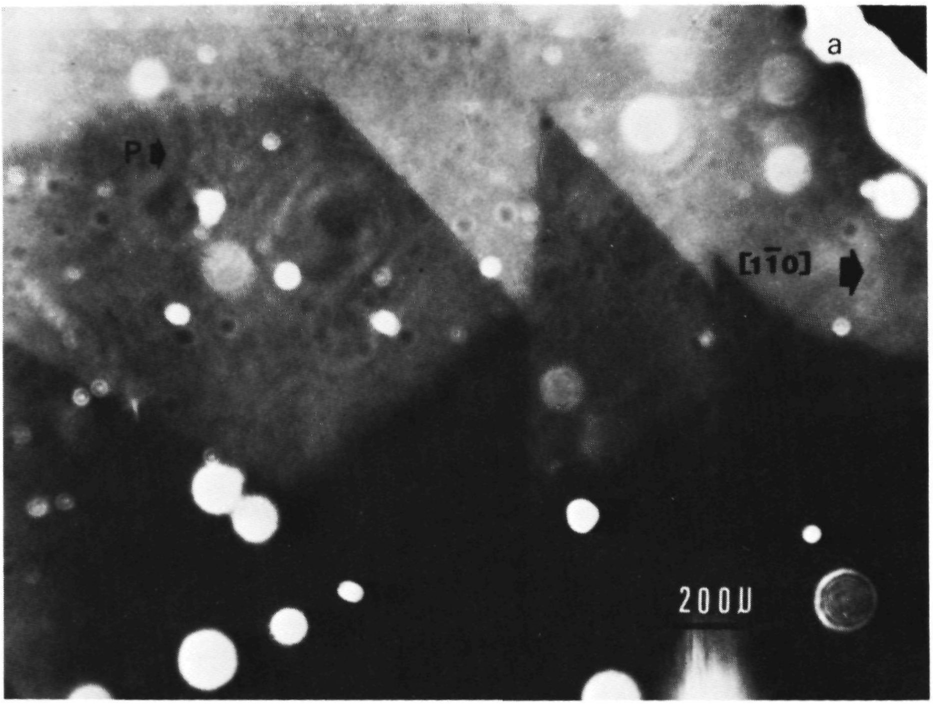

Fig.10. (a) Stress birefringence micrograph showing adjacent (1$\bar{1}$1), (1$\bar{1}$0) and (1$\bar{1}\bar{1}$) sectors.

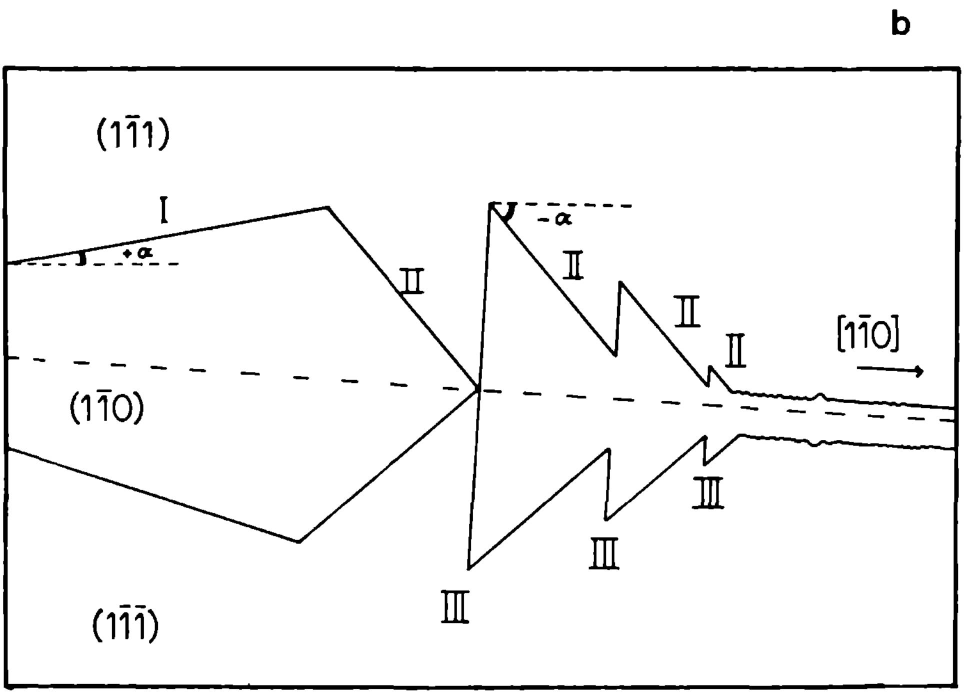

Fig.10. (continued) (b) Schematic representation of (a); the saw-shaped pattern of the (1$\bar{1}$0) sector is due to its extremely high growth dispersion.

served difference in intensity for each sector on the stress birefringence micrographs. However, the lattice bending at the boundaries of these differently distorted growth sectors is too low to be detected by Lang topography. A similar observation of growth sectors by stress birefringence microscopy, which could not be revealed by Lang topography was made by Tanner (1972) for fluorite.

In contrast to the {1$\bar{1}$1} and the {1$\bar{1}$0} sectors, during the present study the {001} sectors could not be distiguished by the stress birefringence method. Growth bands occurring in the {1$\bar{1}$1} growth sectors, were observed on some of the stress birefringence micrographs as thin lines with different contrasts with respect to the background region.

It is well established that growth sector boundaries are "fossiles" of the time sequence of the relative widths of adjacent facets (see for instance: Gits-Leon et al.,1978 and Dam and van Enckevort, 1981). For potash alum the $\{1\bar{1}0\}$ sectors often consist of a row of trigonal patterns, as can be seen in fig. 10. This means that during crystal growth the relative widths of adjacent $(1\bar{1}0)$ and $(1\bar{1}\bar{1})$ sectors varies considerably. From the angle (α) between the sector boundary outcrop at the (110) crystal plate surface and the $|1\bar{1}0|$ direction the ratio of the growth rates of the adjacent $(1\bar{1}0)$ and $(1\bar{1}\bar{1})$ faces can be determined according to:

$$\frac{v_{(1\bar{1}0)}}{v_{(1\bar{1}\bar{1})}} = \frac{\cos\alpha}{\cos(\gamma-\alpha)},$$

where γ is the angle between $(1\bar{1}\bar{1})$ and $(1\bar{1}0)$.

Growth kinetics experiments carried out by Mullin and Garside (1967) and Human (1981) showed that at a given supersaturation the growth rate of the alum {111} faces remains more or less constant throughout a growth experiment (i.e. $v_{(111)}$= constant). Therefore the conclusion can be drawn that the large variation in width of the $(1\bar{1}0)$ growth sector is mainly due to a dispersion in growth rate of the $(1\bar{1}0)$ facet.

In fig. 10 three discrete levels in advancement rate of the $(1\bar{1}0)$ face can be distinguished: I with $v_{(1\bar{1}0)} = 1.0\, v_{(111)}$, II with $v_{(1\bar{1}0)} = 4.2\, v_{(111)}$ and III with $v_{(1\bar{1}0)} \simeq 0$. Similar variations in growth rate and also other advancement rate levels of the $(1\bar{1}0)$ facets were quite commonly observed on the birefringence micrographs. Often no $(1\bar{1}0)$ growth sector could be seen: in these cases only a boundary between the -now adjacent- $(1\bar{1}1)$ and $(1\bar{1}\bar{1})$ sectors was revealed by polarization microscopy.

Probably the enormous growth dispersion of the {110} faces can be interpreted in terms of a presence or non-presence of termination points of dislocation with a screw component at the {110} growth facets, in like manner as for {001} alum, investigated by Gits-Leon et al. (1978). However, during the present study no proof could be given for this suggestion. At this moment the growth dispersion of both the {110} and the {100} alum faces is studied in detail by correlating in situ observations of the crystal growth process with phase contrast surface microtopographs and Lang topographs (Human and van Enckevort, 1981).

4. CONCLUSIONS

It has been shown that the stress birefringence method combined with high contrast photographic emulsions is a simple but powerful tool for studying the dislocation structure in the optically isotropic potash alum crystals. The advantages of this polarization microscopic method are the following: (i) Nearly all dislocations (except those with $\vec{b} = \langle 001 \rangle$) can be revealed. (ii) This method allows to make a direct correlation between the dislocation structure and liquid inclusions by simple removal of the analyser, which turns the polarization microscope into a bright field microscope. (iii) The birefringence method is a convenient, quick and inexpensive means of studying the defect structure in materials such as alum.(iv) The sensitivity for growth bands and sector boundaries is higher than for Lang topography. (v) Since for potash alum the image widths of dislocations on Lang topographs are rather large, the resolution of the birefringence method is higher than for Lang topography.

Disadvantages of the birefringence method are: (i) A lower sensitivety for dislocations with respect to X-Ray diffraction topography. (ii) Determination of the Burgers vectors is impossible, because of an anomalous behaviour of the birefringence images of the dislocations in potash alum.

ACKNOWLEDGEMENTS

The authors wish to thank Prof. P. Bennema for stimulating discussions and critical reading of the manuscript and Mr. W.H. van der Linden for growing the crystals. Further they are grateful to Prof. J. Bloem and Dr. L.J. Giling for their co-operation in setting up the facilities to carry out X-ray diffraction topography.

One of us (W.J.P. van Enckevort) acknowledges the supports of the Netherlands Foundation for Pure Research, ZWO/SON.

REFERENCES

AKIZUKI, Mizuhiko, 1965, Sci.Rep.Tohoko Univ., 9, 217

AUTHIER, A., 1967, Adv. X-ray Analysis (Plenum), 10, 9

BENNEMA, P., 1965, Thesis, Technical University of Delft

BOND W.L., and ANDRUS, J., 1956, Phys. Rev., 101, 1211

BULLOUGH, R., 1958, Phys. Rev., 110, 620

CABRERA, N., LEVINE, M.M., and PLASKETT, J.S., 1954, Phys. Rev., 96, 1153

DAM, B., and ENCKEVORT, W.J.P. van, 1981, J.Crystal Growth, in press

EHRINGHAUS, A., and TRAPP, L., 1958, Das Mikroskop (B.G. Teubner Verlagsgesellschaft, Stuttgart)

EMARA, S.H., LAWN, B.R., and LANG, A.R., 1969, Phil.Mag., 19, 7

ENCKEVORT, W.J.P. van, BENNEMA, P., and LINDEN, W.H. van der, 1981, Chapter II

ENCKEVORT, W.J.P. van, JANSSEN- van ROSMALEN, R., KLAPPER, H., and LINDEN, W.H. van der, 1981, Chapter IX

ENCKEVORT, W.J.P., JANSSEN- van ROSMALEN, R., and LINDEN, W.H. van der, 1980, Chapter VIII

ENCKEVORT, W.J.P. van, and JETTEN, L.A.M.J., 1981, Chapter VI

ENCKEVORT, W.J.P. van, and LINDEN, W.H. van der, 1979, Chapter I

FATHERS, D.J., and TANNER, B.K., 1973 a, Phil. Mag., 27, 17; 1973 b, Ibid., 28, 749

FRANK, F.C., 1951, Acta Cryst., 4, 497

GITS-LEON, S., LEFAUCHEUX, F., and ROBERT, MC., 1978, J. Crystal Growth, 44, 345

GÜLZOW, G., GULZOW, Hj., and LÜDKE, W., 1965, Phys. Stat. Sol. 11, 205

HAHNERT, I., 1972, Kristall und Technik, 7, 419

HOEK, B. van der, EERDEN, J.P. van der, and BENNEMA, P., 1981 a, J. Cryst. Growth, to be published; 1981 b, Ibid., to be published

HUMAN, H.J., 1981, Thesis, Catholic University of Nijmegen

HUMAN, H.J., and ENCKEVORT, W.J.P. van, 1981, Chapters III and IV

INDENBOM, V.L., 1961, Dokl. Akad. Nauk. S.S.S.R., 141, 1360; See also AMELINCKX, S., 1964, The direct observation of dislocations, Solid State Physics Suppl. 6, edited by F. Seitz and D. Turnbull (Academic Press, New York, London) p. 108

INDENBOM, V.L., NIKITENKO, V.I., and MILEVSKII, L.S., 1962, Soviet Phys. Dokl., 6, 1034

INDENBOM, V.L., and TOSHIBOVSKI, G.E., 1957, Soviet Phys. Crystallogr., 2, 183

JENKINS, D.A., and HREN, J.J., 1976, Phil. Mag., 33, 173

KEAR, B.H., and PRATT, P.L., 1958, Acta Met. 6, 457

KLAPPER, H., 1980, private communication

KOVACS, I., and ZSOLDOS, L., 1973, Dislocations and plastic deformations, International series of monographs in natural phylosophy Vol. 60 (Pergamon Press, Budapest, Oxford)

LANG, A.R., 1959, Acta Cryst., 12, 249; 1967, Nature, Lond., 213, 248

LANG, A.R., 1970, Modern Diffraction and Imaging Techniques in Materials Science, edited by S. Amelinckx, R.Gevers, G. Remaut and J. van Landuyt (North-Holland Publishing Co.), p.407

LIPSON, H., and BEEVERS, C.A., 1935, Proc. Roy. Soc. A. 148, 664

LÖSCHKE, K., GOTTSCHALCH, V., JACOBS, K., and TEMPEL, A., 1979, Kristall und Technik, 14, 887

MATTHEWS, J.W., KLOKHOLM, E., PLASKETT, T.S., and SADAGOPAN, V., 1973, Phys. Stat. Solidi (a) 19, 671

MATTHEWS, J.W., PLASKETT, T.S., and AHN, J., 1976, Phil. Mag., 33, 73

MATTHEWS, J.W., PLASKETT, T.S., and BLUM, S.E., 1977, J. Crystal Growth, 42, 621

MULLIN, J.W., and GARSIDE, J., 1967, Trans. Inst. Chem. Engrs., 45, 285

NIKITENKO, V.L., and DEDUKH, L.M., (1970), Phys. Stat. Sol. (a), 3, 383

SATO, K., 1980 a, Jpn. J. Appl. Phys., 19, 1257; 1980 b, Ibid., 19, In press

TANNER, B.K., 1972, Phys. Stat. Sol. (a), 14, K9

TANNER, B.K., 1976, X-ray Diffraction Topography, I.S. Science of the Solid State, Vol. 10 (Pergamon)

TANNER, B.K., and FATHERS, D.J., 1974, Phil. Mag., 29, 1081

WYKOFF, R.W.G., 1965, Crystal Structures, Vol. 3 (John Wiley and Sons), p.872

POTASSIUM HYDROGEN PHTHALATE

CHAPTER VI:
OBSERVATION OF VERY LOW AND HIGHER STEPS ON AQUEOUS SOLUTION GROWN CRYSTALS: CASE OF {010} POTASSIUM HYDROGEN PHTHALATE

W.J.P. van Enckevort and L.A.M.J. Jetten

RIM Laboratory of Solid State Chemistry, Faculty of
Science, Catholic University, Toernooiveld, Nijmegen,
The Netherlands

ABSTRACT

A detailed surface microtopographic study with the aid of highly sensitive differential interference and phase contrast microscopy has been carried out for the {010} faces of potassium hydrogen phthalate single crystals. Two types of growth hillocks could be identified: (i) macroscopic hillocks, emitting steps of considerable height from their centres and (ii) shallow hillocks, being sources of growth steps of very low height. From a relationship between hillock centres and dislocation etch pits, the macroscopic hillocks were identified as a group of cooperating spirals, whereas the shallow hillocks are single spirals originating from single dislocations of unit height. Step height measurements using two beam interferometry showed that for the macro-spirals the step height somewhat away from the centre ranged from 100 to 2500 A. The step height of the small hillocks, however was very low, being equivalent to 14 A. which corresponds to one unit lattice translation normal to the {010} growth face. Several properties of both spiral types are described, among which a relation between inclusion strings and the occurrence of some of the macroscopic hillocks, the phenomenon of bunching of lower steps to higher steps, the formation of liquid inclusions via macrostep overhangs and the equivalence in advancement rates of steps of different heights.

1. INTRODUCTION

During the last three decades numerous kinds of crystal surfaces have been investigated by means of highly sensitive reflection optical phase (PCM) and differential (DIM) contrast microscopy. In the fifties the main purpose of these observations was to give a direct proof for the spiral growth theory of Frank (1) and to study the "internal" structure of crystals in relation to the newly developed dislocation theory, by means of etch pit studies (2). About that time the first unit lattice height and even lower steps were observed and measured by several workers, such as Griffin (3), Amelinckx and Strumane (4), Verma (5) and Sunagawa and Tolansky (6). Later on a lot of additional microtopographic studies on the occurrence of both higher and very low steps were made by other scientists in order to relate more recently developed theories of crystal growth to the experiments (7-9).

Up to very recently unit lattice height and lower steps have only been observed on gas phase grown crystals (4,5,7-10), high temperature flux grown crystals (9,11) and minerals (3,9), but hardly on aqueous solution grown crystals. This is attributed to the fact that separation of crystals prior to surface microtopography, without perturbing the monomolecular step patterns on the surfaces is much more easy to be carried out for gas phase or (lower solubility) flux grown crystals, than for crystals grown from aqueous solutions (12). As far as known to us, at this moment two groups of scientists are working on the topic of ex situ and in situ observations of growth steps of one or a few unit lattice translations in height on aqueous solution grown crystals. The first group, at the University of Sendai made a qualititative ex situ study on KCl (13) and at this moment they are carrying out in situ observations of very low growth steps on CdI_2 crystals by optical transmission microscopy (14). The second group, at the University of Nijmegen made several ex situ investigations on very low growth steps on potash alum (12), $Ni\ SO_4 \cdot 6H_2O$ (15) and the present compound potassium hydrogen phthalate, for which at the moment also in situ studies of the growth processes on the {010} faces are carried out, using optical reflection microscopy.

Potassium hydrogen phthalate (KAP) is chosen as a model compound because of its beautiful surface pattern on the {010} faces consisting of high and very low growth steps, which can relatively easily be observed by means of optical microscopy, because of their large lateral separation. Further this crystal has a practical use as a crystal analyser in long-wavelength X-ray spectrometers (16-18) for two main reasons: (a) Its large lattice parameter perpendicular to the {010} face and (b) Preparation of the crystal plates is very simple, because the crystals can be cleaved easily in a perfect manner parallel to {010} .

The aim of the present study is:

(i) To make a detailed ex-situ microtopographic investigation of the {010} faces of KAP by optical reflection phase contrast (PCM) and differential interference contrast (DIM) microscopy in order to verify a possible relationship between theory and experiment for the very important class of aqueous solution grown crystals.

(ii) To carry out a preliminary study on the {010} faces of KAP, which is of high importance for a better interpretation of present and future in situ observations of moving growth step patterns.

2. EXPERIMENTAL

The platelet-like KAP crystals were grown by a controlled temperature decrease method. A saturated solution of KAP in doubly destilled water was allowed to cool down from 30 °C to 25 °C in a few days, after which period well developed crystals could be gathered.

Prior to observation the crystals were quickly picked up from the supersaturated solution and dipped for a short moment into n-hexane. After this the adhering hexane film was soaked up with a piece of blotting paper or a paper tissue. This procedure has been carried out in order to minimize secondary growth or etching during separation of the crystals from the liquid phase, which may ruin the original step patterns.

The merits of this separation method have been treated extensively in previous work on KDP (19) and potash alum (12).

Surface microtopography has been carried out by making use of a high quality differential interference (DIM) and phase contrast (PCM) microscope, the latter in combination with a high absorption phase plate (12) and high contrast photographic emulsion. By application of this powerful PCM method it is possible to observe height differences as low as about 2 A (20). The crystal surfaces were not silvered before observation.

In order to measure height differences and inclinations two beam interferometry, using a mercury light source combined with a monochromator filter (λ = 5460 A) was applied.

3. OBSERVATIONS AND DISCUSSIONS

3.1. General features

In general the {010} faces of the KAP crystals show one or a few very extended, dominating, growth hillocks, which even can be observed by the naked eye in reflected light. A well developed example of such a macroscopic hillock is given in DIM micrograph 1a. It can clearly be recognized that the two-dimensional point-group of this surface pattern is m (21). This is in accordance with the point-group symmetry of the projection along the $\vec{b}$-axis of the three-dimensional space-group of KAP, $Pca2_1$ (22), which also is m. The orientation of the hillocks with respect to the external morphology of the crystals is presented in figure 1b. From this schematic representation it can be seen that the hillocks are formed by two types of symmetrically non-equivalent steps; both running parallel to <101> directions. One of the step types (indicated by A in figure 1b) has an advancement rate, which is about 10 times faster than the second (denoted by B). Since the absolute configuration of the crystals is not

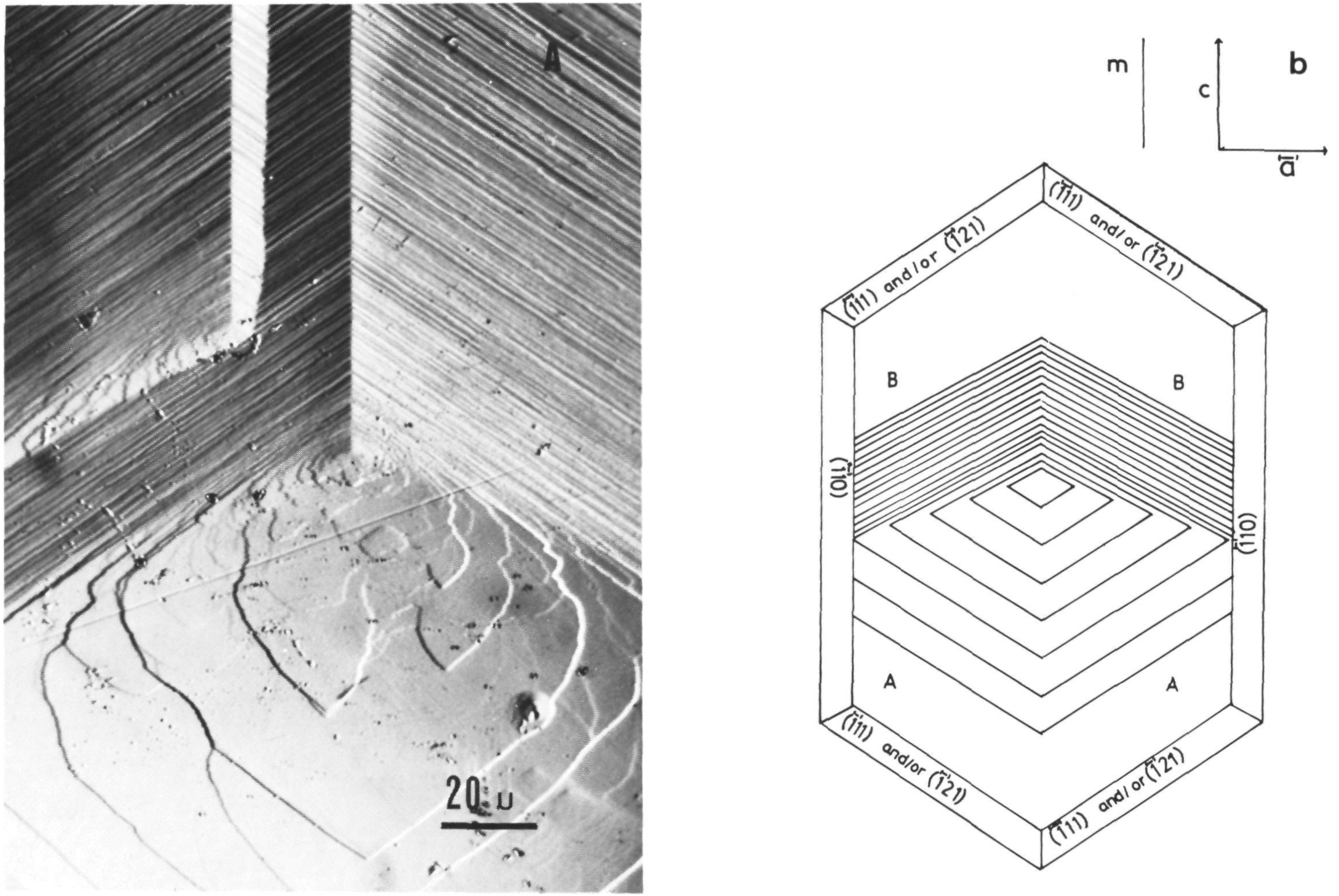

Fig.1. (a) Anisotropic macroscopic growth hillock on {010} KAP (DIM).
(b) Schematic representation of the relative orientation of the asymmetric growth hillocks with respect to the external crystal morphology.

known, no relation between crystallographic structure and step type, i.e. no absolute indices to the steps could be given.

Aside from these dominating macro-hillocks, which often emit very high steps over a large surface area of a given {010} facet, also numerous very small growth hillocks, only visible by DIM and PCM, emerging between the macrosteps could be identified. Typical examples of such shallow hillocks are shown in figure 2. From this PCM micrograph one can deduce that the two-dimensional symmetry of these hillocks as well as the occurrence of two step types and their orientation with respect to the external crystal morphology is exactly the same as for the macroscopic growth hillocks. The main difference between the macroscopic and the smaller hillocks is the considerably lower step height for the latter ones.

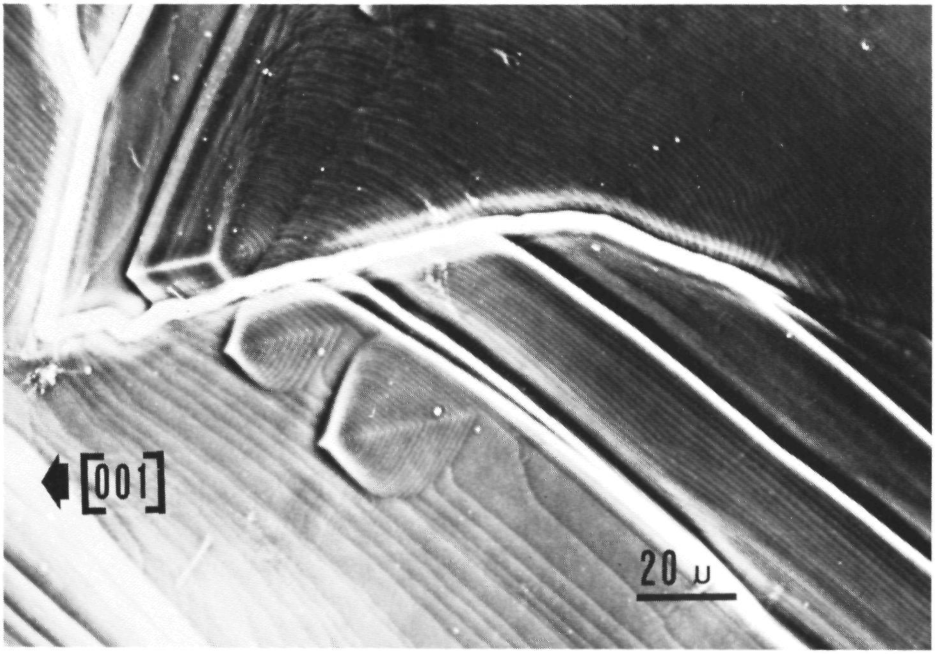

Fig.2. Shallow growth hillocks with unit lattice height steps (∿13 A) between macrosteps (PCM).

3.2. Correspondence between hillock centres and dislocation outcrops at the crystal surface

"Etch pitting" is a powerful technique to relate as grown surface patterns to defects as was demonstrated by

Amelinckx (23), Sato et al. (24) and by one of us (15,19, 25). To correlate growth centres and other surface features to dislocation outcrops (which are marked by pits after etching) in an easy way an etching agent must fulfill two requirements:
(i) The pits formed after etching must almost without any exception correspond to dislocations and should clearly be visible by optical microscopy.
(ii) Etching should proceed very slowly, so that after a given, empirically found, etching time small dislocation pits are formed without serious etching away of the contours of the original growth patterns.

After several attempts using various kinds of etching agents such as water, methanol, ethanol, acetic acid and mixtures of these, ethanol proved to be the most suitable agent for correlating surface features to defects. A typical etch pit pattern on {010} KAP, formed 10 minutes dissolution of the crystal in absolute ethanol is given in figure 3. The etch pits show the same asymmetric pattern (two-dimensional point-group m) bounded by <101> steps, as the hillocks, but now rotated 180°. Concerning the distribution of the etch pits over the {010} faces,

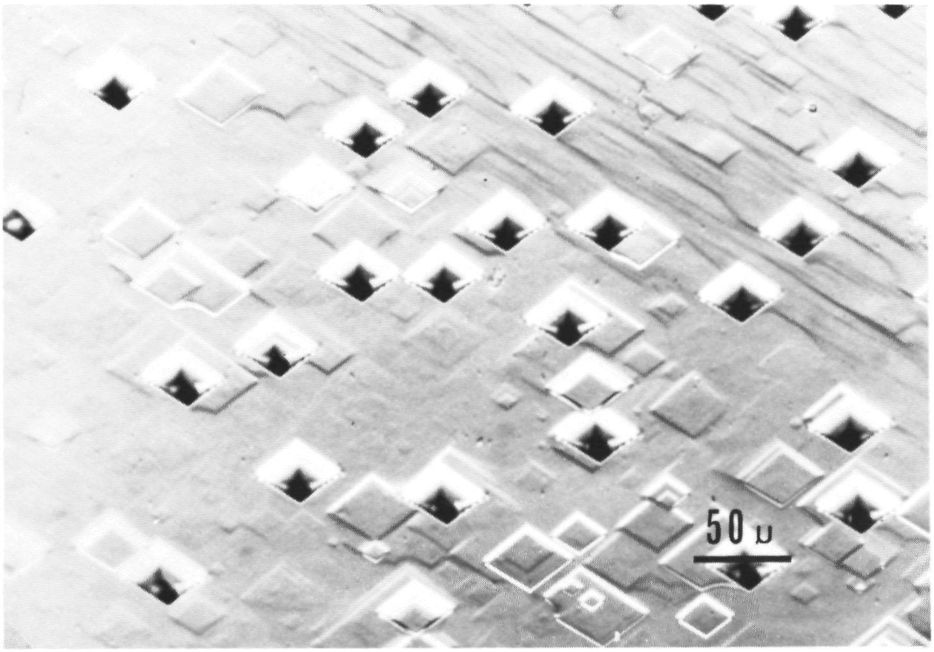

Fig.3. Anisotropic etch pits on {010} KAP formed after 10 minutes dissolution in absolute ethanol (DIM).

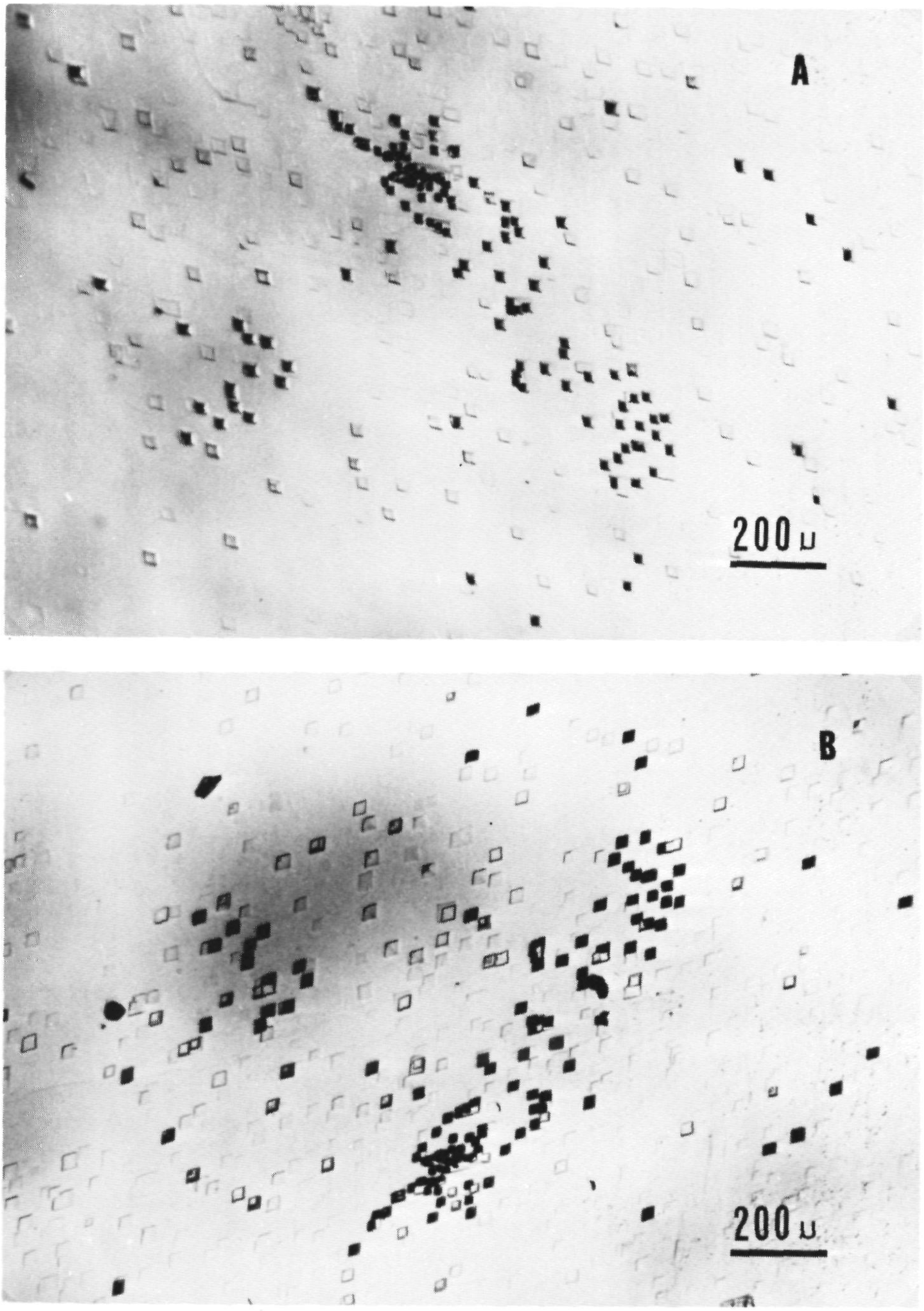

Fig.4. Correspondence between etch pits and dislocations: The etch pit patterns on the two cleaved crystal halves (a) and (b) are, aside from reflection, equivalent to each other.

it is to be mentioned that in general the pit density is much higher at the central region than near the perifery of these faces.

To verify whether the pits are uniquely related to dislocations a "cleavage-etching-matching" experiment was carried out in the same way as for instance by Amelinckx for rock salt (26). This was done as follows: Firstly a crystal was cleaved along {010}. Then the two crystal halves were etched for 10 minutes in ethanol and finally the pit patterns on both parts were compared with each other with the aid of a low power microscope. The result of such an experiment is given in figure 4a and b, showing the two crystal sections: It can clearly be recognized that the etch pit patterns are the same, so the pits are related to line defects intersecting the cleavage plane, i.e. are dislocation etch pits.

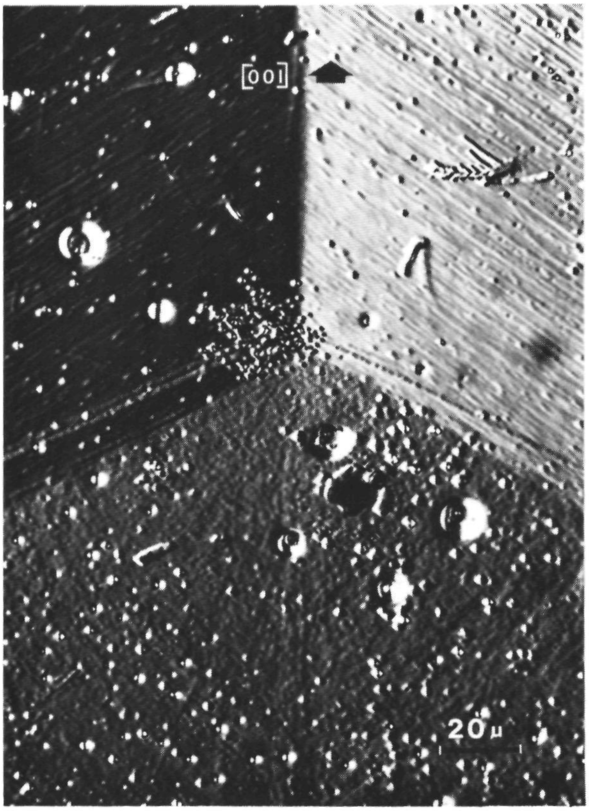

Fig.5. Relation between etch pits and dislocation outcrops: Centre of slightly etched macroscopic hillock decorated by a group of etch pits.

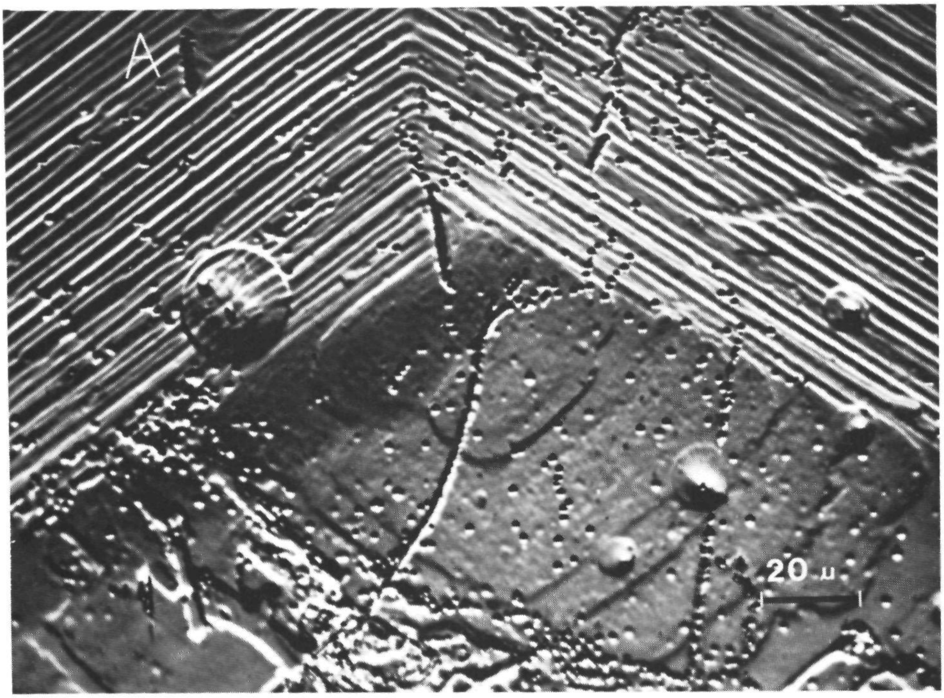

Fig.6. Relation between hillocks and dislocations: Group of cooperating spirals, the starting points of which at the centre are decorated by etch pits (DIM).

On basis of the knowledge that the pits formed by dissolution of KAP in ethanol are related to dislocation outcrops, now the relation between hillock centres and pits can be verified in order to prove that the hillocks are growth spirals. To do this several crystals with both well developed macroscopic hillocks and shallow hillocks were selected and etched for about 10 seconds in ethanol. After etching at all the hillock centres one, a few or a localized cluster of tiny etch pits could be discerned. Two examples of such a relationship between hillocks and pits are given in figures 5 and 6: Figure 5 shows a macroscopic hillock of the common type, the summit of which is decorated by a multitude of pits, which means that this elevation is related to a dislocation bundle and thus probably is a cooperating macrospiral. Figure 6 presents a group of cooperating macrospirals, where a few high steps start from the centre. The starting-points of these steps are marked by etch pits, which means that these starting-points of the cooperating spiral arms are related to dislocation outcrops. Aside from the spiral centre also a perturbation in the step pattern, indicated by A in figure 6, can be seen. The number of steps on the left hand and on the right hand side of A do not equal each other, which means that one or a group of dislocations, with quite a large netto screw component perpendicular to the growth face ends at the crystal surface. The relationship between this pertubation pattern and the occurrence of dislocation outcrops at the surface is confirmed by a group of etch pits at A. The same type of perturbation in a step train due to a dislocation bundle outcrop was reported earlier for {101} KDP, in which case the situation was explained in more detail (19).

For the shallow growth hillocks a similar relation between hillock centre and etch pit was found as for the macroscopic hillocks: After etching each of the shallow hillocks revealed, without any exception one single (sometimes two or more) etch pit at its summit. From this correspondence it can be deduced that the shallow hillocks very probably are growth spirals related to single dislocations, in a similar way as found for {111} potash alum (25) and {101} KDP (19).

From the etching studies it can now be concluded that the macroscopic hillocks in fact are a group of cooperating spirals, whereas the shallow hillocks very probably are single spirals.

3.3. Several properties of the growth hillocks

3.3.1. Measurement of the step height

To get an idea of the heights of the steps emitted from the centres of shallow and macroscopic hillocks two-beam interferometry was applied to the crystal surfaces. The measurement of the height of the spiral steps in the case of a shallow hillock is demonstrated with the aid of figure 7. Firstly a well developed specimen of such a shallow hillock was selected (fig. 7a) and a two-beam interferogram was made of this region (fig. 7b). At the location of the horizontal ridge (denoted by arrows in figures 7a and b) a slight bending of the interference fringes can be recognized. From the magnitude of this bending and the step spacing, measured from PCM photograph 7a the step height was determined to be 14 ± 0.5 A. This height is equivalent to the length of the $\vec{b}$ axis (13.85 A), which is oriented normal to the {010} growth face, so that for the shallow hillocks the growth steps are of unit lattice height. From this observation it can be concluded that the Burgers vector of the screw component normal to the growth face of the dislocation at the centre of the shallow growth spirals must correspond to one unit translation.

Only recently similar unit lattice height and lower steps on aqueous solution grown crystals have been observed and measured on potash alum (12), CdI_2 (14) and $NiSO_4$.

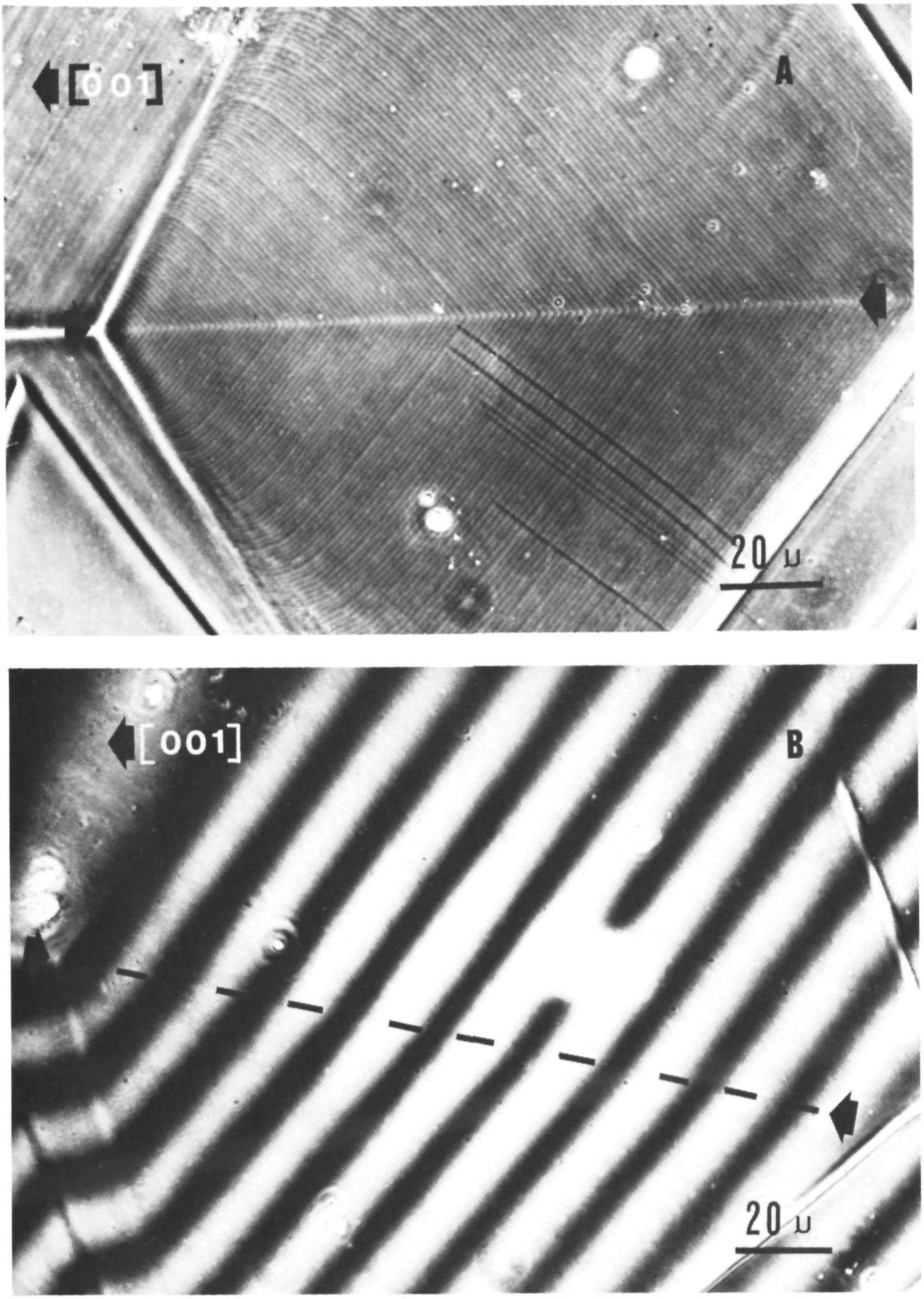

Fig.7. Step height measurement of a shallow growth hillock:
(a) Phase contrast micrograph of a well developed hillock, revealing numerous lower steps (PCM).
(b) Two-beam interferogram of (a).

6 H_2O (15,27). From these surface microtopographic studies it can be concluded that observation of monomolecular or unit lattice height steps on aqueous solution grown crystals by phase contrast microscopy, which was assumed to be impossible for a few years ago, is quite easy to be carried out and can now be considered as a standard technique to study the growth properties of this category of crystals.

Concerning the step heights of the macroscopic hillocks, these heights vary from a few tens of Angströms to about 1500 A, as was deduced from measurements by two beam interferometry. In general, the step height of a given macroscopic hillock increases strongly at further distances from its centre due to bunching as will be pointed out in a subsequent section.

3.3.2. Correlation between a string of inclusions and a macroscopic growth centre

For one of the crystals, which showed a large growth rate of the {010} faces as can be deduced from the rather large thickness of the crystal plates growing at the bottom of the growth vessel, a 'gigantic' macroscopic spiral dominating the complete surface area was found. The centre of this hillock is shown in figure 8a. Application of bright field transmission microscopy to the same crystal revealed a, with respect to the growth face inclined, string of liquid inclusions as can be seen in figure 8b. Careful examination of figure 8b learns that this inclusion string meets the {010} face exactly at the centre of the macroscopic hillock given in figure 8a. The present inclusion string looks very similar to the inclusion strings related to 'heavy' dislocation bundles in potash alum, which were extensively studied using optical transmission bright field and polarization microscopy and Lang topography by van Enckevort and Odekerken (29). Since the centre of a macroscopic hillock must be related to a dislocation bundle outcrop as was pointed out in a previous section, the correspondence between the end point of the inclusion string, which very probably coincides with a dislocation bundle, and the centre of the macroscopic hillock is now obvious. The formation mechanism of the inclusion string is probably the same as for those observed in potash alum (29).

3.4. Step configurations

3.4.1. Bunching

In the composition DIM micrograph presented in figure 9 an extended step train originating from a growth centre (denoted by C) can be seen. The height of the steps just leaving the centre of the hillock is quite low. Further the separation between successive steps in this

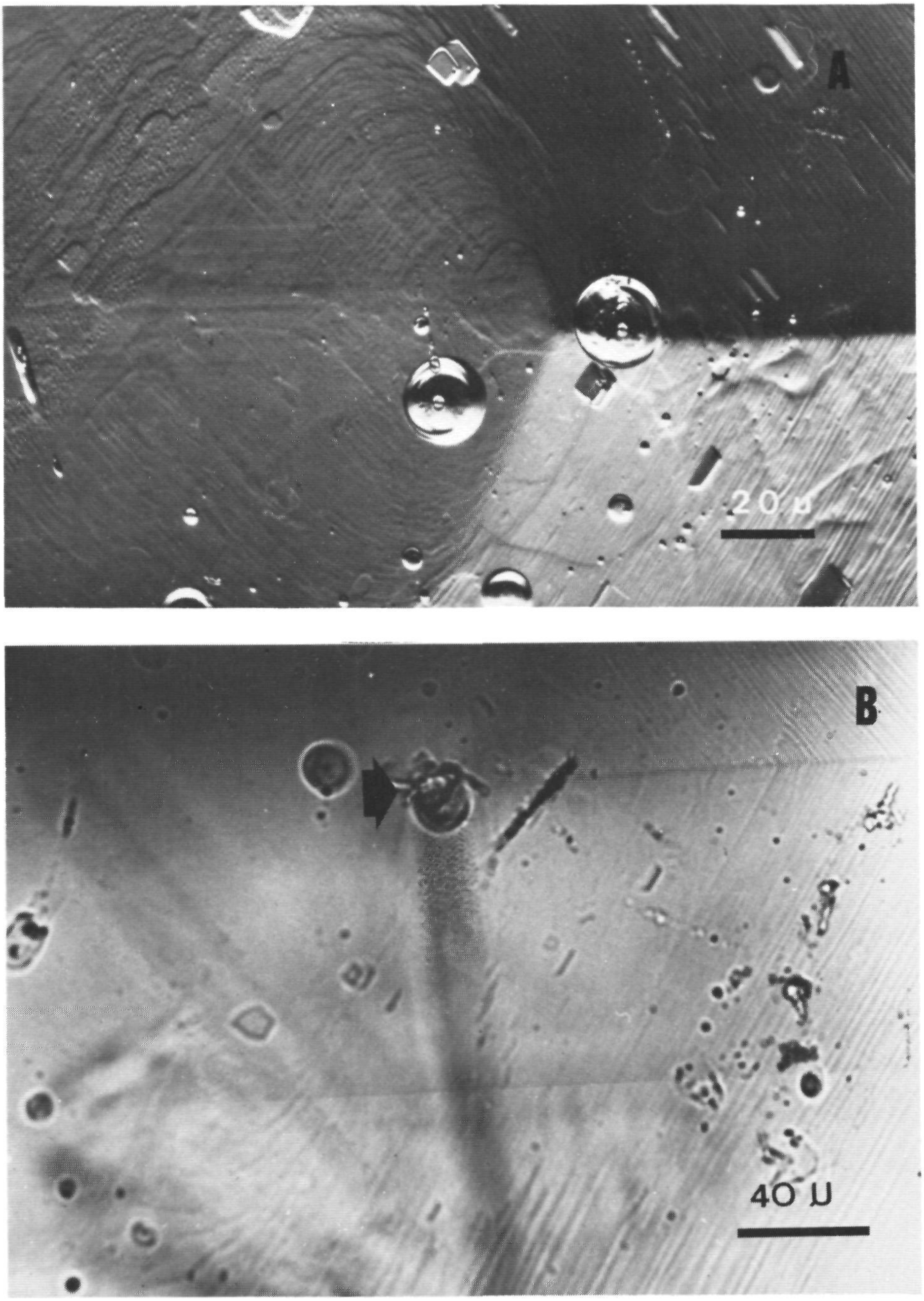

Fig.8. Correspondence between the centre of a well developed macroscopic growth hillock and an inclusion string:
(a) Centre of macroscopic hillock (DIM).
(b) Bright field transmission micrograph of the inclusion string below the summit of the hillock shown in (a).

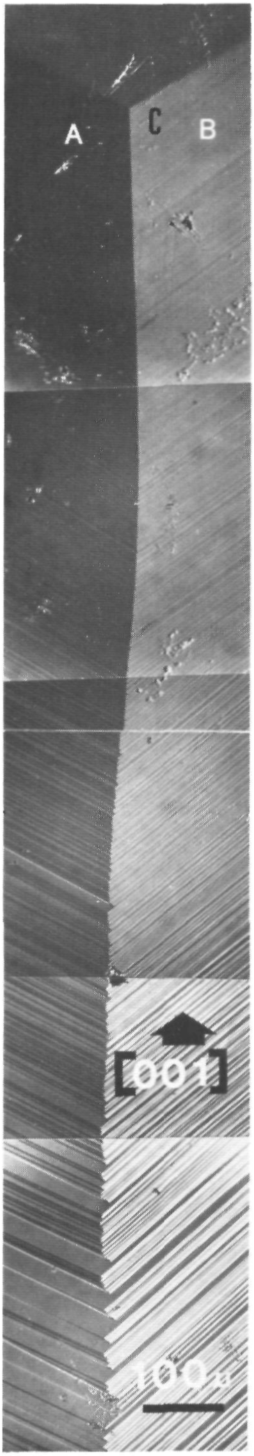

Fig.9. Bunching of a step train originating from a given spiral centre. Lower steps accumulate to higher ones during running away from the growth centre (DIM).

region near the growth centre is too low to be resolved by optical microscopy at the magnification presented in figure 9. On the other hand, far away from the centre the step height (a few hundred to a few thousand Ångströms) as well as the step spacing (∿50 to 100μ) are very high. This points to a 'bunching' of the step train, i.e. during advancing away from the centre lower steps accumulate to higher ones until steps of extreme hights are formed.

This bunching has been observed for all the growth hillocks (both macroscopic and shallow ones) with extended (more than one or a few millimetres) step trains. The origin of this pile up of lower steps to macrosteps is not yet clear and should be investigated in more detail by in situ observations.

3.4.2. Pseudo-interlacing

Since the formation of macrosteps via bunching of lower steps in two adjacent, symmetrically equivalent, spiral sectors (A and B in figure 9) is not correlated with each other, the macrosteps being 'member' of step train A and those that belong to step train B, which intersect each other at the ridge of the hillock do not have the same heights. This implies that these macrosteps of different height can not annihilate each other at the ridge, so that the highest of both steps will continue after the

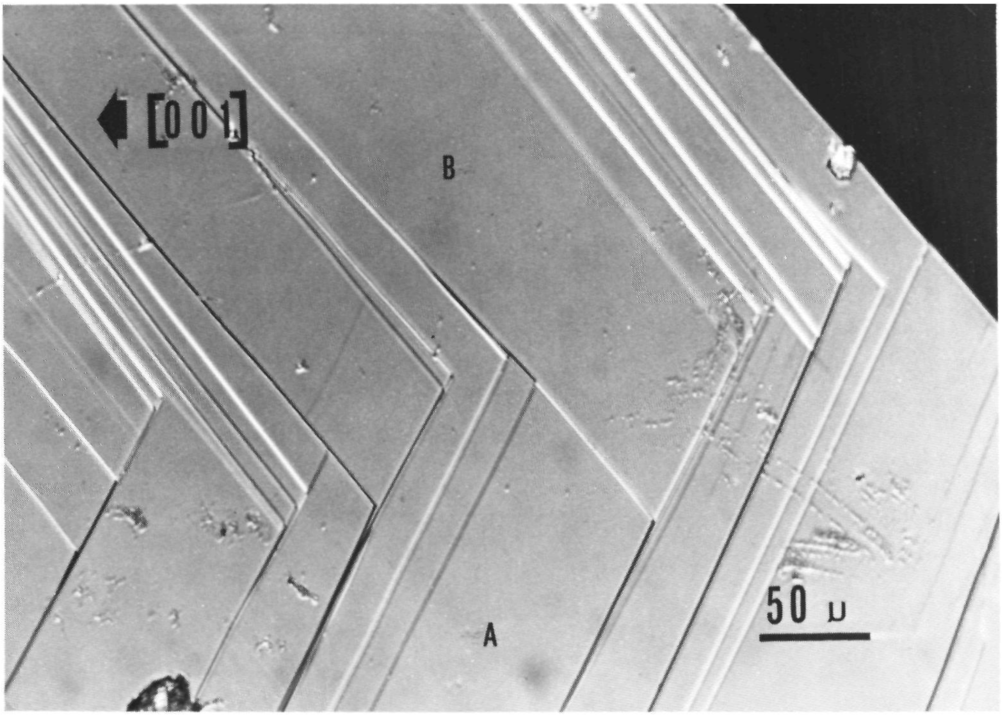

Fig.10. Pseudo-interlacing of macrosteps at the intersection points of growth steps of different orientations and heights (DIM).

point of intersection up to the step ahead, but now having a height equal to the difference in height of the two steps before intersection. This incompetence of the macrosteps to annihilate each other at the ridge of the hillock leads to the formation of a 'pseudo-interlacing' pattern as shown in figure 10. The origin of this 'pseudo-interlacing' is completely different from the commonly observed interlacing patterns of low steps (4,12,29).

3.4.3. Inclusion formation via macrostep overhangs

In some areas the macrosteps can reach such an extreme height that volume diffusion becomes more important, i.e. the supersaturation at the top of the macrostep will be higher than near its bottom. This can lead to the formation of step overhangs, as has been described extensively in a theoretical paper by Chernov and Budurov (30). When the overhang again comes in contact with the basal plane of the crystal an amount of solution is entrapped, which results in the formation of a liquid inclusion. This mechanism is very similar to that observed for the

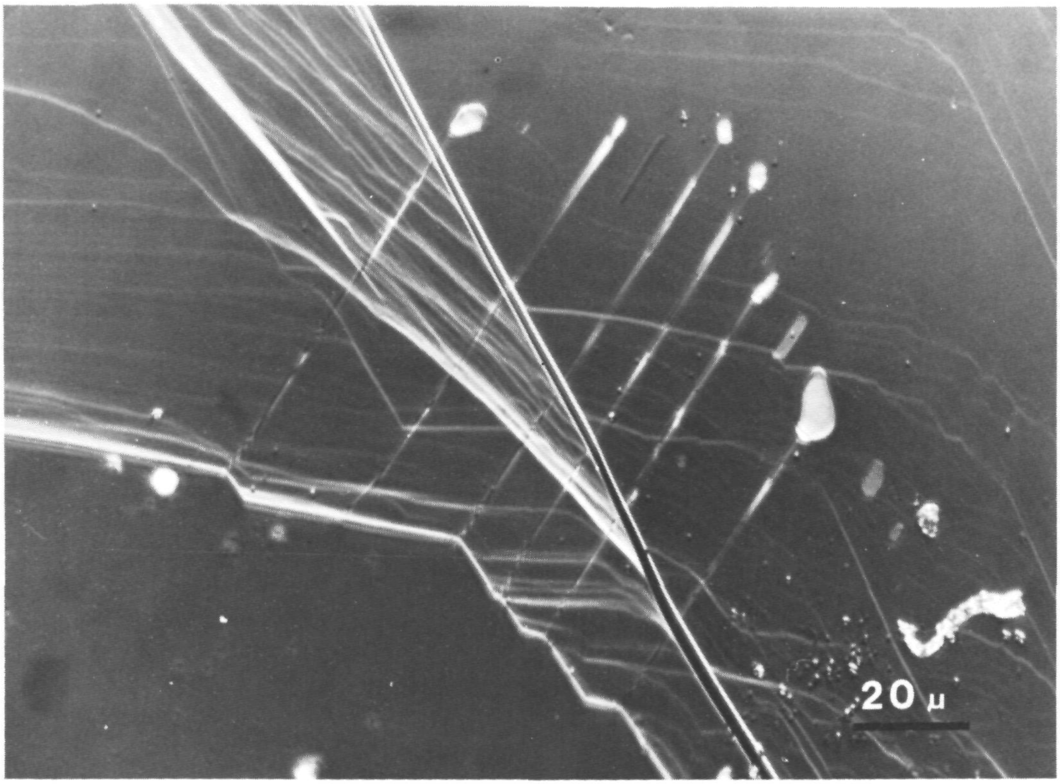

Fig.11. Formation of liquid inclusions via a step overhang mechanism at reentrant corners of the macrostep patterns.

formation of inclusions in stearic acid (31) and synthetic diamond (32). The occurrence of a reentrant corner in the macro-steps reinforces the formation of inclusions as can be seen in figure 11. Reasons for such a preferential inclusion formation at reentrant corners in macrostep patterns have been given elswhere (32).

3.4.4. Step acceleration near reentrant corners in the step patterns

Figure 12 shows 14 A high (estimated from the contrast) steps, a large number of them having a sharp reentrant corner in their patterns. It can clearly be seen that the step separation of step train T strongly increases in the neighbourhood of these reentrant corners, which points to an increase in step advancement velocity in this region. Such a step acceleration due to the presence of a rentrant corner in the step pattern has earlier been obser-

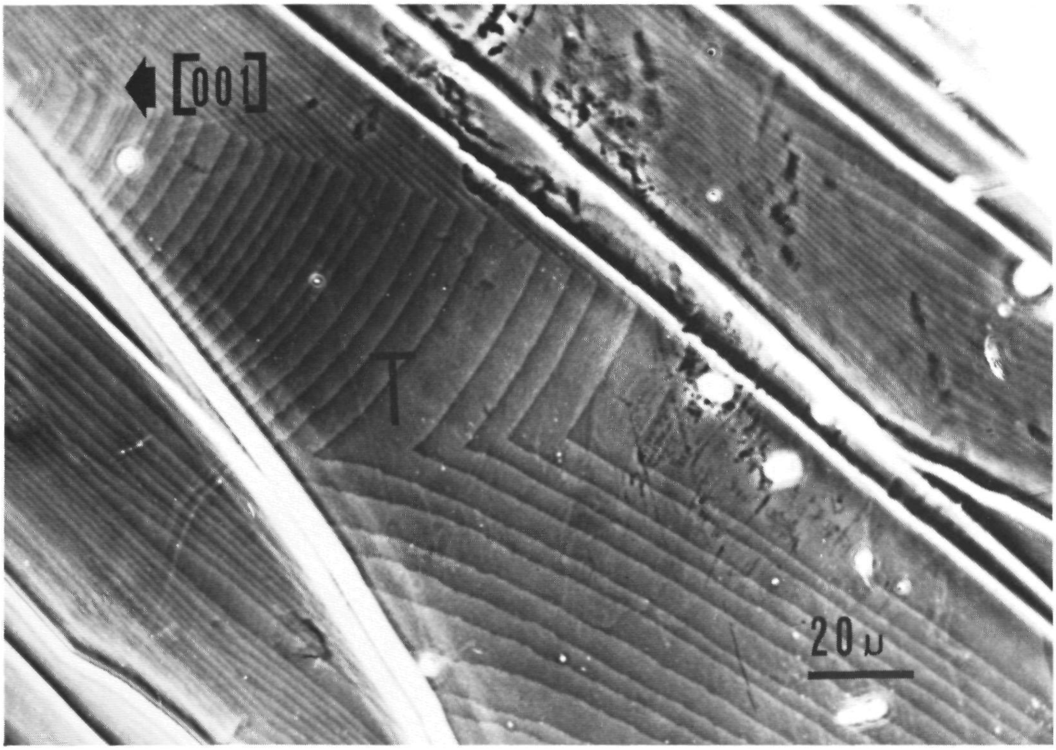

Fig.12. Increase in advancement rate of steps due to the presence of a reentrant corner in the step pattern (PCM).

ved for, among others, potash alum (12) and SiC (7) and is in agreement with the step flow model formulated by Burton, Cabrera and Frank (33). In this model it is derived that the step velocity strongly depends on the step curvature, in such a way that a step with a negative curvature, i.e. concave or bended 'inwards', is accelerated (34). Further the lateral anisotropy in step advancement rate may play an additional role.

3.4.5. Relative advancement rates of parallel steps of different heights

To compare the relative advancement rates of very low (unit lattice height) steps and macrosteps, a shallow hillock, located between very high steps was selected and photographed as shown in figure 13. From this and similar micrographs it can be deduced that the advancement velocities of the low and macro-steps are very similar. This is argued as follows:

Each time a macrostep passes a low shallow hillock, the surface area is cleaned, since the macrostep 'swallows' the hillock completely. Just after the high step has passed the growth centre, this dislocation outcrop again starts emitting new unit lattice height steps in, among others, the two symmetrically equivalent directions 1 and 2, indicated by arrows in figure 13. In this way a new hillock is formed. After some more time the situation presented in figure 13 is attained. Since the distance between the hillock centre and the macrostep is equal to the distance between the hillock centre and the, since the pass by of the macrostep, firstly emitted shallow step in the symmetrically equivalent direction 2, it can be inferred that the advancement rates of both steps have to be more or less equal.

The fact that the step velocity is not or only weakly related to the step height, permits the conclusion that the crystal growth process is not limited by volume or surface diffusion, otherwise higher steps would advance much slower than the lower ones. The only mechanisms that can account for the equivalence in advancement rates of

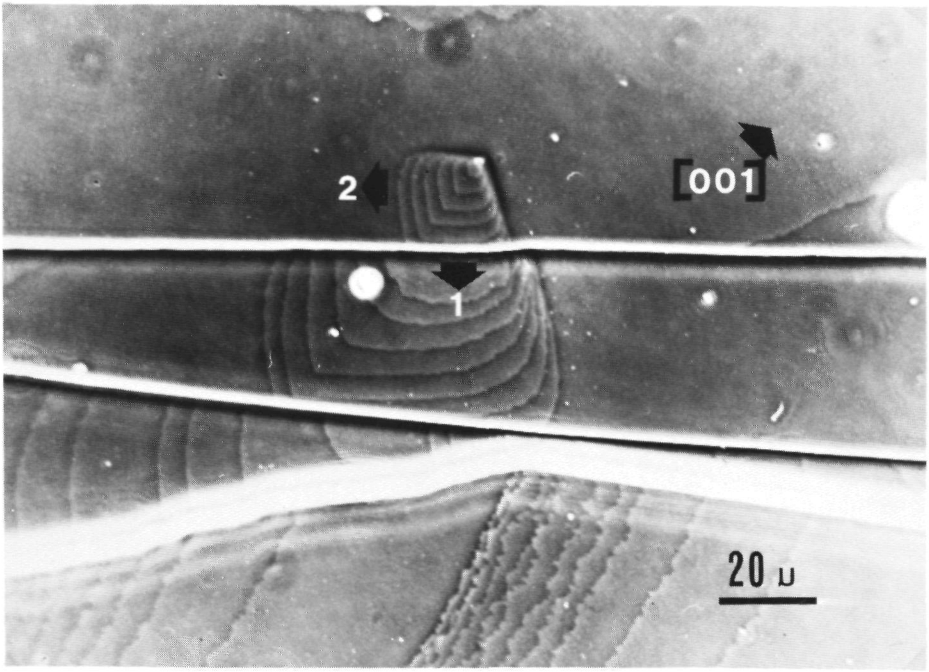

Fig.13. Shallow growth hillock made up of 14 A steps located between macrosteps, demonstrating the equivalence in advancement rate of lower unit lattice height and macrosteps (PCM).

low and high steps are:
(i) A direct integration of growth units from the liquid phase at the step positions as rate determining step in growth.
(ii) Step integration via surface diffusion, for which the incorperation of the first row of step site molecules at the growth steps is rate determining. When the growth units of this row are attached to the steps, the other atoms above or below this row are incorperated quickly, after which a new 'rate determining' first row has to be formed for further step propagation.

4. CONCLUSIONS

From the present detailed a posteriory microtopographic investigation of the {010} faces of potassium hydrogen phthalate, by means of highly sensitive optical interference and phase contrast microscopy, complemented with two-beam interferometry, the following can be inferred:

(i) On the {010} faces of KAP always two types of growth hillocks were found:

(a) 'Macroscopic' hillocks, dominating large surface areas and often even complete crystal faces. These elevations are related to dislocation bundle outcrops, i.e. consist of a group of cooperating spirals. The typical symmetric shape of the hillocks is in agreement with the two-dimensional point-group of the {010} faces. During running away from the growth centre, lower steps pile up to higher ones, forming very high steps near the periphery of the macroscopic hillocks.

(b) Shallow hillocks, frequently located between macrosteps originating from the macroscopic growth hillocks. These reflection symmetric hillocks, which are related to single dislocation outcrops, very probably are single growth spirals. The step height of the arms of these spirals amounts to 14 A, which is equivalent to one unit lattice height.

(ii) The advancement rates of very low and of very high steps are more or less equal to each other. This points to the hypothesis that the rate determining step in the growth process is the integration of growth units, directly coming from the solution phase, at the step positions or a special kind of step integration via surface diffusion.

The present work shows that it is quite possible to carry out a posteriory observations of unit lattice height steps on aqueous solution grown crystals: The preperative technique is based on a careful separation -via rinsing in hexane- of the crystals from the mother liquor. This implies that in future other aqueous solution grown crystals can be investigated by detailed surface microtopography, which is of major importance for both single crystal growth of, for instance, KDP, TGS and CsH_2PO_4 and bulk crystallization of NaCl, sugar, fertilizers and others.

ACKNOWLEDGEMENTS

The authors are indepted to Prof. Dr. P. Bennema and Prof. Dr. J. Bloem for critical reading of the manuscript.
W.J.P. van Enckevort acknowledges the financial support of the Netherlands Foundation for Pure Research, ZWO/SON.

REFERENCES

(1) F.C. Frank, Disc. Faraday Soc. 5 (1949) 48.

(2) R.B. Heimann, Auflösung von Kristallen, Tecnische Mineralogie, Vol.8 (Springer-Verlag, Wien, New-York, 1975).

(3) L.J. Griffin, Phil. Mag. 41 (1950) 196; 42 (1951) 775, 1337; 43 (1952) 651.

(4) S. Amelinckx and G. Strumane, in Silicon Carbide: A high Temperature Semiconductor, Proc. Conf. on Silicon Carbide, Boston, 1959, Eds. J.P. O'Connor and J. Smiltens, Pergamon, New York 1960, pp. 162-201.

(5) Ajit Ram Verma, Phil. Mag. 42 (1951) 1005.

(6) I. Sunagawa, Am. Mineral. 46 (1961) 1216.

(7) B. van der Hoek, J.P. van der Eerden and P. Bennema, J. Crystal Growth (1982) to be published.

(8) I. Sunagawa, K. Narita, P. Bennema and B. van der Hoek, J. Crystal Growth 42 (1977) 121.

(9) I. Sunagawa and P. Bennema, J. Crystal Growth 53 (1981) 490.

(10) M. Shimbo, J. Nishizawa and T. Terasaki, J. Crystal Growth 23 (1974) 267.

(11) K. Tsukamoto and B. v.d.Hoek, J. Crystal Growth 56 (1982) to be published.

(12) W.J.P. van Enckevort, P. Bennema and W.H. van der Linden, Z. Phys. Chemie (Neue Folge) 124 (1981) 171; Chapter II.

(13) I. Sunagawa and K. Tsukamoto, J. Crystal Growth 15 (1972) 73.

(14) K. Tsukamoto, private communication.

(15) W.J.P. van Enckevort and H. Klapper, J. Crystal Growth to be published.

(16) G. Böhm and K. Ulmer, Z. Angew. Phys. 29 (1970) 287.

(17) G. Böhm and K. Ulmer, J. Crystal Growth 10 (1971) 175.

(18) L.M. Belyaev, G.S. Belikova, A.B. Gil'varg and I.M. Sil'vestrova, Sov. Phys-Crystallography 14 (1970) 544.

(19) W.J.P. van Enckevort, R. Janssen-van Rosmalen and W.H. van der Linden, J. Crystal Growth 49 (1980) 502; Chapter IX.

(20) H. Komatsu in: Crystal Growth and Characterization, Eds. R. Ueda and J.B. Mullin (North Holland, Amsterdam, 1975) p. 333.

(21) International Tables for X-ray Crystallography, Vol I (Kinoch Press, Birmingham, 1969).

(22) Y. Okaya, Acta Cryst. 19 (1965) 879.

(23) S. Amelinckx in: Solid State Physics, Suppl. 6, "The Direct Observation of Dislocations", ed. F. Seitz and D. Turnbull (Academic Press, New York,1964) p.16.

(24) K. Sato, K. Yokoyama, H. Kouchi and M. Okada, Jap. J. Appl. Phys. 17 (9) (1978) 1483.

(25) W.J.P. van Enckevort and W.H. van der Linden, J. Crystal Growth 47 (1979) 196; Chapter I.

(26) S. Amelinckx, Phil. Mag. 1 (1956) 264.

(27) P. Bennema, J. van der Eerden, W.J.P. van Enckevort, B. van der Hoek and K. Tsukamoto, Phys. Stat. Solidi (a) 55 (1979) 403.

(28) W.J.P. van Enckevort and J. Odekerken, Phil. Mag. to be published; Chapter V.

(29) B. van der Hoek, J.P. van der Eerden and K. Tsukamoto, J. Crystal Growth to be published.

(30) A.A. Chernov and S.I. Budurov, Soviet Physics Crystallography 9 (1964) 309; Ibid. 9 (1965) 388.

(31) K. Sato, Japanese J. Appl. Phys. 19 (1980) 1257.

(32) W.J.P. van Enckevort and Liu Guang-zhao, J. Crystal Growth to be published; Chapter XX.

(33) W.K. Burton, N. Cabrera and F.C. Frank, Philos. Trans. R. Soc. London 243 (1951) 299.

(34) M. Ohara and R.C. Reid, Modeling Crystal Growth Rates from Solution, Prentice-Hall international series in the physical and chemical engineering sciences (Prentice-Hall, Englewood Cliffs, N.J., 1973).

CHAPTER VII:
IN SITU OBSERVATIONS OF THE GROWTH BEHAVIOUR OF {010} POTASSIUM HYDROGEN PHTHALATE

W.J.P. van Enckevort, B. van der Hoek
and L.A.M.J. Jetten

RIM Laboratory of Solid State Chemistry, Faculty of Science,
Catholic University, Toernooiveld, Nijmegen, The Netherlands

ABSTRACT

The surface morphologies of the {010} faces of potassium hydrogen phthalate crystals, growing in supersaturated aqueous solutions have been studied in situ by means of optical reflection microscopy, combined with analogue contrast amplification via a video system. Several phenomena were investigated by this method, namely: spiral growth via high (∿100 - 1500 A) and low steps (∿28 - 100 A), step acceleration near reentrant corners in step patterns, inclusion formation via step overhangs, etch pits and the occurrence of non-rotating spirals in the neighbourhood of "growing" spirals.

1. INTRODUCTION

During the last few years, several workers succeeded to observe very low (unit lattice height) growth steps on aqueous solution grown crystals like potash alum (1), KCl (2), $NiSO_4.6H_2O$ (3) and potassium hydrogen phthalate (4). The essential point to allow for these a posteriory observations of such low steps on this category of crystals, which was assumed to be impossible for a number of years ago, is a careful separation of the crystal from the mother liquor (1). However, the main disadvantage of such ex situ studies of crystal surfaces is, that only the step pattern at one given moment (namely just before the removal of the crystal from the solution) can be studied, whereas the development of the step patterns in dependence on time can give much more detailed information on the growth process.

Recently Tsukamoto (5) succeeded to observe 15 A steps on the {001} faces of CdI_2 crystals growing in an aqueous solution, by means of optical transmission microscopy, completed with analogue contrast amplification. Inspired by his results, it was attempted to do similar in situ observations for the {010} faces of potassium hydrogen phthalate (KAP) crystals. In the present study, however, optical reflection instead of transmission microscopy was applied.

The aim of the present paper is to summarize the first results of the in situ observations of growth step patterns on {010} KAP, which will form a basis for future, more extended, work on this topic.

2. EXPERIMENTAL

2.1. Crystal growth

The experiments were carried out in a flow system in order to keep both the supersaturation and the flow velocities of the solution, streaming around the crystal, as constant as possible. This flow system consists of a vessel and a heat exchanger, both being placed in a thermostat, a thermostated flow meter and the observation cell, through which elements the solution is circulated by means of a rotation pump. During the experiments the temperature was kept constant within 0.3 °C at a value between 25 and 35 °C.

The crystals for observation, which were grown by a temperature decrease method (4), were placed in the growth cell in such a way that the {010} faces were oriented perpendicular to the optical axis of the microscope used. The cell itself was provided with a "window" made of coated optical glass, to allow for in situ surface microtopography, without blurring the image too much.

2.2. Observation method

The {010} KAP faces growing in the cell were observed by means of an ordinary reflection microscope, using bright field illumination. However, in contrast to "common" microscopy in the present case the aperture diaphragm was closed as much as possible and placed slightly eccentrically with respect to the optical axis. By making use of this special kind of oblique bright field illumination the contrast of the image is strongly increased, so that phase objects, like steps can be revealed in a much better way at a light intensity sufficient for the use of a video system. The growth process is recorded on video tape by means of a video camera, which is connected with an analogue contrast amplifier in order to increase the image contrast to a large extent. In this way very weak contrasts are made visible on the monitor.

3. OBSERVATIONS AND DISCUSSIONS

3.1. Growth

Figure 1 shows a sequence of micrographs of a rotating

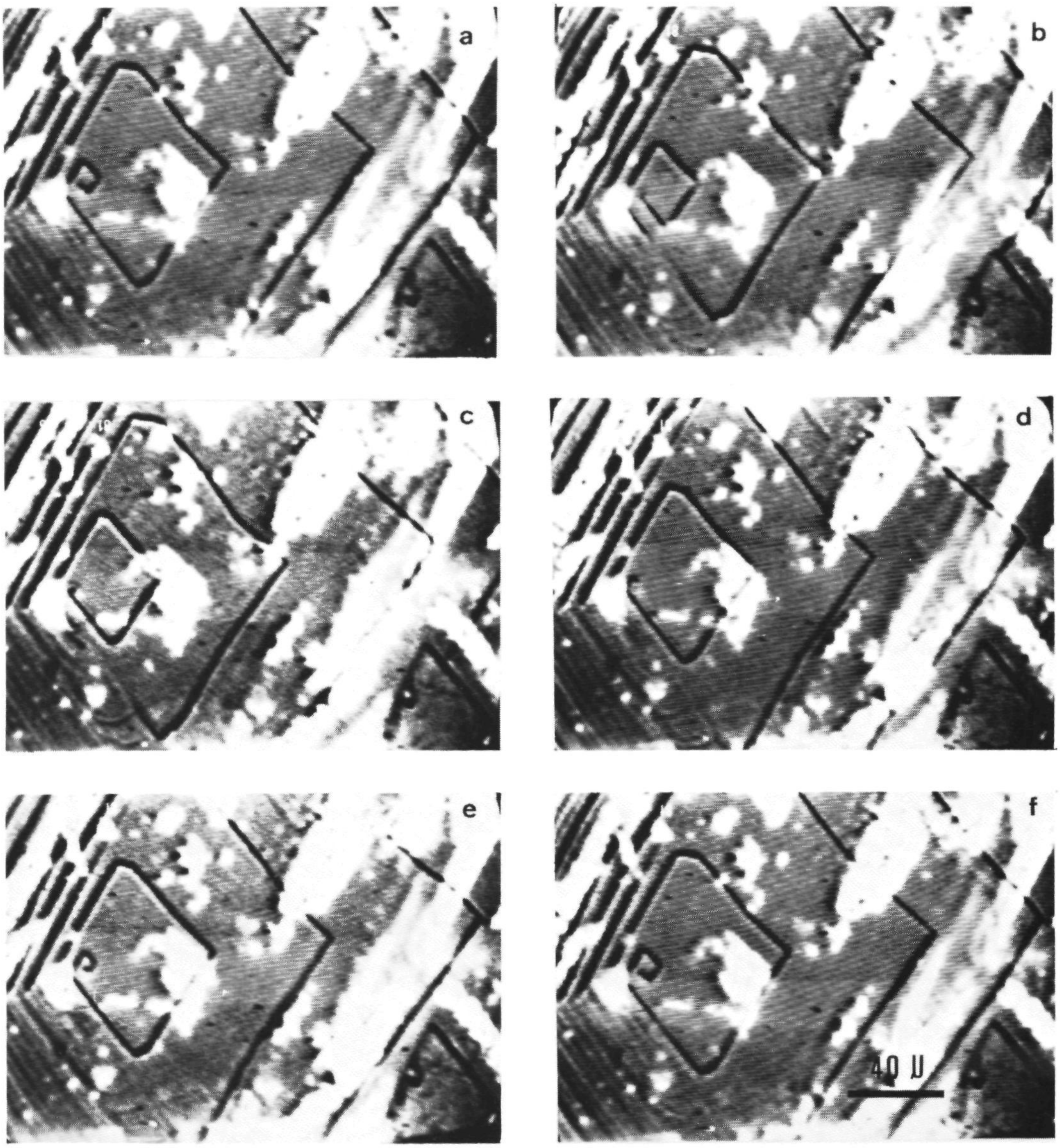

Fig.1. Rotating spiral with large step height, "growing" at moderate supersaturation: (a) t=0 sec.; (b) t=3 sec.; (c) t=6 sec.; (d) t=9 sec.; (e) t=10 sec.; (f) t=11 sec.

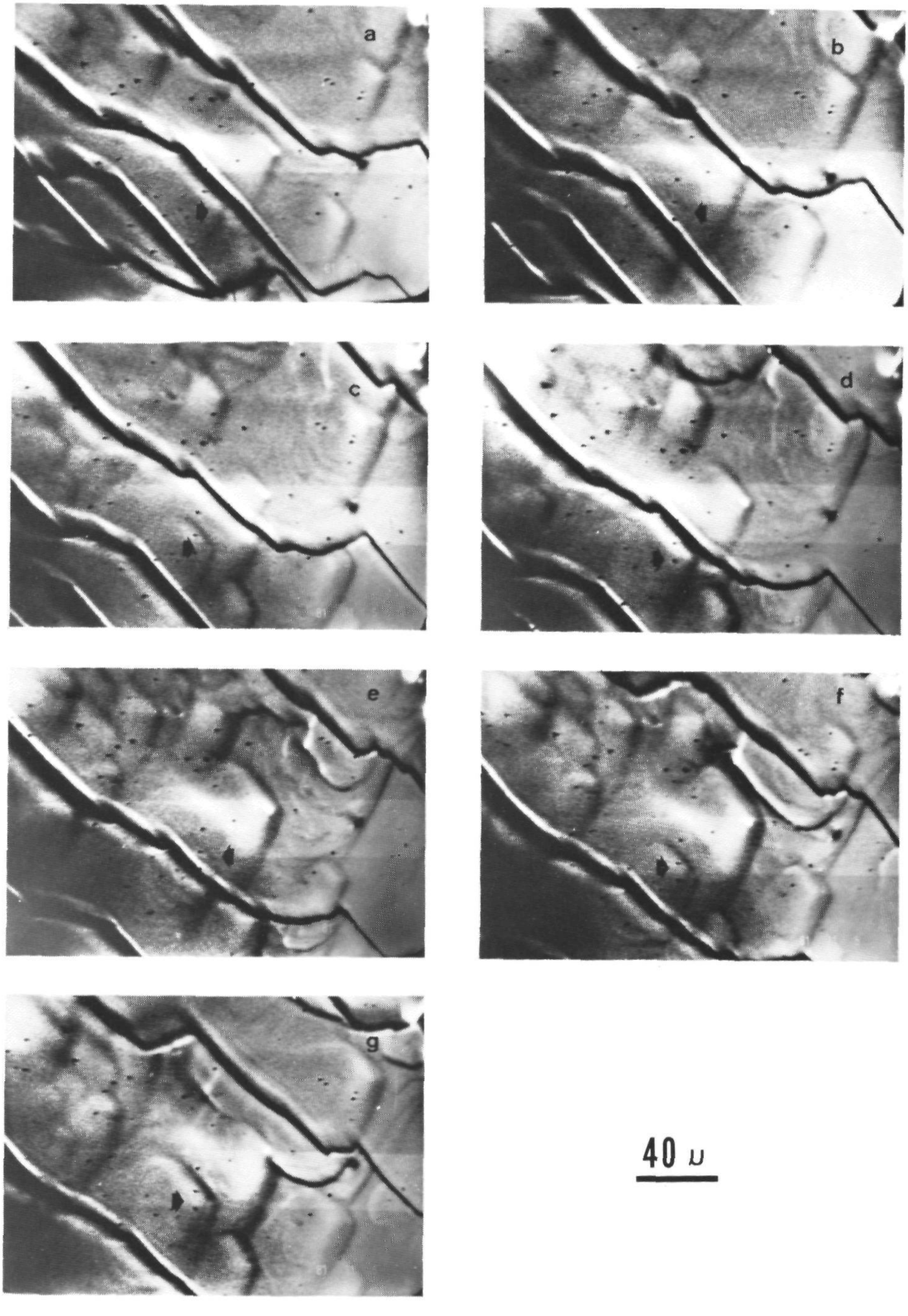

Fig.2. Shallow growth hillocks emerging between macrosteps. The time interval between successive photographs is 4.5 seconds.

macrospiral (4), with a step height of several hundred Angströms. The white spots on the video pictures are images of liquid inclusions just underneath the crystal surface. In this series of micrographs, in which the successive stages of one rotation of the macrospiral is shown, it can be seen that the development of the spiral centre is not stationary. This is caused by a large anisotropy in edge free energy and in advancement rate of the spiral steps.

Figure 2 presents a series of in situ video micrographs, showing macrosteps sweeping over a group of shallow hillocks. In a previous paper (4) it has been shown that these hillocks are single growth spirals with a step height of 14 A. Careful examination of figure 2 learns that these 14 A steps can not be observed by the in situ method, but some bunched steps, probably having a double or triple height (28 - 42 A) can indeed be identified. Another interesting phenomenon, which can be recognized from this figure is that each hillock "reincarnates" after having been "swallowed" by a passing macrostep (see for instance, the hillock indicated by the arrows). This reappearance of shallow hillocks can be understood from the fact that screw dislocations at the crystal surface persist after passing of a macrostep, which implies that they can again act as step sources, forming new growth hillocks.

In figure 3 the one to one correspondence between the

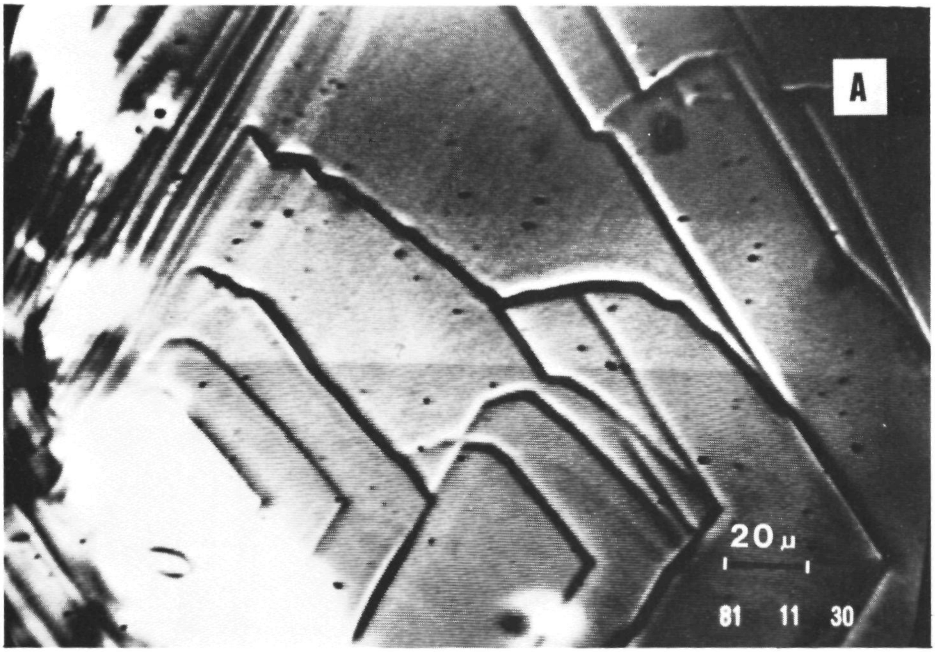

Fig.3. Comparison of the images obtained by in situ and ex situ microtopography. (a) In situ video micrograph of a macroscopic growth spiral.

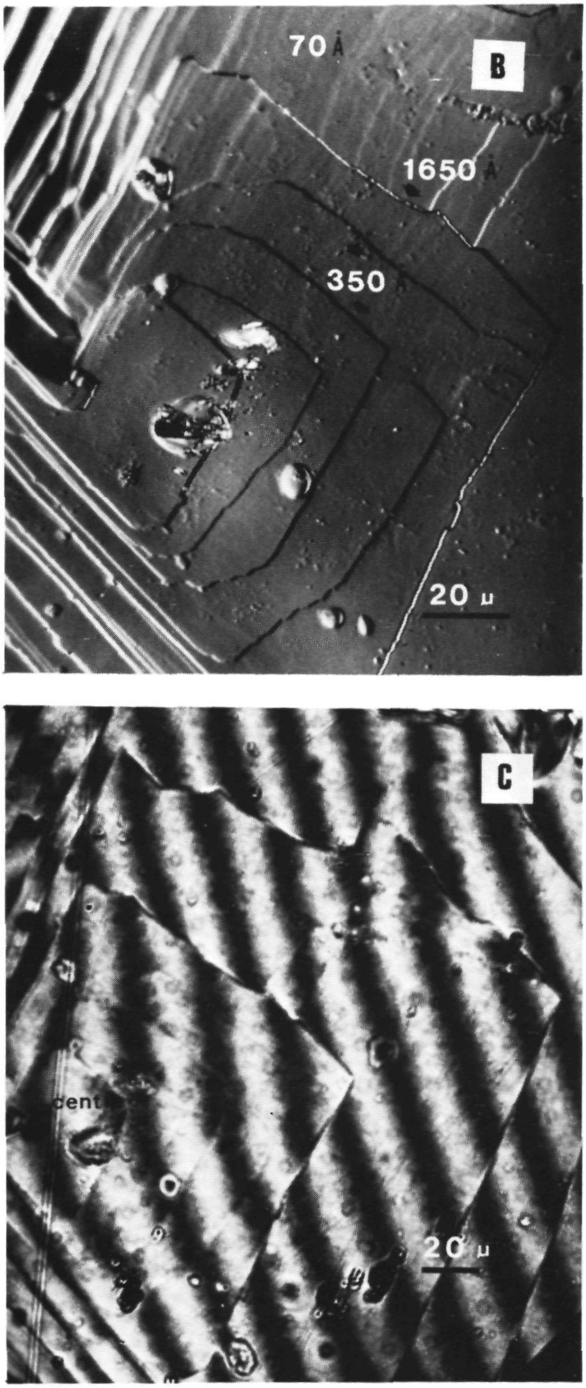

Fig.3 (continued). (b) Ex situ differential interference contrast micrograph of the same area as (a). (c) Two-beam interferogram of (b).

images obtained by in situ -video- surface topography (fig. 3a) and by ex situ surface microtopography, by means of a differential interference contrast microscope in the same way as described elswhere (4) (fig. 3b) can be seen. Comparison of the step heights, which were measured from the two-beam interferogram given in figure 3c, shows that the steps of 350 A and higher give a high contrast by the in situ method, whereas the lower 70 A steps are also clearly visible. A similar comparison of surface areas observed by the in situ method and a posteriory -ex situ- observations of exactly the same surface areas, confirmed that the unit lattice height (14 A) steps were not visible, but steps having a double or triple unit lattice height could be discerned by in situ microtopography as was suggested above.

Figure 4 shows the successive stages of the formation of an inclusion via a macrostep overhang mechanism. The generation of inclusions proceeds in the following manner (4,8). At a given moment a very high step becomes unstable, due to mass or heat transport limited growth, resulting in the formation of an overhang (indicated by an arrow in b), which can be recognized as a bright area, caused by internal reflections between the overhang and the basal plane. After some time the overhang comes in contact with the basal crystal surface, so that an amount of solution is entrapped and the liquid inclusion has been formed.

Figure 5 clearly demonstrates the occurrence of step acceleration due to the presence of a reentrant corner in the step pattern, which both holds for the lower and the higher steps. More details on this phenomenon were discussed in a previous paper (4).

3.2. Dissolution

In the case of undersaturated solutions etch pits were formed as shown in figure 6. Raising the temperature of a supersaturated solution, after observation of a growth spiral, until a considerable undersaturation is obtained, in general, results in the creation of such an etch pit at the spiral centre, which confirms the relation between growth hillocks, etch pits and dislocations mentioned in previous work (4).

Another interesting point is the formation of numerous smaller, flat bottomed etch pits, very probably due to nucleation at micro-inclusions or point defects. The sudden formation and extension of two flat bottomed pits (indicated by arrows), can be seen in figure 7.

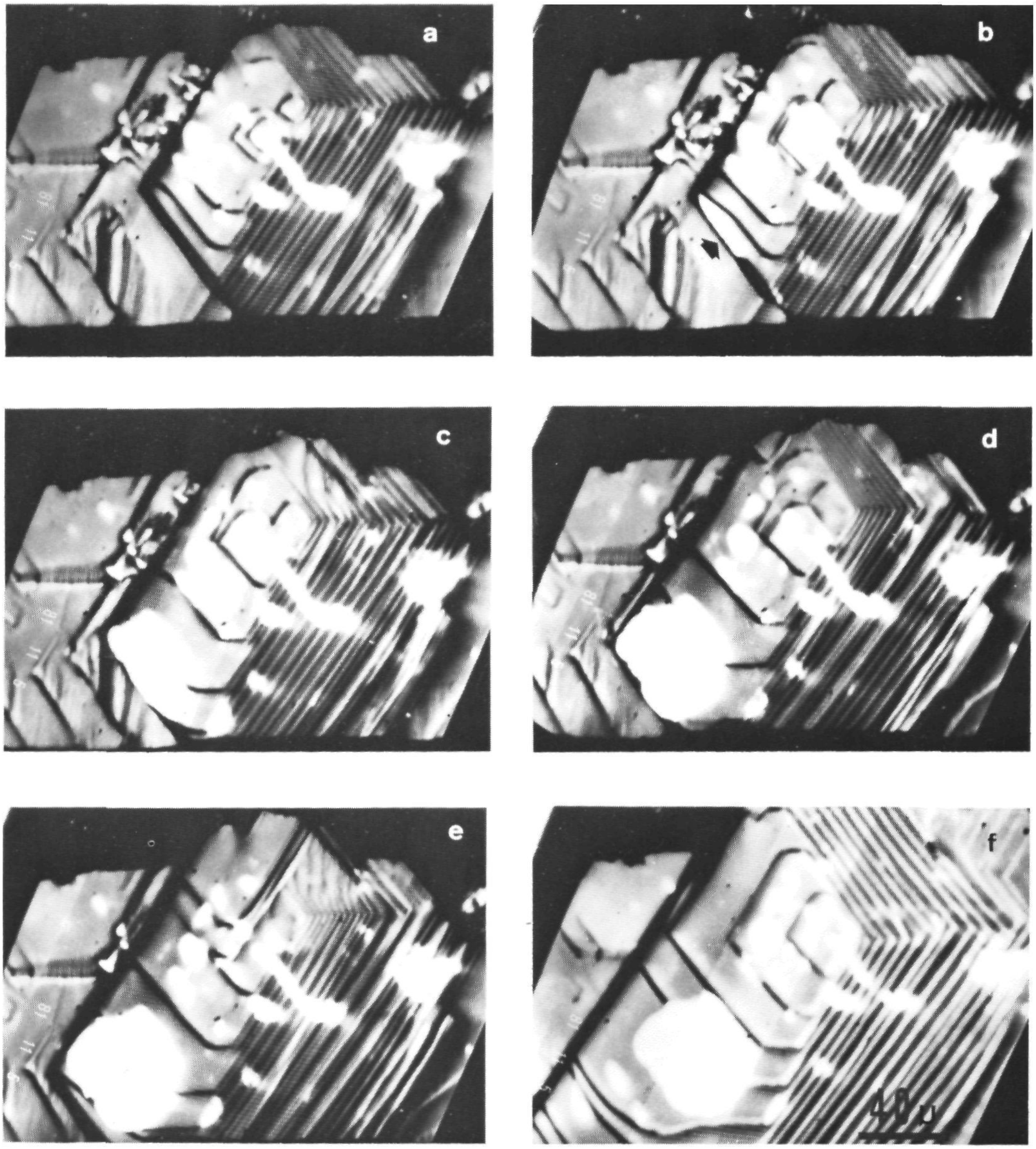

Fig.4. Successive stages of inclusion formation via a macrostep overhang mechanism: (a) t=0 sec.; (b) t=2 sec.; (c) t=20 sec.; (d) t=42 sec.; (e) t=60 sec.; (f) t≈2 min. The creation of the overhang indicated by an arrow starts in (b). The closure of the overhang occurs in (e).

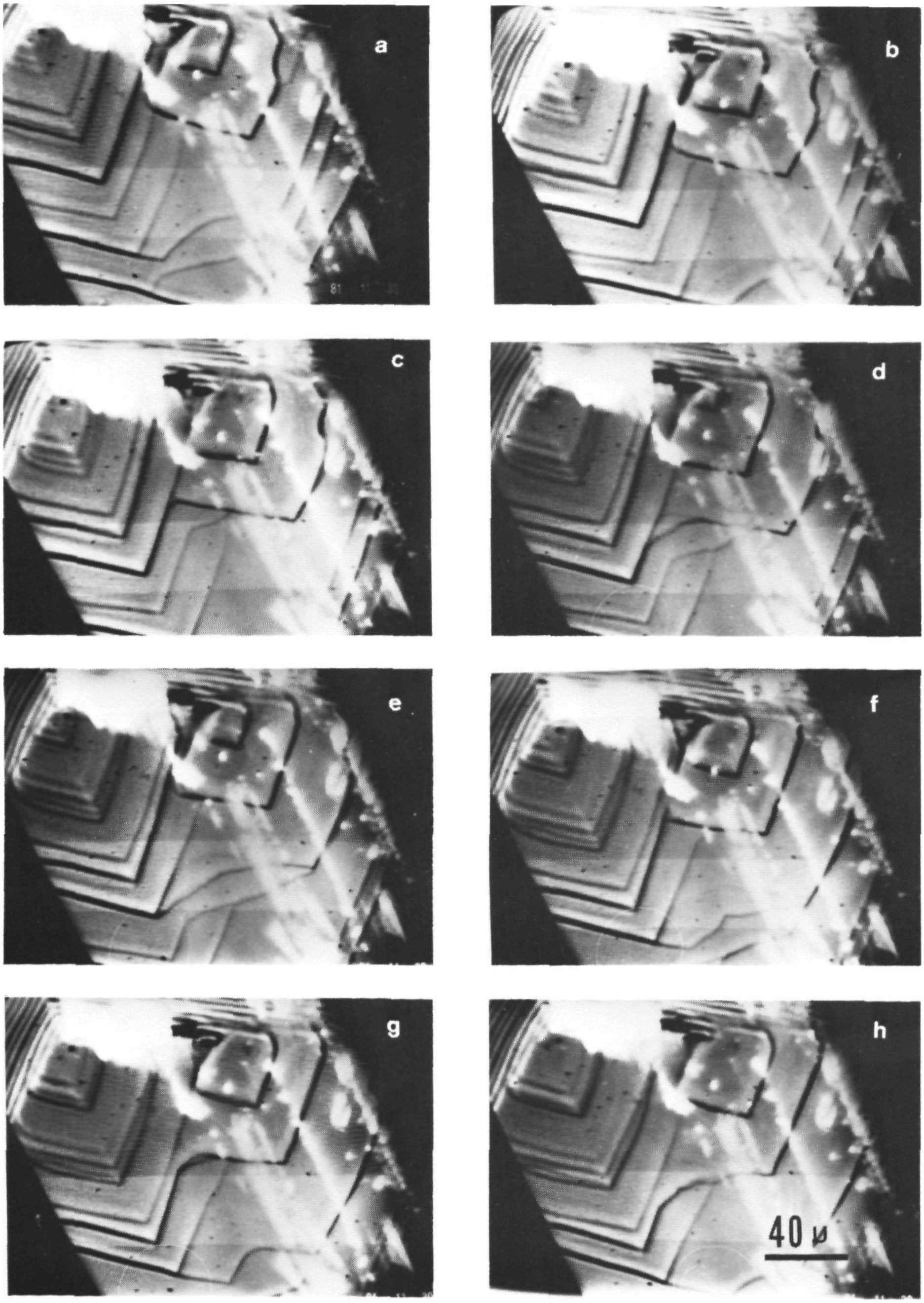

Fig.5. Step acceleration near a reentrant corner in the step pattern. The time interval between successive photographs is one second.

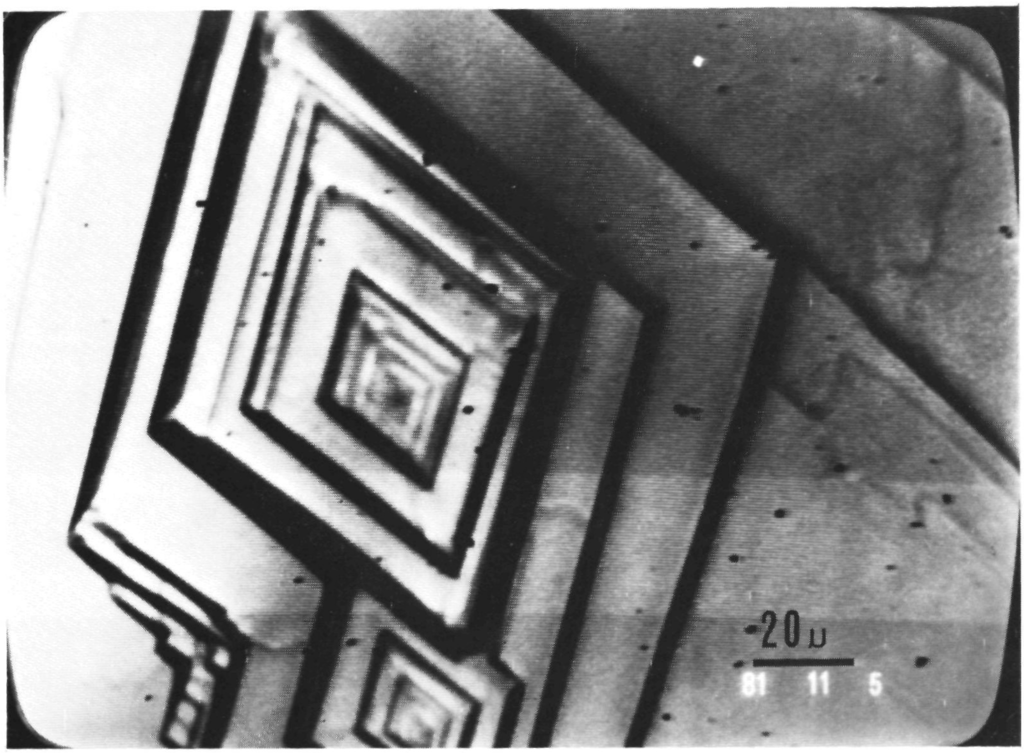

Fig.6. In situ surface microtopograph of a large, well developed etch pit.

3.3. Blocking of growth steps

A particularly intriguing phenomenon is the occurrence of a blocking of steps, for which a typical example is given in figure 8. The in situ micrographs 8a-c present a pair of cooperating macrospirals of equal sign, rotating at normal velocities in a fairly supersaturated solution. After taking these micrographs, the supersaturation was lowered, by increasing the temperature (9), to about equilibrium, so that the steps did not advance any more (fig. 8d). Finally the supersaturation was "turned" back by decreasing the temperature (9), to the original and even a higher level. Quite surprisingly the original step pattern did not move: the growth spiral was completely arrested in growth. Later on a step coming from elswhere overwhelmed this "frozen" spiral, after which a new "fresh" spiral was generated due to the presence of the dislocations that acted as centre of the former spiral (figs. 8e-h). Such a blocking of growth has been deduced earlier for {101} ADP (10), {110} (11) and {100} (12) potash alum from in situ growth rate measurements,

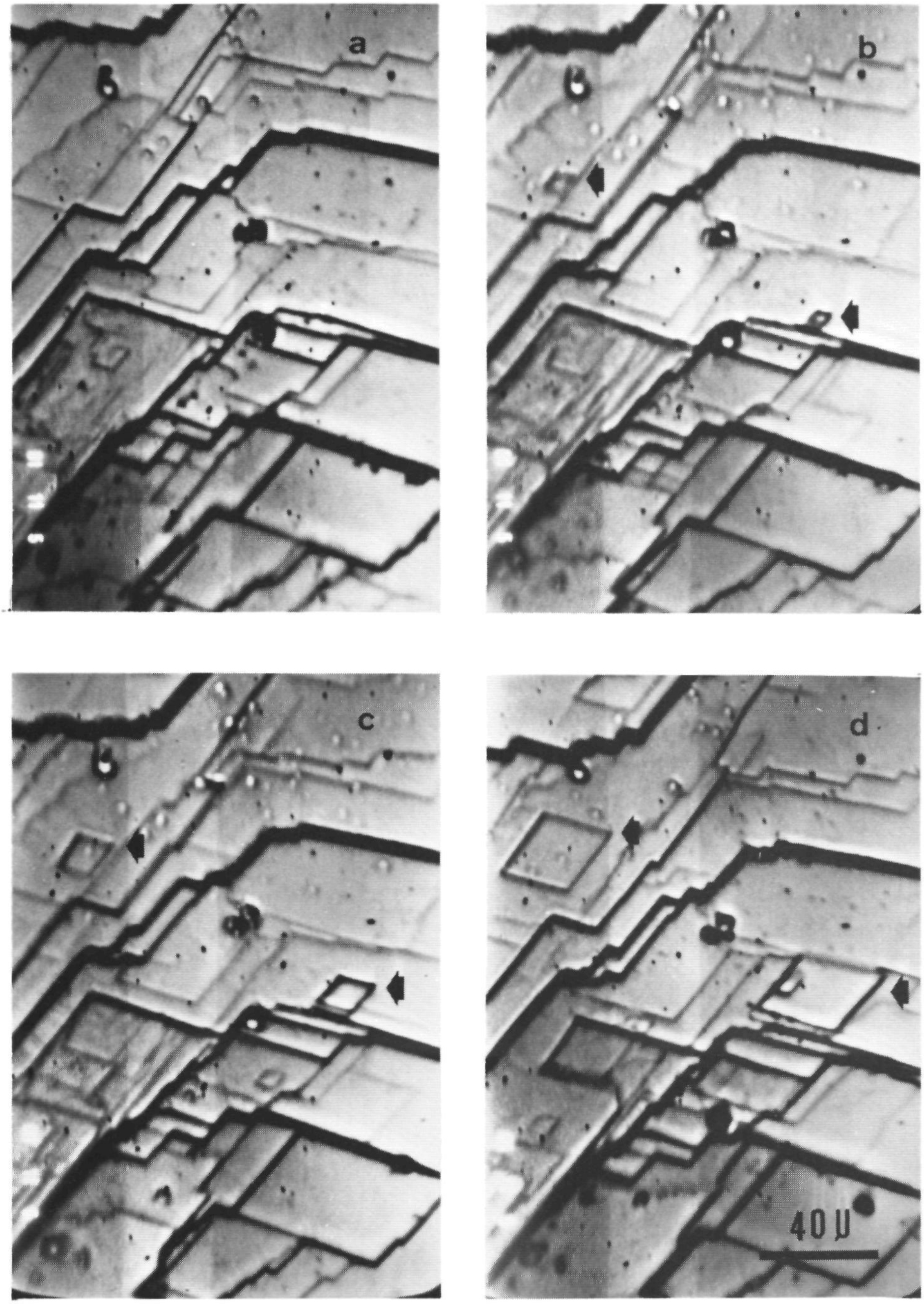

Fig.7. Successive stages of the development of flat bottomed etch pits nucleated at micro-inclusions or point defects: (a) t=0 sec.; (b) t=4 sec.; (c) t=8 sec.; (d) t= 16 sec.

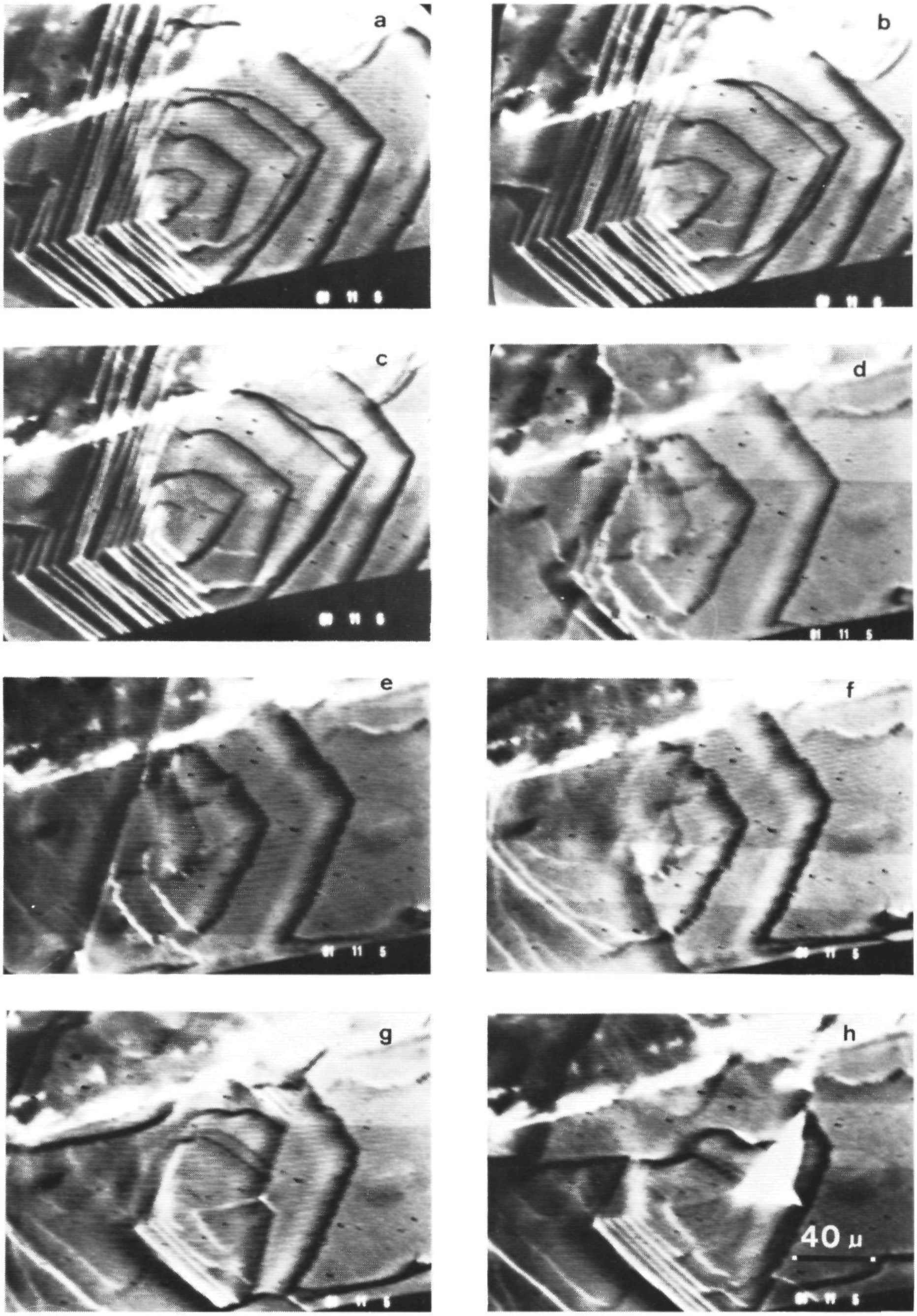
a
b
c
d
e
f
g
h
40 µ

← Fig.8. Blocking of steps:
(a)-(c) Rotating double spiral originating from two large dislocations with screw components of equal sign. $T-T_{eq} \approx -0.7\ ^{o}C$; time interval between successive photographs is 2 seconds. (d) Arrest in growth at very low supersaturation of the same spiral as in (a). $T \sim T_{eq}$.
(e)-(h) Standstill in growth of the same spiral as in (a), despite a large increase in supersaturation ($T-T_{eq}= -1.5^{o}C$). The "frozen" spiral is overwhelmed by steps coming from the left. In photographs g and h the spiral, covered by a "fresh" growth layer, starts to rotate again. Time interval between successive photographs is 5 seconds.

X-ray diffraction topography, stress birefringence microscopy and ex situ surface microtopography. However, in the present case the phenomenon has been observed directly.

This arrest in growth shows that yet unknown surface phenomena can play a decisive role in the crystal growth process, which implies that in crystal growth models more attention has to be paid to the specific configuration of the crystal-solution interface.

4. CONCLUSIONS

From in situ observations of the growth processes on {010} KAP it can, among others, be concluded that:
(i) Aside from high steps (∿100 - 2500 A) it is also possible to observe very low steps (∿28 - 100 A) on the surfaces of crystals, during growth in supersaturated solutions.
(ii) Dislocation outcrops act as spiral sources.
(iii) A decrease followed by a re-increase of supersaturation causes a complete standstill of steps, despite the presence a considerable supersaturation. On neighbouring areas of the same crystal face growth can proceed in a normal manner.

The quite unexpected fact that quite low steps (two or three unit lattice translations in height) can be observed on crystals growing in aqueous solutions by a relatively simple experimental set up, makes it probable that unit lattice height steps can be observed in future by improving the observation method. This improvement can be achieved by using a more sophisticated optical system or by processing the video image with the aid of computers. Such in situ observations of the lowest possible steps on growing crystals is of major importance, because then a direct, quantitative and unambiguous verification of crystal growth theories by experiments can be carried out. This may lead to new ideas in the science of crystal growth.

ACKNOWLEDGEMENTS

The authors are grateful to Ing. J. van Kessel for experimental contributions and to Prof. P. Bennema and Prof. J. Bloem for critical reading of the manuscript.

Two of us (W.J.P. van Enckevort and B. van der Hoek) acknowledge the support of the Netherlands Foundation for Pure Research, ZWO/SON.

REFERENCES

(1) W.J.P. van Enckevort, P. Bennema and W.H. van der Linden, Z. Phys. Chemie (Neue Folge) 124 (1981) 171; Chapter II.

(2) I. Sunagawa and K. Tsukamoto, J. Crystal Growth 15 (1972) 73.

(3) W.J.P. van Enckevort and H. Klapper, J. Crystal Growth to be published.

(4) W.J.P. van Enckevort and L.A.M.J. Jetten, J. Crystal Growth to be published; Chapter VI.

(5) K. Tsukamoto, private communication.

(6) H. Komatsu, in: Crystal Growth and Characterization, Proc. ISSCG-2 Spring School, Japan, 1974, Eds. R. Ueda and J.B. Mullin (North-Holland, Amsterdam, 1975) p.333.

(7) H. Beyer, Theory und Praxis der Interferenzmikroskopie (Akad. Verlagsgeselschaft Geest & Portig, Leipzig, 1974).

(8) A.A. Chernov and S.I. Budurov, Soviet Physics Crystallography 9 (1964) 309; Ibid. 9 (1965) 388.

(9) See for instance: P. Bennema, Thesis, Technical University of Delft, 1965.

(10) A.A. Chernov, I.L. Smolski, V.F. Parvov, Yu.G. Kuznetsov and V.N. Rozhanskii, Sov. Phys. Dokl. 24 (1979) 760.

(11) W.J.P. van Enckevort, H.J. Human and W.H. van der Linden, J. Crystal Growth to be published; Chapter III.

(12) H.J. Human and W.J.P. van Enckevort, J. Crystal Growth to be published; Chapter IV.

POTASSIUM DIHYDROGEN PHOSPHATE

Journal of Crystal Growth 49 (1980) 502–514
© North-Holland Publishing Company

CHAPTER VIII:
EVIDENCE FOR SPIRAL GROWTH ON THE PYRAMIDAL FACES OF KDP AND ADP SINGLE CRYSTALS

W.J.P. VAN ENCKEVORT, R. JANSSEN-VAN ROSMALEN * and W.H. VAN DER LINDEN
RIM Laboratory of Solid State Chemistry, Faculty of Science, Catholic University, Toernooiveld, Nijmegen, The Netherlands

Received 23 November 1979; manuscript received in final form 5 January 1980

Microscopic observations of the pyramidal {101} faces of KDP (KH_2PO_4) and ADP ($NH_4H_2PO_4$) single crystals grown from aqueous solutions revealed that three different types of growth features are possible: growth hillocks, cooperating growth spirals with macro step heights of a few hundreds Ångstroms and nucleation. From the correspondence between the locations of the growth hillocks and the etch pits formed after slightly dissolving the crystal in water, the growth hillocks could be identified as growth spirals, mostly originating from single dislocations. The growth spirals consisting of macro steps could be related to dislocation bundles. These bundles are often formed due to lattice closure errors after the formation of a liquid inclusion. Some typical phenomena as pseudo eccentricity of the growth spirals, step retardation due to strain fields and rhythmical bunching have been observed. In the case of highly perfect KDP crystals with hardly no dislocations ending on the {101} faces, crystal growth is governed by a nucleation mechanism.

1. Introduction

In spite of the large amount of interest for the properties of KDP and ADP single crystals in the last few decennia, only a very few papers describe the surface topography of the {101} faces [1]. The morphological features of both KDP and ADP crystals are given in fig. 1b.

Up to now there is hardly any evidence for the occurrence of growth spirals on these {101} faces and most papers speculate about growth mechanisms in which screw dislocations do not play any role [2]; in that case they assume a nucleation mechanism [3] or a situation where the growth layers on the {101} faces originate from the layers on the {100} faces [1,3].

Three indirect indications for the possibility of spiral growth on {101} KDP or ADP have been reported in literature:

(i) Belouet et al. [4] who reported that in general the growth rate of the {101} faces is higher just after the beginning of the growth than when the growth front is far away from the seed. This could be explained by the decrease of the dislocation outcrop density at the pyramidal faces, when crystal growth proceeds. This observation has been confirmed during our own crystal growth experiments.

(ii) Janssen-van Rosmalen et al. [5,6] reported a linear dependence between the growth rate of the {101} faces of KDP and the interface supersaturation, by means of a rotating disc technique. This observation suggests a growth mechanism dominated by many dislocations in a group of cooperating spirals, which give rise to a second linear law [7].

(iii) Davey and Mullin [8] who studied the growth kinetics of the {101} faces of ADP. They could interpret the growth curve in terms of a modified version [9] of the step model developed by Burton, Cabrera and Frank [10].

The present work describes an extended surface microtopographic study of the {101} surfaces of KDP and ADP single crystals in order to get direct evidence for the mechanisms governing the growth of this particular face.

Contrary to earlier work on this topic by Torgesen and Jackson [1], where the crystals have been observed in the solution using ordinary reflection microscopy, in this study – after removal of the crystals from the solution – the far more sensitive reflection

---

* Present address: Koninklijke / Shell Exploratie en Produktie Laboratorium, Rijswijk (Z.H.), The Netherlands.

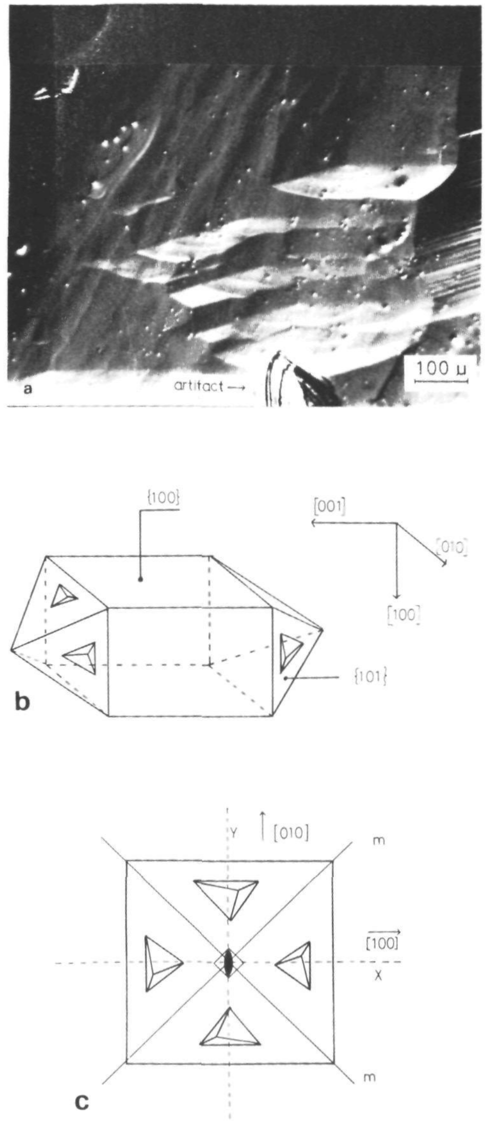

Fig. 1. (a) Typical growth hillock pattern on the {101} surface of ADP after growth from the aqueous solution. (b) Relation between the orientations of the growth hillocks located on the {101} faces and the external morphology of the crystal. (c) Relative orientation of the asymmetric growth hillocks in relation with the point group symmetry $\bar{4}2$ m of the KDP and ADP crystals.

differential interference contrast microscopy, combined with some other techniques has been applied in order to reveal very low inclinations and steps on the surfaces.

2. Experimental

Large (about 3 × 3 × 10 cm^3) KDP crystals were grown in a three-vessel system of the Walker-Kohman type [11] in exactly the same way as described in previous work [5,12]. The bulk supersaturation applied during crystal growth was fixed at 4.2%, whereas the temperature was kept at 29.50°C during all crystal growth experiments. However, the smaller (about 1 × 1 × 3 cm^3) KDP and ADP crystals were obtained by using a temperature decrease method in the following way: Seed crystals ((001) slices taken from previous crystals) mounted on a plastic rod were placed in a thermostated (±0.01°C) and stirred saturated aqueous solution, which was cooled down at a rate of 0.2°C per 24 h. After a period of about ten days a well developed crystal, suitable for surface microtopography could be obtained. In this case of crystal growth using the temperature decrease method the supersaturation was not very well known.

Prior to the growth phenomena on the surfaces being observed, the crystal was quickly taken out of the supersaturated solution and dipped for a moment into n-hexane having the same temperature as the solution. Subsequently adhering n-hexane was removed with a piece of blotting paper. This procedure is based on the following: after removal of the crystal from the supersaturated solution, its surface is covered with a thin solution film, which very quickly contracts to some localized droplets, as a result of a reduction in surface energy.

Evaporation of the adhering solution film would lead to artifacts caused by a sudden increase in growth rate. The n-hexane replaces the solution film, since it is not miscible with water, and at the same time it prevents both cooling down of the surface and evaporation of the adhiring solution film. In this way clean areas between the droplets are formed which are suitable for microtopography.

Finally, the crystal faces were coated with a thin layer of gold or silver in order to increase the reflectivity of the surfaces, necessary for getting a high sensitivity in the application of the reflection differential interference contrast microscopic technique [14]. The gilding or silvering was carried out carefully, using an ordinary sputter coating unit for scanning electron microscopy combined with a water cooled specimen holder and an electron deflection accessory.

This method of coating did not lead to corrosion or other artifacts on the crystal surfaces visible by means of interference contrast microscopy.

Etching of the {101} surfaces for obtaining an etch pit pattern was carried out by dipping the crystal for a few seconds in deionized water or by wiping gently the crystal surface with a wetted paper tissue. In the case of silvered or gilded surfaces, during etching the thin coating layer was removed immediately, so it was not necessary to do this beforehand.

Polishing of the {101} surfaces was carried out using a soft felty cloth pasted on a metal disk and wetted with a water–alcohol mixture.

Observation was carried out using an optical reflection differential interference contrast microscope combined with high contrast photographic emulsions in order to reveal very low contrasts.

Step height and inclination measurements have been performed with an optical microscope fitted with a two beam interferometer using a monochromatic sodium light source ($\lambda = 5892$ Å).

3. Observations and discussion

3.1. Growth hillocks on {101} KDP and ADP

3.1.1. General features

Fig. 1a shows a typical growth hillock pattern on a {101} face of ADP; similar surface features were also observed on the {101} faces of KDP. The occurrence of the growth hillocks on the pyramidal faces was independent of the amount of tapering [15] of the prismatic faces. The orientation of these triangular hillocks with respect to the external crystal faces, as they have been observed are indicated in fig. 1b. The peculiar asymmetry of these hillocks can easily be understood, by keeping in mind that for the point-group $\bar{4}2m$ in which KDP and ADP crystallize [16] the {101} faces have no symmetry. Also the relation between the orientations of the asymmetric growth hillocks on the different {101} faces is in accordance to the point-group symmetry as shown in fig. 1c. In order to prove that the growth hillocks are growth spirals by relating the hillocks to dislocation etch pits in a similar way as described in a previous work on potash alum [13], it was necessary to investigate the properties of the pits formed after etching of the {101} faces.

3.1.3. The relation between the occurrence of etch pits on the pyramidal faces and the dislocation outcrops

Fig. 2 is a photograph of some etch pits on a {101} face of KDP formed after slight dissolution in water. The triangular etch pits show the same typical asymmetric forms as the growth hillocks, the only difference is that now they are 180° rotated with respect to the orientations of the hillocks. A similar 180° rotation of triangular etch pits with respect to the orientations of the growth hillocks has both been observed on the {111} faces of potash alum [13] and on the {111} faces of crystals having a diamond lattice [17]. The relation between the orientations of the asymmetric pits on the different {101} faces is again governed by the point-group symmetry $\bar{4}2m$ of the crystals.

In order to clearify the origin of the etch pits an alternating etching and polishing technique as described in a previous work [13] has been applied. The result is shown in fig. 3. Fig. 3a shows a pit pattern formed after etching in water of {101} KDP.

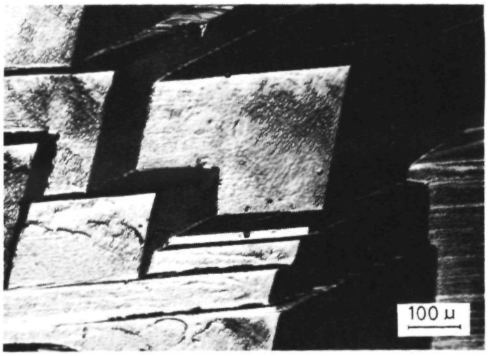

Fig. 2. Typical etch pit pattern on {101} KDP formed after slight dissolution in water. The etch pits are 180° rotated with respect to the growth hillocks as shown in fig. 1.

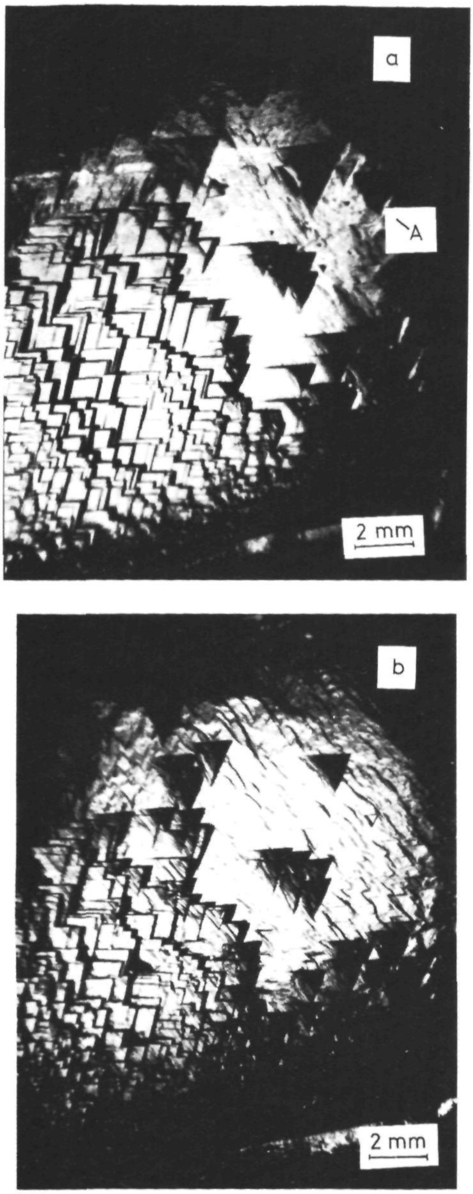

Fig. 3. Relation between etch pits and dislocations: (a) Etch pit pattern on {101} KDP after slightly etching in water. (b) Etch pit pattern after polishing and reetching of the same area as (a).

Fig. 3b shows the same area after polishing (during which procedure so much material was removed that the original etch pit pattern was no longer visible) and reetching. It can clearly be seen that after polishing and reetching the etch pit pattern did not change; obviously the pits are related to line defects, i.e. dislocation outcrops at the surface. By repeating the polish and re-etch procedure as described above it is possible to trace back the paths of the dislocation lines in the crystal. A rather annoying problem using this method is, that due to the slight rounding off near the edges of the crystal face many pits near the edges do not reappear after polishing and etching (for instance etch pit A in fig. 3).

Similar pits on the {101} faces of ADP, formed after slight dissolution in water have been reported by Gülzow et al. [18], who also related these pits to line defects, the so called "primäre Störungen" originating from the seed crystal and propagating in the crystal perpendicularly to the {101} growth faces.

The paths of these primary distortions in ADP as described in their work is very similar to the orientations of most of the dislocation lines observed by means of X-ray diffraction topography in ADP [2] and KDP [2,4,19,20]. So these primary distortions can safely be identified as dislocation lines.

Now it can be concluded that the pits on {101} KDP and ADP formed after etching in water are dislocation etch pits. This conclusion is strongly confirmed by the occurrence of extended rows of etch pits on some crystal faces, which could be understood by relating them to low angle grain boundaries [13,21].

3.1.3. The relation between growth hillocks and dislocation outcrops; evidence for spiral growth

The relation between the locations of the growth hillock centers and the sites of the bottoms of the pits formed after etching is demonstrated in fig. 4. Fig. 4a shows a growth hillock pattern on a {101} face of KDP. Fig. 4b gives the same surface area after application of a slight etch. There is no doubt that etch pits are formed exactly at the locations of the growth hillocks. For all the experiments carried out it appeared that every growth hillock without any exception became an etch pit after dissolution. Because the pits are related to dislocation outcrops, it can be concluded that the centers of the growth

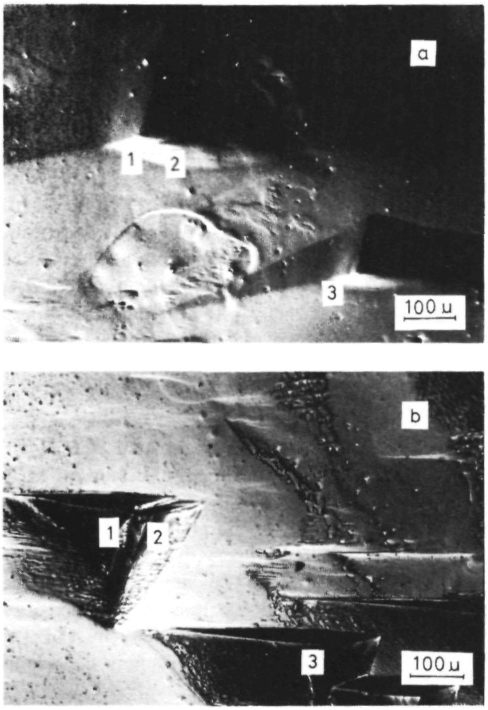

Fig. 4. Relation between growth hillocks and etch pits on the {101} surface of KDP: (a) Hillock pattern on a {101} face formed after growth from the aqueous solution. (b) Etch pit pattern on the same area as (a), formed after slight dissolution in water. The numbers indicate the corresponding pairs of hillocks and pits.

hillocks fall together with dislocation outcrops at the surface. So these elevations are spiral hillocks and crystal growth takes place according to a spiral growth mechanism. Also numerous additional etch pits, not related to a hillock could be observed. Probably these pits originate from edge dislocations or from dislocations containing a different screw component leading to slowly growing spirals, overwhelmed by the growth layers coming from dominating spirals.

The following arguments can be given for the fact that most of these spirals correspond to single dislocations:

(i) After etching of most of the growth hillocks one single etch pit can be seen at the locations of the centres of these hillocks (fig. 4).

(ii) The number of narrow dislocation bundles as has been observed by means of X-ray topography [4,19] is a few orders of magnitude lower than the number of growth hillocks on the {110} crystal surfaces. This only holds when no dominating cooperating macro spirals (which will be treated in detail in a following section) occur.

(iii) The inclinations of the various growth hillocks do not differ too much among themselves. However, when they originate from dislocation bundles a wide variaty in inclination is to be expected [29].

Other evidence for the spiral growth mechanism on the {101} faces of KDP and ADP is given by the following features:

(i) Just after beginning of crystal growth the growth hillock density on the pyramidal faces is in general higher than when the growth front is far away from the seed. This fact is consistent with the observation by Belouet et al. [4] that the dislocation outcrop density on {101} KDP and the growth rate of these faces decrease when crystal growth proceeds.

(ii) From X-ray topographs it could be concluded that for {101} KDP, crystal faces with higher dislocation outcrop densities grow faster [19].

(iii) On {101} KDP many macroscopic growth spirals could be observed as will be treated in a subsequent section.

3.1.4. The morphology of the growth hillocks and etch pits

The inclinations of the side faces of both growth hillocks and etch pits have been measured by means of two-beam interferometry, in order to verify whether these hillocks and pits are limited by F-faces or by – vicinal – S-faces. For the growth hillocks typical values for the inclinations of the three different types of side faces are: 0.07°, 0.20° and 0.4° for a supersaturation of 4.2%, but these can vary to a large extent depending on the growth conditions. On the other hand, the inclinations of the etch pits are somewhat higher, namely about 1.5°, 4.5° and 9° for the three different side faces. All the observed side faces do not belong to the morphological faces (i.e. are no F-faces) as has been deduced by Hartman [23] but are vicinal S-faces. Hence, growth via hillocks or etching via pits can be described in terms of

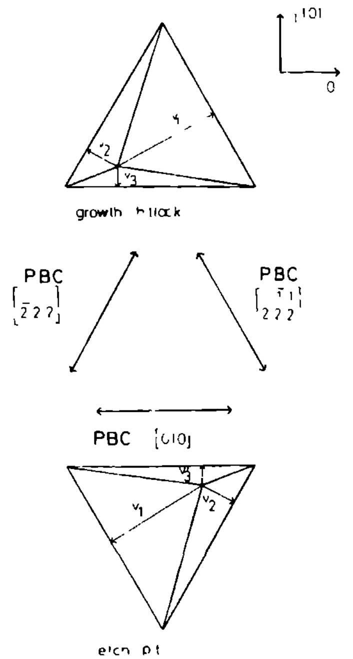

Fig 5 Relation between the morphology of both the growth hillocks and the etch pits on the {101} faces of KDP or ADP and the orientations of the various PBC's in the {101} plane

steps (having the same orientations as the edges of the hillocks or pits) originating from the growth or dissolution centres, running parallel to the lattice vectors $\langle\frac{1}{2}\frac{1}{2}\frac{1}{2}\rangle$ and $\langle 100\rangle$ as can be seen from fig 5.

Since in terms of the morphological PBC method on an F face steps run parallel to the periodic bond chain (PBC) directions [22], the step orientations as mentioned above are in agreement with the $\langle\frac{1}{2}\frac{1}{2}\frac{1}{2}\rangle$ and $\langle 100\rangle$ PBC's on the {011} F faces as deduced by Hartman [23] for the case of KDP as well as for the isostructural ADP

The asymmetry of both the etch pits and the spiral hillocks as reported in a previous section can be explained by a difference in step advancement rate during dissolution or growth between the three step types on the {101} faces $\langle\frac{1}{2}\frac{1}{2}\frac{1}{2}\rangle$, $\langle\frac{1}{2}\frac{1}{2}\frac{1}{2}\rangle$ and $\langle 100\rangle$ The ratio between the step velocities $v_1^{(\prime)}$ ($= v_{\mathrm{step}/\!/\langle\frac{1}{2}\bar{\frac{1}{2}}\frac{1}{2}\rangle}$), $v_2^{(\prime)}$ ($= v_{\mathrm{step}/\!/\langle\frac{1}{2}\frac{1}{2}\frac{1}{2}\rangle}$) and $v_3^{(\prime)}$ ($= v_{\mathrm{step}/\!/\langle 100\rangle}$) is on the average about 6 2 1 (fig 5) This difference in step velocity can be interpreted in terms of different rates for integration of a growth unit at each step type or removal in the case of dissolution Anisotropy of the surface diffusion probably cannot account for these differences in the step advancement rates This can be explained as follows Assuming the diffusion rate of an ad atom has its highest values (= v) when it moves more or less parallel to $v_1^{(\prime)}$ then its component parallel to $v_2^{(\prime)}$ and $v_3^{(\prime)}$ has a value of $\frac{1}{2}v$ So the advancement ratio between $v_1^{(\prime)}$ and $v_2^{(\prime)}$ or $v_3^{(\prime)}$ can be maximal 1 2 This maximal ratio is lower than according to our observations In this explanation it was assumed that along any direction the forward diffusion rate of an ad-atom equals the backward diffusion rate

From the foregoing, and from the conclusion drawn by Davey and Mullin [8] that the dehydration of the ions and their entry into the surface layer is rate determining, it can be concluded that for growth of the {101} faces of KDP or ADP the rate determining step is given by the dehydration of the ions directly at the step sites So probably surface diffusion does not play any role here

Because the absolute configurations of KDP and ADP are unknown it is impossible to relate the advancement rates $v_2^{(\prime)}$ and $v_3^{(\prime)}$ to the crystal structure So a more detailed picture of the difference in step integration kinetics, explaining this difference in step velocity cannot yet been given

3 2 Cooperating growth spirals with macro steps on {101} KDP

3 2 1 General features

A phenomenon quite commonly occurring on the pyramidal faces of the large KDP crystals (especially when the growth front is not too far away from the seed crystal) are cooperating growth spirals with step heights of several hundreds Ångstroms

A typical example of these "macroscopic" growth spirals can be seen in fig 6a, while its interferogram is given in fig 6b From this interferogram it can be deduced that the height difference between each successive turn of the spiral (which corresponds here with two macro steps A and B plus the intermediate region) is about 700 Å (fig 6c)

So the step height of each macro step is maximal 350 Å However, it is quite probable that the region

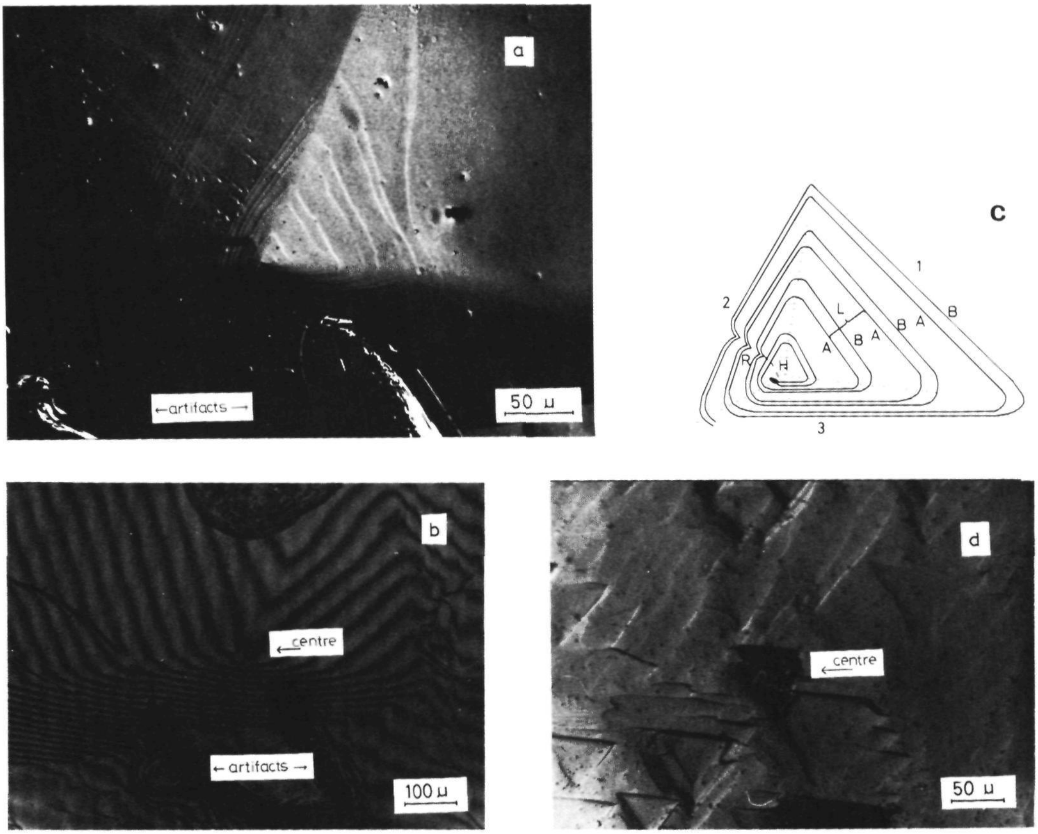

Fig. 6. (a) Macroscopic growth spiral on a {101} face of KDP. (b) Two beam interferogram of the same surface area as (a). (c) Diagram showing some characteristics of the macro spiral: (i) the central hollow core (H); (ii) the periodicity in the "step train" between each successive turn of the spiral (corresponding to length L); (iii) the reentrant corner in the step pattern (R). (d) Group of etch pits located at the position of the centre of the macro spiral mentioned under (a). The etch pits are formed after slightly dissolving the crystal in water.

between these macro steps is occupied by steps of a lower height, because of the difference in intensity in the regions 1, 2 and 3 (see figs. 6a and 6c), which indicates a difference in inclination. So the macro step height may even be lower.

After etching of the surface area as shown in fig. 6a, a group of etch pits can be seen at the location of the centre of the growth spiral (see fig. 6d). This phenomenon holds for most of the observed macroscopic spirals, on KDP and ADP, so it can be concluded that these spirals are related to dislocation bundles. This means that each macro spiral consists of a group of many cooperating single spirals originating from screw dislocations situated closely together in a small centre with their separation less than about $19r^*/2$ (r^* is the radius of a critical two dimensional nucleus) [24,25].

When these cooperating spirals dominate the crystal growth process, a linear dependence between growth rate and supersaturation may be expected [7].

Indeed such a linear dependence for large KDP crystals has been reported by Janssen-van Rosmalen et al. [5,6].

However, in the case of small KDP and ADP crystals the {101} surfaces are only covered by growth hillocks, and most of them originate from single dislocations as has been shown in fig. 4. This is in complete agreement with the parabolic growth rate versus supersaturation curve, which is typical for single spirals, as reported by Davey and Mullin [8].

From the fact that the macro spirals consist of a large group of cooperating spirals, the origin of the macro steps A and B in fig. 6 can be understood in terms of rhythmical bunching as described by Sunagawa and Bennema [25].

Another very peculiar phenomenon to be seen in figs. 6a and 6c is that the reentrant corner R in the step pattern, which is imposed by the complex centre of the growth spiral, remains visible in each spiral arm only far away from the growth centre it seems to fade away. This groove like pattern is not related to stress fields in the crystal, as can be seen in fig 6d, because no etch pits have been formed in this region after etching. So in contrast to the conventional models about reentrant corners in step patterns [26], in this case the step pattern does not quickly restore itself This is in agreement with very recent work on computer simulations of the movement of step patterns on crystal surfaces by Van der Hoek et al. [27].

3 2.2 *Characteristics of the macroscopic growth spirals· an example*

In order to get a better insight in some properties of the macroscopic growth spirals, one particularly beautiful macro spiral has been choosen for detailed investigation (see figs. 7a–7d) Fig. 7a is a differential interference contrast micrograph, showing this growth spiral. A detailed picture of its centre is given in fig. 7b. At the origin of this spiral, a hollow core [28] can clearly be distinguished. Such a phenomenon has been observed for numerous macro spirals. However, it is not clear whether this central hole is formed during crystal growth or a very slight etching has taken place during removal of the crystals from the solution.

From the interferogram (fig. 7c) it could be deduced that the height difference between each successive turn of this spiral is equal to about 1750 Å. Each turn corresponds (similar to the spiral shown in fig. 6) with two macro steps plus the intermediate region where lower steps can be seen (figs. 7a and 7d).

After etching of the surface area as shown in fig. 7a, a group of etch pits appears (fig. 7e), indicating that this spiral is also related to a dislocation bundle. From the fact that this macro spiral is related to a dislocation bundle and that each turn of the spiral corresponds with two macro steps plus an intermediate region with lower steps, it can be concluded that also for this spiral the phenomenon of rhythmical bunching imposed by the centre of the spiral takes place.

Before severe etching of the crystal surface as shown in fig. 7e, first, an extreme slight etching has been applied after removal of the gold coating. From this situation both a transmission micrograph (fig 7f) and a reflection micrograph (fig. 7g) have been made. In fig. 7f an inclusion can be clearly seen below the crystal surface at the former location of the growth centre of the spiral. Now the origin of the dislocation bundle can be understood. After formation of an inclusion (due to some disturbance in the crystal growth process) a lattice enclosure error occurs leading to the formation of a dislocation bundle [2,19], which is energetically much more favourable than one giant single dislocation. The height difference between each successive turn of the macro spiral above the inclusion gives a rough estimate for the length of the Burgers vector of the netto screw component normal to the growth surface of the dislocation bundle generated by the lattice enclosure error. This length has been estimated at about 1750 Å. This value gives some indication of the order of magnitude of the lattice enclosure error. The observation that crystals containing many inclusions grow faster can now be explained, because from these inclusions dislocation bundles are generated. These bundles lead to the formation of macro spirals, consisting of many cooperating spirals, which give according to the classical BCF theory a higher growth rate [29,30] than single spirals. This topic will be treated in more detail in a forthcoming paper [19].

On the micrographs 7a and 7b at region R a retardation of the step advancement can be seen. By relating the location of the dislocation bundle outcrop area with respect to the growth spiral (figs. 7d and 7g) one can see that the main part of the outcrop

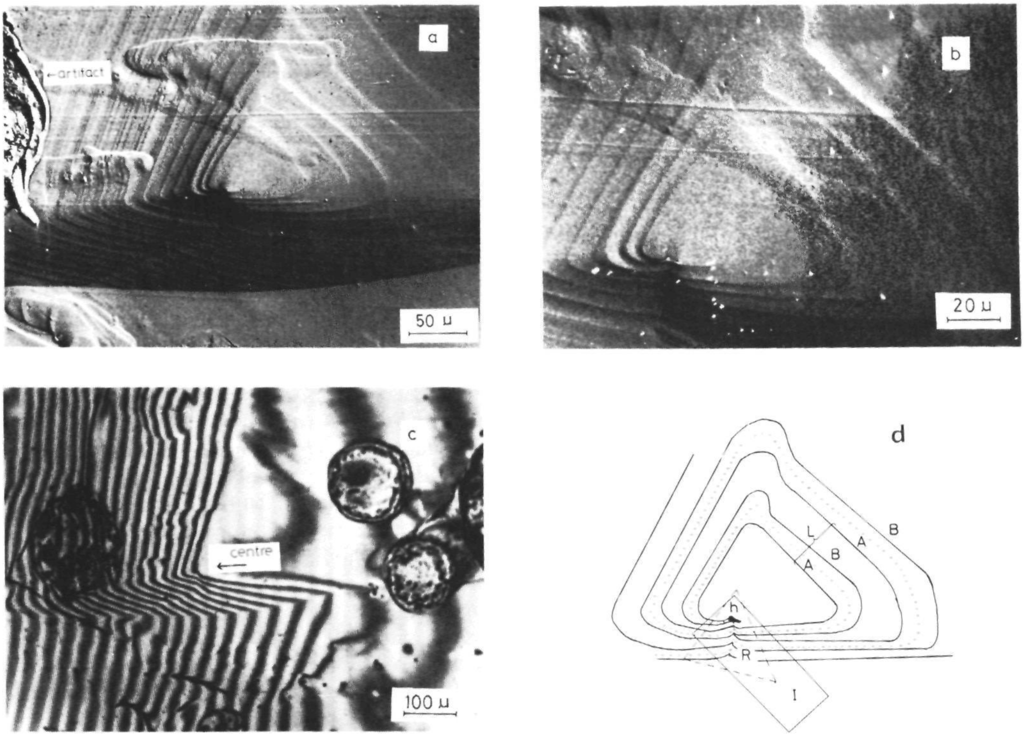

Fig. 7. (a) Macroscopic growth spiral on a $\{101\}$ face of KDP. (b) Detailed picture of the centre of this macro spiral. (c) Two beam interferogram of the same surface area as mentioned under (a). (d) Diagram showing some properties of this macro spiral: (i) the hollow core at its centre H; (ii) the step retardation region R; (iii) the periodicity in the step train between each successive turn of the spiral (corresponding to length L); (iv) the location of the inclusion (I) with respect to the spiral centre; (v) the dashed lined triangle corresponds to the dislocation bundle outcrop area.

area coincides with region R. So the step retardation is due to the local strain field around the dislocation bundle, which slows down the crystal growth process, because of a decrease in effective supersaturation [31]. Similar step retardation due to strain fields has been observed by Komatsu on SiC [32].

Another very interesting phenomenon, which can be seen in region R (see figs. 7a, 7b and 7h) is that the number of steps at the right- and left-hand side of grove g are different, and do not continue at this point. This can be explained by the occurrence of many dislocations having a screw component in the dislocation bundle outcrop area R. The netto screw component normal to the growth surface in area R now leads to a difference in the number of steps between both sides of the dislocation bundle outcrop according to a mechanism as being outlined in fig. 8 [26]. This figure shows the successive stages of the advancement of a step train in a region containing one screw dislocation outcrop (S) belonging to grove g in region R (fig. 7h). The difference in the number of steps between both sides of the dislocation is maintained by one during passage of the step train along this screw dislocation.

Finally, we want to remark that the asymmetry in the step advancement rate as discussed in section 3.1.4 is clearly demonstrated for all the macro spirals observed. It causes a pseudo exentricity of the spiral form.

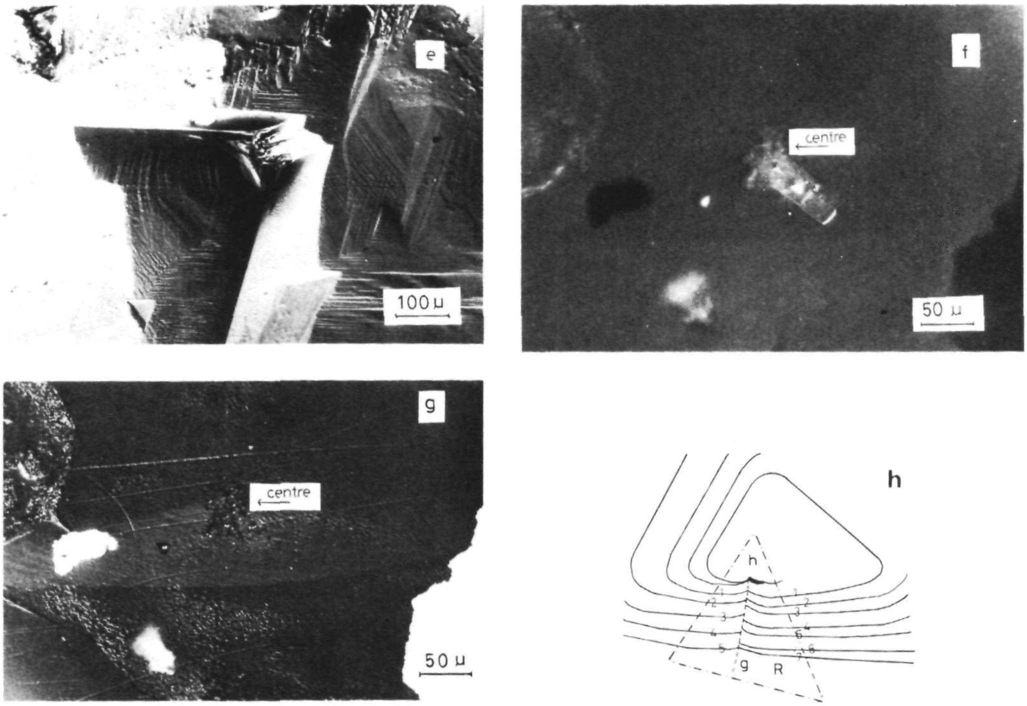

Fig. 7. (e) Etch pit pattern formed after severe etching of the same area as (a); a group of etch pits located at the former position of the spiral centre can be seen. (f) Inclusion below the crystal surface at the location of the spiral centre (transmission micrograph). (g) Dislocation bundle outcrop at the surface: numerous small etch pits can be seen at the location of the spiral centre after extremely slight etching of the crystal surface. (h) Difference in the number of steps between the right-hand side and the left-hand side of grove g; the dot and dash lined triangle corresponds to the dislocation bundle outcrop area R.

3.3. Nucleation growth on {101} KDP

On the {101} faces of large KDP crystals grown under very controlled conditions in a three vessel system, sometimes no growth hillocks nor any cooperating macro spirals could be observed. This only holds when the growth front is far away from the seed. In these cases the step sources, which could easily be traced back by following the step trains are flat, hillock free surface area and are often found near the edges of the crystal faces (fig. 9a). Because it is well known that such crystals grown under very controlled

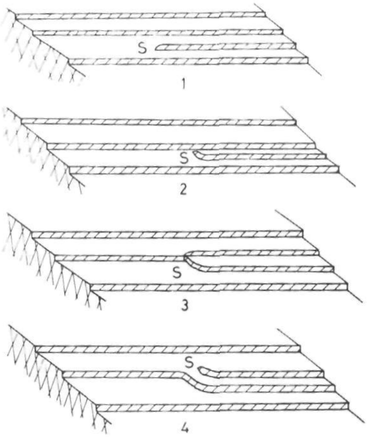

Fig. 8. Successive stages of the pass by of a step train along a screw dislocation outcrop (S). The number of steps at the right-hand side of S is one higher than at the left-hand side.

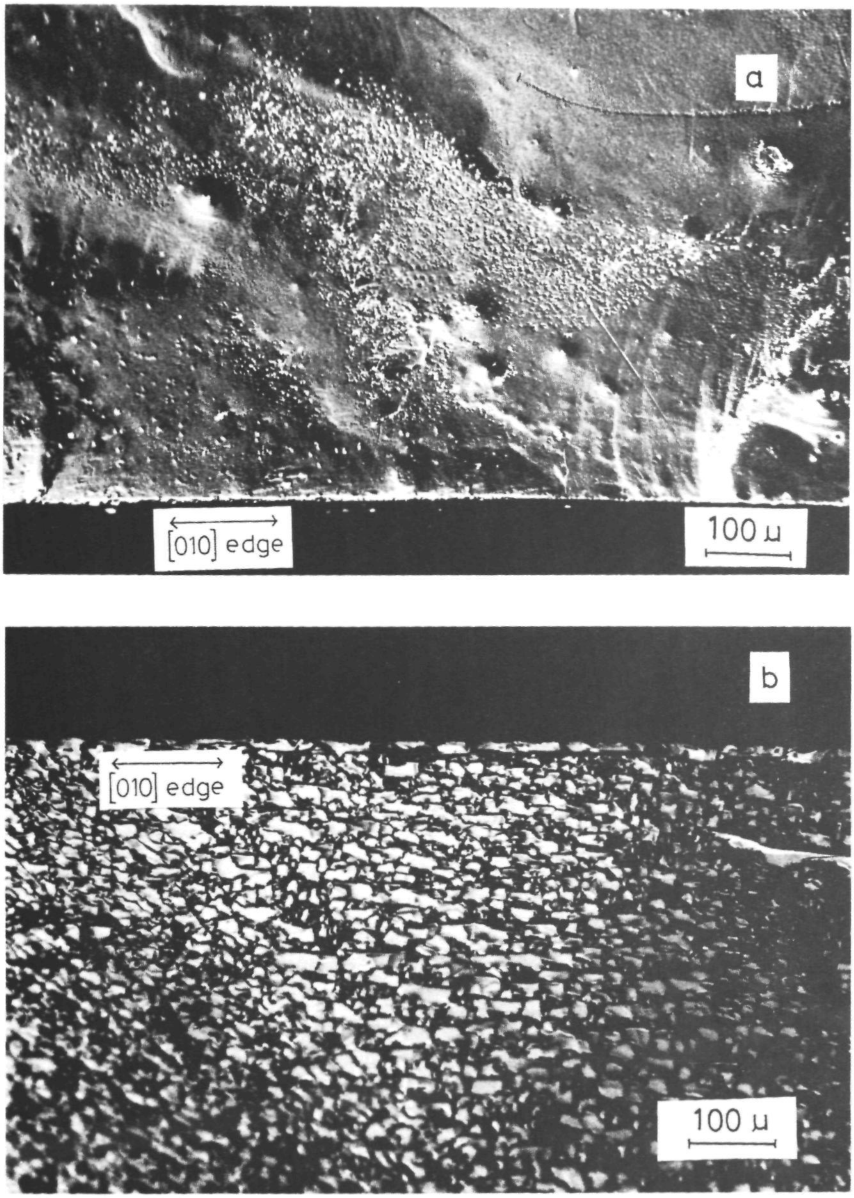

Fig. 9. (a) The surface area on a $\{101\}$ face of KDP near the intersection with an adjacent $\{100\}$ face. The growth is governed by a nucleation mechanism. Neither growth hillocks nor macro steps can be seen (the dots and irregularities are artifacts, formed during the separation of the crystal from the solution). (b) $\{100\}$ surface adjacent to the same $\{101\}$ surface area as mentioned above showing numerous macro steps.

conditions can have dislocation free {101} faces [4,33], it can be concluded that here the growth of the {101} facets is governed by a nucleation mechanism. This is in agreement with the X-ray topographic work carried out by Belouet [34], who observed that pyramidal growth can occur in absence of screw dislocations in any of the four {011} facets.

The growth mechanism for the {101} faces, as postulated by Torgesen and Jackson [1] and elaborated in more detail for dislocation free {101} surfaces by Deslattes et al. [33] and by Belouet and Stacy [3], who suggested that steps on the {100} faces arriving at the [0$\bar{1}$0] edges continue on the {101} faces is in contradiction with our observations, because of the following reasons. First, the growth area where the steps originate are not strictly related to the extreme edge between the pyramidal and prismatic faces. Often they are located at the intersection between two pyramidal faces and sometimes they are found at some distance from the edges. The fact that *the growth centres are mostly situated near the edges* of the {101} facets is simply a result of a difference in supersaturation between the edges and the central region of these faces, due to the hydrodynamics of the system [5,12], and that for a given system for nucleation growth the relative growth rate is more sensitive to differences in supersaturation than for spiral growth, especially at lower supersaturations [35]. Secondly, when the growth centres are located near the intersection prismatic-pyramidal faces, the macro step pattern on {100} does not persist on the {110} faces as can be clearly seen on the micrographs 9a and 9b.

4. Conclusions

Surface microtopography of the {101} faces of KDP and ADP provided very strong evidence for the possible occurrence of the spiral growth mechanism on these faces.

Two types of growth spiral could be distinguished: spiral hillocks mostly originating from single dislocations and macro spirals consisting of a group of cooperating spirals, originating from dislocation bundles. The occurrence of these two kinds of growth spiral can explain the different growth kinetics of the pyramidal faces as has been reported by several authors in literature.

It has also been shown that inclusions formed in the crystals can induce dislocation bundles leading to the formation of macroscopic growth spirals It will be shown in a forthcoming paper [19], that this will give rise to a higher growth rate, which explains the occurrence of quasi-periodic veils of liquid inclusions in large KDP crystals [12].

For highly perfect crystals having their growth fronts far away from the seed, crystal growth on the {101} faces can be governed by a nucleation mechanism.

Acknowledgements

The authors wish to thank B. Dam for experimental contributions and fruitful discussions, and Dr. H. Klapper and Dr P Bennema for stimulating discussions and their kind interest.

One of us (W.J.P. van Enckevort) acknowledges the support of the Netherlands Foundation for Pure Research, ZWO/SON.

References

[1] J L Torgesen and R W Jackson, Science 148 (1965) 952.

[2] V G. Lutsau, Ju.M. Fishman and I.S. Res, Kristall Tech. 5 (1970) 445.

[3] C Belouet and W T. Stacy, J. Crystal Growth 44 (1978) 315

[4] C. Belouet, E. Dunia and J F. Petroff, J. Crystal Growth 23 (1974) 243

[5] R Janssen-van Rosmalen, Thesis, Technical University of Delft (1977).

[6] R. Jansen-van Rosmalen, G.K Richter-van Leeuwen, D. Visser and John M Smith, to be published.

[7] P Bennema and G.H Gilmer, in Crystal Growth, An Introduction, Ed P Hartman (North-Holland, Amsterdam, 1973) ch 10.

[8] R.J. Davey and J.W. Mullin, J. Crystal Growth 23 (1974) 89.

[9] P. Bennema, J. Crystal Growth 1 (1967) 278

[10] W.K. Burton, N. Cabrera and F.C. Frank, Phil. Trans. Roy Soc. (London) 243 (1951) 299.

[11] A.C. Walker and G.T. Kohman, AIEE Trans. 67 (1948) 566

[12] R. Janssen-van Rosmalen, W.H. van der Linden, E. Dobbinga and D. Visser, Kristall Tech. 13 (1978) 17.

[13] W.J.P. van Enckevort and W.H. van der Linden, J. Crystal Growth 47 (1979) 196.

[14] H. Komatsu, in: Crystal Growth and Characterization, Proc. ISSCG-2 Spring School, Japan, 1974, Eds. R. Ueda and J.B. Mullin (North-Holland, Amsterdam, 1975) pp. 333–346.

[15] See, for instance, J. Fontcuberta, R. Rodriguez and J. Tejada, J. Crystal Growth 44 (1978) 593.

[16] A.R. Ubbelohde and I. Woodward, Proc. Roy. Soc. (London) A188 (1947) 358.

[17] W.J.P. van Enckevort and L.J. Giling, J. Crystal Growth 45 (1978) 90.

[18] G. Gülzow and W. Lüdke, Phys. Status Solidi 11 (1965) 205.

[19] W.J.P. van Enckevort, R. Janssen-van Rosmalen, W.H. van der Linden and H. Klapper, J. Crystal Growth, to be published.

[20] H. Klapper, Yu. M. Fishman and V.G. Lutsau, Phys. Status Solidi (a) 21 (1974) 115.

[21] S. Amelinckx, The direct observation of dislocations, in: Solid State Physics, Suppl. 6, Eds. F. Seitz and D. Turnbull (Academic Press, New York, 1964) pp. 23-25.

[22] P. Hartman, in: Crystal Growth: An Introduction, Ed. P. Hartman (North-Holland, Amsterdam, 1973) pp. 358–402.

[23] P. Hartman, Acta Cryst. 9 (1956) 721.

[24] P. Bennema and G.H. Gilmer, in: Crystal Growth: An Introduction, Ed. P. Hartman (North-Holland, Amsterdam 1973) p. 301.

[25] I. Sunagawa and P. Bennema, J. Crystal Growth 46 (1979) 451.

[26] S. Amelinckx and G. Strumane, in: Silicon Carbide: A High Temperature Semiconductor, Proc. Conf. of Silicon Carbide, Boston, 1959, Eds, J.R. O'Connor and J. Smiltens (Pergamon, 1960) pp. 162–201.

[27] B. van der Hoek and J.P. van der Eerden, work in progress.

[28] B. van der Hoek, P. Bennema and J.P. van der Eerden, J. Crystal Growth, to be published.

[29] W.K. Burton, N. Cabrera and F.C. Frank, Phil. Trans. Roy. Soc. (London) 243 (1951) 299.

[30] P. Bennema, in: Industrial Crystallization, Ed. J.W. Mullin (Plenum, New York, 1976) pp. 103–105.

[31] K. Komatsu and B. van der Hoek, to be published.

[32] H. Komatsu, private communication.

[33] R.D. Deslattes, J.L. Torgesen, B. Paretzkin and T. Horton, J. Appl. Phys. 37 (1966) 541.

[34] C. Belouet, Rev. Phys. Appl. 11 (1976) 253.

[35] R. Janssen-van Rosmalen, Thesis, Technical University of Delft (1977) p. 80.

CHAPTER IX:
GROWTH PHENOMENA OF KDP CRYSTALS IN RELATION TO THE INTERNAL STRUCTURE

W.J.P. van Enckevort[*], R. Janssen- van Rosmalen[**], H. Klapper[***] and W.H. van der Linden[*]

[*] RIM Laboratory of Solid State Chemistry, Catholic University, Toernoiveld, Nijmegen, The Netherlands

[**] Present adress: Koninklijke/Shell Exploratie en Produktie Laboratorium, Rijswijk (Z.H.), The Netherlands

[***] Institut für Kristallographie der Technischen Hochschule, Templergraben, Aachen, Germany

ABSTRACT

The influence of the hydrodynamic environment on the perfection of large, single KDP (potassium dihydrogen phosphate) crystals has been studied by means of X-ray diffraction topographic techniques. The crystals were grown from solutions under carefully defined conditions. One of the phenomena caused by the hydrodynamics is the occurrence of quasi-periodic veils of liquid inclusions. This quasi-periodicity can be explained by conflicting growth mechanisms, depending on dislocation density. A strong dependence of growth rate on dislocation density has clearly been observed, also for crystals without liquid inclusions. In addition, the patterns of the growth bands in KDP could also be related to the hydrodynamical environment. A major change in the well known minimum-energy directions of dislocation lines is visible in the growth bands.

1. INTRODUCTION

Single crystals of potassium dihydrogen phosphate (KDP) and its deuterated form (see Fig. 1) are an important material for electro-optical light modulators and solid-state light valves (1,2). Since this application demands large crystals of high quality, much interest has been focussed on the study of crystal defects in KDP and their relation to the conditions of growth (3-11). Large KDP crystals are grown from aqueous solutions by decreasing the temperature.

Lutsau, Fishman and Res (3) present an X-ray topographic investigation of grown-in dislocations in KDP. Their main results are summarized below:

(i) The majority of the dislocations originate from the surface of the seed crystal or from the "capping" region, where in the initial stage of growth many liquid inclusions

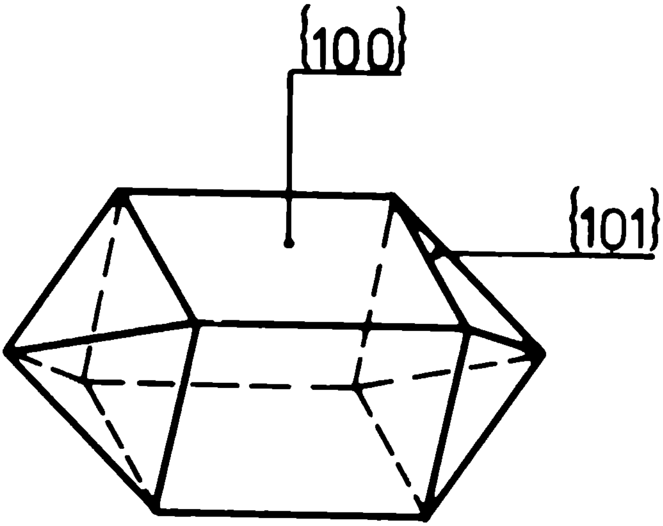

Fig.1. Morphology of KDP crystals grown from aqueous solution.

are formed. Even far from the seed, dislocations arise from inclusions of liquid or foreign particles. They result from lattice closure errors, when the lattice is closed "behind" an inclusion.

(ii) The dislocation lines are essentially straight and have directions depending on the Burgers vector involved. They are refracted when they penetrate a growth sector boundary.

(iii) Since KDP crystals grow practically only on pyramid faces {101} , the dislocations originating from the capping region grow out of the crystal at the prism faces. Thus, the regions far from the seed plate are nearly dislocation-free.

These results have been confirmed by Belouet, Dunia and Pétroff (4). They also found excellent agreement between observed and theoretical dislocation line directions, as calculated by Klapper et al. (5). Belouet et al. have also studied the correlation of impurity segregation and crystal defects. They showed that the tapering angle and the growth bands are strongly influenced by the impurity content of the crystal. Other investigations deal with the X-ray topographic contrast of growth sector boundaries (Fishman and Lutsau (7), Belouet and Stacy (8)), etch grooves related to sector boundaries and growth bands (Dam and van Enckevort (9)) and with the perfection of deuterated crystals (Belouet et al. (10), Fishman (11)).

Much attention has also been given to the growth mechanisms that are active on the pyramid and prisms faces. Torgesen and Jackson (12) observed growth spirals only on the prism faces, but not on the pyramid faces of isomorphous ADP. According to the more refined microscopic observations of van Enckevort et al. (13), however, single and cooperating spirals are present on the pyramid faces of KDP. The major importance of spiral growth on the {101} faces of the isostructural ADP was confirmed by in situ Lang topographic studies carried out by Chernov et al. (14) , who in addition observed a complete arrest in growth not related to a disappearance of a screw dislocation outcrop at the growth face.

The influence of the hydrodynamic environment on the perfection of large KDP crystals grown at constant supersaturation has been studied by Janssen- van Rosmalen et al. (15,16). It has been shown that under certain conditions of solution flow, rows of "quasi-periodic" veils of liquid inclusions are formed in the back part of the crystal (relative to the flow direction), but not in the front part (see section 2). The present study pursues this work. Special attention will be paid to the following four subjects:

- The relationship between dislocation density and growth speed.
- The "quasi-periodicity" of veils in the back part of the crystals.
- The different appearance of growth bands in the back and front part of the crystals.
- The bending of dislocation lines in growth bands.

2. CRYSTAL GROWTH AND FLOW VISUALISATION EXPERIMENTS

The KDP crystals were grown in a three-vessel system of the Walker Kohman type (16,17), consisting of three interconnected vessels, through which a solution of "Baker analyzed" KDP is circulated. The crystals are mounted on a tree which rotates in the solution. The temperature in this system can be kept constant indefinitely to within 0.05 °C. For all the crystal growth experiments the temperature was 29.5 °C and the the bulk supersaturation 5.4%.

The influence of the rotational speed on the perfectness of the crystals has been described in previous work (16). In that study flow visualization experiments have been performed in a low-velocity wind tunnel in order to investigate the hydrodynamic environment of the crystal. Smoke was used as a tracer for the flow profile around the crystal. The flow velocity of the wind tunnel was adjusted in such a way that the Reynolds number related to the cross-sectional areas of the crystals corresponded to the Reynolds number in the three-vessel system at the specific rotational speeds. A large closed wake was observed at the rear of the crystal relative to the flow direction (see Figs. 2a and 2b). The boundary layer separation does not occur at the extreme edge of the crystal, but at some distance from the corner along the pyramid face; the recirculating wake does not reach the prism corner. Since the wake is closed, exhaustion of its solution can occur. As a consequence, a concentration gradient along the crystal surface can exist at the point where the recirculating fluid meets the "fresh" solution coming from the prism

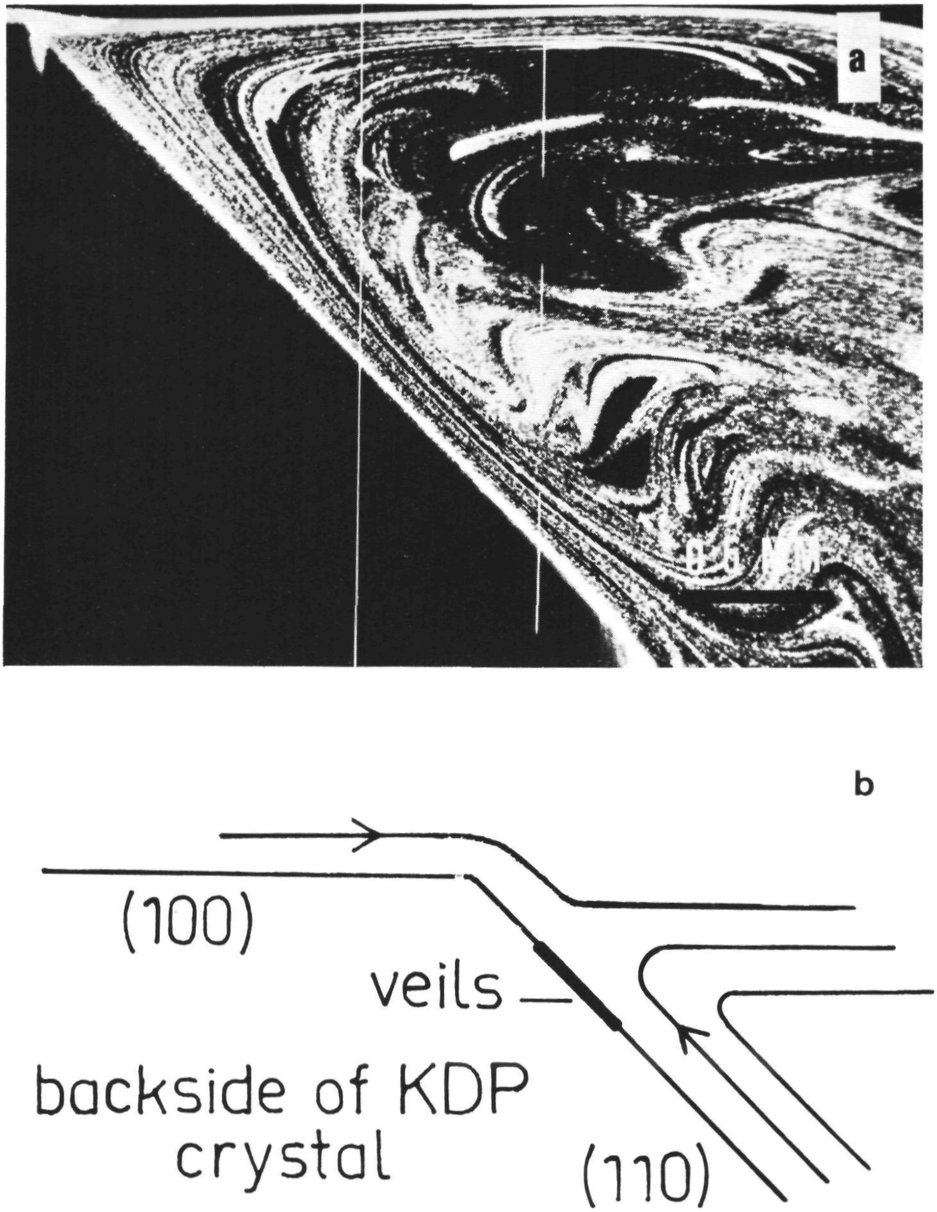

Fig.2. The closed wake at the rear of the crystal:
(a) The streamlines behind the crystal model at Re = 1485, observed in a low-velocity wind tunnel.
(b) Schematic representation of the wake.

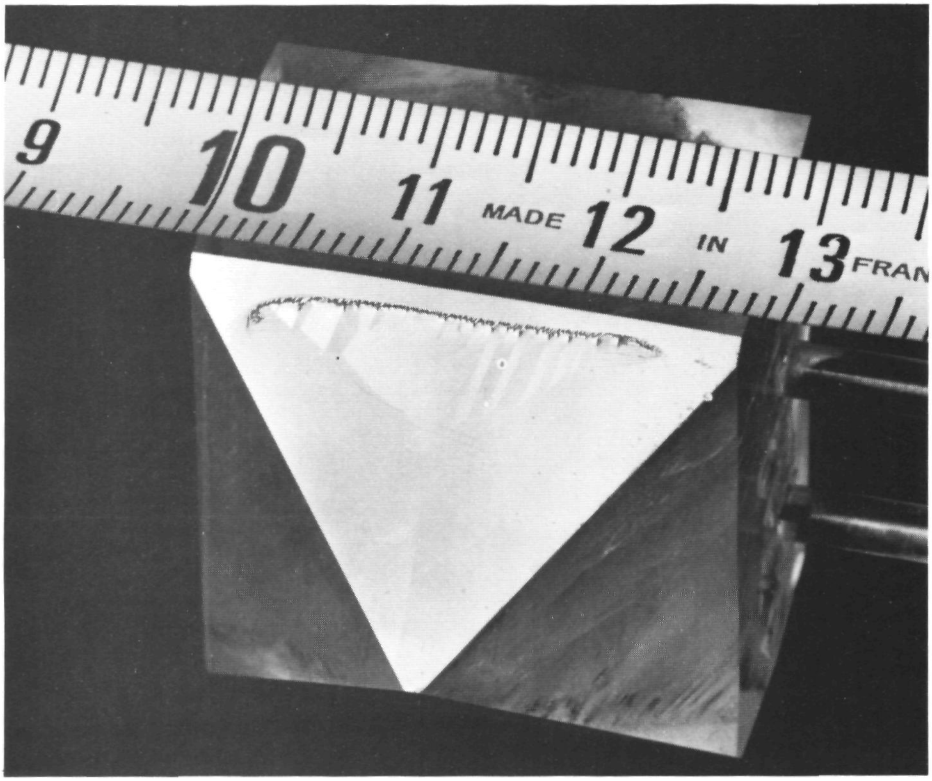

Fig.3. The onset of the formation of a veil at the rear pyramid face.

faces. Since the prism faces have a very low growth rate, the supersaturation of its "fresh" solution is almost equal to the bulk supersaturation. It has been shown (16) that the onset of liquid inclusions starts at this point (see fig.3). As a consequence of these hydrodynamic conditions, three distinct cases of growth can be distinguished:

(i) At very low rotational speeds the whole rear of the crystal is clouded by liquid inclusions.

(ii) At medium speeds veils of liquid inclusions only occur "quasi-periodically". In this case the difference in concentration along the surface is not very high and the growth mechanism seems to be able to overcome this "barrier" under certain conditions, as will be explained later.

(iii) At high rotational speeds the crystals grow without any veils. In this case the turbulence inside the wake is high enough to achieve good mixing.

In the present study we will concentrate on cases (ii) and (iii).

3. PREPARATION OF PLATES AND X-RAY TOPOGRAPHIC PROCEDURE

The samples examined with the topographic techniques were {100} plates 1.5 to 2 mm thick. All cuts were made with a string saw (nylon thread) and using water as solvent. The cut surfaces were smoothed by gently moving the plate on a soft moist cloth. The plates were then immersed for about 30 seconds in distilled water. In this way surface damage (scratches, indentations) was removed.

Two crystals were used for the experiments, one containig "periodical" veils of liquid inclusions (See fig. 4a) and the other without liquid inclusions (grown at high rotational speed). The cutting plan is given in figures 4b and 5 respectively. From both crystals, plates from the front and back part were studied. Although also X-ray topographs have been made from several other cuts, the cuts with the numbers 1, 2, 3a and b have been selected for illustration in this paper.

The Lang transmission method (18) has been applied in order to obtain the X-ray topographs of large specimen area using $AgK\alpha_1$ (λ = 0.5594 A) or Mo $K\alpha_1$ (λ = 0.7093 A)

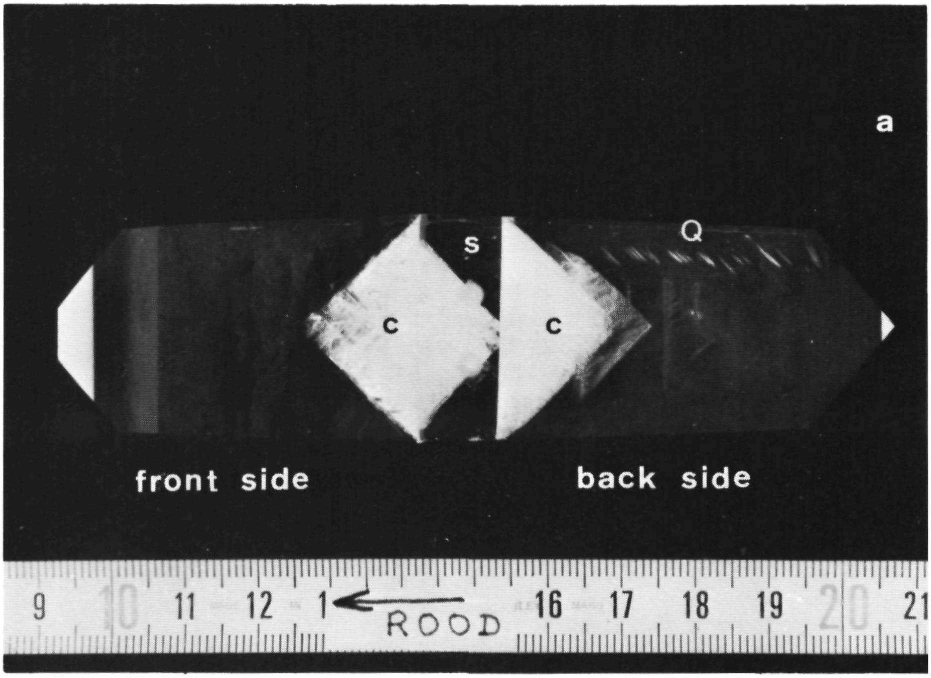

Fig.4. (a) KDP crystal grown on a (001) seed plate. S: seed plate; C: strongly disturbed "capping" region; Q: "quasiperiodic" veils. (The seed plate contains the capping region of a previous growth generation).

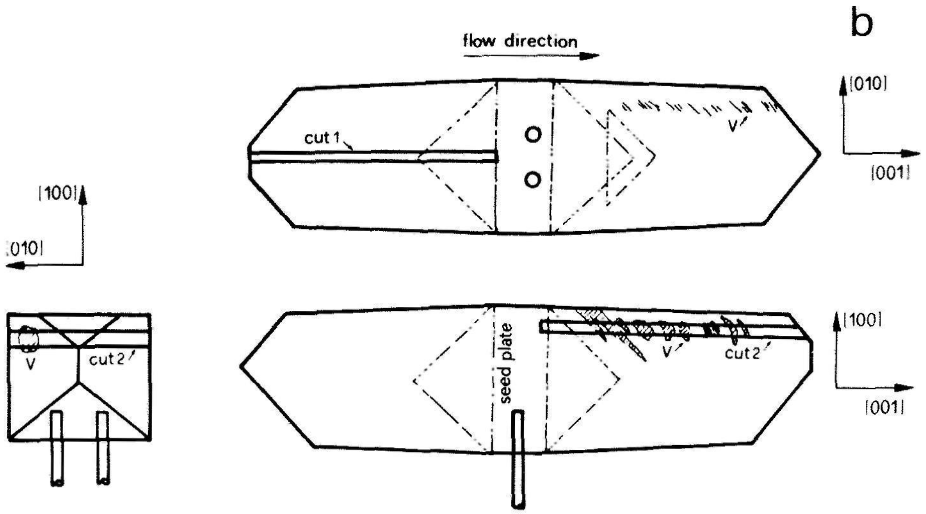

Fig. 4 (continued). (b) Cutting plan of the crystal shown in (a) and the position of the "quasiperiodic" veils (v). X-ray topographs of cuts 1 and 2 are given in figures 6 and 9a, b respectively.

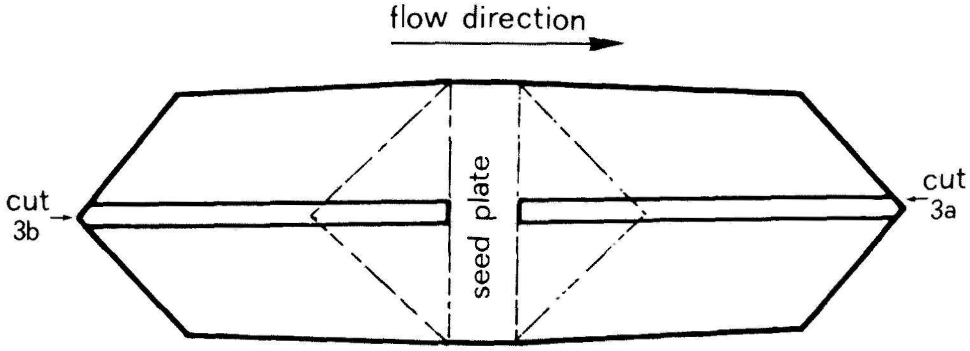

Fig.5. Cutting plan of a crystal grown at high rotational speed (no formation of veils). X-ray topographs of cuts 3a and b are given in figures 12 a and b.

radiation and the high-speed X-ray film Structurix D7 (Agfa Gevaert). The finer grained film Structurix D4 has been chosen for the more detailed pictures. For obtaining the topographs the reflections {200} having a high structure factor and the less intense reflections {101} (medium) and {004} (weak) have been used.

4. RESULTS AND DISCUSSION

4.1. Influence of dislocation density on growth rate

The dependence of the growth rates of the pyramid faces on the dislocation density is clearly visible from

Fig.6. X-ray topograph (reflection 200, AgKα-radiation) of cut 1. Thickness ∿1.5 mm. CR: Capping region; i: inclusion; gb: growth bands; line ABC growth sector boundary between $(\bar{1}0\bar{1})$ and $(10\bar{1})$ sectors.

the topograph in figure 6. The plate (cut 1, see figure 4b) contains numerous dislocation bundles originating from the "capping" region and from isolated inclusions. These dislocations end, or have ended in an earlier stage of growth, on the pyramid faces $(10\bar{1})$ and $(\bar{1}0\bar{1})$. During growth many of them have "travelled" over the edge between the pyramid and the adjacent prism face, and have "vanished" from the pyramid growth face. Because of the higher dislocation density the $(10\bar{1})$ sector had a higher growth speed than the $(\bar{1}0\bar{1})$ sector. The speed ratio of these two faces can be determinated from the orientation of the growth sector boundary (9,19,20), which appears in figure 6 by X-ray topographic contrast and is marked by line A-B-C. Both growth speeds are equal along A-B. At point B the growth sector boundary bends to the right, thus indicating an increase in $(10\bar{1})$ growth speed as compared to $(\bar{1}0\bar{1})$. This increase starts at a stage, where the majority of the dislocations "vanish" from the $(\bar{1}0\bar{1})$ face. The density of dislocations ending on $(10\bar{1})$ remains essentially the same. The speed ratio changes from 1 to about 1.3. The same phenomenon has been observed on the topographs of other cuts shown in figure 5.

A similar relationship between the occurrence of dislocation outcrops at the pyramidal faces and the growth rates of these $\{101\}$ faces has been observed earlier by Chernov et al. (14) by means of in situ X-ray diffraction topography of growing ADP crystals. However, in their work it was dealt with single dislocation outcrops at the crystal surfaces, whereas in the present case dislocation bundles -coexisting with single dislocations in the same crystals- are considered.

The relation between growth rate and dislocation density can be explained from theoretical considerations (21,22). The following three situations have to be distinguished:

(i) Growth by means of (non-cooperating) single spirals;
(ii) Growth by cooperating spirals;
(iii) Growth by nucleation mechanisms.

(i) When spirals do not cooperate with each other (See figure 7a) the growth rate and the dislocation density are not directly related. This situation occurs in regions of relatively low dislocation density and in the absence of dislocation bundles, so that the dislocation outcrops at the surface are separated from each other at a distance larger than $19r^*/2$ (r^* is the radius of the 2D critical nucleus). It leads to a parabolic R-σ curve (See figure 8).

(ii) In the case of cooperating spirals (fig. 7b), where the dislocation outcrop separation is less than $19r^*/2$, the growth rate is approximately proportional to the number of spiral arms (is surface diffusion and changes in step curvature are neglected). This situation

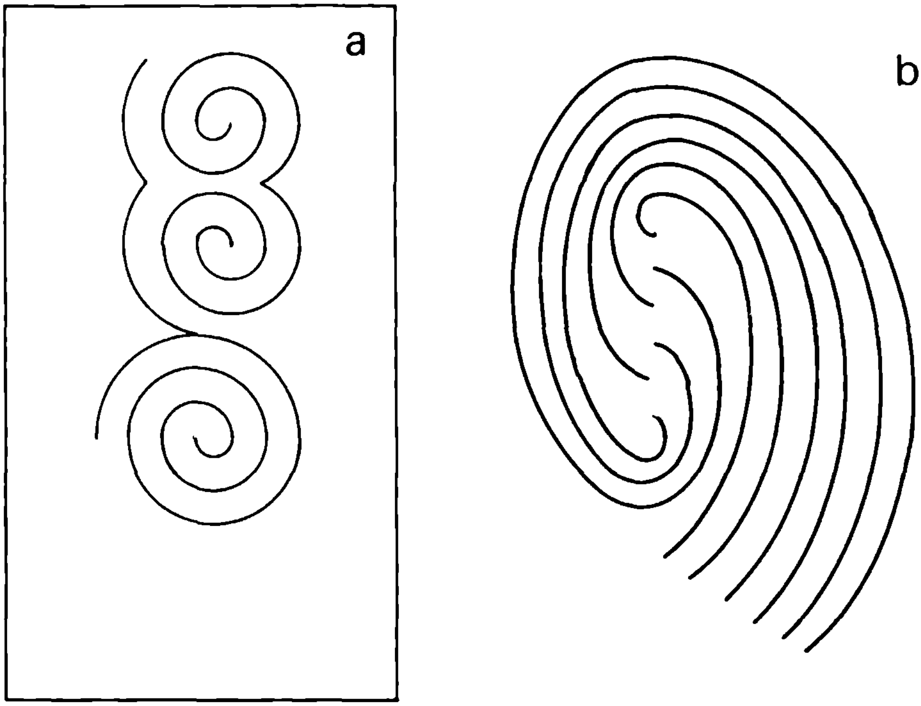

Fig.7. Spiral growth mechanisms: (a) Non-cooperating spirals; (b) Cooperating spirals.

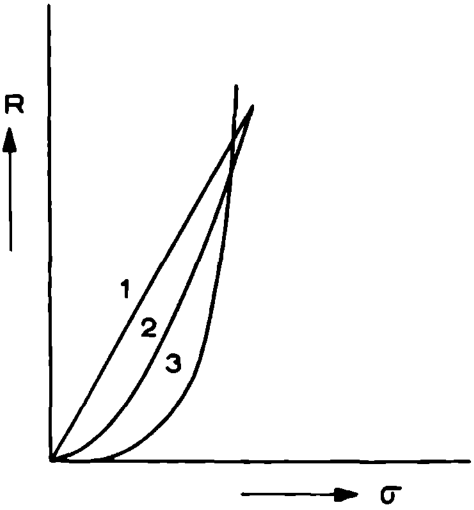

Fig.8. Growth rate versus supersaturation (σ) curves for three different growth mechanisms:
Curve 1: Growth by cooperating spirals.
Curve 2: Growth by single (non-cooperating) spirals.
Curve 3: Growth by nucleation.

results in a linear R-σ curve (fig. 8). The cooperating spirals become more important at higher dislocation densities or in the presence of dislocation bundles, especially in the lower supersaturation range. When a crystal contains both single and cooperating spirals, the group of spirals growing fastest will dominate the others. Mostly, some of the multiple spirals are the fastest and dominate the process.

(iii) If there are no dislocations, with a screw component perpendicular to the growth face ending on the pyramid faces, a nucleation mechanism governs the process. This leads to a lower growth rate in the low supersaturation range (fig. 8).

These three growth mechanisms have indeed been observed on the {101} growth faces of KDP by means of differential interference contrast microscopy (13). We therefore conclude that the dependence of the growth rates of the {101} growth faces of KDP on the dislocation density can be explained in terms of competing growth mechanisms as mentioned above. For the case of {101} ADP studied by Chernov et al. (14), however, -aside from a complete standstill in growth not related to dislocations- only a competition between the mechanisms (i) and (ii) occurs, since no bundles of dislocations were observed on their X-ray topographs.

4.2. "Quasi-periodicity" of veils in large KDP crystals

As has been pointed out in section 2, veils of liquid inclusions occur "quasi-periodically" in the back part of the crystal at intermadiate rotational speeds. Since the hydrodynamic conditions did not change in time during the growth of the crystal, the repeated occurrence of the veils is supposed to be related to internal defects.

X-ray topographs have been made in order to observe the defects in the neighbourhood of the veils. The topograph of cut 2 (cut through the row of veils), given in figure 9, shows that numerous dislocation lines originate from the inclusions. Several groups of dislocations having different line directions and different Burgers vectors can be distinguished. The following examples (4,5) are given: The dislocation lines forming an angle of about 80° with the axis |001| have the Burgers vector $\vec{b}$ = |010| and therefore a predominant screw character. Dislocation lines with an inclination of 10-20° against |001| are also mainly screwlike with Burgers vector $\vec{b}$ = |001|, whereas dislocations with $\vec{b}$ = |011| run almost parallel to the normal of the (011) growth face and have nearly a pure screw character. On the whole, dislocations with $\vec{b}$ = <010>, <001>, <011> and $\frac{1}{2}$<111> have been observed.

Inspection of the topograph 9 shows that the formation of a veil starts when the majority of the end points of the dislocations generated by the foregoing veil have

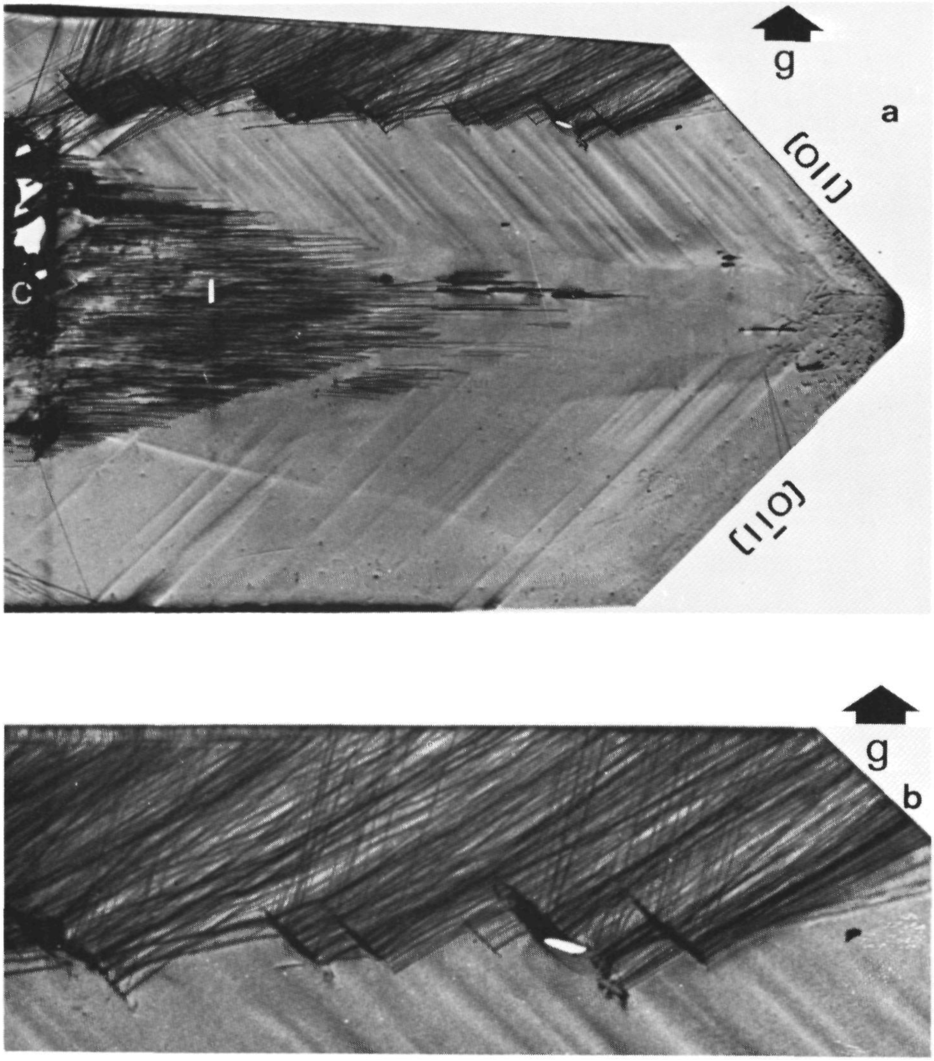

Fig.9. (a) X-ray topograph (reflection 020, AgKα) of cut 2 containing the row of veils. The triangular region T of high dislocation density belongs to one of the growth sectors (101) or ($\bar{1}$01). (b) Enlarged section of (a).

shifted on the growth face from the region of low to that of higher supersaturation, σ (See figures 10a and b). Obviously, the formation of a veil results from a change in the growth mechanism due to the elimination of growth

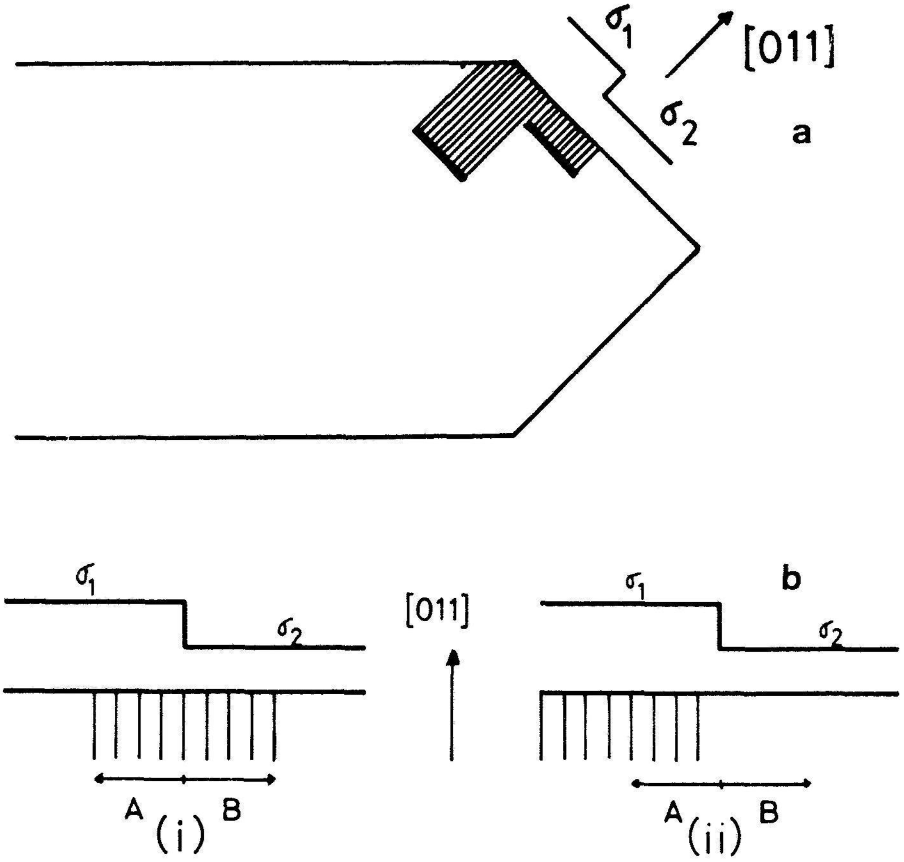

Fig.10. Position of dislocation bundle -related to a liquid inclusion- outcrop with respect to the concentration "jump", caused by the hydrodynamics of the system at the rear of the crystal.
(a) General view (supersaturation $\sigma_1 > \sigma_2$).
(b) Detail of (a). (i) The same number of dislocations in both supersaturation regions: No liquid inclusion will be formed. (ii) Most dislocations in the high supersaturation region: A next liquid inclusion will be formed.

spirals (possibly fast growing cooperating spirals, the centres of which can be related to liquid inclusions (13)) from the closed wake region. This leads to a decrease in growth rate in the lower supersaturation area B and an

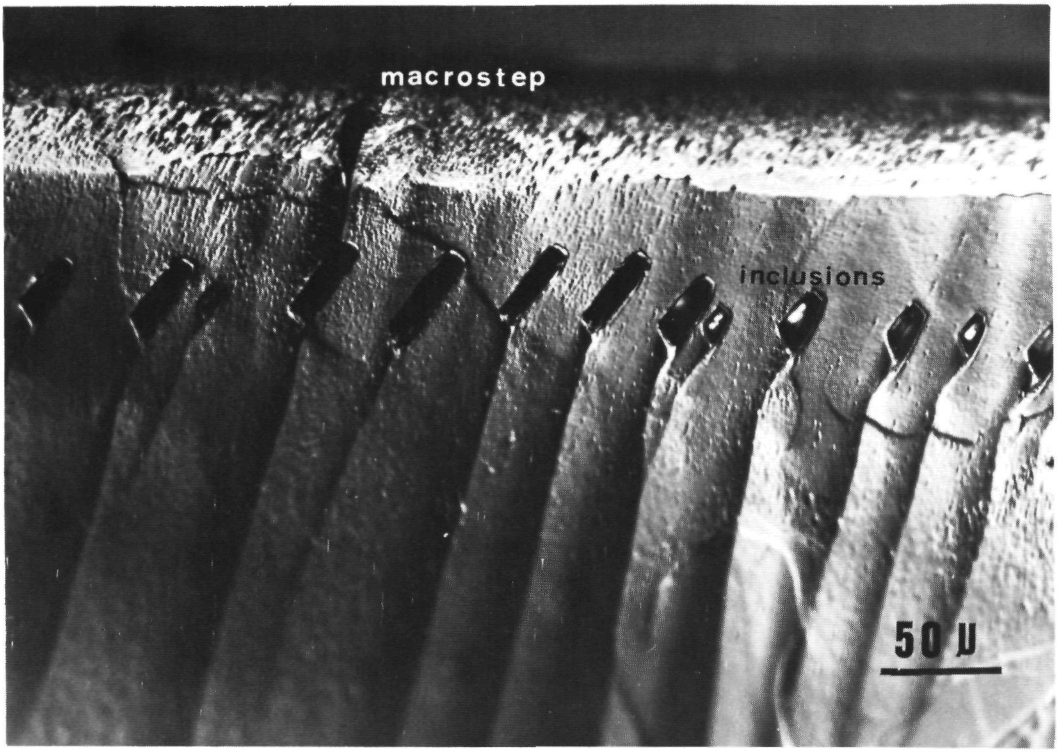

Fig.11. Differential interference contrast micrograph showing the macrostep, related to the "jump" in supersaturation caused by the hydrodynamics of the system, and some inclusions emerging at the crystal surface.

increase in area A, which gives an unstable situation at the concentration "jump". This induces the formation of a macrostep as was derived theoretically in a previous paper (23). That indeed such a macrostep is formed can be seen in figure 3 and better in figure 11, being a differential interference contrast micrograph of the region near the supersaturation "jump". From this figure also clearly the relative positions of the inclusions with respect to the macrostep (i.e. supersaturation jump) can be recognized.

To confirm this hypothesis for the formation of the "quasi-periodic" veils, it has to be established that the dislocations originating from the veils are capable of forming step sources.

A step source is produced by each dislocation having a screw component normal to the growth face. Among the Burgers vectors in KDP mentioned above, dislocations with $\vec{b} = |010|$, $|001|$, $|011|$, $|101|$, $|101|$, $\frac{1}{2}|111|$ and $\frac{1}{2}|111|$ can produce step sources on the (011) growth face. Actually, the majority of the dislocations generated by the inclusions in the veils have such screw components.

4.3. The growth bands

Although crystals grown at high rotational speeds (case (iii) in section 2) do not contain any liquid inclusions, their internal structure seems to be dependent on the hydrodynamical environment. Figures 12a and b are X-ray topographs of the front and rear of the crystal (relative to the flow direction), according to the cutting plan given in figure 5. The front part shows kinked "growth bands", the rear part much more streated bands. It is to be noted that the kinked contrasts on the X-ray topographs can not correspond to former growth horizons, so that in fact they are no growth bands in the true sense of the word. Moreover, the distance between successive bands is larger for the front part. The same phenomenon has been observed on topographs of crystals containing liquid inclusions (compare figure 6 -the front part- and figure 9 -the rear of the same crystal).

Another interesting observation is that the locations of the growth bands in adjacent pyramidal sectors do not correspond with each other (see figures 6, 9 and 12). This latter phenomenon has been observed earlier by means of an etching technique (9), Lang topography (4) and the Schlieren method (24).

These observations indicate that the growth bands are not related to variations in the mother liquor (e.g. temperature), but can be attributed both to differences in the hydrodynamic conditions and to variations in interface kinetics. The main difference in hydrodynamic environment is the following. At the front of the crystal probably a laminar boundary layer exists, resulting in a gradual decrease in supersaturation along the growth face, whereas at the back eddies occur inside the wake, slightly equalizing the concentration at the interface. Such a relation between the occurrence of defects in crystals and the hydrodynamics of the growth system has been established previously for inclusions (15,16,25,26) and dislocations (25,26), but never -as far as known to us- for growth bands.

The occurrence of kinked "growth bands" and growth bands, which X-ray diffraction topographic contrast is not uniform within one single sector indicates that a difference in impurity absorption (which causes growth band formation (4,6,9)) even exists between adjacent area on the same growth face. Since no relation was found between the dislocation structure and this lateral non-uniformity of growth bands, the origin of this phenomenon is not understood.

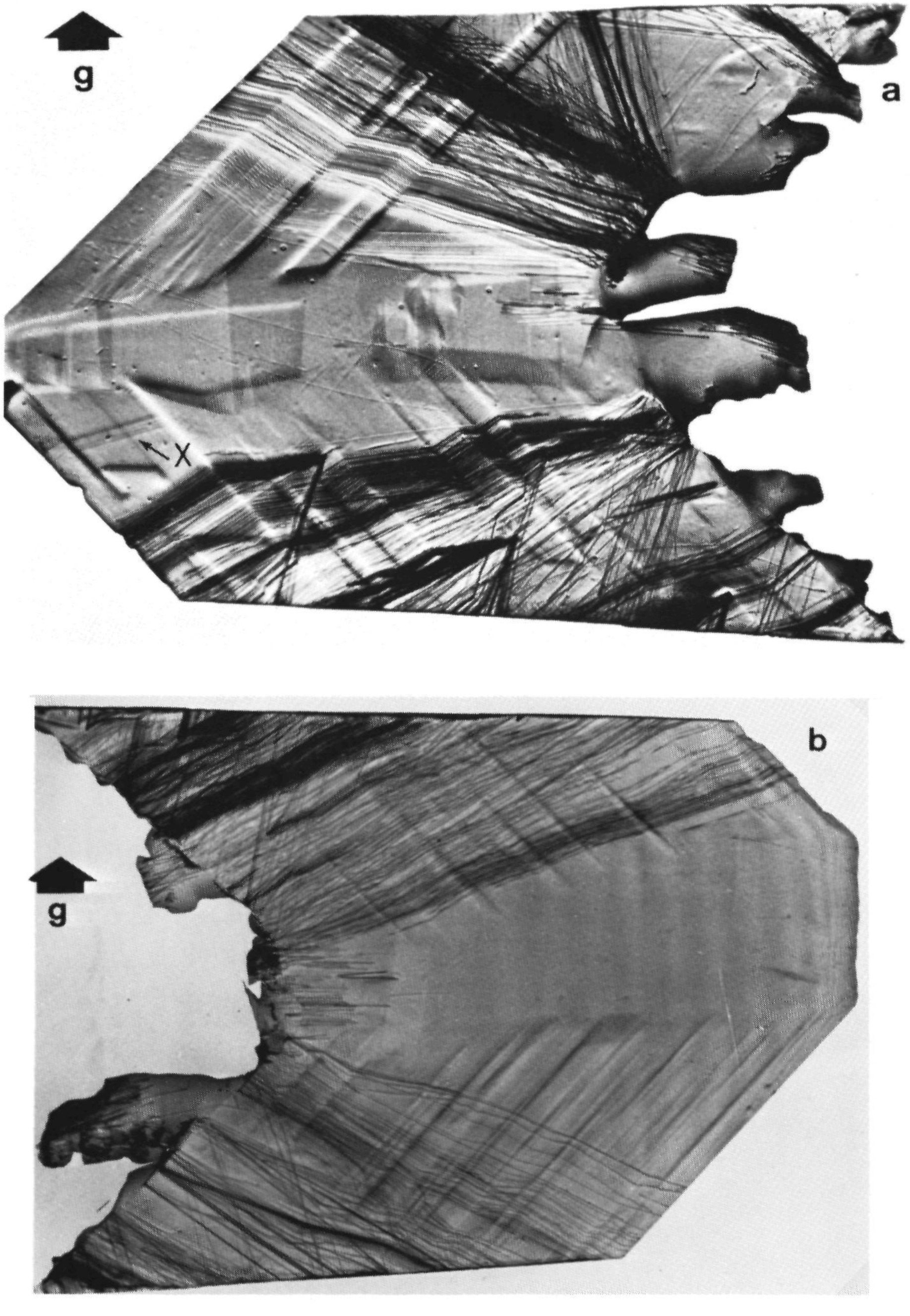

Fig. 12. X-ray diffraction topographs (reflection 020, Ag Kα) of cut 3a and 3b (See figure 5). The plate (thickness ~2 mm) is broken along the seed and capping region.
(a) Front side of the crystal (cut 3a).
(b) Back side of the crystal (cut 3b).

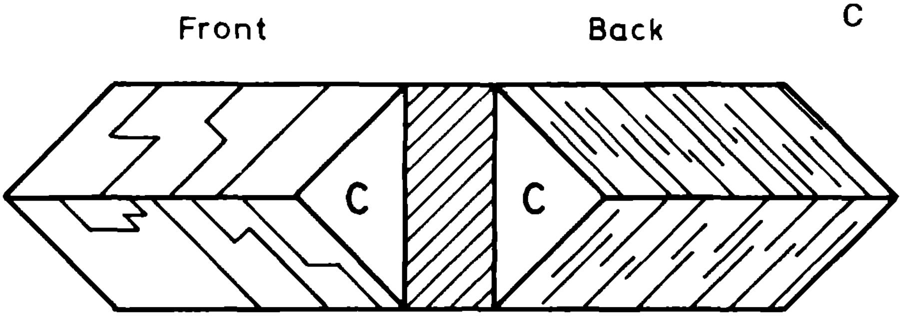

Fig. 12 (continued). (c) Appearance of growth bands in the front and back part of the crystal.
Front: blockwise "growth bands". Back: much more striated growth bands.

4.4. Bending of dislocation lines in growth bands

As a rule, grown-in dislocation lines are straight and follow preferred directions, which depend on the Burgers vector and the orientation of the growth face. These directions are characterized by the minimum of dislocation energy per unit growth length (27,28) or, in another but equivalent approach, by the vanishing of the force, exerted by the growth face upon the dislocation segments close to the surface.

In KDP a change in the preferred dislocation line directions in growth bands is observed. This has been reported by Lutsau et al. (3) and is clearly visible in the topographs given in figure 12. There are two reasons which may be responsible for this feature:

(i) In growth bands, stresses produce forces on the dislocation line, shifting the zero-force direction to an orientation different from that of the unstressed crystal.

(ii) During growth, dislocation lines may be decorated by impurities. The impurity segregation changes the strain field and, consequently, the energy of the dislocation, thus leading to another preferred direction of minimum energy. The decoration of dislocations in KDP, as indicated by an anomalous X-ray diffraction topographic contrast, has been reported by Lutsau et al. (3). An anomalous contrast of dislocation lines is visible on the topograph in figure 12a (label X). It belongs to dislocation lines with Burgers vector |001|. They are out of contrast in reflection 020, except for the segments X lying in a "strong" growth band. Obviously, there is an increased absorption of impurities along these segments.

5. CONCLUSIONS

Conclusions, drawn from the present study on the relation between several growth phenomena and the internal structure of large KDP crystals can be summarized as follows:

(i) The growth rate of KDP is strongly influenced by the dislocation density. This may be explained by a dependence of the growth mechanism (e.g. growth via single or cooperating spirals or 2D nucleation) on the dislocation density.

(ii) The quasi periodicity of veils of liquid inclusions in large KDP crystals has been explained by mutual interaction between the hydrodynamics (i.e. the wake of the crystal) and the internal dislocation structure.

(iii) The growth bands in the front part of the KDP crystals are different from those in the back part. This difference may be explained by a different hydrodynamic environment in combination with variations in interface kinetics.

(iv) A change in the preferred dislocation line directions in growth bands has clearly been shown in the KDP crystals studied. Two possible explanations are given for this phenomenon.

ACKNOWLEDGEMENTS

The authors are indepted to Prof. Dr. P. Bennema for stimulating discussions and for his kind interest in the present study.

One of us (W.J.P. van Enckevort) acknowledges the support of the Netherlands Foundation for Pure Research, ZWO/SON.

REFERENCES

(1) G. Marie, Philips Res. Rept. 22 (1967) 110.

(2) J. Carmine Salvo, IEEE Trans. Electron Devices ED-18 (1971) 748.

(3) V.G. Lutsau, Yu.M. Fishman and I.S. Res, Kristall und Technik 5 (1970) 243.

(4) C. Belouet, E. Dunia and J.F. Pétroff, J. Crystal Growth 23 (1974) 243.

(5) H. Klapper, Yu.M. Fishman and V.G. Lutsau, Phys. Stat. Sol. (a) 21 (1974) 115.

(6) C. Belouet, M. Monnier and J.C. Verplanke, J. Crystal Growth 29 (1975) 109.

(7) Yu.M. Fishman and V.G. Lutsau, Phys. Stat. Sol. (a) 3 (1970) 829.

(8) C. Belouet and W.T. Stacy, J. Crystal Growth 44 (1978) 315.

(9) B. Dam and W.J.P. van Enckevort, J. Crystal Growth 51 (1981) 607; Chapter XI.

(10) C. Belouet, M. Monnier and R. Crouzier, J. Crystal Growth 30 (1975) 151.

(11) Y.M. Fishman, J. Crystal Growth 41 (1977) 296.

(12) J.L. Torgesen and R.W. Jackson, Science 148 (1965) 952.

(13) W.J.P. van Enckevort, R. Janssen- van Rosmalen and W.H. van der Linden, J. Crystal Growth 49 (1980) 502; Chapter VIII.

(14) A.A. Chernov, I.L. Smol'ski, V.F. Parvov, Yu.G. Kuznetzov and V.N. Rozhanskii, Sov. Phys. Dokl. 24 (1979) 760.

(15) R. Janssen- van Rosmalen, Thesis (1977), Delft, The Netherlands

(16) R. Janssen- van Rosmalen, W.H. van der Linden, E. Dobbinga and D. Visser, Kristall und Technik 13 (1978) 17.

(17) A.C. Walker and G.T. Kohman, AIEE Transactions 67 (1948) 5661.

(18) A.R. Lang, J. Appl. Phys. 30 (1959) 1748.

(19) A. Izrael, J.F. Pétroff, A. Authier and Z. Malek, J. Crystal Growth 16 (1972) 131.

(20) H. Klapper, Z. Naturforsch. 28a (1973) 614.

(21) W.K. Burton, N. Cabrera and F.C. Frank, Phil. Trans. Roy. Soc. (London) 243 (1951) 299.

(22) P. Bennema, in: Industrial Crystallization (Ed. J.W. Mullin, Plenum Press, 1976) p. 91.

(23) R. Janssen- van Rosmalen and P. Bennema, J. Crystal Growth 42 (1977) 224.

(24) S.S. Friedmann, N.S. Stepanova and A.W. Beljustin, Kristall und Technik 6 (1971) 77.

(25) S. Gits-Leon, F. Lefaucheux and M.C. Robert, J. Crystal Growth 44 (1978) 659.

(26) S. Gits-Leon, M.C. Robert et Albert Zarka, Bull. Minéral. 101 (1978) 399.

(27) H. Klapper, J. Crystal Growth 10 (1971) 13.

(28) H. Klapper, J. Crystal Growth 15 (1972) 281.

Ann. Chim. Fr., 1979, 4, pp. 451-459

CHAPTER X:

ON THE OCCURRENCE OF A CRITICAL DRIVING FORCE FOR DISSOLUTION: THEORY AND EXPERIMENTAL OBSERVATION ON KDP AND OTHER CRYSTALS

P. BENNEMA, W.J.P. VAN ENCKEVORT

RIM Laboratory of Solid State Chemistry, Catholic University of Nijmegen,
Toernooiveld, Nijmegen, The Netherlands

Summary : The theory of Cabrera and Levine concerning the occurrence of a critical driving force for dissolution,below which the crystal opens up around a dislocation at the surface, forming macroscopic etch pits,is generalized. It is shown that the calculated and observed critical driving force for KDP agree very well. Dissolution experiments on potash alum and silicon which support the theory are also discussed.

Résumé : Sur l'existence d'une force motrice critique de dissolution : théorie et observation expérimentale sur le KDP et d'autres cristaux.- La théorie de Cabrera et Levine, concernant l'existence d'une force motrice critique lors de la dissolution superficielle d'un cristal autour d'une dislocation (formation de piqures d'attaque) est généralisée. Pour le KDP, les valeurs calculées et observées sont en très bon accord. Les résultats obtenus sur l'alun de potassium et sur le silicium confirment également la théorie

1. INTRODUCTION

Already in 1954 Cabrera, Levine and Plaskett [1] and in 1956 Cabrera and Levine [2] (see the last part of ref. [2]) developed a simple thermodynamical theory from which it could be derived that above a certain critical undersaturation a stationary dissolution process is possible and below this critical undersaturation a non stationary very fast dissolution process may occur. In between an undersaturation of zero and the critical undersaturation a stationary spiral dissolution process around a screw dislocation [2] or a repeated negative two dimensional nucleation process favoured by an edge dislocation may occur. Below the critical undersaturation a dissolution catastroph may occur around the screw or edge dislocation and the crystal may open up, so forming etch pits.

It is the first aim of this paper to make the presuppositions of the dissolution theory of Cabrera et al. explicit and to generalize this theory. The second aim is to show briefly that for the pyramidal faces of KDP such a critical value is indeed found using two totally different dissolution experiments and that the results of these experiments are in very good agreement with each other and also with the theoretically calculated value of the critical undersaturation. These two experiments are :
(i) dissolution kinetics measurements by means of the rotating disc technique

---

Reprints : P. BENNEMA, RIM Laboratory of Solid State Chemistry, Catholic University of Nijmegen, Toernooiveld, Nijmegen, The Netherlands.

carried out by R. Janssen-van Rosmalen et al., [3, 4] (ii) etch pit studies carried out by W.J.P. van Enckevort et al. [5].

This paper is a first general paper on the phenomenon of the critical undersaturation. In a forthcoming paper the theory of the critical undersaturation value will be treated as a part of the spiral growth and dissolution process under the influence of stress fields of dislocations and stress fields not related to dislocations [6].

Also the experimental data and their theoretical interpretation are and will be described in more detail elsewere. (See ref. [3], [4] and [7] respectively.)

The structure of this paper is now as follows:

In section 2 the relevant part of the theory is discussed. In section 3 the results of the experiments on {101} faces of KDP will be described. In section 4 we briefly describe some recent etching experiments on the {111} faces of alum and the {111} faces of silicon, where this phenomenon of critical undersaturation is also found. This also will be published in more detail elsewere (work in progress, see ref. [7, 8]).

2. THEORY

In what follows we consider a crystal as a homogeneous body, where each particle (atom, molecule or ion etc.) has a chemical potential μ_s. Also the fluid in contact with the crystal is supposed to be a homogeneous body, where the solute particles have a chemical potential μ_f. We suppose that $\mu_f < \mu_s$ and $\Delta\mu = \mu_f - \mu_s$ is the thermodynamic driving force for dissolution. We asume that the solid and fluid phase are separated by a flat surface and that we have imposed on the solid phase a cylindrically symmetric eleastic stress field, in principle (but not necessarily) related to a screw, edge or mixed dislocation.

The axis of this cylindrical stress field is supposed to be more or less perpendicular to the plane dividing the solid and fluid phases.

The accumulative strain energy function is given by

$$E(r) = C\,F(r) \tag{1}$$

where F(r) is a function of r, r being the radius perpendicular to the axis of the cylindrical coordinate system and C a constant.

The strain density $\rho(r)$ is given by

$$\rho(r) = \frac{\frac{dE(r)}{dr}dr}{2\pi r\ dr} = \frac{C'f(r)}{r} \tag{2}$$

where

$$f(r) = \frac{dF(r)}{dr} \tag{3}$$

and

$$C' = \frac{C}{2\pi} \tag{4}$$

Eq. (2) is obtained from eq. (1) by realizing that the energy of a volume $2\pi r\ dr \times 1$ determined by the surface area of a ring with a surface $2\pi r\ dr$ times the unit length of the cylinder is given by the numerator of the middle part of eq. (2).

It follows from eq. (1) that no "vertical" changes in the stress field which undoubtely will occur upon going from the bulk of the solid state to its surface (due to surface relaxation) are taken into consideration.

Let us now make as a thought experiment a hollow cylinder around the axis of the cylindrically shaped stress field with radius r. We assume, that this cylinder is filled with the homogeneous fluid of the fluid phase in which all the solute particles have the same μ_f. We now change the radius of the hollow core from r to r + dr, where dr is an infinitisimal increase of r.

The free energy of the system hollow core-crystal-surface-supersaturated solution then changes with a value dG due to (i) the transformation of strained crystalline particles with a chemical potential $\mu_s + \Delta\mu_s(r)$ into non strained crystalline particles with μ_s. (ii) the transformation of non strained crystalline particles into supersaturated solute particles. (iii) the increase of the surface of the cylinder.

Contribution (i) gives a decrease in free energy due to a release of the strain $dG_{(i)} = - 2\pi r dr\ \rho_s(r)$

Contribution (ii) gives an increase in free energy due to the increase in μ of the particles : $dG_{(ii)} = \frac{2\pi r dr}{\Omega}\Delta\mu$, where Ω is the molecular volume of the atoms in the crystal.

Contribution (iii) gives also an increase in free energy since the surface of the cylinder with unit length increases with $2\pi dr$ so that $dG_{(iii)} = 2\pi dr\ \gamma$ where γ is the surface free energy of the cylinder wall in contact with the solution.

Adding the three contibutions gives for the total free energy change

$$dG = 2\pi\gamma\left(\frac{r}{r_c} + 1 - \frac{C'f(r)}{\gamma}\right)dr \qquad (5)$$

where r_c is the radius of the critical circular two dimensional nucleus

$$r_c = \frac{\gamma\Omega}{\Delta\mu} \qquad (6)$$

Now a stable hollow core with a radius $r = r_{hc}$ occurs if a minimum is identified in the G(r) plot i.e. if the following two conditions are fulfilled:

$$(a)\ \left.\frac{dG}{dr}\right]_{r=r_{hc}} = 0 \quad (b)\ \left.\frac{a^2G}{dr^2}\right]_{r=r_{hc}} > 0 \qquad (7)$$

In case of a screw, edge or mixed dislocation f(r) is a "convex" monotonously decreasing function of r. In what follows we will investigate a "convex" f(r) function as given in figure 1 below.

Realizing that for dissolution $\Delta\mu$ is negative and according to eq. (6) r_c is also negative we plot the two functions $1 - |\frac{r}{r_c}|$ and $\frac{C'f(r)}{\gamma}$ in one plot (see figure 1).

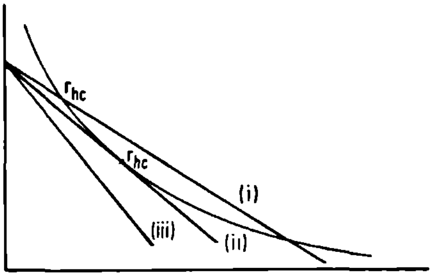

Figure 1: $1 - |\frac{r}{r_c}|$ for different $|\Delta\mu|$ and $\frac{C'f(r)}{\gamma}$ versus r

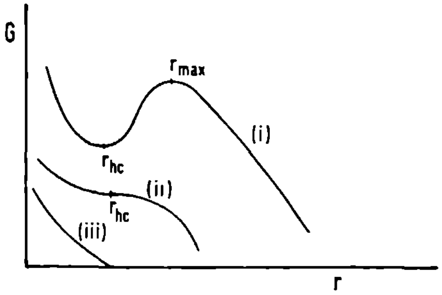

Figure 2: G(r) versus r

It can be seen from eq. (5) that where these functions intersect each other condition (a) of eq. (7) is fulfilled. From figure 1 it can be seen that the following cases can be distinguished:

(i) if $|\Delta\mu|$ is smaller than a certain critical value

$$|\Delta\mu_{cr}|$$

the function

$$1 - \frac{r}{|r_c|}$$

cuts the function

$$\frac{C'f(r)}{\gamma}$$

in two points. Since for the smallest root

$$\left.\frac{C'}{\gamma}\frac{df(r)}{dr}\right|_{r=r_{hc}}$$

is larger than

$$\frac{d}{dr}\left(1 - \frac{r}{|r_c|}\right),$$

it can be concluded that

$$\left.\frac{d^2G}{dr^2}\right|_{r=r_{hc}} > 0$$

giving a stable hollow core. Since for the largest root,

$$\left.\frac{d^2G}{dr^2}\right|_{r=r_{hc}} < 0$$

we have here a maximum in the G(r) plot and this corresponds to an instable hollow core (see also figure 2).

(ii) If $|\Delta\mu|$ becomes equal to a certain critical

$$|\Delta\mu_{cr}|,\ 1 - \frac{r}{|r_c|}$$

is tangent to

$$\frac{C'f(r)}{\gamma}$$

and (a) of eq. (7) is fulfilled, but

$$\left.\frac{d^2G}{dr^2}\right|_{r=r_{hc}} = 0$$

This means that at $r = r_{hc}$ an inflection point occurs, where a minimum and a maximum corresponding to case (i) coincide. We note that $\Delta\mu_{cr}$ is defined as the value for which one inflection point occurs at the G(r) curve (see figure 2).

(iii) If $|\Delta\mu| > |\Delta\mu_{cr}|$, the

$$1 - \frac{r}{|r_c|}$$

curve and the

$$\frac{Cr(r)}{\gamma}$$

curves do not intersect each other, no minimum occurs in the G(r) plot and G(r) becomes a monotonicly decreasing function. This means that even for a very small hollow core with an infinitisimal radius the free energy decreases continuously if the radius of the hollow core increases.
In figure 2 above we have plotted a G(r) curve for three cases (i), (ii) and (iii) respectively. It can be seen that for the first case that if we start with a hollow cylinder with a radius $0 < r < r_{max}$ there will be a driving force to charge r to r_{hc}. If $r > r_{max}$ there is a driving force to make r infinite. For case (iii) there is a driving force for any hollow core with a radius r to go to infinity so in principle the hollow core "opens up", forming a macroscopic etch pit. We note that case (ii) is a transition between case (i) and (iii).

So far we have treated the physical background using as a tool figure 1 and qualitative G(r) plots (figure 2) among others of the dissolution theory of Cabrera et al.

In order to obtain numerically testifyable values for $|\Delta\mu_{cr}|$ we will specify F(r) and f(r) as used in eqs. (1) and (2). The generally accepted accumulative elastic stress function E(r) somewhat away from the core of a dislocation for an isotropic medium is given by

$$E(r) = \frac{\mu b^2}{4\pi} K(\psi) \ln r + C'' \qquad (9)$$

where μ is the shear modulus, b is the height of the Burgers vector and C" a constant. K(ψ) is given by the following expression

$$K(\psi) = \frac{\sin^2\psi}{1-\nu} + \cos^2\psi \qquad (10)$$

where ν is the Poisson ratio and ψ the angle between the Burgers vector and the dislocation line. In case of a pure screw dislocation $\psi = 0$ and for a pure edge dislocation $\psi = \pi/2$. Using eq. (2) we obtain from eq. (9)

$$\rho_s(r) = \frac{\mu b^2}{8\pi^2} K(\psi) r^{-2} \qquad (11)$$

This makes f(r) proportional to r^{-1}, so giving a monotonicly decreasing "convex" function (see eq. (2). If we substitute this into eq. (5) we obtain

$$d6 = 2\pi\gamma\left(\frac{r}{r_c} + 1 - \frac{r_o}{r}\right) dr \qquad (12)$$

where

$$r_o = \frac{\mu b^2}{8\pi^2\gamma} K(\psi) \qquad (13)$$

Again realizing that for dissolution r_c given by eq. (6) is negative we see that making $dG/dr = 0$ gives a quadratic equation (obtained after multiplying eq (12) by r) so that

$$r_{hc} = \tfrac{1}{2}|r_c|\left(1 \mp \sqrt{1 - 4\frac{r_o}{|r_c|}}\right) \qquad (14)$$

As discussed for case (i) above the smallest root corresponds to a minimum in the G(r) plot and gives the radius of the stable hollow core. The largest root corresponds to an instable hollow core since G(r) is maximal. The case (i) corresponds to

$$|\Delta\mu| < |\Delta\mu_{cr}| = \frac{2\pi^2\gamma^2\Omega}{\mu K(\psi)b^2} \qquad (15)$$

For

$$|\Delta\mu| > |\Delta\mu_{cr}|$$

no solutions exist as can be seen from eq. (14) and the hollow core opens up. This corresponds to case (iii) discussed above.

We note that it can be seen from eq. (14) that if $|\Delta\mu|$ goes to zero $r_c \to \infty$ we get

$$\lim_{|\Delta\mu| \to 0} r_{hc} = r_o \qquad (16)$$

This gives the definition of r_o. It is defined as the radius of the stable hollow core if $\Delta\mu = 0$. This expression was first derived by Frank[7]

3. EXPERIMENTAL CHECK OF THE GENERALIZED CABRERA LEVINE THEORY FOR THE {101} FACES OF KDP

In the previous part of this paper we have treated the formation of macroscopic dislocation etch pits below a certain critical undersaturation from a purely thermodynamic point of view. This has the advantage that the critical value $\Delta\mu_{cr}$ can be calculated from our thermodynamic formalism. Here the kinetics were not taken in consideration, however. In the following part we will describe briefly experiments which enabled us to determine $\Delta\mu_{cr}$. For a more detailed description of the experiments and the necessary calculations of $\Delta\mu_{cr}$ we refer to ref. [3, 4] and especially ref. [5]. The following experiments were carried out:

(i) Crystals of KDP (KH_2PO_4) were embedded in plastic in such a way that only one pyramidal face of the set {101} could be exposed to the undersaturated solution. The cylindrical bloc of embedded crystal and plastic was mounted in a very precisely constructed rotating disc system, where the rate of dissolution in dependence of the angular velocity of the embedded crystal and the undersaturation was measured for a KDP solution, which was saturated at 30°C. Since for this rotating disc system the hydrodynamic regime is very well defined, the undersaturation at the crystal surface could be calculated precisely. Upon plotting the negative growth rate in dependence of the undersaturation at the surface, it was found that below a certain critical supersaturation given by

$$\sigma_{cr} = -0.70 \pm 0.07\%$$

the dissolution process goes very fast and the slope $\frac{dR}{d\sigma}$ becomes almost infinite. The observation of a rapid dissolution below $\Delta\mu_{cr}$ at the surface - observed during the first stages of the dissolution process suggests convincingly the formation of macroscopic pits below $\Delta\mu_{cr}$.

(ii) The next group of experiments to determine $\Delta\mu_{cr}$ were etching experiments.

The following observations were made upon observing the surface of KDP crystals with an optical interference contrast microscope. If $\sigma_{cr} < \sigma < 0$ where σ_{cr} has about the same value as given above, almost no etch pits could be observed. If, however, $\sigma < \sigma_{cr}$ a lot of etch pits could be seen. The number of etch pits varied between 30 to 1000 per cm^2. This number corresponds to the normal concentrations of dislocations which for rather perfect crystals may vary from 10^2 to 10^3 per cm^2.
That the etch pits indeed correspond to dislocation outcrops at the crystal surface will be shown elsewhere (ref [5] and [8]).

Upon comparing the results of the totally different experiments (i) and (ii), which lead to the same σ_{cr} we may conclude, that the idea of $\Delta\mu_{cr}$ is strongly supported.

In order to calculate $\Delta\mu_{cr}$ from σ_{cr} the data of the highly concentrated non ideal electrolytic KDP solutions concerning activity coefficients have to be taken into account (see ref. [5]).

The $\Delta\mu_{cr}$ resulting from the theory is calculated using eq. (15) derived above. Choosing relevant dislocations which intersect the surface at an angle which is not very different from 90° and taking into consideration the anisotropy of the crystal and the character of the dislocation leading to a proper value for μ and $K(\psi)$ and using an experimentally determined γ value one obtains (see ref. [5])

$$\left(\frac{\Delta\mu}{kT}\right)_{cr}^{theor.} = -0.0080$$

From the two types of experiments one gets:

$$\left(\frac{\Delta\mu}{kT}\right)_{cr}^{exp.} = -0.0067$$

Taking into consideration uncertainties in the value of the surface free energy and the neglect of surface relaxation effects, the agreement between observed and calculated values for $\Delta\mu_{cr}$ is very good. (For the calculations we refer to ref. [5].)

4. ETCHING EXPERIMENTS FOR ALUM AND Si

Similar etching experiments as described above for KDP were also carried out for the octahedral {111} faces of potash alum. In between a relative undersaturation of -1% and minus a few percents a certain amount of etch pits were formed which is obviously due to dislocations with a somewhat high Burgers vector. Below the lowest σ value just mentioned many etch pits were formed, which correspond to dislocations, which obviously have a sufficiently large Burgers vector to give macroscopic etch pits for this range of undersaturations.
The change from very flat etch pits (due to a spiral dissolution or repeated nucleation process) to steeper etch pits due to the formation of macroscopic pits is very critical; this was observed as follows:
A droplet of a largely undersaturated alum solution was planed on a {111} facet of an alum crystal and the formation of many etch pits was found. After a while - due to dissolution - the undersaturation of the droplet decreases and the in depth etching stops abrubtly. Now only the side faces of the etch pits were moving leaving a flat bottomed etch pit. This observation suggests convincingly the occurrence of a critical $\Delta\mu_{cr}$ (see ref. [9]).

It is interesting to note that due to evaporation after a while the droplet becomes supersaturated which causes the formation of a shallow hillock in the center of the flat bottom. This obviously is a spiral hillock formed around the screw dislocation which gave dissolution. That this kind of growth hillocks indeed are growth spirals has been shown in an earlier paper (ref. [10]). Experiments are now carried out to determine precisely $\Delta\mu_{cr}$ (work in progress, ref. [9]). In figure 3 the above described observations can be seen.

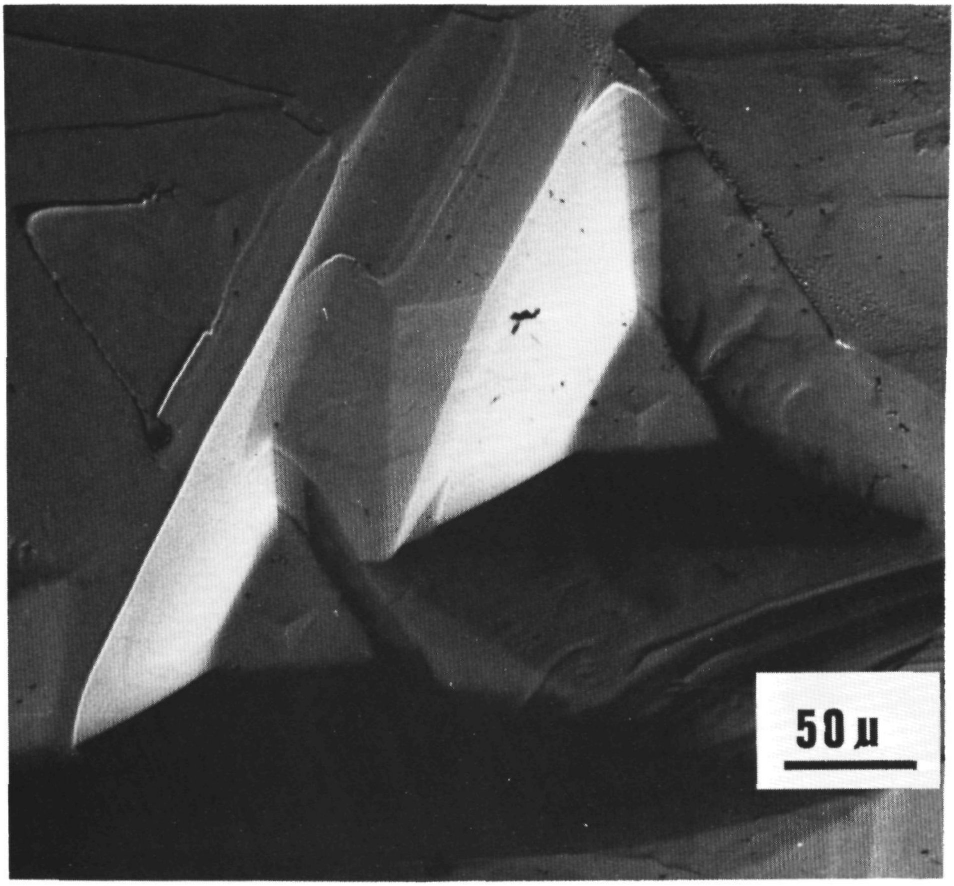

Figure 3 : **Photograph of a {111} potash alum surface. The flat bottomed etch** pits developed after the undersaturation decreased. When the undersaturated solution became supersaturated a shallow hill developed.

We finally mention the formation of etch pits on the {111} faces of Si as another experimental evidence for the occurrence of a $\Delta\mu_{cr}$. Gas phase etching of Si (111) wafers may lead to etch pit formation depending on temperature and HCl input concentration. In ref. [11] it was shown that a transition line was found in the P_{HCl}-T diagram separating two areas in the P_{HCl}-T plane; one region where the silicon surface remains smooth and the other one where the silicon surface becomes covered with etch pits. It was recently found by Tsukamoto et al. from extensive X-ray topographical studies that the etch pits are correlated to dislocations (ref. [12]). In a similar way as described above for alum it was found that if the undersaturation becomes less due to a reduction of the HCl concentration in the gas atmosphere the bottoms of the etch pits again abrubtly become flat. This abrubt transition corresponds with the observed boundary in the P_{HCl}-T diagram. The sudden change from flat to steep etching was also shown by the observation, that the macroscopic etch pits having the lowest inclination of the side faces have still an edge steepness of 33°. Lower inclinations were not observed.

5. CONCLUSIONS

From the simple generalized thermodynamic dissolution theory of Cabrera et al. it can be derived that due to stress fields, originating from dislocations, macroscopic pits are formed below a certain critical undersaturation.

It has been shown that the observed and calculated $\Delta\mu_{cr}$ for KDP agree very well. Strong evidence supporting the idea of $\Delta\mu_{cr}$ were discussed for the totally different systems of alum dissolving in an aqueous solution and Si etched in HCl atmosphere.

6. REFERENCES

[1] CABRERA (N.), LEVINE (M.M.), PLASKETT (J.S.), Phys. Rev. 96, 1954.
[2] CABRERA (N.), LEVINE (M.M.), Phil. Mag. 1, 1956, 450.
[3] JANSSEN-VAN ROSMALEN (R.), Thesis Technical University of Delft, 1977, Chapter VII.
[4] JANSSEN-VAN ROSMALEN (R.), VAN LEEUWEN (C.), RICHTER-VAN LEEUWEN (G.K.), SMITH (J.M.), Delft Progress Report 1, 1976, 150.
[5] VAN ENCKEVORT (W.J.P.), JANSSEN-VAN ROSMALEN (R.), VAN DER LINDEN (W.H.), BENNEMA (P,), to be published.
[6] VAN DER HOEK (B.), BENNEMA (P.), VAN DER EERDEN (J.P.), SUNAGAWA (I.), to be published in Journal of Crystal Growth.
[7] FRANK (F.C.), Acta Cryst. 4, 1951, 297.
[8] VAN ENCKEVORT (W.J.P.), JANSSEN-VAN ROSMALEN (R.), VAN DER LINDEN (W.H.), J. of Crystal Growth, to be published.
[9] VAN ENCKEVORT (W.J.P.), VAN DER LINDEN (W.H.), J. of Crystal Growth, to be published.
[10] VAN ENCKEVORT (W.J.P.), VAN DER LINDEN (W.H.), J. of Crystal Growth, 47, 1979, 196.
[11] VAN DER PUTTE (P.), GILING (L.J.), BLOEM (J.), J. of Crystal Growth, 41, 1977, 133.
[12] TSUKAMOTO (K.), YASUDA (T.), GILING (L.J.), to be published.

(Remis à l'éditeur le 25 octobre 1979)

Journal of Crystal Growth 51 (1981) 607-623

CHAPTER XI:

ON THE FORMATION OF ETCH GROOVES AROUND STRESS FIELDS DUE TO INHOMOGENEOUS IMPURITY DISTRIBUTION IN KH_2PO_4 SINGLE CRYSTALS

B DAM and W J P VAN ENCKEVORT *

RIM Laboratory of Solid State Chemistry Faculty of Science Catholic University Toernooiveld Nijmegen The Netherlands

Received 30 September 1980

It is shown that planar strain fields in potassium dihydrogen phosphate (KDP) single crystals, can be made visible as macroscopic etch grooves by etching polished {100}, {101} and {001} slices These planar strain fields are due to inhomogeneous impurity distributions in the crystal, for instance at the boundary of two growth sectors with different impurity contents or at the boundaries of the growth bands within a single growth sector The sensitivity of this method is similar as for X ray diffraction topography, but by etching a higher resolution (less than 1 μm) can be obtained The formation of the etch grooves and the increasing sensitivity of the etch method for the {100}, {101} and {001} plates successively is explained analogous to the thermodynamic dislocation theory of dissolution of crystals as formulated by Cabrera and Levine, combined with a consideration of some nucleation models for the initial opening up of the groove

1 Introduction

The habit of solution grown potassium dihydrogen phosphate (KDP) single crystals, space group $I\bar{4}2d$, is formed by a combination of prismatic {100} and pyramidal {101} faces as shown in fig 1 For these crystals two types of growth sectors can be distinguished (a) prismatic sectors, corresponding to growth in the ⟨100⟩ directions and (b) pyramidal sectors corresponding to growth in the ⟨101⟩ directions These growth sectors and the boundaries between them are shown schematically in fig 2 fig 2a shows a projection on a {001} face, whereas fig 2b gives a projection on {100}

The impurity content in the prismatic growth sectors can be a few orders of magnitude higher than in the pyramidal sectors This was first noticed by Jaffe and Kjellgren [1], who found that if the crystals were grown in a solution slightly contaminated with Cr^{3+} ions, those parts of the crystals where growth was governed by prismatic faces (in other words the prismatic growth sectors) showed a greenish colour By means of autoradiography of KDP {001} slices, Belouet et al [2,3] were able to confirm this difference in impurity content between both sectors On the same autoradiographs growth bands within the prismatic sectors could be observed These bands are due to slight variations in the growth conditions resulting in an inhomogeneous impurity capture Very detailed information about the strain fields originating from inhomogeneous impurity distributions can be obtained from Lang topographs [2-7] Besides the very strong contrasts at the prismatic-pyramidal sector boundaries pyramidal pyramidal sector boundaries and growth bands within the prismatic as well as within the pyramidal sectors were

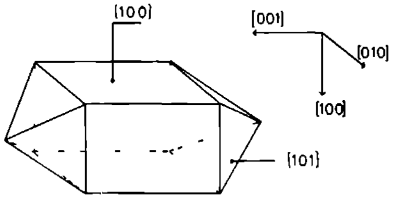

Fig 1 External morphology of KDP crystals, bounded by {100} and {101} faces

---

* All correspondence concerning this paper should be sent to W J P van Enckevort

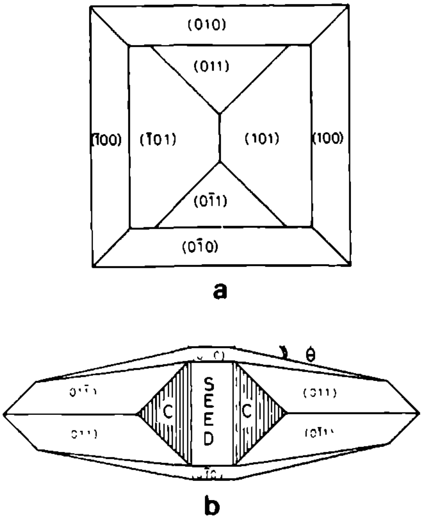

Fig. 2. Schematic representation of the growth sectors and the boundaries between them for an idealized situation (a) projection on the (001) plane, (b) projection on the (100) plane θ denotes the tapering angle and C the capping region [16,20].

revealed. The contrasts observed on the X-ray topographs at both the sector boundaries and the boundaries of the growth bands were found to be due to a strain field resulting from a difference in lattice parameters between both sides of these boundaries, induced by an inhomogeneous impurity distribution [2–6]

In the present work an etch method to reveal all the above mentioned strain fields is described. After application of this method the strained areas become visible as etch grooves on the surfaces of {001}, {101} and {100} plates.

Etching has rarely been applied to reveal sector boundaries or growth bands, one of the few cases reported in literature is HgI_2 etched with a 2% bromine solution in methanol [8]. On the other hand etching is a very common technique to reveal dislocation outcrops at the crystal surfaces [9,10]. Also from a theoretical point of view etching of planar defects such as sector boundaries or growth bands has hardly been treated in literature, this in contrast to the numerous papers about the formation of dislocation etch pits [9,11–15]. The only paper in which the formation of etch grooves due to planar defects perpendicular to the surface is discussed theoretically, has recently been written by Van der Hoek et al. [15].

Now the second aim of the present study is to interprete qualitatively the experimental work, using a modified version of the above-mentioned dissolution theory of crystals in presence of a planar stress field.

2. Experimental

2.1. Crystal growth

Large (about 12 X 3 X 3 cm^3) single crystals of KDP were grown by two different methods:

(i) By slow cooling (0.15°C/day) of a thermostated (±0.05°C) saturated solution in which the seeds, {001} slices, were mounted on the arms of a slowly rotating tree in a similar way as described by Janssen-van Rosmalen et al. [16]. The crystals, which could be "harvested" after a period of 6 to 8 weeks, were severely tapered [17,18], the tapering angle θ (see fig. 2) being 10–15°, but free from inclusions. During growth of crystals by this method the supersaturation was not well known.

(ii) By making use of a three vessel system of the Walker–Kohman type [19] in exactly the same way as pointed out in previous work [16,20] During growth of crystals by this method the conditions, such as temperature and bulk supersaturation were very well defined and in the present case fixed at 29.50°C and 4.2% respectively. Depending on the rotational velocity the crystals were flawed sometimes [16], but the amount of tapering, which is a measure for impurity capture [5,17], was much less ($\theta = 2$–$8°$).

For both methods of crystal growth pro analyse KDP containing 0.001% Fe was used.

2.2. Specimen preparation and observation technique

Specimens for observation of the etching pattern were plates, a few millimetres in thickness, cut with a metal-wire saw and polished on a clothed turn-table. The felty cloth was wetted with a mixture of 50%

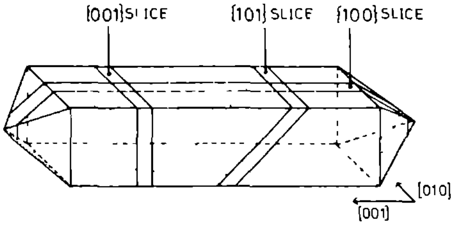

Fig. 3. Positions of the specimen plates {001}, {101} and {100} with respect to the external crystal form.

ethyl alcohol and 50% water. The alcohol was added in order to reduce the etch rate and thus to prevent a severe rounding off of the corners and edges of the plate. The final polishing was carried out using a thick, wetted soft cloth, upon which the crystal was moved gently. In this way a mirror-like smooth surface could be obtained.

The specimen plates were prepared in three different orientations (i) slices cut parallel to {100}, (ii) parallel to {101}, and (iii) parallel to {001}. All the three types of specimens have been pictured out in fig. 3.

Etching of the plate surfaces for obtaining an etch groove pattern, in order to reveal the strain fields in the crystal, occurred during the polishing procedure, though in the case of {100} slices it was sometimes necessary to whipe the crystal face with a wetted paper tissue.

Observation of the surfaces of the etched specimens was carried out by means of an optical reflection differential interference contrast microscope. In order to enhance the sensitivity of this microscopic method the plate surfaces were coated with a thin layer of silver or gold, using a sputter coating unit for scanning electron microscopy.

X-ray diffraction topographic observation of the specimen plates (thickness 1–2 mm) was carried out by means of a Lang camera using Ag Kα_1 radiation.

3. Results and discussion

3.1 Slices parallel to {001}

3.1 1. General features

Fig. 4a shows a typical etch pattern on a {001} slice consisting of numerous etch grooves. From comparison of this groove pattern with a schematized representation of all the kinds of growth bands and sector boundaries as have been observed by means of X-ray diffraction topography of {001} plates [2-5], as shown in fig. 4b, it can be concluded that all the etch grooves are related to these phenomena The grooves corresponding to the prismatic–pyramidal (sb1) and the pyramidal-pyramidal (sb2) sector boundaries and the growth bands in the prismatic sector (gb1) can be recognized most clearly, whereas the prismatic-prismatic sector boundaries (sb3) and the pyramidal growth bands (gb2) give less contrasted grooves. It was shown by means of X-ray diffraction topography, that both growth bands and sector boundaries originate from lattice deformations, due to a difference in lattice parameters in adjacent regions, caused by a variation in impurity content, which leads to local strain fields in these crystal area [2,5,6] Because of an increase in effective undersaturation at the – rectilinear – outcrops of these local strain fields at the slice surfaces, these are preferred sites for dissolution, leading to the formation of etch grooves

Comparing this etch technique with X-ray diffraction topography (see figs. 4c and 4d), it can be concluded that for etching the resolution (about 1 μm) is slightly higher as well as it is less laborious to be carried out. The sensitivity of this etch method is similar (and in some cases even higher!) as for X-ray diffraction topography, except for long range strain fields where Lang topography is superior.

The difference in growth method of the crystals clearly established itself in a variation of the etch groove pattern For crystals grown by the temperature decrease method (section 2.1 (i)) numerous growth bands, originating from instabilities in the growth conditions, which are typical for this method, could be seen (fig. 4a). On slices of crystals grown in the three-vessel system (section 2.1 (ii)) the etch grooves related to growth bands were much less abundant. Crystals grown from recrystallized, highly pure, material, which were not tapered at all and showed no optically visible defects, did not reveal any groove pattern – nor related to sector boundaries, nor to growth bands - at all From this observation it can be concluded that the major cause of the growth bands and sector boundaries is a local variation in impurity content.

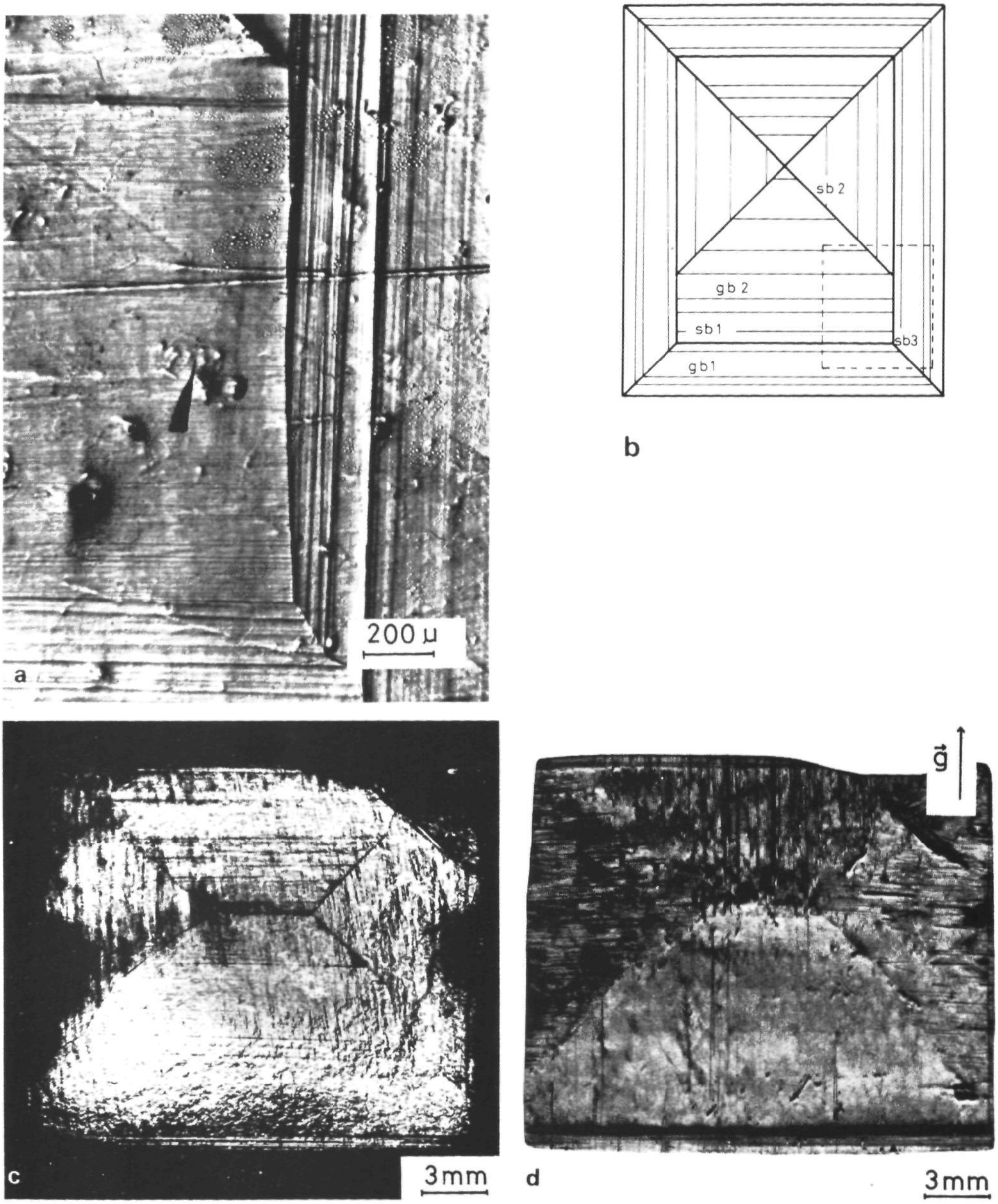

Fig. 4. Typical etch groove pattern on a $\{001\}$ KDP slice: (a) interference contrast micrograph; (b) schematic diagram showing the various sector boundaries and growth bands, visible on the $\{001\}$ plates. The dashed lined rectangle indicates the area of (a); (c) general view of an etched $\{001\}$ slice; (d) Lang topograph of the same specimen plate as (c). Ag $k\alpha_1$ radiation, $\mu t \approx 1.5$.

3.1.2. Pyramidal sectors

Often the four pyramidal growth sectors are separated by four well developed etch grooves corresponding with the pyramidal–pyramidal sector boundaries (see figs. 2a and 4–6). Belouet et al. [5] concluded from X-ray diffraction topography, that the strain field around these sector boundaries can be caused in two ways: (i) by a slight angular misorientation between two neighbouring sectors or (ii) by a distortion in lattice parameter due to a segregation of impurities, leading to a difference in unit cell parameters between adjacent sectors. From the fact that after etching no groove pattern could be obtained on slices of crystals grown from highly pure recrystallized material, it can be concluded that cause (ii) is actually predominant.

In addition, in the pyramidal sectors themselves many grooves related to growth bands, originating from fluctuations in impurity segregation [4,5] could be distinguished. Usually it could be seen that within one single growth sector the growth bands were uniform, but in general they did not correspond with the growth bands in adjacent sectors (see figs. 4–6). This phenomenon has also been observed by means of Lang topography [5,7] and by means of the Schlieren method [21]. From these observations it can be concluded that besides fluctuations in the liquid phase, also the surface processes play an essential role in the formation of the growth bands.

Another feature showing that surface kinetics are highly important in the formation of growth bands and can lead to variations in difference in growth rate between adjacent sectors is the occurrence of stepped pyramidal–pyramidal sector boundaries as shown in fig. 5. The steps in the sector boundary are clearly related to the growth bands. This phenomenon was observed especially for lower quality crystals grown by the temperature decrease method at higher supersaturations. The stepped boundaries can be explained in terms of short-time (~30 min) fluctuations in growth rate of the pyramidal facets, keeping in mind that for adjacent faces these rapid changes are not related to each other. Probably these fluctuations in growth rate of the pyramidal facets are similar to the oscillations in growth rate of {101} ADP, due to a variation in impurity coverage of the crystal surfaces as has been reported by Davey and Mullin [22]. These variations in growth rate, leading to differences in impurity segregation, cause the growth bands related to the step sites in the sector boundaries.

Fig. 5. Stepped pyramidal–pyramidal sector boundary, visible on an etched {001} plate, demonstrating the short time fluctuations in difference in growth rate between two adjacent pyramidal sectors (interference contrast micrograph).

Apart from the small stepped perturbations in the pyramidal–pyramidal sector boundaries, also large curvatures can occur as shown in fig. 6. These are very similar to some kinds of the parasitic growth gosts that have been observed by Belouet et al. [2], but are here regarded as long-time (~30 h) variations in the growth rates of the individual {101} facets. As the groove pattern related to the sector boundaries on the {001} slices in fact reveals a time sequence of the relative widths of the pyramidal facets during crystal growth, the angle (β) between the pyramidal–pyramidal sector boundary outcrop at the slice surface and the ⟨100⟩ direction is a measure for the relative growth rate of the adjacent facets. From simple geometrical considerations it could be concluded that

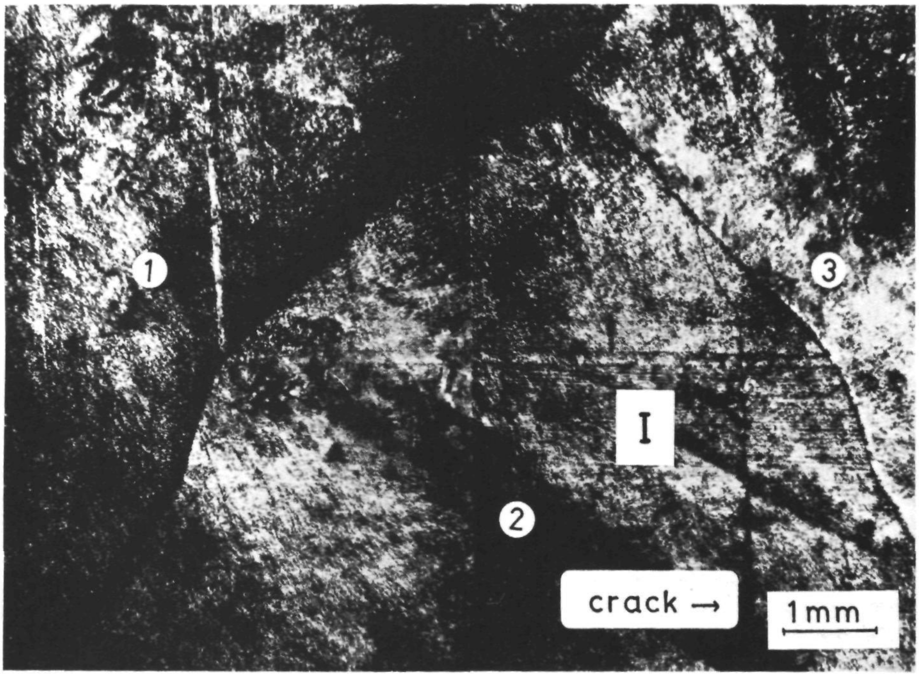

Fig. 6. Etched {001} plate showing long range curvatures in the pyramidal–pyramidal sector boundaries, indicating long time variations in difference in growth rate between adjacent pyamidal facets (optical micrograph).

the ratio between the growth rates of two adjacent pyramidal sectors equals the tangent of this angle β. For instance in region I of fig. 6, where $\beta \approx 70°$, the growth rate of face 2 was about 2.8 times higher than of faces 1 and 3. Probably these long-time variations in growth rate are caused by an appearance and disappearance of cooperating spirals with different activities [23] on the {101} facets. Similar changes in growth rate related to dislocation bundle outcrops at the crystal surfaces have been observed with the aid of Lang topography by van Enckevort et al. [7], while Davey [24] reported different growth velocities between adjacent pyramidal facets too. Moreover these cooperating spirals on {101} KDP actually have been observed by means of optical interference contrast microscopy [25]. Often these variations in growth rate are accompanied by growth bands, as shown in fig. 6. It is suggested that these growth bands originate from a change in impurity segregation due to the increase in growth rate.

In nearly all cases the prismatic–pyramidal sector boundaries gave the most well developed etch grooves. This can easily be understood from the fact that the impurity content can differ as much as a few orders of magnitude for the two types of sectors [2,26]. This extremely large difference in impurity content gives a highly developed strain field around the prismatic–pyramidal sector boundaries, leading to the most clearly visible etch grooves.

3.1.3. Prismatic sectors

After etching an {001} slice, in the prismatic sectors the growth band pattern can easily be revealed as etch grooves as shown in fig. 7. Numerous parallel lines with different contrasts, caused by a variation in strain as a result of a difference in impurity content

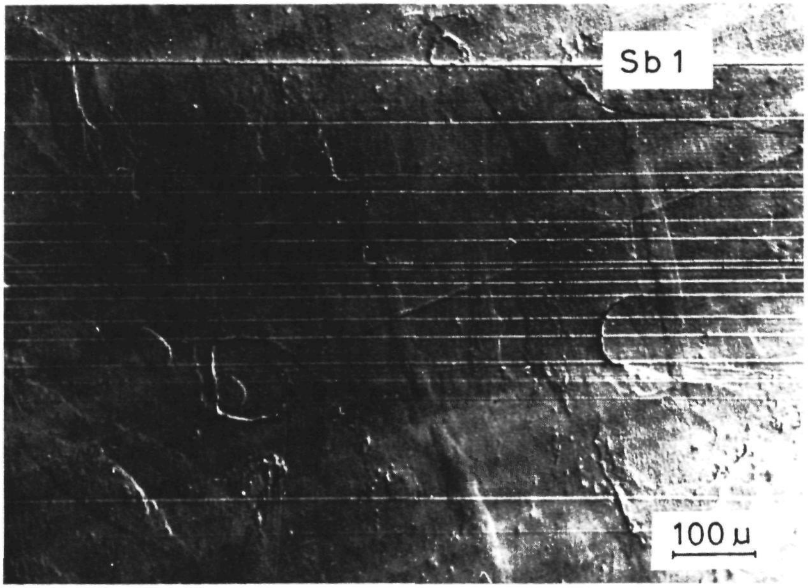

Fig. 7. Prismatic growth bands and prismatic–pyramidal sector boundary (Sb1) visible on an etched {001} slice (interference contrast micrograph).

for the individual growth bands, can be seen. In general, on the same slice these etch grooves are more clearly developed than those who are related to the growth bands in the pyramidal sectors. This is in agreement with the observation by Belouet et al. [2] that for the prismatic sectors the variations in iron content with growth parameters was found to be relatively large as compared to those in the pyramidal sectors.

In contrast to the growth bands in the pyramidal sectors, those in the prismatic sectors mostly continue on adjacent sectors (fig. 8). This indicates that the growth bands in the prismatic sectors usually originate from fluctuations in the mother liquor from which the crystals grow. However, in lower quality crystals (especially some of those grown by the temperature decrease method) many prismatic growth bands do not continue on neighbouring sectors (fig. 4). From this observation it can be concluded that in these cases, surface kinetics also plays an important role in the formation of the growth bands.

Another indication for a difference in growth rate between adjacent prism faces of some – especially lower quality – crystals is that the prismatic–prismatic sector boundaries (which were found only in the presence of prismatic growth bands) often have a stepped nature (fig. 4), similar to some of the pyramidal–pyramidal sector boundaries as treated in the foregoing section. In general some of the prismatic growth bands are correlated to the steps in the sector boundaries showing a correspondence between the fluctuations in growth rate and impurity capture. The origin of these differences in growth rate and impurity capture between adjacent {100} faces is not very clear, maybe these are related to a disparity in the macrostep pattern [18,25] or in the activities of the cooperating growth spirals operative [27] on these faces.

3.2. Slices parallel to {101} and {100}

On {101} slices after etching a similar etch groove pattern as observed on {001} slices can be revealed as shown in fig. 9. Clearly the groove corresponding to

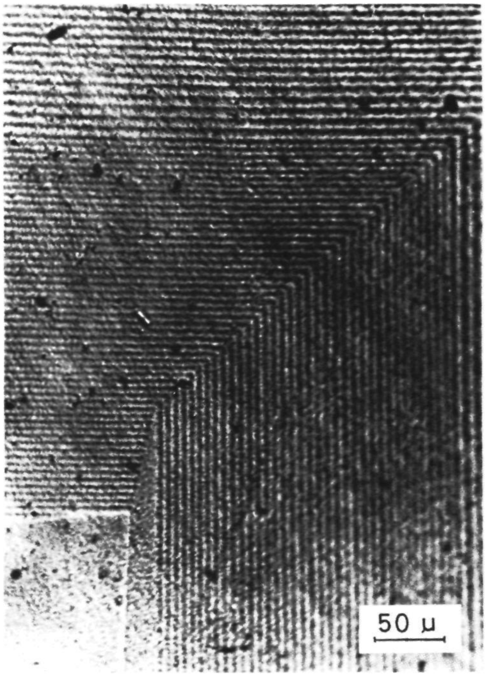

the pyramidal–prismatic sector boundary (sb1) and also some grooves related to prismatic growth bands can be recognized, but the contrasts are considerably lower than for {001} slices. By comparing etched {001} and {101} slices of the same crystal it was found that the number of etch grooves in the prismatic sectors was much lower for the {101} plates. As for the growth bands and the sector boundaries in the pyramidal sectors, in contrast to the {001} slices on the {101} plates they could not even be revealed.

In most areas also a few deformed dislocation etch pits [25,28], which did not interfere seriously with the groove pattern could be seen. However, often their number was much less than observed on etched asgrown {101} faces, because of the misorientation of the real crystal surface with respect to the {101} plane, due to a non-exact cutting of the slice. In the few cases of very low misorientated surfaces, which were studded with etch pits, often the most impor-

Fig. 8. Numerous prismatic growth bands near a prismatic–prismatic sector boundary, demonstrating the high resolution of the etch method. Note that the growth bands continue on adjacent sectors (interference contrast micrograph).

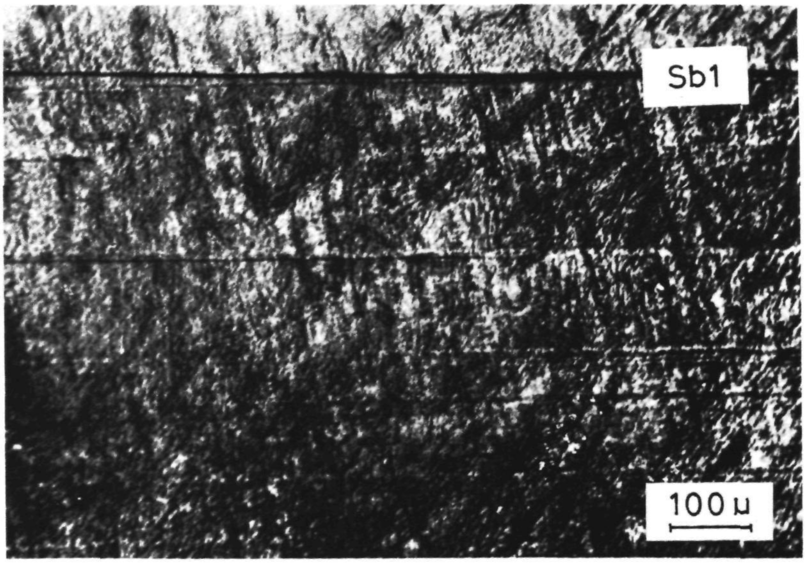

Fig. 9. Prismatic–pyramidal sector boundary (Sb1) and prismatic growth bands on an etched {101} slice. This {101} plate and the {001} plate shown in fig. 4a were cut from the same crystal (interference contrast micrograph).

tant grooves still remain visible, traversing the etch pits.

In contrast to the {001} and {101} slices on {100} slices hardly any groove pattern could be observed, even after etching in pure water. In some cases the prismatic–pyramidal sector boundary could be revealed on the bunched surface. However, usually the groove pattern is overwhelmed by the numerous bunches and macrosteps, caused by the low misorientation of the crystal surface with respect to the crystallographic {100} plane as a result of a non-exact cutting of the slice. A similar bunch pattern due to such a misorientation has also been observed on gas phase etched silicon slices [29]. When the misorientation is very large, i.e. the real surface is revolved 20 degrees or more around the [001] axis with respect to the exact {100} plane, the sector boundaries and prismatic growth bands become clearly visible as shown in fig. 10. In these cases the contrast is still lower than for the {001} slices.

The trajectory of the pyramidal–prismatic sector boundary shows, going from the seed to the top faces of the crystal, a gradual decrease in size of the pyramidal sector (fig. 2b), which indicates that the tapering theory of Byteva [18,30] is incorrect. According to this hypothesis tapering is caused by an inhomogeneous dislocation distribution on the {100} faces. These dislocations, mainly emerging at the centre of the crystal are the sources of the – due to impurity effects – slowly advancing (macro) steps, whose distribution on the prismatic faces is responsable for the tapering. According to this model the prismatic–pyramidal sector boundaries must run parallel to {100}, which does not agree with the observed inclinations of these boundaries. The definite explanation of the tapering should take in account the gradual decrease in size of the pyramidal sector [31].

For a few crystals the prismatic–pyramidal sector boundary had a stepped nature, as shown in fig. 10. This indicates sudden changes in growth rate of one of both adjacent faces, in a similar way as discussed in foregoing sections for the stepped prismatic–prismatic or pyramidal–pyramidal sector boundaries.

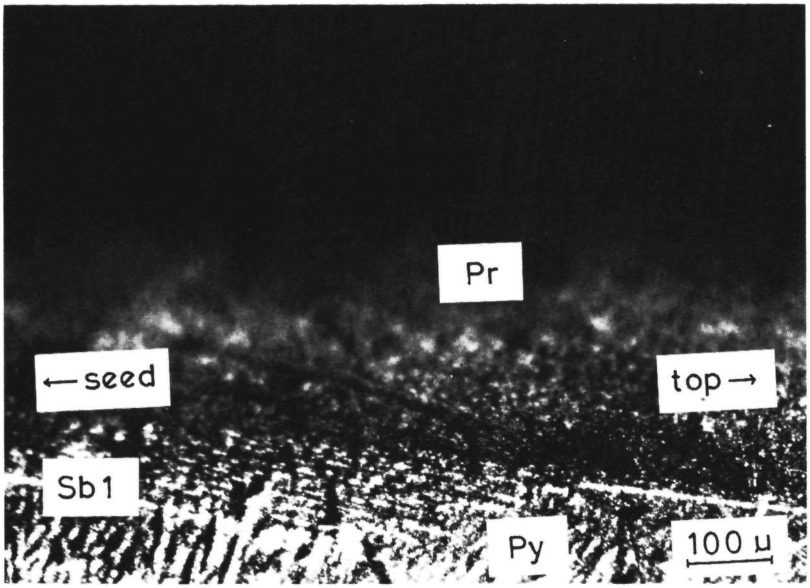

Fig. 10. Etch groove pattern revealing a stepped prismatic–pyramidal sector boundary (Sb1) and some prismatic growth bands on an about 25° misoriented {100} plate. Py pyramidal sector, Pr prismatic sector (interference contrast micrograph).

3.3. Etching parallel to the strain field

Etching of small ($5 \times 5 \times 15$ mm^3) heavily tapered (tapering angle $\theta \approx 20°$) KDP crystals, with only very thin prismatic growth sectors, often revealed cavities, which were not normal to the tapered or the central non-tapered prismatic surfaces, but rather undercut them (fig. 11). The mechanism of this process, which is outlined schematically in fig. 11c, is as follows: First after a vertical etching, for instance via the formation of a dislocation etch pit, the heavily strained area near the prismatic–pyramidal sector boundary is reached. Then a horizontal etch starts along this sector boundary, because of a preferred dissolution at this planar, heavily strained, region. In this way, soon some etch holes below the crystal surface are formed.

3.4. Comparison of the sensitivity of the etch method on the various slices

As mentioned in the foregoing sections the sensitivity (i.e. the number of grooves which can b revealed) of the etch method successively increases for the KDP {100}, {101} and {001} slices. On the

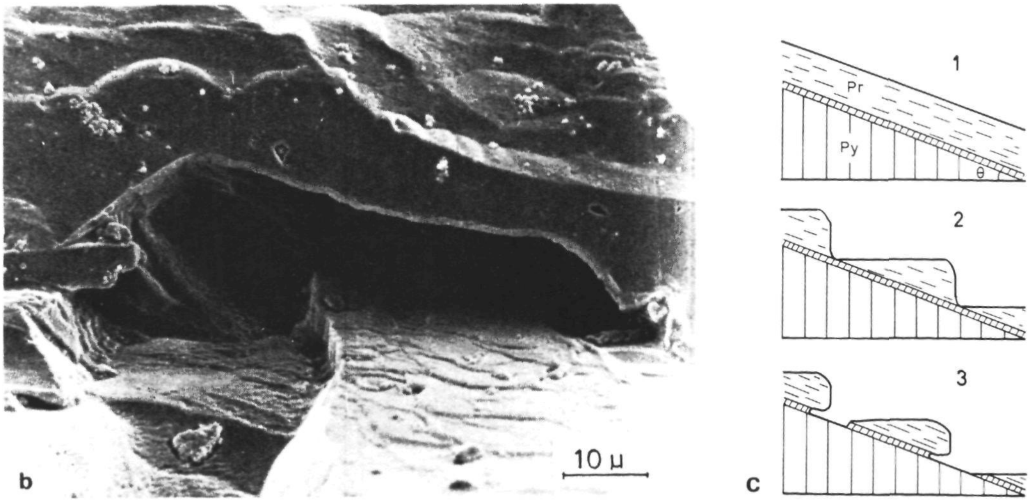

Fig. 11. Etching parallel to the strain field: (a) cavities undercutting the heavily tapered prismatic faces of a slightly etched KDP crystal, grown in a highly impure solution (SEM photograph); (b) detail of (a); (c) schematic representation showing the successive stages of the formation of "caves" paralleling the tapered prismatic surface. Py pyramidal sector, Pr prismatic sector, θ tapering angle.

{100} slices only in some cases the prismatic–pyramidal sector boundary could be revealed after etching in pure water On the {101} slices some grooves related to the prismatic sectors could be revealed, even after etching in a slightly undersaturated solution whereas on {001} all the types of growth bands and sector boundaries as have been observed by means of X ray diffraction topography [5] could clearly be recognized after etching in slightly undersaturated solutions So it can be concluded that for a given undersaturation the minimum stress which leads to etch groove formation decreases in the slice order {100}, {101}, {001} In the following chapter this sequence in sensitiveness will be interpreted in terms of a theoretical model for etch groove formation

4 Theory of etch groove formation

4 1 Thermodynamical model for groove expansion

Analogous to the "dislocation theory for evaporation of crystals" developed by Cabrera, Levine and Plasket [11,12,32] which describes from a thermodynamical point of view the formation of macroscopic etch pits around dislocations, a similar thermodynamic model for the formation of etch grooves will be given in this section An excellent general description of the influence of stress fields on the growth or dissolution of crystals is given by Van der Hoek et al [15]

In the following we consider the non strained crystal as a homogeneous body, in which each particle (atom, ion or molecule) has the same chemical potential μ_s In the solution – also considered as a homogeneous body – which is in contact with the crystal, the solute particles have a chemical potential μ_f Because in the case of dissolution, which is considered here, $\mu_f < \mu_s$, the thermodynamic driving force for crystal growth $\Delta\mu = \mu_f - \mu_s$ is negative

It is assumed that the solid phase and the liquid phase are separated by a flat solid–fluid interface Now a planar stress field with a strain density (= strain energy per unit volume) function $\rho(x, y, z) = \rho(x)$ is imposed as shown in fig 12 This kind of planar stress field is typical for the strained area around sector boundaries or growth bands [3,6] Because the strain density function $\rho(x)$ is hardly known for both the sector boundaries and the growth bands, it is assumed that $\rho(x)$ can be any function of x The only restrictions to $\rho(x)$ are (i) $\rho(x) > 0$ because here a negative strain field has no physical relevance and $\rho(x \to \infty) = 0$, for at an infinite distance from the sector boundary or growth band its stress field goes to zero

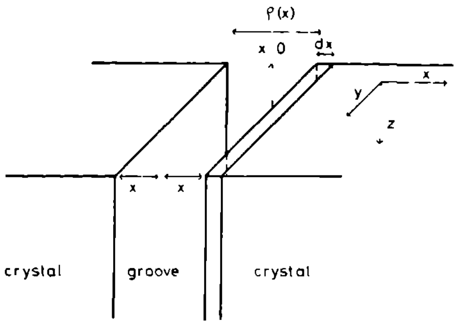

Fig 12 Representation of the expansion of an etch gorge over an infinitesimal distance dx

Now we make as a thought experiment a groove with plan parallel flat boundaries perpendicular to the crystal surface with a length and a depth of unit length and a width $x + x$ (see fig 12) We assume that the right wall of the groove makes an infinitesimal shift of dx Because the situation for the left wall is the same as for the right wall, in the following the left one will not be considered explicitly The infinitesimal increase in free energy dG due to the shift dx of the right wall consists of three parts [11,32]

(i) $\mathrm{d}G(\mathrm{i}) = -\rho(x)\,\mathrm{d}x$, due to a transformation of strained crystalline particles into non-strained particles with a chemical potential μ_s

(ii) $\mathrm{d}G(\mathrm{ii}) = (\Delta\mu/\Omega)\,\mathrm{d}x$ (Ω is the volume of one crystalline particle), resulting from a transformation of non-strained solid particles into undersaturated solute particles

(iii) $\mathrm{d}G(\mathrm{iii}) = 2\sigma\delta(x)$, where σ is the surface free energy of the side faces of the groove and $\delta(x)$ the Dirac delta function

This means that in contrast to the cases of etch pit formation around cylindrical stress fields of dislocations [11,15,32], the surface, and so also the surface energy, does not change during opening up of an etch groove, except for $x = 0$, where the cleavage energy barrier has to be overcome

Adding the three contributions gives a total free energy change of

$$dG(x) = [\Delta\mu/\Omega + 2\sigma\,\delta(x) - \rho(x)]\,dx \qquad (1)$$

Realizing that $\rho(x)$ is always positive (except when $x \to \infty$) and $\Delta\mu$ is negative, the conclusion can be drawn that $(dG(x)/dx)_{x \neq 0}$ is always negative, so $G(x)$ is a monotonously decreasing function. This means that even for a very narrow groove, having an infinitesimal width, the free energy decreases continuously if the width of the groove increases In other words as soon as for some reason an infinitesimal narrow groove has been formed, it opens up, forming a macroscopic etch groove visible by optical microscopy This opening up will -- from a thermodynamical point of view -- always occur, independently of the type of face or stress field, so this model cannot explain the observed difference in sensitivity of etch groove formation on the various KDP slices. Therefore it can be concluded that the initial nucleation (i e the first formation of a narrow groove) must account for this difference in sensitivity.

An important point, which can affect seriously the final shape of the etch grooves is the volume diffusion of the solute particles in the liquid phase However, since this hardly influences the relative sensitivity of the etch method on the various slices, it will not be discussed in this paper An excellent treatise on the two-dimensional volume diffusion problem in relation to crystal growth or dissolution, which is also applicable in the case of etch groove formation, is given by Chernov and Budurov [33,34]

4.2 *Initial nucleation*

In principle the initial nucleation of an etch groove at $x = 0$, here defined as the locus where $\rho(x)$ is maximal, can take place according to both a two-dimensional and an one-dimensional nucleation mechanism as shown in figs 13a and 13b

Two-dimensional nucleation will occur, when the nucleus density is high and the dependence of $\rho(x)$ on x at $x \approx 0$, i e.

$$|(\partial^2\rho(x)/\partial x^2)_{x=0}|\,,$$

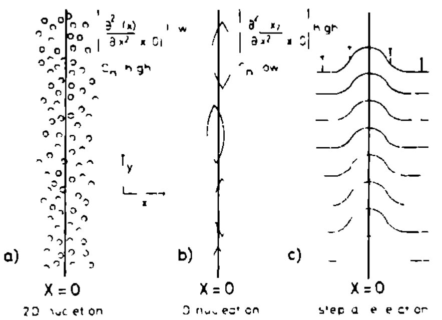

Fig 13 Diagram giving three possible mechanisms for the initial nucleation of etch grooves (a) two-dimensional nucleation (C_n = nucleus density) (b) one dimensional nucleation (c) step acceleration near the stress field during the dissolution of surfaces having a misorientation with respect to the exact crystallographic plane

is relatively small (fig. 13a) On the other hand, one-dimensional nucleation will occur at $x \approx 0$, when the density of the nuclei is low and

$$|(\partial^2\rho(x)/\partial x^2)_{x=0}|$$

is high (fig 13b) An intermediary case between both nucleation mechanisms is also possible

In the expressions for the growth rates and so also for the etch rates, since growth and etching are complementary processes, for both one and two-dimensional nucleation the nucleation rate which can be written as [35,36]

$$I = k^+ C_1(X_s)(\beta\,\Delta^0\mu_{tot})^{1/2}\exp(-C_2\beta\gamma^2/\Delta^0\mu_{tot})\,, \qquad (2)$$

and the step advancement rate, given by [35,36]

$$v_{step} = k^+ A_{st}(X_s)[1 - \exp(-\beta\,\Delta^0\mu_{tot})]\,, \qquad (3)$$

are both involved [35–37] In these equations $C_1(X_s)$ and $A_{st}(X_s)$ are constants depending on the mean surface diffusion distance of an adatom, X_s, C_2 is a geometrical constant, γ the edge free energy of a growth unit in a step and β equals $1/kT$ (k Boltzmann's constant, T absolute temperature) The attachment frequency of the solute particles on the crystal surface [35,36] is given by k^+, whereas $\Delta^0\mu_{tot}$ is the overall difference in chemical potential between the solid and the solute particles at $x \approx 0$, which is equivalent to

$$|(\mu_f - \mu_s) - \rho(x)_{x\approx 0}\,\Omega|$$

For two-dimensional nucleation, when γ is not too low the etch rate is given by [35,36]

$$R_{etch} \propto (I^{\alpha} v_{step}^{1-\alpha}), \tag{4}$$

with $\alpha \approx \frac{1}{3}$, which yields for not too high values of $\beta\Delta^0\mu_{tot}$

$$R_{etch} = k^{+} A_1 (\beta\,\Delta^0\mu_{tot})^{A_2} \exp(-A_3\beta\gamma^2/\Delta^0\mu_{tot}), \tag{5}$$

where A_1, A_2 and A_3 are numerical constants depending on the choice of the elementary processes and the spreading mechanisms of the nuclei. A_1 is strongly dependent on X_s in contrast to A_2 and A_3. A similar dependence of the etch rate on the effective supersaturation $\beta\Delta^0\mu_{tot}$ was also found by Monte Carlo computer simulations [35,36,50].

In contrast to two-dimensional nucleation, the one dimensional nucleation problem could be treated exactly. This was done by Frank [37], who was able to give an implicit expression for the growth (etch) rate in terms of the nucleation rate per unit length (which again depends on I and $\rho(x)$) the step advancement rate and the length of the substrate (here etch groove).

For the formation of an etch groove it is necessary that the "initial nucleation" rate near the center of the groove (R_{groove}) is higher than the etch rate of the crystal surface outside this groove ($R_{crystal}$). Steps on the crystal surface, which are responsible for $R_{crystal}$ can originate from the following sources:

(i) A (local or non-local) misorientation of the crystal surface, resulting from a non-exact cutting of the crystal slice.

(ii) The edges of the crystal, from which often the dissolution process starts.

(iii) Dislocation etch pits or dissolution spirals.

(iv) Two-dimensional nucleation.

From the foregoing it can be concluded that numerous factors determine the condition $R_{groove} > R_{crystal}$, necessary for etch groove formation. A difference in fulfilment of this condition on the various KDP slices is the final cause for the difference in sensitivity of the etch method for these slices.

A special kind of initial opening up, which only occurs on crystal surfaces with a considerable misorientation with respect to the exact crystallographic plane, is caused by a local increase of the advancement rate of the steps on the crystal surface due to the stress field, also leading to the formation of etch grooves as shown in fig. 13c. This phenomenon was especially observed on {101} slices studded with dislocation etch pits, where some grooves remained faintly visible on the side faces (often these were inclined up to about 15–20° with respect to the exact {101} plane) of the pits. This feature was also seen on a few very carefully polished and non bunched {100} slice surfaces with a large misorientation. Such a relation between stress field and step advancement rate has been treated for the case of growth – where instead of an acceleration a step retardation takes place – both theoretically [38] and experimentally [25].

The above mentioned possible mechanisms for initial opening up of the etch grooves only hold for surfaces where the edge free energy of steps does not approach zero. For crystal surfaces, where the step edge free energy goes to zero (the so called rough faces [35,36]) there is no nucleation barrier for the initial opening up of the etch grooves. This means that the etch rate inside the groove is always higher than elsewhere on the crystal surface as will be shown in section 4.3.2, so that during etching independently of the undersaturation and stress field always etch grooves are formed.

4.3. Application to the etch groove formation on KDP

4.3.1. {101} and {100} KDP plates

It is well established that the {101} and {100} faces of KDP are F-faces [39]. This could be concluded both from periodic bond chain (PBC) analysis [40,41] and from experimental observations of steps on these surfaces [25,42]. From this PBC analysis, carried out by Hartman [40], it was deduced that a KDP {101} slice [39] is very similar as a {111} slice of the sphalerite or diamond lattice, having three laterally bonded nearest neighbours. On the other hand, a KDP {100} slice is similar to a {001} slice of a Kossel crystal [43], having four laterally bonded nearest neighbours.

In the following discussion, as a rough approximation, only the nearest neighbour interactions (i.e. the strong bonds between ions in the first coordination sphere) are considered This assumption has successfully been applied by Hartman for the construction of the PBC's in his periodic bond chain analysis of KDP [40] The first order lateral bonds of the {101} slices are purely formed by bonds of type (a) (cf Hartman [40] p 722), having a first order electro static bonding energy of $-0\ 2603\ e^2/\text{Å}^{-1}$, whereas the {100} slices have lateral bonds consisting of 50% type (a) and 50% type (b) [40], the latter having an electrostatic bonding energy of $-0\ 2866\ e^2/\text{Å}^{-1}$ So for the {101} and {100} slices the average first order bonding energy ϕ_{ss} [44] differs only about 5% So it can be concluded that the standard temperature θ [35] which is defined as

$$\theta = \frac{0\ 88kT}{\frac{1}{2}(\phi_{ss} + \phi_{ff}) - \phi_{sf}}, \tag{6}$$

where ϕ_{ss} ϕ_{ff} and ϕ_{sf} denote the potential energies of solid–solid, fluid -fluid and solid–fluid bonds respectively, is nearly equal for the {101} and the {100} faces, since ϕ_{sf} and ϕ_{ff} do not vary with a change in crystallographic orientation

Recent Monte Marlo simulation results of nucleation growth (or dissolution, since growth and etching are more or less complementary processes) of a {111} diamond face [45] show that for a given θ and $\Delta\mu/kT$ the etch rate of a {111} diamond-like surface is much higher than of a {001} Kossel face [46,42] This especially holds for standard temperatures below the roughening point [35], which is the case for both the {101} and the {100} faces of KDP as can be concluded from the observation of steps on both faces [25,42] So the conclusion can be drawn that R_{groove}, which is governed by nucleation, will be much higher for {101} KDP plates than for {100} plates

Also from a point of view of more "classical" nucleation theories there is evidence that the etch rate in the groove, governed by nucleation, will be higher for the {101} plates This is shown as follows For both one and two-dimensional nucleation the etch rate in the groove, R_{groove}, depends strongly on γ, the edge free energy of a growth unit in a step, since in the etch rate expressions for both mechanisms the nucleation rate I, which is given by eq (2), is involved So for a given $\beta\Delta^0\mu_{\text{tot}}$, R_{groove} will increase strongly for decreasing γ, because the edge free energy appears squared in the exponential term of I

In order to compare $\gamma\{101\}$ and $\gamma\{100\}$, one can use the relation between the edge free energy per growth unit in a step, γ, and some properties of growth spirals, as given by Sohnel [47]

$$\gamma = f(v)\,(y/h)\,kT \ln S_a/19, \tag{7}$$

where S_a is the supersaturation based on activities, $f(v)$ is the ratio between the advancement rate of a monomolecular step and a (macro-)step of the spiral, y is the distance between the (macro)-steps and h is the step height The ratio (y/h) is also equal to the reciprocal value of the tangent of the inclination of a spiral hillock From this equation the ratio between the edge free energies of the {101} and {100} faces can be estimated

$$\frac{\gamma\{101\}}{\gamma\{100\}} = \frac{f(v)\{101\}}{f(v)\{100\}}\ \frac{[(y/h)\ln S_a]\{101\}}{[(y/h)\ln S_a]\{100\}} \tag{8}$$

For KDP {100} the data in eq (6) are [47,48] y/h = 330, $S_a \cong 1{,}083$ (according to Sohnel et al [49] for KDP the supersaturations based on activities and molalities are very similar) and $f(v) = 1$ On the other hand, data for {101} KDP were obtained from Van Enckevort et al [25] being $(y/h)_{\text{averaged}} = 420$ $S_a \approx 1\ 042$ and $f(v) = 1$ Here only the growth hillocks originating from single (unit) dislocations have been considered (where $f(v) = 1$), since for cooperating macrospirals [25], eqs (7) and (8) do not hold

Substitution of these values in eq (6) yields a ratio between $\gamma\{101\}$ and $\gamma\{100\}$ of 0 65 Because $\gamma\{101\}$ is lower than $\gamma\{100\}$, it can be concluded that for a given $\beta\Delta^0\mu_{\text{tot}}$ R_{groove} will be higher for the {101} than for the {100}-plates

Also from a more theoretical point of view it can be understood that $\gamma\{101\}$ must be lower than $\gamma\{100\}$, since for a given standard temperature θ the diamond-like {101} face is much nearer to the roughening transition temperature than the Kossel like {100} face This means that the edge free energy for nucleation will be much lower for {101} than for {100} KDP, because γ decreases to zero near the roughening temperature [35,50,51]

As for the etch rate outside the groove R_{crystal}, it could be concluded from surface topography that in general, this etching proceeds via steps originating from a misorientation of 1–2° of the crystal surface with respect to the exact crystallographic plane, due to a non-exact cutting of the slice, or from a local misorientation visible as an orange peel surface or as bunches. So the etch rate on the crystal is given by

$$R_{crystal} = \rho_{steps}\, v_{step}, \qquad (9)$$

where ρ_{steps} is the number of steps per unit length and v_{step} is the advancement rate of the steps.

Since nucleation in the grooves requires that the average distance between two nuclei has to be less than the step distance on the surface, ρ_{steps}^{-1}, it can be deduced that the average distance between the nuclei in the etch grooves on KDP must be less than ~100 Å On the other hand, from X-ray diffraction topography it was determined that the widths of the stress fields near sector boundaries and growth bands in KDP have an order of magnitude of 10^6 Å and also that $(\partial^2\rho(x)/\partial x^2)_{x=0}$ is not too large, otherwise the Penning and Polder theory would not be applicable [6]. This means that probably the initial nucleation is governed by a two-dimensional nucleation mechanism, since the variation of $\rho(x)$ at $x \approx 0$ is small with respect to the average nucleus distance in the groove.

Monte Carlo simulations [43] showed that the dependence of the step advancement rate, and the two-dimensional nucleation rate on the mean surface diffusion length was very similar, so for the same face the ratio between R_{groove} and $R_{crystal}$ will not be affected seriously by a variation in surface diffusion. Compared to the two- (or one-)dimensional nucleation rate, or R_{groove}, the dependence of the step advancement rate, or $R_{crystal}$, on the type of crystal lattice or edge free energy is, aside from the above mentioned surface diffusion, very much lower.

From the foregoing it can be concluded that the ratio $R_{groove}/R_{crystal}$, the most important criterion for groove formation, is mainly affected by a variation in crystallography of a slice or in edge free energy, being strongly dependent on the former This ratio is higher for the diamond-like {101} KDP face with a lower edge free energy, than for the Kossel-like {100} face, which explains the higher sensitivity of the etch method for the {101} plates compared to the {100} plates.

Anisotropy in $\rho(x)$, which depends on the anisotropy in difference in lattice parameter between two adjacent regions with different impurity content, can not account for the observed differences in $R_{groove}/R_{crystal}$ for the various plate orientations For this two arguments can be given (i) The anisotropy of the difference in lattice parameters between the adjacent regions near the prismatic–pyramidal sector boundaries or the prismatic growth bands is rather low This was demonstrated by comparing the contrasts of these features on the X-ray topographs of an {001} and an {100} plate, cut from the same crystal As diffraction vector, g, a vector parallel to the plate surface and perpendicular to the sector boundary or growth bands was chosen, because in this case the contrast – after taking into consideration the effects resulting from a departure from Friedel's law – is a measure of the lattice parameter difference component perpendicular to the plate surface [6] Since the contrasts for the {100} and the {001} plates (for both $g = \langle 200 \rangle$) were very similar it can be concluded that the anisotropy in lattice parameter difference and so also in $\rho(x)$ is rather low. (ii) The dependence of $R_{groove}/R_{crystal}$ on variations in $\rho(x)$ (e.g caused by anisotropy) is much less than on differences in edge free energy, as can be concluded from eq. (5).

4 3.2. {001} KDP slices

From surface topographic investigations it is strongly suggested that {001} KDP behaves like a rough face [35] In terms of the periodic bond chain theory this means as an F face above the roughening transition temperature [35] or as a face composed of two S faces belonging to two different zones, similar to {001} fluorit [41], or as an ordinary S or K face The conclusion that in an aqueous solution {001} KDP is a rough face was drawn from the following experimental observations (i) Neither steps, nor a bunch like pattern, indicating that growth takes place by a layer by layer (step flow) mechanism, were ever observed (by means of interference contrast microscopy) on etched {001} faces. (ii) Growth of this face resulted in the formation of numerous {101} microfacets, covering the surface This is the beginning of the so-called capping process as has been observed during growth of KDP crystals from {001} slices as seeds [16,20]. (iii) Slight growth of single crystal spheres of KDP did never reveal {001} facets [52]

Also from a theoretical point of view, the {001} face can be considered as a rough face as was deduced by several PBC analyses of KDP or the isostructural ADP. At first Hartman concluded that {001} KDP is an F face formed by two very weak periodic bonds chains ⟨110⟩ However, F_{slice} is very low [40], so if this holds, probably {001} will be an F face around or above the roughening transition temperature In a later paper [41] Hartman concluded from energetical calculations that the periodic bond chains ⟨110⟩ have no physical relevance and that it is better to consider {001} KDP as an S face This face can be considered as composed of two S_1 faces belonging to different zones, which appear simultaneously Since a step at $T > 0$ K is to be considered as rough [35], it can be concluded that an S_1 face, which is purely made up of steps behaves like a rough face Finally Aguilo [53] concluded from a new PBC analysis of ADP that {001} is a K face

From the fact that {001} KDP is a rough face, it can be concluded that dissolution of this face is governed by a "normal growth" mechanism where the dissolution rate is given by a modified Wilson–Frenkel law [35]

$$R_{etch} = k^{+} A [1 - \exp(-\beta \Delta\mu_{tot})] \qquad (9)$$

In this equation A is a proportionality constant depending on the standard temperature θ and the mean surface diffusion distance of the adatoms, while $\Delta\mu_{tot}$ equals $|\Delta\mu|$ for the unstrained surface area and $|\Delta\mu - \rho(x)\,\Omega|$ for the strained area Hence it follows that the ratio between the etch rates in the groove and at the unstrained crystal surface on the {001} slices is given by

$$\frac{R_{groove}\{001\}}{R_{crystal}\{001\}} = \frac{1 - \exp(-\beta|\Delta\mu - \rho(x)\,\Omega|)}{1 - \exp(-\beta|\Delta\mu|)} \qquad (10)$$

From this equation the conclusion can be drawn that the etch rate inside the groove is always higher than elsewhere on the crystal surface, independently of the undersaturation or stress field So the extreme high sensitivity of the {001} face for groove formation can now be understood from the consideration that this face is a rough face

Also the enormous increase in sensitivity, mentioned in section 3 2, of the etch method in comparison with the exact {100} plane, on surfaces with a misorientation of 20° or more to this crystallographic plane, can be explained in terms of rough faces This kind of misoriented face can be considered as an S_n face between the F faces [40] (100) and (010) with $n \approx 2$–3 or between the F faces (100) and (110) with $n \approx 1$ So this surface can be regarded more or less as a rough face, leading for similar reasons as mentioned earlier for the {001} face, to the observed increase of the sensitivity of the etch method

5 Conclusions

Sector boundaries and growth bands in potassium dihydrogen phosphate single crystals can be made visible on cutted crystal plates by a simple etch technique combined with reflection differential interference contrast microscopy During this etching procedure the planar stress fields near the sector boundaries and growth bands (caused by a lattice deformation due to a difference in impurity contents between adjacent areas) lead to a local increase in effective undersaturation, which can enhance locally the dissolution rate, resulting in the formation of etch grooves at the outcrops of these planar stress fields at the plate surfaces Compared with X ray diffraction topography; for {001} plates this etch method gives a higher resolution and is more convenient to be carried out, without any loss in sensitivity

Several growth features concerning growth bands and sector boundaries were studied in detail by this method For instance, from the etch groove pattern it could be deduced that both short time and long time variations in the relative growth rates of adjacent faces were very common during crystal growth

A theoretical model both for expansion and for initial nucleation of the etch grooves explains the increasing sensitivity of the etch method for the {100}, {101} and {001} plates respectively From this model it is suggested that for revelation of sector boundaries and growth bands in crystals it is better to apply etching on "rough" faces than on "flat" surfaces with high slice energies

Acknowledgements

The authors wish to thank W H van der Linden for growing the crystals and Ing A W Dicke for making the SEM micrographs Further they are grateful to Dr K Tsukamoto for his valuable comments on the surface topographs and to Ing J Odekerken for making the X ray topographs They are also thankful to Professor P Bennema, Dr J.P van der Eerden and Ir B van der Hoek for stimulating discussions and critical reading of the manuscript One of us (W J P van Enckevort) acknowledges the support of the Netherlands Foundation for Pure Research, ZWO/SON

References

[1] H Jaffe and B R E Kjellgren, Disc Faraday Soc 5 (1949) 319
[2] C Belouet, M Monnier and J C Verplanke, J Crystal Growth 29 (1975) 109
[3] C Belouet and W T Stacy, J Crystal Growth 44 (1978) 315
[4] V G Lutsau, Ju M Fishman and I S Res, Kristall Tech 5 (1970) 445
[5] C Belouet, E Dunia and J F Petroff, J Crystal Growth 23 (1974) 243
[6] Yu M Fishman and V G Lutsau, Phys Status Solidi (a) 3 (1970) 829
[7] W J P van Enckevort, R Janssen-van Rosmalen, H Klapper and W H van der Linden, J Crystal Growth, to be published
[8] M Schieber, I Beinglass, G Dishan and A Holzer, in Current Topics in Materials Science, Vol 2, Eds E Kaldis and H J Scheel (North-Holland, Amsterdam, 1977) p 279
[9] R B Heimann, Auflosung von Kristallen, Technische Mineralogie, Vol 8 (Springer, Berlin, 1975)
[10] W J P van Enckevort and W H van der Linden, J Crystal Growth 47 (1979) 196
[11] N Cabrera and M M Levine, Phil Mag 1 (1956) 450
[12] N Cabrera, M M Levine and J S Plaskett, Phys Rev 96 (1954) 1153
[13] W Schaarwachter, Phys Status Solidi 12 (1965) 375
[14] W Schaarwachter, Phys Status Solidi 12 (1965) 865
[15] B van der Hoek, P Bennema and J P van der Eerden, J Crystal Growth, to be published
[16] R Janssen-van Rosmalen, W H van der Linden, E Dobbinga and D Visser, Kristall Tech 13 (1978) 17
[17] R J Davey and J W Mullin, Kristall Tech 11 (1976) 229
[18] J Fontcuberta, R Rodriguez and J Tejada, J Crystal Growth 44 (1978) 593
[19] A C Walker and G T Kohman, AIEE Trans 67 (1948) 566
[20] R Janssen-van Rosmalen, Thesis, Technical University of Delft (1977)
[21] S S Friedmann, N S Stepanova and A W Beljustin, Kristall Tech 6 (1971) 77
[22] R J Davey and J W Mullin, J Crystal Growth 23 (1974) 89
[23] W K Burton, N Cabrera and F C Frank, Phil Trans Roy Soc (London) 243 (1951) 299
[24] R J Davey, Thesis, University of London (1973)
[25] W J P van Enckevort, R Janssen van Rosmalen and W H van der Linden, J Crystal Growth 49 (1980) 502
[26] C Belouet, Acta Electron 16 (1973) 339
[27] P Bennema, J P van der Eerden, W J P van Enckevort, B van der Hoek and K Tsukamoto, Phys Status Solidi (a) 55 (1979) 403
[28] H Gulzow, in Growth of Crystals, Vol 7, Ed N N Sheftal (Consultants Bureau, New York, 1968) p 82
[29] P van der Putte, W J P van Enckevort, L J Giling and J Bloem, J Crystal Growth 43 (1978) 659
[30] I M Byteva in Growth of Crystals, Vol 5B, Ed N N Sheftal (Consultants Bureau, New York, 1968) p 26
[31] W J P van Enckevort and B Dam, work in progress
[32] P Bennema and W J P van Enckevort, Ann Chim 4 (1979) 451
[33] A A Chernov and S I Budurov, Soviet Phys -Cryst 9 1964) 309
[34] A A Chernov and S I Budurov, Soviet Phys -Cryst 9 (1965) 388
[35] J P van der Eerden, P Bennema and T A Cherepanova, in Progress in Crystal Growth and Characterization, Vol 1 (Pergamon, Oxford, 1978) p 219
[36] J P van der Eerden, Thesis, Catholic University of Nijmegen (1979) p 56
[37] F C Frank, J Crystal Growth 22 (1974) 233
[38] B van der Hoek, P Bennema and J P van der Eerden, J Crystal Growth, to be published
[39] P Hartman, in Crystal Growth, An Introduction, Ed P Hartman (North-Holland, Amsterdam, 1973) pp 358–402
[40] P Hartman, Acta Cryst 9 (1956) 721
[41] P Hartman, Neues Jahrb Mineral Monatsh 4 (1959) 73
[42] J L Torgesen and R W Jackson, Science 148 (1965) 952
[43] G H Gilmer and P Bennema, J Appl Phys 43 (1972) 1347
[44] P Bennema and J P van der Eerden, J Crystal Growth 42 (1977) 201
[45] W J P van Enckevort and J P van der Eerden, J Crystal Growth 47 (1979) 501
[46] G H Gilmer and P Bennema, J Crystal Growth 13/14 (1972) 148
[47] O Sohnel, Kristall Tech 13 (1978) 1163
[48] Z Solc and O Sohnel, Kristall Tech 8 (1973) 811
[49] O Sohnel, J Garside and S J Jančic, J Crystal Growth 39 (1977) 307
[50] S W H de Haan, V J A Meeussen, B P Veltman, P Bennema, C. van Leeuwen and G H Gilmer, J Crystal Growth 24/25 (1974) 491
[51] P Bennema, J Boon, C van Leeuwen and G H Gilmer, Kristall Tech 8 (1973) 659
[52] B Dam, unpublished
[53] M Aguilo, Thesis, University of Barcelona (1979)

SILICON

Journal of Crystal Growth 45 (1978) 90–96

CHAPTER XII:

THE INFLUENCE OF ADSORPTION AND STEP RECONSTRUCTION ON THE GROWTH AND ETCHING VECTORS OF SILICON (111)

W.J.P. VAN ENCKEVORT and L.J. GILING
Laboratory of Solid State Chemistry, RIM, Catholic University, Toernooiveld, Nijmegen, The Netherlands

The lateral growth and etching vectors which are published for silicon and related materials appear to differ between the vacuum(or gas)–solid systems and the liquid–solid system: the vectors are 180° rotated with respect to each other. A theoretical analysis based on a first order broken bond model and assuming either unaffected dangling bonds or completely saturated dangling bonds leads to growth and etching vectors consistent with the vector orientations observed in the liquid–solid system. When step reconstruction is taken into account a similar treatment leads to the 180° rotated vector orientations which are found in the vacuum(or gas)–solid systems.

1. Introduction

Although considerable interest exists in the chemistry of the chemical vapour deposition of silicon, only a few papers are published on the morphological aspects connected with growth and etching. Only recently the growth kinetics and the influence of input concentrations and temperature on the morphology have been studied in more detail [1–4]. In the course of our studies on the etching of silicon, interest arose in the theoretical background of the orientations of the lateral growth and etching vectors on (111) orientated silicon, especially because in the last few years many contradicting observations have been published by several workers [5–8]. A systematic study of the existing literature of this phenomenon soon revealed that, although the vectors in the vacuum(gas)–solid system differ from those in the liquid–solid system, there is a perfect ordering within both systems itself. From table 1 which covers more than 20 references, and which contains both growth and etching experiments, it is evident that within one system no discrepancies are present with the exception of experiments involving oxygen. The relationship between the observed growth and etching vectors within one group can easily be understood. However, the discrepancy between the two systems is more fundamental. It is the purpose of this paper to try to give more insight in the mechanism which underlies this phenomenon.

2. Crystallographic growth and etching vectors

In order to interpret the differences between the morphologies of the gas(or vacuum)–solid system and the liquid–solid system the atomic network of the silicon lattice itself has to be studied. From this and from the assumption that broken bonds do not recombine one should be able to deduce the directions of the slowest and of the fastest lateral growth and etching vectors. This then has to be combined with the 4 main rules which govern the growth and etching phenomena, viz.

(1) etching of a hill reveals edges which are determined by the fastest etching directions;
(2) growth of a hill develops edges determined by the slowest growth vectors;
(3) etching of a pit reveals edges formed by the slowest vector;
(4) growth inside a pit gives edges formed by the fastest vector.

Fig. 1 gives the atomic network of a (111)-Si crystal which consists of a number of strong bond chains in the $\langle\bar{1}10\rangle$ directions, the so called periodic bond chains [30].

From this figure it follows that etching of the fully kinked $[\bar{1}\bar{1}2]$ oriented step in the [112] direction proceeds by first removing simultaneously the atoms numbered 1 by breaking two bonds for each Si atom, then in the same way the atoms numbered 2 follow where also two bonds have to be broken, again fol

Table 1
Experimentally observed lateral growth and etching vectors on a (111) surface of the diamond structure

System	Experiment	Observed pattern	Refs
	Etching experiments		
	High vacuum etching of Si	step $[\bar{1}\bar{1}2]$	[5,8,10]
Gas (vacuum) solid	Vacuum etching of Si HCl etching in CVD system		[11,12,13] [2 3 4]
	Growth experiments CVD of Si at atmospheric pressure Molecular beam epitaxy Gas phase transport	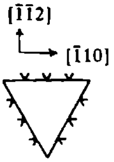	[1,2] [5,8,10] [14]
	Etching experiments		
Liquid solid	Dissolution of Si in molten metals Dissolution of Ge in molten metals Sirtl etching of Si Wright etching of Si Magma etching of natural diamond	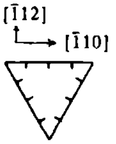 and (111) faces	[6] [15,6] [7] [16] [17] [18]
	Growth experiments Growth of Si from the melt Growth of Ge from the melt	ridges in $[1\bar{1}2]$ gives steps in $[11\bar{2}]$	 [19] [20]
Etching involving oxygen	Gaseous etching of diamond in oxygen at 1200°C	both 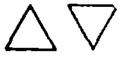	[21]
	Liquid etching of germanium by HF, H_2O_2		[22]

lowed by the atoms 3, etc The etching of the $[11\bar{2}]$ oriented step in the $[\bar{1}\bar{1}2]$ direction on the other hand proceeds according to a mechanism similar to the classical Kossel model after removal of the threefold bonded atom numbered 1 the step is stripped away sideways by etching successively the atoms numbered 2, 3, 4, etc by breaking two bonds For the following step again an atom which is 3 fold bonded has to be etched away first From an energetic point of view the continued breaking of 2 bonds will be favoured compared with the bond breaking sequence 3, 2, 2, 2 etc In addition the simultaneous attack which is possible at all the kinks on a $[\bar{1}\bar{1}2]$ step allows for a much faster etching than the stripping mechanism at a $[11\bar{2}]$ step So $[11\bar{2}]$ will be the fastest etching vector and $[\bar{1}\bar{1}2]$ the slowest For the

Table 2
Growth and etching vectors for a diamond (111) face based on a simple broken bond model, adsorption or reconstruction is not taken into account

	Slowest vector	Fastest vector
Etching	$[\bar{1}\bar{1}2]$	$[11\bar{2}]$
Growth	$[11\bar{2}]$	$[\bar{1}\bar{1}2]$

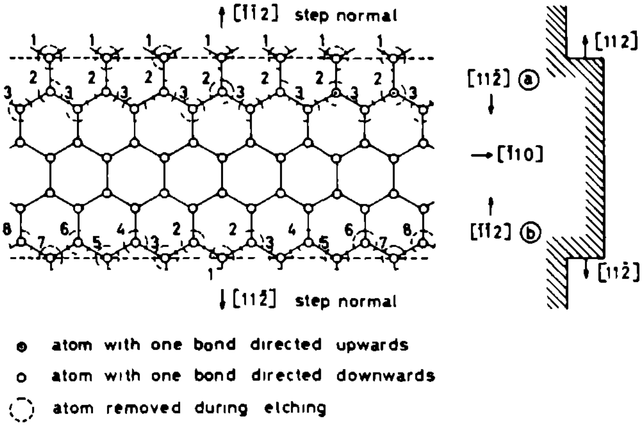

Fig 1 Etching of a [11$\bar{2}$] step and a [$\bar{1}\bar{1}$2] step on Si (111) according to the first bond order model Projection on the (111) surface (a) Etching of the fully kinked [112] step occurs in the [112] direction (b) Etching of the [112] step without kinks takes place in the [112] direction See text for the meaning of the numbered atoms

growth process, the situation is reversed, i e for growth processes [$\bar{1}\bar{1}$2] will be the fastest and [11$\bar{2}$] the slowest growth vector In summary the same step, i e the fully kinked step, etches and grows fastest although their lateral movement will be opposite in either case Table 2 summarizes these results

Using these growth and etching vectors it is easy to deduce the 4 main rules given above for a diamond lattice, this is illustrated for the rules 1 and 2 in figs 2 and 3 Starting with a spherical cap, the final form after the etching process is characterized by ⟨$\bar{1}\bar{1}$2⟩ sides, whereas the growth of a hill, the resulting morphology is determined by ⟨11$\bar{2}$⟩ sides

The theoretically expected morphologies for growth or etching now can be deduced using the 4 main rules as given in the introduction combined

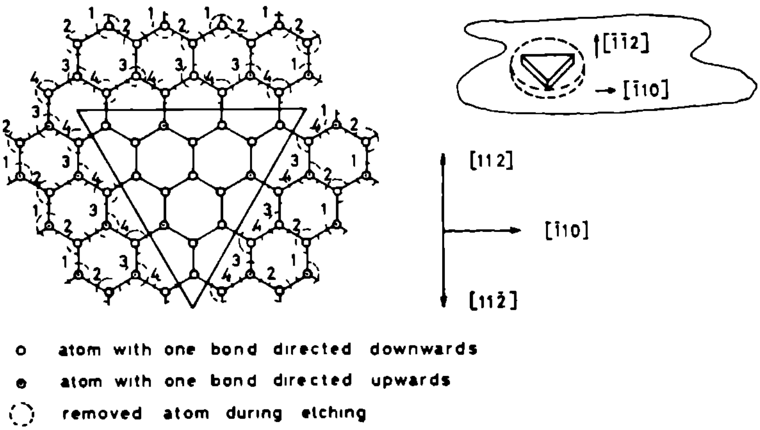

Fig 2 The etching of an originally round hill The etching takes place by removing successively the twofold and single bonded atoms 1, 2, 3, 4 The final triangular form is characterized by the ⟨112⟩ orientated fully kinked steps

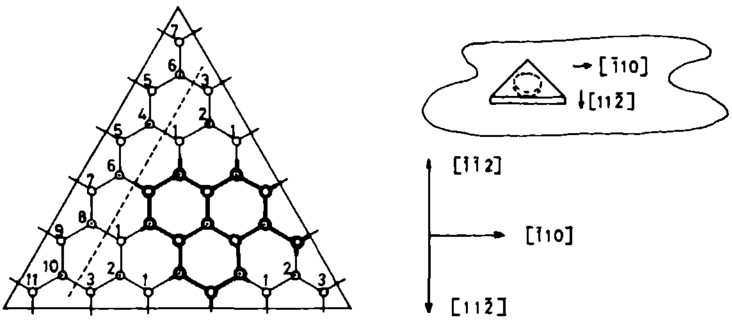

● atom of the original nucleus with one bond directed downwards
◉ atom of the original nucleus with one bond directed upwards
○ added atom after growth with one bond directed downwards
⊙ added atom after growth with one bond directed upwards

Fig. 3. The growth of a hill. Starting with a round hill the growth takes place by adding successively the atoms 1, 2, 3 etc. The addition of the single bonded atom 4 initiates the growth of a complete row of atoms (4–10). In the final triangular shape the edges are characterized by $\langle 11\bar{2}\rangle$ steps without kinked positions.

with the vector orientations as listed in table 2. The result for a diamond lattice is given in fig. 4.

We are now in a position to compare experiment with theory. From table 1 and the theoretically deduced patterns as given in fig. 4 it follows that only the liquid–solid systems behave according to the patterns deduced by the first order broken bond model. On the other hand the gas(or vacuum)–solid systems appear to be 180° reversed to the expected patterns.

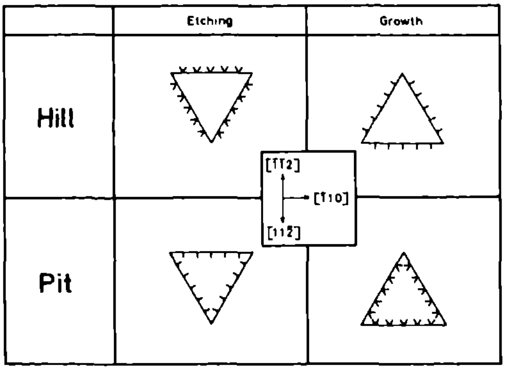

Fig. 4. Theoretically expected patterns after growth or etching of a pit or hill on a (111) surface of a diamond lattice. Adsorption or step reconstruction is not taken into account.

The reversal of the vector orientation going from the gas–solid to the liquid–solid system appears not to be associated with the temperature of the experiment. Inspection of the literature mentioned in table 1 revealed that for both systems the experimental temperatures ranged from low (137°C) to high (1412°C). So the effect is definitely not associated with a particular temperature range and we have to look for other factors which are responsible for the effect.

3. Adsorption and step reconstruction

In the above given model it was assumed that all dangling bonds were not reactive with respect to each other or to foreign species. This of course is not realistic. Especially in a liquid with a high density of molecules or atoms near the step, the dangling bonds will almost instantly be saturated by the neighbouring molecules and be stabilized in this way.

So in a solution (or melt) it will be expected that as soon as a dangling bond is formed it will be stabilized by the adsorption of surrounding molecules (or atoms). In fact, this gives a similar situation as is used in the first order broken bond model because, for the deduction of the slowest or fastest growth or etching vectors, it does not make any difference whether a dangling bond remains "dangling" or is completely saturated This is only true if to each dangling bond an atom or molecule is adsorbed, i e in the completely saturated situation no bridges between two dangling bonds are allowed The other extreme is when there is time enough for the dangling bonds to interact with each other (reconstruction) In that case the response to growth or etching will also be different, because the number of bonds to be broken will have changed This situation will occur when the density of the surrounding molecules is very low (vacuum or low vapour pressures) For step reconstruction to take place it will be necessary therefore to fulfill the following two requirements

(1) the adsorption probability must be low,

(2) the geometry of the step must allow for the recombination of the dangling bonds.

The second point has to be elucidated in more detail In fig 5 it is seen that because of the sideways pointed dangling bonds, reconstruction geometrically is possible for the [$\bar{1}\bar{1}2$] step, whereas the forward pointed lobes of dangling bonds at the step [$11\bar{2}$] are too far away from each other in lateral direction to make reconstruction likely

For the [$\bar{1}\bar{1}2$] step a reconstruction in vertical direction is also possible When the atom row numbered 1 in fig 5 is etched away reconstruction can take place between the forward (and somewhat downward) pointed lobes of the atoms of the second row and the upward pointed bonds of the surface. This can account for the observed decrease in step height of 4% compared to bulk values of this step as mentioned by Henzler [9] Such possibilities for reconstruction between step and surface do not exist for the [$11\bar{2}$] step Step [$\bar{1}\bar{1}2$] closely resembles a (100) surface where surface reconstruction in a (2 × 1) pattern is known to take place, at all temperatures to at least 1160°C [28], whereas the other step [$11\bar{2}$] is more like a (111) surface where reconstruction is more difficult [23,24], and is known to convert to a (1 × 1) pattern above 900°C [29] More experimental evidence that the reconstructed step [$\bar{1}\bar{1}2$] is more stable than the other is given by Rowe et al [25] This is in agreement with calculations made by Schluter [26] Assuming that the reconstruction at step [$\bar{1}\bar{1}2$] indeed takes place, a similar analysis as given above on the fastest growth and etching vectors now leads to the oppposite results as obtained without reconstruction because the reconstructed step possesses many atoms from which 3 bonds have to be broken, requiring more energy than the bond breaking sequence 3, 2, 2, 2 etc of the unreconstructed step [$11\bar{2}$]

The vector orientations which are obtained in this way are consistent with the vectors observed in the gas(vacuum)–solid systems Although for the vacuum system step reconstruction is likely to occur, adsorp-

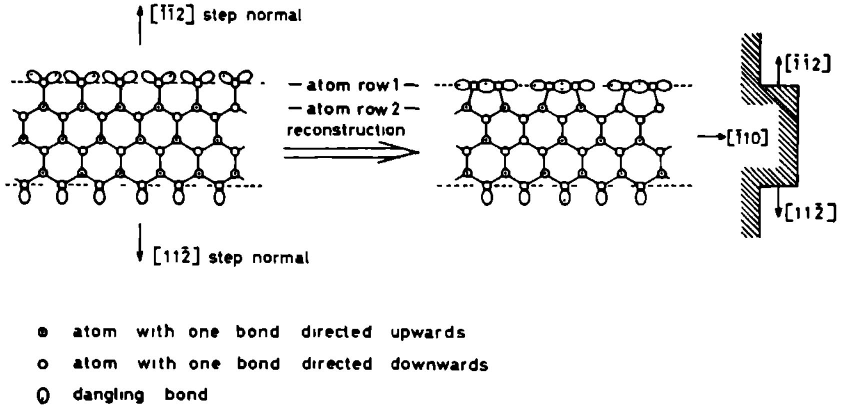

Fig. 5 Step reconstruction assuming no adsorption at the dangling bonds Geometrically the reconstruction is more likely to occur at the [$\bar{1}\bar{1}2$] step and on the [$11\bar{2}$] step

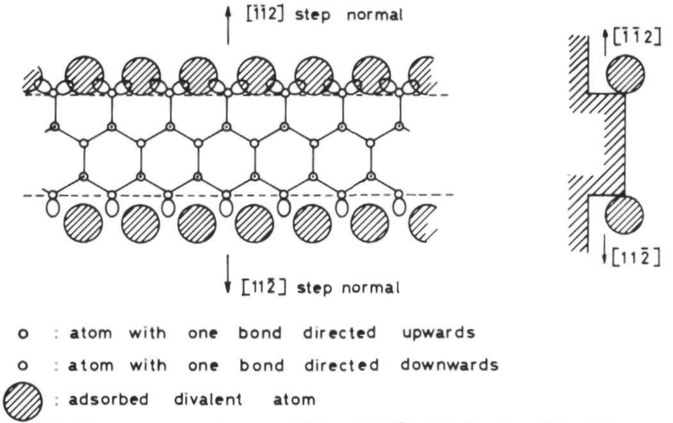

Fig. 6. Adsorption of a divalent atom at the steps [$\bar{1}\bar{1}2$] and [$11\bar{2}$]. Stabilization will be highest at the [$\bar{1}\bar{1}2$] steps.

tion certainly has to be considered in gaseous systems. The experimental evidence given above rules out the possibility that, e.g., during chemical vapour deposition of silicon in a hydrogen atmosphere at a pressure of 1 bar and a high temperature ($T >$ 1300 K) hydrogen or chlorine are adsorbed in large quantities at the step. If that would be the case the vector orientations would be equal to the ones observed in the liquid–solid system. So the above given analysis leads to the conclusion that step reconstruction is more likely to occur than H or Cl adsorption at the step. This is also true for other monovalent gaseous atoms. Such a low coverage of the step by H or Cl is in contrast with surface coverages calculated by Chernov [31,32], who comes up to the surface coverages of nearly 100%.

This idea of a monoatomic coverage of the surface by adsorbed species as yet has not been proven experimentally, but it will not be in real conflict with the above given concept, because the discussed reconstruction occurs at the steps where the etching takes place. The reconstruction of the freshly broken bonds requires a very low activation energy and therefore this relaxation process will be fast compared to the adsorption process at the steps. But it is to be expected that adsorption at the steps will become more important when the species has a high concentration in the gas phase.

In the last paragraph of this paper an example is given that indeed high step coverages are by all means probable at higher chlorine concentrations and low temperatures. So it may be that Cl can be adsorbed in reasonable quantities at the steps, when it is present in high concentrations in the gas phase. We, however, think that H adsorption is not likely to occur. That hydrogen adsorption indeed plays a minor role during the etching of silicon was proven by Van der

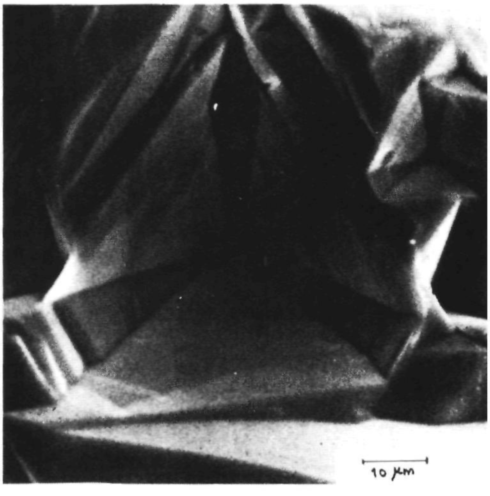

Fig. 7. Hexagonal etchpit in a Si (111) surface developed at high HCl pressures (5.7%) in hydrogen at T = 1150°C demonstrating the equivalence of the etching directions [$\bar{1}\bar{1}2$] and [$11\bar{2}$] under conditions of partly reconstruction and adsorption.

Putte et al [27] in the Si-argon–HCl system The analysis, however, does not rule out the possibility of adsorption of a divalent gaseous atoms such, e g , oxygen between these dangling bonds leading to bridge formation on both steps (fig 6) Because of a larger overlap this bridge formation might be favoured at the $[\bar{1}\bar{1}2]$ step and may explain the deviating experimental results given in table 1 of the etching with oxygen [21,22] It may also explain remarkable influence of small quantities of oxygen (≥25 ppm) on the growth morphology of silicon [33] It is to be noted that the bond energies increase from SiH to SiCl and SiO

In conclusion it can be said that the physical picture is the following in the vacuum or gas systems step reconstruction can take place because of the low density of gaseous atoms or molecules near the dangling bonds at the step, whereas in the liquid system all the dangling bonds are saturated with adsorbed atoms It is to be expected that in a gas atmosphere containing many active monovalent molecules, an intermediate case may exist where adsorption and reconstruction more or less cancel each other This will lead to the equivalence of vector orientations $\langle 11\bar{2}\rangle$ and $\langle\bar{1}\bar{1}2\rangle$ and a hexagonal hill or etch pit will be the result This indeed has been observed at high HCl concentrations during the gas phase etching of silicon (fig 7) [2]

References

[1] J Nishizawa, Y Kato and M Shimbo, J Crystal Growth 31 (1975) 290

[2] J Bloem and L J Giling, Mechanisms of the Chemical Vapour Deposition of Silicon, in Current topics in Material Science, Vol I, Ed E Kaldis (North-Holland, Amsterdam, 1977)

[3] P van der Putte, W J P van Enckevort, L J Giling and J Bloem, J Crystal Growth 43 (1978) 659

[4] P van der Putte, L J Giling and J Bloem, J Crystal Growth, to be published

[5] B A Joyce, R R Bradley and G R Booker, Phil Mag 15 (1967) 1167

[6] J W Faust Jr , A Sagar and H F John, J Electrochem Soc 109 (1962) 824

[7] E Sirtl and A Adler, Z Metallk 52 (1961) 529

[8] H C Abbink, R M Broudy and G P McCarthy, J Appl Phys 39 (1968) 4673

[9] M Henzler, Surface Sci 36 (1973) 109

[10] G R Booker and B A, Joyce, Phil Mag 14 (1966) 301

[11] G R Booker and B A Unvala, Phil Mag 11 (1965) 11

[12] H E Farnsworth, R E Schlier and J A Dillon, J Phys Chem Solids 8 (1959) 116

[13] H E Farnsworth, R L Schlier and J A Dillon, Solid State Electron 1 (1960) 602

[14] J W Faust Jr , H F John and C Pritchard, J Crystal Growth 3/4 (1968) 321

[15] R Goldstein, RCA Rev 18 (1957) 213

[16] M Wright-Jenkins, in Proc Symp on Etching for Pattern Definition, Eds H E Hughes and M J Rand (Electrochem Soc , New York, 1976) p 63

[17] K Tsukamoto and I Sunagawa, J Crystal Growth, to be published

[18] H Kanda, S Yamaoko, N Setaka and H Komatsu, J Crystal Growth 38 (1977) 1

[19] T F Ciszek, J Crystal Growth 10 (1971) 263

[20] T Surek, C B Hari Rao, J C Swartz and L C Gazone, J Electrochem Soc 124 (1977) 112

[21] T Evans and D H Sauter, Phil Mag 6 (1961) 429

[22] J Bloem and J C van Vessum, J Electrochem Soc 109 (1962) 33

[23] E Tosatti, in Proc 13th Intern Conf on the Physics of Semiconductors, Rome, 1976, p 21

[24] J C Phillips, in Proc 13th Intern Conf on the Physics of Semiconductors, Rome, 1976, p 12

[25] J E Rowe, S B Christman and H Ibach, Phys Rev Letters 34 (1975) 874

[26] M Schluter, in Proc 13th Intern Conf on the Physics of Semiconductors, Rome, 1976, p 646

[27] P van der Putte, L J Giling and J Bloem, J Crystal Growth 41 (1977) 133

[28] B Z Ol'shanetskii, A V Rzhanov and E L Edel'man, Soviet Phys -Semiconductors 7 (1974) 1538

[29] J V Florio and W D Robertson, Surface Sci 24 (1971) 173

[30] P Hartman and W G Perdok, Acta Cryst 8 (1955) 49, 521

[31] A A Chernov and N S Papkov, Soviet Phys -Dokl 21 (1976) 300

[32] A A Chernov, J Crystal Growth 45 (1978) 73

[33] H J Rijks, L J Giling and J Bloem, J Crystal Growth, to be published

Journal of Crystal Growth 47 (1979) 501–508
© North-Holland Publishing Company

CHAPTER XIII:
MONTE CARLO SIMULATION OF A (111) DIAMOND FACE AROUND THE ROUGHENING TRANSITION

W.J.P. VAN ENCKEVORT and J.P. VAN DER EERDEN
Laboratory of Solid State Chemistry, RIM, Catholic University, Toernooiveld, Nijmegen, The Netherlands

Received 6 June 1979

Monte Carlo simulations have been applied to study the roughening transition on the (111) solid–fluid interfaces of the diamond model, without a solid on solid condition. The following interface properties as a function of the temperature and array size have been calculated: Interface width, surface energy, heat capacity, step energy and the growth rate in dependence of the supersaturation. From all these measurements the estimated value for the roughening temperature was within five percent of the critical temperature of the hexagonal simple Ising model.

1. Introduction

In the last two decennia a considerable interest for growth of crystals having a diamond lattice has arosen, both in experimental and in theoretical field.

Many papers have been published about experimental work on the topic of growth or dissolution of natural diamond [1,2] and numerous papers about the same features of silicon [3–5] and germanium [6,7]. Another interesting group of compounds having a diamond lattice are of the AB type, for instance GaAs, GaP and ZnS [8,9]. These compounds have been grown or etched both from the gasphase and from the melt or solution. Particularly the (111) surfaces of these crystals have been studied extensively by means of optical and electron microscopy.

On the other hand much work has been performed on Monte Carlo simulations of the equilibrium structure and growth of Kossel type crystals and crystals having a fcc or a bcc structure, using a solid on solid (SOS) condition [10,11].

These computer experiments confirmed the existence of a roughening transition at a temperature T_R at the solid–fluid interface below the critical bulk temperature T_C^{3D} for a three dimensional Ising model, as suggested by Burton and Cabrera [12].

Recently Swendsen [13] and Van der Eerden and Knops [14] showed that the edge free energy of the SOS Kossel model was equivalent to the spin–spin correlation length in the X–Y model, and vanishes for $T > T_R$. Subsequent Monte Carlo simulation of the height correlation function in the Kossel model by Shugard, Weeks and Gilmer [15] confirmed the conjecture of Kosterlitz [16,17] that these models possess a textural (or infinite order) phase transition. An interesting point is to investigate whether a roughening transition is present in non SOS models, and, if so, its character.

In this paper a Monte Carlo simulation is carried out on a non SOS nearest neighbour diamond lattice model, concentrating on a possible roughening transition. For the (111) solid–fluid interface the temperature dependence is studied of the interface width, the surface energy, the specific heat, the step energy and the growth curves. These features show the same qualitative behaviour as in the Kossel model. Hence the existence of a roughening transition in this diamond model is strongly suggested. T_R is close to the critical temperature of a two dimensional hexagonal simple Ising model [18]. The results of these simulations can be used for systems for which the first order broken bond model is a reasonable approximation. Recently it has been shown that for Si and Ge the solid–liquid systems belong to this class, in contrast to vapour–solid systems [19]. Examples are VLS whisker growth [20], liquid phase epitaxy [21] and growth from the melt.

2 Simulation model

2 1 Three-dimensional storage array and boundary conditions for the (111) diamond model

For a Monte Carlo simulation of the (111) solid–fluid interface of a diamond model a SOS restriction would be too severe to study surface roughening, because of the crystal lattice

Two important implications of working with a non SOS model are first the necessity to use a three dimensional array for defining the atom location instead of the usual two dimensional array in a SOS system, second, the bulk phase now plays an important role and the effects of the bulk phase have to be considered in the interpretation of the surface properties

The three-dimensional array for atom storage in the computer (figs 1 and 2) has been defined in the following way (All vectors are in reference to the cubic space group Fd3m, having a unit lattice vector of length a)

(a) The x axis is parallel to the lattice vector $[\bar{1}\bar{1}2]$ The distance between each storage location is $(\sqrt{2}/2\sqrt{3})\,a$ One third of them has not been used because of the structural properties of the diamond lattice (fig 2)

(b) The y axis is parallel to $[2\bar{1}\bar{1}]$ and the distance between each storage location equals $(\sqrt{2}/2\sqrt{3})\,a$

(c) The z axis is parallel to [111], while the distance between successive x–y layers in this direction equals $(\sqrt{3}/3)\,a$

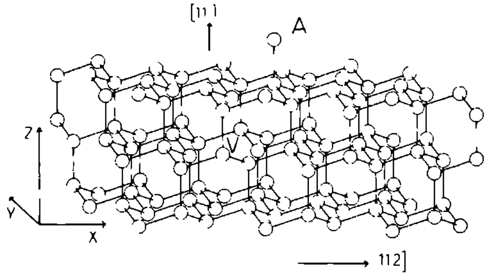

Fig 1 Diamond lattice model, with one vacancy (V) in the bulk phase and with one adatom (A) at the (111) interface, in relation with the three dimensional array (x, y, z) for computer storage The array size ($3L \times 3M$) equals (9×6)

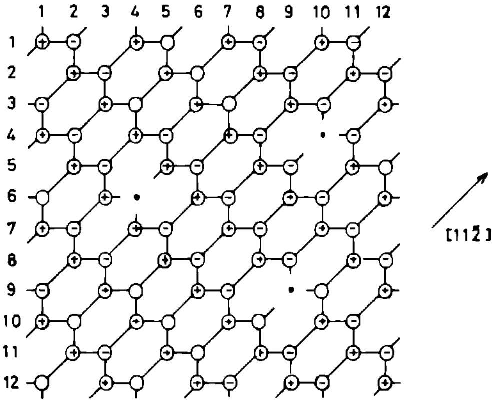

Fig 2 One x–y layer of the three-dimensional computer array related with a distorted (111) layer without step in the diamond lattice The array size ($3L \times 3M$) equals (12×12), so according to the periodic boundary conditions row 13 is equivalent to row 1 and column 13 to column 1 (•) fluid site (+) and (−) solid sites with upward and downward bond directions respectively

In this array a site at a certain location (in the following defined as (l, m, n), which means $x = l(a\sqrt{2}/2\sqrt{3})$, $y = m(a\sqrt{2}/2\sqrt{3})$, $z = n(a\sqrt{3}/3)$, l, m, n are integers) can be in two states solid or fluid

In order to simulate the properties of the diamond lattice (111) interface without steps the following boundary conditions have been used

(1) The array size is restricted as follows in order to fulfill the periodic boundary conditions The total length of the array in the x direction (L_x) has to be equal to $3L(a\sqrt{2}/2\sqrt{3})$, in the y direction (L_y) to $3M(a\sqrt{2}/2\sqrt{3})$, and the total height of the array to $N(a\sqrt{3}/3)$ The height of the solid fluid interface is not restricted (L, M and N are integers)

(2) The states of the atoms located at $(3L + 1, m, n)$ are equal to the states at $(1, m, n)$, whereas the states of the atoms at $(l, 3M + 1, n)$ equal to the states at $(l, 1, n)$

(3) The sites located at $(l, m, 1)$ (the bottom layer) always remain solid, whereas the sites located at (l, m, N) (the top layer) are kept always fluid

Steps without kinks on a diamond (111) interface in the case of a nearest neighbour model, having similar properties as steps in the classical Kossel model run parallel to the $\langle\bar{1}10\rangle$ directions and are oriented to the $\langle 11\bar{2}\rangle$ directions as shown in fig. 3 [19] So in order to simulate the diamond (111) interface with one step, slightly different boundary conditions have been introduced (fig. 3)

(1) The array size is restricted as follows in order to fulfill the periodic boundary conditions and to get a good crystallographic fitting The total length of the array in the x direction (L_x) has to be equal to $(3L + 1)(\sqrt{2}/2\sqrt{3})a$, in the y direction (L_y) to $(3M + 1)(\sqrt{2}/2\sqrt{3})a$, and the total height ($L_z$) of the array to $(N(\sqrt{3}/3)a)$. The height of the solid–fluid interface is not restricted

(2) The states of the atoms located at $(3L + 2, m, n)$ are equivalent to the states at $(1, m, n + 1)$, whereas the states at $(1, m, n)$ equal those at $(3L + 2, m, n - 1)$ The states of the sites located at $(l, 3M + 2, n)$ equal the states at $(l, 1, n \quad 1)$ and the states at $(l, 1, n)$ are equivalent to those at $(l, 3M + 2, n + 1)$.

(3) All the sites at the bottom of the array ($n = 1$) and also the atom located at $(1, 3M + 1, 2)$ are kept solid during the simulation, whereas the sites in the top layer ($n = N$) and the site located at $(3L + 1, 1, N \quad 1)$ remain fluid

In order to give the simulation more physical relevance, another condition has been introduced in both the simulations without step and the cases with step A solid atom having three fluid nearest neighbour atoms is converted to the fluid state immediately after getting its fourth fluid neighbour, because a single solid atom completely surrounded by fluid nearest neighbours has no physical significance.

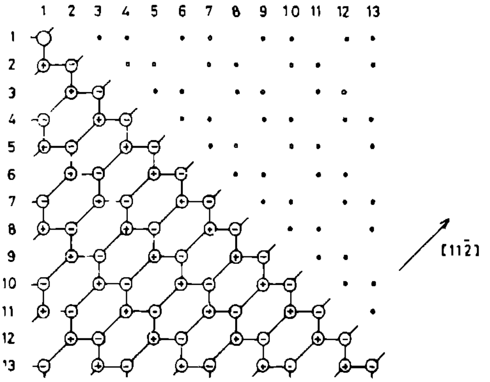

Fig 3. One x–y layer of the three dimensional computer array in relation with a distorted (111) layer with one step in the diamond lattice. The array size $(3L + 1 \times 3M + 1)$ equals (13×13), so denoting the height of this layer by n, the periodic boundary conditions are as follows. (a) Row 14 in layer n is equivalent to row 1 in layer $n - 1$. (b) Row 1 in layer n is equivalent to row 14 in layer $n + 1$ (c) Colum 1 in layer n is equivalent to colum 14 in layer $n - 1$ (d) Colum 14 in layer n is equivalent to colum 1 in layer $n + 1$.

Table 1 shows the array sizes which have been used in this paper for the Monte Carlo simulations of the diamond (111) interface, with and without introduction of a step.

2.2 *Transition probabilities and simulation procedure.*

During the Monte Carlo simulations of the properties of the diamond (111) interface, no surface diffusion is assumed to take place To convert an atom at a certain location from the fluid state to the solid state the transition frequency P_i^+ has been introduced and for the reverse process the transition frequency P_i^- has been used in a similar way as defined by Gilmer and Bennema [22].

$$P_i^+ = \nu\, e^{\Delta\mu/kT} \qquad (i = 1, 2, 3), \tag{1}$$

$$P_{i=0}^+ = P_{i=4}^+ = 0\,, \tag{2}$$

$$P_i^- = \nu \exp\left[(2 - i)\frac{2\varphi}{kT}\right] \qquad (i = 1, 2, 3), \tag{3}$$

$$P_{i=4}^- = 0\,, \quad P_{i=0}^- = \infty\,, \tag{4}$$

where ν is the characteristic frequency for the material in consideration. $\Delta\mu$ is equal to the difference in chemical potential between the fluid and solid phase, and i equals the number of solid nearest neighbours. During the simulations the relative transition probabilities,

$$P_i^{(+,-)} = P_i^{(+,-)}/\max\{P_i\}_{i\neq 0}\,, \tag{5}$$

have been used. The formation energy of a solid–fluid bond is given by.

$$\varphi = -(\tfrac{1}{2}\varphi_{\rm ff} + \tfrac{1}{2}\varphi_{\rm ss} - \varphi_{\rm sf})\,, \tag{6}$$

where $\varphi_{\rm ff}$, $\varphi_{\rm ss}$ and $\varphi_{\rm sf}$ denote the potential energies of the fluid–fluid, solid–solid and solid–fluid bonds respectively. In order to give the simulation more physical relevance $P_{i=4}^-$ is set to zero, for a solid atom completely surrounded by four solid nearest neigh-

Table 1

	Length L_x in x-direction	Length L_y in y-direction	Total height L_z in z-direction	Height solid fluid interface
Equilibrium without step	24	24	40	20
	36	36	40	20
	48	48	15	9
Equilibrium with step	49	49	15	9
Growth without step	24	24	40	7

bours cannot get fluid. $P_{i=0}$ is assumed to be infinite, whereas $P^+_{i=0}$ equals zero, because a solid atom completely surrounded by fluid nearest neighbours does not exist, as described in the foregoing section.

Finally $P^+_{i=4}$ is set to zero, because a vacancy cannot change into a solid atom.

From the foregoing it can easily be understood that the assumption has been made that the probability to convert a fluid site to the solid state is independent of the local configuration, except for the cases where $i = 0$ or $i = 4$. In the following instead of φ/kT the standard temperature as defined by Van der Eerden et al. [10] will be used

$$\theta = 0.88138\ kT/\varphi \tag{7}$$

During the simulations, the sites having 1, 2 or 3 solid fluid bonds have been stored both in the three-dimensional array described above and in two additional arrays one containing the characteristics of the fluid sites and the other one of the solid sites.

To carry out one Monte Carlo step it is first decided whether a transition from solid to fluid or from fluid to solid possibly takes place, by choosing one of these additional arrays, using the probabilities:

$$P_{\text{solid array}} = N_s/(N_s + N_f P^+_{i=1}) , \tag{8}$$

$$P_{\text{fluid array}} = N_f P^+_{i=1}/(N_s + N_f P^+_{i=1}) , \tag{9}$$

where N_s equals the number of atoms stored in the solid additional array and N_f the number of atoms in the fluid array.

Then one site in the just chosen array is selected at random and in the case of a fluid site it is changed to the solid state immediately, whereas in the case of a solid site the transition takes place with the probability given by eq. (3).

After this both the three-dimensional array and the solid and fluid arrays are readjusted to the new situation, when a transition has taken place and now the next Monte Carlo step can follow.

The total number of Monte Carlo steps (N_{cycli}) per unit surface area defined as

$$N_{\text{steps}} / \tfrac{2}{3} L_x L_y , \tag{10}$$

where L_x and L_y are the array lengths in the x and y directions respectively and N_{steps} the total number of cycli, is taken as 4.5 × 10^3 for the simulation of an equilibrium surface. However, for the simulations of growth properties execution stops, when 20 layers have been grown or when the total number of Monte Carlo cycli per unit surface area has reached the value of 18.2 × 10^3.

3. Simulation results and discussion

3.1. Equilibrium surfaces

3.1.1. Interface width

The width of the interface is not uniquely defined and many measures of it have been used in literature [23,24]. Most of these measures cannot be used in the present non-SOS model since the height of the interface at a certain location is not uniquely defined and also the role of the vacancies in the bulk phase has to be taken in consideration.

A suitable measure of the interface width is obtained through the interface profile, i.e. the solid site concentration $c_s(n)$ in a layer in dependence on the layer number n. As an example we present in fig. 4 the interface profile of a 36 X 36 X 40 array for three temperatures θ. It is easily seen that the maximum value of the gradient dc_s/dz (z is the real version of the integer n) decreases when the interface extends over more layers. Accordingly the interface width Δ is defined by,

$$\Delta = [\max(dc_s/dz)]^{-1}, \qquad (11)$$

In order to determine the maximum value of the solid atom concentration gradient (dc_s/dz) for a certain array size and temperature a third degree polynomial has been fitted to sets of four successive $c_s(n)$ points resulting from a simulation for the given array size and temperature as shown in fig. 4.

The results of these interface width measurements are shown in fig 5, where the reciprocal values of the maximal concentration gradients have been plotted as a function of the temperature θ for three different array sizes. During all these simulations the array is kept several times higher than the interface width in order to minimize the influence of the array height on the determination of the interface width.

It is assumed that for infinite systems the interface width diverges at and above the roughening temperature [10,15]. A finite array size, however, tends to stabilize the interface. Hence it is to be expected that the divergence in finite systems is announced by a point of inflection in the interface width versus temperature curve. For the 24 X 24, 36 X 36 and 48 X 48 arrays the point of inflection is situated at θ = 0.69, 0.68 and 0.67 (all ±0.01) respectively. Upon extrapolating these values, assuming a $(L_xL_y)^{-1/2}$ dependence, to infinite systems we find $\theta_R = 0.65 \pm 0.03$. Note also that the increasing slope at the point of inflection of the curves in fig. 5 for increasing system sizes supports the hypothesis of a singularity for infinite systems.

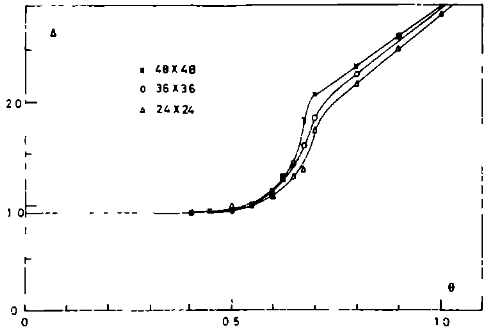

Fig 5 Interface width Δ versus standard temperature θ for three different array sizes

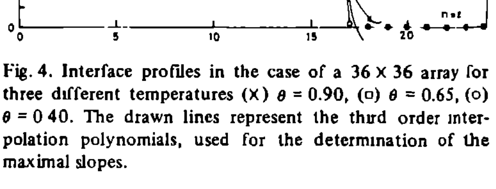

Fig. 4. Interface profiles in the case of a 36 X 36 array for three different temperatures (X) θ = 0.90, (□) θ = 0.65, (o) θ = 0 40. The drawn lines represent the third order interpolation polynomials, used for the determination of the maximal slopes.

3.1.2. Surface energy and specific heat

For the calculation of the surface energy in a non-SOS model it is necessary to consider the energy of the bulk phase due to vacancies or vacancy clusters, so in this case the surface energy for a system in equilibrium has to be defined as the total energy of the system minus the total number of solid atoms in this system times their specific energy in the bulk phase.

The number of solid--fluid bonds can be used as a measure of energy [10]. The number of broken bonds to be ascribed to the surface N_{sf}^{surf} is the total number of solid–fluid bonds in the system minus the total number of solid atoms times the average number of solid–fluid bonds per solid atom in the bulk phase. The surface energy is φN_{sf}^{surf}.

During the simulations of the equilibrium surface, it appeared that the lower part of the bulk phase did not reach its equilibrium state in the number of Monte Carlo steps carried out here. Also the boundary condition that the bottom layer always remains solid does affect the number of solid–fluid bonds per atom in the lower part of the bulk phase.

Because of these two reasons the solid phase (this is the bulk phase plus the surface layers) has been splitted in two parts the higher part which is in equilibrium and the lower part which did not reach its equilibrium state. Consequently from a simulation run $N_{sf}^{surf}(\theta)$ is calculated as (The total number of solid- fluid bonds in the system) -- (the total number of atoms in the equilibrium upper part of the solid phase times the average number of solid - fluid bonds per atom in the equilibrium bulk phase) – (the total number of solid- fluid bonds in the lower non-equilibrium part of the bulk phase). In fig. 6 the specific surface roughness is defined as:

$$\rho^\sigma = \frac{N_{sf}^{surf}(\theta) - \frac{1}{3}L_xL_y}{L_xL_y}, \qquad (12)$$

where $\frac{1}{3}L_xL_y$ is equivalent to $N_{sf}^{surf}(\theta = 0)$, is plotted as a function of θ for three different array sizes. In this figure it can be seen that above the roughening temperature θ_R, as determined from the interface width in the foregoing section, the specific rougheness increases with increasing array size, whereas near the roughening transition an inflection point can be seen for each ρ^σ versus θ curve. The specific heat is defined as the temperature derivative of the surface energy.

$$c_v = \left(\frac{\partial \varphi\rho^\sigma}{\partial T}\right)_v = 0.88138k\left(\frac{\partial \rho^\sigma}{\partial \theta}\right)_v, \qquad (13)$$

where φ and k have been defined in section 2.2. The value of $c_v/0.88138$ k has been determined from the ρ^σ versus θ curves in fig. 6 by means of a second order interpolation, and is plotted in fig. 7 versus the standard temperature θ, again for three different array sizes. The maxima of the $c_v(\theta)$ curves are located at the θ values 0.68, 0.66 and 0.67 (all ±0.02) for the 24 X 24, 36 X 36 and 48 X 48 arrays respectively. this is very near the roughening temperature as determined in the foregoing section Within the accuracy of the measurements, it can be concluded from fig. 7 that the temperature θ where $c_v(\theta)$ reaches its maximal value is not significantly below the roughening temperature determined from the interface width, this in contrast to the SOS and XY model [13,14]

Another interesting point is that with increasing array size the peak in the c_v versus θ curve becomes broader, whereas the maximum value of the specific heat does not alter too much.

From this it is suggested that for an infinite array size the c_v versus θ curve will not show a singularity at θ_R. This behaviour was proved for the SOS and XY models, and is typical for a textural phase transition.

3.1.3. Step energy

Recently several autors [23,25] suggested on the basis of their Monte Carlo simulation results that for a SOS model the energy associated with a step should vanish at the roughening transition This has exactly been proved by Swendsen [13] and by Van der

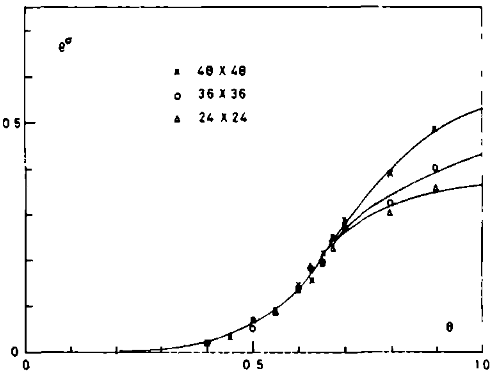

Fig. 6. Specific surface roughness ρ^σ versus standard temperature θ for three different array sizes.

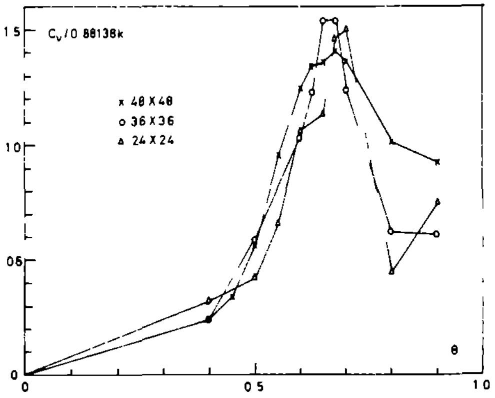

Fig. 7. Specific heat $c_v/0.88138k$ versus standard temperature θ for three different array sizes

Eerden and Knops [14] on the basis of the equivalence of the SOS model to the classical XY model

In this section step energy measurements are discussed which have been performed on the (111) interface of the non SOS diamond model in order to investigate whether also in this case the step energy decreases to zero near the roughening transition

For the diamond model the step roughness per unit length ρ^{st} for a square array ($L_x = L_y = L = 3K + 1$ where K is an integer) is calculated according to the relation

$$\rho^{st} = \frac{1}{L}\left(N_{sf}^{surf}{}_{L}(1\ \text{step}) - \frac{1}{L-1} N_{sf}^{surf}{}_{L-1}(\text{no step})\right), \tag{14}$$

where $N_{sf}^{surf}{}_{L}(1\ \text{step})$ is the number of solid fluid bonds at the surface as defined in the foregoing section for a $L \times L$ array with one step whereas $N_{sf}^{surf}{}_{L-1}(\text{no step})$ equals the number of solid fluid bonds at the surface for a $(L-1) \times (L-1)$ array without steps

The results of the step energy measurements are shown in fig 8 where the step roughness per unit length is plotted as a function of the standard temperature θ for a 49 X 49 array with a single step

It can clearly be seen that after an increase at low θ values near 0 5 the step energy decreases rapidly to zero near the roughening temperature $\theta \approx 0\ 65$ So it can be concluded that the properties of the step energy as a function of the temperature for the non SOS diamond model and for the conventional SOS models are similar after an increase of the step energy compared to the situation at $\theta = 0$ at temperatures somewhat below the roughening point it goes to zero around θ_R

3 2 *Non equilibrium surfaces growth*

3 2 1 *Growth rate versus supersaturation*

Fig 9 gives the growth rate R as a function of the supersaturation $\beta\Delta\mu$ in the case of the diamond model (111) interface without steps for various θ values on a 24 X 24 array In this figure it can be seen that at θ values below the roughening point (θ = 0 4 0 5 and 0 6) there is a nucleation barrier for growth, resulting in a non linear dependence between the growth rate and the supersaturation More precisely $dR/d(\beta\Delta\mu)$ approaches zero if $\beta\Delta\mu$ goes to zero

On the other hand for θ values above the roughening transition (θ = 0 70 and 0 80) no nucleation barrier for growth is present giving a linear dependence between the growth rate and the supersaturation i e $dR/d(\beta\Delta\mu)$ does not approach zero if $\beta\Delta\mu$ goes to zero

This observation is in complete agreement with the results of the measurement of the growth rate versus supersaturation carried out by Gilmer and Bennema [22 26] for a SOS model who also observed a linear dependence of the growth rate versus supersaturation above the roughening transition and a non linear behaviour below θ_R

The growth rate R during the simulations of the

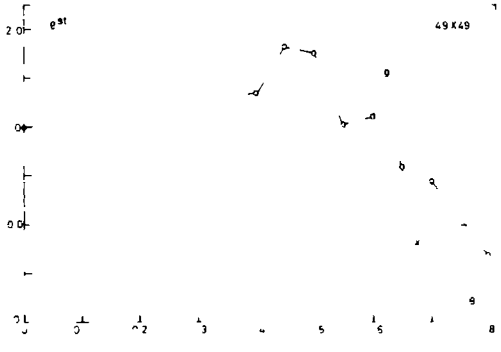

Fig 8 Step roughness per unit length ρ^{st} versus temperature θ for a 49 X 49 array

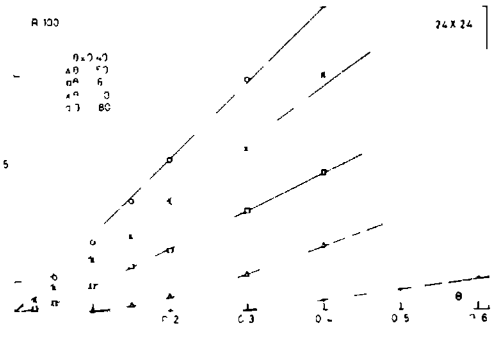

Fig 9 Growth rate versus supersaturation curves for various standard temperatures θ The array size is 24 X 24

growth properties of the (111) diamond interface is defined as

$$R = \frac{N_{f\to s} - N_{s\to f}}{L_x L_y} \left[\sum_{i=1}^{N_{f\to s}} \frac{1}{N_f(i)} \right]^{-1} \qquad (15)$$

where $N_f(i)$ is the number of fluid sites having 1, 2 or 3 solid neighbours (in other words the size of the fluid additional array) before the ith time that a fluid to solid transition takes place. $N_{f\to s}$ is the number of these transitions during the simulation, whereas $N_{s\to f}$ denotes the number of solid to fluid transitions. For the above mentioned definition of the growth rate the implication of eq. (1) that the probabilities for a fluid to solid transition for fluid sites with 1, 2 or 3 solid–fluid bonds are equal has been used.

4. Conclusions

Monte Carlo simulations of the (111) interface of the non-SOS diamond model showed that many properties of this type of interface are very similar to those of the (001) interface of the Kossel model.

Interface width measurements revealed clearly a roughening transition at the standard temperature value of $\theta = 0.65 \pm 0.03$. This is very close to the transition point for a hexagonal simple Ising model [18].

The absence of a singularity in the specific heat supports the idea that the roughening transition is of the textural (infinite order) type.

Step energy measurements confirmed strongly this type of roughening transition near $\theta = 0.65$.

Finally it could be observed that the growth rate versus supersaturation curves showed a linear dependence at temperatures above the roughening transition, whereas they show a non-linear behaviour below the roughening point, similar to the SOS model.

Acknowledgements

One of us (W.J.P. van Enckevort) acknowledges supports of the Netherlands Organisation for the Advancement of Pure Research ZWO/SON. We wish to thank Dr. P. Bennema for stimulating discussions.

References

[1] I. Sunagawa, K. Tsukamoto and I. Yasuda, J. Crystal Growth, to be published.
[2] H. Komatsu and A.R. Lang, Mineral. Soc. Japan Spec. Pap. 1 (1971) 35.
[3] P. van der Putte, W.J.P. van Enckevort, L.J. Giling and J. Bloem, J. Crystal Growth 43 (1978) 659.
[4] J. Nishizawa, Y. Kato and M. Shimbo, J. Crystal Growth 31 (1975) 290.
[5] J.W. Faust Jr., H.F. John and C. Pritchard, J. Crystal Growth 3/4 (1968) 321.
[6] J. Bloem and J.C. van Vessem, J. Electrochem. Soc. 109 (1962) 33.
[7] G.A. Wolff, Am. Mineralogist 41 (1956) 60.
[8] J.B. Theeten, L. Hollan and R. Cadoret, in: Current Topics in Materials Science, Vol. 2, Eds. E. Kaldis and H.J. Scheel (North-Holland, Amsterdam, 1977).
[9] E.I. Givargizov and P.A. Babasian, J. Crystal Growth 37 (1977) 129.
[10] J.P. van der Eerden, P. Bennema and T.A. Cherepanova, Progr. Crystal Growth Characterization 1 (1978) 219.
[11] G.H. Gilmer and K.A. Jackson, in: Current Topics in Materials Science, Vol. 1, Ed. E. Kaldis (North-Holland, Amsterdam, 1978).
[12] W.K. Burton, N. Cabrera and F.C. Frank, Phil. Trans. Roy. Soc. London 243 (1951) 299.
[13] R.H. Swendsen, Phys. Rev. B17 (1978) 3710.
[14] J.P. van der Eerden and H.J.F. Knops, Phys. Letters 66A (1978) 334.
[15] W.J. Shugard, J.D. Weeks and G.H. Gilmer, to be published.
[16] J.M. Kosterlitz, J. Phys. C7 (1974) 1046.
[17] S.T. Chui and J.D. Weeks, Phys. Rev. Letters 40 (1978) 733.
[18] See e.g. C. Domb and M.S. Green, Eds., Phase Transitions and Critical Phenomena, Vol. 2 (Academic Press, London, 1972).
[19] W.J.P. van Enckevort and L.J. Giling, J. Crystal Growth 45 (1978) 90.
[20] E.I. Givargizov, in: Current Topics in Materials Science, Vol. 1, Ed. E. Kaldis (North-Holland, Amsterdam, 1978).
[21] C. Kimura, T. Yamaki, H. Hoshino, J. Crystal Growth 38 (1977) 233.
[22] G.H. Gilmer and P. Bennema, J. Appl. Phys. 43 (1972) 1347.
[23] R.H. Swendsen, Phys. Rev. B15 (1977) 5421.
[24] G. J.D. Weeks and G.H. Gilmer, Phys. Rev. Letters 31 (1973) 549.
[25] H.J. Leamy and G.H. Gilmer, J. Crystal Growth 24/25 (1974) 499.
[26] G.H. Gilmer and P. Bennema, J. Crystal Growth 13/14 (1972) 148.

Growth Mechanisms of Silicon Crystallites Grown on Top of a Metal-Coated Graphite Substrate

W. J. P. van Enckevort and M. W. M. Graef

RIM Laboratory of Solid State Chemistry, Faculty of Science,
Catholic University, Toernooiveld, Nijmegen, The Netherlands

ABSTRACT

Microscopic *in situ* observations and *a posteriori* surface topography by means of optical and scanning electron microscopy have been carried out in order to study the growth of large-grain polycrystalline silicon films from the gas phase onto a graphite substrate coated with a liquid layer of tin or aluminum In the present study, only the initial stages of the process, where crystal growth is governed by vapor-liquid-solid mechanisms, are considered For the growth of the crystallites in the polycrystalline layers, which occur in two morphological forms, *viz*, needles and platelets two different mechanisms could be identified (*i*) a twin plane reentrant edge (TPRE) mechanism leading to a fast lengthwise growth of needles and a fast sidewise growth of platelets, and (*ii*) a nucleation mechanism, accounting for a slow thickness growth of the needles and a slow expansion of the platelike crystals On the upper surfaces of some needles and platelets a capricious surface pattern (always in conjunction with the occurrence of some solidified metal droplets) could be identified, which could be interpreted in terms of a two-dimensional VLS growth mechanism

The interest in the preparation of photovoltaic silicon solar cells via inexpensive processes has resulted in the publication of a variety of studies dealing with the growth of silicon onto nonsilicon substrates, particularly graphite (1-4) One of the main problems in the chemical vapor deposition (CVD) of silicon onto foreign substrates is the poor crystallinity of the grown layers It was found that the crystallinity could be enhanced by means of coating the graphite with liquid tin prior to the deposition of silicon (5) In this CVDOLL process (chemical vapor deposition on liquid layers) the purpose was to grow large-grain polycrystalline silicon layers on top of graphite substrates The deposition of silicon onto graphite plates coated with a 10 μm thick molten tin film resulted in the growth of polycrystalline films having a mean grain size exceeding 100 μm which is a requirement for satisfactory solar cell operation (typical conditions 0 75% $SiHCl_3$ and 1 0% HCl in H_2 ambient surface temperature 1500 K) The formation of large grains is evidently associated with the presence of a liquid film that influences the nucleation and growth of silicon Although it was assumed that the presence of liquid tin (or, alternatively liquid aluminum) (*i*) reduces the density of the silicon nuclei and (*ii*) feeds the growing crystals from a solution of silicon in the solvent (6) a detailed investigation into the nature of this growth process has not yet been carried out

The purpose of the present studies was to characterize the growth mechanism for the growth of silicon on a liquid-metal coated substrate This was done by the analysis of the polycrystalline silicon deposits by means of scanning electron microscopy and optical microscopy

Experimental

Preparation of samples —The growth process was carried out in a conventional horizontal epitaxial quartz reactor tube provided with water cooling and rf heating Trichlorosilane was used as a silicon source hydrogen chloride as an etching agent and hydrogen as a carrier gas The substrates were graphite plates, coated with pyrolytic graphite and with dimensions 2 0 × 2 5 × 0 1 cm^3, placed on a graphite susceptor Tin or aluminum were deposited onto these graphite plates via sublimation *in vacuo* prior to the deposition of silicon The thickness of the metal layer amounted to 10 μm The substrate temperature during growth was kept at 1500 K

The formation of a liquid metal layer was brought about as follows (6) upon melting, the metal contracted to droplets, due to its high surface tension The surface tension could be reduced by dissolving silicon into the droplets This was done by an injection of several pulses of 0 75% $SiHCl_3$ in H_2 each one lasting about 10 sec This caused the droplets to spread out over the graphite, eventually forming a continuous liquid layer

The growth of silicon on tin-coated graphite was initiated by the continuous addition of 0 75% $SiHCl_3$/1% HCl, which resulted in the formation of silicon needles and platelets Simultaneously, the tin was evaporated due to the etching activity of HCl After completion of the evaporation of tin, the growth process continued in a way essentially comparable to conventional CVD of polycrystalline silicon layers [cf for instance, Ref (7)]

The growth of silicon on aluminum-coated graphite was carried out by (*i*) dissolving silicon into liquid aluminum [forming a 70 atomic percent (a/o) Si/30 a/o Al liquid mixture at 1500 K], and (*ii*) the removal of aluminum by the addition of HCl to the gas phase, causing silicon needles to grow from a supersaturated solution This process was described by Graef and Monkowski (8)

For the purpose of this work it was necessary to interrupt the growth process before the evaporation of the liquid metal was completed, since the grain boundaries had not yet developed during this stage, and thus the crystallites could be studied separately

Observational techniques —The growth of silicon needles and platelets from solution could be studied *in situ* by means of a binocular microscope placed over an epitaxial reactor tube provided with a quartz window

A more refined study of these crystallites was performed by means of optical reflection differential interference contrast microscopy in order to reveal low contrast surface patterns In order to obtain a three-dimensional view at higher magnifications a

Key words polycrystalline silicon, vapor liquid solid growth twin plane reentrant edge mechanism

scanning electron microscope (SEM) was used. Most of the microscopic observations were carried out on as-grown samples. However, some SEM observations were realized on samples which were etched during 2 hr in a solution 50 volume percent (v/o) concentrated HNO_3/50 v/o H_2O in order to remove residual

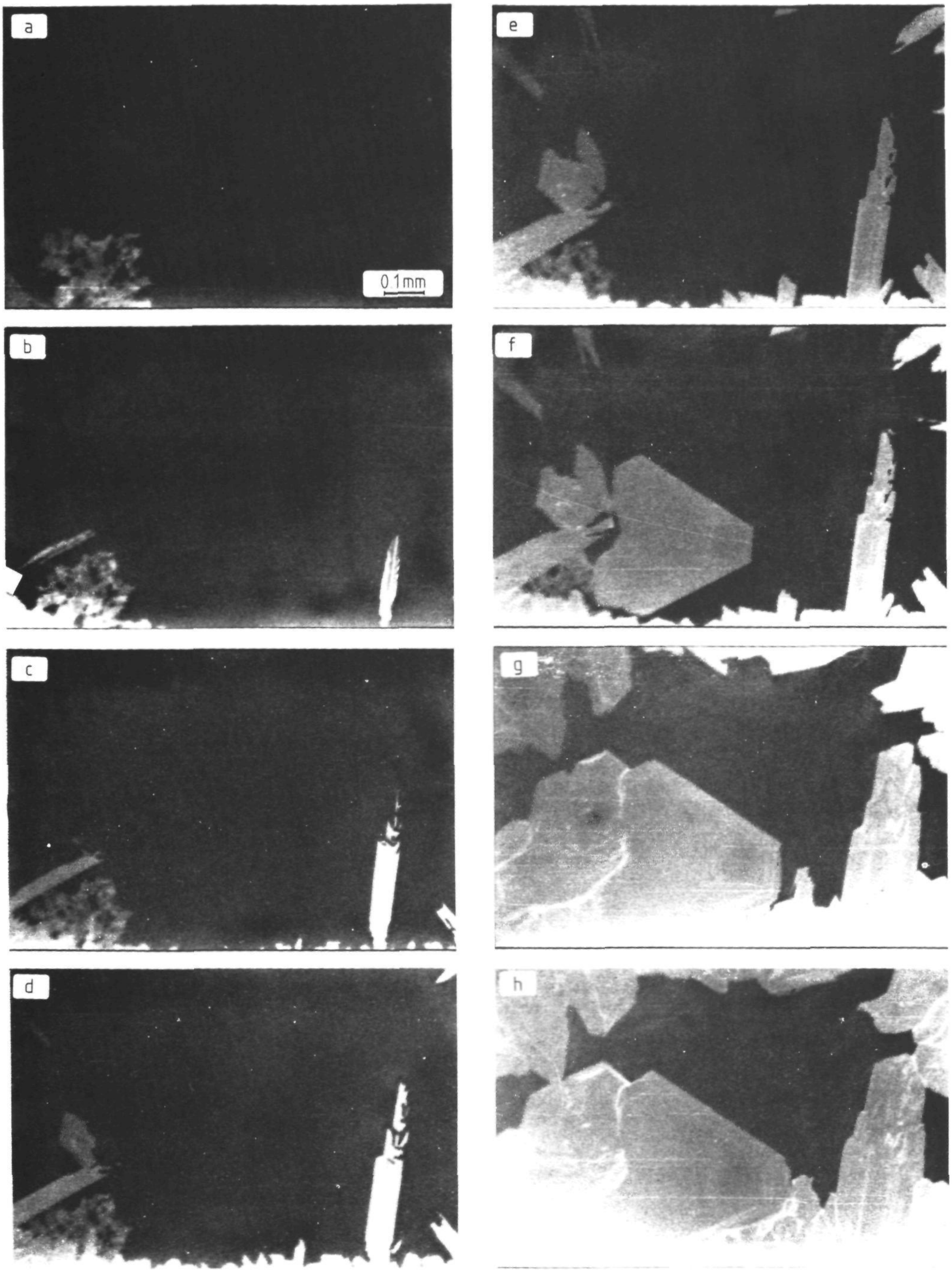

Fig. 1. Successive stages of the growth of silicon crystallites on tin-coated graphite. The addition of 0.75% $SiHCl_3$ and 1% HCl started at $t = 0$. Light regions: silicon; dark regions: tin. a. $t = 1'00''$; b. $t = 1'20''$; c. $t = 2'30''$; d. $t = 3'00''$; e. $t = 4'30''$; f. $t = 4'45''$; g. $t = 6'00''$; h. $t = 8'40''$.

droplets of tin or aluminum. This etching was carried out in order to reveal the areas of the silicon crystallites that had been covered by solidified metal. For studying the perfection of the crystals and to reveal stacking faults and twin planes, Sirtl etching (9) was applied.

The Growth of Needles and Platelets

The growth of silicon needles and platelets was observed to be typically associated with the presence of liquid metal droplets on top of the graphite substrate. These crystallites could be studied both during their formation, and *a posteriori*. In order to study the growth mechanism of needles and plates, investigations were made on the morphology of large crystallites that were grown on isolated droplets.

In situ observations.—Figure 1 shows a sequence of micrographs that was made during the deposition of silicon onto tin-coated graphite substrate. It can be observed that the initial growth of needles (*e.g.*, Fig. 1, a and b) and plates (Fig. 1, e and f) proceeds very rapidly, but after a short time, the rapid growth stops, after which the crystallites grow in all directions at a much slower rate. It was estimated that the initial growth rate of the needles lengthwise was more than 60 times larger than the thickness growth rate. The initial expansion velocity of the platelets was of about the same order of magnitude as the needle propagation rate. This observation permits the conclusion that two growth mechanisms are operative: one for the rapid growth and one for the slow growth.

Needle growth.—*Characteristics*.—The growth of needles is characterized by the following features:

1. The growth of needle-shaped crystallites always starts on the edge of a liquid droplet, and the growth continues in a direction more or less toward the center of the droplet. Figure 2 gives a survey of a group of needles grown from liquid aluminum, whereas Fig. 3 shows silicon needles that were grown from a liquid tin droplet.

2. The upper surfaces of the needles are curved, while the lower ones are in contact with the graphite substrate. For the Sn/Si system the morphology of the needles could be elucidated by the removal of the solidified tin using a 1:1 HNO_3/H_2O etchant, which does not affect the silicon needles and the graphite. Figure 4 shows a typical large needle in the Sn/Si system. The profile of the upper surface is determined by the curvature of the droplet (Fig. 4a and d). This is similar to the way in which the external shape of cylindrical or rectangular crystals is determined by the shape of the meniscus in the case of Czochralski (10) or edge-defined film-fed growth (11). Figure 4b shows that the bottom side of the needle follows the morphology of the graphite substrate.

Both features, *viz.*, the fact that the top surfaces of the needles are determined by the gas-liquid interface and the fact that the bottom surfaces are determined by the substrate, have also been observed clearly in the Si/Al system. Furthermore, it was found that the upper and lower surfaces of the needles are no crystallographic faces in general.

3. The top surfaces of the needles, both in the Si/Sn and in the Si/Al system exhibit a reentrant corner (Fig. 4c and Fig. 5). Associated with a reentrant corner, a group of twin planes running parallel to the needle axis may always be observed (Fig. 4 and 5). These twin planes can be recognized by means of SEM, but particularly by means of differential interference contrast microscopy. The twin planes may be revealed more clearly by slight etching, *e.g.*, by gas phase etching using HCl (Fig. 6a, for Si/Al) or by Sirtl etching (Fig. 6b).

It appears that the needle axis and consequently the twin planes always run parallel to one of the sides of the stacking fault triangles that were created by the deposition of epitaxial silicon layers onto the needles (12) (Fig. 6b). This indicates that the twin lines always run parallel to a {111} plane. Also, the twin planes are virtually always parallel to the lateral faces of the needles. These faces constitute {111} planes, being the only stable F-face for the growth

Fig. 2. Silicon needles grown on graphite coated with liquid aluminum. Differential interference contrast micrograph showing that the growth of the needles starts at the edge of the liquid droplet.

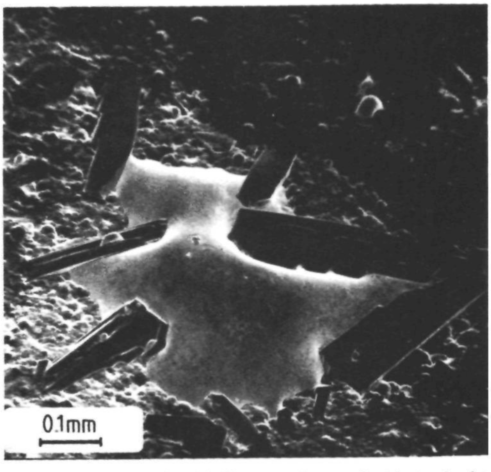

Fig 3. Silicon needles (dark) grown from a liquid tin droplet (light). The growth of the needles starts at the edge of the droplet (SEM micrograph).

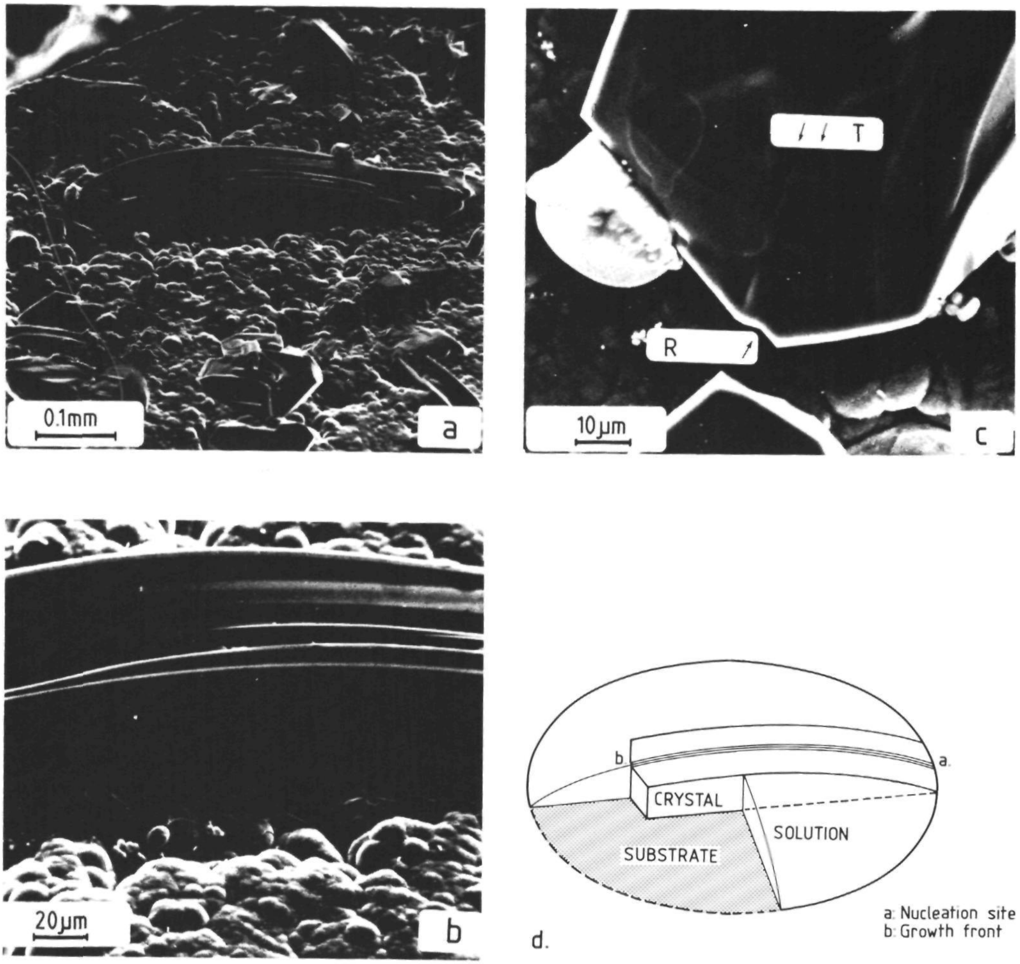

Fig. 4. SEM micrographs showing a typical large needle grown in the Si/Sn system. The tin has been removed by chemical etching. a. Overall view: the profile of the upper surface of the needle is determined by the curvature of the droplet. b. Detail of (a): the lower surface of the needle is in close contact with the substrate. c. Detail of the needle in (a): the top surface shows a reentrant corner (R) and some twinning lines (T) running parallel to the needle axis. d. Schematic representation of the characteristic features of needle growth.

of silicon from the metal melt (13). Hence it can be concluded that the twinning is of the type {111} normal twin (the twin axis <111> is normal to the {111} composition plane). This type of twinning is the most common one that occurs in the diamond lattice (14) (Fig. 7).

The growth mechanism that accounts for the generation of steps at a twin plane reentrant edge (TPRE) has been extensively studied both theoretically (15-17) and experimentally (18-21) for germanium, silicon, and diamond. The easy nucleation at a reentrant corner explains the high growth rate of the needles; Bennett and Longini (18) have been able to grow germanium crystals at a rate of 15 cm/min using TPRE growth.

The rate-determining step in this VLS mechanism is unknown in the present case; it is possible that the growth is limited by surface kinetics, volume diffusion, or heat transport.

It was shown by Wagner (19) and by Hamilton and Seidensticker (15) that at least two twin planes are required for a continued reentrant edge growth mechanism. As a matter of fact, on virtually all needles two or more twin planes could be discerned; the separation was sometimes less than 0.5 μm.

Growth history of the needles.—The growth process of the silicon needles can be summarized as follows (cf. Fig. 8):

1. The growth starts in the vicinity of the edges of the liquid droplets. Some of the microcrystals (having a size of a few microns) that are formed contain two or more parallel {111} twins. If these twins are directed toward the liquid, the formation of needles will start (Fig. 8a).

2. Needle growth (Fig. 8b): the TPRE-defined needle growth takes place at a very high rate (roughly 1000 μm/sec) and stops suddenly. In the Si/Al system the needle growth is stopped only by collision against other needles (cf. Fig. 2), but in the Si/Sn system, the needle growth often stops without an evident reason (this might be due to poisoning of the reentrant corner, or exhaustion of the solution due to the poor solubility of Si in Sn, 2 a/o at 1500 K). In principle, the needle size in the Al/Si system is unlimited (needles having a length up to 10 mm have been grown); the top and bottom surfaces are deter-

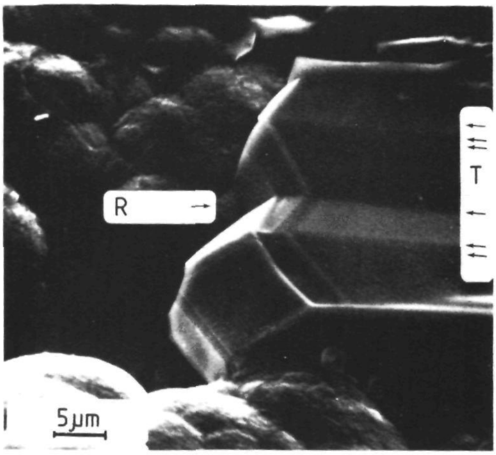

Fig. 5. Reentrant corner (R) and twinning lines (T) on the top surface of a silicon needle grown in the Si/Sn system (SEM micrograph).

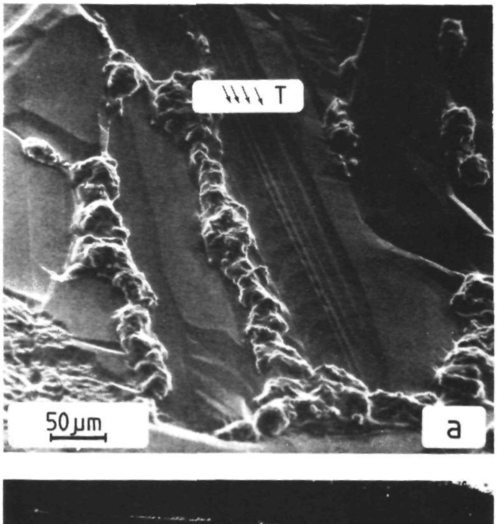

Fig. 6. Twinning lines (T) on silicon needles, revealed by etching. a. Silicon needle grown in the Si/Al system, etched by gaseous HCl at 1500 K (SEM micrograph). b. Silicon needle grown in the Si/Al system, etched by Sirtl solution, and showing stacking fault triangles. The twinning lines run parallel to one of the sides of the triangles (optical micrograph).

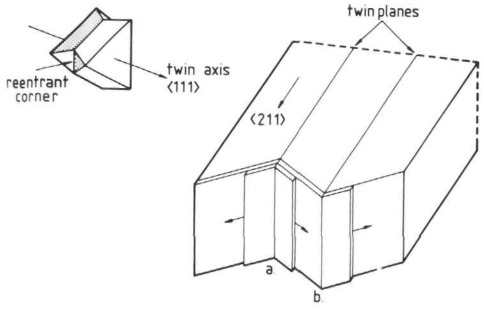

Fig. 7. Schematic representation of the twin plane reentrant edge growth mechanism at the tip of silicon needles.

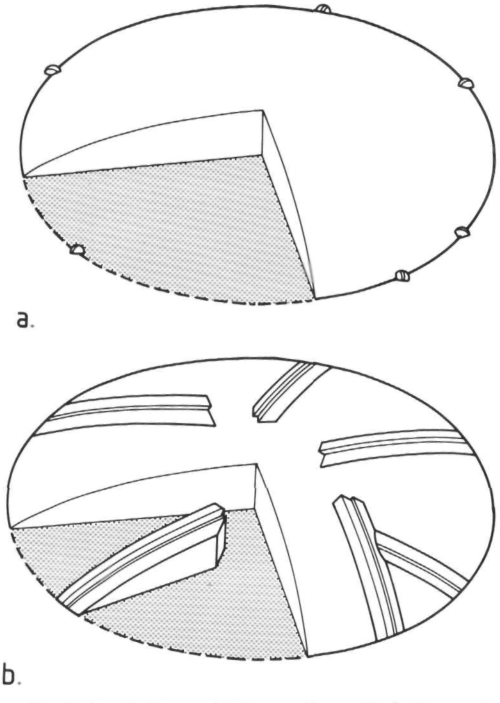

Fig. 8. Growth history of silicon needles. a. Nucleation on the edges of a droplet. b. Needle growth by a TPRE growth mechanism, followed by two-dimensional nucleation.

mined by the shape of the aluminum liquid and by the substrate, respectively.

3. Thickness growth: subsequently, the growth of the needles in the directions perpendicular to the silicon-liquid interfaces starts. Here, the growth rate is less than 1/60 of the TPRE growth. From this sharp decrease in growth rate, it can be concluded that for the thickness growth, the surface kinetics constitute the rate-determining step in the process. Very probably, this growth process is determined by a nucleation mechanism. This is indicated by the fact that the TPRE mechanism only occurs if no spiral growth mechanism is operative (17). It is well known that VLS growth can result in the formation of highly perfect crystals (22, 23). The defects that were revealed by Sirtl etchant were typically twins, stacking faults, and many points defects (the latter were presumably created due to tin inclusions, or after growth).

Only in a few cases dislocations or dislocation arrays (which might have been formed during cooling) have been found. The relatively low dislocation density is in agreement with the assumed nucleation mechanism.

Platelet growth.—Characteristics.—The growth of platelets is characterized by the following features:

1. The platelets usually originate in the liquid metal (homogeneous nucleation; Fig. 1e and f) and subsequently grow rapidly over the liquid surface via a VLS mechanism. In some cases platelets were observed to originate from the edge of a droplet (Fig. 9). Platelet growth was found to occur only in the Si/Sn system, and not in the Si/Al system.
2. The platelets always exhibit a hexagonal shape (Fig. 1f and Fig. 9), so it can be concluded that the top and bottom surfaces are usually {111} crystal faces. However, since the curved surface of the liquid determines the upper surface of the platelet (analogous to the morphology of needles), this surface can be slightly curved. The bottoms of the platelets are usually not in contact with the substrate; in some cases a movement of platelets over the liquid surface has been observed.
3. Sirtl etching and surface topography did not reveal any twinning lines (intersection lines of a twin plane with a crystal face) on the upper surfaces of the platelets originating from a central point to the corners. Careful observation, however, revealed the presence of twinning lines and associated reentrant corners on the narrow side faces of the {111} plates (Fig. 10). These lines were parallel to the {111} surface.

This indicates that the growth of platelets is governed by two or more twin planes parallel to the {111} surface. Thus, the growth of platelets proceeds via the TPRE mechanism that is also responsible for the growth of needles, as described by Faust and John (20) and Wagner (19). The growth mechanism has been pictured schematically in Fig. 10b.

Growth history of the platelets.—The growth process of the platelets can be summarized as follows (Fig. 11):

1. Probably, homogeneous nucleation in the liquid metal is responsible for the formation of platelets. Alternatively, nucleation may be initiated at the liquid-vapor interface (which might be explained by the existence of a concentration gradient in the liquid metal). Nucleation at the liquid metal-substrate interface is improbable, since after etching of the solidified metal no traces of silicon on the graphite could be detected. In some cases heterogeneous nucleation on the graphite on the edge of a droplet caused the formation of platelets; in this case the twin planes run parallel to the liquid surface.

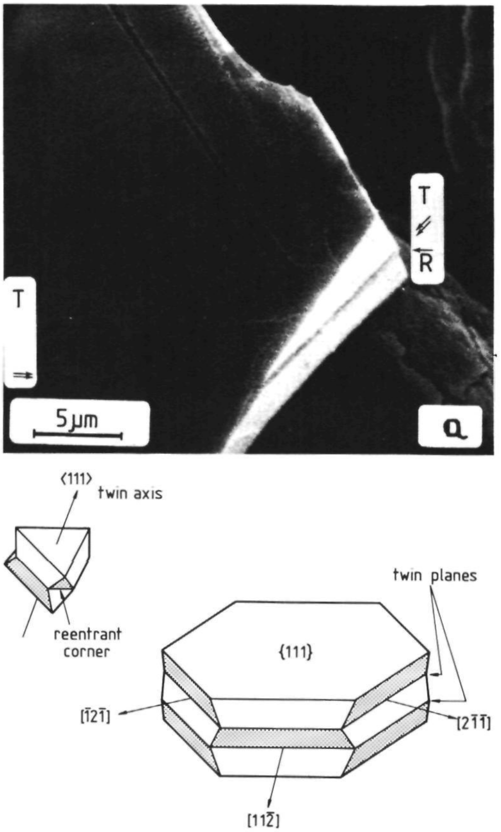

Fig. 10. Twin lines (T) and reentrant corners (R) on the narrow side faces of silicon platelets grown on a tin droplet. a. Twinning line on a side face of a platelet, revealed by Sirtl etching (SEM micrograph). b. Schematic representation of a TPRE grown platelet.

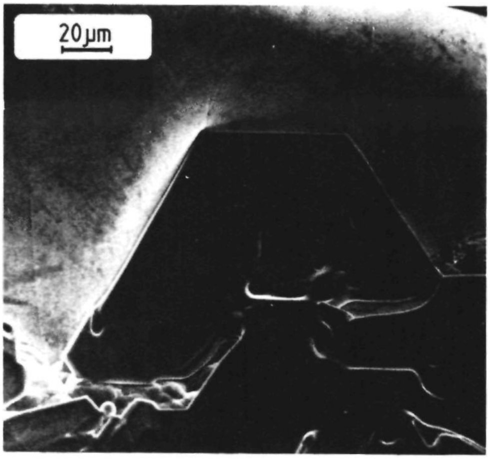

Fig. 9. Silicon platelet, nucleated on the edge of a tin droplet (SEM micrograph).

In the case of homogeneous nucleation inside the liquid, a microcrystal migrates to the liquid surface (due to its small density compared with that of tin), where the platelet adjusts itself to the surface (*i.e.*, the twin planes become directed parallel to the surface). Any other geometry will result in the growth of needles.

2. Subsequently, a rapid lateral growth of the platelets takes place. Since the curvature of the droplet determines the curvature of the crystal top surface, the platelet will be slightly bent. As a consequence of this bending, after some time the twin planes will come out at the top surface instead of at the side facets, and lose contact with the liquid (Fig. 11b). Then, the growth rate decreases suddenly (Fig. 1f). On the upper surface of some platelets twin lines have indeed been found, running parallel to the edges.
3. If there are no twinning lines left on the side faces of the platelets (and consequently the reentrant corners are no longer operative), the subsequent growth continues via a nucleation mechanism. This is the slow growth (about 1/60 times the TPRE growth rate) that has been observed after the rapid growth

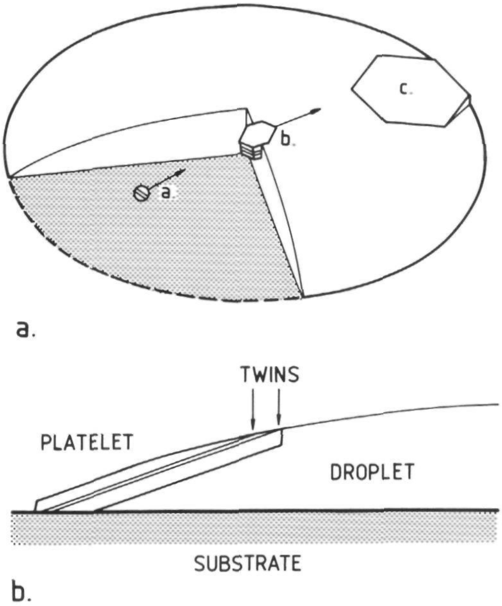

Fig. 11. Growth history of silicon platelets. a. Nucleation and TPRE growth of a platelet. b. Cross section showing that the twin planes lose contact with the liquid.

(Fig. 1g and h). The arguments for the assumption that this growth is governed by a nucleation mechanism, and that the surface process is the rate-determining step, are similar to the reasons given for the growth via nucleation for needles.

Two-dimensional VLS Growth

In some cases it was observed that some small tin droplets remained present on the top surfaces of the needles and platelets. Here the crystal surface always exhibited a very complicated pattern in which these few isolated tin droplets could be detected (see Fig. 12a). These patterns can be understood in terms of a two-dimensional VLS growth mechanism and are similar to the ones that have been observed on ice by Kobayashi (24) (however, in the present case there is no repeatable process for the formation of multiple terraces) and on CuGaS$_2$ by van Enckevort *et al.* (25). This two-dimensional VLS growth mechanism for the advancement of a macrostep has been outlined schematically in Fig. 12b. The growth of such a step is governed by the presence of a liquid tin front, which accelerates the process via a VLS mechanism. The observed solidified tin droplets are the remnants of these liquid "frills" at the edges of the macrosteps.

Conclusions

Silicon crystallites that resulted from the isothermal growth of silicon by means of chemical vapor deposition onto a graphite substrate coated with a liquid metal have been analyzed. It was found that the initial growth of the crystallites proceeds via a VLS mechanism. Two stages in this growth process could be discerned:

1. A rapid growth of needles and platelets according to the twin plane reentrant corner (TPRE) mechanism: the twin planes that are responsible for this mechanism run parallel to the needle axis in the case of needles and parallel to the surface in the case of platelets. There is no essential difference between the growth of needles and platelets. The distinction in morphology is determined by geometrical factors.

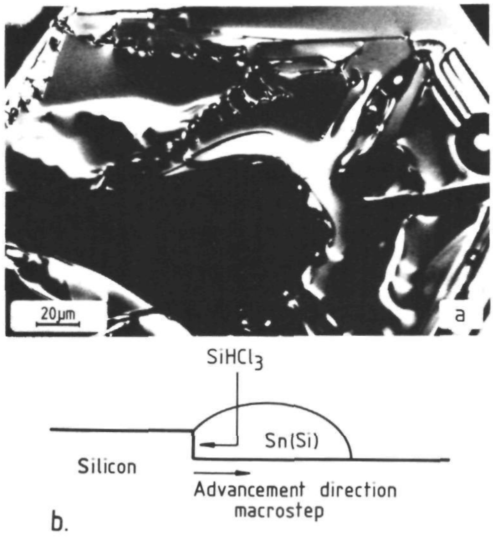

Fig. 12. Two-dimensional VLS growth of silicon in the Si/Sn system. a. Differential interference contrast micrograph showing an irregular surface pattern caused by two-dimensional VLS growth on the upper surface of a silicon platelet. Various solidified tin droplets are present. b. Schematic cross section showing a liquid "frill" at the edge of an advancing step.

2. A slow growth via a nucleation mechanism: in the case of needles this process is observed as the thickness growth perpendicular to the needle axis. In the case of platelets it is observed as a slow lateral growth of the platelets if the twinning lines are no longer in contact with the liquid. Crystallites without twin planes have not been observed. This is caused by the overgrowth of these slow-growing clusters by crystallites possessing two or more parallel twin planes. Two-dimensional VLS growth has been observed on the upper surfaces of needles and platelets. The velocity of macrosteps appeared to be influenced considerably by the presence of a liquid metal frill at the step front. From the fact that even for higher supersaturations growth of the $\{111\}$ faces of silicon and germanium from the melt or metallic solution is strongly accelerated by the occurrence of a TPRE mechanism as compared to two-dimensional nucleation, it can be concluded that the standard temperature θ [for definition of θ, see Ref. (26) and (27)] of these systems is far below the roughening transition point as was determined by Monte Carlo simulation (27). In a forthcoming paper (28), in which a comparison will be made between the Monte Carlo simulation results and growth experiments of $\{111\}$ Si and Ge from the liquid phase, special attention will be paid to the relation between the parameters, which rule the simulations (such as θ), and experimentally known values. A closer investigation into the thermodynamic and kinetic phenomena that are associated with the described growth process may lead to an augmented knowledge of the growth of thin large-grain polycrystalline silicon layers onto nonsilicon substrates, and enable the preparation of inexpensive materials for photovoltaic solar cell fabrication.

Acknowledgments

The authors wish to thank H. A. v. d. Linden and Ing. A. W. Dicke for their help in making the SEM photographs. They also want to thank Prof. Dr. P. Bennema, Prof. Dr. J. Bloem, and Dr. L. J. Giling for stimulating discussions and for their kind interest in the present study. W. J. P. van Enckevort acknowledges the support of The Netherlands Foundation for Pure Research (ZWO/SON), whereas M. W. M. Graef acknowledges the Commission of the European Communities for an EC grant Contract No. 442-78-2 ESN.

Manuscript submitted March 28, 1980; revised manuscript received July 29, 1980.

Any discussion of this paper will appear in a Discussion Section to be published in the December 1981 JOURNAL All discussions for the December 1981 Discussion Section should be submitted by Aug. 1, 1981.

Publication costs of this article were assisted by Catholic University.

REFERENCES

1. T. L. Chu, H. C. Mollenkopf, and S. S. Chu, *This Journal*, **123**, 106 (1976).
2. C. Belouet, J. Hervo, R Martres, Ngo-Tich Phuoc, and M Pertus, Proceedings of the XIIth IEEE Photovoltaic Specialists Conference, Washington, D.C., p 131 (1978).
3. C.-A. Chang and W. J. Siekhaus, *J. Appl. Phys.*, **46**, 3402 (1975).
4. T. F. Ciszek, G. H. Schwuttke, and K. H. Yang, *J. Cryst. Growth*, **46**, 527 (1979).
5. M. W. M. Graef, L. J Giling, and J. Bloem, *J. Appl. Phys*, **48**, 3937 (1977).
6. J. Bloem, L. J. Giling, M. W M. Graef, and H. H. C. de Moor, Proceedings of the 2nd E.C. Photovoltaic Solar Energy Conference, Berlin p. 759 (1979).
7. C. H J van den Brekel and J. Bloem, *Philips Res. Rep.*, **32**, 134 (1977).
8. M W. M. Graef and J. R. Monkowski, To be published.
9. E. Sirtl and A. Adler, *Z. Metallk.*, **52**, 529 (1961).
10. W. Bardsley, F. C. Frank, G. W. Green, and D. T. J. Hurle, *J. Cryst. Growth*, **23**, 341 (1974).
11. T. Surek, C. B. Hari Rao, J. C. Swartz, and L. C. Garone, *This Journal*, **124**, 112 (1977).
12. B H. Berry, in "Fundamentals of Silicon Integrated Device Technology," Vol. 1, R. M. Burger and R. P. Donovan, Editors, p 434, Prentice-Hall Inc., Englewood Cliffs, N J. (1967).
13. J W Faust, A. Sagar, and H. F. John, *This Journal*, **109**, 824 (1962).
14. G. A Wolff, *Am. Mineral*, **41**, 60 (1956).
15. D R. Hamilton and R G. Seidensticker, *J. Appl. Phys*, **31**, 1165 (1960).
16. A. A. Davydov and V. N. Maslov, *Soviet Phys.-Cryst.*, **9**, 393 (1965).
17. M Kitamura, S Hosoya, and I. Sunagawa, *J. Cryst. Growth*, **47**, 93 (1979).
18. A. I Bennett and R. L. Longini, *Phys. Rev.*, **116**, 53 (1959).
19. R. S. Wagner, *Acta Metall*, **8**, 57 (1960).
20. J W. Faust and H. F. John, *J. Phys. Chem. Solids*, **25**, 1407 (1964).
21. C. Lemaignan and Y. Malmejac, *J. Cryst. Growth*, **46**, 771 (1979).
22. E I. Givargizov, in "Current Topics in Materials Science," Vol 1 E Kaldis Editor, p. 79, North-Holland Publishing Co. (1978).
23. B. J. Baliga, *This Journal*, **125**, 598 (1978).
24. T. Kobayashi, *J. Cryst Growth*, **26**, 6 (1974).
25. W J. P. van Enckevort, H. Binsma, and G Staarink, *ibid.*, To be published.
26. J P van der Eerden, P. Bennema, and T. A. Cherepanova, "Prog. Crystal Growth and Charact.," Vol 1, p. 219, Pergamon, Oxford (1978).
27. W J P. van Enckevort and J P. van der Eerden, *J. Cryst. Growth*, **47**, 501 (1979).
28. W. J P. van Enckevort, P. Bennema, and L. J. Giling, Work in progress.

Journal of Crystal Growth 43 (1978) 659–675
© North-Holland Publishing Company

CHAPTER XV:
SURFACE MORPHOLOGY OF HCl ETCHED SILICON WAFERS

II Bunch formation

P VAN DER PUTTE, W J P VAN ENCKEVORT, L J GILING and J BLOEM
University of Nijmegen R I M Department of Solid State Chemistry Toernooiveld Nijmegen The Netherlands

Received 1 December 1977 manuscript received in final form 1 February 1978

Gas phase etching of silicon (111) wafers not only results in the formation of etch pits, but also may lead to bunch formation depending on temperature and HCl input concentration Analogous to a transition line pitted smooth, a second transition line can be given between bunched and smooth surface structures, the position of this transition line in the p_{HCl} T diagram strongly depends on the type of carrier gas (hydrogen or argon) It appears that the individual shape of the observed bunches is determined by the misorientation of the exposed surface from the real (111) plane and by the directions of the crystallographic preferential etching vectors in the (111) surface Both positive and negative bunches are observed corresponding to bunch formation without and with impurities Their formation can be described in a satisfactory way by the kinematic wave theory as given by Frank and represents a good example in this field In addition to Cabrera's type I and type II curves, a third type of curve is introduced at the limit of very high impurity concentrations on the surface An analysis is given of the process leading to bunch formation based upon the assumption that bunches develop when the rate of advance of a step is comparable with the velocity of the surface diffusion of individual adatoms In this way the temperature dependence of the transition line from smooth to bunched can be explained

1 Introduction

In a previous paper, [1] (referred to as part I in the following), in which the reaction mechanisms were described for the etching of silicon with gaseous HCl at 1400 to 1600 K, a transition was reported separating areas in the p_{HCl} T diagram where the silicon surface remains smooth and where the surface becomes covered with the etch pits

Prior to this pit formation, another surface phenomenon can be observed during the etching process which is due to bunch formation Bunch formation or the macroscopic pile up of steps on a crystal surface – can be observed during the growth or etching from the vapor phase or from solution. Revesz and Evans [2] reported bunch formation on silicon, but further evidence on silicon material is scarce In the present paper a more systematic study is made of this phenomenon in which attention is given to the development, the nature and the existence of bunches found after etching of (111) silicon, followed by a theoretical interpretation based on the kinematic wave theory as given by Frank and Cabrera [4,5].

2 Experimental procedure

The etching process of silicon was performed in a water cooled epitaxial reactor according to the conditions described in part I Several silicon crystal orientations with different misorientations were used A survey of the substrates used in the experiments is given in table 1 After the etching process the evaluation was performed with an optical microscope fitted with a Tolanski interferometer In all experiments about 25 μm was etched away from the slices, at etch rates, depending on the HCl input concentration, between 0 25 and 20 μm/minute for the hydrogen system, and between 3 5 and 28 μm/minute for the argon system

Table 1
Specific misorientations of the different silicon substrates used in the etching experiments with gaseous HCl in hydrogen or argon

Crystal orientation		Deviation from real crystal plane	In the direction of
(111)	a	2°49′	Nearest (100)
		0°23′	Nearest $(\bar{1}31)$
	b	4°30′	Nearest (110)
	c	Less than 0.5° in all directions	
(110)		5°	Nearest (111)
(100)		0°45′	Nearest (110)
		0°57′	(110) perpendicular to the first (110)

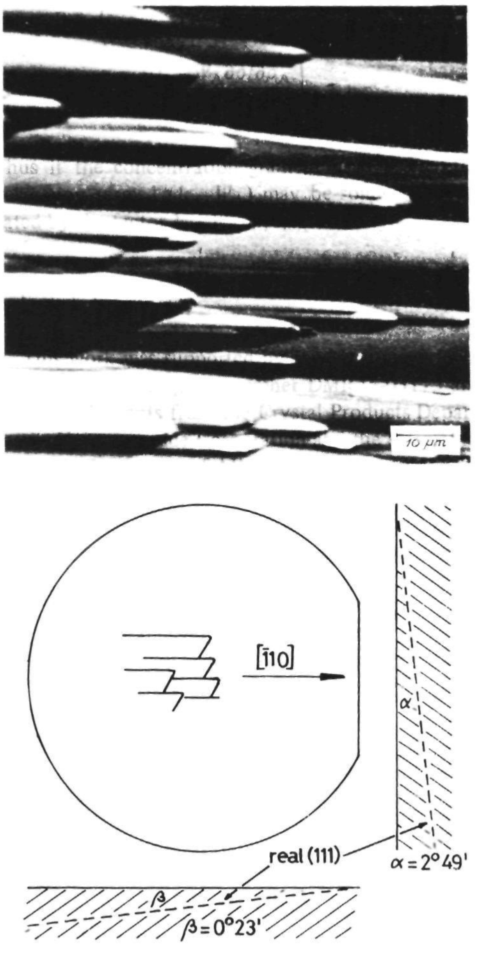

Fig. 1. Misorientation of silicon (111)a substrates, and bunch pattern found after etching with HCl at 1450 K.

3. Experimental results

In the temperature and concentration range of interest, bunches could only be detected on (111) silicon surfaces. No bunch formation could be observed on the (100) and (110) orientated surfaces specified in table 1, i.e. the (100) surfaces showed no structure at all, whereas on (110) surfaces only some grooves were observed in the surface. (See section on (110) and (100) surfaces.) On all three orientations however, etch pits are formed at high etch rates as shown in part I.

As regards the bunch formation on the (111) substrates, it can be said that depending on the orientation of the exposed surface with respect to the real (111), the following types of bunch pattern could be observed:
(i) Substrates (111)a exhibit long stretched positive bunches (for definition of positive and negative bunch formation see the section on discussion). The shape of these bunches is given in fig. 1, together with the position of the bunches with respect to the crystallographic direction of the substrate. The height of the bunches did not exceed 1 μm. Besides this type of bunch formation sometimes large hillocks were observed (fig. 14a);
(ii) Substrates (111)b developed droplet-like positive bunches, shown in fig. 2. In the same picture some examples of hillocks are given, which are also found on this type of misorientation;
(iii) On crystals (111)c with a misorientation less than 0.5° from (111), a completely different surface structure developed. On these surfaces the exposed surface broke up, resulting in facets having a deviation from the real (111) of about 1.0° (fig. 3). On these facets again bunch formation of the type mentioned under (i) could be observed.

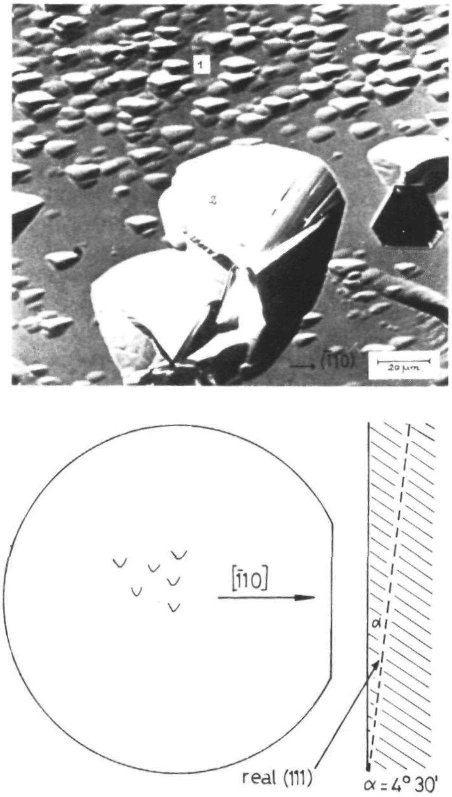

Fig. 2. Misorientation of silicon (111)b substrates, and bunch pattern found after etching with HCl at 1435 K. The photograph shows both droplet like bunching (1) and hillocks (2).

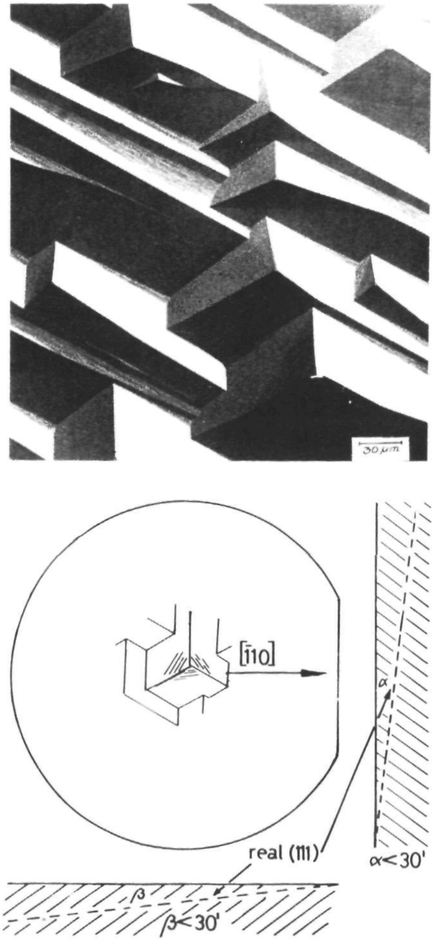

Fig. 3. Misorientation of silicon (111)c substrates, and surface structure found after etching with HCl at 1450 K.

The observed shape and position of the bunches were independent of the type of carrier gas or the direction of the gasflow with respect to the position of the crystal. When impurities are introduced (e.g. oxygen or water vapour) the nature of the bunches changed. When viewed in a vertical cross-section the form was converted from positive into negative, i.e. the discontinuity point shifts from the bottom to the top side of the bunch. Negative bunches are most commonly observed when argon is used as a carrier gas, probably because of the presence of ≈10 ppm H_2O. With argon as the carrier gas the surface becomes very rough due to the high density of negative bunches. A lower density of negative bunches can be observed in the $H_2/HCl/O_2$ system, although even then the bunches are very small (fig. 4).

An overview, showing under which conditions of p_{HCl} and temperature bunches will develop is given in fig. 5. The situation for the hydrogen system is given by the drawn line; the dotted line represents the transition from smooth to bunched surface structures when argon is used as a carrier gas. It can be seen that this transition line is shifted to lower input concen-

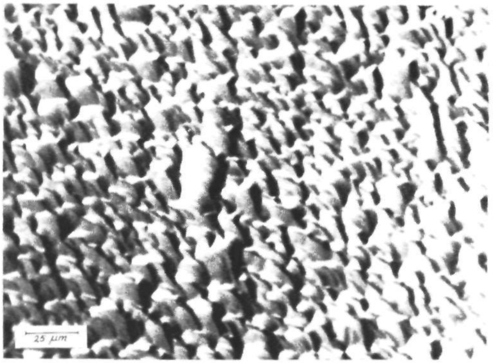

Fig. 4. A typical negative bunch pattern on (111)b silicon after etching with HCl in hydrogen with 50 ppm oxygen.

trations of HCl and higher temperatures. An explanation for this difference between the hydrogen and argon system will be given later on in this paper. In the same figure the transition line from a smooth to a pitted surface, as given in part I, is shown. In the regime of high p_{HCl} and low temperature both etch pits and bunches are present. In general etch pits are created on a bunched surface.

4. Discussion

4.1. *Crystallographic etching vectors, step flow mechanism and kinematic wave theory*

It is known [2,3] that the growth of silicon on (111) surfaces proceeds by a stepflow mechanism as described by Burton, Cabrera and Frank [4] with steps moving in the $\langle\bar{1}\bar{1}2\rangle$ directions. Consequently it follows that, during the etching process, steps will move in the opposite direction viz the $\langle 11\bar{2}\rangle$ directions. This can easily be deduced from fig. 6, which gives a top view of the silicon (111) face. Crystallographically the etching of silicon can take place in the $\langle 11\bar{2}\rangle$ or in the $\langle\bar{1}\bar{1}2\rangle$ directions. By going in the $\langle 11\bar{2}\rangle$ directions the step is etched by breaking 2 Si–Si bonds for every silicon atom, whereas by going in the $\langle\bar{1}\bar{1}2\rangle$ directions etching will proceed by breaking alternatingly 1 and 3 Si–Si bonds. Etching in the $\langle 11\bar{2}\rangle$ directions therefore is energetically favoured compared with etching in the $\langle\bar{1}\bar{1}2\rangle$ directions. Accordingly, it has to be expected that on a silicon (111) surface, etching in the $\langle 11\bar{2}\rangle$ directions will dominate; only under extreme conditions is it to be expected that the $\langle\bar{1}\bar{1}2\rangle$ directions will become visible. Which of the three possible $\langle 11\bar{2}\rangle$ directions will

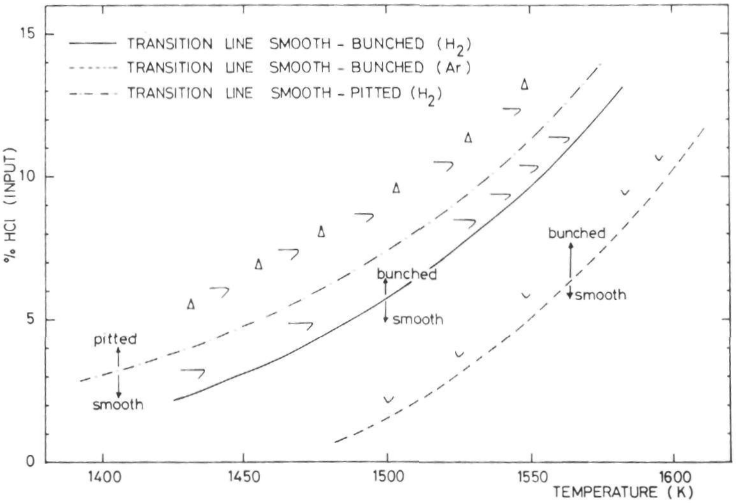

Fig. 5. Transition lines from smooth to bunched surface structure for the H_2/HCl and Ar/HCl system, and the transition line from smooth to pitted surface structure for the H_2/HCl system. All lines are for (111) oriented substrates; on all slices about 25 μm was etched away.

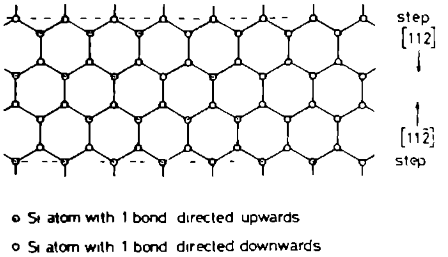

Fig 6 Top view of the silicon (111) surface, showing the two theoretically possible etching directions

become operative in practice will depend on the specific misorientation of the substrate. This will be illustrated in greater detail later on in this paper

When a row of steps moves across the surface, a perturbation in the equidistant train of steps may either be damped out or may develop into a macroscopic compilation of steps, called a bunch

Theoretically the form and development of bunches from such a row of steps can be described by the kinematic wave theory of Frank [5] and Cabrera [6] This theory, developed for traffic flows, does not apply to microscopic processes such as the diffusion of adatoms between the steps, only the movement of steps is involved in the calculation

When a surface has a declination from the real crystallographic plane the step density k (the number of steps per unit length) is determined by the misorientation of the surface and the step height (h) The step flux q (i e the number of steps passing a point on the surface per unit time) is related to the etch rate R by

by

$$R = hq, \tag{1}$$

whereas the velocity of an individual step (v_{st}) is given by

$$v_{st} = q/k, \tag{2}$$

in which the step flux q is a function of the step density Besides the velocity of an individual step, a group velocity v_{gr} can be defined, i e the velocity of a surface formation called a kinematic wave

$$v_{gr} = dq/dk \tag{3}$$

The relation between q and k depends on the amount of impurities on the surface Cabrera postulated two types of q-k relations

(1) Cabrera's type I relation is shown in fig 7a The curve is valid for the case where no impurities are present on the surface The shape of the curve reflects the effects of shorter step distances on the growth or etch rate As the step distance decreases, giving a higher step density the supply of reactants and the removal of reaction products is more and more hampered, and thus the step flux will deviate from the linear q-k dependence For this type of curve the formation of a bunch can be understood to take place in the following way a disturbance in an equidistant train of steps moving across the surface results in a group as given in fig 8a As the velocity of the group is lower than the individual step velocity, at the upper

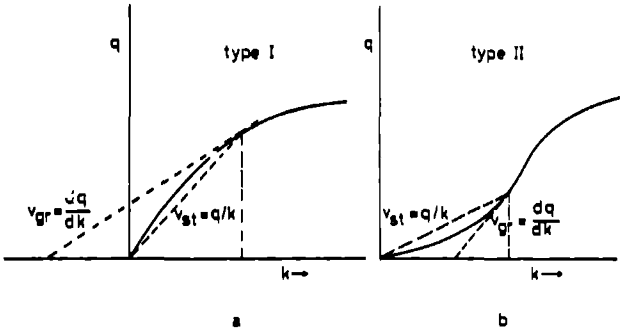

Fig 7 Relation between step flux (q) and step density (k) according the Cabrera's type I (a) and type II (b) curves, v_{gr} is group velocity, v_{st} is the individual step velocity

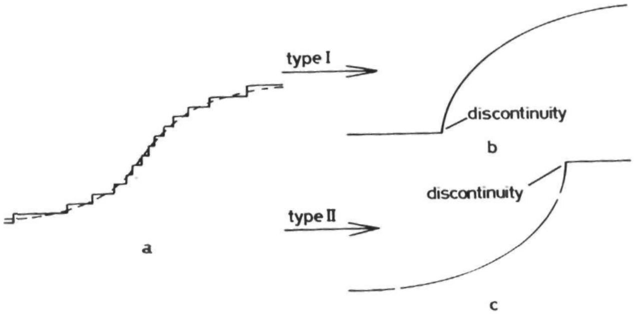

Fig. 8. Schematic picture of a group resulting from statistical fluctuations in the equidistant train of steps (a) and the development into a positive (b) or a negative (c) bunch, according to Cabrera's type I and type II curve respectively.

edge of the group the steps will leave without difficulty, but at the lower side the fast steps will collide with the group forming a discontinuity (fig. 8b). Such a group in time will develop to a visible macroscopic bunch with a discontinuity at te lower side: a positive bunch.

(ii) Cabrera's type II $q-k$ relation (fig. 7b) describes the situation in which below a critical value for the step density the group velocity is higher than the velocity of the individual steps. This type is valid for the case of time dependent adsorption of impurities from the gas-phase, i.e. when the concentration of adsorbed species at the surfaces between the steps becomes higher at longer exposure times. The steps will move more slowly as the amount of impurities that covers the surface becomes higher. So when a disturbance in the steptrain is formed, as given in fig. 8a, the shorter step distances in the group will be less affected than the longer step distances on the rest of the surface. Now the group will collide with the slow steps at the top, giving rise to a so called negative bunch (fig. 8c).

Using the kinematic wave theory an explantion can now be given for the surface structures which are experimentally observed on the silicon slices with the given misorientations.

4.2. *Shape of the bunches on silicon (111)*

4.2.1. *Positive bunch formation*

Misorientation (111)a. Fig. 9 shows the misorientation of the exposed silicon surface from the real

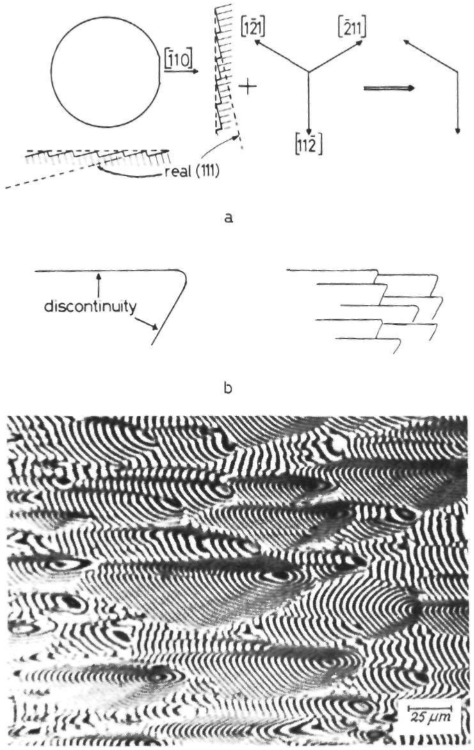

Fig. 9. (a) Direction of moving step trains resulting from a combination of misorientation and preferential etching vectors on the silicon surface with misorientation (111)a; (b) predicted shape of a bunch and accumulation of bunches on (111)a; (c) interference photograph of a bunched silicon surface with misorientation (111)a.

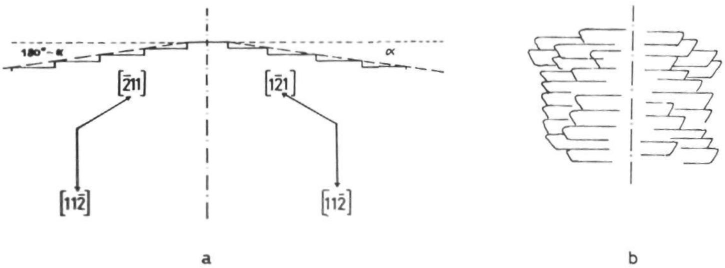

Fig. 10 Predicted bunch patterns near the edge of a silicon (111) slice with misorientation (111)a, where the silicon surface is rounded off. The step train in the [12̄1] direction is replaced by a step train in the [2̄11] direction.

(111), measured for the directions parallel and perpendicular to the reference side of the slice. The combination of this misorientation with the preferential etching directions results in rows of steps moving only in the [12̄1] and [112̄] directions. The etching vector in the [2̄11] direction is ineffective because of a lack of steps in this direction. Fluctuations in the step density will result in bunch formation with discontinuities at the lower side, perpendicular to the [12̄1] and [112̄] directions. As the overall misorientation has to remain constant, at the top of the bunch large perfect (111) facets must develop compensating for the larger step densities at the flank of the bunch. So for the given misorientation ((111)a), the length of the bunch in the [11̄0] direction must be about 6 times as large as the length of the bunch in the [112̄] direction, which indeed is observed. On these facets an undersaturation of $SiCl_2$ adatoms can easily develop as required for the nucleation of etch pits as described in part I.

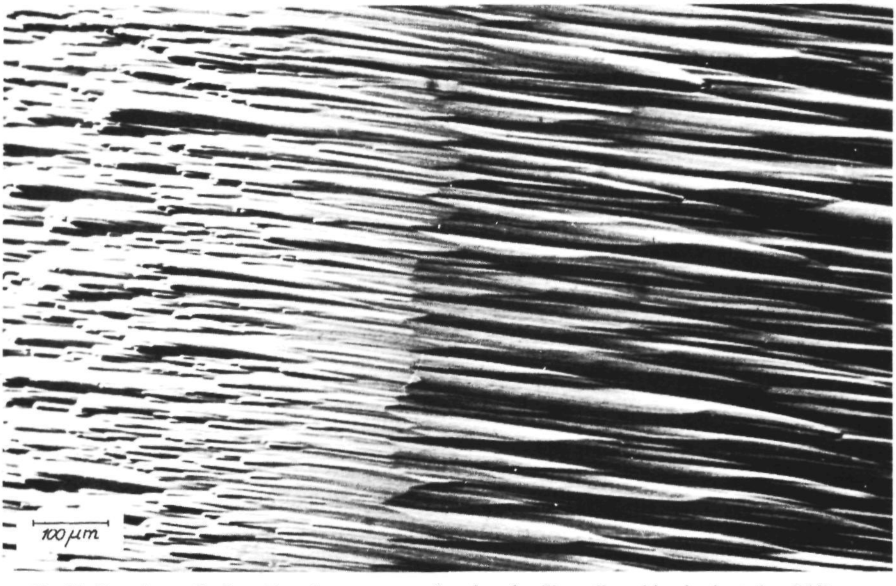

Fig. 11. Experimentally found bunch pattern near the edge of a silicon slice with misorientation (111)a.

Fig. 9b shows the theoretical shape of a bunch for this type of silicon slice. An accumulation of this kind of bunch will finally result in a surface structure as depicted in the same figure. From fig. 1 and fig. 9c it follows that the observed bunches indeed are positive and possess the predicted discontinuities perpendicular to the directions of the active etching vectors.

It is evident from this analysis that the shape and position of the bunches is determined solely by the etching vectors in operation and the existing misorientation. There is no influence of the gas stream above the crystal on the shape of the bunches. This could be nicely demonstrated by the following experiment. Near the edge of the silicon slice the surface is rounded off. Consequently a place can usually be found where the misorientation shifts from α (the original declination) to $180^\circ - \alpha$ (fig. 10a). Accordingly, when the misorientation of the exposed surface is the decisive parameter, the shape of the bunches in that region has to change because now the etching vector in the $[\bar{2}11]$ direction becomes effective instead of the vector in the $[1\bar{2}1]$ direction. The bunch pattern should thus correspond to the form depicted in fig. 10b, as indeed was found experimentally (fig. 11).

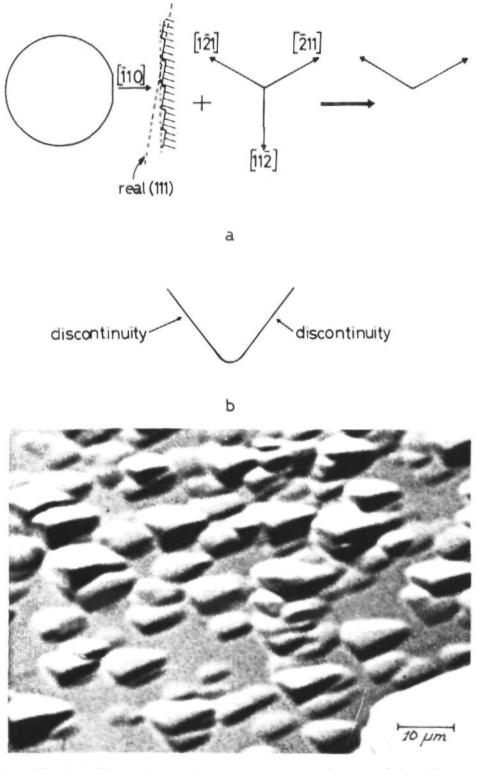

Fig. 12. (a) Direction of moving step trains resulting from a combination of misorientation and preferential etching vectors on the silicon surface with misorientation (111)b; (b) predicted shape of a bunch; (c) photograph of bunches on silicon (111) slices with misorientation (111)b.

Misorientation (111)b. Fig. 12a shows the misorientation of the exposed silicon surface from the real (111). Only the two etching directions $[1\bar{2}1]$ and $[\bar{2}11]$ can be operative. Application of the kinematic wave theory results in bunches with the shape predicted in fig. 12b. Fig. 12c shows the experimenrally observed bunch formation for this misorientation, and it will be seen that it has the same shape as that predicted theoretically.

4.2.2. Negative bunch formation

The formation of negative bunches is to be expected when impurities are present in the system. In the etching of silicon indeed negative bunch formation is found, especially in the experiments where argon was used as a carrier gas; probably because the concentration of oxygen in the argon gas from time to time exceeded 10 ppm (O_2 and H_2O together). During the experiments a maximum concentration of 25 ppm was measured. This concentration appeared to be high enough for the formation of negative bunches, especially at low temperatures. Fig. 13 shows an example of negative bunch formation in the argon/HCl system on a slice with misorientation (111)b. In the hydrogen/HCl system oxygen had to be introduced deliberately in the gas stream to obtain negative bunches. Fig. 4 gives an example of negative bunch formation on a slice with misorientation (111)b in the hydrogen/HCl system. It can be seen that the bunches are too small to detect a relation with the given misorientation.

4.2.3. The formation of hillocks

In addition to bunch formation, as described sofar, another type of surface structure exists, called hillocks, which differs in three respects from the bunches: (a), they are isolated elevations on the sur-

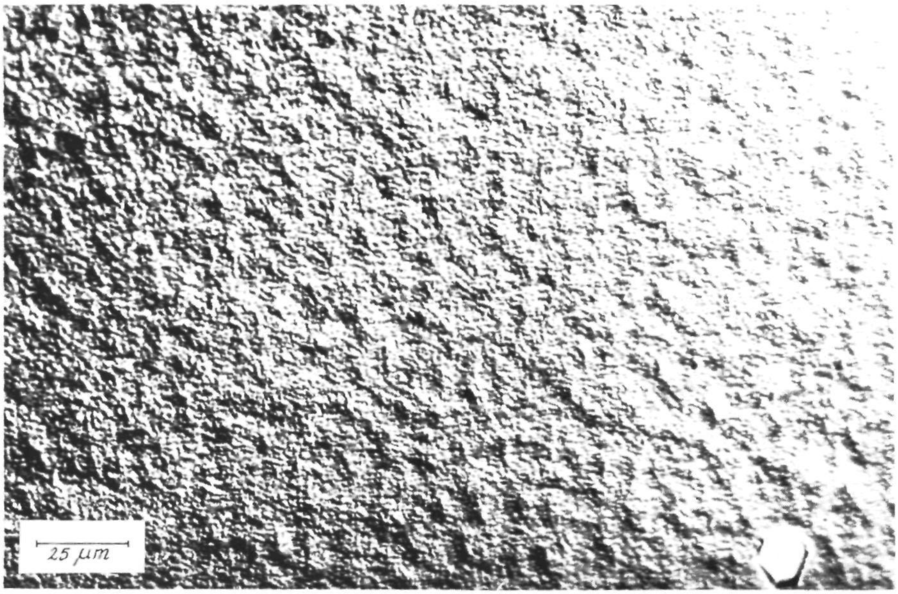

Fig. 13. Typical negative bunch pattern on (111) silicon with misorientation (111)b after etching in an argon/HCl mixture.

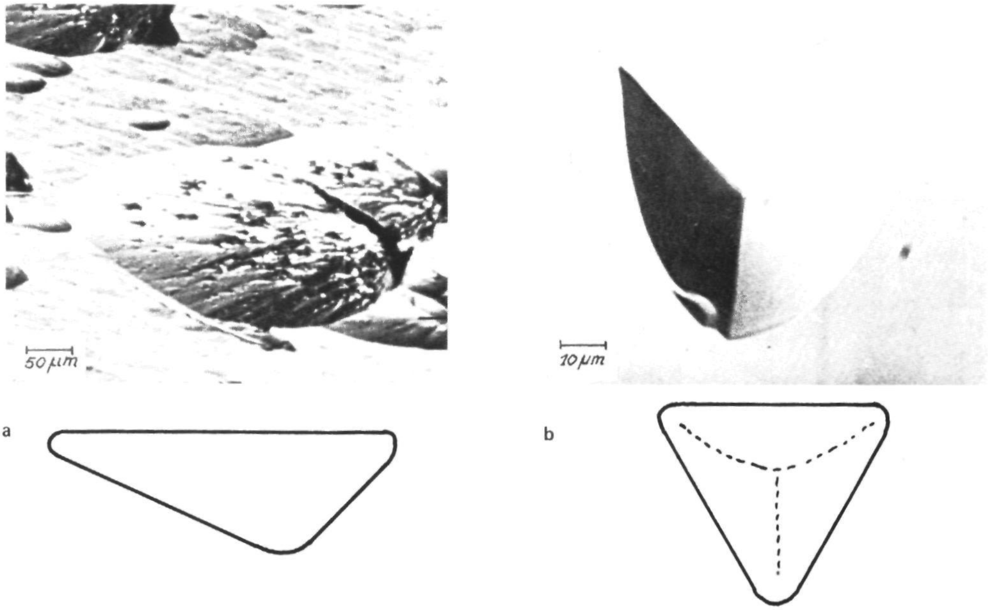

Fig. 14. Predicted and experimentally found hillocks on silicon (111). (a) Misorientation (111)a; (b) misorientation (111)b.

face (I), the size of these hillocks is much larger than the size of normal bunches [illegible] at all three sides the transition from the hillocks to the exposed surface is discontinuous when type I curve is valid. Figs 14a and 14b show the types of hillocks observed on the silicon slices with misorientation (111)a and (111)b respectively. These hillocks appear to be associated with impurities because it was observed that they followed a striated pattern on the surface indicating that micro defects in the silicon crystal [7] are probably responsible for their existence. At a strongly bound impurity on the silicon surface (e g SiC) the etching may be retarded with respect to the silicon surface around the hillock.

This could explain why the hillock becomes higher than its surroundings, eventually so high that step trains are present in all three crystallographic directions ⟨11$\bar{2}$⟩ This leads to a discontinuity at all three sides of the hillock.

4 2 4 Facet formation on near (111) silicon

On (111) surfaces with a very small misorientation (≤0.5°) an entirely different morphology develops which is not directly related to bunch formation. On these nearly perfect (111) surfaces no bunch formation could be detected. This is not surprising since, because of the small misorientation the step density is low and thus the step velocity and the group velocity derived from the lineare region in fig 7 are nearly identical, viz., when $v_{st} = v_{gr}$ bunch formation will not take place. However beyond a critical HCl concentration the surface breaks up and facets are formed (fig 15, fig 3). The surface is covered with very shallow triangular pits. The observed symmetry is due to the threefold symmetry of the (111) plane. The facets make an angle of about 1.0° with the real (111) plane.

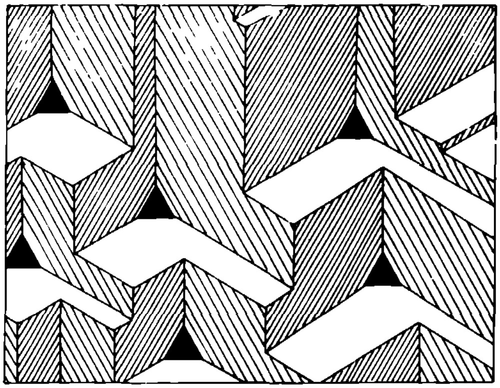

Fig 15 Facet formation in 3 directions for silicon (111) crystals with a small (≈0 5°) misorientation.

Such facet formation has earlier been reported by Burmeister [8] in growth and etching experiments. The formation of these facets is not due to the bouncing of steps in a step flow mechanism as described by the kinematic wave theory. In our opinion, the facets are created, because the original surface can not respond properly to the etch rate imposed on it by the increasing HCl concentration, since the density of steps is too low.

When the input concentration of HCl is increased above a critical point an undersaturation of $SiCl_2$ develops between the steps, and nucleation of the surface between the steps, as described in part I will occur. As soon as a surface vacancy, or a group of vacancies is formed, a set of three new steps is created in the three etching directions as shown in fig 16. The effect of repeated nucleation is such that the surface breaks up into facets and creates its own local misorientation. By this procedure enough new steps are created to respond properly to the desired etch rate. On these facets bunch formation, as described in section A, can again take place, as is observed. Burmeister explained this facet formation on the basis of the stability of crystallographic planes covered with adsorbed species, the gain in free surface energy being the driving force for the facet formation. To test this hypothesis, silicon samples were heated at 1100°C in a closed tube in contact with different mixtures of hydrogen and HCl. The amounts of gas and reactants were such as to give a total pressure near to 1 atm. In

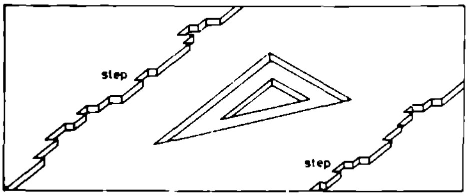

Fig 16. The formation of additional steps on nearly (111) substrates resulting in facets with a deviation from (111) of about 1.0 degrees.

this way the same gaseous composition and the same adsorption conditions were present as in a CVD reactor After heating for 24 h no facet formation could be observed for any of the different mixtures In our opinion this excludes the possibility that the facet formation is an equilibrium phenomenon The alternative explanation for the formation of facets, based upon kinetic nucleation as outlined above, will be treated in more detail in a paper on nucleation

4 2 5 Type III q-k relation

It was observed that for very high etch rates (e g 10 μm/min at 1450 K) the bunches tend to disappear This cannot be explained by Cabrera's type I or type II $q-k$ relations However an explanation for this effect can be given according to the following analysis Cabrera's type II $q-k$ relation is valid when the concentration of adsorbed species is time dependent However, a situation can exist where the impurity flux towards the surface is so large that adsorption equilibrium is established almost instantly, i e adsorption becomes time independent Under such circumstanes the step velocity is only determined by the presence of the adsorbed species and thus becomes independent of the step density, i e $v_{step}(k) = v_{group}$ = constant, and disturbances in the step train will not develop into bunches This leads to the introduction of a new type of q k relation, the type III $q-k$ relation (fig 17), which is a straight line over the entire k range

This explanation requires the presence of large amounts of impurities at the surface In part I it has been shown that the etch rate of the silicon surface is determined by the surface diffusion of $SiCl_2$ adatoms away from the steps This means that in the direct neighbourhood of the steps the concentration of the reaction product $SiCl_2$ is very high, equal for every step, and independent of the step density As the surface becomes smooth at large HCl input concentations, which implies large $SiCl_2$ adatom concentration at the steps, it can be assumed that $SiCl_2$ itself acts as the impurity which causes the observed stability of the surface against disturbances

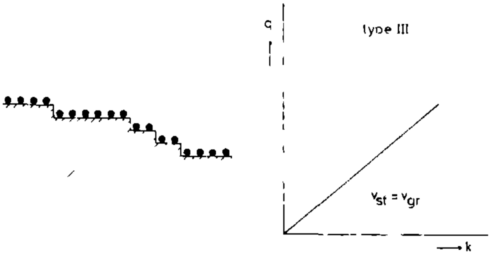

Fig 17 Relation between step flux (q) and step density (k) for the case where very high impurity concentrations are present on the surface the type III q k relation Every step is hindered to the same amount and so the step velocity is independent of the step density

4 3 The transition smooth to bunched qualitative interpretation based on the stability-instability criterium

Although the formation of bunches can be described in a satisfactory manner by the kinematic wave theory, the theory is not able to predict when, and under what conditions of p_{HCl} and temperature, instabilities in the step train will develop into macroscopic bunches For that purpose the movement of the individual steps has to be considered in more detail

It is assumed [9] that the velocity of a step is a function of the length of the surfaces in front of (λ_+), and behind, (λ_-), a particular step (fig 18) The velocity of a step is then determined by the number of adatoms on both surfaces Allowance is made for a different dependence on these two distances

$$v_{step} = f_+(\lambda_+) + f_-(\lambda_-) \qquad (4)$$

When an equidistant train of steps is disturbed, the

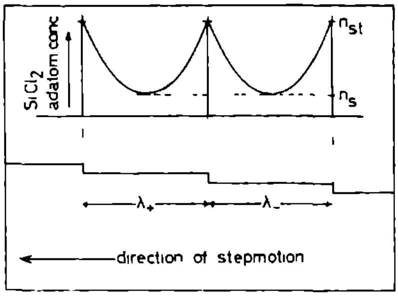

Fig 18 Step train moving across the surface λ_+ is step distance in front of the step, λ_- is step distance behind the step n_{st} is $SiCl_2$ adatom concentration at the step, n_s is $SiCl_2$ adatom concentration between the steps

amplitude of the disturbance, u (= distance of the step from its unperturbed position), can be treated mathematically like the motion of an infinite chain of masses attached by springs The corresponding time dependent solution is

$$u_q(t) = \exp(bt + iwt), \tag{5}$$

where

$$b = \left[\frac{df_+(\lambda)}{d\lambda} - \frac{df_-(\lambda)}{d\lambda}\right][(\cos q\lambda) - 1)]$$

$$w = \left[\frac{df_+(\lambda)}{d\lambda} + \frac{df_-(\lambda)}{d\lambda}\right] \sin q\lambda,$$

and q is inversely proportional to the wavelength of the corresponding normal mode of vibration

When

$$\frac{df_+(\lambda)}{d\lambda} = \frac{df_-(\lambda)}{d\lambda},$$

$b = 0$ and any small perturbation will continue with a constant amplitude This is the case for a symmetrical dependence of the step velocity on the spacing in front and behind, a disturbance in the spacing will continue unabated

It can be shown that when $f_+(\lambda) > f_-(\lambda)$, also

$$df_+(\lambda)/d\lambda > df_-(\lambda)/d\lambda,$$

and b becomes negative, since $(\cos q\lambda) < 1$ In this case the amplitude of the perturbation will decay exponentially When

$$df_+(\lambda)/d\lambda < df_-(\lambda)/d\lambda,$$

the amplitude of the perturbation will grow exponentially, and, if the perturbation growth rate is fast enough multiple steps and bunch formation will be the result Physically, a difference in f_+ and f_- will result in unequal concentration profiles of adatoms on both sides of the steps (cf the Schwoebel effect [10]) As was pointed out in part I the etching of silicon takes place at the steps, with the overall reaction being given by

$$Si + 2\,HCl \rightleftharpoons SiCl_2 + H_2 \tag{6}$$

It was shown that near the transition line smooth—pitted the etch rate of silicon, in the temperature range studied, is governed by the surface diffusion of $SiCl_2$ adatoms away from the steps on the surface Since the transition line smooth bunched is very near to the line smooth pitted the same condition will apply At low HCl input concentrations the etch rate and, therefore, the step velocity is low much lower than the diffusion velocity of the individual $SiCl_2$ adatoms The diffusion away from the steps is equal in both directions and $f_+ = f_-$ Perturbations therefore will not grow out to give bunches At larger HCl input concentrations the velocity of the steps will increase and the relative velocity of adatoms in front of the step will decrease while the relative velocity of adatoms behind the step increases In fact the diffusion of $SiCl_2$ adatoms in the direction in front of the steps is hampered, and $f_+ < f_-$

A disturbance in the train of steps will grow exponentially, resulting in bunch formation For very high HCl concentrations $f_+ \approx f_-$, because the adatom concentrations at both sides of the steps are equally high (curve III) Hence, on the basis of the instability criterium the formation of bunches can be adequately described The temperature dependence of the transition line can be understood as follows At constant p_{HCl} the etch rate, and thus the step velocity, will only depend on temperature As this temperature dependence is small (±4 kcal/mol [11]) the step velocity is only weakly dependent on temperature However, the surface diffusion velocity of $SiCl_2$ adatoms will change with temperature according to

$$v_{diff} = a\nu \exp(-E_{diff}/kT), \tag{7}$$

where E_{diff} = activation energy for diffusion, ν = vibration frequency, and a = atomic distance This means that the diffusion velocity decreases with decreasing temperature A smooth surface will be stable for $v_{step} \ll v_{diff}$ and bunches will only develop when v_{step} and v_{diff} become of the same order of magnitude At low p_{HCl} (low v_{step}) this condition will be met at low temperatures, while for high temperatures only at high p_{HCl} bunches will occur This is shown schematically in fig 19 The combination of the influence of temperature and HCl input concentration can thus give a qualitative explanation for the shape of the experimentally found transition line, shown in fig 5 In the next section a quantitative analysis will be presented

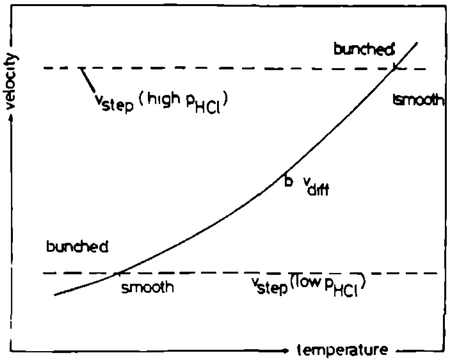

Fig 19 Illustration of the condition for bunch formation For $v_{step} - bv_{diff}$ bunch formation is expected $v_{diff} = \exp(-E_{diff}/kT)$ Two situations are given one for low v_{step} (= low p_{HCl}) and one for high v_{step} (- high p_{HCl})

4 4 *The transition line smooth-bunched quantitative treatment*

As stated previously the etching of the silicon surface is governed by surface diffusion of $SiCl_2$ adatoms away from the steps

Therefore an undersaturation of $SiCl_2$ on the surface between the steps is present The velocity of the steps is proportional to the diffusional flux of $SiCl_2$ adatoms from the steps [4]

$$v_{step} = 2\frac{D_s}{x_s}\frac{n_{st} - n_s}{n_0}\tanh\frac{\lambda}{2x_s}, \tag{8}$$

where n_{st} = adatom concentration at the step, n_s = adatom concentration between the steps, n_0 = total number of surface sites (cm^{-2}), x_s = mean diffusion length determined by $D_s = x_s^2/\tau_{des}$ $\tau_{des} = \nu^{-1}\exp(E_{des}/kT)$, D_s = surface diffusion coefficient of $SiCl_2$ and E_{des} = activation energy for desorption of $SiCl_2$

If it is assumed that $x_s > \lambda$, $\tanh \lambda/2x_s = \lambda/2x_s$ and eq (8) becomes

$$v_{step} = \frac{\lambda D_s}{x_s^2}\frac{n_{st} - n_s}{n_0} = \frac{\lambda}{\tau_{des}}\frac{n_{st} - n_s}{n_0}, \tag{9}$$

using the definition of D_s Introducing in eq (9) the undersaturation

$$\gamma = (n_{st} - n_s)/n_{st}, \tag{10}$$

the step velocity can be written

$$v_{step} = (\lambda/\tau_{des})\,\gamma(n_{st}/n_0), \tag{11}$$

and with help of the expression for τ_{des} given above, eq (11) becomes

$$v_{step} = \nu\lambda\gamma(n_{st}/n_0)\exp(-E_{des}/kT) \tag{12}$$

As pointed out in part I, the concentration of adatoms at the steps is in equilibrium with the concentration of $SiCl_2$ in the gas phase, hence

$$SiCl_2(adatom)_{step} \underset{k_{-1}}{\overset{k_1}{\rightleftharpoons}} SiCl_2(gas)(eq)$$

It follows that

$$K_1 = k_1/k_{-1} - p_{SiSl_2}(eq)/n_{st}, \tag{13}$$

in which p_{SiCl_2} (eq) equals the equilibrium concentration of $SiCl_2$ in the gas phase just above the surface Because

$$K_1 = K_0\exp(-E_{des}/kT), \tag{14}$$

from eq (13) the concentration of adatoms at the steps is

$$n_{st} = K_0^{-1}\,p_{SiCl_2}(eq)\exp(E_{des}/kT) \tag{15}$$

Accordingly, the step velocity is given by

$$v_{st} = \nu\lambda\gamma\, n_0^{-1} K_0^{-1}\, p_{SiCl_2}(eq) \tag{16}$$

From this equation it is evident that the temperature dependence of v_{step} has to be very small, because in this expression only p_{SiCl_2} (eq) will be responsible for a small temperature dependence [1] This is in good agreement with experiment as can be seen from fig 20 * In this figure the etch rates given by Kuyer et al [11] are plotted versus $1/T$, with, however, constant p_{SiCl_2} (eq) instead of a constant input value of p_{HCl} The observed temperature dependence varies between +6 and 4 kcal/mole The expression for the

---

* All partial pressures used in the calculations are taken from part I

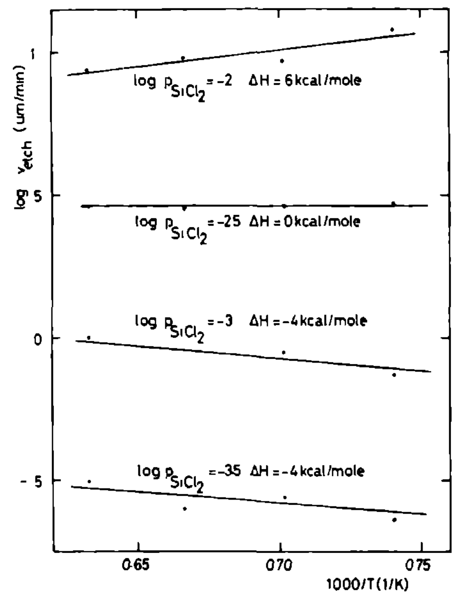

Fig 20. The logarithm of the etch rate as a function of $1/T$ at constant $SiCl_2$ equilibrium pressures (calculated from ref [11])

step velocity, eq. (16), now can be used as follows. It is assumed that bunch formation will occur when v_{step} is of the same order of magnitude as v_{diff} The diffusion velocity can be written as

$$v_{diff} = a/\tau_{diff} = a\nu \exp(-E_{diff}/kT), \qquad (17)$$

where a = atomic distance, ν = vibration frequency and E_{diff} = activation energy for the diffusion process

The condition, that the step velocity must be of the same order of magnitude as the diffusion velocity of the $SiCl_2$ adatoms, can be written as

$$v_{step} = b v_{diff}, \quad b = \text{constant} < 1 \qquad (18)$$

Using eqs. (16) and (17), this condition becomes

$$\nu\lambda\gamma n_0^{-1} K_0^{-1} p_{SiCl_2}(\text{eq}) = ba\nu \exp(-E_{diff}/kT), \qquad (19)$$

or

$$\lambda\gamma(a n_0 K_0)^{-1} p_{SiCl_2}(\text{eq}) \exp(E_{diff}/kT) = b \qquad (19a)$$

This equation in terms of p_{SiCl_2} (eq) and temperature expresses the condition for the instability of a train of steps For the process of bunch formation another effect has also to be taken into account Raising the temperature not only results in higher diffusion velocities but also in roughening of the steps For high temperatures, the steps can be roughened to such an extent that individual steps disappear This means that a second condition for the formation of bunches has to be fulfilled, i e individual steps have to be present on the surface Thus the conditions for bunch formation are given by a combination of the probability of steps being present on the surface and the condition for the instability of a train of steps As for the presence of steps it can be said that a step is well defined when the mean distance x_0 between two kinks on the step is large, in that case the step roughening will be small According to Burton, Cabrera and Frank [4] this mean distance is given by

$$x_0 = \tfrac{1}{2}a \exp(E_b/kT), \qquad (20)$$

where E_b is the energy to form a kink in a step The probability of having well defined steps will be proportional to $\exp(E_b/kT)$ Combining this with (19a) the probability W of bunch formation can be given as

$$W \propto \lambda\gamma n_0^{-1} K_0^{-1} p_{SiCl_2}(\text{eq}) \exp[(E_{diff} + E_b)/kT] \qquad (21)$$

Assuming that W is constant on the transition line from smooth to bunched surface structure, and assuming in addition that the temperature dependence of γ is small, the following equation holds on the transition line

$$p_{SiCl_2}(\text{eq}) = C \exp[-(E_{diff} + E_b)/kT] \qquad (22)$$

This relation gives the transition from smooth to bunched surface structure in terms of p_{SiCl_2} (eq) and temperature

As the experimentally observed transition, depicted in fig 5 is given in p_{HCl} (input) and temperature, a conversion has to be made from p_{HCl} (input) to p_{SiCl_2} (eq) Using the equilibrium values as given in part I, fig 5 was reconstructed, the result being given in fig 21 It appears now that the transition line for

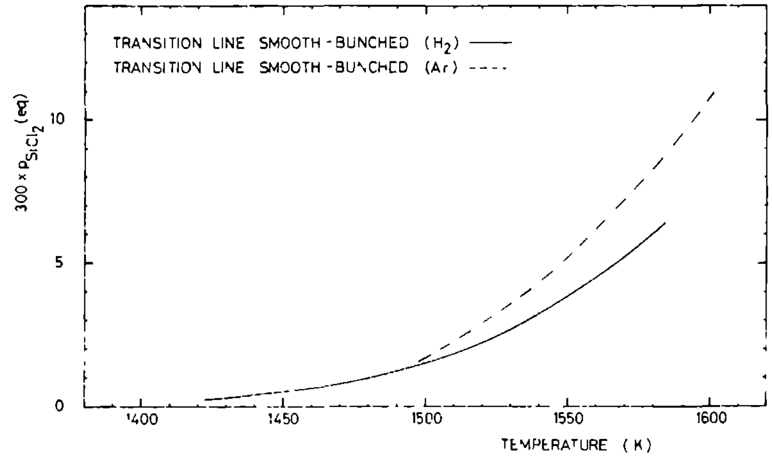

Fig. 21. The transition lines from smooth to bunched surface structure as a function of the $SiCl_2$ equilibrium concentration for the hydrogen and the argon system (replot of fig. 5).

the hydrogen and argon systems also come close together, thus removing the apparent discrepancy of fig. 5. This is a strong indication that bunch formation in both systems is governed by the same process. The small remaining difference between the transition lines for the hydrogen and the argon system may be due to the fact that different misorientations, i.e. different λ's were used.

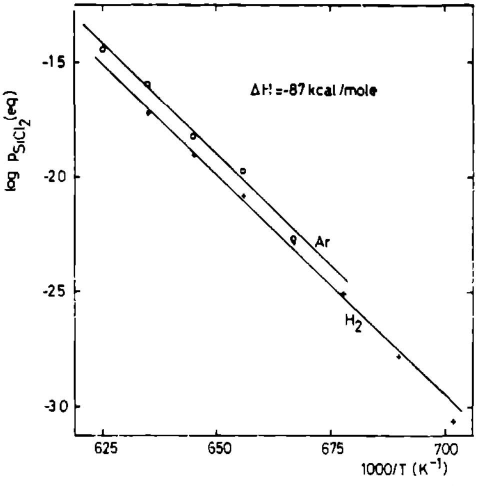

Fig. 22. Arrhenius plot of the transition line from smooth to bunched surface structure for the hydrogen and the argon system.

The activation energy for bunch formation can now be deduced from a plot of the logarithm of the $SiCl_2$ equilibrium concentration of the transition line versus $1/T$. This has been done for both the hydrogen and the argon system in fig. 22. From this figure it follows that

$$E_{diff} + E_b = 87 \text{ kcal/mole}. \tag{23}$$

When E_b is taken to be equal to the Si-Si bond energy of 55 kcal/mole, a value of 32 kcal/mole results for the activation energy for surface diffusion of $SiCl_2$. According to the literature the activation energy for surface diffusion of Si has a value ranging from 5 to 35 kcal/mole [12,13]. A value of 32 kcal/mole for E_{diff} of $SiCl_2$ therefore seems reasonable.

4.5. The surface structure on silicon (110) and (100)

It was mentioned in the beginning of this paper that on the (110) and (100) substrates, with the particular misorientations used in the experiment, bunch formation could not be observed. Knowing now the conditions for bunch formation, an explanation can

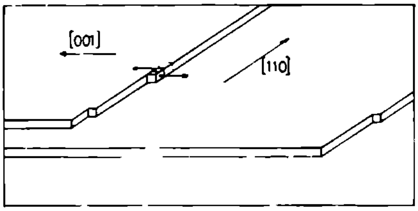

Fig 23 Schematic picture of the etching mechanism on the (110) surface with the misorientation used in the experiments The etching direction is [110], the steps move in the [001] direction

be given for this behaviour

On (110) substrates the preferential etching vectors are lying in the [1̄10] and [11̄0] directions However, the substrates used have a misorientation in the [001̄] direction, i e perpendicular to the preferential etching directions Therefore the etching can be supposed to take place in the following way (fig 23)

Rows of Si atoms will be etched away in the [11̄0] and/or [1̄10] direction This will lead to a step motion, imposed by the misorientation, in the [001̄] direction

In this configuration the diffusion of $SiCl_2$ atoms away from the steps will take place in the [001] and [001̄] direction, parallel to the macroscopic step motion, but perpendicular to the direction in which Si atoms are etched from the step As the direction in which the adatoms diffuse from the step is perpendicular to the microscopic etching direction the adatoms can not effectively hamper the etching process, and disturbances in the train of steps will not develop into bunches

The explanation for the absence of bunches on the (100) substrate is more trivial The (100) substrates which were used possessed only a slight deviation from the real (100) This means that on these substrates the step density was very low As can be seen from fig 7, Cabrera's curves type I and type II show an almost linear q–k dependence for very low step densities, or, in other words, on surface with low step densities the step velocity will be equal to the group velocity As was pointed out earlier, in such cases bunch formation will not occur

Therefore on the (100) substrates, used in the experiments, bunch formation is not to be expected The etching via steps is also thought to be operative on (100) surfaces, in a similar manner as for the (111) and (100) cases in that etch pits are formed at high etch rates (part I)

In general, however, bunch formation must be possible on both the (110) and the (100) surface The fact that no bunch formation was found in the experiments reported here was due to the specific misorientations of the substrates This is supported by the fact that on some (100) substrates near the edge of the slice, where the silicon slice is rounded off and thus the misorientation becomes higher, bunch formation has been observed

5 Conclusion

The geometrical shape and the position of the bunches observed on silicon (111) slices with different misorientations appears to be determined by the specific deviation of the surface from real (111) in combination with the preferential etching vectors for the (111) surface ([12̄1], [112̄] and [2̄11]) The formation of bunches can be explained by the kinematic wave theory of Frank and Cabrera The theoretically predicted positive and negative bunches are observed on these silicon surfaces It is deduced that for low HCl input pressures the surface will remain smooth, that for higher HCl input pressures bunch formation can be expected, and that for very high HCl input concentrations the surface becomes smooth again For the last case a new q–k relation is introduced A theoretical analysis shows that bunch formation can be expected when the velocity of an individual step becomes of the order of the velocity of a diffusing adatom, thus inducing a distortion of the symmetrical dependence of the step velocity on the spacings in front of and behind the step The combination of experiment and analysis gives a value for the activation energy of bunch formation which can be expressed as a combination of the activation energies for surface diffusion of $SiCl_2$ adatoms, and the formation of a kink in a step on the surface

Acknowledgement

The authors wish to thank Dr P Bennema for stimulating discussions and Mr R Grevink and Mrs J a d Brugh for experimental contributions

References

[1] P van der Putte, L J Giling and J Bloem, J Crystal Growth 41 (1977) 133

[2] A G Revesz and R J Evans, Trans. Met Soc AIME 230 (1964) 581

[3] H C Abbink, R M Broudy and G P McCarthy, J Appl Phys. 39 (1968) 4673

[4] W R. Burton N Cabrera and F C. Frank, Phil Trans Roy. Soc London A243 (1950) 299

[5] F C Frank, in Growth and Perfection of Crystals (Wiley, New York, 1958) p 411

[6] N Cabrera and D A Vermilya, in Growth and Perfection of Crystals (Wiley, New York, 1958) p 393

[7] A J R de Kock, thesis, Catholic University of Nijmegen (1973)

[8] J Burmeister, J Crystal Growth 11 (1971) 131.

[9] P Bennema and G H Gilmer, in Crystal Growth, An Introduction, Ed P. Hartman (North-Holland, Amsterdam, 1973) p 317

[10] R L. Schwoebel, J Appl Phys 40 (1969) 614.

[11] Th J M Kuyer, L J Giling and J Bloem, J Crystal Growth 22 (1974) 29

[12] R.C Henderson and R F Helm, Surface Sci 30 (1972) 310

[13] R F C. Farrow, J Electrochem Soc 121 (1974) 899

$CuInS_2$ AND $CuGaS_2$

CHAPTER XVI:
CVT GROWTH OF $CuInS_2$ AND $CuGaS_2$

PART I: EVIDENCE FOR VLS GROWTH WITH CuI AS LIQUID PHASE

J.J.M. Binsma, W.J.P. van Enckevort
and G.W.M. Staarink

RIM Laboratory of Solid State Chemistry, Faculty of Science,
Catholic University, Toernooiveld, Nijmegen, The Netherlands

ABSTRACT

Single crystals of the chalcopyrite compounds $CuInS_2$ and $CuGaS_2$ were grown by chemical vapour transport (CVT), with iodine as transporting agent. Surface microtopographic studies of these crystals by means of optical microscopy, scanning electron microscopy and X-ray microanalysis showed that vapour-liquid-solid (VLS) growth with CuI as liquid phase plays a main role during crystal growth. The VLS mechanism gives an explanation for the discrepancy between the experimental morphology -hollow needles and thin platelets generally- and the theoretical octahedron-like morphology. The occurrence of a liquid CuI phase is confirmed for both the Cu-In-S-I and the Cu-Ga-S-I system by thermodynamic calculations of the vapour phase composition.

1. Introduction

Chemical vapour transport (CVT) is a well known technique for growth of single crystals with high melting points. This method can be quite useful for lower temperature growth of crystals, which cannot be grown from their melt or from a high temperature flux, because of several reasons, such as a solid state phase transition which must be passed during cooling or evaporation of one or more of the components out of the melt or flux. A detailed description of this CVT technique is given in a monograph by Schäfer [1], whereas more theoretical aspects of the gasphase transport mechanism are reported by Noläng and Richardson [2,3].

Crystals grown by this method show a wide variety of non-equilibrium shapes, such as prismatic columns [4], hollow and solid rods or needles [5,6,7], very thin platelets [8] and dendrites [9]. Even one and the same kind of crystal can manifest itself in numerous growth forms as was shown by Kaldis for CdS crystals [9]. Most of these forms, especially the hollow needles, thin platelets and dendrites, indicate that at least in directions with the highest growth rates, growth is mainly controlled by volume diffusion or heat transport. This in agreement with the results of Noläng and Richardson. On the basis of a comparison of the actual growth rate of the crystals with a calculated rate they showed that crystal growth in CVT systems is generally limited by gas phase transport [3].

Up to now only a few authors have examined the growth mechanisms of CVT grown crystals using surface microtopography in order to verify whether growth takes place via spiral growth nucleation or by another mechanism [7,9]. In addition, most interest was focussed in these studies on the side faces of the plates, needles or prisms, the growth rate of which was in general limited by surface kinetics. A microtopographic investigation that particularly dealt with the growth mechanism of the top faces of needles and the narrow side faces of plates was carried out by Nittono et al. [10]. They grew copper whiskers via hydrogen reduction of cuprous iodine vapour, by making use of rather a chemical vapour deposition (CVD) than a CVT technique. It was concluded from their observations by means of scanning electron microscopy and X-ray microanalysis that growth of the needle tops and lateral expansion of the needles and platelets proceed via a vapour-liquid-solid (VLS) mechanism, with CuI as liquid agent. In the present paper and in a subsequent one [11] (referred to as part II in the follo-

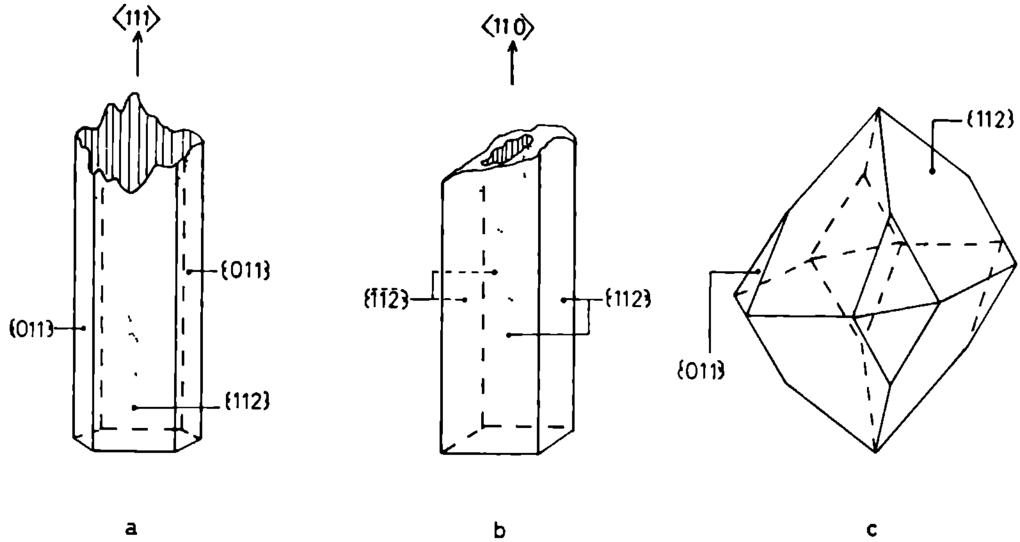

Fig. 1 *Morphologies of CVT grown $CuInS_2$ and $CuGaS_2$ crystals. (a) Needle-like shape with the longitudinal axis parallel to <111>, observed for both chalcopyrite compounds. (b) Needle-like shape with the axis parallel to <110> observed for a part of the $CuGaS_2$ crystals. (c) Theoretically predicted octahedron-like shape limited by {112} and {011} planes.*

wing), the growth properties of CVT grown $CuInS_2$ and $CuGaS_2$ single crystals are described in detail.

The $CuInS_2$ and $CuGaS_2$ crystals were grown in order to obtain suitable samples for further optical and electrical experiments. For $CuInS_2$ this method is particularly important, because growth from its own melt is hindered by the solid state phase transition from zincblende to chalcopyrite [12,13]. The first to report on CVT growth of chalcogenide chalcopyrites was Honeyman [14], who in this way obtained $CuAlS_2$ needles (2 cm long and several mm wide) and platelets (several mm wide and about 100 µm thick). Paorici et al. [15] dealt with CVT growth of $CuInS_2$ and $CuGaS_2$. They compared growth in a stationary temperature profile with that in a time-varying temperature profile. The time-varying temperature profile method leads to a two to four fold increase in crystal dimensions.

Verheijen [16] carried out CVT growth of $CuInS_2$ and $CuGaS_2$. He obtained crystals with a needle-like shape, as shown in figs. 1a and 1b, and plate-like crystals. Both kinds of crystals were limited by $\{112\}$, $\{\bar{1}\bar{1}2\}$ and

{011 } facets. On the basis of a periodic bond chain (PBC) analysis it was shown by Verheijen and Bennema [16,17] that the theoretical shape for crystals with chalcopyrite structure is octahedron-like (see fig. 1c), the bounding facets being the also experimentally observed {112 }, $\{\bar{1}\bar{1}\bar{2}\}$ and {011} faces. In spite of the agreement between observed and predicted faces, the $CuInS_2$ and $CuGaS_2$ crystals do not have the predicted octahedron-like shape. In the present study it will be shown that this difference between theory and experiment can be explained on the basis of VLS growth, which takes place especially at the tops of the needles. In part II an extended description will be given of the VLS mechanisms as well as of the occurring vapour-solid (VS) growth forms.

2. Experimental

2.1 *Crystal Growth*

Crystals of $CuInS_2$ and $CuGaS_2$ were grown by the "ordinary" stationary temperature profile or the time-varying temperature profile method [15]. In both cases, the quartz ampoules employed were 200 mm in length with a diameter of 15 mm. They were cleaned according to the procedure given in ref. [18]. $CuInS_2$ or $CuGaS_2$, prepared as described in ref. [12], were added to the ampoule together with an amount of iodine (5 mg cm^{-3}). In the stationary profile method source temperatures of 800 to 850°C and deposition temperatures of 750 to 800°C were used, the temperature difference always being 50°C. A better control of the nucleation can be achieved using the time varying temperature profile method by slowly increasing the temperature difference between source and deposition ends up to its final value of 50°C. This method was carried out in a similar way as reported by Paorici et al. [15], with a final source temperature of 850°C and a deposition temperature of 800°C. For both methods the growth period was about 10 days. The experiments were terminated by shifting the ampoule out of the furnace in such a way that the source end was the first to cool down with about half of the ampoule still inside the furnace. In this way a small temperature gradient was maintained over the ampoule during cooling in order to prevent precipitation of iodine on the crystals. This shut off procedure at the end of the experiment, during which the ampoule was allowed to cool down within a few minutes, was carried out in order to minimize secondary effects, leading to artifacts on the surface topographs. The stationary temperature profile method yielded about hundred, generally needle-like, crystals with a maximum size of 10x1.5x1 mm^3. By means of the time varying temperature profile method the number of crystals decreased to about ten, while their size increased, up to a maximal size of 20x4x2 mm^3. These observations are similar to those reported by Paorici et al. [15] .

No differences in surface morphology between crystals prepared by either method were observed (see section 3).

2.2 *Characterization*

Observation of the side faces of the needles and the upper and lower faces of the platelets was carried out with the aid of a reflection differential interference contrast microscope, combined with standard fine grain photographic emulsions. In this way it was possible to reveal rather low inclinations and height differences, at the crystal surface.

For obtaining a clear three-dimensional view of needle tops and of solidified droplets on the crystal faces use was made of a scanning electron microscope (SEM). Determination of the composition of the solidified remnants of the liquid agent, that governed the VLS growth process, was carried out by means of X-ray (EDAX) microanalysis.

3. Observations and interpretation

3.1 *Surface microtopography*

Figures 2a and b show characteristic examples of two-dimensional VLS growth patterns on the {112 } needle side faces or top and bottom platelet surfaces of $CuInS_2$ of $CuGaS_2$ crystals respectively. Similar VLS growth features, due to the presence of a liquid phase on the crystal surface in the shape of droplets or liquid "frills" at step edges were also observed by Lemmlein et al. on paratoluedine [19] , Tairov et al. on SiC [20] , Kobayashi on ice [21] and van Enckevort and Graef on silicon [22] . In contrast to these cases, where each crystal established its own particular two-dimensional VLS growth pattern, for the two chalcopyrite-like crystals a wide variety of surface morphologies caused by this mechanism was found. This abundance of growth forms will be treated in detail in part II.

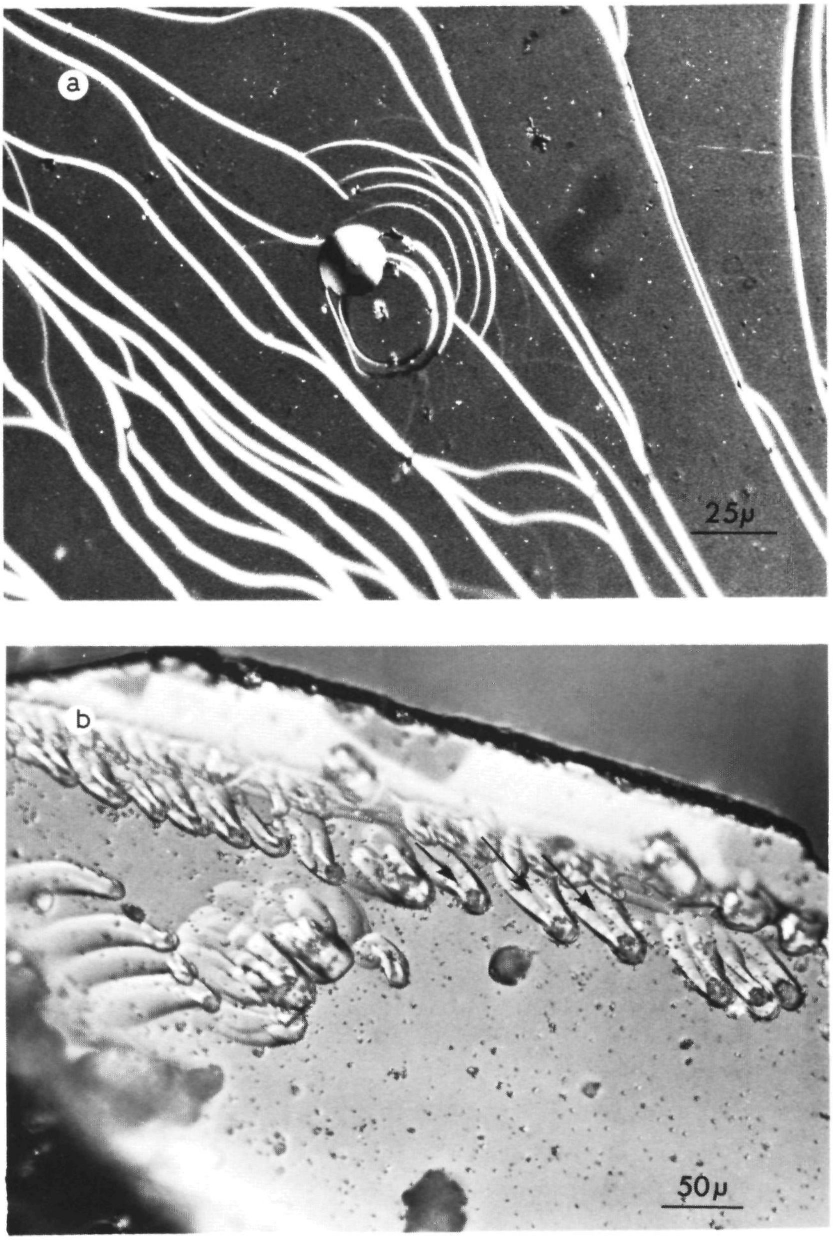

Fig. 2 Examples of two-dimensional VLS growth patterns. (a) Closed loop steps generated by repeated nucleation via a droplet on $CuInS_2$. (b) Protuberances, with a central depression on $CuGaS_2$. (Differential interference contrast micrographs).

The limiting faces of the $CuInS_2$ needles appear to be {112 } and {011} as was determined by optical goniometry. The longitudinal axis is parallel to <111 > (fig. 1a). These observations were also reported by Verheijen and Bennema [16,17]. For $CuGaS_2$ two kinds of needles were found: (i) Needles with exactly the same habit as $CuInS_2$; (ii) needles, of which the axis coincides with the <110> direction and with only {112} faces parallel to the needle axis (fig. 1b). Most needles are hollow and posses inclusions as indicated in figures 1a and b. A description of the shape and the formation mechanism of these cavities will be presented in part II.

In general the top faces of the needles are not limited by crystallographic planes but are rounded off smoothly as can be seen in fig. 3. For some of the $CuGaS_2$ needles very rough top faces were observed as shown in fig. 4. From morphological considerations, however, it is to be expected that these top faces are limited by crystallographic {112 } and { 011} planes, just like the side faces of the needles. This rounding off of the needle tops can be understood in terms of the presence of a liquid-like film covering the surface which induces VLS growth at these tops. This VLS growth -which accelerates growth along the needle axis and thus accounts for the oblong form of the crystals- can easily lead to normal growth

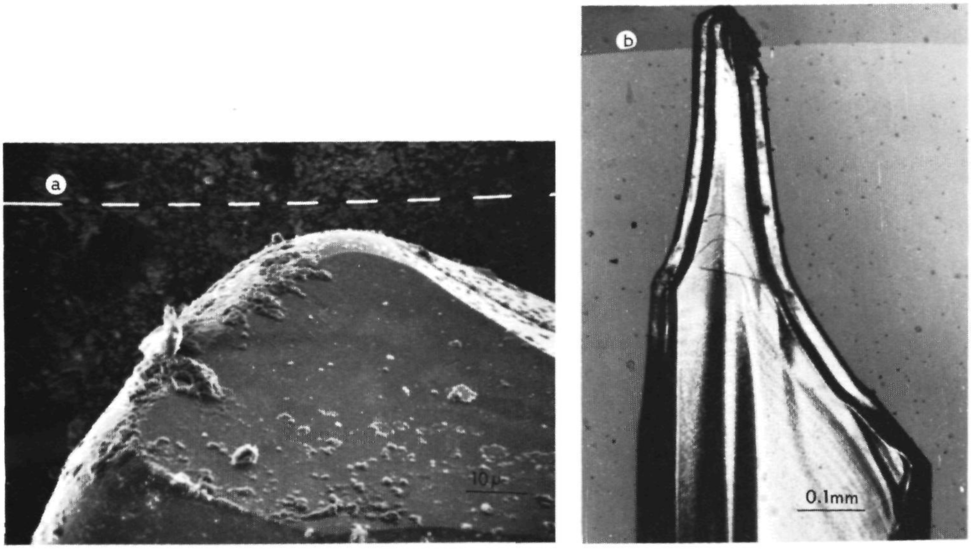

Fig. 3 Non-facetted needle tops. (a) $CuInS_2$ (SEM micrograph) (b) $CuGaS_2$ (optical micrograph).

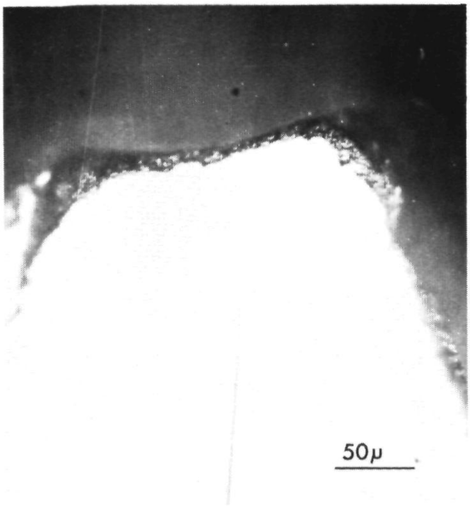

Fig. 4 Rough needle top, showing a granular surface structure, observed for $CuGaS_2$*. Similar growth features were also observed on the narrow side faces of* $CuGaS_2$ *platelets (optical micrograph).*

[23,24] so that the faces are no longer singular but become rounded off [24,25]. Also the roughness of the top faces of some $CuGaS_2$ needles is a result of a VLS growth process. Here the liquid-film might have been much thicker than in the case of the smooth top faces ($CuInS_2$ and remaining $CuGaS_2$ needles). The same growth features as observed at the needle tops were also seen on many of the narrow side faces of the $CuInS_2$ and $CuGaS_2$ platelets, indicating that platelet expansion also proceeds via a VLS growth mechanism. A similar VLS growth of platelet-like crystals was reported earlier by Givargirov for CdSe [26,27]. Further details of the vapour-liquid-solid growth mechanisms at needle tops and platelet side faces will be given in part II.

From the microtopographic observations (see also part II) it is evident that VLS growth plays an essential role during CVT growth of $CuInS_2$ and $CuGaS_2$ crystals. The occurrence of VLS growth at needle tops and at the narrow side faces of platelets (giving higher growth rates than for the other faces, where growth generally proceeds via a vapour-solid (VS) mechanism [27] as shown in part II) explains the discrepancy between the theoretically deduced octahedron-like shape and the observed needle- or platelet-like habit.

3.2. *X-ray microanalysis*

On the surface of many crystals for which the temperature gradient during the shut off procedure (section 2.1) was kept as low as possible, but just sufficiently high to prevent iodine precipitation, or of crystals with very well developed VLS growth patterns, numerous particles can be seen as shown in figure 5. These particles being 0.5 to 5 μm in diameter are colourless or brownish white and transparant as could be verified by means of optical microscopy. Often they occur as cubic-like or rectangular crystallites, in other cases they do not have a crystal-like appearance. These deposits cannot be attributed to iodine precipitates, formed during cooling at the end of the growth experiment, since the iodine particles have a black and opaque appearance. From the close relationship between the

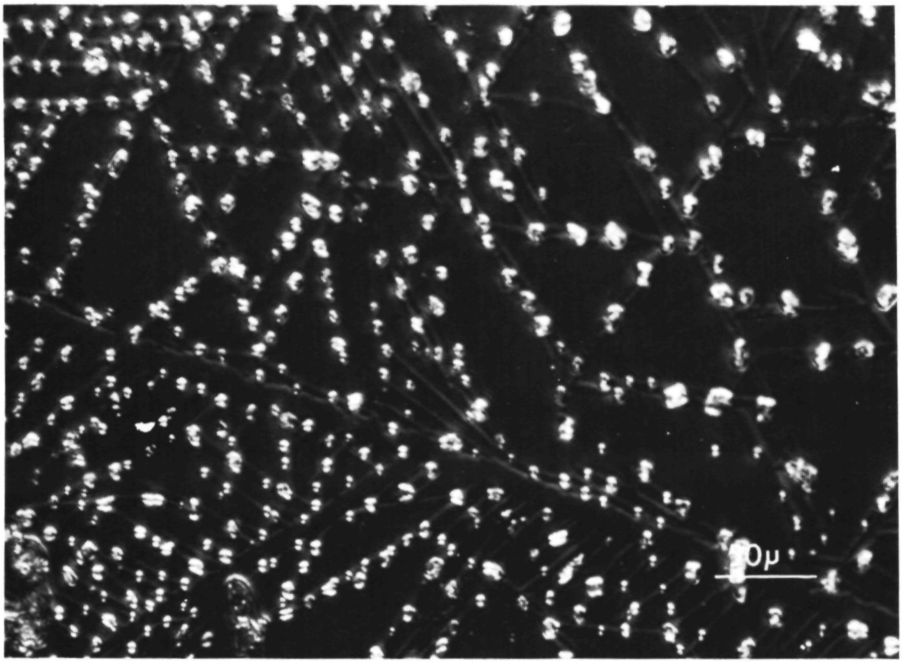

Fig. 5. Two dimensional VLS growth pattern on a $CuInS_2$ *crystal with solidified remnants of the liquid phase (differential interference contrast micrograph).*

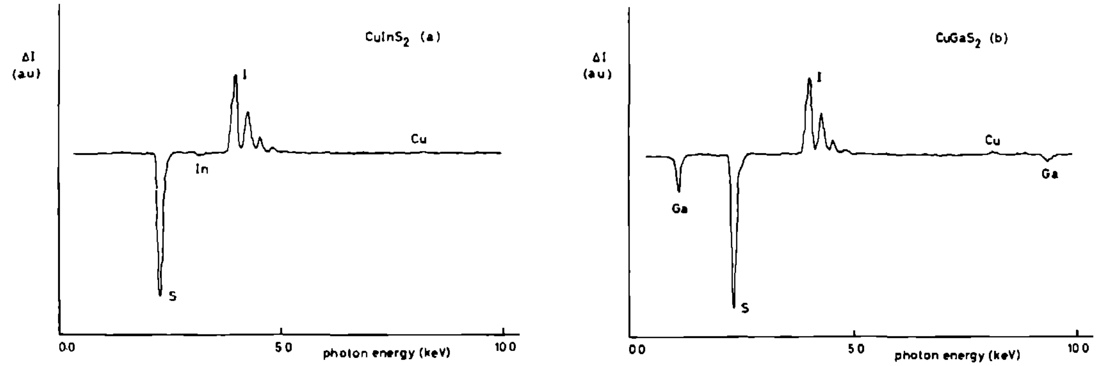

Fig. 6 Difference in X-ray intensity ΔI (arbitrary units) between an area covered with a solidified remnant of a former liquid phase and an adjacent clean surface area versus the photon energy as determined by EDAX-analysis. (a) $CuInS_2$, (b) $CuGaS_2$.

locations of the transparant deposits and the surface patterns characteristic for two-dimensional VLS growth (see fig. 5), it can be concluded that these deposits are solidified remnants of the liquid phase that governed the VLS growth process.

In order to obtain information on the chemical composition of these solidified remnants X-ray microanalysis (energy dispersive: EDAX) was carried out. Since the penetration depth of the electron bundle (∿5-20μm) was much higher than the particle thickness (½-3μm) it was necessary to make a correction for the "background" region, being the $CuInS_2$ or $CuGaS_2$ crystal itself. This was carried out by measuring the X-ray intensity (counts per second) as a function of the photon energy, both in the region of a particle and for a clean surface area in the neighbourhood. From this the dependence of the difference in X-ray intensity between both surface areas on the photon energy, which is a measure for the difference in composition between the particle and the crystal, can be obtained. Examples of such curves are given in figures 6a and 6b for $CuInS_2$ and $CuGaS_2$ respectively. From these curves the conclusion could be drawn that the liquid agent for VLS growth of $CuGaS_2$ crystals is almost pure CuI, whereas for $CuInS_2$ the liquid consists of a mixture of CuI and InI/InI_3 with a widely varying composition. Analysis of a clean surface area alone showed that no detectable amount of iodine (i.e. less than 2 mol %) is present in the bulk of the crystals. A similar X-ray microanalysis of solidified remnants of the liquid phase was also carried out for needle tops. This yielded the same results as for the two-dimensional VLS growth patterns.

From the microtopographical observations and the X-ray microanalysis it is evident that VLS growth mechanisms with CuI as liquid agent play a main role in the CVT growth of $CuGaS_2$ and $CuInS_2$. In addition to VLS growth also VS growth is commonly encountered on the crystal faces, especially on $CuGaS_2$ platelets and needles and $CuInS_2$ platelets (see part II).

4. Thermodynamic analysis

In this section the results of equilibrium calculations will be presented for the systems Cu-In-S-I and Cu-Ga-S-I. These calculations were carried out under the assumption that the reaction rates for the heterogeneous reactions are so high that the equilibrium state is reached in the immediate vicinity of the growing surface. In that case thermodynamic calculations can give information about the influence of temperature and input composition on the vapour phase and the presence of condensed phases [1]. This information may be useful for the interpretation of the observed crystal morphology and the choice of suitable conditions for crystal growth.

Equilibrium compositions for a given temperature, pressure and input composition were calculated by means of a computer program, using minimalization of the Gibbs energy, for the systems Cu-In-S-I and Cu-Ga-S-I at temperatures in the range 720-830 °C. In this range the crystal growth experiments of $CuInS_2$ and $CuGaS_2$ were carried out (see section 2.1).
The program was capable of handling a condensed phase of a species, which does not occur in the gasphase, viz. the ternary compounds, $CuInS_2$ and $CuGaS_2$. The thermodynamic data (enthalpy, entropy and specific heat values) needed for the equilibrium calculations were taken from refs [28-34] and in some cases estimated according to Sirtle [35] or Kubaschewski [36].

For the Cu-In-S-I system, the following components were taken into account: $CuInS_2$(s), Cu (s) and (g), In (l) and (g), S_n(g) with n=1 to 8, I(g), I_2(g), InS(s) and (g), CuS (s) and (g), CuI(l) and (g), $(CuI)_n$ (g) with n=2,3,4, CuI_2(g), InI(g), InI_3(g), In_2S(g) and In_2S_2(g). In the calculations for the Cu-Ga-S-I system the following components were included: $CuGaS_2$(s), Cu(s) and (g), Ga(l) and (g), S_2(g) with n=1 to 8, I(g), I_2(g),

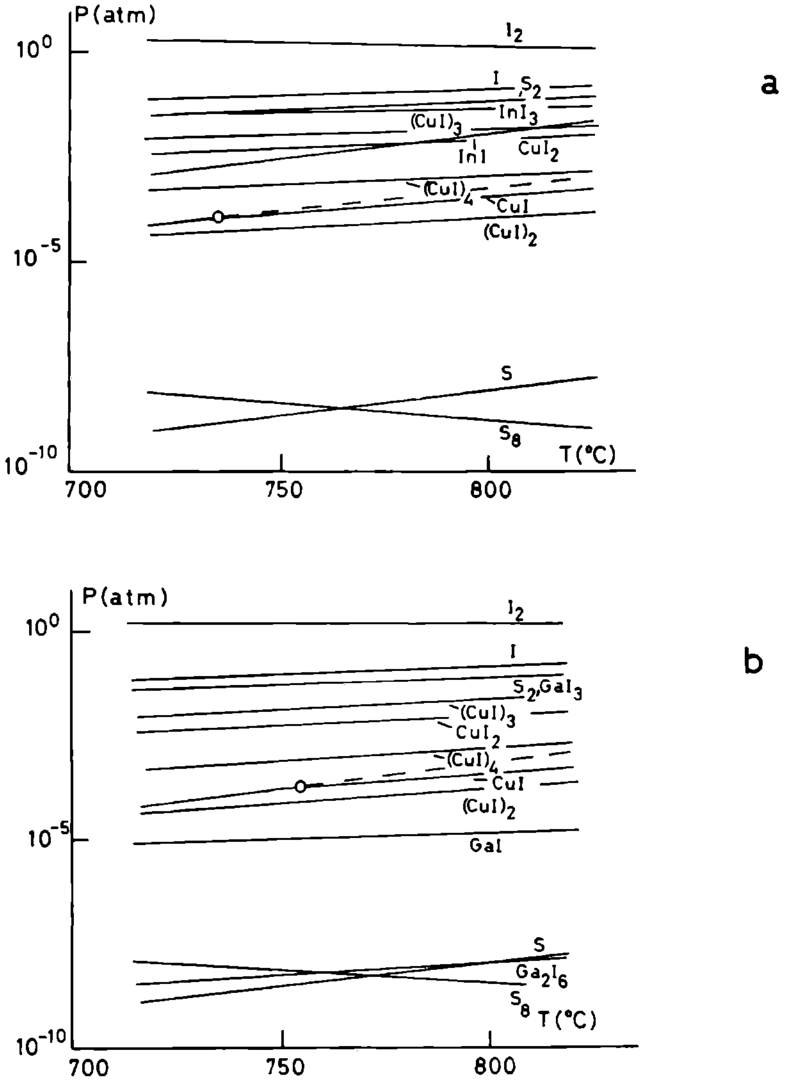

Fig. 7 Computed partial pressures at a total pressure of 1.8 atm corresponding to an amount of iodine of 5 mg cm^{-3}: (a) for the system Cu-In-S-I, (b) for the system Cu-Ga-S-I. The dashed lines indicate the saturation vapour pressure of CuI. At temperatures below the intersection point-indicated by a circle-liquid CuI is present in the system.

GaS(s) and (g), CuS(s) and (g), CuI(l) and (g), $(CuI)_n(g)$ with n=2,3,4, $CuI_2(g)$, GaI(g), $(GaI_3)_n(g)$ with n=1,2 and $Ga_2S(g)$. The input-composition consisted of solid $CuInS_2$ or $CuGaS_2$ and an amount of iodine in the gas-phase in accordance with the experimental quantity of 5 mg cm^{-3}. The results of the calculations for the Cu-In-S-I system and the Cu-Ga-S-I system are shown in figures 7a and b respectively. Components having partial pressures less than 10^{-10} atm have been excluded from these graphs. $CuInS_2$ and $CuGaS_2$ are present as a solid over the whole temperature range considered. For the Cu-In-S-I system no other condensed phases are stable above 735 °C, but be-below 735°C CuI reaches its saturation vapour pressure, which leads to the presence of liquid CuI. In the Cu-Ga-S-I system CuI(l) is present as an additional condensed phase up to 755 °C. All other components only occur in the gas phase. The formation of liquid CuI according to the thermodynamic calculations is in good agreement with the experimental observations (see section 3), which show the presence of liquid CuI, although the actual growth temperatures (750 - 800 °C) were slightly higher than the critical values of 735 and 755 °C. This can be explained by the uncertainty of these critical values due to the uncertainty of the thermodynamic data of some components. Further the saturation pressure of CuI will decrease by dissolution of GaI, InI and other components in the liquid. This dissolution was especially observed for InI, see section 3. The lowering of the saturation pressure means that the intersection -temperature of the saturation pressure curve and the P_{CuI} curve increases. So it can be concluded that at the growth temperatures CuI is likely to be present as a liquid phase.

Preliminary growth experiments for $CuInS_2$ at high temperatures (900-1000 °C) yielded crystals with only vapour-solid (VS) growth patterns. Thus in these cases no VLS growth takes place, which indicates that no liquid CuI ($CuI-InI/InI_3$) is formed. These experiments are in agreement with the prediction -based on thermodynamical calculations- that there should be a transition from simultaneous VLS-VS growth to pure VS growth at higher temperatures.

5. Conclusions

In the present study it is shown that during growth of the chalcopyrite crystals $CuInS_2$ and $CuGaS_2$ by the CVT method with iodine as transporting agent, VLS mechanisms with CuI as liquid phase play a main role. This was deduced both experimentally by means of microtopography and X-ray microanalysis and theoretically by equilibrium calculations of the vapour phase composition. The occurrence of VLS growth strongly affects the final shape of the crystals, resulting in the formation of crystals with a needle-like or platelet-like shape instead of the theoretically predicted octahedron-like shape. Since in literature the same needle and platelet-like shapes were reported for numerous other CVT grown crystals, it may be quite interesting to carry out a detailed surface microtopographic study of these crystals from the point of view of VLS growth.

Acknowledgements

The authors wish to thank Dr. A.L.H. Stols, Mr. A. Boekestein and Mr. H.A. van der Linden for their help in making the SEM micrographs and carrying out the X-ray microanalysis. Further they are grateful to Dr. K. Tsukamoto for his valuable comments on the surface microtopographs and to Dr. A.W. Verheijen for growing the $CuGaS_2$ and some of the $CuInS_2$ crystals. They also want to express their thanks to Prof. P. Bennema, Prof. J. Bloem and Dr. L.J. Giling for their profound interest in the present work and for critical reading of the manuscript. The present investigations have been carried out under the auspices of the Netherlands Foundation for Chemical Research (SON) with financial support from the Netherlands Organization for the Advancement of Pure Research (ZWO).

References

[1] H. Schäfer, Chemical Transport Reactions (Academic Press, New York, 1964).
[2] B.I. Nolång and M.W. Richardson, J. Crystal Growth 34 (1976) 198.
[3] B.I. Nolång and M.W. Richardson, J. Crystal Growth 34 (1976) 205.
[4] M. Shiloh and J. Gutman, J. Crystal Growth 11 (1971) 105.
[5] M. Ritschel and H. Opperman, Kristall und Technik 15 (1980) 535.
[6] C. Paorici, J. Crystal Growth 5 (1969) 315.

[7] R.A.M. Lieth, Phys. Stat. Sol. (a) 12 (1972) 399.

[8] R. Nitsche in: Proceedings of the International Conference on Crystal Growth, Boston 1966, Ed. H. Steffen Peiser (Pergamon Press, Oxford, 1967).

[9] E. Kaldis, J. Crystal Growth 5 (1969) 376.

[10] O. Nittono, H. Hasegawa and S. Nagakura, J. Crystal Growth 42 (1977) 175.

[11] W.J.P. van Enckevort and J.J.M. Binsma, to be published, Chapter V.

[12] J.J.M. Binsma, L.J. Giling and J. Bloem, J. Crystal Growth 50, (1980) 429, Chapter II.

[13] J.J.M. Binsma, L.J. Giling and J. Bloem, Phys. Stat. Sol. (a) 63 (1981) 595, Chapter III.

[14] W.N. Honeyman, J. Phys. Chem. Solids 30 (1969) 1935.

[15] C. Paorici, L. Zanotti and G. Zuccalli, J. Crystal Growth 43 (1978) 705.

[16] A.W. Verheijen, Thesis, University of Nijmegen, Nijmegen (1979).

[17] A.W. Verheijen and P. Bennema, J. Crystal Growth accepted.

[18] E. Kaldis, in: Crystal Growth, Theory and Techniques, Vol. 1, Ed. C.H.L. Goodman (Plenum, London, 1974).

[19] G.G. Lemmlein, E.D. Dukova and A.A. Chernov, Soviet Phys. - Cryst. 2 (1957) 426.

[20] Yu. M. Tairov, V.F. Tsvetkov and I.I. Khlebnikov, J. Crystal Growth 20 (1973) 155.

[21] T. Kobayashi, J. Crystal Growth 26 (1974) 6.

[22] W.J.P. van Enckevort and M.W.M. Graef, J. Electrochemical Soc. 128 (1981) 154.

[23] J.P. van der Eerden, P. Bennema and T.A. Cherepanova, Prog. Cryst. Growth Charact. Vol. 1 (1978) p 219.

[24] J.P. van der Eerden, Thesis, University of Nijmegen, Nijmegen (1979).

[25] H.J. Human, J.P. van der Eerden, L.A.M.J. Jetten and J.G.M. Odekerken, J. Crystal Growth 51 (1981) 589.

[26] E.I. Givargizov, Dokl. Akad. Nauk. SSSR 211 (1973) 332.

[27] E.I. Givargizov, in: Current Topics in Materials Science, Vol. 1, Ed. E. Kaldis (North-Holland, Amsterdam, 1978) p. 79.

[28] I. Barin and O. Knacke, Thermodynamic Properties of Inorganic Substances (Springer, Berlin, 1973).

[29] K.C. Mills, Thermodynamic Data of Inorganic Sulfides, Selenides and Tellurides (Butterworth, London, 1974).

[30] Selected Values of Chemical Thermodynamic Properties, US Department of Commerce, Nat. Bur. Stand.

[31] D.R. Stull and H. Prophet, Janaf Thermochem. Tables (NSRDS - NBS 37, Washington, 1971).

[32] K.J. Bachmann, F.S.L. Hsu, F.A. Thiel and H.M. Kasper, J. Electronic Mater. 6 (1977) 431.

[33] K. Krasnov et al., Handbook of Molecular Constants of Inorganic Compounds (Israel Progr. Scientific Translations, Jerusalem, 1970).

[34] T.E. Joyce and E.J. Rolinski, J. Phys. Chem. 76 (1972) 2310.

[35] E. Sirtl, Z. Naturforschg. 21a (1966) 2001.

[36] O. Kubaschewski, E.L.L. Evens and C.B. Alcock, Metallurgical Thermodynamics (Pergamon Press, Oxford, 1967).

CHAPTER XVII: CVT GROWTH OF $CuInS_2$ AND $CuGaS_2$

PART II: DETAILED SURFACE MICROTOPOGRAHIC STUDY ON THE VARIOUS VLS GROWTH MECHANISMS

W.J.P. van Enckevort and J.J.M. Binsma

RIM Laboratory of Solid State Chemistry, Faculty of Science,
Catholic University, Toernooiveld, Nijmegen, The Netherlands

ABSTRACT

Detailed surface microtopographic studies of $CuInS_2$ and $CuGaS_2$ crystals grown by chemical vapour transport (CVT), with iodine as transporting agent, by means of highly sensitive optical reflection differential interference and phase contrast microscopy, completed with scanning electron microscopy revealed a wide variety of vapour-liquid-solid (VLS) growth patterns, with CuI as liquid phase. Two modes of VLS growth could be discerned: (i) Two-dimensional VLS growth, leading to the formation of closed loop steps, surface dendrites, protuberances, macro steps with liquid fronts and surface patterns resulting from growth via a liquid film. (ii) Growth of needle tops and narrow side faces of platelets, which are mostly non-facetted, via a liquid CuI film, leading to normal growth above the roughening point. The observed large diversity in morphology of the crystals, which occurred as generally hollow needles, thin platelets, whiskers, spheroids and goblet-like crystals is interpreted in terms of an interplay of this second mode of VLS growth and mass or heat transport limited growth. Besides VLS, also vapour-solid growth patterns, such as growth spirals with very low step heights (∿ 3-50 Å), were commonly observed on the needle side faces and the top and bottom surfaces of platelets. The observed wide variety of surface morphologies is discussed in terms of surface roughness in relation to the occurrence of a roughening transition, deduced from recent Monte Carlo simulation experiments.

1. Introduction

In the previous paper, [1] (referred to as part I in the following it was shown that VLS growth, with CuI as liquid agent, plays a main role during growth of $CuInS_2$ and $CuGaS_2$ crystals by the CVT (Chemical Vapour Transport) method. This was demonstrated with the aid of surface microtopography by application of optical and scanning electron microscopy and by means of X-ray microanalysis (EDAX). Thermodynamic calculations of the vapour phase composition in the closed tube systems confirmed the occurrence of liquid CuI for both the Cu-In-S-I system and the Cu-Ga-S-I system. On both chalcopyrite-like crystals a wide variety of the many types of VLS growth patterns, each being particularly interesting, were observed.

VLS (Vapour-Liquid-Solid) growth is a well known and thoroughly studied crystal growth mechanism, discovered by Wagner and Ellis [2,3] for the case of whisker growth via a liquid droplet at the tops of the needles. Characteristic for VLS growth is the occurrence of a liquid layer or droplet, situated between the vapour and the growing crystal. This liquid layer - the surface of which being a preferred site for decomosition from the vapour [4] in addition - lowers the nucleation barrier for crystal growth at the liquid-solid interface with respect to the vapour-solid interface [5]. Crystal growth via VLS can thus proceed at a much higher rate than via a VS (Vapour-Solid) mechanism. VLS growth manifests itself in a wide variety of forms such as: (i) Growth of whiskers via a liquid droplet at their tops, which is the most extensively investigated type of VLS growth [2-8]. (ii) Two-dimensional VLS growth [4], yielding several kinds of growth patterns on crystal surfaces, like closed loop steps generated by a central liquid droplet [4,9,10], protuberances [7,9,11-13] and macro steps, the advancement of which is controlled by a liquid "frill" at the step fronts [10,14]. (iii) Growth via a liquid film on the surface of the crystal [15]. (iv) Thin platelet growth via the vapour-liquid-solid mechanism [4,6,16].

The aim of the present study is to carry out a very detailed surface microtopographic examination of the numerous kinds of growth features related to VLS growth, as well as of a few characteristics connected with VS growth, on the faces of $CuInS_2$ and $CuGaS_2$ crystals in order to get a deeper understanding of these pehnomena. The observations on the crystal faces are performed with the aid of highly sensitive optical reflection differential interference contrast and phase contrast microscopy as well as with scanning electron microscopy. Both optical methods, combined with high contrast photographic emulsions, have proven to be extremely powerful to reveal very low inclinations and step heights, typically 10 Å, as was shown by the surface microtopographic studies of hematite [17], SiC [18], KCl [19], potash alum [20,21] and KDP [22]. This detailed examination subsequently serves as a starting point for a phenomenological interpretation of the various VLS (and some VS) growth patterns on basis of several crystal growth models. These include concepts like nucleation and normal growth [23], spiral growth [24], roughening transition [23] and mass or heat transport as a crystal shape controlling factor [25].

2. Observation methods

The needle or platelet-like [1,26,27] $CuInS_2$ and $CuGaS_2$ crystals, which were grown by the chemical vapour transport method (with iodine as transporting agent) in the manner as described in part I, were characterized by the following microtopographic techniques:

(i) Optical reflection differential interference contrast microscopy after Nomarski [28] and Françon [29] combined with standard fine grain photographic emulsions. This method, which is applied to observe the side faces of needles and the top and bottom faces of platelets, is capable to reveal extremely low inclinations (∿ 0.05 degrees) and height differences as small as 10 Å. This method is especially suitable to inspect slightly waved or rugged surfaces.

(ii) Optical reflection phase contrast microscopy after Zernike [30], combined with a high contrast photographic film. By making use of a good quality microscope (in the present case a metallurgical Reichert Me F II microscope was used), fitted with a high absorption (∿ 95%) phase plate, height differences as low as 2 Å can be revealed. This extremely high sensitivity allows the observation of very low steps on the side faces of needles and the upper and lower faces of platelets. Especially for studying VS growth surface patterns on both kinds of chalcopyrite-like crystals this method has proven to be extremely powerful. Reviews on surface microtopography by optical reflection microscopy are written by Komatsu [31] and Sunagawa [32].

(iii) Optical bright field transmission microscopy in order to investigate the bulk of the crystals, for examination of inclusions and negative dendritic growth forms, using visible light for $CuGaS_2$ and infrared light for the opaque $CuInS_2$ crystals.

(iv) Scanning electron microscopy (SEM) for obtaining a clear three-dimensional view of several VLS growth features, in particular those occurring at needle tops or narrow side faces of platelets.

3. Some aspects of two-dimensional VLS growth

Two-dimensional VLS growth occurring on the $\{112\}$ and $\{\bar{1}\bar{1}\bar{2}\}$ faces of $CuInS_2$ and $CuGaS_2$ crystals manifests itself in a wide variety of surface patterns. These growth forms can be classified into three main categories, viz. stationary VLS, non-stationary VLS and growth via a liquid film.

3.1. *"Stationary" VLS growth*

In this category are classified all the growth features resulting from a localized liquid phase, which does not move on the crystal faces during the growth process. These were found in three principal configurations:

(i) Concentric closed loop steps (Fig. 1 and also fig. 2a in part I) Near the centre of these growth features clearly a remnant of the liquid phase, manifesting as a solidified droplet, can be recognized. During growth this droplet functioned as a step source, generating more or less periodically new thick layers, which expand laterally over the crystal surface. Probably this expansion proceeds via a VS mechanism, since no remnants of a liquid phase were ever observed near the steps. The preferred nucleation of new growth layers underneath the droplet can be understood in terms of a VLS growth mechanism, for which the nucleation barrier for the formation of a new layer is much lower for the solid-fluid interface under the droplet than for the gas-solid interface elswhere on the crystal surface. A similar periodic generation of closed loop steps via VLS growth was observed by Yoda on MoO_3 [9] and by Kobayashi on ice [10]. Each of them gave his own explanation for

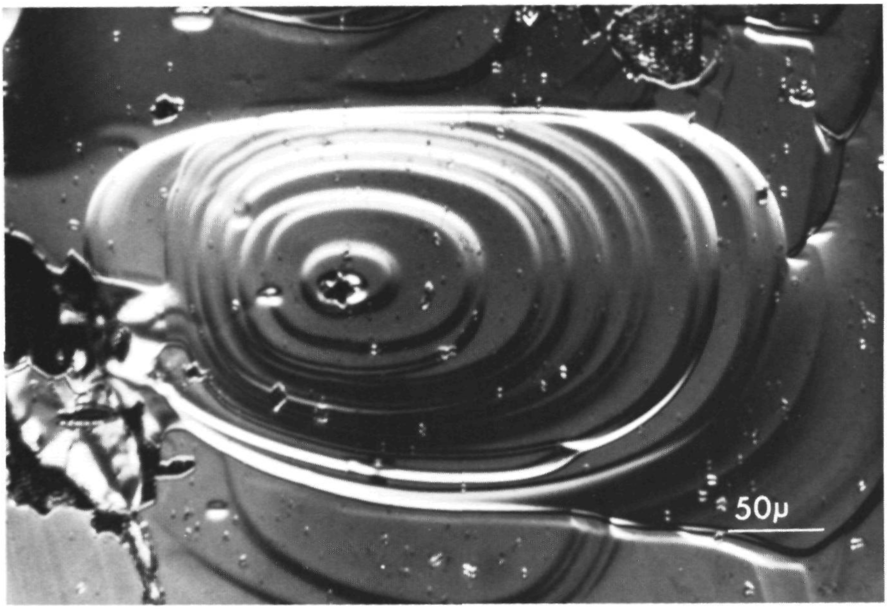

Fig. 1. Repeated formation of closed loop steps by a central droplet on $CuGaS_2$ (differential interference contrast micrograph).

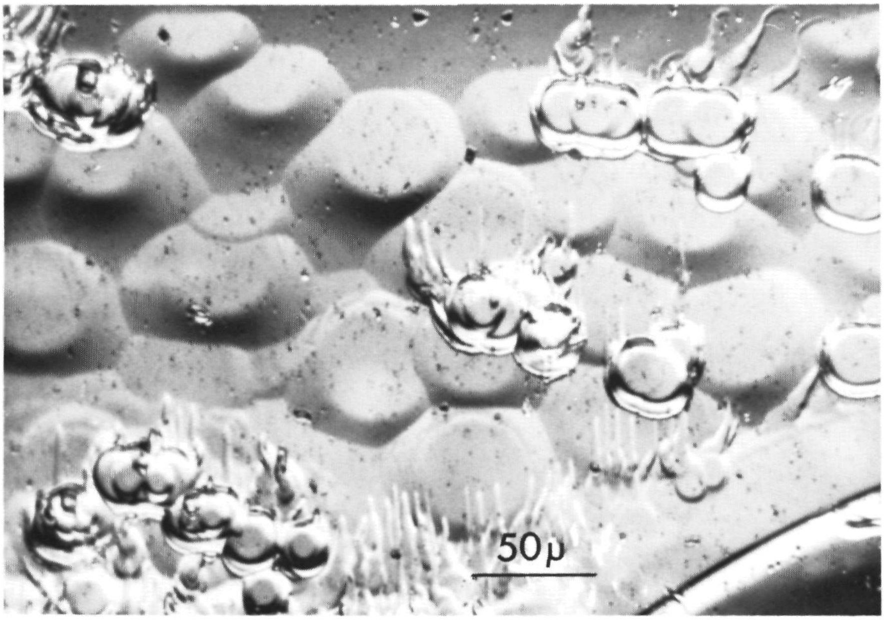

Fig. 2. Growth islands on $CuGaS_2$, formed via a two-dimensional VLS growth mechanism. All stages of development can be discerned (differential interference contrast micrograph).

this periodicity. For the present case it is not clear whether the periodicity in the repeated nucleation process should be interpreted analogous to Yoda's model, where nucleation takes place around the droplet or to Kobayashi's model where new layer generation occurs below the droplet.

(ii) Flat-topped growth islands (fig. 2). The growth mechanism of these elevations is very similar to the former case: the occurrence of a droplet generates a circular growth hillock due to VLS growth. But now for some reason the droplet disappears and thus no repeated nucleation takes place. On hillocks in the first stage of development often some remnants of the liquid phase in the shape of crystalline particles can be recognized. Further - lateral - growth of the islands proceeds via a VS growth mechanism or via VLS growth due to the presence of a liquid front at the edges of the islands, leading to a flattening of the hillock followed by a weakening of the contours until they become invisible. That the formation of these elevations is not a secondary effect due to the shut off procedure at the end of the growth experiment can clearly be deduced from micrograph 2 in which all stages of the growth history of the hillocks can be recognized. When these hillocks were an artifact caused at the termination of the experiment it is to be expected that these would appear more or less at the same stage of development, which is in contrast to the actual observation.

(iii) Rectilinear growth forms related to twin boundaries, slip lines but also on defect free surface area (fig. 3). On many $CuGaS_2$ crystals (rarely on $CuInS_2$) numerous solidified droplets, well developed growth hillocks and protuberances were found to occur in extended rows. The protuberances are formed by non-stationary VLS growth (see section 3.2.). Since all the growth hillocks and protuberances were at the same stage of development and no older remnants, being more or less faded out by VS growth, were observed, it can be concluded that these surface phenomena were formed during the shut off procedure at the end of the experiment. From this it is strongly suggested that, due to a change in surface tension during cooling off, a rectilinear liquid layer contracted to droplets leading to the formation of these artifacts ordered in a row. Very often the location of this linear liquid layer coincides with a twin boundary (or other planar defect) outcrop at the crystal surface.

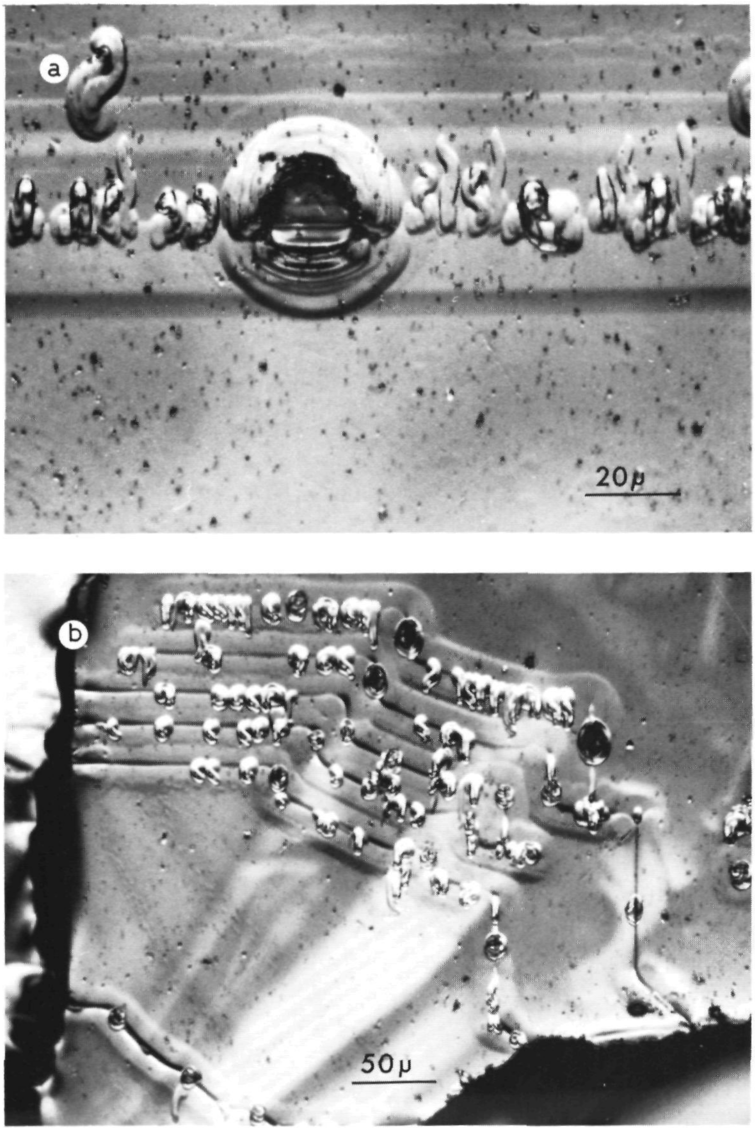

Fig. 3. Two-dimensional VLS growth from rectilinear surface area on $CuGaS_2$. The protuberances are due to a contraction of the liquid layer during cooling off at the end of the growht experiment. (a) VLS growth governed by a 'liquid line along' twin boundary (T). (b) VLS growth from an array of parallel 'liquid lines'. (Differential interference contrast micrographs).

Also parallel steps originating from the former position of the rectilinear liquid line - i.e. the ordered row of protuberances and hillocks - could be observed. In fig. 3a these steps arose from a liquid line at a twin boundary (TB in fig. 3, also appearing at the opposite face of the crystal) along which the artifacts, formed during cooling off, are ordered. In fig. 3b a kind of grooves at the former locations of the liquid lines become apparent; probably most of them are not related to crystal defects, since they could not be revealed at the back side of the crystal. From these observations it is suggested that during crystal growth a rectilinear liquid layer coinciding with a planar defect outcrop, such as a twin line and sometimes occurring in a perfect region, generates new - laterally spreading - growth layers due to a VLS growth mechanism. A similar VLS mechanism, where the liquid, functioning as a step source, is concentrated near (micro) twin lines was reported by Givargirov for epitaxially grown Si and Ge [4].

3.2. *"Non Stationary" VLS growth*

In contrast to the stationary VLS growth patterns, to this category belong all the surface patterns that are a result of two-dimensional VLS growth in which a moving liquid phase is involved. This non-stationary VLS growth can manifest itself in the following two ways:

(i) Growth via droplets running over the crystal surface, leading to the formation of protuberances (figs. 3, 4 and also fig. 2b in part I). Since these protuberances were always found to occur at the same stage of development it can be concluded, for the same reasons as mentioned in the foregoing section, that these growth features are a result of the shut off procedure at the end of a growth experiment. During this cooling off a more extended liquid layer contracts to droplets, which run over the crystal surface, leaving a trace like a snail. This may be caused by VLS growth or be generated by liquid-solid (LS) growth due to a decrease in solubility of $CuGaS_2$ or $CuInS_2$ in the liquid droplet with decreasing temperature. Similar growth features were also observed by Lemmlein et al. on paratoluidine crystals [11], Yoda on MoO_3 [9], Sickafus and Barker on $NiBr_2$ [12] and by Tairov et al. on SiC [13].

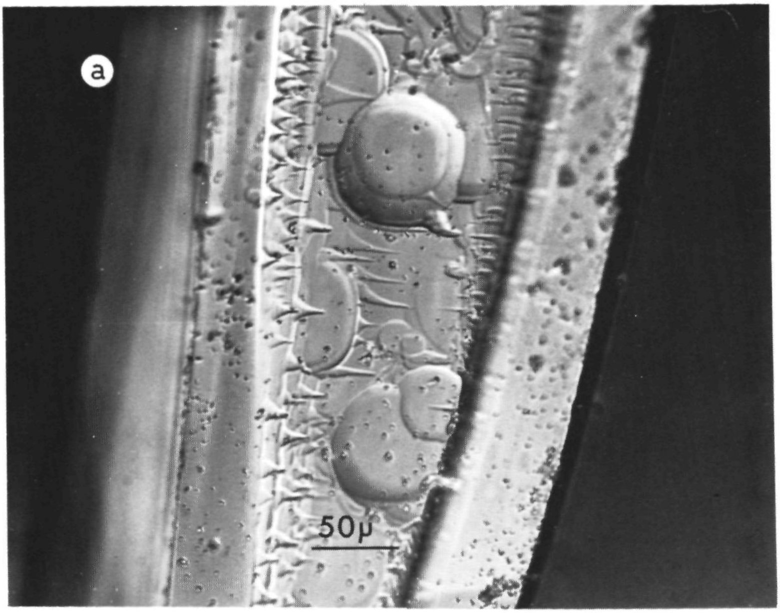
a
50µ

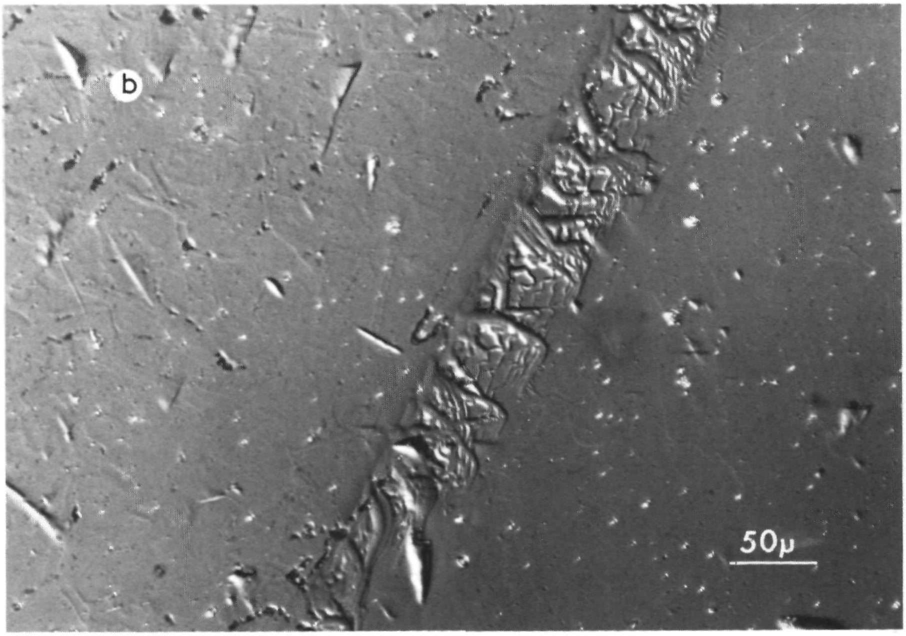
b
50µ

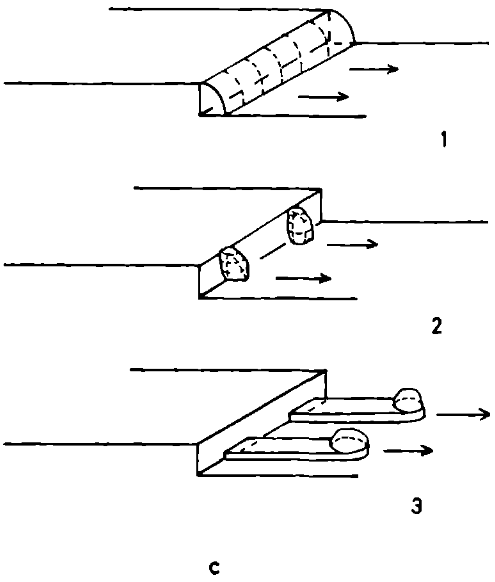

Fig. 4. Advancement of macrosteps governed by the presence of a liquid front. During cooling off at the end of the experiment the liquid contracts to isolated droplets, leading to the formation of protuberances in front of the step. (a) Differential interference contrast micrograph of such a step on $CuGaS_2$*. (b) Differential interference contrast micrograph of a macrostep on* $CuInS_2$*. (c) Schematic representation of the formation of protuberances at the end of the growth experiment.*

In the cases reported in literature, however, these protuberances play an essential role during growth and are not an artifact formed during the termination procedure of an experiment; also their formation mechanism is quite different.

A quite interesting phenomenon is that, in general, the droplets run more or less in the same direction during cooling of, as can be deduced from the parallel orientations of the protuberances. This can clearly be seen in figures 2-4 and fig. 2b of part I. The preferred orientation of the protuberances can be understood on basis of the occurrence of a temperature gradient over the crystal surface during cooling off, in the same way as described by Weyher for horizontal VLS growth of Si via a Si-Pt alloy which is enhanced by a horizontal temperature gradient over the substrate [7].

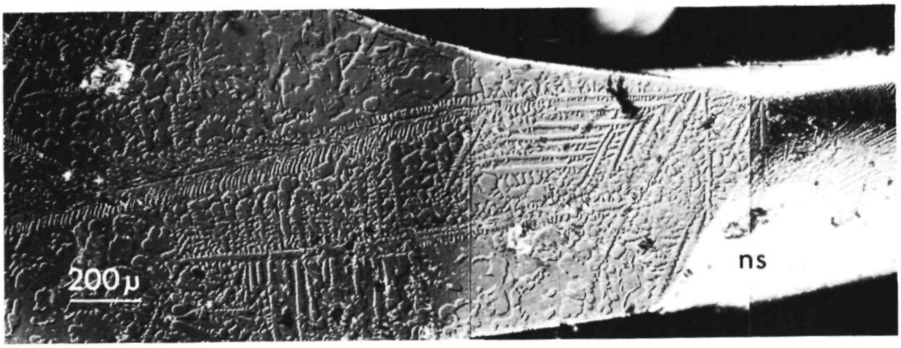

Fig. 5. Surface dendrites and growth islands on a singular and a non-singular side-face of a $CuInS_2$ *needle (differential interference contrast micrograph).*

(ii) Growth via macro steps, the advancement of which is accelerated by VLS growth, induced by the presence of a liquid "frill" at the step fronts (fig. 4 and also fig. 2b in part I). The protuberances commonly observed at the step edges are caused by a contraction of the - rectilinear - liquid growth front at the steps to - moving - droplets during the cooling off procedure as depicted in fig. 4. Similar steps accelerated via two-dimensional VLS growth were observed by Kobayashi on ice [10] and by van Enckevort and Graef on silicon [14].

Often these steps originate from the edges of the crystal, especially for $CuGaS_2$ platelets as can for instance be seen in figs. 2, 4 and fig. 2b in part I. It is strongly suggested that this generation of VLS accelerated steps at the platelet edges is induced by the presence of a well developed liquid layer at the narrow side faces of the crystal plates, that was responsible for the platelet expansion as pointed out in part I and in section 4.1. An analogous mechanism for step generation was given by Nittono et. al. for growth of the side faces of copper whiskers [33].

A special case of growth via steps with a liquid front is the formation of two-dimensional - surface - dendrites and islands on the side faces of many $CuInS_2$ needles as shown in fig. 5. The height of these surface features ranges from a few tens to several hundred of Angströms. On the interference contrast micrograph it can clearly be seen that these dendrites even continue on a non-singular surface (NS), a phenomenon which cannot be explained by ordinary VS growth. The only possible mechanism which can account for this is two-dimensional VLS growth that proceeds via a liquid phase present at the step fronts of the surface dendrites and islands. During this growth process the step advancement rate is so high that mass or heat transport becomes rate determining, leading to dendrite formation.

3.3. *VLS growth via a liquid film on the crystal surface*

For numerous $CuInS_2$ needles and $CuGaS_2$ platelets and needles a completely flat and featureless surface morphology could be revealed. Even after application of highly sensitive phase contrast microscopy, combined with high contrast photographic emulsions, no steps, nor hillocks, nor bunch formation, but only irregular height variations of a few Angstroms, which can be recognized as dots of a few microns in diameter could be observed (fig. 6). In many cases also faces which are not crystallo-

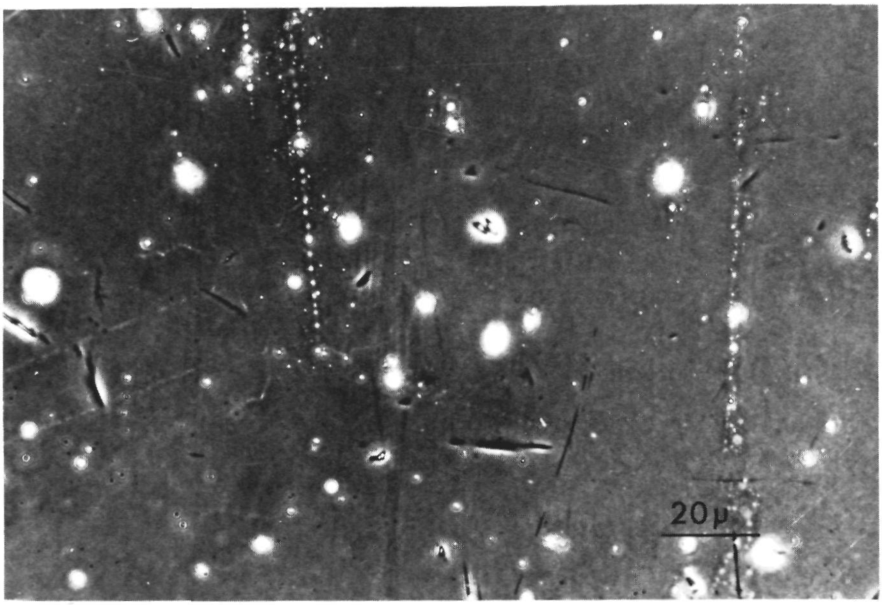

Fig. 6. Phase contrast micrograph of a typical surface area on a side face of a $CuInS_2$ needle, where growth proceeds via a VLS mechanism involving a liquid-like layer.

graphic but rounded off in all possible directions could be discerned. These surface phenomena point to the occurrence of a liquid layer on the crystal surface, so that growth proceeds via 2D nucleation, involving a small critical nucleus size. For the non-crystallographic surfaces this critical nucleus size approaches one growth unit so that the solid-liquid interface behaves like a rough face and growth proceeds via a normal growth mechanism [23]. A detailed discussion on the phenomena of 2D nucleation via a small critical nucleus and of normal growth, due to the occurrence of a liquid layer, which lowers the interfacial energy at the crystal surface with respect to the VS system, will be given in chapter 5.

During the shut off procedure at the end of the experiment this liquid layer can contract to droplets, leading to the formation of some isolated protuberances or growth hillocks. A similar rupture of a liquid layer on gas phase grown crystals leading to the formation of growth hillocks was observed by Zlomanov et al. on lead selenide [15].

3.4. *Various other aspects*

(i) The shut off procedure leads for the $CuGaS_2$ platelets to the formation of protuberances and growth hillocks of the type as shown in fig. 3 and fig. 2b in part I. The rate determining step in this VLS growth process is obviously volume diffusion in the liquid droplet. This is demonstrated with the aid of fig. 7: Volume diffusion of solute via path 1, near the edge of the droplet, will proceed considerably faster than via path 2, near the centre, since the concentration gradient in region 1 is much higher than in region 2. Here it is assumed that the supersaturation is constant at the whole solid-fluid interface as well at the whole liquid-gas interface. So, when volume diffusion is rate determining the growth rate will be highest near the edge and lowest

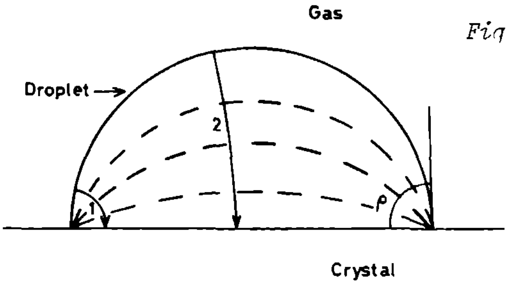

Fig. 7. Volume diffusion controlled VLS growth. The dashed lines are equiconcentration lines. ρ is the contact angle of the droplet.

near the centre of the droplet, which means that under the droplet the formation of a crater can be expected. Indeed, craters have been developed as can for instance be seen in fig. 3a. When the droplet moves on the surface, leaving a protuberance, it is now to be expected that the edges of this trace are higher than the central part. Actually these groove-like protuberances were very commonly observed. A few well developed specimens are given in fig. 2b in part I, where the depressed areas are denoted by an arrow.

(ii) Besides VLS growth also VS growth occurs very commonly on the crystal faces, especially on $CuGaS_2$ platelets and needles and on $CuInS_2$ platelets. This can give rise to the formation of single or groups of cooperating growth spirals on the crystal surfaces [24] as shown in fig. 8. On this phase contrast micrograph some spiral centres (step height, estimated from the contrast, about 5 Å), which are indicated

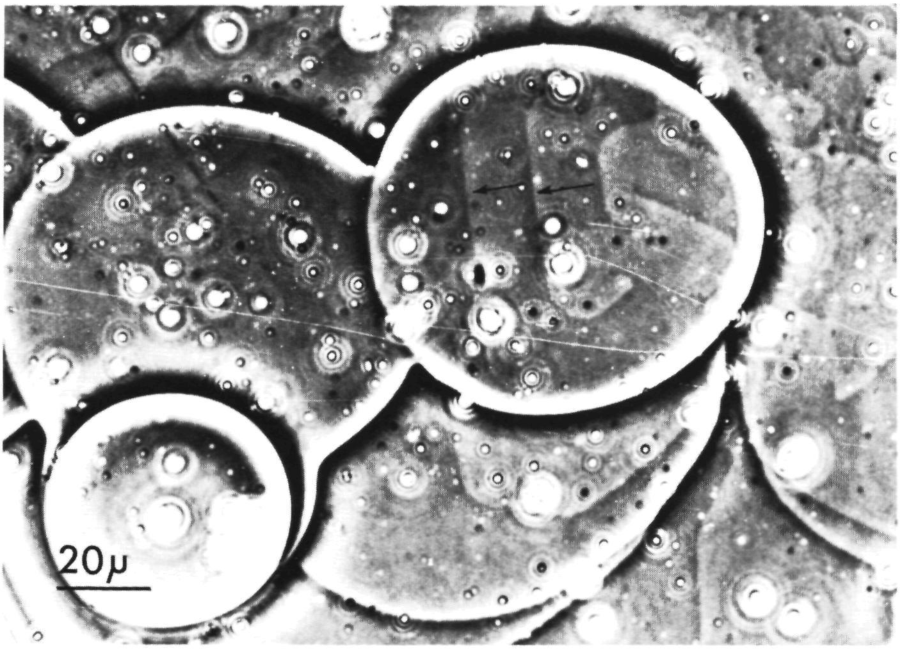

Fig. 8. Phase contrast micrograph of VS and VLS growth patterns on $CuInS_2$. The well developed growth islands, bounded by macrosteps are remnants of VLS growth, whereas the spirals on top of one of these islands are a result of VS growth.

by arrows can be seen on top of one of the circular islands, formed via a VLS growth mechanism as described in section 3.1. (ii). In general the separation between successive spiral arms, y_o, has an order of magnitude of 10 μ, which means that the radius of the critical two-dimensional nucleus for growth via a VS mechanism ($y_o/19$, [34]) equals about 0.5 μ. For VLS growth this 2D nucleus size is much smaller, approaching one growth unit for the case of normal growth via a liquid film giving curved non-crystallographic faces as will be pointed out extensively in chapter 5. That the growth islands are not a result of spiral growth, but must originate from two-dimensional VLS growth, is simply deduced from the fact that the neighbouring growth island does not contain any spiral.

(iii) It appears that the {112} and the $\{\bar{1}\bar{1}\bar{2}\}$ faces of $CuInS_2$ and $CuGaS_2$ needles and platelets show quite different VLS growth forms. For instance, for $CuGaS_2$ platelets, on one face protuberances and solidified droplets are found, whereas on the opposite face they hardly occur. This difference has already been predicted by Verheijen en Bennema in their PBC analysis of crystals with chalcopyrite structure [16,27], in a similar way as for {111} and $\{\bar{1}\bar{1}\bar{1}\}$ ZnS [35]. One of these faces is expected to have only sulphur atoms in its outermost layer, whereas the opposite face will be bounded by metal atoms [36]. Experimental confirmation of the difference between both kinds of {112} faces was obtained for $CuInS_2$ by a selective etching agent consisting of HCl, HNO_3 and H_2O in the ratio 1:1:4. After etching clearly a difference between both faces can be seen by means of optical microscopy One of these faces is always severely attacked and looks very rough, whereas the opposite face nearly remained unattacked and very smooth. A similar etching technique for determination of the polarity of a face of a crystal with a ZnS structure was used by e.g. White and Roth [37] and by Warekois et al. [38].

With the aid of this etching method it could be shown that the surface morphology resulting from a simultaneous occurrence of VLS and VS growth differed for the {112} and the $\{\bar{1}\bar{1}\bar{2}\}$ faces of especially the $CuInS_2$ platelets and to a lesser extent of the $CuInS_2$ needles. This difference is beautifully demonstrated in figure 9 showing an as-grown twinned region of a $CuInS_2$ platelet: After etching surface area of type A be-

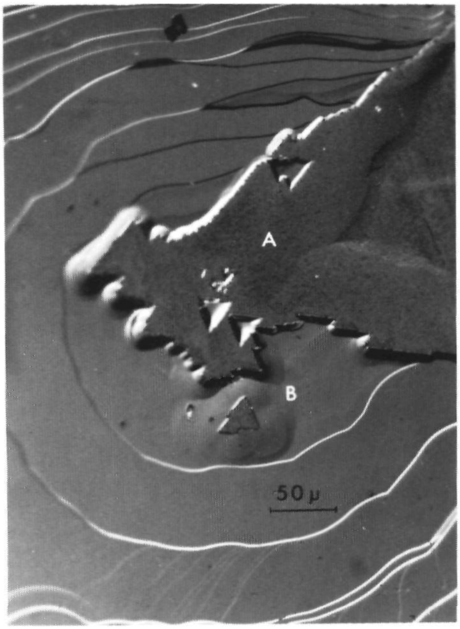

Fig. 9. Twinned surface area in $CuInS_2$*, revealing both* $\{112\}$ *and* $\{\bar{1}\bar{1}\bar{2}\}$ *faces, each having a different surface morphology (differential interference contrast micrograph).*

comes rough, whereas surface area of type B remains unaffected. It is interesting to note that for $CuInS_2$ platelets the VS growth spirals discussed in the preceding section were only found on surfaces of type B, as was verified by etching. Surfaces of type A showed no spirals, nor hillocks but only growth features pointing to 2D nucleation and VLS growth. For $CuGaS_2$, no verification by etching has taken place, since the above mentioned etchant did not reveal any difference between both faces. Earlier observations of a difference in VLS and VS growth patterns between opposite faces of a polar crystal with a ZnS-like structure were carried out by Swridersky on the carbon and silicon faces of SiC [39] and by Givargizov for the gallium and arsenic faces of GaAs [6]. In chapter 5 the correlation between the difference in surface morphology of opposing $\{112\}$ and $\{\bar{1}\bar{1}\bar{2}\}$ faces and the type of surface (sulphur or metal atoms in its outermost layer) will be discussed in detail for the case of VS grown $CuInS_2$ platelet surfaces.

3.5. *Resumé*

For all the growth experiments carried out, two-dimensional VLS growth patterns became apparent on the crystal surfaces, however, these always manifested themselves more or less in a different way. Even for crystals obtained from the same growth experiment these patterns were not completely uniform. So the reproducibility of the shapes of the two-dimensional VLS growth patterns is rather low, which means that minor changes in temperature, composition, impurity-content and supersaturation can affect their appearance considerably.

Nevertheless some general tendencies were observed:

$CuInS_2$: Besides VLS growth the platelets also show a large amount of VS growth patterns and establish a great difference in surface morphology between the $\{112\}$ and $\{\bar{1}\bar{1}\bar{2}\}$ faces. The needles nearly always reveal surface dendrites or growth features related to growth via a liquid film covering the surface. Minor differences are manifest between the $\{112\}$ and $\{\bar{1}\bar{1}\bar{2}\}$ faces.

$CuGaS_2$: Both the platelets and the needles show, besides VS growth patterns, numerous VLS growth forms related to stationary or moving droplets and to steps with liquid fronts. In some cases also remnants of liquid films could be seen, but never dendrites. A clear difference between the $\{112\}$ and $\{\bar{1}\bar{1}\bar{2}\}$ faces is present.

Finally it is to be mentioned that growth forms related to the occurrence of localized droplets were more commonly observed on $CuGaS_2$ than on $CuInS_2$, where surface patterns related to liquid films are somewhat more dominant. From this it is suggested that generally the contact angle of the liquid layer with respect to the crystal surface [40] is higher for $CuGaS_2$. An explanation for this difference may be the different composition of the liquid, viz. a mixture of CuI and InI for $CuInS_2$ and almost pure CuI for $CuGaS_2$ (see part I).

4. VLS growth of the top faces of needles and the narrow side faces of platelets

4.1. *Normal growth via a liquid film of non-singular needle tops and platelet side faces*

As shown in part I the unidirectional growth of needles and the lateral expansion of platelets can be interpreted in terms of VLS growth. The observation of non-singular top faces for most of the needles (and whiskers, which were also observed, having typical dimensions of 4 mm in length and 100 μ in width) rules out the dislocation whisker model for needle growth after Sears [41,42]. This can be understood from the fact that for this model, where spiral growth induced by a screw dislocation parallel to the needle axis, only occurs at the needle top face, a singular - facetted - top face is required to occur, otherwise no spiral growth can take place. Also the model for platelet growth involving a dislocation network parallel to the top and bottom faces, leading to spiral growth only at the narrow side faces [43] does not hold, since the side faces (especially at locations where the growth centres are expected to occur) were in numerous cases not facetted.

The occurrence of non-facetted (or rough) needle top faces and platelet side faces points strongly to VLS growth, where growth proceeds above the kinetical roughening transition, as mentioned in part I. Since the phenomenon of normal growth has extensively been studied with the aid of the Monte Carlo method [23,44,45] it will be quite useful to interprete this observation in terms of computer simulation results. This will be done in chapter 5.

The preferential length-wise growth of the needles and the sidewise expansion of the plates proceed via a mechanism, which is very similar to the "secondary whisker growth" of Cu whiskers observed by Nittono et. al. [33]. In this mechanism the liquid is preferentially deposited on terraced (in the present case rough) faces, especially occurring at the whisker tops (here the needle tops or the lateral faces of platelets) leading to uni-directioral VLS growth. In the same article, also the occurrence of rounded needle tops was reported, similar to those observed for $CuInS_2$ and $CuGaS_2$, as was shown in their figure 8b.

The most evident case for needle or platelet growth is the situation where the - generally rounded - needle tops or narrow side faces of the plates grow via a fast VLS mechanism and the - generally facetted - needle side faces or platelet top and bottom faces via a VS mechanism, as was already pointed out in part I. However, in addition also numerous - thicker - needles of $CuInS_2$ were found, of which also the side faces to a great extent had grown via a VLS mechanism giving non-facetted surface area as discussed in section 3.3. For these crystals the needle-like growth form can be developed, because of the following reasons:

(i) The final shape of the crystals, the growth of which is governed by a normal growth mechanism is largely controlled by mass or heat transport. This means that when a crystallite is slightly elongated, the lines of diffusive (or heat transport) flux will concentrate to regions with higher crystal surface curvatures so that this initial crystal shape will be accentuated leading to the observed needle-like form [46].

(ii) It is well known that VLS growth mainly proceeds in the direction of the highest temperature (better: thermodynamic driving force) gradient [7]. Probably the needle tops point to the direction of the highest gradient in temperature. This might be the case here, but it should be noted, that this explanation mainly holds for VLS growth via a localized liquid layer (or droplet) as discussed in section 4.3.

(iii) The liquid layer on the needle side faces is formed at a later stage after that needle growth via VLS growth at the top and VS growth at the side faces has taken place. For this possibility, however, up to now no proof could be given.

4.2. *Non-facetted crystals: an extreme case of normal growth*

In several cases some completely non-facetted, mostly smaller, $CuInS_2$ crystals were observed, on which neither $\{112\}$, nor $\{\bar{1}\bar{1}\bar{2}\}$, nor $\{011\}$ faces could be discerned. They showed many rounded shapes, such as spheroids, ellipsoids or worm-like growth forms. Such crystals are representative of the most extreme case of normal growth - via a liquid film covering the surface - for which no correlation exists between adjacent surface area, so that no facets are formed [54]. In these cases the final shape of the crystals is nearly completely determined by environmental conditions, such as mass or heat transport or chemical reactions on or in the liquid phase.

4.3. *VLS growth of facetted needle tops*

For a number of $CuGaS_2$ crystals facetted needle tops were observed, however, the edges often revealed a certain microscopic roughness. A clear example of such a needle top is given in fig. 10. The - microscopic - rough areas are former locations of a localized liquid (this crystal was washed in an aqueous KI solution and alcohol in order to remove surface contaminants). This liquid, preferentially deposited on the terraced, or rough edges of the needle top functions as a step source for the facetted top faces, leading to needle growth. This situation is very similar to the "secondary whisker growth" of Cu whiskers, involving facetted needle tops as reported by Nittono et al. [33].

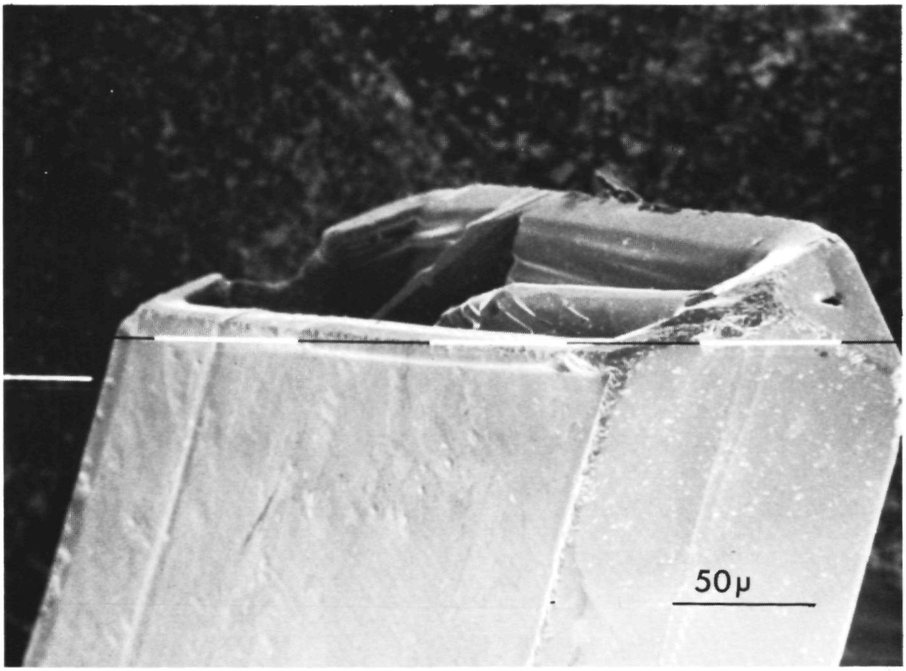

Fig. 10. Facetted needle top of a $CuGaS_2$ *crystal, showing rough edges, being the former locations of the liquid phase (SEM micrograph).*

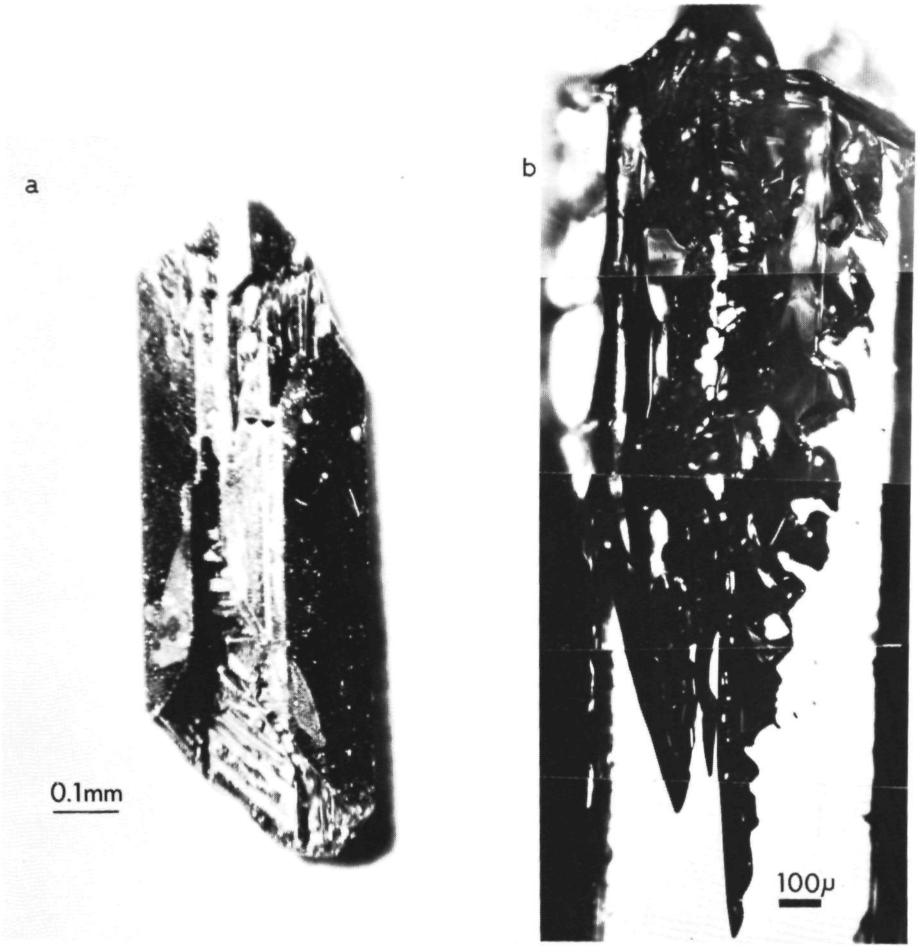

Fig. 11. Hollow needles, with a negative dendritic pattern inside. (a) $CuInS_2$ needle with a non-closed lateral face (optical micrograph). (b) $CuGaS_2$ needle with a well developed negative dendritic cavity (transmission optical micrograph).

4.4. *Growth of hollow needles*

A large extent of the observed $CuInS_2$ and $CuGaS_2$ needles are hollow and reveal a beaker-like shape as shown in figs. 11a and b. The interior of these crystals reveals a negative dendritic pattern as well as numerous inclusions. Also goblet-like crystals were commonly observed. These consist of a whisker needle at the bottom that turns into a hollow, conically shaped, crystal at the top. Hollow needles were also reported for CdS [47,48], CdSe [49] and ZnS [50] crystals. A very detailed SEM study of goblet-like crystals was carried out for CdTe by Simov et al. [51].

Since for most of the hollow crystals the top faces were not facetted, the growth mechanism for hollow crystals as proposed by Chandrasekharaiah and Krishna [47] and by Simov et al. [51] does not hold for the present case, since it requires the occurrence of facetted top faces. This mechanism is analogous to the dislocation mechanism for the mass or heat transport limited growth of cone crystal planes of salol crystals developed by Amelinckx [52]. On the other hand, a growth mechanism based on an interplay of VLS growth and volume diffusion or heat transport limited growth can explain the formation of the hollow chalcopyrite crystals. According to such a model growth proceeds as follows: Firstly a needle with a non-facetted top face is formed, as a result of VLS growth via a liquid film. When transport phenomena play a role in the growth process, the supersaturation gradient and thus also the growth rate is expected to be highest near the edges of this top face [53]. Since growth of the needle tops proceeds via normal growth, a mechanism for which no correlation in growth rate exists between adjacent surface areas [54], the top surface will show no tendency to flatten out. This means that the outward regions of the top face grow faster, leaving a central depression. This hopper like face enhances the difference in supersaturation, caused by transport limiting factors, between the edges and the centre and so reinforces the formation of a hollow crystal shape. In contrast to the above mentioned dislocation mechanism this model also explains the formation of hollow needles with non-closed lateral faces [51], which were observed quite commonly (fig. 11a).

Besides hollow needles with unfacetted tops also needles which did have facetted top faces have been observed (fig. 10). This phenomenon can be explained by the preferential occurrence of the liquid at the edges of the top face as pointed out in the foregoing section. This liquid, in conjunction with transport phenomena, strongly enhances the growth rate near the edges, leading to hollow needle formation in a similar way as for the unfacetted tops.

From the foregoing it is concluded that formation of hollow needles via VLS growth can take place when the contact angle of the liquid approaches zero, giving normal growth, or when the liquid is mainly deposited on the edges of the top face. This situation is completely different from the extensively studied VLS growth of Si or Ge whiskers with a liquid metal globule, where growth is nucleation limited [4,6] - thus no normal growth - and where the droplet is located centrally on the needle top. Here never hollow needles were observed.

Finally it should be mentioned that in the light of the preceding Givargizov's suggestion that the formation of hollow conical crystals of CdS and CdTe may be related to VLS growth [4] is worth a closer examination.

5. Discussion in terms of computer simulation experiments

In Monte Carlo simulation studies the influence of two factors on the crystal growth process was studied, viz. (i) the standard temperature 0 characterizing the equilibrium structure of the surface and (ii) the factor $\Delta\mu/kT$ which is the driving force for crystallization. 0 is defined as [23] :

$$0 = 0.88138\ kT/-(\tfrac{1}{2}\varphi_{ff} + \tfrac{1}{2}\varphi_{ss} - \varphi_{sf}) \quad , \qquad (1)$$

where φ_{ff}, φ_{ss} and φ_{sf}, which are negative numbers denote the potential energies of the fluid-fluid, solid-solid and solid-fluid nearest neighbour interactions. $\Delta\mu/kT$ is defined as $(\mu_f - \mu_s)/kT$ (μ_f is the chemical potential of the fluid phase, μ_s is the chemical potential of the solid phase).

Application of the Monte Carlo method to crystal growth, both for the Kossel model [23,44,45] and the {111} diamond face [55], which is very similar to the {112} and $\{\bar{1}\bar{1}\bar{2}\}$ $CuInS_2$ and $CuGaS_2$ faces, showed among others the following:

(i) The higher the standard temperature 0, the lower is the critical nucleus size for 2D nucleation, due to a lower step edge free energy, γ [56,57]. This results in a strong increase in nucleation growth rate for a given $\Delta\mu/kT$ [23,55].

(ii) In the case of equilibrium ($\Delta\mu/kT = 0$), there is a phase transition at a certain critical value of the standard temperature 0_R (the roughening temperature). This transition has the following properties: if $0 < 0_R$, the edge free energy of a step, γ, is larger than zero, if $0 \geqslant 0_R$, $\gamma = 0$ [55,57-61]. This implies that for $0 < 0_R$ layer growth mechanisms occur (spiral growth and 2D nucleation), giving well defined crystallographic faces and for $0 \geqslant 0_R$ normal growth is present, yielding faces without any crystallographic orientation. Therefore at temperatures above 0_R the crystal face is no longer facetted but rounded off [62]. The faces show no tendency to flatten out, because no or only a very weak correlation exists between adjacent surface regions at $0 > 0_R$ [23,54,55]. Thus the growth form of the crystal now depends largely on external factors, such as heat or mass transport.

For vapour-solid systems the fluid-fluid (φ_{ff}) and fluid-solid (φ_{sf}) nearest neighbour interactions are approximately zero [45], so the standard temperature equals:

$$0_{VS} \approx 0.88\ kT/-\tfrac{1}{2}\varphi_{ss}\ . \tag{2}$$

For liquid-solid (and so also for VLS systems) $\varphi_{ff} \approx \varphi_{sf} \neq 0$ - case of complete wetting [63] -, so:

$$0_{LS} \approx 0.88\ kT/-\tfrac{1}{2}(\varphi_{ss} - \varphi_{ff}). \tag{3}$$

Since for solution (or VLS) growth, in general, φ_{ff} is considerably less then zero, $0_{(V)LS}$ will be higher than 0_{VS}. This means that the critical nucleus for 2D nucleation for VS growth is much larger than for LS (VLS) growth, which is in agreement with the observations mentioned in section 3.4 (ii).

It should be noted, however, that equation (2) only holds when no adsorption layer is present on the vapour-solid surface. Introduction of such a layer may lead to a considerable lowering of the surface free energy, due to saturation of the "dangling bonds" of the surface atoms as was pointed out by Chernov and Papkov [64,65]. This causes a strong increase in standard temperature 0_{VS}, since 0 is roughly inversely proportional to the - vapour-solid - interfacial free energy [23,63,65]. From this it can be concluded that on crystal faces, covered with a dense adsorption layer, which saturates the "dangling bonds", 2D nucleation is facilitated and sometimes normal growth may occur [65].

For VS growth of $CuInS_2$ and $CuGaS_2$, it is very probable that the {112} face with the metal atoms in its outermost layer is completely covered by an adsorption layer, consisting of monoatomic iodine. This was verified by applying the same calculation method as used by Chernov and Papkov [64], using some typical values for the Cu-I, Ga-I and In-I bond strengths. The monoatomic layer saturates all the dangling bonds of Cu and In (Ga) and thus lowers the surface free energy considerably. On the other hand, the opposite {112} face, having only sulphur atoms in its outermost layer will not be covered by iodine, but rather by species like InI_3 (not more than roughly ½ to 2/3 th of the surface sites, since a higher coverage will lead to an enormous sterical hindering), InI, $(CuI)_n$ and CuI_2 as a result of their high metal-sulfur interactions. Since after adsorption these molecules have - except for InI_3 - still one or two "dangling bonds" left and also because of the higher number of iodine atoms - belonging to the adsorbed metal (mono-, di- or tri-) iodides - per unit surface area compared to the adsorbed M-face it is to be expected that the surface energy will not become very much lower with respect to the unadsorbed surface. The coverage at steps is expected to be similar to the coverage at the surface area in between, because the main supply of adsorbed atoms at steps will proceed via surface diffusion from the remaining surface. Thus the edge free energy per step atom will not differ too much from the surface free energy per surface atom. From the foregoing it can now be concluded that the standard temperature of the S faces will be in the same order of magnitude as the value derived on basis of equation (2), leading to spiral growth or may - be extremely slow 2D nucelation, involving a large 2D nucleus. On the contrary, VS growth of the M faces, which have a lower interfacial free energy (and thus a lower step free energy), probably will proceed via fast 2D nucleation growth, almost similar to melt growth.

In the light of the proceeding it is interesting to note that the VS growth spirals were only found on one of the two opposite $CuInS_2$ platelet surfaces, as discussed in section 3.4 (iii). Since these spirals indicate a large 2D critical nucleus, this face very probably corresponds to the S face. After etching, the {112} faces with spirals always remained unaffected. This means that the surfaces of type B (section 3.4 (iii)) correspond to the {112} faces with the S atoms in the outermost layer.

Confirmation was obtained by the observation, that after etching of $CuInS_2$ needles -also those which were grown via VLS involving a liquid film- the smooth S-face was always the larger of the two opposing faces. This is in complete agreement with the conclusion of Cadorets study on acentric crystals [36,66], that the face with the most polarizable atoms in its outer layer (here the S-face) is the largest one of two opposing polar faces.

From the occurrence of non-facetted faces, generated by VLS growth via a liquid film covering these surface areas and leading to normal growth, the following can be concluded:

(i) The solubility of $CuInS_2$ and $CuGaS_2$ in liquid CuI is not very low. This can be derived from the relation between the standard temperature and the ratio of particle densities in the solution and in the crystal, $X_{s\ eq}$ as given in refs [62] and [63], modified for the case of several solid state phase transitions before melting:

$$0 \cong 0.88/\ \{\ \sum_i \Delta H_i/kT_i + (\Delta H_m/T_m - \ln x_{eq})\}\ . \qquad (4)$$

In this equation s denotes the number of nearest neighbours of a growth unit, ΔH_m the heat of melting, T_m the temperature of melting and $\sum_i \Delta H_i/kT_i$ is the sum of the heats of transition of all phase transitions occurring in the temperature range between the experimental temperature and the melting point, divided by the corresponding temperatures of transition. For $CuInS_2$ grown at 750°C, $\Sigma\Delta H_i/kT_i + \Delta H_m/kT_m$ equals 5.8 using the heats and temperatures of the two solid state transitions and melting determined by Binsma et al. [67].

For the non-facetted $CuInS_2$ faces the standard temperature exceeds the roughening point, 0_R. Assuming that the growth and dissolution units are equivalent to one single metal or sulphur atom, 0_R must equal about 0.65 for the {112} faces of the chalcopyrite crystals in the case of equilibrium. This can be concluded from the structural similarity of these faces to the {111} facets of diamond, for which the roughening temperature

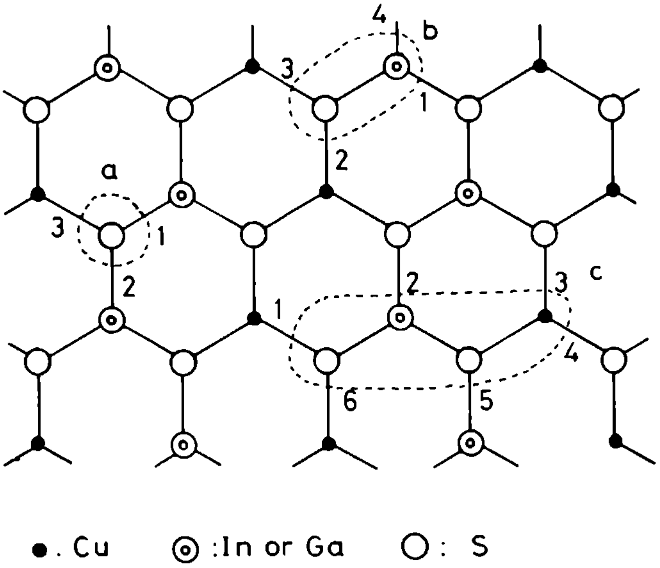

Fig. 12. Representation of a {112} slice of the chalcopyrite structure showing three in size differing creation and annihilation units. (a) Single atoms: three lateral bonds. (b) Diatomic units: four lateral bonds. (c) four-atomic units, like $CuInS_2$ or $CuGaS_2$ units: six lateral bonds.

was determined to be 0.65 ± 0.03 [55]. Using relation (4) it can now be concluded that for obtaining rough faces the mole fraction of $CuInS_2$ in CuI(l) must exceed 0.01. In the case of diatomic metal-sulphur growth and dissolution units, the {112} faces are very similar to a {001} Kossel face, because each growth unit has four lateral and two vertical bonds (See figure 12). The roughening temperature of a {001} Kossel face equals ~ 1.1 [23], which means that now the mole fraction of $CuInS_2$ in CuI(l) must be higher than 0.07 in order to obtain non-facetted growth. Finally for four-atomic $CuInS_2$ creation and annihilation units (six lateral bonds (fig. 12) resulting in $\Theta_R \approx 2.0$ [68]) even for a mole fraction of 1.0 Θ is less than Θ_R, so no roughening can occur at all! Since this is in contradiction to the observed roughening it can be concluded that the growth and "dissolution" units cannot be equivalent to complete $CuInS_2$ molecules, but must correspond to smaller fractions, such as single metal or sulphur atoms, metal-sulphur pairs or species like CuS, Cu_2S, CuI, InI and InI_3.

For the system Cu-In-S-I, there is indeed some evidence for a higher solubility of Cu, In and S in liquid CuI. This is firstly based on the observations that the solubility of InI/InI_3 in liquid CuI is very high as was found with the aid of X-ray microanalysis in part I. In addition, since Cu_2S dissolves well in CuCl(l) (15 mole % at 500°C [69,70]), it is quite probable that it also dissolves fairly in CuI(l), which has thermodynamic and structural properties very similar to CuCl(l).

(ii) Since 0_{VLS} is high, as can be concluded from the fact that this standard temperature exceeds the roughening point, the liquid-solid interfacial free energy, y_{LS}, should be low, because 0 is roughly inversely proportional to y_{LS} [23,54]. The contact angle ρ (see fig. 7) of a liquid phase on a - crystal - surface equals $\cos^{-1} [(y_{GS} - y_{LS})/y_{LG}]$ [40], where y_{GS} and y_{LG} are the gas-solid and liquid-gas interfacial energies. From this expression it can be concluded that for low y_{LS}, ρ should be minimal. Indeed, this is in agreement to the observed growth via a liquid film, for which ρ is zero. During cooling off, due to a decrease in solubility of Cu, In, Ga and S-compounds in CuI, 0 decreases and y_{LS} increases giving a higher value for ρ, manifesting in a contraction of the liquid layer to droplets during the shut off procedure at the end of the experiments.

6. Conclusions

The numerous sorts of VLS growth patterns present on CVT grown $CuInS_2$ and $CuGaS_2$ crystals were studied in detail, with the aid of several surface microtopographic methods. These VLS growth features could be classified into two groups.

(i) Two-dimensional VLS growth, manifesting in a wide range of surface patterns, that are a result of growth involving a stationary or moving localized liquid phase or a liquid film at the crystal faces. The shapes of the 2D VLS patterns differ for each growth experiment, indicating that minor changes in growth conditions strongly influence the 2D VLS growth behaviour.

(ii) VLS growth of the top faces of needles and the narrow side faces of platelets, giving various morphologies like hollow needles, whiskers, thin platelets, prisms, spheroids and goblet-like crystals. Often this VLS growth is governed by a liquid film at the surfaces leading to an enhanced growth and non-facetted faces. This morphology is interpreted in terms of crystal growth above the roughening temperature, due to a low liquid-solid interfacial energy.

The present work permits the conclusion that it would be highly interesting to make a general and thorough theoretical study of the complicated phenomenon of VLS growth. This may result in a better understanding of the relations between the numerous different manifestations of VLS growth, reported in literature and in this work, and the physical properties of the system such as, interface energies, solubility and diffusion rate in the liquid phase and surface roughness at the liquid-solid interface.

Acknowledgements

The authors wish to thank Dr. K. Tsukamoto for his valuable comments on the surface microtopographs and Dr. A.W. Verheijen for growing some of the crystals. They are also indebted to Prof. P. Bennema, Prof. J. Bloem and Dr. L.J. Giling for their kind interest and for critical reading of the manuscript. The present investigations have been carried out under the auspices of the Netherlands Foundation for Chemical Research (SON) with financial support from the Netherlands Organisation for the Advancement of Pure Research (ZWO).

References

[1] J.J.M. Binsma, W.J.P. van Enckevort and G.W.M. Staarink, J. Crystal Growth to be published, Chapter IV.

[2] R.S. Wagner and W.C. Ellis, Appl. Phys. Letters 4 (1964) 89.

[3] R.S. Wagner and W.C. Ellis, Trans. Met. Soc. AIME 233 (1965) 1053.

[4] E.I. Givargizov in: Current Topics in Materials Science, Vol. 1, Ed. E. Kaldis (North Holland, Amsterdam, 1978) p. 79.

[5] B. Mutaftschiev, R. Kern and C. Georges, Phys. Letters 16 (1965) 32.

[6] E.I. Givargizov, J. Crystal Growth 31 (1975) 20.

[7] J. Weyher, J. Crystal Growth 43 (1978) 235.

[8] J. Weyher and M. Surowiec, J. Crystal Growth 43 (1978) 245.

[9] E. Yoda, J. Phys. Soc. of Japan 15 (1960) 821.

[10] T. Kobayashi, J. Crystal Growth 26 (1974) 6.

[11] G.G. Lemmlein, E.D. Dukova and A.A. Chernov, Soviet Phys. Cryst. 2 (1957) 426.

[12] E.N. Sickafus and B.D. Barker, J. Crystal Growth 1 (1967) 93.

[13] Yu. M. Tairov, V.F. Tsvetkov and I.I. Khlebinikov, J. Crystal Growth 20 (1973) 155.

[14] W.J.P. van Enckevort and M.W.M. Graef, J. Electrochemical Soc. 128 (1981) 154.

[15] V.P. Zlomanov, E.V. Masyakim and A.V. Novoselova, J. Crystal Growth 26 (1974) 261.

[16] E.I. Givargizov, Dokl. Akad. Nauk. SSSR 211 (1973) 332.

[17] I. Sunagawa, Am. Mineralogist 46 (1961) 1216.

[18] S. Amelinckx and G. Strumane, in: Silicon Carbide: A high temperature semiconductor, Proceedings of the Conference on Silicon Carbide, Boston Masachusetts. (1959), Eds. J.R. O'Connor and J. Smiltens (Pergamon, 1960) pp. 162-201.

[19] I. Sunagawa and K. Tsukamoto, J. Crystal Growth 15 (1972) 73.

[20] W.J.P. van Enckevort and W.H. van der Linden, J. Crystal Growth 47 (1979) 196.

[21] W.J.P. van Enckevort, P. Bennema and W.H. van der Linden, Z. Physikalischen Chemie 124 (1981) 171.

[22] W.J.P. van Enckevort, R. Janssen- van Rosmalen and W.H. van der Linden, J. Crystal Growth 49 (1980) 502.

[23] J.P. van der Eerden, P. Bennema and T.A. Cherepanova, in: Progress in Crystal Growth and Characterization, Vol. 1 (Pergamon, Oxford, 1978) p. 219.

[24] W.K. Burton, N. Cabrera and F.C. Frank, Phil. Trans. Roy. Soc. 243 (1951) 299.

[25] A.A. Chernov, J. Crystal Growth 24/25 (1974) 11.

[26] A.W. Verheijen, thesis, University of Nijmegen, Nijmegen (1979).

[27] A.W. Verheijen and P. Bennema, J. Crystal Growth, accepted.

[28] H. Beyer, Theorie und Praxis der Interferenzmikroskopie (Akad. Verlaggesellschaft Geest & Portig K.-G., Leipzig, 1974) p. 107.

[29] H. Beyer, Theorie und Praxis der Interferenzmikroskopie (Akad. Verlaggesellschaft Geest & Portig K.-G., Leipzig, 1974) p. 104.

[30] Born and Wolf, Principles of Optics (Pergamon Press, 1975) p. 424.

[31] H. Komatsu, in: Crystal Growth and Characterization, Eds. R. Ueda and J.B. Mullin (North Holland, Amsterdam, 1975) p. 333.

[32] I. Sunagawa, in: Crystal Growth and Characterization, Eds. R. Ueda and J.B. Mullin (North Holland, Amsterdam, 1975) p. 347.

[33] O. Nittono, H. Hasegawa and S. Nagakura, J. Crystal Growth 42 (1977) 175.

[34] N. Cabrera and M.M. Levine, Phil. Mag. 1 (1956) 450.

[35] P. Hartman, in: Crystal Growth: an Introduction, Ed. P. Hartman (North-Holland, Amsterdam, 1973) p. 367.

[36] R. Cadoret, Thesis, University of Caen, Caen (1965).

[37] J.G. White and W.C. Roth, J. Appl. Phys. 30 (1959) 960.

[38] E.P. Warekois, M.C. Lavine, A.N. Mariano and H.C. Gatos, J. Appl. Phys. 33 (1962) 690.

[39] I. Swiderski, J. Crystal Growth 32 (1976) 350.

[40] E.A. Moelwijn-Hughes, Physikalischen Chemie (Georg Thieme Verlag, Stuttgart, 1970) p. 502.

[41] G.W. Sears, Acta Met. 1 (1953) 457.

[42] G.W. Sears, Acta Met. 3 (1955) 361, 367.

[43] G.W. Sears and R.V. Coleman, J. Chem. Phys. 25 (1956) 635.

[44] G.H. Gilmer and P. Bennema, J. Crystal Growth 13/14 (1972) 148.

[45] G.H. Gilmer and P. Bennema, J. Appl. Phys. 43 (1972) 1347.

[46] See for instance: B.J. Mason in: The art and Science of Growing Crystals, Ed. Gilman (John Wiley and Sons, New York, 1963) p. 119.

[47] M.N. Chandrasekharaiah and P. Krishna, J. Crystal Growth 5 (1969) 213.

[48] D.H. Mash and F. Firth, J. Appl. Phys. 34 (1963) 3636.

[49] C. Paorici, J. Mater. Sci 5 (1970) 918.

[50] E.J. Soxman, J. Appl. Phys. 34 (1963) 948.

[51] S.B. Simov, P.R. Kamadjiev, M.M. Gospodinov and V.F. Gantcheva, J. Crystal Growth 26 (1974) 294.

[52] S. Amelinckx, Phil. Mag. 44 (1953) 337.

[53] A. Seeger, Phil. Mag. 44 (1953) p. 8 and 9.

[54] W.J. Shugard, J.D. Weeks and G.H. Gilmer, Phys. Rev. Letters 41 (1978) 1399.

[55] W.J.P. van Enckevort and J.P. van der Eerden, J. Crystal Growth 47 (1979) 501.

[56] P. Bennema, J. Boon, C. van Leeuwen and G.H. Gilmer, Kristall und Technik 8 (1973) 659.

[57] J.P. van der Eerden, C. van Leeuwen, P. Bennema, W.L. van der Kruk and B.P.Th. Veltman, J. Appl. Phys. 48 (1977) 2124.

[58] H.J. Leamy and G.H. Gilmer, J. Crystal Growth 24/25 (1974) 499.

[59] R.H. Swendsen, Phys. Rev. B15 (1977) 5421.

[60] R.H. Swendsen, Phys. Rev. B17 (1978) 3710.

[61] J.P. van der Eerden and H.J.F. Knops, Phys. Letters 66A (1978) 334.

[62] H.J. Human, J.P. van der Eerden, L.A.M.J. Jetten and J.G.M. Odekerken, J. Crystal Growth 51 (1981) 589.

[63] P. Bennema and J.P. van der Eerden, J. Crystal Growth 42 (1977) 201.

[64] A.A. Chernov and N.S. Papkov, Sov. Phys. Dokl. 21 (1976) 300.

[65] A.A. Chernov, J. Crystal Growth 42 (1975) 55.

[66] R. Cadoret and J.C. Monier, J. Cryst. Growth 1 (1967) 59.

[67] J.J.M. Binsma, L.J. Giling and J. Bloem, J. Cryst. Growth 50 (1980) 429, Chapter II.

[68] J.P. van der Eerden, Phys. Rev. B 13 (1976) 4942.

[69] A. Rabenau, in: Crystal Growth: an introduction, Ed. P. Hartman (North Holland, Amsterdam (1973)) p. 152.

[70] A. Rabenau and H. Rau, Z. Physik, Chem., Neue Folge 53 (1967) 155.

CHAPTER XVIII:
CVT GROWTH OF $CuInS_2$

PART III: CHARACTERIZATION OF GROWTH SPIRALS ON $CuInS_2$ FORMED BY VAPOUR-SOLID GROWTH

W.J.P. van Enckevort, K. Tsukamoto
and J.J.M. Binsma

RIM laboratory of Solid State Chemistry, Faculty of Science,
Catholic University, Toernooiveld, Nijmegen, The Netherlands

ABSTRACT

Growth spirals with very low step heights (3-50Å) occurring on the {112} faces of $CuInS_2$ crystals have been investigated by means of optical phase and differential interference contrast microscopy. In contrast to earlier observed surface patterns formed via Vapour-Liquid-Solid growth, the present patterns are related to Vapour-Solid growth. Several properties of the spirals, such as central dimples, eccentricity of the spiral pattern and the occurrence of monoatomic growth steps are treated in more detail.

In two preceding papers [1,2], referred to as part I and part II in the following, the surface morphology of $CuInS_2$ and $CuGaS_2$ crystals grown via Chemical Vapour Transport (CVT) has been described extensively. From observations by means of optical differential interference (DIM) and phase contrast (PCM) microscopy, combined with scanning electron microscopy (SEM) and X-ray microanalysis (EDAX) it was pointed out that growth of these crystals was mainly governed by Vapour-Liquid-Solid (VLS) mechanisms, with CuI as liquid agent. However, (in part II) it was already argued that a Vapour-Solid (VS) mechanism also can play an essential role in the CVT growth of these crystals, manifesting in the occurrence of growth steps with low step heights on the {112} faces.

The present work describes the occurrence and properties of growth spirals on $CuInS_2$ platelets in more detail. The $CuInS_2$ crystals were grown in the same manner as described in part I, but for the investigation of growth spirals very thin platelet-like crystals (∿ 5-10 mm in width, ∿ 50-100µ in thickness) have been selected, since, in general, these show the clearest VS growth patterns.

The crystals have been observed by means of highly sensitive optical reflection PCM and DIM, combined with high contrast photographic emulsions in order to reveal the very low step patterns on the crystal faces. These observation methods have been described extensively elsewhere [2,3,4,5].

A first example, of a growth spiral on CVT grown {112} $CuInS_2$ is given in figure 1. The step height amounts about 25-60Å, as can be estimated from the contrast by comparison with calibrated step patterns. It can clearly be recognized that here a group of cooperating spirals is active starting from a small array of dislocations with equal signs. The black rectangular feature is a former contact point of another crystallite touching the crystal face, which also functioned as a step source.

A great number of VS grown crystal surfaces did not reveal any growth spiral, even when the extremely sensitive phase contrast method, which is capable to detect step heights as low as 2Å[3,4], was applied. From this it can be concluded that the platelet-like crystals are nearly free from dislocations, which might act as spiral centres.

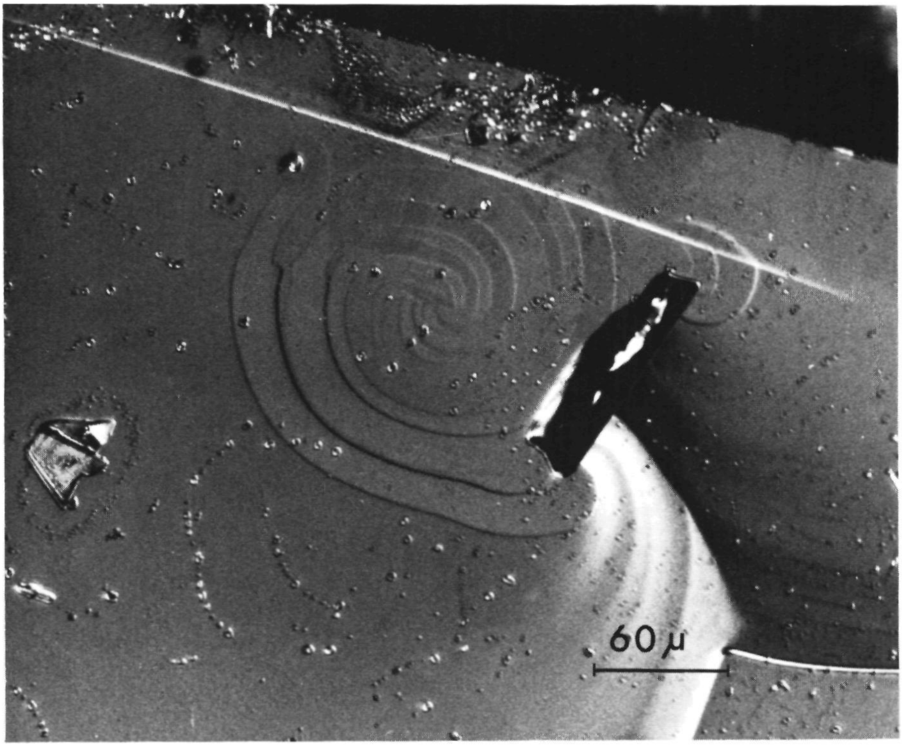

Fig. 1 Group of cooperating spirals on {112} $CuInS_2$ (DIM micrograph).

Further it is to be noted that on all the opposite - $\{\bar{1}\bar{1}\bar{2}\}$- faces of crystal plates showing VS growth spirals never such helixes could be identified, due to the occurrence of VLS growth via a liquid like film as mentioned previously in part II.

On one of the $CuInS_2$ crystals an exceedingly beautiful, partly polygonized, spiral was found, a general view of which is presented in figure 2. Such well shaped specimens were not commonly found on the $CuInS_2$ crystals. In order to measure the step height of this spiral a multiple beam interferogram (MBI) after Tolansky [3,6] was made as shown in figure 3. From this interferogram it was derived that the height of the spiral arms, somewhat further away from the centre equals 29 ± 1Å.

From figure 4, a detailed view of the spiral centre, it can be seen that this spiral is not a single one, but is composed of three cooperating spirals of equal sign. Since the contrasts of the arms of the spirals are quite similar it can be deduced that the height of each step at the centre amounts 9 to 10Å. This means that the screw components, perpendicular to the growth faces, of the dislocations from

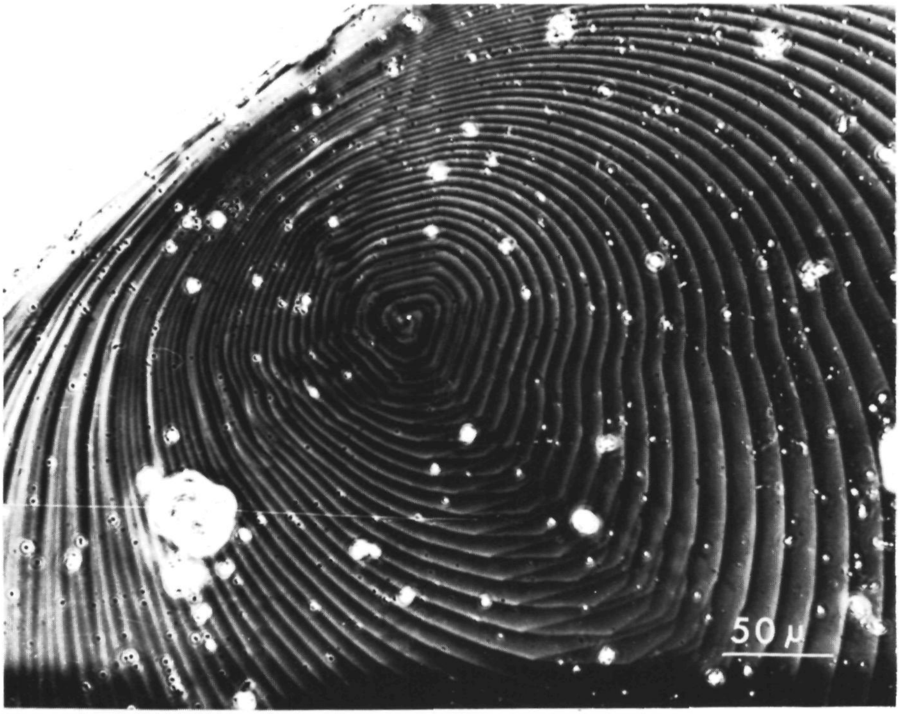

Fig. 2 General view of a partly polygonized spiral (PCM micrograph).

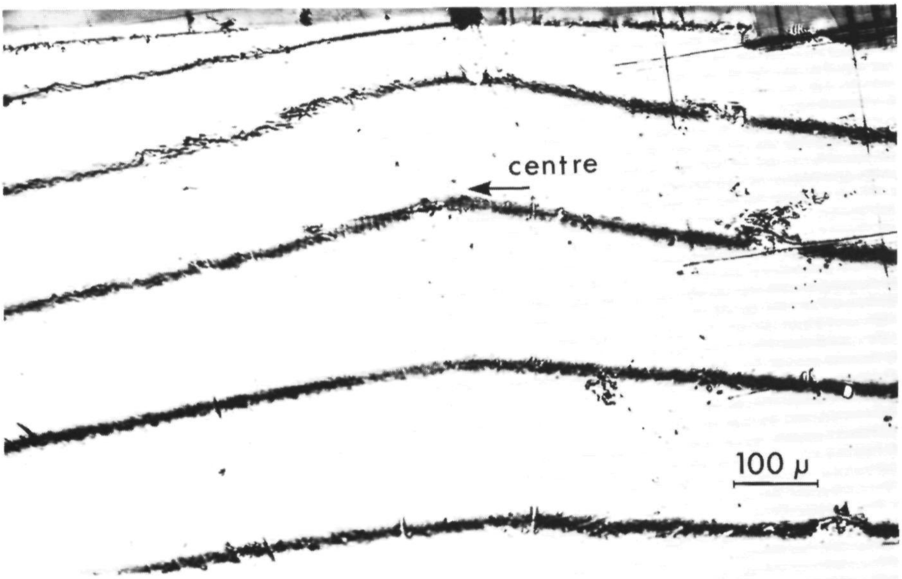

Fig. 3 Multiple beam interferogram of the spiral presented in fig. 2.

which the spiral steps originate also are equivalent to 9 to 10Å. At some distance from the centre the three 10Å steps collide with each other forming 29Å steps.

Another feature which can be recognized from figure 4 is the occurrence of a black dot at the spiral centre, which points to a shallow depression at that position (on all the phase contrast micrographs presented here, bright regions are located at a higher level than adjacent dark areas). This local depression may be an end-dimple of a dislocation meeting the crystal surface as described by Frank [7] or may be attributed to a preferred slight dissolution due to the stress field around the dislocations at the end of the growth experiment. It is not a hollow tube around the dislocation line as treated in ref. [7], since the depth of the central dimple measures only a few tens of Angströms.

Further a very low slip line (height, estimated from the contrast,

Fig. 4 Detailed view of the centre of the spiral presented in fig. 2 (PCM micrograph).

∿ 3Å) starting from the spiral centre can be seen in figure 4 (indicated by S). Since the line is completely unaffected, i.e. no growth took place at the slip line, which actually is a step, it can be concluded that slip occurred after growth, probably due to stress in the crystal during cooling off.

From the low magnification micrograph presented in figure 2 it can be recognized that the spiral is polygonized (trigonal or hexagonal-like pseudo-symmetry) at its centre, whereas the perifery is, aside from the eccentricity (which will be discussed next) more or less isotropic. This points to the fact that the step edge free energy is anisotropic for the lower centrally located 10Å steps and that the advancement rate for the higher 29Å steps at the perifery of the spiral is isotropic [8]. Since spirals with higher steps (25-75Å) are not polygonized at their centres (see, for instance, figure 1), it can be concluded that also the step free energy of the higher steps is isotropic.

A second point which can be inferred from the general spiral shape is that during growth a considerable gradient in supersaturation existed over the crystal face. This can be deduced from the eccentric shape of the spiral, as was found by Sunagawa et al. [9] and Muller-Krumbhaar [10]. At the side where the supersaturation is low, the step spacing is much less than at the high supersaturation side, due to the lower relative advancement rates of these steps, which are emitted from the spiral centre at a constant frequency. This observation shows that for CVT growth of crystals large supersaturation gradients may exist in the growth system.

A final pecularity of the growth spiral presented here is the occurrence of a complicated interlacing pattern at one side as can be seen in figure 2. A detailed view of this pattern is presented in figure 5a, while figure 5b gives a schematic representation of it. The origin of this interlacing pattern is not clear; probably the complicated spiral centre plays an essential role in the splitting up of the steps. However, this pattern can serve very well to determine the height of the lowest possible steps on CVT grown {112} $CuInS_2$, which are indicated by A in figure 5a. In figure 5b, the heights of the various lower steps, which make up the interlacing pattern, are given. These values are obtained from a careful comparison of the relative contrasts of the lower steps. Firstly the 29Å step splits up (via an intermediate state of 2 steps,

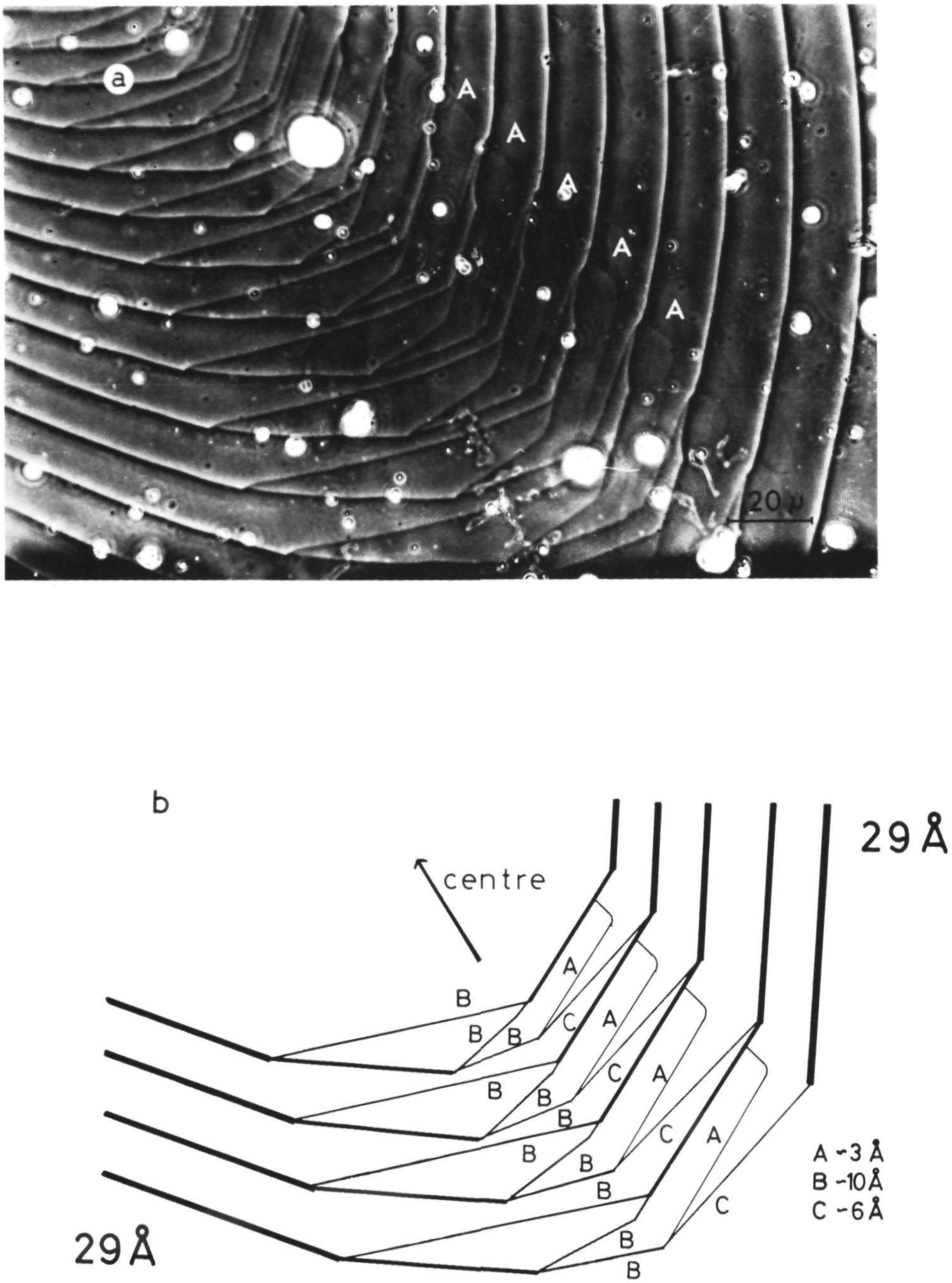

Fig. 5 Detailed view of the interlacing pattern observed on the spiral presented in fig. 2. PCM micrograph (a), schematic representation (b).

10 and 20Å in height) into three steps of about 10Å (B in fig. 5b), then one of these 10Å steps splits into one lower (A) and one higher step (C). Since 10Å must correspond to three F slices $d_{\{112\}}$, each having a thickness of 3Å as was deduced from a PBC analysis of the chalcopyrite structure [11], step A must be equal to 3Å and step C to 6Å. Since the 3Å steps correspond to one F-slice thickness, being equivalent to one monoatomic layer [11], now a direct proof has been given that monoatomic layer steps occur on CVT grown crystals grown via a VS mechanism.

Two of the authors (W.J.P. van Enckevort and J.J.M. Binsma) acknowledge the financial support of the Netherlands Foundation for Pure Research (ZWO/SON).

References

[1] J.J.M. Binsma, W.J.P. van Enckevort and G.W.M. Staarink, J. Crystal Growth to be published, Chapter IV.

[2] W.J.P. van Enckevort and J.J.M. Binsma, J. Crystal Growth to be published, Chapter V.

[3] H. Komatsu, in: Crystal Growth and Characterization, Eds. R. Ueda and J.B. Mullin (North Holland, Amsterdam, 1975) p. 333.

[4] I. Sunagawa, in Crystal Growth and Characterization, Eds. R. Ueda and J.B. Mullin (North Holland, Amsterdam, 1975) p. 347.

[5] W.J.P. van Enckevort, P. Bennema and W.H. van der Linden, Z. Phys. Chemie Neue Folge 124 (1981) 171.

[6] S. Tolansky, Surface Microtopography (Longmans, London, 1960).

[7] F.C. Frank, Acta Cryst. 4 (1951) 497.

[8] H. Müller-Krumbhaar, T.W. Burkhart and D.M. Kroll, J. Crystal Growth 38 (1977) 13.

[9] I. Sunagawa, K. Narita, P. Bennema and B. van der Hoek, J. Crystal Growth 42 (1977) 121.

[10] H. Müller-Krumbhaar, J. Crystal Growth 44 (1978) 135.

[11] A.W. Verheijen and P. Bennema, J. Crystal Growth to be published. See also: A.W. Verheijen, Thesis, University of Nijmegen (1979).

SYNTHETIC DIAMOND

CHAPTER XIX:
MICROTOPOGRAPHY OF SYNTHETIC DIAMONDS

PART I: SURFACE FEATURES IN RELATION TO CRYSTAL GROWTH OR DISSOLUTION

W.J.P. van Enckevort and Liu Guang-zhao*

RIM Laboratory of Solid State Chemistry, Catholic University,
Toernooiveld, Nijmegen, The Netherlands

ABSTRACT

Detailed surface microtopographic studies, by means of hihgly sensitive differential interference and phase contrast microscopy, completed with two and multiple beam interferometry have been carried out in order to study the growth and dissolution properties of synthetic diamonds grown from molten metal solutions at ultrahigh pressures. The as-grown {111} faces revealed growth steps of 25-50 Å and lower in height, which originate from trigonal growth hillocks, the summits of which are often related to -solidified- liquid inclusions below the surface. These hillocks could be correlated to dislocation outcrops at the surface by an etch pit method, which gives strong evidence for a spiral growth mechanism. Also on the {001} faces shallow growth hillocks could be discerned. The in the growth chamber slightly dissolved octahedral facets revealed both high and extremely low (about 5 to 20 A) steps, whereas on the cubic faces square etch pits were found. A very few of the {111} faces showed positively oriented etch pits, formed via a different dissolution mechanism. Finally a new model for the formation of the very commonly occurring surface dendrites on the {111} faces is presented. All the observations favour the conclusion that growth of synthetic diamonds is a typical case of solution growth.

1. INTRODUCTION

Troughout all ages, mankind was facinated by the beauty and rareness of diamond, which has a long history as a gem stone. This and the fact that the crystallographic structure is very simple lead to a great scientific interest

---

*Present adres: Shanghai Institute of Ceramics, Chinese Academy of Sciences, Shanghai, The Peoples Republic of China for this crystal. Especially the surface morphology has been studied in great detail during the last few decennia in order to get an insight in the genesis of the diamonds in earth. A main contribution to these surface studies has been given by Tolansky in the fifties and sixties (1-4). Further important work has been carried out by, for instance, Sunagawa, Tsukamoto and Kasuda (5) and by Komatsu and Lang (6). The most important studies on the inner structure of natural diamond was performed by Lang, using high resolution X-ray diffraction topography (7-9). These investigations showed that natural diamond is a typical case of a solution grown crystal, with magma saturated with carbon as liquid phase. This has most beautifully been demonstrated by Sunagawa et al. (5,10), who were able to observe very shallow growth hillocks, the summits of which were occupied by etch pits related to screw dislocations, which strongly points to the occurrence of spiral growth on {111} natural diamond.

The occurrence of small trigonal depressions, the so-called trigons, on the octahedral faces of nearly all natural diamonds is still a point of controversy. According to Tolansky (2,3) these features are caused by growth, whereas Frank and Lang consider them as a result of etching during the transport from the depth of the earth to its surface (8). More recent work by among others Komatsu and Lang (6), Kanda et al. (11), Angus and Dyble (12) and Sunagawa et al. (5) strongly supports the etching hypothesis for the origin of the trigons.

The beauty as well as the industrial importance of the diamonds urged many experimentists to synthetize these crystals in the past (13). However, it took up to 1954 before a group of scientists, formed at General Electric Co. succeded to obtain synthetic diamonds in a reproducable way (13,14). At the present time synthetic diamond is produced on a large industrial scale (a few tens of tons per year) over the world.

Soon after that the first synthetic diamonds were grown, several investigators, such as Tolansky (4, 15-17), Sunagawa (16,17), Bovenkerk (18) and Bezrukov et al. (19) studied the surface morphology by application of bright field or phase contrast microscopy and/or multiple beam interferometry. Typical surface features on the {111} faces were surface dendrites, higher growth steps and slip lines, whereas on the {001} facets in addition to these phenomena also growth spirals with relatively high steps were found. The inner structure of synthetic diamonds was studied by Kamiya and Lang (20), Lang (7,21), Woods and Lang (22) and Vishnevsky (23). Despite this work, still a lot of uncertainties on the growth mechanism of synthetic diamonds exists, for instance manifesting in the discussion whether growth proceeds via a catalytic process or via ordinary solution growth (24).

The aim of the present work is to carry out a very detailed surface microtopographic study of synthetic diamonds, using highly sensitive phase contrast and interference contrast microscopy, completed with two- or multiple beam interferometry. Both as-grown and "as-dissolved" (which means, slightly dissolved in the high pressure cell at the end of the growth experiments) surfaces were observed in order:

(i) To verify whether crystal growth and dissolution proceeds via a catalytic process or according to a solution growth mechanism.

(ii) To apply the models of crystal growth to the case of synthetic diamond growth in a qualitative manner. Up to now this has hardly been done.

(iii) To verify the two conflicting hypotheses for the formation of the trigons on the octahedral faces of natural diamonds on basis of an analogy between synthetic and natural diamond.

The internal structure of synthetic diamond in relation to its growth will be treated in a following paper, referred to as part II (25).

2. EXPERIMENTAL

2.1. Crystal Growth

The synthetic diamond crystals that were examined during the present investigation were grown at the Shanghai Institute of Ceramics (Chinese Academy of Sciences).

The crystals were grown in a cubic high pressure chamber made of pyrophyllite, mounted in a high pressure apparatus that compresses the chamber from six directions (27). In the cylindrical core of this chamber a sample composed of graphite as source material and metal as solvent was placed. The graphite and metal can be made to have many kinds of shapes in order to obtain uniform temperature and pressure distributions and thus better growth conditions in the chamber.

During crystal growth the pressure was kept about 55 - 60 Kb and the temperature about 1400 - 1500 °C. The phase transition of Ba at about 53 Kb was used to calibrate the pressure, whereas the temperature was measured using a thermocouple.A 40 % Ni - 30% Fe - 30% Mn alloy was frequently used as metal solvent. Under these ultra-high pressure and high temperature conditions graphite dissolves into the molten alloy. Because at high pressure diamond is stable, carbon crystallizes from the molten metal solution as diamond. The driving force of crystallization of diamond is given by the difference between the solubilities of diamond and graphite at high pressure (27). The growth period of the diamond crystals at high pressure and high tempera ture was about one hour.

Most of the crystals, the size of which varies from 0.5

mm to 1.5 mm, have a deep yellow colour and cubo-octahedron shapes. The crystalline quality veries considerably.

2.2. Observation methods

The characterization of the surface morphology of the diamonds was carried out both in a qualitative and a quantitative way, by making use of the following optical microscopic techniques:

(i) Reflection differential interference contrast microscopy (DIM) after Nomarski (28). This method, which is very sensitive to observe slight relief and low inclinations is used to obtain general views of growth features and to study etch pits. In combination with high contrast photographic emulsions DIM is capable to detect extremely low inclinations (0.05 degrees and sometimes even less), so it is also very powerful to observe the very shallow growth hillocks.

(ii) Reflection phase contrast microscopy (PCM), using a high absorption phase plate (29)(95% instead of the commonly used 60% absorption), combined with high contrast photographic emulsion. By this method it is possible to observe extremely low step heights, as low as 2 A (30). By making use of an oil-immersion objective (in microscopy commonly used to obtain higher lateral resolution up to about 2500 A) the sensitivity of PCM can be increased even more. This can be understood by realizing that now the refractivity of the medium between object-lens and specimen, and thus also the optical path difference between two adjacent area of a phase object (28), is increased by a factor 1.5, being the refractive index of the immersion-oil used. On all the PCM photographs presented in this work, the brighter area are situated at a higher level than adjacent darker regions. The power of PCM to study crystal surfaces has been well established in the past as can be deduced from numerous papers written on this subject by, for instance, Sunagawa (30,31), Komatsu (32), Tsukamoto et al. (33), Amelinckx and Strumane (34), Verma (35), van Enckevort et al. (36,37) and Bennema et al. (38).

(iii) Two beam (TBI) and multiple beam interferometry (MBI) after Tolansky (39) in order to obtain quantitative information, such as height differences and inclinations, on the the surface morphology. As a monochromatic light source, which is required for this technique, a mercury lamp combined with an interference filter (λ = 5460 A) was used.

Prior to observation a lot of the diamond surfaces were coated coated with a thin layer of silver in order to increase the sensitivity of the observation techniques. For application of MBI and for using the oil-immersion lens, the silver coating on the crystal surfaces was even essential! The silvering was carried out carefully by means of an ordinary sputter coating unit for scanning electron microscopy, combined with a water cooled specimen holder and an electron deflection accesory.

Exellent reviews on the use of optical microscopy for the characterization of crystal surfaces have been written by Komatsu (29) and Sunagawa(40).

3. GROWTH PHENOMENA

3.1. General features

During the present investigation several hundreds of diamond {111} faces were examined. Nearly all these octahedral faces showed the typical dendrite pattern, which has been observed earlier by numerous workers (15,16,18,19), or were completely rough. However, in some cases clean, somewhat depressed areas between the over the whole surface dominating dendritic or rough regions were found. In all cases these surface areas revealed a growth step pattern, often dotted with a few growth hillocks as shown in figure 1. From this and similar phase contrast micrographs it can be deduced that the growth step and hillock pattern presents the original surface morphology during crystal growth. On the other hand, the at a higher level situated rough regions as well as the dendrite pattern covering the surfaces are

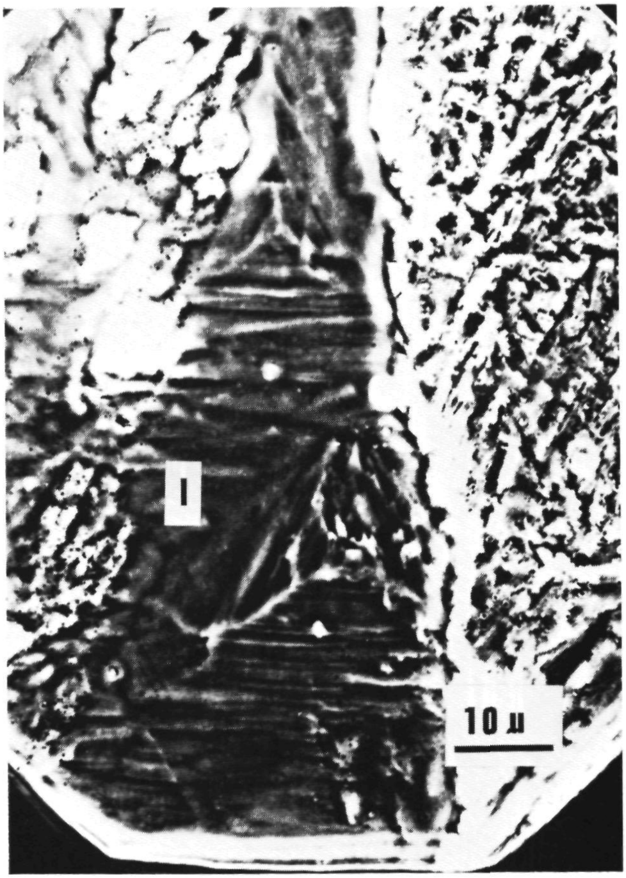

Fig.1. Triangular growth hillocks and step patterns in a clean surface region emerging from the, due to contamination, generally rough or dendritic surface pattern.

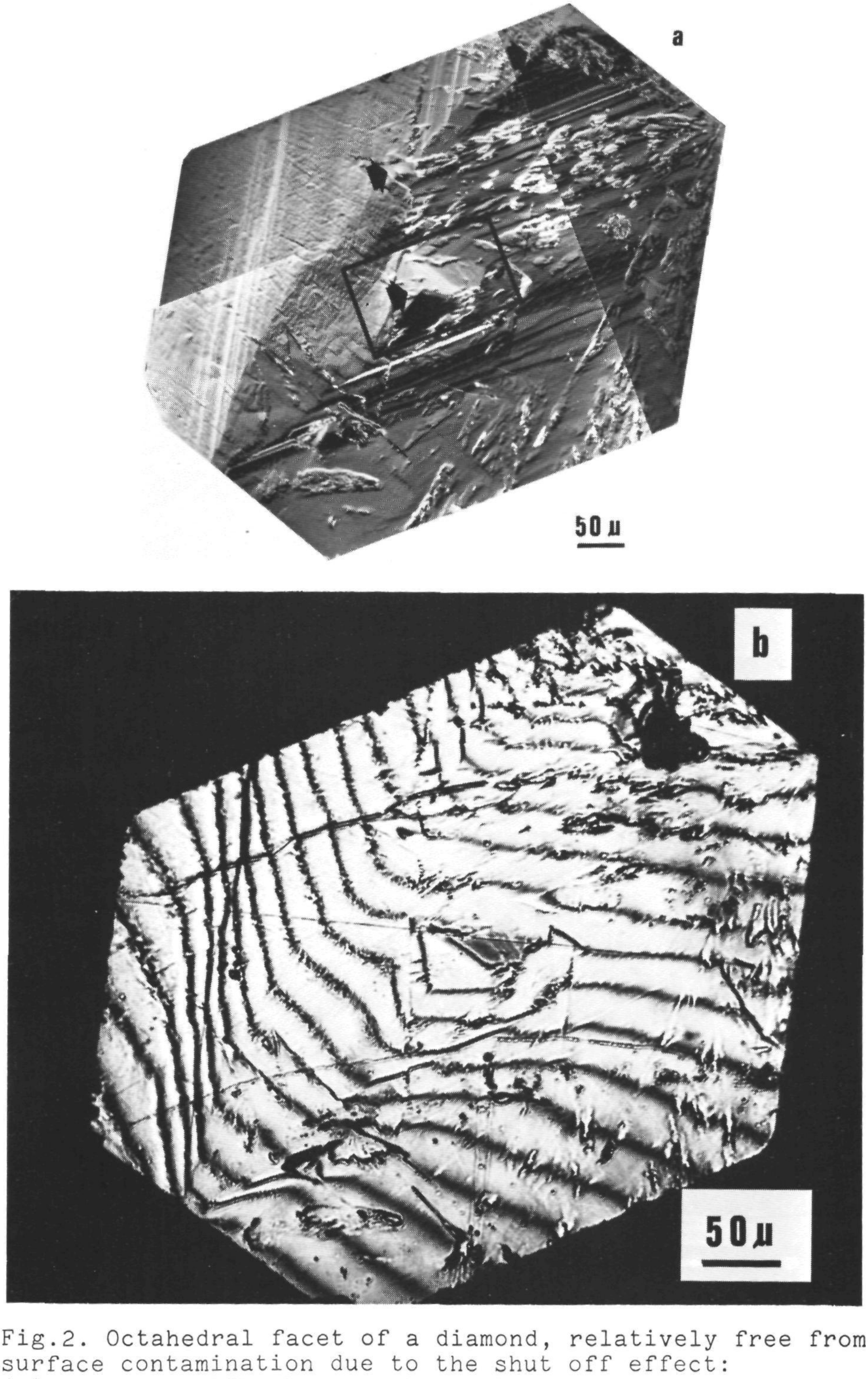

Fig.2. Octahedral facet of a diamond, relatively free from surface contamination due to the shut off effect:

(a) Composite DIM photograph showing growth hillocks and steps

(b) Two beam interferogram of the same facet as (a).

a result of the so-called "shut off effect", i.e. secondary effects due to local growth or etching at the end of the growth experiment that ruins the original surface pattern. This perturbation is one of the main problems for detailed surface microtopography of, especially solution grown, crystals and has been treated in detail for the case of potash alum (36,38,41) and KDP (38,42). It should be noted that in contrast to aqueous solution grown, flux grown and other crystals for diamond no way exists to minimize the shut off effect, that causes the artifacts on the surfaces. Therefore the only possibility to overcome this difficulty in some way is to inspect numerous diamonds for some surface areas that show the original structure just before cessation of growth.

In rare cases octahedral facets that were almost completely free from surface contamination, due to the shut off effect -and thus showing the original pattern- were found. One of these "unperturbed" faces is given in figure 2a, while its multiple beam interferogram is shown in figure 2b. Clearly three distinct growth centres (denoted by arrows) from which steps laterally spread over the crystal face can be recognized. On other "unaffected" octahedral faces often one hillock dominating the whole surface area or a multitude of smaller hillocks (fig. 3) was found. It

Fig.3. Group of growth hillocks and slip lines (S) on {111} synthetic diamond (PCM).

is quite remarkable that nearly all the observed growth features on {111} diamond show a quite large similarity to surface phenomena on solution grown crystals, such as potash alum (36,37) and, apart from the symmetry {101} KDP (42).

Another phenomenon commonly observed on the diamond faces are slip lines (in figure 3 indicated by S) running parallel to the {110} directions. The occurrence of similar slip lines on synthetic diamonds has been reported by several workers like Tolansky and Sunagawa (15), Tolansky (15) and Bezrukov et al. (19). Since the slip lines (which actually are steps located between two opposite screw dislocations or edges of the face) never show indications of any interaction with the original step pattern, but is just superimposed on it, the conclusion can be drawn that these slip lines are formed after termination of growth, probably during cooling off. This observation confirms the supposition that slip occurred after that the crystal was completely formed, made by Tolansky, two decennia earlier(15).

3.2. Growth steps

On all surface regions, not perturbed by the shut off effect, numerous growth steps, mostly appearing as extended step trains originating from one or more growth centres can be seen by application of differential interference contrast and phase contrast microscopy (See figures 1,4 and 5). In practically all cases one or more triangular growth hillocks, the properties of which will be discussed in the following section, function as step source. Similar step trains originating from triangular centres have been observed earlier on natural diamonds by Tolansky (4) and Sunagawa et al. (5).

The advancement directions of the growth steps -which nearly always are oriented parallel to <110> - with respect to the external morphology of the cubo-octahedral crystals is given in figure 6a. The observed -positive (44,45)- hillock orientation is in agreement with the theoretically expected hillock orientation deduced on basis of the first order broken bond model by van Enckevort and Giling (46). This means that during growth of synthetic diamond from the liquid metal solution no (or weak) step reconstruction takes place at the kinked $|\bar{1}\bar{1}2|$ steps (46) and that the lateral anisotropy of the step advancement vectors is typical for solution growth. From this it can now be concluded that it is highly interesting to relate the observed surface morphology of {111} synthetic diamind to the results of a Monte Carlo simulation study of {111} diamond (47), which is also based on the first order broken bond model.

In order to obtain an estimate of the heights of growth steps occurring on the {111} faces, manifesting as more or less wel developed step trains, several phase contrast

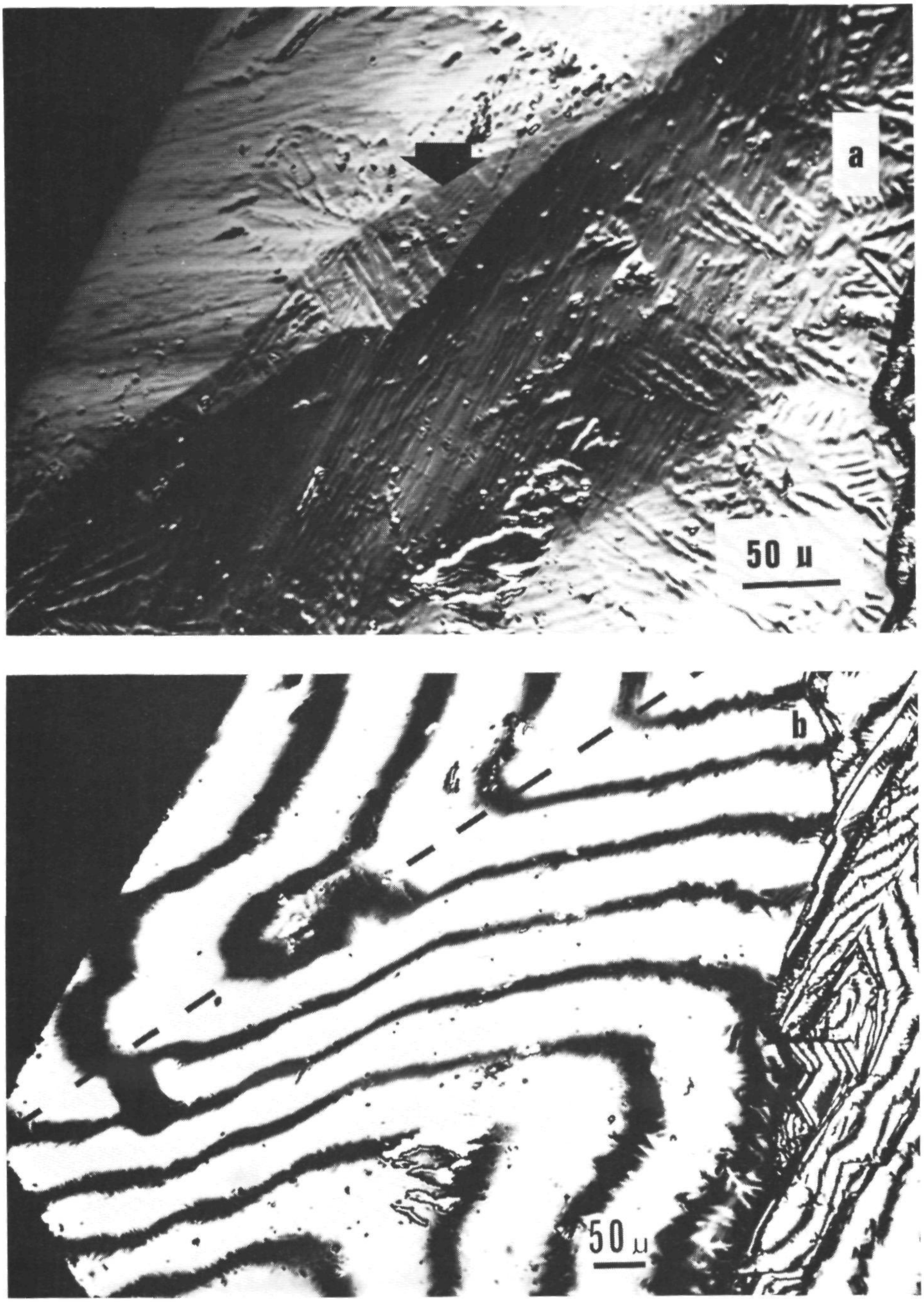

Fig.4. Measurement of the step height on a {111} diamond face:

(a) Low magnification DIM photograph giving a general view of a step train.

(b) Two beam interferogram of the same area as (a).

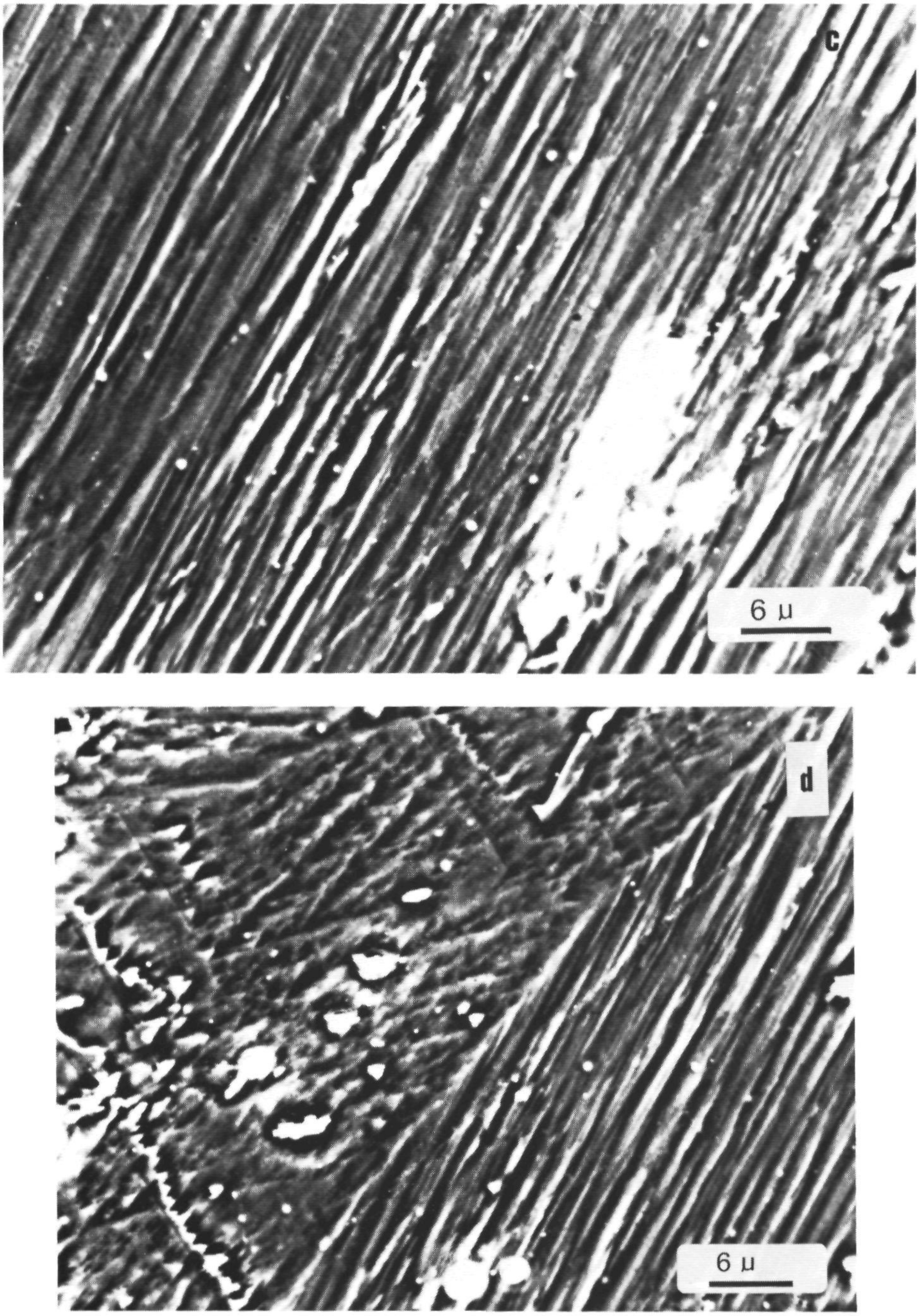

Fig.4. (continued):
(c) High magnification oil-immersion PCM photograph revealing individual steps in the step train.
(d) High magnification PCM micrograph showing saw tooth like shaped $\{\bar{1}\bar{1}2\}$ steps.

Fig.5. Growth hillocks dominating the complete step pattern on a {111} facet:
(a) General view (DIM).
(a') Inclusions below the summit of the hillock presented in (a).
(b) Two beam interferogram of the major part of the same {111} face as in (a). C: growth centre.
(c) Detailed view of the hillock (PCM).

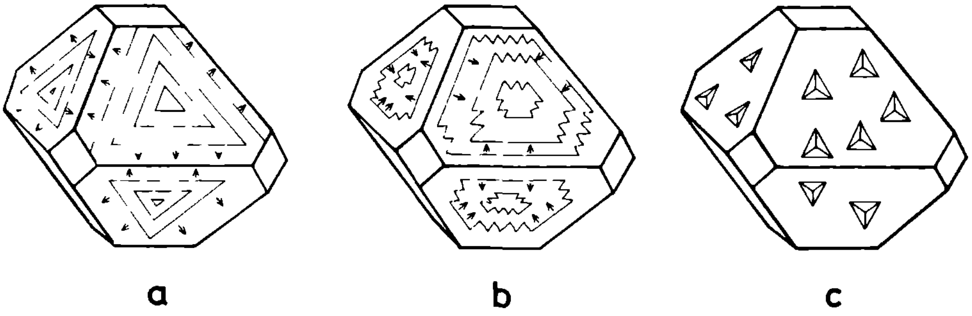

Fig.6. Schematic representation of the orientations of the step patterns on the octahedral diaomond faces with respect to the external morphology:
(a) Growth via $|11\bar{2}|$ steps; (b) Dissolution starting from the edges via $|11\bar{2}|$ steps. (c) Dissolution via $|\bar{1}\bar{1}2|$ steps involving the formation of positively oriented etch pits.

micrographs and two- or multiple beam interferograms were made. Three examples are given in figures 4,5 and 8. The case given in figure 4 will be elucidated in some detail: Photograph 4a presents a DIM micrograph showing a ridge, which forms a boundary between two step trains having an angle of 60^{o} with respect to each other. Of this region also a two beam interferogram, shown in figure 4b, has been made, in which the ridge (indicated by a dashed line) can easely be recognized by a strong bending outwards of the fringes. From this TBI micrograph it can be deduced that the inclination -perpendicular to the step orientations- of the step trains with respect to the exact {111} plane amounts 0.5 degrees. From figure 4c, being a high magnification oil immersion micrograph, the step density is determinated to be about 25.10^{2} steps per millimeter. It is to be noted, however, that very probably the actual step density is higher, since numerous steps in micrograph 4c have a bunched appearance and thus consist of two or more superimposed lower steps. From this it can be concluded that the step height for this hillock is 35 A or lower. A similar analysis applied to figures 5 and 8 shows that for these elevations the step height is less than 25-50 A and 25-40 A respectively. So now the conclusion can be drawn that, in general, the step height on {111} diamond, for the case of growth is equal to 25-50 A or less.

This observation permits the conclusion that growth of {111} diamond from a molten metal solution proceeds via low steps and that the layer models for crystal growth developed by Kossel (48), Stransky (49) and Burton, Cabrera and Frank (50) can be applied to the case of synthetic diamond.

In a very few cases a different step orientation for growth of {111} diamond was found, as can for instance be seen in figure 4a, in which steps parallel to <110> but advancing towards the $|\bar{1}\bar{1}2|$ direction instead of the common $|11\bar{2}|$ direction are indicated by an arrow. Close examination of these steps at higher magnifications (see figure 4d) shows that these $|\bar{1}\bar{1}2|$ steps often consist of a saw tooth shaped pattern made up of $|11\bar{2}|$ steps. The reason for this phenomenon is not clear. A further interesting phenomenon observed on numerous octahedral facets is the occurrence of reentrant corners in the step patterns. These are mainly found in the region between two growth hillocks as can be seen in phase contrast micrographs 1, 2a, 7a and b and 8, where the reentrant corners are indicated by I.

Fig.7. Reentrant corners (I) in step patterns: (a) PCM micrograph.

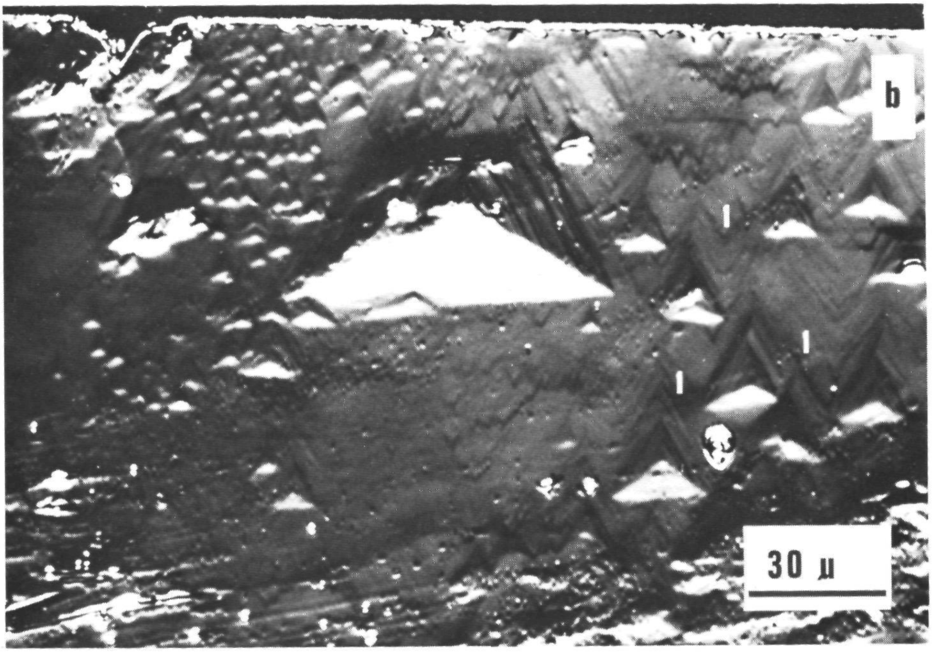

Fig.7. (continued) (b) DIM micrograph showing a group of hillocks and lower (∿20 A) steps.

From these photographs it can be gathered that the steps with a reentrant corner have a slightly increased advancement rate. A similar effect, which can be deduced from the dependence of the step advancement rate on the step curvature derived by Burton, Cabrera and Frank (50) was observed earlier for {111} potash alum (36). However, in contrast to potash alum here the step orientations near the reentrant corners only slightly change and the "legs" of the V-shaped patterns maintain roughly parallel to the <110> directions. So the conclusion made from computer simulations that the shape of the reentrant corner (or cusp) in a step is stable in time, also holds for the anisotropic case of 111 diamond.

A final point to be mentioned is the occurrence of bunching in the step patterns as can for instance be seen in figures 1-5 and 8, where higher and lower steps often alternate in step trains. These perurbations in step trains may be explained by the extremely high growth rates of the diamonds, due to which local and time dependant variations in supersaturation may occur. These instabilities lead to fluctiations in the step advancement rates, which causes the observed bunching of steps. Further, the bunching may be imposed by complicated growth centres as was pointed out by Sunagawa and Bennema (52). Probably the bunching of the hillock shown in figure 8 is caused by this phenomenon.

3.3. Growth hillocks

In the preceding sections, several properties of the trigonal growth hillocks occurring on the {111} faces of synthetic diamond have been mentioned, such as the orientation with respect to the external morphology and the step height. In this section some other characteristics of the hillocks which give a deeper insight in the origin of these elevations will be elucidated.

Firstly, in several cases the centres of the growth hillocks are related to "liquid" (i.e. during crystal growth liquid) inclusions just below the crystal surface. This correspondence is demonstrated with greatest clearness for the hillock shown in figure 8a, being a phase contrast micrograph of the boxed area in the composite DIM photograph 2a. In figure 8c, a high magnification PCM photograph made without previous silvering of the surface, at the centre of this hillock an extended bright area can be recognized. Application of bright field transmission microscopy shows that this spot corresponds to a "liquid" inclusion just below the surface as can be seen in figure 8c'. Such a relation between a growth centre and a liquid inclusion underneath is also demonstrated in figure 5: PCM photograph 5a and c show the growth hillock, while transmission micrograph 5a' gives the inclusion -denoted by an arrow- below its summit.

In order to verify whether a particle or a crater exists at the summit of the hillocks or not, high magnification DIM (fig. 8d) and PCM (fig 8e) photographs were made of the same, but now silvered so that the inclusion can not interfere the image, surface region as shown in figure 8c. On these pictures it can clearly be seen that no recognizable irregularities exist at the hillock centre. From this the conclusion can now be drawn that during crystal growth no solid particle that functioned as a step source, leading to the formation of this triangular elevation was present at the hillock centre.

To obtain an understanding of the actual cause of the formation of the growth hillock in figure 8, after the previous close examination etching has been applied to mark dislocation outcrops at the surface as etch pits. The dislocation etch pits were produced by slightly dissolving the crystal surface in fused KNO_3, a well known dislocation etchant for diamond (53,54) at 655 °C during 12 minutes. This etching time was just long enough to enable the formation of well developed etch pits, but was unsufficient to obscure the contours of the growth hillock. The surface pattern after etching is given in figures 8f and g. It can clearly be seen that at the hillock centre a point bottomed etch pit (indicated by an arrow) has been formed. Careful examination of this pit shows that its pointed bottom is

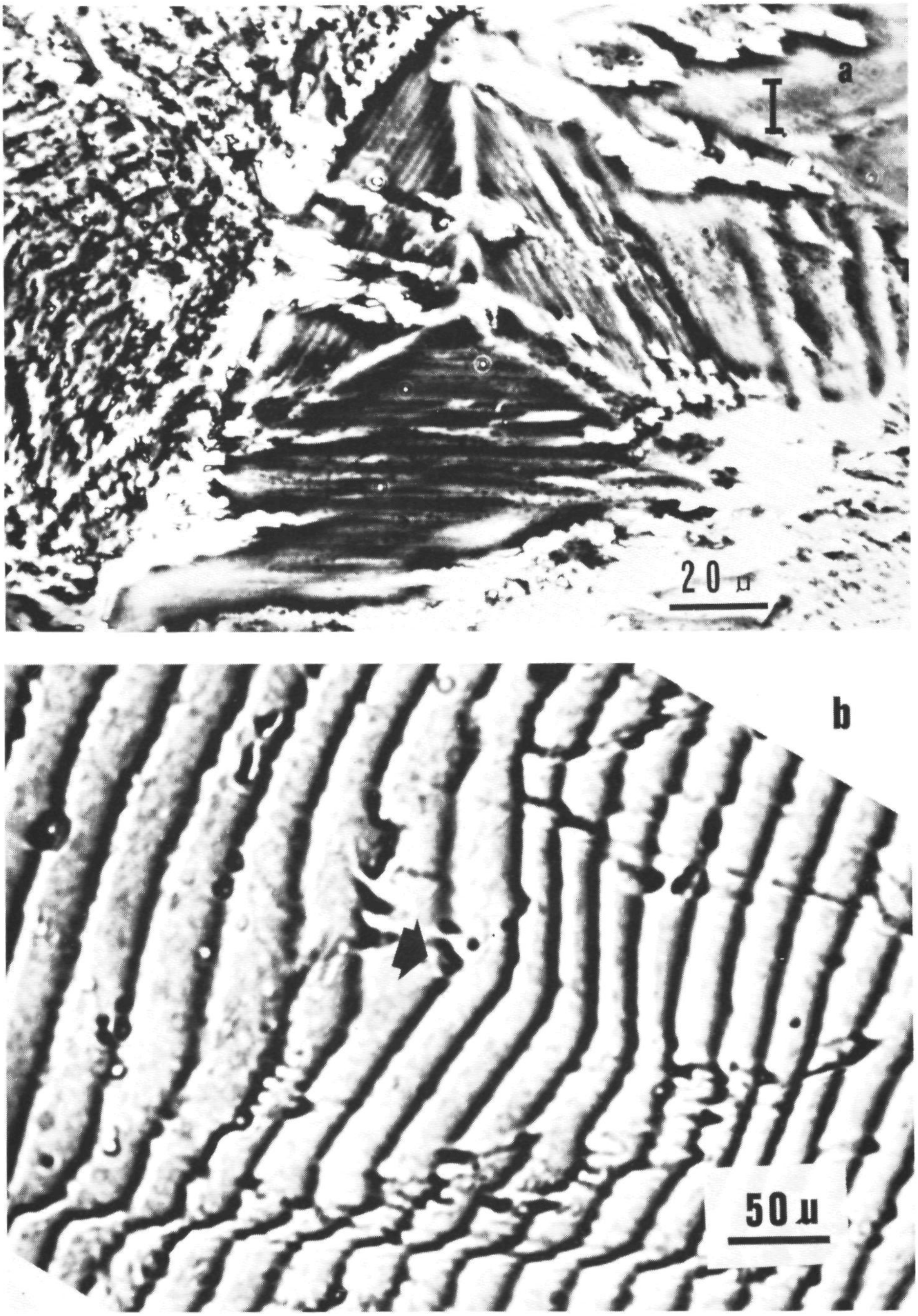

Fig.8. Relation between hillock centres, inclusions and dislocations:
(a) General view of a well developed growth hillock (PCM).
(b) MBI micrograph of the same area as (a).

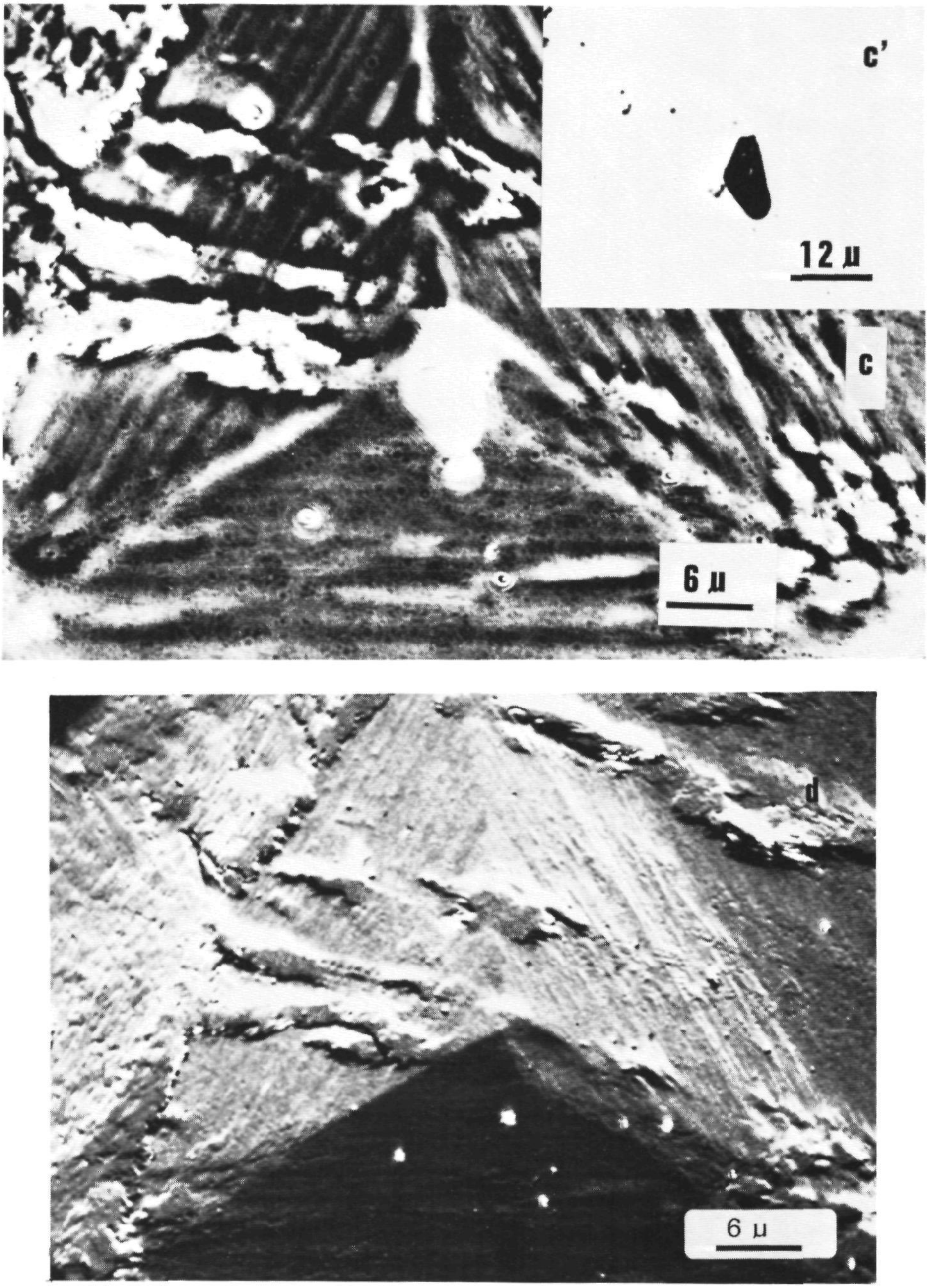

Fig.8. (continued) (c) PCM photograph of the unsilvered surface showing the hillock and the -solidified- liquid inclusion below its summit. (c') Bright field transmission micrograph of the inclusion shown in (c).
(d) DIM micrograph of the same area as (c) after silvering the crystal surface.

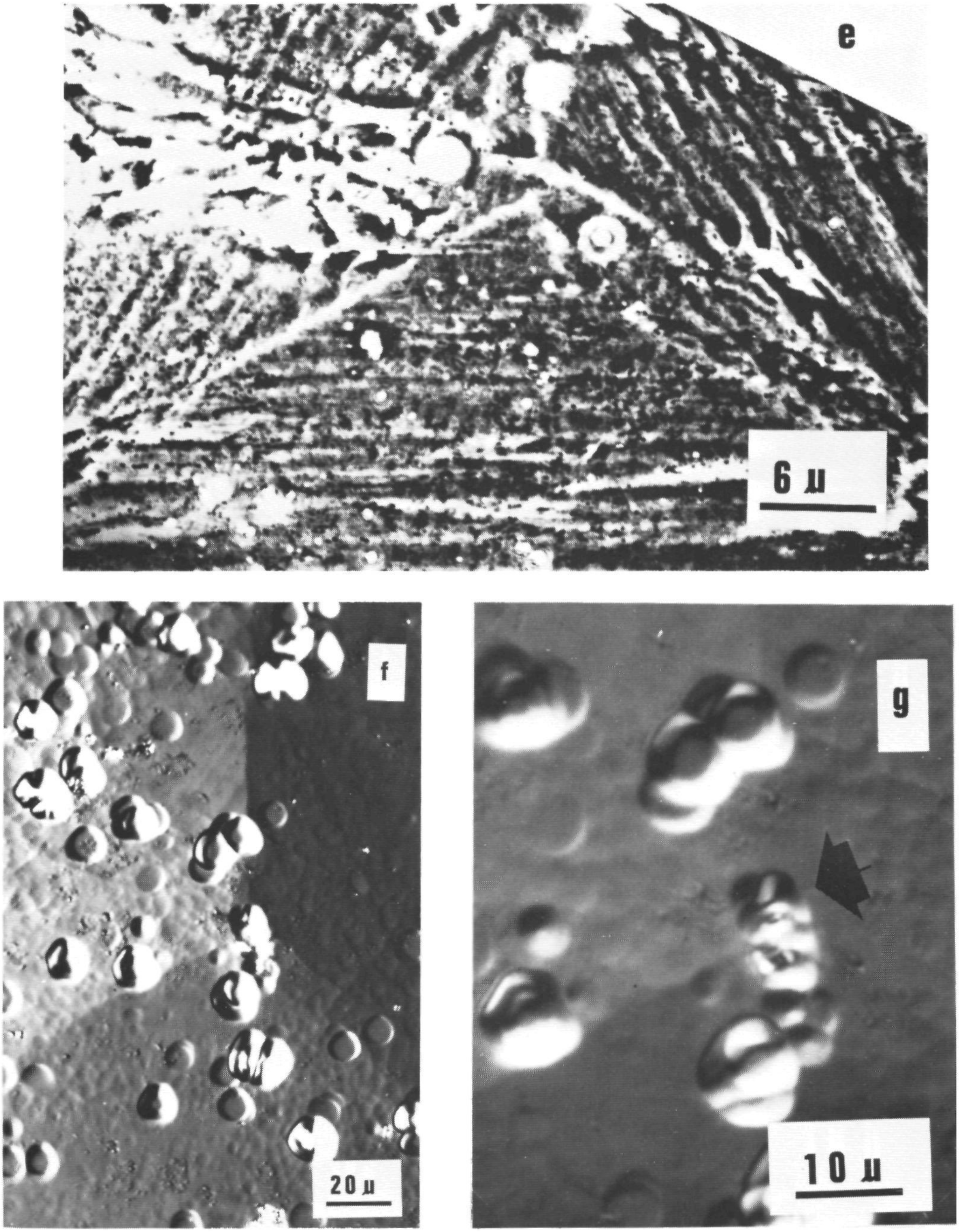

Fig.8. (continued) (e) PCM of the area given in (c) after silvering the crystal surface.
(f) Etch pits at the summit of the growth hillock after slight dissolution in fused KNO_3.
(g) Detail of (f).

not in contact with the inclusion underneath. This means that the pit is not created by the presence of the inclusion itself, but rather by the occurrence of dislocation lines running from this inclusion to the crystal surface. The neighbouring pits are nearly all flat bottomemd as can be verified from the low contrast DIM photograph 8g, which means that these pits are not related to dislocation outcrops but rather to point defects near the surface.

From this correspondence between growth hillock centre and dislocation outcrops it can be inferred that it is quite probable that these elevations are spiral hillocks, i.e. crystal growth of {111} synthetic diamond proceeds via a spiral growth mechanism. A similar correspondence between hillocks and dislocation outcrops was found for {111} (43), {001} (55,56) and {101} (41,56) potash alum, SiC (57), stearic acid (58) and {101} KDP (42). Now also the occurrence of some hillock centres above "liquid" inclusions can be understood easily: After formation of the inclusion lattice closure errors occur, leading to the creation of a few -screw- dislocations or a dislocation bundle, which again causes spiral growth, resulting in the formation of a spiral hillock above the inclusion. This phenomenon has been observed earlier for {101} KDP (42) and has been studied in detail by Sato et al. for stearic acid (59,60).

All the observed surface patterns, such as the occurrence of low steps originating from a few or numerous growth centres, which probably are growth spirals, show a very large resemblance to surface features of solution grown crystals like potash alum (36,43,55,56), KDP (42), garnet (33) and others. This gives very strong evidence that synthetic diamond growth does not proceed via a catalytic mechanism (23), or via a kind of solid state transition (61), but is a typical case of "ordinary" solution growth, which confirms the hypothesis given by Litvin (62,63), Sunagawa (64) and others (24,27).

From the viewpoint of the spiral growth model, also the difference of the growth hillock pattern on each face, viz. one or a few hillocks dominating the whole surface (figs. 2 and 5) or the occurrence of multitudenious hillocks (fig. 7b) can now be explained in terms of a "struggle for life" between numerous competing growth spirals. According to this hypothesis the growth spirals on a given crystal face that produce the highest growth rates (mostly cooperating spirals with a greater activity (50)) overwhelm the slower "growing" spirals and thus determine the growth rate and the step pattern of this face. This competition of growth spirals, which results in a for each {111} face unique surface pattern, may be one of the causes of the dispersion in growth rate (65) of the {111} faces deduced from cathodoluminicence studies of the growth sectors in diamond (22,23).

Finally it is to be noted that the distribution of growth hillocks on the {111} facets is quite random, with a slight preference for the edges. This suggests that the dislocation outcrops are also roughly randomly distributed over the octahedral faces, which is in contrast to other solution grown crystals, like natural diamond (9,66), potash alum (67,68), urotropine (69) and others (66). Such a random distribution is in agreement with observed -dislocation-etch pit patterns on synthetic diamonds as will be elucidated in section 4 and part II.

3.4 {001} faces

Application of DIM and PCM to the 001 surfaces of the synthetic diamonds revealed, at least when the surface is not obscured by the shut off effect, a featureless surface pattern, which was often slightly undulated with inclinations up to 0.05 degree. Macrosteps as have been seen by for instance Tolansky and Sunagawa (15,16), Bovenkerk (18), Strong and Hanneman (70) and Bezrukov et al. (19) were never observed. Also the extremely flat surfaces reported by Tolanky and Sunagawa (16) could never be revealed. In many cases, however, growth centres, from which concentric un-

Fig.9. Growth centre emitting bunched step patterns on an {001} face of synthetic diamond (DIM).

dulated bunches spread over the whole crystal face as well as square growth centres could be seen by DIM. A clear example of such a growth centre is given in figure 9. The presence of these growth hillocks strongly points to the occurrence of low growth steps, laterally expanding from one or more centres over the whole cubic surface as was suggested previously by Kamiya and Lang (20). The bunches can be considered as a pile up of steps as described in the kinematic wave theory of Frank and Cabrera (71-73).

According to the Periodic Bond Chain method (74), {001} diamond is a K-face (74), which means that it does not show steps but is rough and growth proceeds very rapidly via a "normal growth" mechanism (75). This means that from a theoretical point of view the {001} faces should not occur on diamond since the external morphology of crystals is only determined by the slowest growing faces. So it is quite intriguing that the cubic faces of synthetic diamond, which should be K-type, have a low growth rate involving low steps. A similar growth via low steps on a K-face was found by Bauser et al. for {001} GaAs (76).

Possible explanations for this phenomenon are:

(a) Adsorption of metal atoms on the {001} planes, resulting in a decrease in growth rate as postulated by Kamiya and Lang (20).

(b) Surface reconstruction (2x1 type) of the {001} faces, which reduces the number of dangling bonds to more than 50% (77) and thus lowers the interfacial free energy. It was pointed out by van Vechten (78) that surface reconstruction not only occurs at gas -or vacuum- solid interfaces, but also may take place at a liquid-solid interface.

Further investigation to the F-face like appearance of the {001} -"K"- diamond faces would be of great interest.

4. DISSOLUTION

A few diamonds obtained by the previously described growth method showed a completely different surface morphology: From the observation that for these diamonds the edges of the facets were slightly rounded off it was concluded that these deviating surface patterns can be attributed to a short time dissolution at the end of the growth experiments. Probably these crystals were located at a, during the shut off procedure, slightly undersaturated region in the growth chamber. It is more possible, however, that at the final period of an experiment a rise in temperature makes these diamonds slightly dissolved. Somewhat dissolved synthetic diamonds were also found by Bovenkerk (18) and Bezrukov et al. (19).

4.1. Step patterns formed via dissolution

For several of the dissolved diamonds on the {111} faces numerous higher and lower steps could be revealed by application of phase contrast microscopy as can be seen in figures 10 and 11. The orientation and the advancement directions of these steps are represented schematically in figure 6b. From this figure it can be deduced that here the dissolution steps originate from the edges of the crystal faces, which is a commonly occurring phenomenon observed on practically all kinds of slightly dissolved crystals without etch pits. Since on natural diamonds, besides the well known trigons, also steps starting from the edges (many of these diamonds are even rounded off near the edges!) were found (79) it can be concluded that for these crystals after cessation of growth always a slight dissolution occurred.

Another point that can clearly be recognized from figure 6b is that the steps are of $<11\bar{2}>$ type (46), with one dangling bond per step site atom. This can be concluded from the fact that the $<11\bar{2}>$ steps originating from the edges, which represent the intersection lines between two adjacent {111} faces remain straight, whereas the $<\bar{1}\bar{1}2>$ steps originating from the intersection lines between {111}

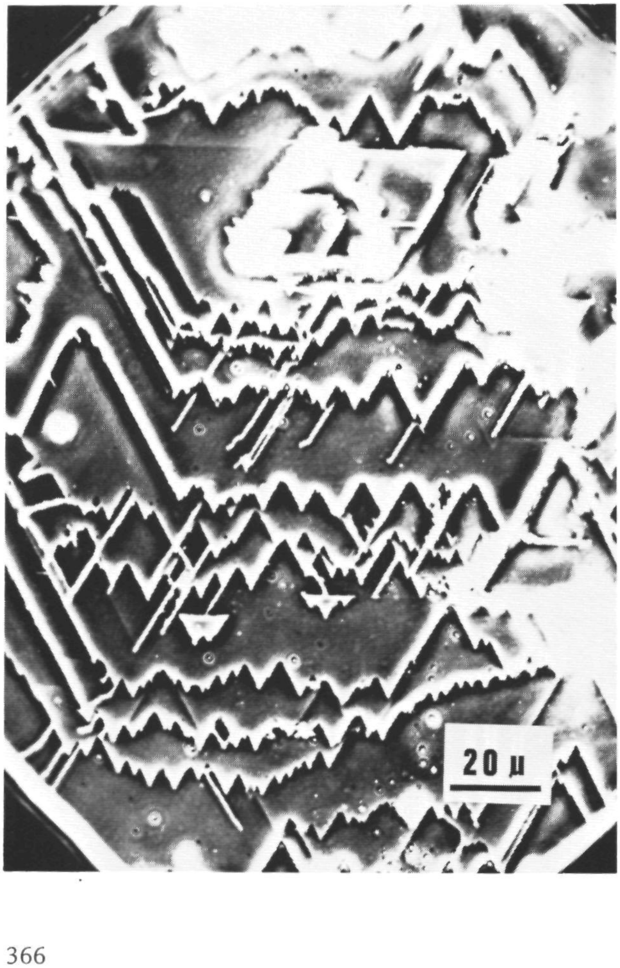

Fig.10. Kinked macrosteps and surface dendrites on a {111} face of a slightly dissolved diamond (PCM).

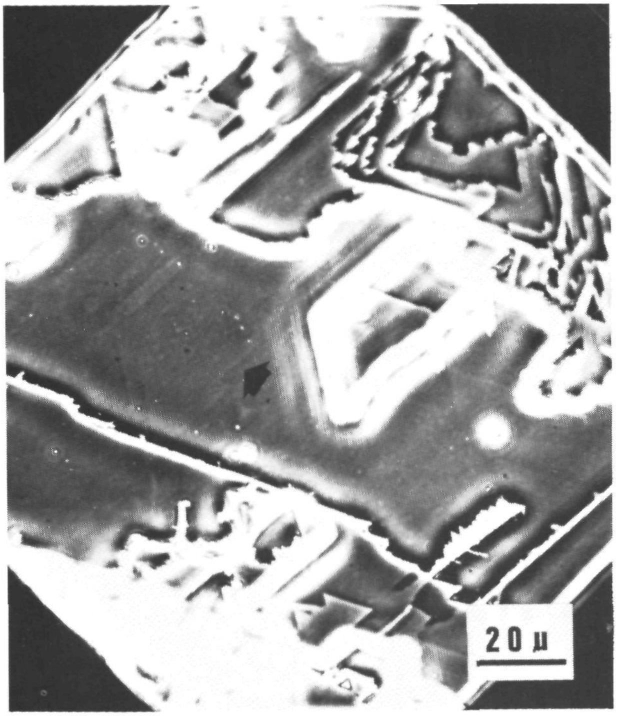

Fig. 11. Extremely low steps situated between macrosteps on a slightly dissolved {111} face. The step indicated by the arrow is about 5 A in height (PCM).

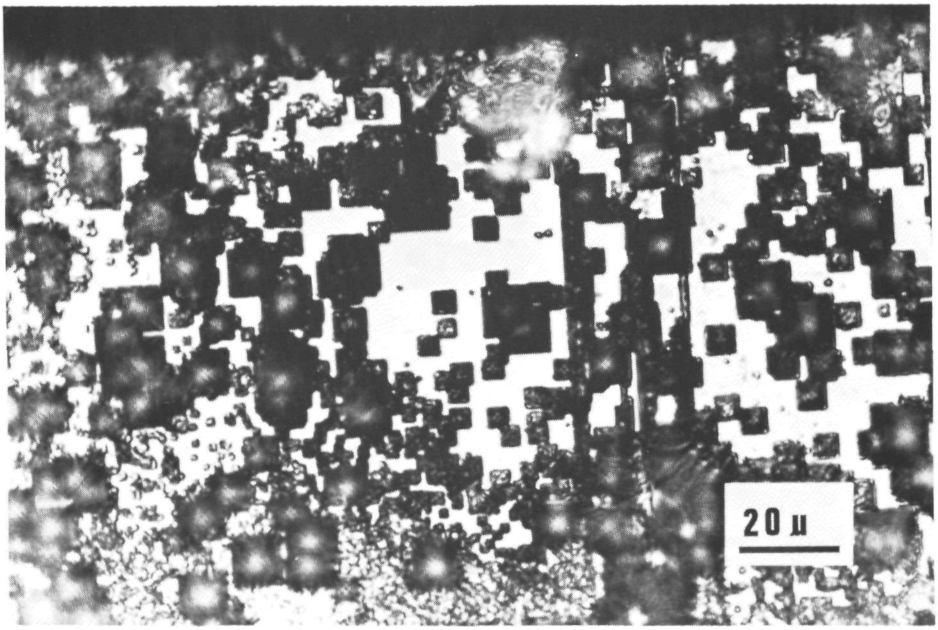

Fig. 12. Etch pit pattern on the {001} faces of the same crystal as shown in figure 10 (Bright field micrograph)

and {100} faces split up into <11$\bar{2}$> steps and thus have a kinked appearance. This means that dissolution of synthetic diamond in molten metal solutions at ultra high pressure also proceeds via a first order broken bond model just like its growth. So dissolution and growth of synthetic diamond can be considered as complementary processes.

On the {111} faces of this type never point bottomed etch pits were found. However, on the {100} faces of the same crystals numerous square point bottom pits, having their edges parallel to the <110> directions could be identified (fig. 12). This observation strongly reinforces the conclusion that these diamonds have been exposed to a slight dissolution after termination of growth.

The dissolution steps on the dissolved {111} faces can be classified into two catagories: Firstly the macrosteps, having heights varying from hundred to several thousand Ångströms as can be seen in figure 10. The steps shown in this micrograph originate from the edge between the {111} face and an adjacent {100} faces and thus have a saw-tooth like appearance consisting of stable <11$\bar{2}$> type steps as described before. Similar zig-zag shaped macrosteps were obseved earlier by Tolansky (4); probably his crystal was also subjected to a slight dissolution. The macrosteps are not a result of a piling up of lower steps (bunching): Observation by phase contrast microscopy showed that these steps were immediately formed at the perifery of the crystal face.

A particularly interesting phenomenon is the occurrence of the second catagory of steps, which are extremely low, at the flat area in between the dissolution macrosteps as can be seen in figure 11. Estimated from the contrast these steps are about 20 Å and lower in height. For instance the step indicated by an arrow in figure 11 probably has a height of 5 Å or maybe even lower! The orientations of the low steps are the same as for the macrosteps. As far as known to us, these steps are by far the lowest ones ever observed on {111} synthetic diamond. Very low steps have been reported earlier for {100} synthetic diamond (16) and for {111} natural diamond (4,5). This observation of dissolution steps and of growth steps (mentioned in section 3.1), both having a height of a few atomic layers permits the conclusion that crystal growth here proceeds via growth (creation (80)) and dissolution (annihulation (80)) units of one or several atoms in size. So the observation of slightly dissolved surfaces strongly strengthens the conclusion drawn in section 3.2. that crystal growth (and dissolutio) of synthetic diamonds can be described in terms of the atomistic or "molecular" layer models developed by Kossel, Stranski and Burton, Cabrera and Frank.

A final point that can be inferred from the dissolution patterns shown in figure 10 is the origin of the dendritic patterns on the {111} diamond faces, observed by several workers (4,14,16,18,19). Up to now two possible explanations for this phenomenon have been given: (i) The surface dendrites represent imprints of the dendritic structure of the solidified metal in contact with the diamond faces, i.e. reflections of the dendrites formed in the freezing metal solution during cooling off at the end of the experiment (18). (ii) The dendrites are formed due to dissolution (4).

In general, the number of surface dendrites covering the crystal faces is so high that it is extremely difficult to study them separately. However, on the slightly dissolved surfaces the number of dendrites is very low, and they have a very well defined appearance in addition. Clear examples of such dendrites can be seen in figure 10: Firstly it can be perceived that the - on the phase contrast micrographs brightly appearing- dendrites are elevations, so these can not be formed via dissolution. Secondly it can be clearly be seen that the dendrites show a crystallographic orientation, namely they are orientated parallel to the <110> directions. This means that these dendrites can not be formed due to a replication of solidifying metal solution dendrites, since these are not expected to follow any crystallographic direction on the substrate.

A better explanation for the formation of the surface dendrites is the occurrence of very fast two-dimensional dendritic growth of diamond due to the occurrence of a -short- extremely high supersaturation at the end of the growth experiment. This hypothesis is strengthened by the observation that the dendrites always originate from a step and that in many cases the heights of the dendrites and the step in question are the same.

So now the formation history of the dendrites can be described in more detail in the following way: During cooling off the supersaturation of the molten metal increases strongly, so that the straight steps are no longer stable. This may lead to the formation of a "fold" that immediately grows out to a dendrite. The dendritic patterns observed by Bovenkerk in the solidified metal (18), probably are replicas of the dendrites formed on the diamonds.

4.2. Etch pits

On a very few of the dissolved diamonds, instead of the previously described step pattern consisting of higher and lower steps numerous etch pits were found. A representative octahedral surface region dotted with pits is shown in figure 13a, while their orientation with respect to the external morphology of the crystals is given in figure 6c. From these pictures it can be recognized that the etch pits have a positive orientation (9,44), which means that, quite surprisingly, here etching proceeds via $\langle\bar{1}\bar{1}2\rangle$ steps instead of the $\langle 11\bar{2}\rangle$ steps observed on all the other growth and dissolution {111} faces. Similar positively oriented etch pits formed via a dissolution process in the growth chamber have been reported earlier by Bovenkerk (18). The positive

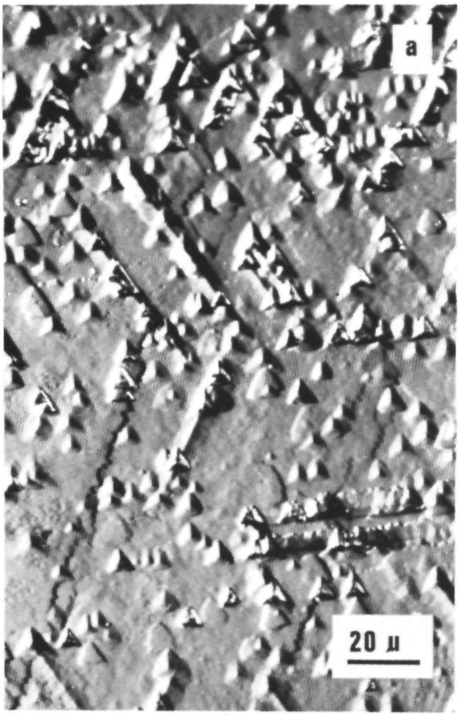

Fig.13. (a) Positively oriented point bottomed etch pits on a slightly dissolved diamond {111} face (DIM).

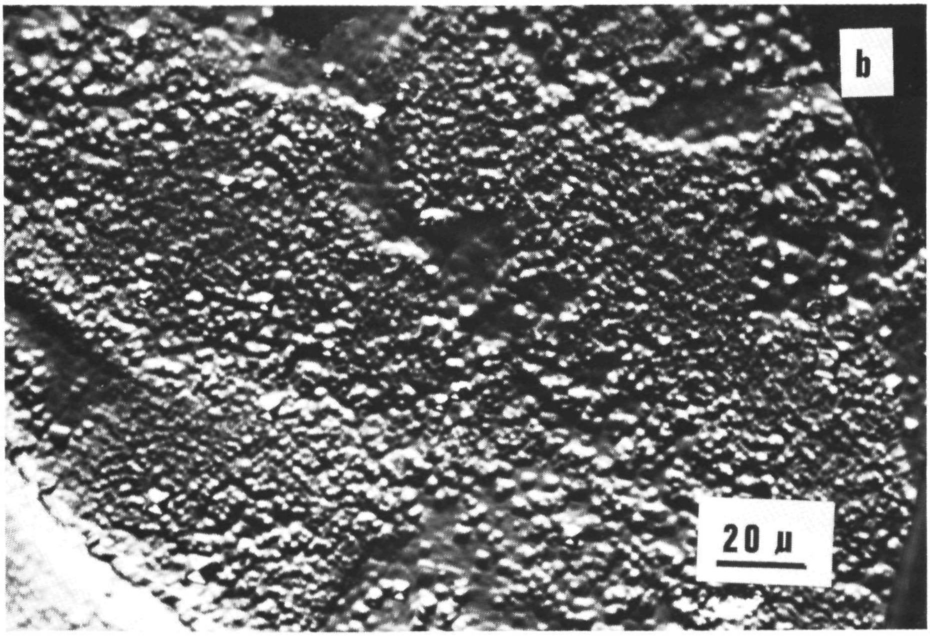

Fig.13. (b) Dissolved {001} face of the same crystal as in (a)(DIM).

orientation of the trigons implies that the formation of these pits proceeded via a mechanism differing from the growth and dissolution processes described before. Possibilities for the sudden stabilisation of the according to the first order broken bond model kinked <$\bar{1}\bar{1}2$> steps are, for instance, adsorption of impurity atoms, like oxygen, forming a bridge between adjacent step atoms (46,81,82) or maybe even step reconstruction.

The etch pattern on the {001} faces of the same crystal as given in micrograph 13a is shown in figure 13b. It can clearly be seen that also for the cubic faces the surface morphology is completely different from the surface pattern of the other slightly dissolved crystals presented in figure 12. This confirms the deviating etching process for the present case.

It is very likely that the trigonal etch pit are dislocation pits and thus mark the outcrops of dislocations at the {111} faces. Two reasons for this supposition can be given: Nearly all pits are point bottomed and uniform in size; (ii) Often the pits are arranged in rows, which can be interpreted as low angle grain boundaries.

The inclinations of the pit sides is not equal for all the pits; several pits are steeper than other ones as can be deduced from the variations in contrast on DIM micrograph 13a. A similar variation in slopes of etch pits was also observed for the trigons on {111} natural diamond (9). Probably this diversity in slope is due to a difference in Burgers vector of the dislocations related to the pits. A further point is that the distribution of the etch pits over the octahedral facets is, aside from the frequently occurring ordering in rows, quite random. This is in agreement with the uniform dislocation outcrop distribution, already elucidated in section 3.3. and discussed in full detail in part II.

Aside from the crystallographic orientation the -positive- etch pits appear very similar to the -negative- trigons on natural diamond. On as-grown non-dissolved surfaces of synthetic diamonds never pits but only hillocks have been observed, which means that during growth no pits are formed. So on basis of an analogy between synthetic and natural diamond it is now strongly suggested that the "growth" trigons on natural diamonds are formed via a dissolution process. This once more confirms the dissolution theory for the trigon formation on natural diamond, which was already gaining ground during the last ten to twenty years.

5. CONCLUSIONS

From the present detailed surface microtopographic study of synthetic diamonds, employing highly sensitive phase and differential interference contrast microscopy combined with two and multiple beam interferometry the following conclusions can be formulated:

(i) Crystal growth of the octahedral faces of synthetic diamonds proceeds via low growth steps, 25-50 Å or lower in height oriented in conformity with the first order broken bond model.

(ii) In general, these steps originate from triangular growth hillocks, which in several cases are located above inclusions underneath the crystal surfaces. From the relation between hillock centres and dislocation outcrops it is strongly suggested that these hillocks are growth spirals.

(iii) The occurrence of very shallow square hillocks and bunches on the {001} faces strongly points to the occurrence of a stepflow mechanism involving very low steps for these faces. This is in contradiction to the PBC theory according to which {001} diamond should be a K (i.e. a non-stepped, rough) face.

(iv) Diamonds that are slightly dissolved in the growth chamber at the end of the growth experiment show high and very low (sometimes as low as 5Å!) dissolution steps on the {111} faces, the orientation of which is the same as for growth. On the {001} faces of the same diamonds well developed square point bottomed etch pits could be discerned.

(v) The well known surface dendrites on {111} diamond are not a result of dissolution or an imprint of metal dendrites near the diamond surfaces, but are due to very fast two-dimensional dendritic growth of diamond.

(vi) On a very few diamonds on the {111} faces positively oriented etch pits were found, the step orientation of which is opposite from all the other observed diamonds. In this case dissolution proceeds via an other -unknown- mechanism.

All the observed surface patterns on the synthetic diamonds grown from liquid metal alloys at ultra high pressures are very similar to the surface morphologies of solution grown crystals. This gives strong evidence that synthetic diamond does not grow via a catalytic process or via a solid state transition but is a typical case of solution growth.

ACKNOWLEDGEMENTS

One of the authors (Liu Guang-zhao) wishes to thank all the collaborators of the Laboratory of Solid State Chemistry, Catholic University of Nijmegen, where this work was carried out, for their kind help.

W.J.P. van Enckevort acknowledges the support of the Netherlands Foundation for Pure Research (ZWO/SON).

REFERENCES

(1) S. Tolansky, The Microstructure of Diamond Surfaces (N.A.G. Press Ltd., London, 1955).

(2) S. Tolansky, Surface Microtopography (Longmans, London, 1960) p.71.

(3) S. Tolansky, in: Physical Properties of Diamond, Ed. R. Berman (Claradon, Oxford,1965).

(4) M. Moore, in: Properties of Diamond, Ed. J. Field (Academic Press, 1979) pp. 245-277.

(5) I.Sunagawa, K. Tsukamoto and T. Kasuda, to be published.

(6) H. Komatsu and A.R. Lang, Mineral. Soc. Japan, Proc. IMA Vol., Spec. Pap. 1.

(7) A.R. Lang, in: Properties of Diamond, Ed. J. Field (Academic Press, 1979) pp. 425-469.

(8) F.C. Frank and A.R. Lang in: Physical Properties of Diamond, Ed. R. Berman (Claradon, Oxford, 1965) pp. 69-115.

(9) A.R. Lang, Proc. Roy. Soc. (London) A278 (1964) 234.

(10) P. Bennema, J.P. van der Eerden, W.J.P. van Enckevort, B. van der Hoek and K. Tsukamoto, Phys. Stat. Sol. (a) 55 (1979) 403.

(11) H. Kanda, S. Yamaoka, N. Setaka and H. Komatsu, J. Crystal Growth 38 (1977) 1.

(12) J.C Angus and T.J. Dyble, Surface Science 50 (1975) 157.

(13) K. Nassau and J. Nassau, J. Crystal Growth 46 (1979) 157.

(14) F.P. Bundy, H.T. Hall, H.M. Strong and R.H. Wentorf Jr., Nature 176 (1955) 51.

(15) S. Tolansky, Proc. Roy. Soc. A 263 (1961) 31.

(16) S. Tolansky and I. Sunagawa, Nature, London 184 (1959) 1526.

(17) S. Tolansky and I. Sunagawa, Nature, London 185 (1960) 203.

(18) H.P. Bovenkerk, in: Progress in Very High Pressure Research, Eds. F.P. Bundy, W. Hibbard and H.M. Strong (John Wiley and Sons, Inc., New York, 1961) p.58.

(19) G.N. Bezrukov, V.P. Butuzov and D.F. Korolev, in: Growth of Crystals, vol 7, Ed. N.N. Sheftal (Cons. Bureau, New York, 1969) p. 91.

(20) Y. Kamiya and A.R. Lang, J. Appl. Phys. 36 (1965) 579.

(21) A.R. Lang, Phil. Mag. B 41 (1980) 689.

(22) G.S. Woods and A.R. Lang, J. Crystal Growth 28 (1975) 215.

(23) A.S. Vishnevsky, J. Crystal Growth 29 (1975) 296.

(24) G. Muncke, in: Properties of Diamond, Ed. J. Field (Academic Press, 1979) pp. 473-499.

(25) W.J.P. van Enckevort and Liu Guang-zhao, J. Crystal Growth to be published; Chapter XX.

(26) Li Da-miy, Liu Guang-zhao and Zhia Jien-xie, Scientific Bulletin 6 (1978) 356 (in Chinese).

(27) Liu Guang-zhao, Acta Physica Sinica 28 (1979) 334 (in Chinese).

(28) H. Beyer, Theorie und Praxis der Interferenzmikroskopie (Akad. Verlaggesellschaft Geest & Portig K.-G, Leipzig, 1974).

(29) H. Komatsu in: Crystal Growth and Characterization, Eds. R. Ueda and J.B. Mullin (North Holland, Amsterdam, 1975) p.333.

(30) I. Sunagawa, Amer. Mineralogist 46 (1961) 1216.

(31) I. Sunagawa, J. Crystal Growth 45 (1978) 3.

(32) H. Komatsu, private communication.

(33) K. Tsukamoto, private communication.

(34) S. Amelinckx and G. Strumane in: Silicon Carbide: A High Temperature Semiconductor, Proc. Conf. of Silicon Carbide, Boston, 1959, Eds. J.R. O'Connor and J. Smiltens (Pergamon, New York, 1960) pp. 162-201.

(35) Ajit Ram Verma, Nature 167 (1951) 939.

(36) W.J.P. van Enckevort, P. Bennema and W.H. van der Linden, Z. Phys. Chemie (Neue Folge) 124 (1981) 171; Chapter II.

(37) W.J.P. van Enckevort and H. Klapper, J. Crystal Growth to be published.

(38) P. Bennema, J.P. van der Eerden, W.J.P. van Enckevort, B. van der Hoek and K. Tsukamoto, Phys. Sat. Sol. (a) 55 (1979) 403.

(39) S. Tolansky, Surface Microtopography (Longmans, London, 1960).

(40) I. Sunagawa, in: Crystal Growth and Characterization, Eds. R. Ueda and J.B. Mullin (North Holland, Amsterdam, 1975) p.347.

(41) W.J.P. van Enckevort, H.J. Human and W.H. van der Linden, J. Crystal Growth to be published; Chapter III.

(42) W.J.P. van Enckevort, R. Janssen van Rosmalen and W. H. van der Linden, J. Crystal Growth 49 (1980) 502; Chapter VIII.

(43) W.J.P. van Enckevort and W.H. van der Linde, J. Crystal Growth 47 (1979) 196; Chapter I.

(44) F.C. Frank, K.E. Puttick and L.M. Wilks, Phil. Mag. 3 (1958) 1262.

(45) A.R. Lang, Proc. Roy. Soc. (London) A278 (1964) 234.

(46) W.J.P. van Enckevort and L.J. Giling, J. Crystal Growth 45 (1978) 90; Chapter XII.

(47) W.J.P. van Enckevort and J.P. van der Eerden, J. Crystal Growth 47 (1979) 501. Chapter XIII.

(48) W. Kossel, Nachr. Ges. Wiss. Goettingen, Math. Physik Kl II a (1927) 135-143.

(49) I.N. Stranski, Z. Phys. Chem. 136 (1928) 259.

(50) W.K. Burton, N. Cabrera and F.C. Frank, Philos. Trans. R. Soc. London 243 (1951) 299.

(51) B. van der Hoek, P.Bennema and J.P. van der Eerden, J. Crystal Growth accepted.

(52) I. Sunagawa and P. Bennema, J. Crystal Growth 46 (1979) 451.

(53) A.R. Patel, Physica 27 (1961) 1097.

(54) A.R. Patel, Physica 28 (1962) 44.

(55) H.J. Human and W.J.P. van Enckevort, J. Crystal Growth to be published; Chapter IV.

(56) H.J. Human, Thesis, University of Nijmegen, The Netherlands (1981).

(57) S. Amelinckx in: Solid State Physics, Suppl. 6, "The Direct Observation of Dislocations", Ed. F. Seitz and D. Turnbull (Academic Press, New York, 1964) p.16.

(58) K. Sato, K. Yokoyama, H. Kouchi and M. Okado, Jap. J. Appl. Phys. 17 (1978) 1483.

(59) K. Sato, Jap. J. Appl. Phys. 19 (1980) 1257.

(60) K. Sato, M. Komikado, M. Okada and T. Seto, Jap. J. Appl. Phys. 20 (1981) 495.

(61) L.S. Palatnik and L.I. Gladkikh, Soviet Phys. Dokl. 16 (1972) 763.

(62) Y.A. Litvin, Inorgan. Mater. 4 (1968) 144.

(63) K. Nassau and J. Nassau, J. Crystal Growth 46 (1979) 157.

(64) I. Sunagawa, private communication.

(65) P. Bennema, in: Industrial Crystallization (Ed. J.W. Mullin, Plenum Press, 1976) p. 91.

(66) B.K. Tanner, X-Ray Diffraction Topography, I.S. Science of the Solid State, Vol 10 (Pergamon,1976).

(67) S. Gits-Leon, F. Lefaucheux and M.C. Robert, J. Crystal Growth 44 (1978) 345.

(68) W.J.P. van Enckevort and J. Odekerken, Phil. Mag. to be published; Chapter V.

(69) R.A. Ducket and A.R. Lang, J. Crystal Growth 18 (1973) 135.

(70) H.M. Strong and R.E. Hanneman, J. Chem. Physics 46 (1967) 3668.

(71) F.C. Frank, in: Crystal Growth and Perfection of Crystals (Wiley, New York, 1958) p.411.

(72) N. Cabrera and D.A. Vermilya, in: Growth and Perfection of Crystals (Wiley, New York, 1958) p.393.

(73) P. van der Putte, W.J.P. van Enckevort, L.J. Giling and J. Bloem, J. Crystal Growth 43 (1978) 659; Chapter XV.

(74) P. Hartman, in: Crystal Growth: An Introduction, Ed. P. Hartman (North Holland, Amsterdam, 1973) p.367.

(75) B. Dam and W.J.P. van Enckevort, J. Crystal Growth 51 (1981) 607.

(76) E. Bauser and H. Strunk, J. Crystal Growth 51 (1981) 362.

(77) W.S. Verwoerd, Surface Science 103 (1981) 404.

(78) J.A. van Vechten, IBM Research Report RC 6418 (27697) 3/3/77 Solid State Physics.

(79) H. Kanda, S. Yamaoka, N. Setaka and H. Komatsu, J. Crystal Growth 38 (1977) 1.

(80) G.H. Gilmer and P. Bennema, J. Appl. Phys. 43 (1972) 1347.

(81) T. Evans and D.H. Sauter, Phil Mag. 6 (1961) 429.

(82) A.V. Varshavsky, Extended Abstracts ICCG6, Moscow (1980), Volume IV p. 149.

CHAPTER XX:
MICROTOPOGRAPHY OF SYNTHETIC DIAMONDS

PART II: DEFECTS IN RELATION TO GROWTH

W.J.P. van Enckevort and Liu Guang-zhao*

RIM Laboratory of Solid State Chemistry, Catholic University, Faculty of Science, Toernooiveld, Nijmegen, The Netherlands

ABSTRACT

The internal defect structure of synthetic diamond grown from molten metal solutions at ultra-high pressures has been studied by a wide variety of characterization methods, viz. etch pit techniques, optical transmission and stress birefringence microscopy, scanning electron microscopy, Lang topography, X-ray absorption topography and optical absorption topography. From these studies it was shown that the dislocation outcrop distribution at the crystal faces was quite random, since most of these dislocations were generated from inclusions located at growth sector boundaries. For lower quality crystals "hollow" tubes, filled with solidified metal or graphite, at the cores of dislocations with high Burgers vectors were found. In addition to the dislocations two types of inclusions were identified: (i) Type A, being solidified metal solution inclusions formed via a mechanism involving step overhangs and (ii) Type B, occurring near sector boundaries and the trajectories of the vertices of the crystal, which very probably are graphite inclusions formed due to a higher local supersaturation occurring near the edges or angular points of the crystals. Finally the distribution of paramagnetic nitrogen impurity over the different growth sectors was studied by application of optical absorption topography, demonstrating that the nitrogen concentration was by far higher for the {001} sectors compared to the {111} sectors.

1. INTRODUCTION

Up to now the internal defect structure of synthetic diamonds, grown from molten metal solutions at ultra-

---

*Present adress: Shanghai Institute of Ceramics, Chinese Academy of Sciences, Shanghai, The people's Republic of China.

high pressures, has been investigated by several workers. One of the earliest was van Bovenkerk (1), who used optical transmission microscopy to obtain an impression of the occurrence of inclusions and the colours of the diamonds. The most important work in this field has been carried out by Lang and coworkers, who applied a wide diversity of characterization methods to study the defect structure of artificial diamonds (2). In the first place they employed X-ray diffraction projection and section topography, combined with X-ray absorption topography in order to clarify the dislocation structure and the distribution of solidified metal inclusions in the crystals (3). In a later work Woods and Lang (4) presented a very detailed study in which a few synthetic diamonds were characterized by a multitude of topographic techniques, such as X-ray diffraction topography, visible light cathodoluminicence topography, optical absorption topography and Nomarsky interference microscopy of polished crystal sections to differentiate the various growth sectors . By these methods several aspects of the internal structure were uncovered, among others a difference in growth banding and overall cathodolunminicence for the various growth sectors, a dependence of the content of paramagnetic nitrogen impurity on the type of growth sector and the generation of -decorated or nondecorated- dislocations from sector boundaries. A similar cathodoluminicence study of growth sectors and growth bands was also carried out by Vishnevsky (5). In addition to the visible light cathodoluminicence Lang recently also reported the occurrence of infrared cathodoluminicence, which was only detectable for the {111} growth sectors (6).

For natural diamonds similar studies of the defect structure were made by numerous workers, such as Lang (2, 7,8), Woods (9), Kiflawi and Lang (10), Sunagawa et al. (11) and Harrison and Tolansky (12). In addition to above mentioned techniques also UV absorption (13), stress birefringence microscopy (13) and electron microscopy (2) was applied.

In the above cited studies of the inner structure of synthetic diamonds, hardly any relation was made between crystal growth and defect formation, probably because of a lack of knowledge about the growth mechanism of these artificially grown crystals. However, in a previous work (14), in the following referred to as part I, a deeper insight in the growth mechanism of synthetic diamonds was obtained from a detailed study of the surface morphology using highly sensitive optical microscopic techniques. The main conclusion drawn in this work was that, despite a lot of speculations in literature, growth of synthetic diamond is a typical case of crystal growth from solution and can be described qualitatively by the generally accepted spiral growth theory formulated by Burton, Cabrera and Frank (15). Since it is well established that the majority of defects in crystals is formed during the growth process (See for instance (16,17)) it is highly important to study the internal structure of the synthetic diamonds from the viewpoint of theories of crystal growth from solution. Therefore in the present work several types of defects are studied by making use of a wide variety of techniques in order to get a better understanding of their formation mechanisms in terms of these solution growth models. Such an insight is essential to find the way to grow -almost- defect free crystals of highest gem quality.

2. Experimental

The specimen crystals used for the present investigation of the internal defect structure of synthetic diamond were grown from molten metal solutions at ultra-high pressures at the Shanghai Institute of Ceramics, Chinese Academy of Sciences, as described in part I.

In order to study the dislocation structure of the crystals three different characterization methods were applied:
(i) Selective etching, to mark the end points of dislocation lines at the crystal surfaces as etch pits, with the aim of getting an insight of the dislocation outcrop distribution over the crystal surfaces. Etching was carried out by slightly dissolving the diamonds in fused KNO_3 at 655 ^oC for varying periods of time (from 5 to 30 minutes). In this way well developed point bottomed dislocation etch pits and flat bottomed pits related to surface or localized -point- defects can be obtained as described by Patel (18,19) and in part I.
(ii) Lang topography (20), using $CuK\alpha_1$ radiation (λ = 1.5406 A) in combination with the ultra-fine grained photographic Ilford L4 Nuclear Emulsion in order to record as much as possible detailed picture of the tiny ($\sim$1 mm in size) crystals. For obtaining the topographs use was made of the strong reflections {220} and {111}.
(iii) Stress birefringence microscopy, by making use of a high quality polarization microscope. This method, maybe less current than X-ray diffraction topography, is a well approved technique to observe dislocations in -mostly optically isotropic- crystals (21,22,23). An earlier stress birefringence study on natural diamonds was carried out by Lang (13), who suggested that small bundles of dislocations with a resultant Burgers vector of 3 to 4 unit Burgers vectors can be detected by this method. The birefringence method is an extremely powerful tool for investigating the relationship between dislocations and inclusions as was demonstrated for potash alum by van Enckevort and Odekerken (24).

The properties of inclusions in the synthetic diamonds were investigated by three other characterization techniques:
(i) Optical bright field transmission microscopy, to observe all kinds of inclusions and "hollow" tubes, filled with foreign opaque materials, occurring at the cores of

some dislocations with high Burgers vectors.
(ii) X-ray absorption topography in order to get information on the composition of the various types of inclusions, namely whether they are metal or graphite inclusions. The clue of this method is that due to an extremely large difference between the absorption coefficients of diamond and solvent metal for copper X-ray radiation, metal inclusions as small as a few microns can easily be identified in the crystals. In contrast to the work carried out by Kamiya and Lang (3), in the present case no monochromatic CuKα or CuKβ radiation, but unfiltered copper radiation was used. This non-monochromaticy did not affect the results because now no pure Ni, but an alloy of Ni, Fe and Mn (14) was used as a solvent to grow the diamonds, which implies that, in contrast to the pure Ni case, the absorption coefficients for CuKα and CuKβ are are approximately similar and thus the monochromaticy of the radiation is less important. The absorption coefficient for copper radiation of the 40% Ni - 30% Fe - 30% Mn alloy used for growing the diamonds equals very roughly about 1800 cm^{-1} , which means that inclusions of ∿4μ in diameter already give rise to a local intensity decrease of 50%. The absorption topographs were recorded on the ultrafine grain Ilford L4 Nuclear Emulsion.
(iii) Scanning electron microscopy (SEM) to get a clear three-dimensional view of the "entrances" of inclusions at the diamond surfaces at higher magnifications. This is of high importance to unravel the formation history of the various kinds of inclusions.

For studying the distribution of paramagnetic nitrogen, manifesting as a yellowish colour in the diamonds, optical absorption topography was applied in a similar manner as described by Woods and Lang (4). This optical topographic method was carried out by making use of a standard optical transmission microscope combined with a high pressure mercury light source, fitted with a wide band monochromator filter (wavelength: ∿425 nm).

3. OBSERVATIONS AND DISCUSSIONS

3.1. Dislocation structure

3.1.1 Etch pits

Figure 1 shows a typical etch pit pattern on a {111} surface of synthetic diamond, formed after etching in fused KNO_3. As to be expected hardly no difference between the present etch pattern and the pattern observed by Patel (18, 19) on etched natural diamonds can be seen. Several types of pits can be distinguished:
(i) Flat bottomed pits, formed as a result of dissolution around localized stress fields, which probably are rela-

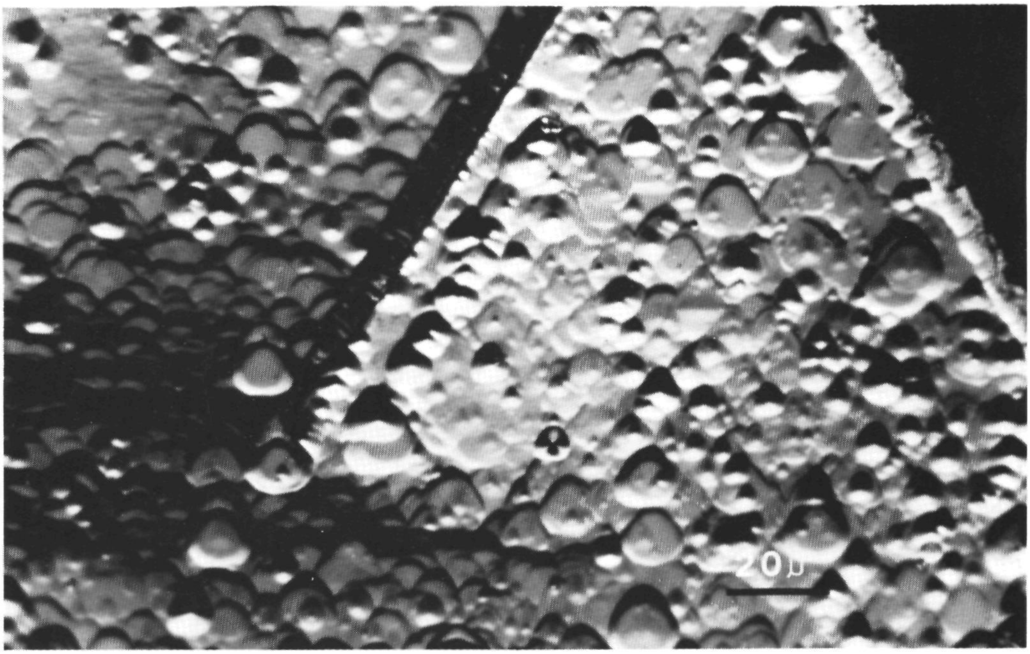

Fig. 1. Typical etch pit pattern on {111} diamond, formed after slight dissolution in fused KNO_3 (Differential interference contrast micrograph).

ted to point defects or inclusions. After etching away of such a local defect, only lateral expansion of the side faces of the pits occurs, whithout continuation of the vertical etching, which leads to the formation of flat bottomed pits. Since nearly all flat bottomed pits are of equal and, compared to the other pits, of maximal size it can be concluded that these are formed at the first beginning of the dissolution process. This allows the conclusion that this kind of etch pits are generated due to localized surface defects, probably formed during the shut off procedure at the end of the growth experiment.
(ii) Point bottomed pits of varying size and with various inclinations of the side walls. Probably these are related to line defects, i.e. dislocations (18) with different orientations and Burgers vectors. Despite the fact that no one to one relation between dislocations and etch pits has been established, the density of point bottomed pits still gives a good qualitative indication of the crystalline quality.
(iii) Etch grooves, very probably related to outcrops of two-dimensional (planar) defects, for instance stacking

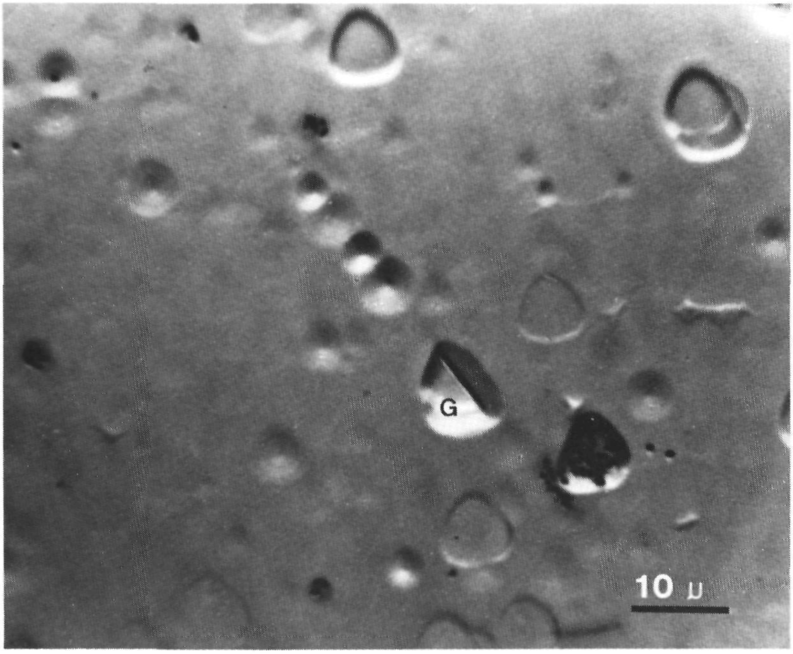

Fig.2. Etch groove (G) and etch pits on {111} diamond, formed after slight dissolution in molten KNO_3 (Differential interference contrast micrograph).

faults (2) or nitrogen platelets (2) at the crystal surfaces. A characteristic example of such a localized groove is given in figure 2. For a detailed treatise on the topic of etch groove formation the reader is referred to reference (25).

Concerning the distribution of the point bottomed dislocation etch pits over the {111} surfaces it is to be noted that there is no strong preferential occurrence of etch pits near the centres of the {111} faces. This means that the dislocation outcrop distribution over a given octahedral facet is quite random, which is in conformity with the random distribution of growth hillocks related to dislocations as discussed in part I. Such a random occurrence of dislocation outcrops at the 111 synthetic diamond faces is in complete contradistinction to the preferred occurrence of dislocations at the central regions of crystal faces as was observed for other solution grown -cubic- crystals like natural diamond (7), potash alum (24,26), urotropine (17,27), NaCl (28) and others (17). This topic will be treated further in a subsequent section.

Another typical aspect of the point bottomed etch pits is their preferential ordering in rows as can be seen in figure 1 and 2. These rows can be interpreted as low angle grain boundaries in a similar way as for potash alum (29) and $NiSO_4$ aq (30). In a few cases a weak relationship was found between a local increase in etch pit density at the crystal surface and the occurrence of a liquid inclusion just underneeth.

Finally it is to be mentioned that the density of the point bottomed dislocation etch pits (as well as of the flat bottomed pits) varies strongly from crystal to crystal, which indicates that the crystalline perfection of the diamonds differs largely for each individual crystal.

3.1.2. Lang topography

To carry out X-ray diffraction topography, better quality specimen crystals, with a minimum of inclusions

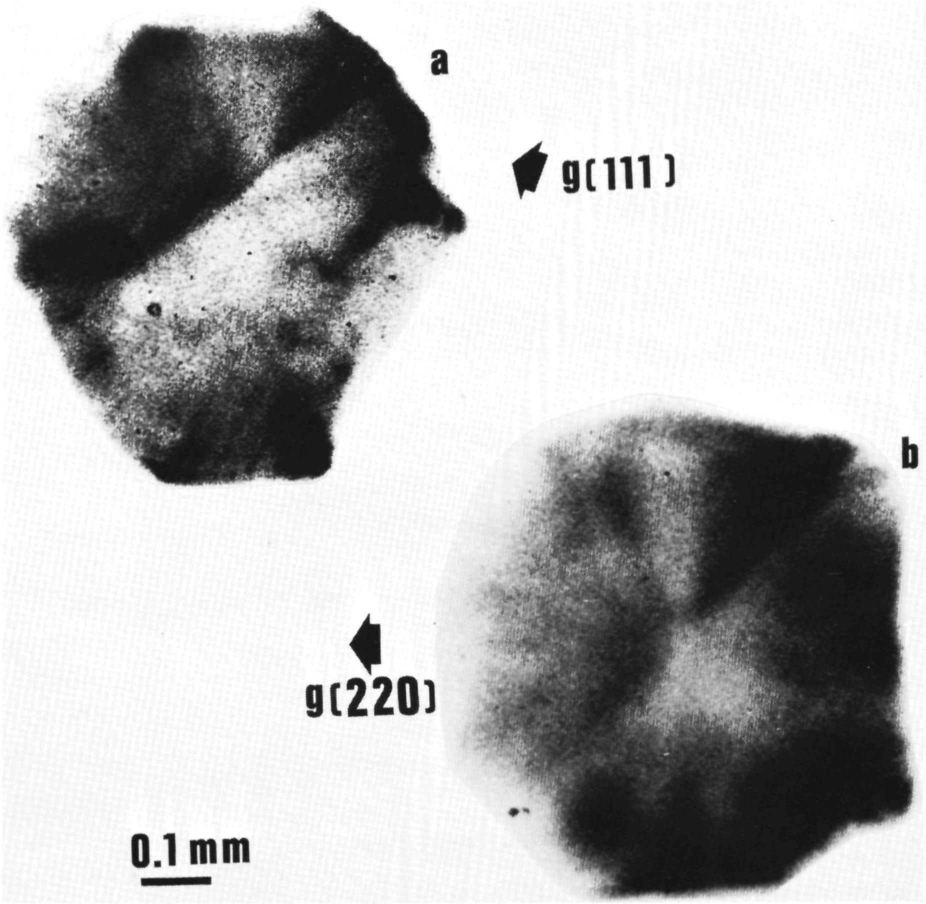

Fig.3. Lang topographs of a better quality specimen crystal: (a) {111} reflection; (b) {220} reflection.

and a very low amount of stress birefringence were selected. Prior to Lang topography the crystals were slightly etched in fused KNO_3 , so that surface defects, which may strongly disturb the X-ray topographic images (3) are eliminated. A typical result is presented in figures 3a and b, showing two topographs of the same crystal, but with the different reflections {111} and {220} respectively.

From the topographs it can be deduced that: (i) No mosaic structure occurs in the better quality crystals, since only extinction and no orientation contrast was found. (ii) Dislocation bundles radiating outwards from central regions and from inclusions to the surfaces dominate the defect structure of the crystals. (iii) Also single dislocations or very narrow dislocation bundles, manifesting as isolated lines on the topographs (indicated by an arrow in figure 3a) could be identified. Whether these lines present dislocations having a Burgers vector of unit length is not clear. All the topographs have a very similar appearance as the topographs of synthetic diamonds made by Kamiya and Lang (3), so for further details the reader is referred to their paper.

3.1.3. Stress birefringence micrography

In contrast to Lang topography, stress birefringence microtopography is a very powerful method to study the

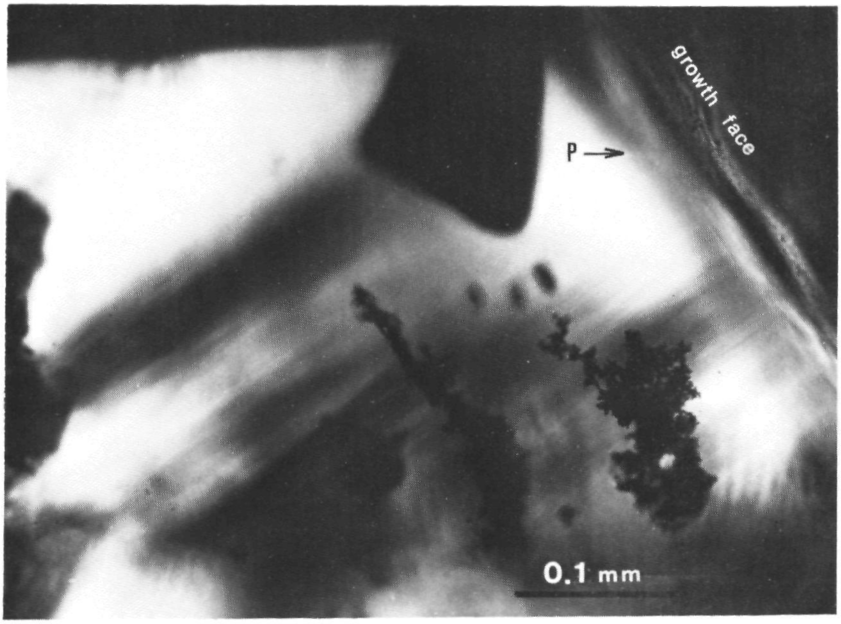

Fig.4. Stress birefringence micrograph of a lower quality diamond crystal showing numerous dislocation lines ending perpendicularly to the crystal surface (P: orientation polarizer).

dislocation structure in lower quality, high dislocation density diamond crystals. A representative birefringence micrograph of such a lower quality crystal is given in figure 4. Clearly numerous dislocation lines running parallel to each other and ending more or less perpendicular to the growth faces can be seen. In general, the dislocations originate from the central nucleus of the diamonds or from inclusions in the crystals. The relationship between inclusions and dislocations can easily be recognized in figure 5. In this polarization micrograph numerous dislocation lines and bundles, starting from a row of inclusions located at the trajectory of one of the vertices of the diamond crystal during growth can be seen. A similar behaviour of inclusions as starting points of dislocation lines was also found for good quality, commercial grade General Electric diamonds. The generation of grown-in dislocations starting from inclusions probably is due to lattice enclosure errors after inclusion formation during crystal growth in the same manner as for KDP (16,31), stearic acid (32) and potash alum (24). Sometimes such a group of dislocations originating from an inclusion may lead to the formation of a growth spiral as described in part I.

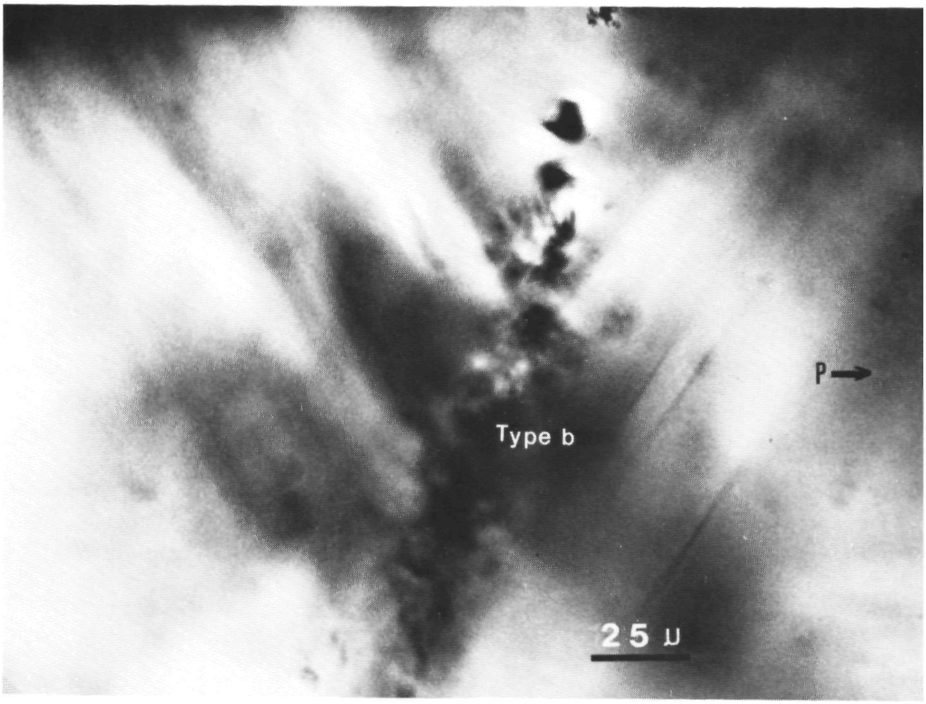

Fig. 5. Stress birefringence micrograph of grown-in dislocation lines originating from a row of type b inclusions (P: orientation polarizer).

In general, the dislocation lines run more or less perpendicular to the growth faces, which is typical for cubic solution grown crystals like potash alum (24,26), urotropine (17,27) and others (17). From the fact that the inclusions from which the dislocations originate are not concentrated in a single central region in the crystal, the more or less uniform distribution of dislocation outcrops over the crystal faces can now easily be understood.

3.1.4. "Hollow" tubes around dislocation lines

At the cores of several dislocation lines "hollow" tubes, filled with solidified metal or another foreign opaque material, were found as shown in figures 6a and b. Figure 6a presents a stress birefringence micrograph, showing a bundle of parallel dislocation lines. A few of them have a very strong contrast, pointing to a high Burgers vector for these lines. As can be seen in figure 6b, application of bright field microscopy revealed a narrow black line of about 0.5µ in width at the core of the dislocation line denoted by an arrow in figure 6a.

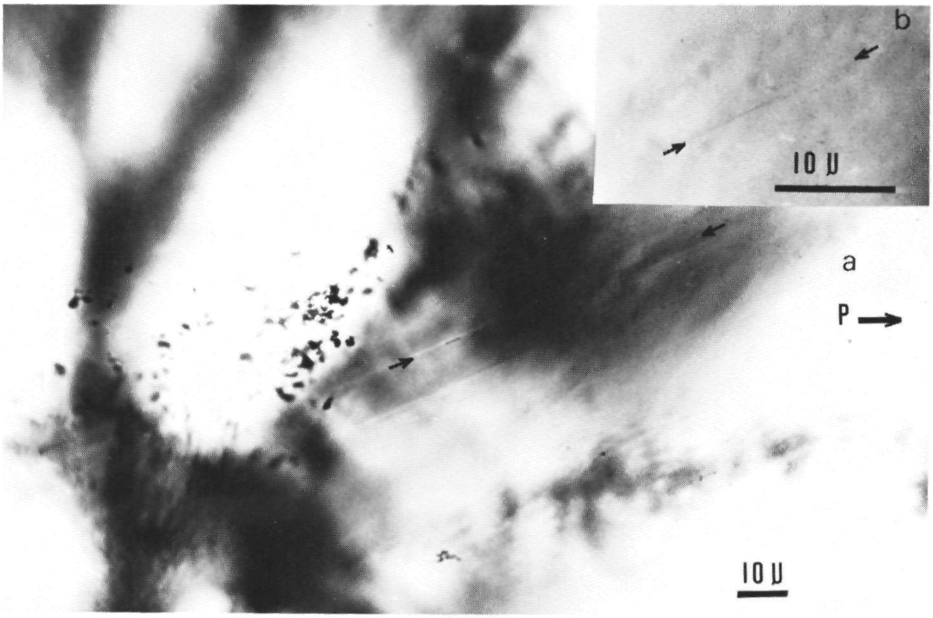

Fig.6. "Hollow" tubes at the cores of dislocations with high Burgers vectors: (a) Stress birefringence micrograph showing a bundle of dislocation lines, a few of which having a high Burgers vector (P: orientation polarizer).(b) High magnification optical transmission micrograph revealing the "hollow" tube at the core of the dislocation indicated by an arrow in (a).

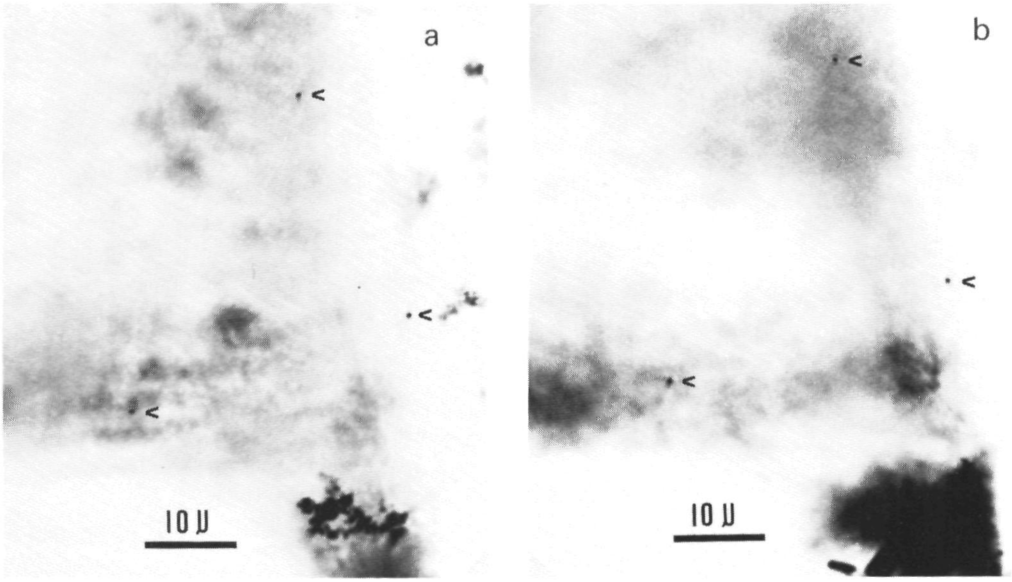

Fig.7. Top view of three "hollow" tubes at the cores of dislocation lines, manifesting as three black dots indicated by arrows. The optical transmission micrographs (a) and (b) show the same area but at different focussing levels.

The black lines at the cores of some dislocations can better be seen from above as shown in figure 7: Bright field micrograph 7a gives such a top view of three "hollow" cores, identificable as three black dots, whereas micrograph 7b gives a similar view but now at a different focussing level. By changing the height of the plane imaged in sharp focus by raising or lowering the specimen with respect to the front lens of the microscope it was possible to trace the "hollow" dislocation lines through the crystal. In general, these "hollow" dislocations originate from the central nucleus or from an inclusion occurring throughout the crystal.

Verification by polarization microscopy showed that the "hollow" cores were only found for dislocations with highly contrasted birefringence images, i.e. with high Burgers vectors, which mostly occur in lower quality crystals. This strongly points to the hypothesis that these "hollow" tubes are the same ones as described theoretically by Frank (33), Cabrera, Levine and Plaskett (34) and by van der Hoek et al. (35). Similar hollow tubes, formed due to high stress fields at the centres of dislocation lines were found for SiC (35) and potash alum (24).

3.2. Inclusions

By application of bright field transmission microscopy two kinds of inclusions could be identified in the synthetic diamonds. Both types of inclusions are shown in figure 8: In the first place, solid, rounded, dendritic or droplet like inclusions can be discerned, which are denoted as "type a" inclusions in the following. Secondly an irregularly shaped, granular, spongy-like inclusion can be recognized, which will further be denoted as "type b". In the following part the specific properties and formation mechanisms of both kinds of inclusions will be discussed in detail.

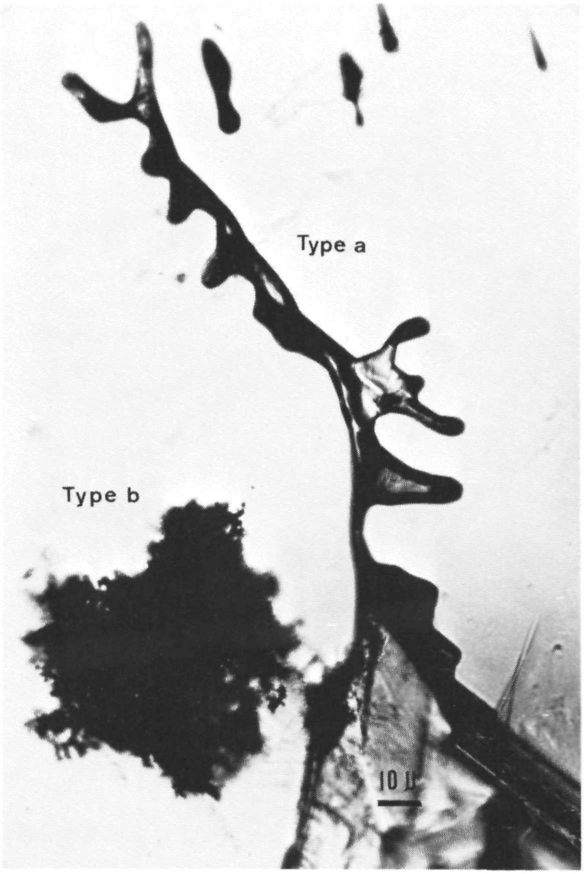

Fig.8. Bright field transmission micrograph presenting characteristic examples of both type a and type b inclusions.

3.2.1. Type a inclusions

To obtain a deeper insight in the formation history of the type a inclusions, a general view SEM micrograph (figure 9a) was made of the very {111} facet, below which the inclusions shown in figure 8 were photographed. This micrograph clearly shows a central depression surrounded by high (∿5μ) macrosteps. In order to clarify the relationship between the type a inclusions and macrostep patterns, of the same surface area as shown in figure 9a a second overall picture was made, but now by application of optical transmission microscopy. From this micrograph, which is presented in figure 9b and the SEM micrograph it can be recognized that numerous type a inclusions are "connected" with the macrosteps. A detailed SEM micrograph of the same region as shown in figure 8, which is given in figure 9c, clearly shows a cavity at the point of connection of the large dendritic type a inclusion of figure 8 with the macrostep. A further aspect of the relationship between inclusions and macrosteps is the preferential formation of type a inclusions at reentrant corners in the macrostep patterns as can be deduced from figure 9b.

The existence of a strict relation between the creation of type a inclusions and the occurrence of macrosteps permits the conclusion that these inclusions are formed in the following manner:

(i) Due to the existence of a large gradient in supersaturation over a given crystal surface, caused by mass or heat transport limited growth, macrosteps are formed (36) (fig. 10a). Since in the case of transport limited growth the supersaturation near the edges of a crystal facet is higher than at the central part (37), the macrosteps move from the periphery towards the centre of this facet. This results in the formation of a central depression bounded by macrosteps as shown in figure 9a and as was observed previously by Tolansky (38).

(ii) When the macrostep reaches a given height, such a step may become unstable, because due to the transport determined growth kinetics, the supersaturation at the top of the step becomes essentially higher than at its lower part. This leads to the formation of an overhang (fig. 10b) as described extensively by Chernov and Budurov (39,40). If a reentrant corner is present in the step pattern, the overhang formation is even facilitated, because now the difference in supersaturation between the top and the bottom part of the macrostep is larger. This can be understood from the fact that now the bottom part is limited by three -solid- faces from which no solute can be supplied. Another phenomenon that provides inclusion formation at reentrant corners is that the reentrant corner may function as a step source for the overhang formation, whereas for simple macrosteps (often being stable crystallographic planes!) growth of over-

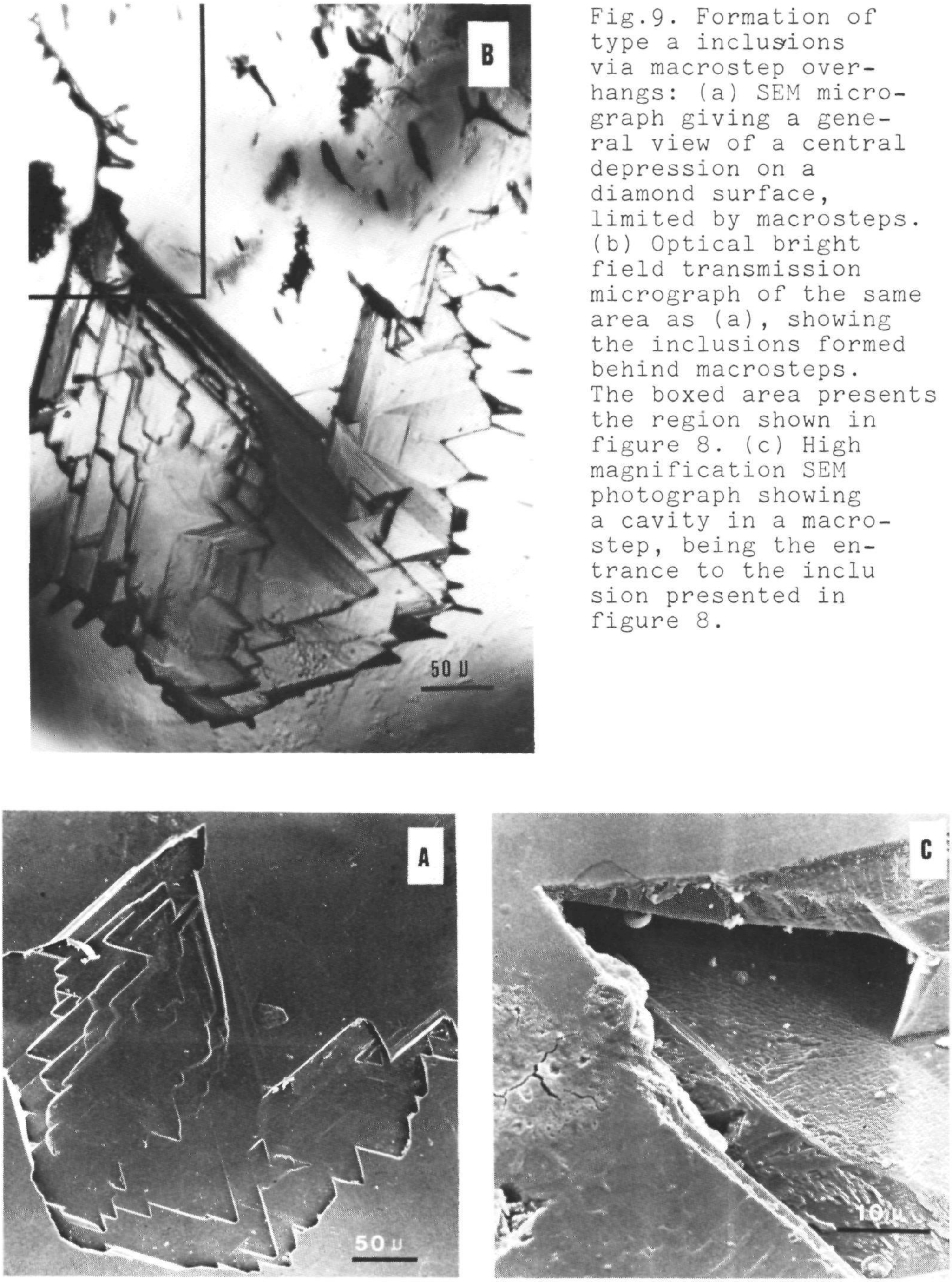

Fig.9. Formation of type a inclusions via macrostep overhangs: (a) SEM micrograph giving a general view of a central depression on a diamond surface, limited by macrosteps. (b) Optical bright field transmission micrograph of the same area as (a), showing the inclusions formed behind macrosteps. The boxed area presents the region shown in figure 8. (c) High magnification SEM photograph showing a cavity in a macrostep, being the entrance to the inclusion presented in figure 8.

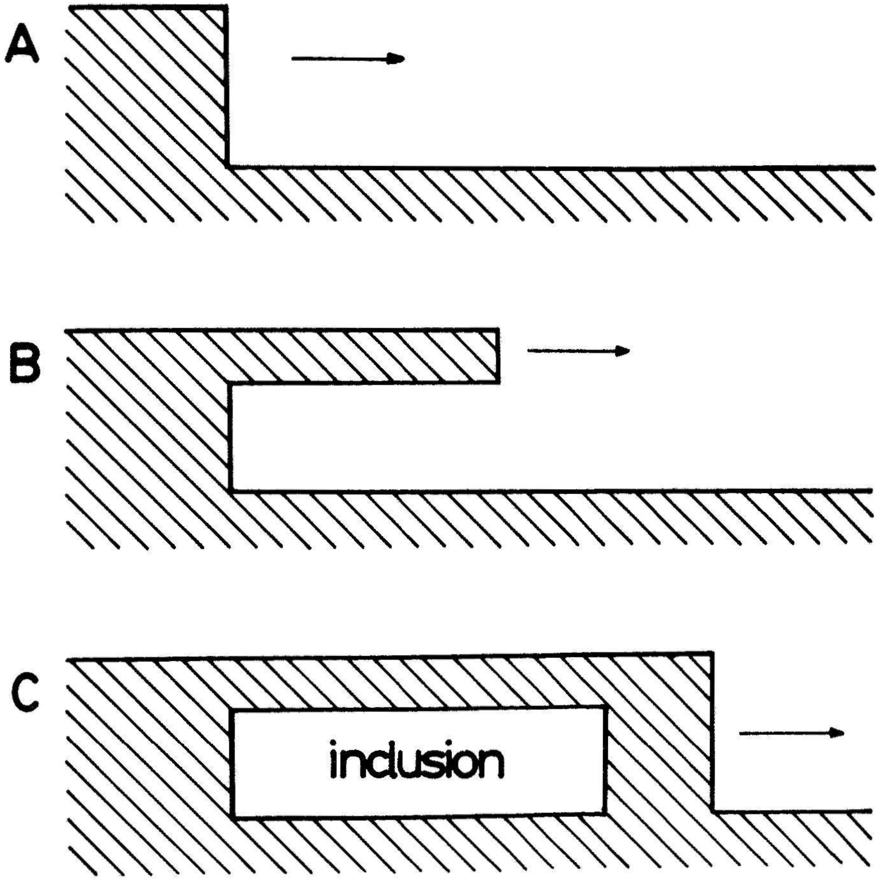

Fig.10. Successive stages of the formation of a type a inclusion involving macrostep overhangs:
(a) Macrostep prior to inclusion formation;
(b) Generation of a step overhang;
(c) Closure of the overhang, entrapping an amount of solution.

hangs must proceed via a slower two-dimensional nucleation mechanism.
(iii) Finally the overhang comes in contact with the basal crystal surface (fig. 10c), leading to a closure of the cavity, after which the type a inclusion is formed.

According to this model for inclusion formation the type a inclusions are entrapments of metal solvent and thus should consist of solidified metal. Application of X-ray absorption topography indeed demonstrates that the type a inclusions contain a large amount of metal, as can be inferred from figure 11: Figure 11b shows an X-ray ab-

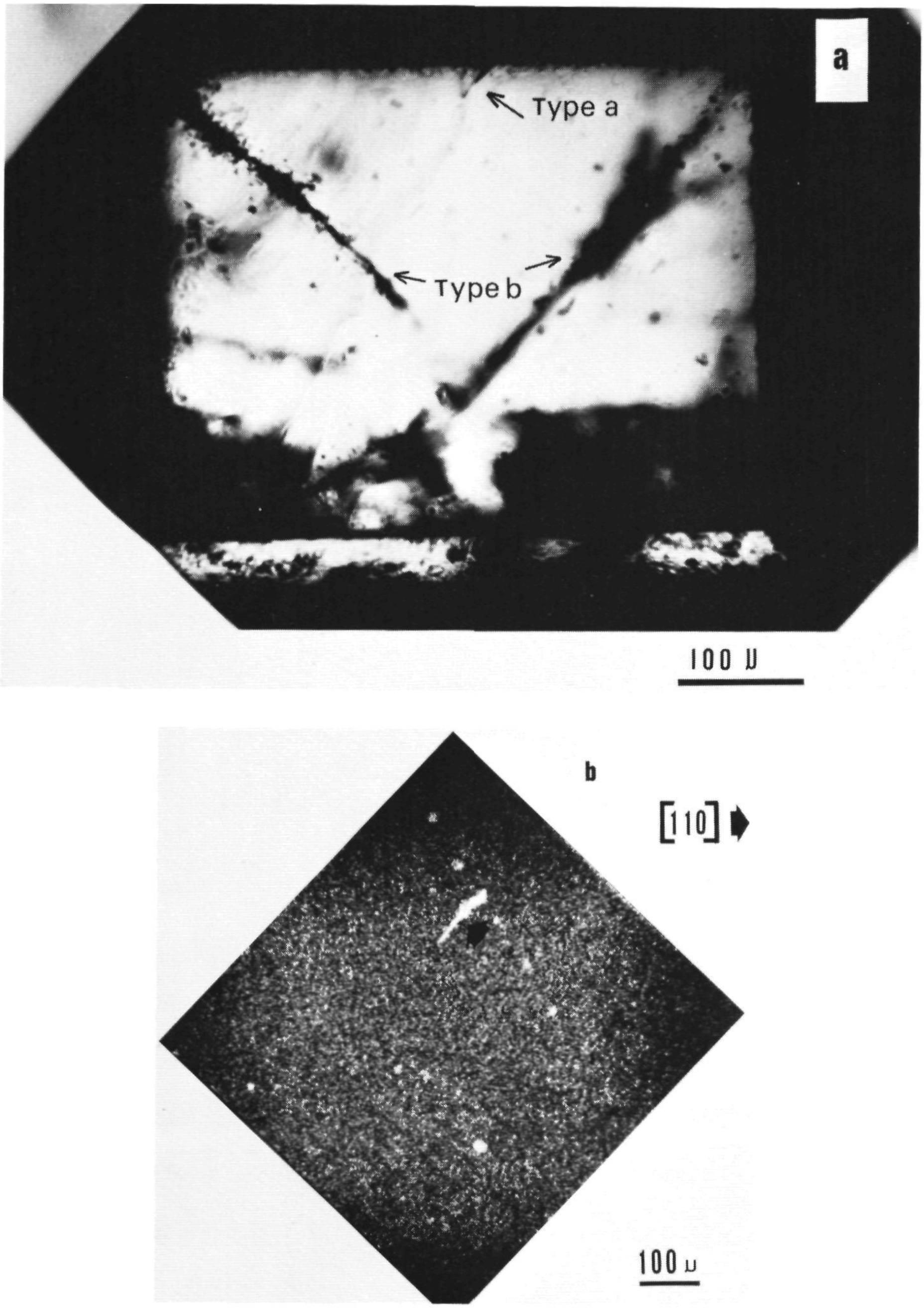

Fig.11. X-ray absorption topography of a diamond containing a large number of type b inclusions and one -small- type a inclusion. (a) Optical transmission micrograph giving a general view of the distribution of inclusions. (b) X-ray absorption topograph of the crystal shown in (a) using unfiltered Cu radiation.

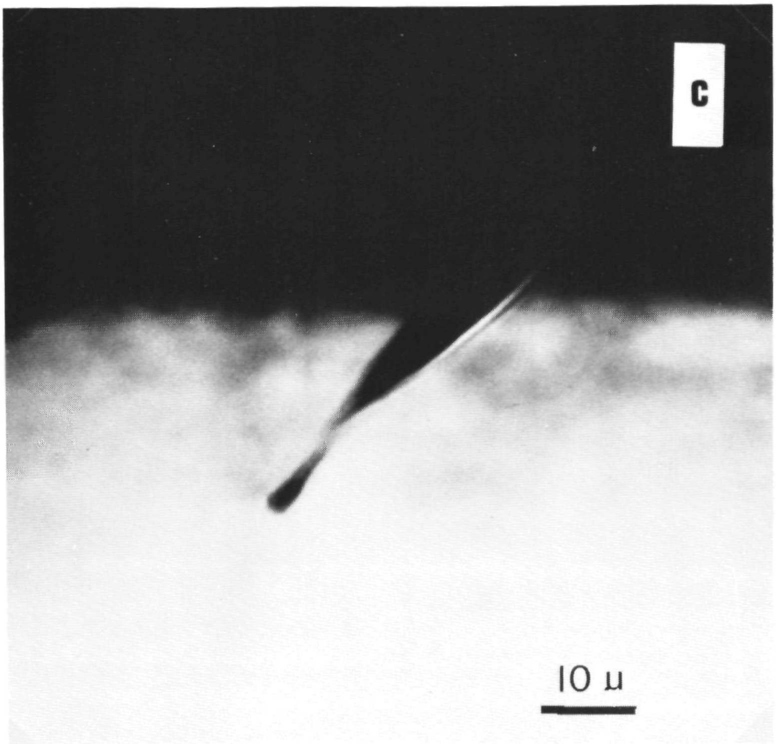

Fig.11 (continued). (c) Detailed view of the single type a inclusion, indicated by an arrow in (a) and (b) (Optical transmission micrograph).

sorption topograph of the crystal presented in figure 11a, which contains only one, small, type a inclusion. A high magnification optical transmission micrograph of this inclusion, which is marked by an arrow in the figures 11a and 11b is presented in figure 11c. Inspection of the X-ray absorption topographs learns that the inclusion in question is clearly recognizable as a white elongated spot, so that here the X-rays were strongly absorbed, which implies that the type a inclusion contains a very large amount of solidified metal. It is to be mentioned, that the occurrence of these "bubble-like" metal inclusions has been reported earlier by Kamiya and Lang (3), but no details about the formation mechanism were given.

3.2.2. Type b inclusions

In contrast to the type a inclusions, the type b inclusions are not randomly distributed in the synthetic diamond crystals, but are preferentially located along the trajectories of the vertices of the cubo-octahedrons (figs. 11a and 12a) and near the boundaries between different growth

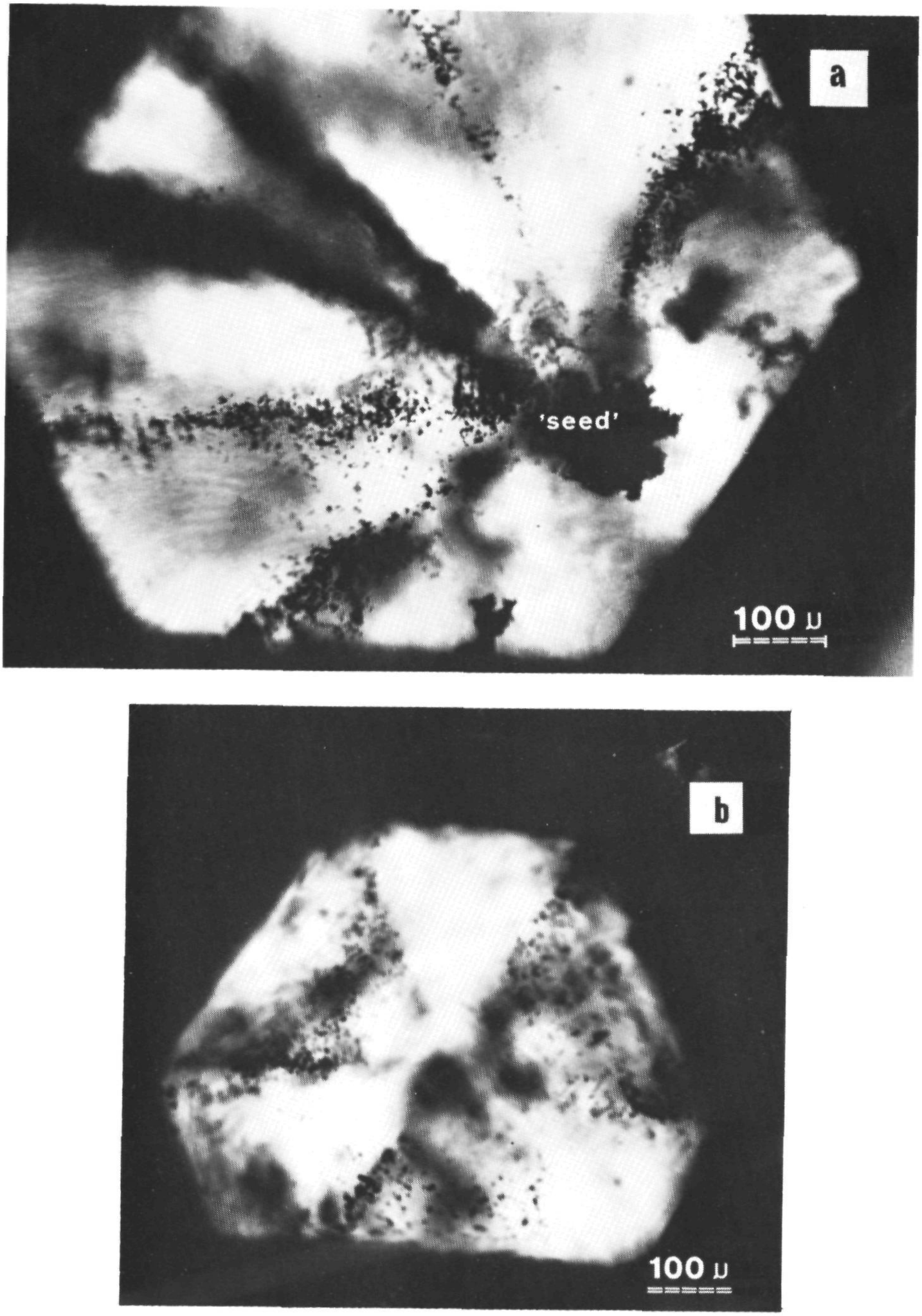

Fig. 12. Distribution of type b inclusions in the synthetic diamond crystals. (a) preferential ordering around the trajectories of the vertices of the cubo-octahedral crystals. (b) Preferential ordering near the boundaries of adjacent {111} growth sectors.

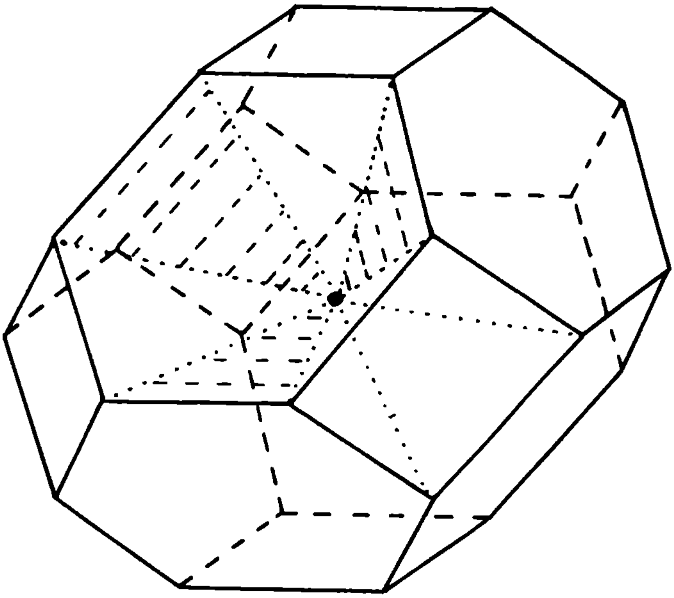

Fig.12 (continued). (c) Schematic representation of inclusion distribution in one {111} and one {100} growth sector.

sectors (fig. 12b). Further, in several cases a larger type b inclusion was found at the central nucleus of the crystals (fig. 12a) being the initial growth seed of the crystal as was verified by tracing back the trajectories of the vertices of the crystal, which are decorated by strings of type b inclusions. The preferential ordering of the type b inclusions is represented schematically in figure 12c.

Application of high magnification optical transmission microscopy showed that the inclusions are particles (∿1μ and less to 20μ in size) with a crystallite-like structure, having a random orientation and, aside from being limited by more or less flat faces, an irregular shape (fig.13). To obtain a three dimensional view of type b inclusions emerging at the crystal surface, SEM micrographs were taken as shown in figures 14a and b. Since the inclusions themselves were dissolved during the rinsing procedure in perchloric acid dihydrate prior to surface microtopography, only cavities, being the former peripheries of the type b inclusions can be seen. Again the irregular, unpredictable, but still crystalline-like shape as was observed by optical microscopy can be discerned. From

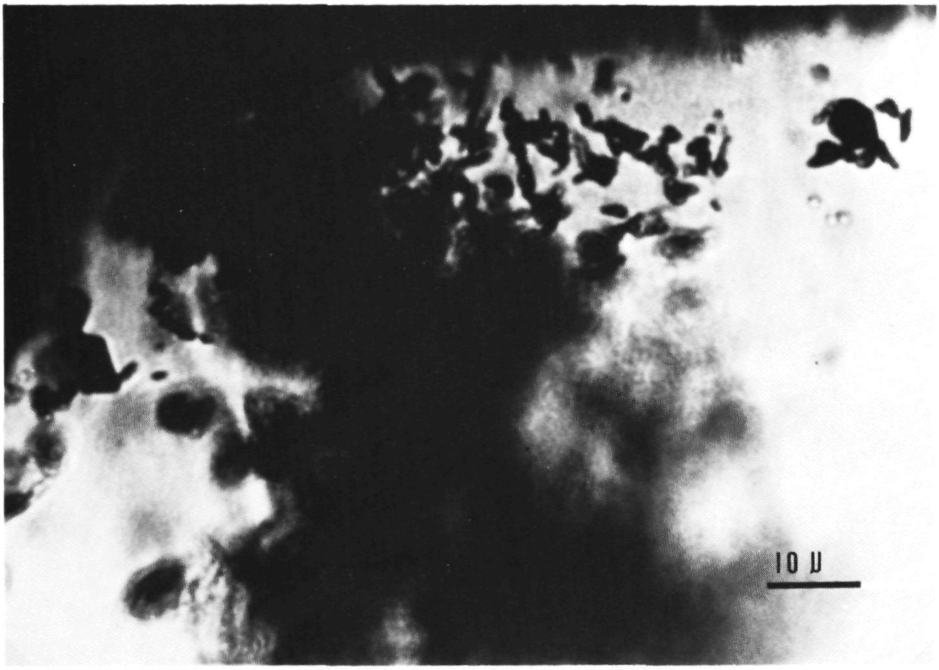

Fig.13. High magnification optical transmission micrograph showing the crystallite-like structure of type b inclusions.

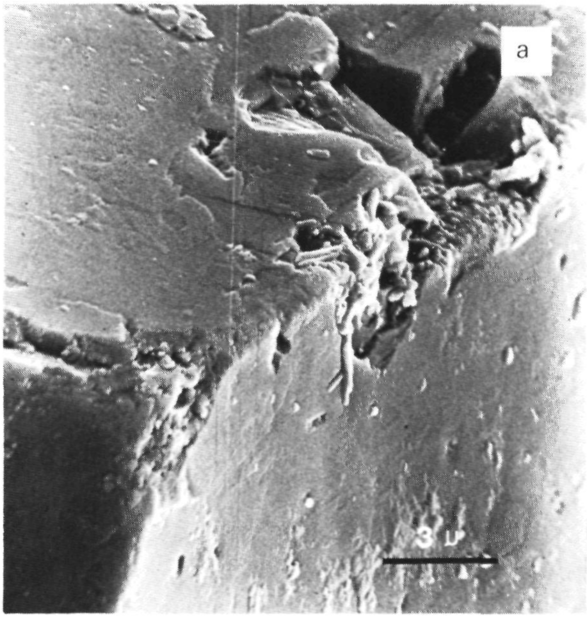

Fig.14.'Three-dimensional' views of type b inclusions meeting the crystal surface (SEM micrographs):
(a) At the edge and a corner of the crystal.

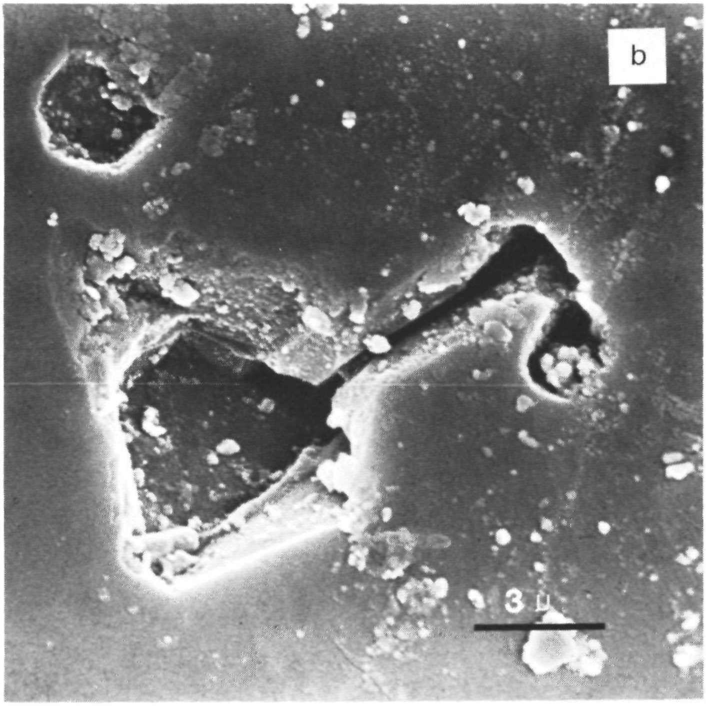

Fig.14 (continued). (b) At the central region of a growth face.

the SEM micrographs it can clearly be seen that no relation exists between macrosteps and these inclusions, which implies that type b inclusions must be formed in a completely different way compared to type a inclusions. Moreover, it is to be noted that the type b inclusions can not be formed via the conventional inclusion formation mechanisms in crystal growth, involving heat or mass transport limited growth, since the inclusions are preferentially formed at the edges and corners of the crystal, where the supersaturation in such transport limited growth is higher than elswhere on the crystal surface (37).

To verify whether the type b inclusions are formed during crystal growth or later on, via preferential precipitation of impurity along the trajectories of the corners of the crystals or near sector boundaries, releasing the stress in these area, the relation between type b inclusions and dislocations was studied by means of stress birefringence microscopy. By this polarization microscopic method, it was found that for lower quality crystals the type b inclusions can act as a source of single or bundles of dislocations as is shown in figure 5. In this polarization micrograph a row of type b inclusions (located near a sector boundary or a trajectory of a crystal corner), emitting dislocations in two different sectors can be seen. A similar generation of dislocations at sector boundaries can also be recognized from the cathodoluminicence topograph in figure 4 and the surface reflection X-ray topograph in figure 7 presented in the work by Woods and Lang (4). Since the dislocations originating from these inclusions, for each growth sector only run in one particular direction, being more or less perpendicular to the growth face belonging to the growth sector in question, it can be concluded that these line defects are typical grown-in dislocations (17). This means that these dislocations are formed during the growth process, just after inclusion formation, as a result of lattice enclosure errors (16,24) and can not be caused by strain release due to the generation of inclusions via precipitation of an impurity. In this case the dislocation lines should run in completely different directions, not related to growth sectors and probably should be curved. Now it can be concluded that the inclusions are formed during the growth process and are not a result of precipitation of an unknown impurity. This conclusion is reinforced by the fact that never dislocation lines -even those with very high Burgers vectors- were decorated by type b inclusions, as was to be expected when these inclusions were a result of a release in strain via precipitation.

Finally X-ray absorption topography, the result of which is presented in figure 11, has been applied, in order to obtain information concerning the composition of the type b inclusions. To carry out this technique, firstly a crystal with a large amount of type b inclusions was selected. A general view of this specimen is shown in the optical transmission bright field micrograph 11a. Of this crystal, mounted in the same orientation as in the optical micrograph, the X-ray absorption topograph given in figure 11b was made. On this topograph no sign is found of type b inclusions, which are much larger in size than the type a inclusion identified in the previous sector. This means that the type b inclusions do not or minute quantities contain solidified matal or metal carbides. Since the growth system only contains solvent metal and carbon in larger amounts, the only possiblity left is that type b inclusions are graphite particles. This is confirmed by the completely black appearance of these micro-crystallites in the diamonds. That the formation of graphite does occur in the growth system was already pointed out by Strong and Hanneman and by Liu Guang-zhao (42).

Using the assumption that the type b inclusions are graphite crystallites, their preferential occurrence near the sector boundaries and the trajectories of the vertices of the crystals can be understood from the following consideration:

It is well established that in non-stirred, more or less mass or heat transport limited growth systems, the supersaturation is higher near the edges and corners than at central regions of the growth faces of the crystals (37, 43). In the work of Liu Guang-zhao (42), it was shown that under growth conditions where diamond is stable, metastable graphite might be formed at higher supersaturations. Since these higher supersaturations, which promote graphite crystallization, preferentially occur near the edges and corners of the diamonds, the formation of graphite inclusions in the diamonds is enhanced in these regions. This means that the graphite, type b, inclusions *mainly occur at the former positions of the* edges and corners of the faces during crystal growth, i.e. at the sector boundaries and the trajectories of the vertices of the crystals.

3.3. Distribution of paramagnetic nitrogen impurity

Investigation of the crystals, using a low power optical transmission microscope showed, that for all the diamonds some regions were yellowishly coloured, whereas other regions in the same crystals were colourless. Since it is well known that the yellow colour in synthetic diamond originates from the presence of paramagnetic singly substituted nitrogen impurity (44), it can be concluded that the distribution of this impurity in the crystals is not uniform.

To get more detailed information on this non-uniformity of the nitrogen impurity distribution, use was made of optical absorption topography (4) employing monochromatic light of about 425 nm. This specific wavelength has been chosen, because of the fact that in the visible light region the nitrogen impurity is strongly absorbing this -violet- wavelength (45). By this method it was found that the nitrogen impurity distribution was related to the type of growth sector: The strongly absorbing {100} growth sectors have a much higher nitrogen content than the weakly or non-absorbing {111} sectors.

To demonstrate this specific nitrogen distribution over the {111} and {100} sectors in a clear manner, a twinned crystal, illustrated schematically in figure 15a, was selected. From this diamond an optical absorption topograph was made in such a manner, that the monochromatic light traverses perpendicular to its twin plane. In this way each individual ray of light passes, aside from the growth sectors related to the upper and lower basal planes of the twinned crystal, only one type of growth sector, so that the difference in absorption for each growth sector type can separately be recognized. The result is presented in figure 15 b: A large difference in intensity between the dark -highly absorbing- {100} and the bright -hardly absorbing- {111} growth sectors, due to the much higher paramagnetic nitrogen impurity content in the cubic sectors with respect to the octahedral sectors, can be seen.

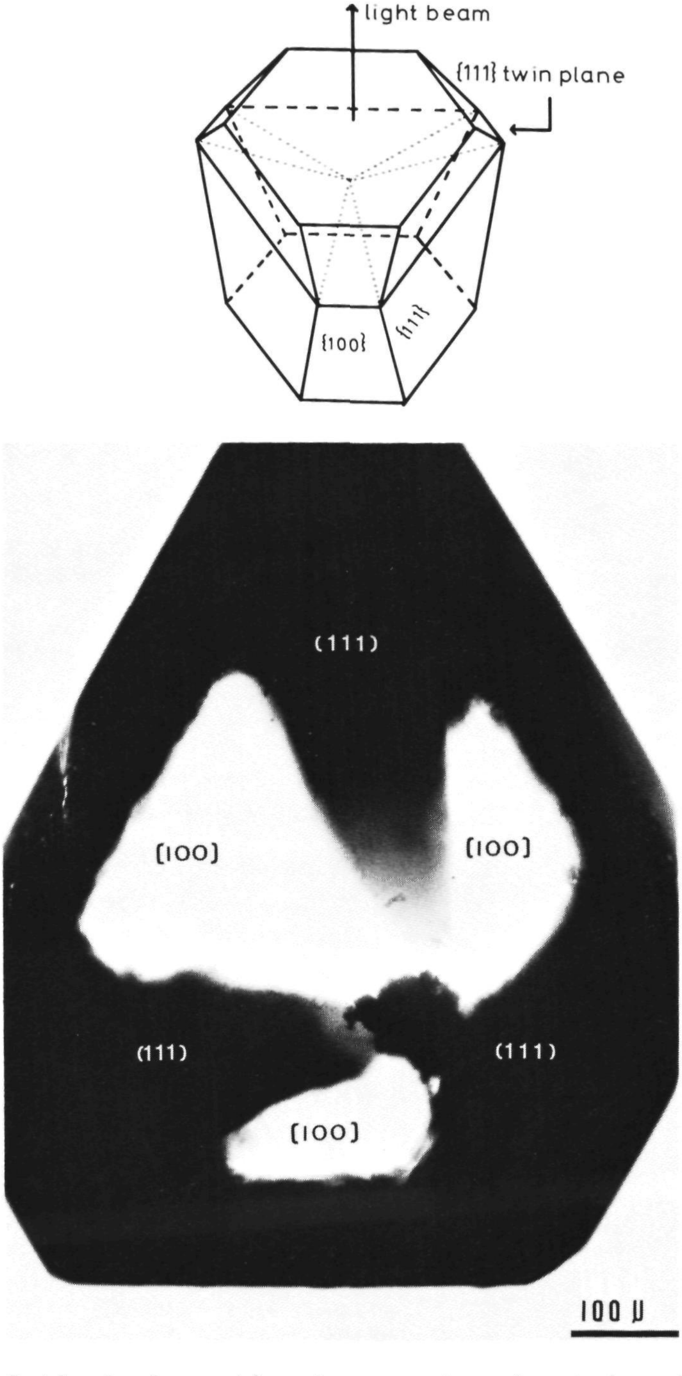

Fig.15. Optical absorption topography of a twinned specimen crystal: (a) Schematic representation of the twinned diamond; (b) Optical absorption micrograph, using monochromatic light (∿400 nm). The dark areas on the micrograph correspond to strong absorption, i.e. to higher paramagnetic nitrogen impurity contents.

The present observation of a considerably higher nitrogen content in the {100} growth sectors is in contradiction with the work by Woods and Lang (4), who applied the same optical absorption topographic method to "de Beers" synthetic diamonds. They found that the nitrogen content in the {111} growth sectors was much higher than in the {100} sectors, in which the nitrogen concentration was highly variable. Possibly this disparity in nitrogen distribution is caused by a difference in growth method or in composition of the metal solvent, however, no definite conclusions can be drawn, since in the paper by Woods and Lang no details of the growth method of the diamonds were given.

4. CONCLUSIONS

From the present detailed investigation of the internal defect structure of synthetic diamonds, by making use of a wide variety of complementary optical and X-ray topographic characterization techniques the following conclusions can be summarized:

(i) In general, dislocations in synthetic diamond run more or less perpendicular to the growth faces in a similar manner as often found for solution grown crystals.
As sources of dislocations function: (a) The central nucleus in the crystal, often being a -larger- graphite particle; (b) Inclusions occurring in all kinds of regions in the diamonds.
The crystalline perfection of the diamonds varies considerably, leading to a large difference in dislocation density for each individual crystal. In low quality crystals only enormous bundles of dislocations were found, whereas in better quality crystals also individual dislocation lines could be seen.
(ii) At the cores of a few dislocation lines with a high Burgers vector, "hollow" tubes, filled with opaque material were discerned.
(iii) In synthetic diamond two types of inclusions can be distinguished: (a) Type a inclusions, being entrapments of -solidified- metal solution, which are formed via a macrostep overhang mechanism; (b) Type b inclusions, which very probably are graphite inclusions. The preferential occurrence of these inclusions near sector boundaries and the trajectories of the vertices of the cubo-octahedral crystals is caused by a local increase in supersaturation near the edges and corners of the crystals, which enhances graphite formation in these surface areas.
(iv) In the {001} growth sectors the concentration of singly substituted nitrogen is by far higher than in the 111 sectors, which is in flat contrast to earlier work.

The main point that can be inferred from this characterization study of synthetic diamonds is that, if it is desired to grow high quality crystals, care should be taken in one or another way, that the supersaturation at the crystal-solution interface is kept constant over the whole surface area of each crystal (for example, by a kind of stirring). This prevents the formation of both type a and type b inclusions, which again prevents the formation of a major part of the dislocations in the crystals.

ACKNOWLEDGEMENTS

One of the authors (Liu Guang-zhao) wishes to thank all the collaborators of the Laboratory of Solid State Chemistry, Catholic University of Nijmegen, where this work was carried out, for their kind help. Further the authors are grateful to Ing. A.W. Dicke for his assistance in making the SEM photographs.

W.J.P. van Enckevort acknowledges the support of the Netherlands Foundation for Pure Research (ZWO/SON).

REFERENCES

(1) H.P. Bovenkerk, in: Progress in Very High Pressure Research, Eds. F.P. Bundy, W. Hibbard and H.M. Strong (John Wiley and Sons Inc., New York, 1961) p.58.

(2) A.R. Lang, in: Properties of Diamond, Ed. J. Field (Academic press, 1979) pp. 425-469.

(3) Y. Kamiya and A.R. Lang, J. Applied Phys. 36 (1965) 579.

(4) G.S. Woods and A.R. Lang, J. Crystal Growth 28 (1975) 215.

(5) A.S. Vishnevsky, J. Crystal Growth 29 (1975) 296.

(6) A.R. Lang, Phil. Mag. B 41 (1980) 689.

(7) A.R. Lang, Proc. Roy. Soc. (London) A278 (1964) 234.

(8) A.R. Lang, Brit. J. Appl. Phys. 14 (1963) 904.

(9) See: A.R. Lang, in: Properties of Diamond, Ed. J. Field (Academic press, 1979) p. 463.

(10) I. Kiflawi and A.R. Lang, Phil. Mag. 33 (1976) 697.

(11) I. Sunagawa, K. Tsukamoto and T. Kasuda, to be published.

(12) E.R. Harrison and S. Tolansky, Proc. Roy. Soc. (London) A279 (1964) 490.

(13) A.R. Lang, Nature 21 (1967) 248.

(14) W.J.P. van Enckevort and Liu Guang-zhao, J. Crystal growth to be published; Chapter IXX.

(15) W.K. Burton, N. Cabrera and F.C. Frank, Trans. Roy. Phil. Soc. (London) A243 (1951) 299.

(16) W.J.P. van Enckevort, R. Janssen -van Rosmalen, H. Klapper and W.H van der Linden, J. Crystal Growth to be published; Chapter IX.

(17) B.K. Tanner, X-ray Diffraction Topography, I.S. Science of the Solid State, Vol. 10 (Pergamon,1976).

(18) A.R. Patel, Physica 27 (1961) 1097.

(19) A.R. Patel, Physica 28 (1962) 44.

(20) A.R. Lang, J. Appl. Phys. 30 (1959) 1748.

(21) W.L. Bond and J. Andrus, Phys. Rev. 101 (1956) 620.

(22) D.J. Fathers and B.K. Tanner, Phil. Mag. 28 (1973) 749.

(23) B.K. Tanner and D.J. Fathers, Phil. Mag. 29 (1974) 1081.

(24) W.J.P. van Enckevort and J. Odekerken, Phil. Mag. to be published; Chapter V.

(25) B. Dam and W.J.P. van Enckevort, J. Crystal Growth 51 (1981) 607.

(26) S. Gits-Leon, F. Lefaucheux and M.C. Robert, J. Crystal Growth 44 (1978) 345.

(27) R.A. Ducket and A.R. Lang, J. Crystal Growth 18 (1973) 135.

(28) S. Ikeno, H. Maruyama and N. Kato, J. Crystal Growth 3/4 (1968) 683.

(29) W.J.P. van Enckevort and W.H. van der Linden, J. Crystal Growth 47 (1979) 196; Chapter I.

(30) W.J.P. van Enckevort and H. Klapper, J. Crystal Growth to be published.

(31) W.J.P. van Enckevort, R. Janssen-van Rosmalen and W.H. van der Linden, J.Crystal Growth 49 (1980) 502; Chap-

ter VIII.

(32) K. Sato, Jap. Journal of Aplied Physics 19 (1980) 1257.

(33) F.C. Frank, Acta Cryst. 4 (1951) 497.

(34) N. Cabrera, M.M. Levine and J.S. Plasket, Phys. Rev. 96 (1954) 1153.

(35) B. van der Hoek, J.P. van der Eerden and P. Bennema, J. Crystal Growth 56 (1982) to be published.

(36) R. Janssen-van Rosmalen and P. Bennema, J. Crystal Growth 42 (1977) 224.

(37) A. Seeger, Phil. Mag. 44 (1953) 1.

(38) S. Tolansky, Proc. Roy. Soc. (London) A 263 (1961) 31.

(39) A.A. Chernov and S.I. Budurov, Sov. Phys. Crystallography 9 (1964) 309.

(40) A.A. Chernov and S.I. Budurov, Sov. Phys. Crystallography 9 (1965) 388.

(41) H.M. Strong and R.E. Hanneman, J. Chem Physics 46 (1976) 3668.

(42) Liu Guang-zhao, Acta Physica Sinica 28 (1979) 334 (in Chinese).

(43) A.A. Chernov, J. Crystal Growth 24/25 (1974) 11.

(44) H.M. Strong and R.H. Wentorf Jr., Naturwissenschaften 59 (1970) 1.

(45) R.M. Chrenko, H.M. Strong and R.E. Tuft, Phil. Mag. 23 (1971) 1.

SAMENVATTING

Ondanks het feit dat er gedurende de laatste paar eeuwen een veelvoud aan kristalgroei experimenten is uitgevoerd en dat de theorie der kristalgroei sedert de twintiger jaren, met als hoogtepunt het spiraalgroei model door Burton, Cabrera en Frank in 1951, tot volle wasdom is gekomen, is een gedetailleerde correlatie tussen theorie en experiment, met name voor de groei uit de oplossing, nog steeds een witte plek op de landkaart van onze kennis. Om dit "terra incognita" te verkennen zijn gedurende het huidige promotie onderzoek (naast elders uitgevoerde groeikinetiek metingen) oppervlakte microtopografie m.b.v. zeer verfijnde fasencontrast microscopie, differentiële interferentiecontrast microscopie, "two" of "multiple beam" interferometrie en "scanning electron" microscopie evenals röntgen diffractie -Lang- topografie de belangrijkste hulpmiddelen geweest. M.b.v. deze technieken was het mogelijk om zowel de interne (met name dislocatie en groeisector configuraties) als de externe (oppervlakte morfologie) structuur in relatie tot de groeihistorie der kristallen te doorvorsen.

Twee hoofdgroepen van kristallen werden bestudeerd:

(i) Uit de waterige oplossing gegroeide ionogene kristallen, zoals kalium aluminium aluin, kalium en ammonium waterstof fosfaat en kalium waterstof ftalaat.

Bij deze kristallen werden, kort samengevat, de volgende fenomenen ontdekt en/of uitgebreid bestudeerd:

(a) Voor het eerst werd onweerlegbaar aangetoond dat kristalgroei uit de waterige oplossing verloopt via zeer lage groeistappen met een hoogte variërende van 6 tot 20 A. Als stapbronnen kunnen fungeren: Uitmondingen van schroefdislocaties aan het kristaloppervlak welke aanleiding geven tot spiraalgroei en daarnaast tweedimensionale kiemen op defectvrije oppervlakte gebieden.

(b) Etspatronen (zowel putten als groeven), welke geinterpreteerd konden worden met behulp van een aantal theoretische modellen.

(c) Diverse aspecten, zoals de vorming van insluitsels in verband met de dislocatiestructuur en hydrodynamica, een interpretatie van het voorkomen van groeidispersie van kristalvlakken, nucleatiegroei en spannings dubbelbreking microscopie van dislocatie configuraties in relatie met Langtopografie.

(d) In situ waarnemingen van zeer lage stappen (26 A) op kristallen groeiende in de waterige oplossing m.b.v. optische microscopie. Een bijzonder intrigrerende ontdekking hierbij is dat op een gegeven kristaloppervlak in een gegeven oplossing roterende -groeiende- spiralen naast stilstaande -niet groeiende- spiralen gelijktijdig kunnen voorkomen.

(ii) Kristallen met een diamantrooster of een hiervan afgeleide kristalstructuur

Allereerst werd een aantal theoretische modellen ontwikkeld voor deze groep van kristallen, waarbij Monte Carlo simulaties en "stap"-reconstructie een sleutelrol spelen. Daarna werden een aantal kristallen specifiek onder de loep genomen:

(a) Polykristallijn silicium gegroeid op een substraat dat bedekt is met een dunne laag vloeibaar metaal, voor de produktie van goedkoop fotovoltaīsch zonnecelmateriaal. Deze microkristallen bleken verrassenderwijs te groeien volgens een heel specifiek "twin plane reentrant edge" mechanisme, waarbij "twin"lijnen fungeren als stappenbron.

(b) Eén-kristallijn silicium geetst met gasvormig HCl; de op deze kristallen uitgebreid bestudeerde "bunch"-vorming kon worden geinterpreteerd m.b.v. de kinematische golftheorie voor groeistappen patronen, ontwikkeld door Frank.

(c) $CuInS_2$ en $CuGaS_2$, gegroeid m.b.v. de "chemical vapour transport" (CVT) methode met jodium als transporteur. Hier blijkt "vapour-liquid-solid" (VLS) groei met CuI als vloeibare fase een cruxiale rol te spelen in het groeiproces.

(d) Synthetische diamant, gegroeid uit een vloeibare metaalflux van 1400 ^{o}C bij een druk van ca. 60 Kbar. Uit oppervlakte microtopografie blijkt dat deze kristallen typische representanten zijn voor kristalgroei uit de oplossing, hetgeen vroegere speculaties omtrent katalytische groei weerlegt. De kristalgroei vindt plaats via zeer lage stappen (5-50 A), welke gegenereerd worden door groeispiralen of tweedimensionale kiemen. Naast de oppervlakte morfologie werd er eveneens uitvoerig aandacht besteed aan de inwendige defectstructuur van deze kristallen, hetgeen resulteerde in de waarneming en interpretatie van dislocaties, twee soorten insluitsels en specifieke verdelingen van onzuiverheden.

Als voornaamste eindconclusie van het onderzoek kan worden gegeven, dat ondanks het feit dat de kristalgroeimodellen -al dan niet in gemodificeerde vorm- goed toepasbaar zijn op de vele kristalsoorten, elk kristal, ja zelfs elk symmetrisch equivalent vlakje van het zelfde kristal uniek is qua oppervlakte morfologie en defect structuur.

CURRICULUM VITAE

W.J.P. van Enckevort werd geboren op 16 april 1952 te Blerick-Venlo. Na het behalen van het HBS-b diploma aan het Blariacum College in zijn geboorteplaats is hij in 1969 begonnen aan zijn scheikunde studie aan de Katholieke Universiteit te Nijmegen. In 1972 behaalde hij zijn kandidaatsexamen (S3, cum Laude) en in 1977 zijn doctoraalexamen (cum laude) met als hoofdvakken Vaste Stof Chemie (onderwerp: karakterisatie van met gasfase HCl geetst één-kristallijn silicium) en Kristallografie (onderwerp: structuur analyses m.b.v. directe methoden). Sindsdien heeft hij als wetenschappelijk medewerker een promotieonderzoek verricht inzake de karakterisatie van een grote diversiteit van één-kristallen in relatie tot de theorie van de kristalgroei onder de bezielende begeleiding van Prof. Dr. P. Bennema. Gedurende deze tijdspanne assisteerde hij een aantal jaren "traditiegetrouw" bij het werkcollege electrochemie.

Naast het hier beschreven promotieonderzoek heeft hij ook meegewerkt aan een aantal andere onderzoeksprojecten, welke resulteerden in de volgende artikelen:

(1) A.W. Verheijen, W.J.P. van Enckevort, J. Bloem and L.J. Giling: Flux growth, analysis and crystallographic aspects of alkali rare earth sulfides, J. de Physique 36 (1975) C3-39.

(2) W.J.P. van Enckevort, Paul T. Beurskens, E.M. Menger and W.P. Bosman: Structure analysis of Catena[-µ-(2,6-diethylamino-1,3,5,7-tetra-thiahepta-1,6-diene)di-µ-iodo-di(iodomercury(II))], Cryst. Struct. Comm. 6 (1977) 417.

(3) W.J.P. van Enckevort, H.M. Hendriks and Paul T. Beurskens: Structure analysis of Trichloro-bis-(triethylphosphine)cobalt, Cryst. Struct. Comm. 6 (1977) 531.

(4) P. Bennema, J.P. van der Eerden, W.J.P. van Enckevort B. van der Hoek and K. Tsukamoto: Observation and interpretation of spirals for spiral growth from the liquid state, Phys. Stat. Sol. (a) 55 (1979) 403.

alsmede aan een aantal, -momenteel nog niet gepubliceerde- andere onderzoekingen zoals:
(i) Gedetailleerde kwantitatieve etsputstudies op {111} aluin en {101} KH_2PO_4;
(ii) De vorming van insluitsels in KH_2PO_4 kristallen in relatie tot de hydrodynamica van het groeisysteem;
(iii) Een uitgebreide microtopografische oppervlaktestudie van {001} $NiSO_4.6H_2O$;
(iv) Een rontgen-topografisch onderzoek van de inwendige defect structuur van $(NH_4)_2SO_4$ kristallen.

STELLINGEN

1

De toepassing van het directe stepintegratie model volgens Chernov op metingen aan misoriënteerd {110} granaat films, gegroeid volgens de LPE techniek door Görnert et al. is aan bedenkingen onderhevig.

P. Görnert, G.G. d'Ambly, R. Hergt and S. Bornman, phys. stat. sol. (a) 57 (1980) 163.
A.A. Chernov, J. Crystal Growth 24/25 (1974) 11.

2

Het veelvuldig voorkomen van de K-vlakken {100} op uit de gasfase gegroeide diamant en silicium kristallen kan geinterpreteerd worden in termen van het vóórkomen van een 2x1 oppervlakte reconstructie.

3

Voor het opsporen en identificeren van "scatter centra" in kristallen te gebruiken als frequentieverdubbelaar voor hoog vermogen lasers kan "scattered light tomografie" een waardevol hulpmiddel zijn.

K. Moriya and T. Ogawa, J. Crystal Growth 44 (1978) 53.

4

Bij het vergelijken van de resultaten van een Periodic Bond Chain (PBC) analyse met de fysische werkelijkheid, is de overeenkomst verheugend, maar vaak verwonderlijk.

5

In de beschrijving die Hitchman en Kane geven over de vorming van SIPOS lagen, is ten onrechte de mogelijkheid van nucleatie van SiO_2 in de gasfase buiten beschouwing gelaten.

M.L. Hitchman and J. Kane, J. Crystal Growth 55 (1981) 485.

6

De in het "Handbook of Chemistry and Physics" en in de thermodynamische tabellenboeken vermelde waarde voor de enthalpie van gasvormig CuI is zeer waarschijnlijk onjuist.

Dit proefschrift.

7

Het in de wereld der kristallografen veelvuldig gebruikte mozaïekstructuur-model ter correctie van de extinctie voor niet "ideaal imperfecte kristallen" heeft in het algemeen geen fysische relevantie.

8

Kristalgroeiers hebben doorgaans een minimale kennis van kristallografie.

9

Kristallografen hebben doorgaans een minimale kennis van kristalgroei.

10

Uitgaande van Machiavelli's stelling, dat een 'goed' heerser zich in vredestijd altijd moet blijven voorbereiden op oorlogsvoering kan men concluderen dat het streven naar permanente vrede bij voorbaat kansloos is.

N. Machiavelli, De Heerser (Atheneum, Polak & van Gennep, Amsterdam, 1977) p.123 - 126.

11

Amoralismen zijn niet noodzakelijkerwijs immoreel.

12

Voor een verantwoorde uitvoering van "Supply-Side Economics" is ook een bezuiniging op de defensiebegroting van niet te onderschatten belang.

Arthur B. Laffer, De fiscus onder het mes (Acropolis, Amsterdam, 1981).

13

Gevorderde amateurastronomen zien over het algemeen door andermans kijkers geen sterren, doch hooguit afbeeldingsfouten.

W.J.P. van Enckevort Nijmegen, 26 februari 1982